Stony Brook University

On the Subject of Analyzing Iron and Sulfur Bearing Minerals from Three Extreme Environments: Geological Carbon Sequestration, Acid Mine Drainage, and Mars

A Dissertation Presented

by

Elizabeth Christ Sklute

to

The Graduate School

in Partial Fulfillment of the

Requirements

for the Degree of

Doctor of Philosophy

in

Geosciences

Stony Brook University

August 2014

Stony Brook University
The Graduate School

Elizabeth Christ Sklute

We, the dissertation committee for the above candidate for the
Doctor of Philosophy degree, hereby recommend
acceptance of this dissertation.

Dr. Timothy Glotch – Dissertation Advisor
Associate Professor, Department of Geosciences

Dr. Richard Reeder - Chairperson of Defense
Professor, Department of Geosciences

Dr. Martin Schoonen
Professor, Department of Geosciences

Dr. Deanne Rogers
Assistant Professor, Department of Geosciences

Dr. Ed Cloutis
Professor, Department of Geography,
The University of Winnipeg, Canada

This dissertation is accepted by the Graduate School

Charles Taber
Dean of the Graduate School

On the Subject of Analyzing Iron and Sulfur Bearing Minerals from Three Extreme Environments: Geological Sequestration, Acid Mine Drainage, and Mars

by

Elizabeth Christ Sklute

Doctor of Philosophy

in

Geoscience

Stony Brook University

2014

Abstract

The global iron and sulfur cycles are linked to some of the most ancient metabolisms on our planet, and, therefore, possibly other planetary bodies. They are also linked to some of our most pressing environmental problems on Earth. Understanding their interactions and monitoring their occurrence is, therefore, an important aspect of exploring planetary bodies and sustainable resource management. This dissertation reports investigations into the identification and analysis of iron and sulfur bearing phases in three extreme environments: Acid-gas/CO_2 co-sequestration, acid mine drainage (AMD), and Mars.

H_2S and SO_2 (acid gases) are often co-contaminants in CO_2 streams. Co-sequestration of these gases lowers the cost of sequestration, but these sulfur-bearing gases can increase the reactivity of the injection site, particularly if iron-bearing minerals are present. Analyzing iron

and sulfur reactivity in these systems is, therefore, crucial to further development of carbon sequestration technology. Experiments examining the simulated co-injection of CO_2, H_2S and/or SO_2 are reported for hematite-bearing and hematite-free sandstones. The iron mineralogy of the sandstones, which is monitored using Mössbauer spectroscopy, is key to the reactivity of the sandstones.

Jarosite is an iron sulfate found primarily in areas of AMD, but it has also been identified on Mars. On Earth, using remote sensing to quantify jarosite concentrations could be a time and cost saving measure for AMD detection and cleanup. On Mars, quantifying jarosite may help constrain surface processes responsible for its formation. Quantitative mineral abundance determination using remote sensing requires knowledge of the optical constants of minerals present on the surface. The optical constants of jarosite are determined and the methodology for optical constant determination (Hapke formulation), including an open source computer code, is reported.

The Martian surface has an abundance of amorphous material that is rich in iron and sulfur. There is also evidence for a current brine hydrologic cycle. Under the low atmospheric pressure of the Martian surface, iron and sulfur rich brines could form amorphous phases. Since our ability to interpret spectra from other planets is dependent upon the breadth of our spectral library, amorphous iron sulfates are synthesized and analyzed so that they may be considered in future analyses.

This work is dedicated to the late Dr. Paul Alpers

- an unparalleled researcher of bright mind and steady hand,

who found poetry in even the most pedestrian subjects.

You are missed.

Frontispiece

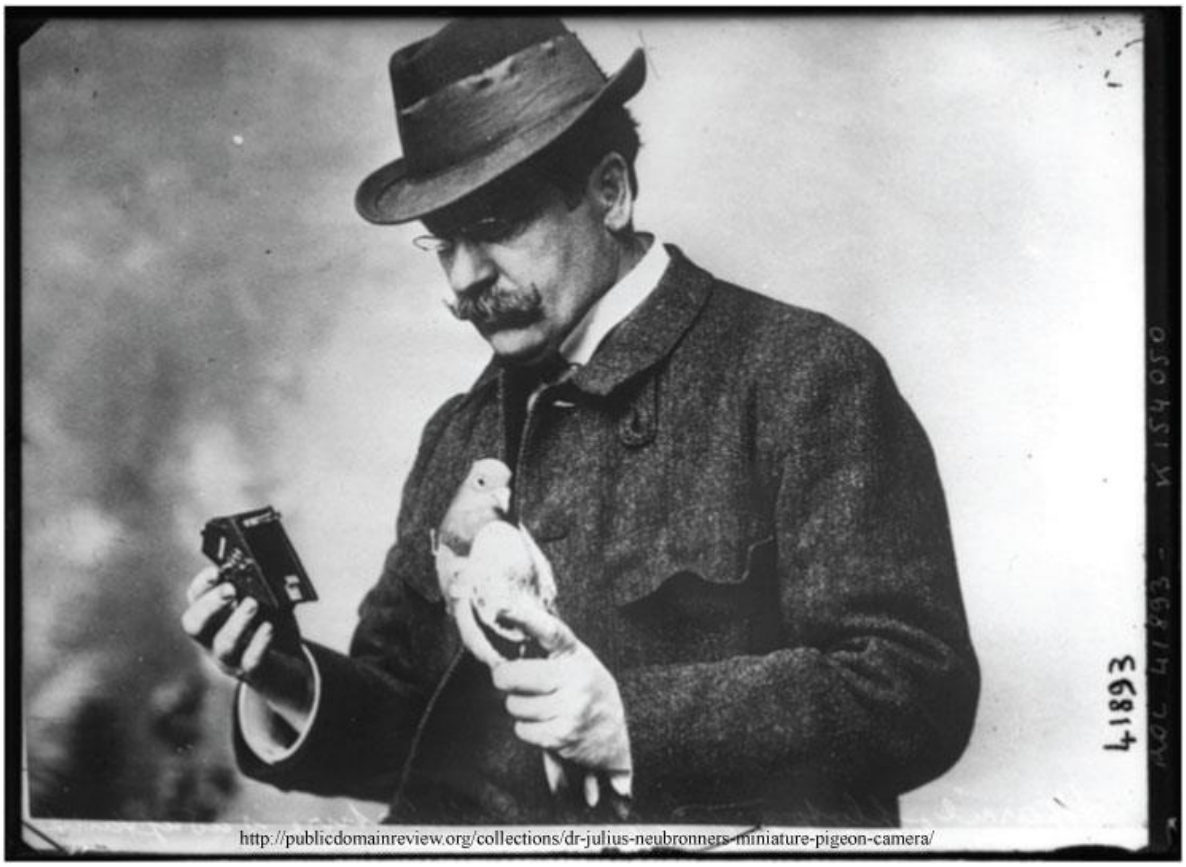

Because in every field, there is a man who wants to strap a camera to a pigeon.

And thus, remote sensing was born.

TABLE OF CONTENTS

LIST OF FIGURES

LIST OF TABLES

Preface

“The Golden Age

The golden age was first; when Man yet new,
No rule but uncorrupted reason knew:
And, with a native bent, did good pursue.
Unforc'd by punishment, un-aw'd by fear,
His words were simple, and his soul sincere;
Needless was written law, where none oppress:
The law of Man was written in his breast:
No suppliant crowds before the judge appear'd,
No court erected yet, nor cause was heard:
But all was safe, for conscience was their guard.
The mountain-trees in distant prospect please,
E're yet the pine descended to the seas:
E're sails were spread, new oceans to explore:
And happy mortals, unconcern'd for more,
Confin'd their wishes to their native shore.
No walls were yet; nor fence, nor mote, nor mound,
Nor drum was heard, nor trumpet's angry sound:
Nor swords were forg'd; but void of care and crime,
The soft creation slept away their time.
The teeming Earth, yet guiltless of the plough,
And unprovok'd, did fruitful stores allow:
Content with food, which Nature freely bred,
On wildings and on strawberries they fed;
Cornels and bramble-berries gave the rest,
And falling acorns furnish'd out a feast.
The flow'rs unsown, in fields and meadows reign'd:
And Western winds immortal spring maintain'd.
In following years, the bearded corn ensu'd
From Earth unask'd, nor was that Earth renew'd.
From veins of vallies, milk and nectar broke;
And honey sweating through the pores of oak.

The Silver Age

But when good Saturn, banish'd from above,
Was driv'n to Hell, the world was under Jove.
Succeeding times a silver age behold,
Excelling brass, but more excell'd by gold.
Then summer, autumn, winter did appear:
And spring was but a season of the year.
The sun his annual course obliquely made,
Good days contracted, and enlarg'd the bad.
Then air with sultry heats began to glow;
The wings of winds were clogg'd with ice and snow;
And shivering mortals, into houses driv'n,
Sought shelter from th' inclemency of Heav'n.
Those houses, then, were caves, or homely sheds;
With twining oziers fenc'd; and moss their beds.
Then ploughs, for seed, the fruitful furrows broke,
And oxen labour'd first beneath the yoke.

The Brazen Age

To this came next in course, the brazen age:
A warlike offspring, prompt to bloody rage,
Not impious yet...

The Iron Age

Hard steel succeeded then:
And stubborn as the metal, were the men.
Truth, modesty, and shame, the world forsook:
Fraud, avarice, and force, their places took.
Then sails were spread, to every wind that blew.
Raw were the sailors, and the depths were new:
Trees, rudely hollow'd, did the waves sustain;
E're ships in triumph plough'd the watry plain.

Then land-marks limited to each his right:
For all before was common as the light.
Nor was the ground alone requir'd to bear
Her annual income to the crooked share,
But greedy mortals, rummaging her store,
Digg'd from her entrails first the precious oar;
Which next to Hell, the prudent Gods had laid;
And that alluring ill, to sight display'd.
Thus cursed steel, and more accursed gold,
Gave mischief birth, and made that mischief bold:
And double death did wretched Man invade,
By steel assaulted, and by gold betray'd,
Now (brandish'd weapons glittering in their hands)
Mankind is broken loose from moral bands;
No rights of hospitality remain:
The guest, by him who harbour'd him, is slain,
The son-in-law pursues the father's life;
The wife her husband murders, he the wife.
The step-dame poyson for the son prepares;
The son inquires into his father's years.
Faith flies, and piety in exile mourns;
And justice, here opprest, to Heav'n returns.”

Ovid’s Metamorphosis, Translated by Sir Samuel Garth, John Dryden, et al.

Acknowledgements

Thanks belong

to the bank of Mom

Without thee

I'd not be debt free

at the end

of this PhD

Yet, perhaps

more importantly

it is your choice

and need to voice

a belief in me

that maintained

my sanity

(and of course

that dog and horse

who now will see

a lot more of me)

Chapter 1

Introduction

The identification and analysis of iron and sulfur bearing phases is important across a broad spectrum of scientific problems. The global cycles of iron and sulfur are linked to some of the most basic and ancient metabolisms on our planet (Stetter 1996; Canfield and Raiswell 1999; Canfield and Farquhar 2012; Kendall et al. 2012); and iron and sulfur have been called the most important elements for biogeochemical interactions on a global scale (Krumbein and Gorbushina 2010). On Earth, since the Paleoproterozoic (2.5 Ga), surface geology has been either directly or indirectly affected by surface biology (Hazen et al. 2008); the redox cycles of sulfur and iron have been central to those interactions (Stetter 1996; Canfield and Raiswell 1999; Sievert et al. 2007; Krumbein and Gorbushina 2010). Thus, the search for life on other planets should include a focus on the identification of these two elements in the rock record. Iron and sulfur cycles are also inextricably linked to some of our most pressing environmental problems, individually (Chestnut and Mills 2005) and through their direct and indirect interaction with the carbon cycle (Raiswell and Canfield 2012). Because iron and sulfur are major elements in industry (Ober 2002; UNEP 2013), tracking the interaction of iron and sulfur byproducts with the natural world is important in mitigating and remediating contamination. Therefore, investigating the interactions of these two species in extreme environments provides interesting challenges to, and

opportunities for, the development of techniques that enhance our understanding of Earth and other planetary bodies.

This work is divided into three sections, each representing an extreme environment in which the interaction of iron and sulfur plays a pivotal role: 1) acid gas - carbon co-sequestration, 2) acid mine drainage, and 3) Martian surface geochemisty. Analysis of the interactions of iron and sulfur in each of these environments provides critical information about the systems in question.

Acid gas - carbon co-sequestration. Acid gases like H_2S and SO_2 are often co-contaminants in CO_2 streams from thermal power stations (Chialvo et al. 2013). Co-sequestration of these gases lowers the cost of sequestration by limiting the cost of gas purification steps (GHG 2003; Anheden et al. 2005). But these sulfur-bearing gases can increase the reactivity of the injection site, particularly if iron-bearing minerals are present (DePaolo and Cole 2013). Often, modeling cannot account for all the variables in these complex systems (Bertier et al. 2006). Experimental investigations of these systems are, therefore, crucial to further the development of carbon sequestration technology. Tracking the reactivity between the iron and sulfur phases provides key insights into potential reactivity of sequestration systems. In this dissertation, I report on experiments examining the simulated co-injection of CO_2, H_2S and/or SO_2 for hematite-bearing and hematite-free sandstones. The iron mineralogy, which is monitored using Mössbauer spectroscopy, is central to the reactivity of the sandstones.

Acid mine drainage. Acid mine drainage (AMD) is a highly acidic, potentially hazardous runoff from mining sites that is caused by the oxidative weathering of sulfides, usually pyrite (FeS_2) (Jambor and Blowes 1994). AMD often results in the precipitation of iron and sulfur-bearing minerals that can be used as tracers and indicators of this contamination (Swayze et al.

2000). Detecting and monitoring these minerals is, therefore, a key step in prevention and cleanup efforts. The use of remote sensing for mineral monitoring can save both time and money (Swayze et al. 2000). Remote sensing using visible and near infrared spectroscopy is particularly useful, since iron sulfates display characteristic and differentiable absorptions in this wavelength range (Cloutis et al. 2006). But obtaining quantitative mineral abundances from VNIR spectra of mixed samples requires that the optical constants (the real and imaginary indices of refraction) of the minerals in the mixture be known. Optical constant determination of key iron and sulfur bearing minerals is, therefore, crucial to the analysis of iron and sulfur on global scales. The iron oxyhydroxy sulfate, jarosite, in particular, is linked to the acidification potential of the soil and is often present in large enough quantities that it can be detected using remote sensing (Swayze et al. 2000). This dissertation presents the optical constants of three synthetic jarosites, along with detailed methodology for optical constant determination using the Hapke formulation of radiative transfer theory. A Matlab computer code, which can be used for the determination of optical constants of additional materials, is also included.

Mars surface geochemistry. The Martian surface is rich in iron and sulfur bearing minerals (McLennan 2012), including jarosite (Klingelhofer et al. 2004). The central role of iron and sulfur to past and present life on Earth (Konhauser and Riding 2012) makes concentrations of these two elements attractive places to look for evidence of life on Mars. In the absence of sample return, our ability to accurately identify and quantify the abundance of such minerals through remote sensing provides one of our primary sources of information about the Martian surface. Iron sulfates like jarosite, in particular, are important remote sensing target minerals because they form under a limited set of conditions and are associated with microbial activity on Earth (Bigham et al. 1996a; Bigham et al. 1996b; Norlund et al. 2010). Therefore, their accurate

identification and quantification provide valuable constraints on Martian surface geochemistry and possible indications of Martian surface biology. Here, too, optical constant determination is key to enhancing our interpretations of the Martian surface environment.

Our ability to interpret remote sensing data is also dependent upon the breadth of the spectral library we use for comparison. Recent findings show that parts of the Martian surface are made up of large percentages of amorphous material that is rich in both iron and sulfur (Bish et al. 2013; Morris et al. 2013). There is also evidence of a brine hydrologic cycle that may currently be active on the surface and in the shallow subsurface of Mars (Chevrier and Altheide 2008; Altheide et al. 2009; McEwen et al. 2011; Martinez and Renno 2013; Masse et al. 2014). Iron and sulfur form brines that would be stable over much of the Martian surface and subsurface, at least for short periods of time (Chevrier and Altheide 2008). Upon evaporation or boiling under Mars' low atmospheric pressure, amorphous iron sulfates can form. An interesting feature of amorphous and poorly crystalline materials on Earth is that they are often associated with biological activity (Konhauser and Riding 2012). In either case, library spectra of amorphous iron sulfates are required for identification of these phases on Mars. Here I report the synthesis and characterization of amorphous iron sulfates so that these phases may be considered in future analyses.

This introductory chapter will briefly introduce the global cycles of sulfur and iron and how they interconnect on Earth. I then use this background to discuss how they may cycle on Mars.

1.1 The Sulfur Cycle

Sulfur, an essential element for life, cycles globally through the atmosphere, hydrosphere, biosphere, and lithosphere (Ivanov 1983) in valence states ranging from -2 to +6. Although sulfur's transit through these spheres is not separable, it is convenient to divide atmospheric sulfur cycling from geologic sulfur cycling, a convention that arises from a historical separation in the field (Eriksson 1963).

1.1.1 Geologic Sulfur Cycle

Mantle derived sulfur, brought to the surface primarily through volcanic out-gassing, hydrothermal activity, and weathering of igneous material in oxic seawater (Canfield and Farquhar 2012) is geologically stored mainly as gypsum ($CaSO_4 \cdot 2H_2O$) or pyrite (FeS_2) (Canfield 2004). Continental weathering (both biotic and abiotic) and interactions between the lithosphere and hydrosphere result in the oxidation and transport of sulfur to the oceans in the form of sulfate (SO_4^{2-}). Here, biologically mediated reduction transforms sulfate back to sulfide (S^{2-}), and, as such, it is deposited and buried. Uplift and erosion can continue cycling S through the surface reservoir, and subduction can deliver it back to the mantle (Canfield 2004).

1.1.2 Atmospheric Sulfur Cycle

The hydrosphere is the most prominent intersection between the atmospheric sulfur cycle and the geologic sulfur cycle. Non-anthropogenic sulfur emissions to the atmosphere are primarily from algal blooms in the form of the volatile compound dimethyl sulfide (DMS), a metabolic product of marine photoautotrophs (Sievert et al. 2007). Other sources include volcanic out-gassing of SO_2 and H_2S and non-anthropogenic weathering of sulfur-containing sediments transported by aeolian processes (Brimblecombe et al. 1989). Anthropogenic inputs, however, overshadow all natural atmospheric sources, making up 70-80% of all sulfur emissions

to the atmosphere (Rasch et al. 2000). In the atmosphere, sulfur exists as SO_2 for only a short while before being converted to sulfuric acid (H_2SO_4) and sulfate aerosols (Karnieli et al. 2009). Sulfur is re-deposited on the surface through precipitation, adsorption, and particulate deposition over continents and oceans, but most continental inputs wind up in rivers (Brimblecombe et al. 1989), thus becoming part of the hydrosphere and making their way back to the ocean.

1.1.3 Anthropogenic Contributions to the Sulfur Cycle

Anthropogenic contributions to the sulfur cycle are multifaceted. Although the largest contribution to anthropogenic sulfur emissions is the burning of fossil fuels (Smith et al. 2001), it is not the only way in which anthropogenic activities influence the sulfur cycle. Humans act as agents of continental erosion through direct mining and through land use that leads to desertification, thus increasing sulfur input to both the hydrosphere and atmosphere. Indirectly, nutrient enrichment of coastal waters may also contribute to increased DMS production (Brimblecombe et al. 1989). These combined contributions are responsible for acidification of precipitation (Galloway 2001) and surface waters (Galloway 2001; Johnson 2003), increases in particulate pollution (Chestnut and Mills 2005), and climate forcing (Boucher and Anderson 1995).

1.2 The Iron Cycle

Iron is the 4th most abundant component of the Earth's crust and is required as a micronutrient by almost every living organism (Kendall et al. 2012). Like sulfur, iron redox chemistry has likely been central to microbial metabolisms since the beginning of life on our planet (Kendall et al. 2012). However, in today's oxygen-rich atmosphere, iron is actually the

limiting reactant in photosynthesis carried out by marine phytoplankton and is thus intimately linked to the carbon cycle (Raiswell and Canfield 2012).

Iron makes up 7 wt% of the crust in a variety of minerals (McLennan 2001). As these minerals weather (biotically and abiotically), iron, as Fe^{2+} and Fe^{3+}, is released. This iron either enters the hydrosphere or the atmosphere. In oxic waters, Fe^{2+} is quickly oxidized to Fe^{3+}, which hydrolyzes to form a variety of Fe-(O)-OH species. Much of this Fe^{3+} then quickly precipitates as (oxyhydr)oxides. The Fe^{3+} that remains in solution is primarily bound in complexes or colloids, most of which precipitate in coastal environments when high ionic strength fluids mix with riverine inputs and neutralize the colloids' surface charge that has kept them suspended (Kendall et al. 2012). The primary delivery method of iron to the surface oceans is thought to be nanoparticulate aeolian dust (Raiswell 2011). Other surface ocean inputs include iceberg melt and recycling of shelf sediments (Raiswell and Canfield 2012). Iron enters the deep ocean through hydrothermal systems (Chu et al. 2006; Bennett et al. 2008). Here, anoxic waters stabilize Fe^{2+} in solution, but in the presence of sulfur, which is prevalent in hydrothermal environments, iron sulfides form and quickly precipitate (Kendall et al. 2012). These sediments can then be brought to the surface again through tectonic activity.

1.3 Where the Iron and Sulfur Cycles Meet

It is in the deep oceans that the iron and sulfur cycles are most firmly linked. The microbial oxidation of organic matter in marine sediments, crucial to the carbon cycle, is accomplished through sulfate reduction to sulfide. This sulfide is primarily deposited as pyrite, making pyrite an integral mineral in the carbon, iron, and sulfur cycles (Raiswell and Canfield 2012). These deep sea accumulations of pyrite and other sulfides are what later become the

economically important massive sulfide deposits (Huston et al. 2010) that are mined for a variety of metals.

While it is iron sulfides that are the main link between the iron and sulfur cycles, in Earth's oxidizing conditions, and mediated by a host of different bacteria, it is iron sulfate that is most often seen at the surface. These sulfates, however, provide a wealth of information about their depositional environments. Since sulfate transformations are often path dependant (Xu et al. 2009), they can be used to deduce details about the fluid from which they formed. That fluid composition can be used to interpret the conditions under which the original sulfide weathered (Jambor et al. 2000). In addition, in arid environments, sulfate mineral assemblages can be used to track climate variations (Murad and Rojik 2005).

1.3.1 Iron and Sulfur on Mars

The sensitivity of iron sulfates to changes in climate and depositional environment makes them important indicator minerals to find on the surface of Mars. In fact, iron sulfates, which are relatively rare on Earth, are quite common on the surface of Mars (Dyar et al. 2013). This abundance is due to the fact that Mars seems to be dominated by a sulfur cycle, unlike earth, which is dominated by a carbon cycle (King and McLennan 2010; McLennan 2012; Gaillard et al. 2013). On Mars, it is believed that a sulfur rich core and at least two distinct eras of magmatic degassing have contributed to the varied sulfur content of the surface (Gaillard et al. 2013). Although there is no clear consensus on the weathering processes that have led to the formation of sulfates in general, and iron sulfates, in particular (Gaillard et al. 2013), sulfur on Mars is often associated with iron (Christensen et al. 2001; Glotch and Rogers 2007; Sowe et al. 2012; Weitz et al. 2012). The abundance of both these elements is likely due to the increased FeO content of the Martian mantle, allowing for greater S solubility in silicate melts (Gaillard et al.

2013). Regardless of origin, an interesting implication of plentiful iron sulfates is the possibility of liquid brines at the surface and in the near subsurface (Chevrier and Altheide 2008; Altheide et al. 2009; Chevrier and Rivera-Valentin 2012) for much of Martian history (Fairen et al. 2009). If liquid water is required for life, then the stability of liquid brines (provided that they are of low enough activity) increases the potential for life on Mars. More importantly, perhaps, brines set up a location where disequilibria can be exploited (e.g. the interaction of acidic brines with silicic rocks), a factor that may be of primary importance for developing and sustaining life (Russell et al. 2014).

1.4 Background for Chapters

1.4.1 Geological Carbon Sequestration (GCS)

Chapters 2 and 3 focus on experiments that simulate geological carbon sequestration (GCS) in deep saline aquifers using a mixed acid-gas CO_2 gas stream.

The burning of fossil fuels has been aptly described as taking carbon out of long-term geological storage and putting it in the atmosphere, and geological carbon sequestration simply as the reversal of this process (DePaolo and Cole 2013). Because efforts to curb our consumption of fossil fuels are, at present, not producing substantial changes in global carbon emissions (DePaolo and Cole 2013), strategies that mitigate the effects of CO_2 in the atmosphere are a pressing concern (IPCC 2014). The majority of CO_2 emissions emanate from large point sources, such as thermal power stations that use fossil fuels to generate steam power (Chialvo et al. 2013). Sequestering CO_2 from these sources, or capturing it and injecting it into deep geological formations, would serve as a way to mitigate carbon emissions as we transition to alternative fuels.

Carbon sequestration becomes relevant in the sulfur cycle because sulfur is a common co-contaminant in flue gas from thermal power plants. Because human emissions of sulfur gasses into the atmosphere are the greatest source of atmospheric SO_2 and SO_3 (4 to 100 times greater than natural sources depending on region; Galloway (2001)), and have led to environmental problems like acid rain, regulations have been instituted to limit sulfur emissions. Meeting these regulations necessitates the separation of sulfur species from power plant flue gas (Chestnut and Mills 2005). If CO_2 were being captured for sequestration, it is possible to reduce the overall capture costs by 10-20% through co-capturing sulfur-bearing gases and CO_2 (GHG 2003; Anheden et al. 2005; Chialvo et al. 2013). The presence of these species in the injection gas has the potential to make the injected fluid more reactive (DePaolo and Cole 2013). Where supercritical CO_2 acts as a non-wetting fluid, essentially immiscible in the deep saline fluids at the injection depth, sulfate species have the potential to acidify the solutions (Chialvo et al. 2013). These acidified fluids can lead previously stable minerals (like clays) in contact with the fluids to react and become more mobile (Mohan et al. 1993).

For GCS, increasing the reactivity of the system can both hinder and facilitate sequestration, depending on the type and location of the reactions. The drop in pH generally increases the dissolution of the host mineral matrix, freeing divalent cations, and thus increasing the mineralization rates of CO_2. Although this outcome would be considered beneficial, such an increase in reactivity also has the potential to change the permeability of the host matrix, clog the injection site, or even lead to cap rock failure (Ellis et al. 2011). Therefore, understanding the effects of these phases on the reactivity of potential carbon sequestration systems is of utmost importance to the advancement of sequestration technology. While modeling and experimental

studies are increasing for mixed gas systems (see Chialvo et al. 2013 for a review), there are substantial gaps, particularly concerning basic geochemical reactivity (Chialvo et al. 2013).

The work on carbon sequestration is divided into two chapters, which represent papers two and three of a set of experiments designed to investigate the reactivity of sandstones to sulfur-bearing fluids exposed to $scCO_2$. Paper one focused on the reactivity of a hematite (Fe_2O_3)-bearing sandstone in flow-through and low fluid:rock ratio experiments, simulating conditions near the injection site and in interfacial regions, where gas and fluid begin to mix (Schoonen et al. 2012). Paper two (Chapter 2; Sklute et al. (In Preparation-a)) deals with the same hematite–bearing sandstone in high fluid:rock ratio experiments, using saline fluids to simulate reactions far from the CO_2 source. Paper three (Chapter 3; Sklute et al. (In Preparation-b)) deals with several hematite-free sandstones in near, interfacial, and far-field experiments. These experiments show that iron in hematite is key to the reactivity of these sandstones. Papers two and three are being prepared for submission to Chemical Geology.

1.4.2 Optical Constants of Jarosite

Chapter 4 describes the determination of optical constants for the iron oxyhydroxy sulfate mineral, jarosite.

The mining of sulfur, sulfur bearing minerals, and sulfur containing deposits plays a pivotal role in the United States and world economies (Ober 2002). However, the disruption of large volumes of sulfide-containing soil and sediment, characteristic of mining practices, results in highly acidic runoff known as acid mine drainage (AMD). When buried, sulfides are stable in the reducing conditions present below the water table (Ward et al. 2004).When sulfides are

brought to the surface and exposed to oxygen and water, sulfur oxidizes, and large amounts of acidity and sulfate are produced (e.g. pyrite oxidation; Equations 1.1-1.3).

$$2FeS_2 + 2H_2O + 7O_2 \rightarrow 2Fe^{2+} + 4SO_4^{2-} + 4H^+(aq) \quad (1.1)$$

$$4Fe^{2+} + 4H^+(aq) + O_2 \rightarrow 4Fe^{3+} + 2H_2O \quad (1.2)$$

$$FeS_2 + 14Fe^{3+} + 8H_2O \rightarrow 15Fe^{2+} + 2SO_4^{2-} + 16H^+(aq) \quad (1.3)$$

This oxidation is largely the result of the metabolic transformation of sulfide to sulfate by sulfur oxidizing bacteria, and Fe^{2+} to Fe^{3+} by iron oxidizing bacteria. Fe^{3+} is then used for further sulfide oxidation (Equation 1.3; Nordstrom and Southam 1997). This oxidation occurs any place where sulfide, oxygen, and water come together (Johnson and Hallberg 2005), like mine shafts, open pits, slag heaps, tailings piles, and construction in sulfidic soils. In the absence of mitigating procedures, once sulfides have become exposed, they will continue to oxidize and produce acidity until they are gone. For many sites, this can last decades or even centuries (Christensen et al. 1996).

Unlike other point source emissions, where on-site monitoring and emission regulations can be effective (Chestnut and Mills 2005), AMD does not necessarily flow from a single point source (Johnson 2003), and it is primarily a problem after mine closure (Younger 2002; Johnson 2003). These factors can lead to difficulties in both enforcement and monitoring. However, the oxidation of iron sulfides, like pyrite, and the subsequent production of sulfate, lead to the precipitation of a predictable sequence of sulfate minerals and their oxidation products (Jambor et al. 2000; Jerz and Rimstidt 2003) that can be used to identify areas of acid mine drainage (Swayze et al. 2000). The assemblages of minerals present can also be used to predict the acidification potential of the site. Where sulfates represent a higher acidification potential, the oxides, which they weather to over time, or that precipitate from higher pH fluids, represent a lower acidification potential (Swayze et al. 2000).

Remote sensing has the ability to survey large areas of land for these minerals and has been successfully utilized to identify areas of AMD contamination (Swayze et al. 2000; Dalton et al. 2004; Riaza et al. 2011). Each pixel in a remotely acquired hyperspectral image provides a spectrum of the combined reflectances (at visible and near infrared (VNIR) wavelengths), or emissivity (at thermal infrared wavelengths) of the materials within that area. The VNIR is especially useful in identifying iron sulfates because iron sulfates display characteristic combinations of absorptions that make them differentiable from each other and other common minerals in this wavelength region (Cloutis et al. 2006).

Mineral identification through remote sensing on Earth (concerning AMD) has been mainly qualitative (Clark et al. 1998; Swayze et al. 2000; Dalton et al. 2004). Although qualitative information of mineral distributions can show changes with time of the *spatial* distribution of key AMD precipitates, quantitative information would allow assessment of the change in *concentration* of a mineral in a given pixel with time. However, in the VNIR, contributions from minerals in a mixture are not linearly correlated with mineral concentrations (Hapke 1981). Therefore a model is required to relate abundance to spectral character.

It is understood that the interaction of the electromagnetic spectrum with minerals can be modeled using radiative transfer theory (Hapke 1981; Hapke and Wells 1981; Hapke 1993; Lucey 1998; Poulet et al. 2009a; Poulet et al. 2009b; Li and Li 2011), provided that key optical properties, namely the real and imaginary indices of refraction (optical constants) of the minerals in the mixture are known. This modeling process can be applied in both the forward and backwards direction (Poulet et al. 2009a), such that a laboratory spectrum of a pure mineral can be used to determine optical constants, and those optical constants can be used to reproduce the spectrum of that mineral. The latter becomes useful in analyzing remote sensing data, but the

former is required before any analyses can be performed. Thus optical constants of AMD associated minerals are required to enhance our ability to monitor and remediate AMD affected areas. Specifically, optical constants for the mineral jarosite ($AFe^{3+}_3(SO_4)_2(OH)_6$; $A=K^+$, Na^+, H_3O^+), which both correlates with the acidification potential of the soil and occurs on spatial scales useful for remote sensing, (Swayze et al. 2000), have not been determined.

On Earth, remote sensing can be accompanied by ground truthing, but remote sensing is our primary means of studying other planets and icy satellites. Much of our understanding of planetary surface composition is derived from instruments like Galileo's Near Infrared Mapping Spectrometer (NIMS), Cassini's Visual and Infrared Mapping Spectrometer (VIMS), the Compact Imaging Reconnaissance Spectrometer for Mars (CRISM), and l'Observatoire pour la Minéralogie, l'Eau, les Glaces et l'Activité (OMEGA), (e.g.Bibring et al. 2005; Cruikshank et al. 2007; Murchie et al. 2009; Dalton 2010; Dalton et al. 2010), which collect reflected sunlight in part of the VNIR wavelength range. Even on planets where landers and rovers are deployed, remote sensing can provide global and regional surveys, where mineralogical trends can clarify important processes and provide insight into current and past geological settings. For instance, OMEGA and CRISM facilitated the identification, distribution analysis, and interpretation of sulfates on Mars (Bibring et al. 2005; Gendrin et al. 2005; Murchie et al. 2009) over areas and on timescales not possible for rovers. Therefore, enhancing our ability to interpret planetary data through facilitating the determination of quantitative mineral abundance is similarly useful in planetary science.

Here, again, jarosite plays an important role. Jarosite was one of the first sulfates to be unambiguously detected on the surface of Mars (Klingelhofer et al. 2004). The detection of jarosite on the surface of Mars supports the hypothesis that Mars experienced wet, acidic

conditions at some point in its history (Bishop et al. 2004) since these are the conditions responsible for the formation of jarosite on Earth (Bigham and Nordstrom 2000). Due to the constraints that jarosite can place on surface processes (Rye and Stoffregen 1995; Lueth et al. 2005; Papike et al. 2006; Swayze et al. 2008; Madden et al. 2009), quantitative abundance estimates of jarosite on the surface could enhance our ability to interpret past and present Martian surface geochemistry.

Chapter 4 presents the optical constants for synthetic potassium, sodium, and hydronium jarosite and details how optical constants can best be determined for minerals. A manuscript based on this chapter is currently in review at American Mineralogist. Appendix 1 is the Matlab computer code developed to determine these optical constants and Appendix 2 is the tabulated values of those optical constants.

1.4.3 Amorphous Iron Sulfates on Mars

Chapter 5 focuses on the synthesis and characterization of amorphous iron sulfate and its potential occurrence on Mars.

Because there are global differences in the geologic cycles between Earth and Mars (McLennan 2012), it should not be surprising that there are drastic differences in surface mineralogy. However, the emerging evidence that the Martian surface is rich with amorphous material (Bish et al. 2013) requires that hypotheses on Martian surface processes be re-examined. Amorphous materials on Earth often result from the rapid deposition of minerals from saturated fluids since amorphous phases nucleate more readily than their crystalline counterparts (Nielsen and Sohnel 1971; Konhauser and Riding 2012). These metastable phases may persist, however, until conditions are energetically favorable for their transformation (Morse and Casey 1988;

Konhauser and Riding 2012). The low temperatures of the Martian surface may facilitate the perseverance of metastable, amorphous phases.

Given the iron- and sulfur-rich nature of the Martian surface, the possibility exists that some of the amorphous material, which is iron- and sulfur-rich (Morris et al. 2013; McAdam et al. 2014), is amorphous iron sulfate. Amorphous iron sulfates will crystallize if the relative humidity raises above 11% for an extended period of time (Wang et al. 2012). Some authors have argued that amorphous iron sulfates may not be stable on Mars due to the expected relative humidity fluctuations (diurnally 1-100%; Savijarvi (1995)), combined with slowed kinetics for dehydration but unaltered kinetics for hydration at the depressed Martian temperatures and pressures (Wang et al. 2013; Zhou and Wang 2013). However, the discovery of recurring slope lineae (a seasonal albedo change associated with channels that is predominantly on equator facing slopes; Chevrier and Rivera-Valentin (2012)) has been used to hypothesize an active brine hydrologic cycle on the surface of Mars (Chevrier and Altheide 2008; Altheide et al. 2009; McEwen et al. 2011; Martinez and Renno 2013; Masse et al. 2014). Ferric (Fe^{3+}) iron sulfate fluids are one of the best candidates for these brines due to the relative abundance of iron and sulfur on the surface and the low eutectic of Fe^{3+} and SO_4^{2-} saturated solutions (Chevrier and Altheide 2008). Due to the low relative humidity and pressure of the Martian surface, brines that upwell would likely boil or evaporate depending on surface location (Martinez and Renno 2013). Both of these processes could lead to the formation of amorphous iron sulfates. Thus, even if Wang et al. (2012) are correct, and the stability of the amorphous phase is on the order of years on Mars rather than centuries, the active brine cycle could be continually reforming them.

The absence of spectral data for amorphous sulfates from the literature has limited consideration of these phases as possible components of the Martian surface. In Chapter 5, I

morphologically and spectrally characterize these phases so that they may be added to the spectral library. A paper based on this chapter is being prepared for submission to the Journal of Geophysical Research-Planets.

Works Cited

Altheide, T., Chevrier, V., Nicholson, C., and Denson, J. (2009) Experimental investigation of the stability and evaporation of sulfate and chloride brines on Mars. Earth and Planetary Science Letters, 282 (1-4), 69-78.

Anheden, M., Andersson, A., Bernstone, C., Eriksson, S., Yan, J., Liljemark, S., and Wall, C. (2005) CO_2 quality requirement for a system with CO_2 capture, transport and storage. In: M. Wilson et al. (Eds.), Greenhouse Gas Control Technologies 7. Elsevier, pp. 2559-2564.

Bennett, S.A., Achterberg, E.P., Connelly, D.P., Statham, P.J., Fones, G.R., and German, C.R. (2008) The distribution and stabilisation of dissolved Fe in deep-sea hydrothermal plumes. Earth and Planetary Science Letters, 270 (3-4), 157-167.

Bertier, P., Swennen, R., Laenen, B., Lagrou, D., and Dreesen, R. (2006) Experimental identification of CO_2-water-rock interactions caused by sequestration of CO_2 in Westphalian and Buntsandstein sandstones of the Campine Basin (NE-Belgium). Journal of Geochemical Exploration, 89 (1-3), 10-14.

Bibring, J.P., Langevin, Y., Gendrin, A., Gondet, B., Poulet, F., Berthe, M., Soufflot, A., Arvidson, R., Mangold, N., Mustard, J., Drossart, P., and Team, O. (2005) Mars surface diversity as revealed by the OMEGA/Mars Express observations. Science, 307 (5715), 1576-1581.

Bigham, J.M., and Nordstrom, D.K. (2000) Iron and aluminum hydroxysulfates from acid sulfate waters. Sulfate Minerals - Crystallography, Geochemistry and Environmental Significance, 40, 351-403.

Bigham, J.M., Schwertmann, U., and Pfab, G. (1996a) Influence of pH on mineral speciation in a bioreactor simulating acid mine drainage. Applied Geochemistry, 11 (6), 845-849.

Bigham, J.M., Schwertmann, U., Traina, S.J., Winland, R.L., and Wolf, M. (1996b) Schwertmannite and the chemical modeling of iron in acid sulfate waters. Geochimica Et Cosmochimica Acta, 60 (12), 2111-2121.

Bish, D.L., Blake, D.F., Vaniman, D.T., Chipera, S.J., Morris, R.V., Ming, D.W., Treiman, A.H., Sarrazin, P., Morrison, S.M., Downs, R.T., Achilles, C.N., Yen, A.S., Bristow, T.F., Crisp, J.A., Morookian, J.M., Farmer, J.D., Rampe, E.B., Stolper, E.M., Spanovich, N., and Team, M.S.L.S. (2013) X-ray diffraction results from Mars Science Laboratory: Mineralogy of Rocknest at Gale Crater. Science, 341 (6153).

Bishop, J.L., Darby Dyar, M., Lane, M.D., and Banfield, J.F. (2004) Spectral identification of hydrated sulfates on Mars and comparison with acidic environments on Earth. International Journal of Astrobiology, 3 (04), 275-285.

Boucher, O., and Anderson, T.L. (1995) General circulation model assessment of the sensitivity of direct climate forcing by anthropogenic sulfate aerosols to aerosol size and chemistry. Journal of Geophysical Research-Atmospheres, 100 (D12), 26117-26134.

Brimblecombe, P., Hammer, C., Henning, R., Ryaboshapko, A., and Boutron, C.F. (1989) Human influence on the sulfur cycle. In: A.Y. Lein, P. Brimblecombe, and U. International Council of Scientific (Eds.), Evolution of the global biogeochemical sulphur cycle. Wiley, Chichester, West Sussex, England ; New York, pp. 77-121.

Canfield, D.E. (2004) The evolution of the Earth surface sulfur reservoir. American Journal of Science, 304 (10), 839-861.

Canfield, D.E., and Farquhar, J. (2012) The Global Sulfur Cycle, Fundamentals of Geobiology. John Wiley & Sons, Ltd, pp. 49-64.

Canfield, D.E., and Raiswell, R. (1999) The evolution of the sulfur cycle. American Journal of Science, 299 (7-9), 697-723.

Chestnut, L.G., and Mills, D.M. (2005) A fresh look at the benefits and costs of the US Acid Rain Program. Journal of Environmental Management, 77 (3), 252-266.

Chevrier, V.F., and Altheide, T.S. (2008) Low temperature aqueous ferric sulfate solutions on the surface of Mars. Geophysical Research Letters, 35 (22).

Chevrier, V.F., and Rivera-Valentin, E.G. (2012) Formation of recurring slope lineae by liquid brines on present-day Mars. Geophysical Research Letters, 39.

Chialvo, A.A., Vlcek, L., and Cole, D.R. (2013) Acid gases in CO_2-rich subsurface geologic environments. In: D.J. DePaolo, D.R. Cole, A. Navrotsky, and I.C. Bourg (Eds.), Geochemistry of Geologic CO_2 Sequestration. Reviews in Mineralogy & Geochemistry, pp. 361-398.

Christensen, B., Laake, M., and Lien, T. (1996) Treatment of acid mine water by sulfate-reducing bacteria; Results from a bench scale experiment. Water Research, 30 (7), 1617-1624.

Christensen, P.R., Morris, R.V., Lane, M.D., Bandfield, J.L., and Malin, M.C. (2001) Global mapping of Martian hematite mineral deposits: Remnants of water-driven processes on early Mars. Journal of Geophysical Research-Planets, 106 (E10), 23873-23885.

Chu, N.C., Johnson, C.M., Beard, B.L., German, C.R., Nesbitt, R.W., Frank, M., Bohn, M., Kubik, P.W., Usui, A., and Graham, I. (2006) Evidence for hydrothermal venting in Fe isotope compositions of the deep Pacific Ocean through time. Earth and Planetary Science Letters, 245 (1-2), 202-217.

Clark, R.N., Vance, J.S., Livo, K.E., and Green, R.O. (1998) Mineral mapping with imaging spectroscopy: the Ray Mine, AZ. In: R.O. Green (Editor), 7th annual JPL Airborne Earth Science Workshop. JPL Publication, pp. 67-76.

Cloutis, E.A., Hawthorne, F.C., Mertzman, S.A., Krenn, K., Craig, M.A., Marcino, D., Methot, M., Strong, J., Mustard, J.F., Blaney, D.L., Bell, J.F., and Vilas, F. (2006) Detection and discrimination of sulfate minerals using reflectance spectroscopy. Icarus, 184 (1), 121-157.

Cruikshank, D.P., Dalton, J.B., Ore, C.M.D., Bauer, J., Stephan, K., Filacchione, G., Hendrix, A.R., Hansen, C.J., Coradini, A., Cerroni, P., Tosi, F., Capaccioni, F., Jaumann, R., Buratti, B.J., Clark, R.N., Brown, R.H., Nelson, R.M., McCord, T.B., Baines, K.H., Nicholson, P.D., Sotin, C., Meyer, A.W., Bellucci, G., Combes, M., Bibring, J.P., Langevin, Y., Sicardy, B., Matson, D.L., Formisano, V., Drossart, P., and Mennella, V. (2007) Surface composition of Hyperion. Nature, 448 (7149), 54-56.

Dalton, J.B. (2010) Spectroscopy of icy moon surface materials. Space Science Reviews, 153 (1-4), 219-247.

Dalton, J.B., Bove, D.J., and Mladinich, C.S. (2004) Remote sensing charachterization of the Animas River watershed, southwest Colorado, by AVIRIS imaging spectroscopy. 2004-5203, USGS.

Dalton, J.B., Cruikshank, D.P., Stephan, K., McCord, T.B., Coustenis, A., Carlson, R.W., and Coradini, A. (2010) Chemical Composition of Icy Satellite Surfaces. Space Science Reviews, 153 (1-4), 113-154.

DePaolo, D.J., and Cole, D.R. (2013) Geochemistry of geologic carbon sequestration: An overview. In: D.J. DePaolo, D.R. Cole, A. Navrotsky, and I.C. Bourg (Eds.), Geochemistry of Geologic CO_2 Sequestration. Reviews in Mineralogy & Geochemistry, pp. 1-14.

Dyar, M.D., Breves, E., Jawin, E., Marchand, G., Nelms, M., O'Connor, V., Peel, S., Rothstein, Y., Sklute, E.C., Lane, M.D., Bishop, J.L., and Mertzman, S.A. (2013) Mössbauer parameters of iron in sulfate minerals. American Mineralogist, 98 (11-12), 1943-1965.

Ellis, B.R., Peters, C.A., Fitts, J., Bromhal, G., McIntyre, D., Warzinski, R., and Rosenbaum, E. (2011) Deterioration of a fractured carbonate caprock exposed to CO_2-acidified brine flow. Greenhouse Gases-Science and Technology, 1 (3), 248-260.

Eriksson, E. (1963) Yearly circulation of sulfur in nature. Journal of Geophysical Research, 68 (13), 4001-&.

Fairen, A.G., Davila, A.F., Gago-Duport, L., Amils, R., and McKay, C.P. (2009) Stability against freezing of aqueous solutions on early Mars. Nature, 459 (7245), 401-404.

Gaillard, F., Michalski, J., Berger, G., McLennan, S.M., and Scaillet, B. (2013) Geochemical reservoirs and timing of sulfur cycling on Mars. Space Science Reviews, 174 (1-4), 251-300.

Galloway, J.N. (2001) Acidification of the world - Natural and anthropogenic. Water Air and Soil Pollution, 130 (1-4), 17-24.

Gendrin, A., Mangold, N., Bibring, J.P., Langevin, Y., Gondet, B., Poulet, F., Bonello, G., Quantin, C., Mustard, J., Arvidson, R., and LeMouelic, S. (2005) Sulfates in Martian layered terrains: the OMEGA/Mars Express view. Science, 307 (5715), 1587-1591.

GHG (2003) Potential for improvements in Gasification Combined Cycle Power Generation with CO_2 Capture. International Energy Agency Greenhouse Gas R&D program, IEA GHG, Chetenham, UK.

Glotch, T.D., and Rogers, A.D. (2007) Evidence for aqueous deposition of hematite- and sulfate-rich light-toned layered deposits in Aureum and Iani Chaos, Mars. Journal of Geophysical Research-Planets, 112 (E6).

Hapke, B. (1981) Bidirectional reflectance spectroscopy 1. Theory. Journal of Geophysical Research, 86 (NB4), 3039-3054.

Hapke, B. (1993) Theory of Reflectance and Emittance Spectroscopy. Topics in Remote Sensing Cambridge University Press, New York, NY.

Hapke, B., and Wells, E. (1981) Bidirectional reflectance spectroscopy 2. Experiments and observations. Journal of Geophysical Research, 86 (NB4), 3055-3060.

Hazen, R.M., Papineau, D., Leeker, W.B., Downs, R.T., Ferry, J.M., McCoy, T.J., Sverjensky, D.A., and Yang, H.X. (2008) Mineral evolution. American Mineralogist, 93 (11-12), 1693-1720.

Huston, D.L., Pehrsson, S., Eglington, B.M., and Zaw, K. (2010) The geology and metallogeny of volcanic-hosted massive sulfide deposits: Variations through geologic time and with tectonic setting. Economic Geology, 105 (3), 571-591.

IPCC (2014) IPCC, 2014: Summary for policymakers., IPCC, Cabridge, United Kingdom and New York, NY, USA.

Ivanov, M.V. (1983) The Global biogeochemical sulphur cycle. In: J.R. Freney, M.V. Ivanov, U. International Council of Scientific, and S.U.W.o.t.G.B.S. Cycle (Eds.), SCOPE ;19. Published on behalf of the Scientific Committee on Problems of the Environment of the

International Council of Scientific Union by Wiley, Chichester [Sussex] ; New York, pp. 61-78.
Jambor, J.I., Nordstrom, D.K., and Alpers, C.N. (2000) Metal-sulfate salts from sulfide mineral oxidation. Sulfate Minerals - Crystallography, Geochemistry and Environmental Significance, 40, 303-350.
Jambor, J.L., and Blowes, D.W. (1994) Short course handbook on environmental geochemistry of sulfide mine wastes, 22. Mineralogical Association of Canada, Waterloo, Ontario, 438 pp.
Jerz, J.K., and Rimstidt, J.D. (2003) Efflorescent iron sulfate minerals: Paragenesis, relative stability, and environmental impact. American Mineralogist, 88 (11-12), 1919-1932.
Johnson, D.B. (2003) Chemical and Microbiological Characteristics of Mineral Spoils and Drainage Waters at Abandoned Coal and Metal Mines. Water, Air and Soil Pollution: Focus, 3 (1), 47-66.
Johnson, D.B., and Hallberg, K.B. (2005) Acid mine drainage remediation options: A review. Science of the Total Environment, 338 (1-2), 3-14.
Karnieli, A., Derimian, Y., Indoitu, R., Panov, N., Levy, R.C., Remer, L.A., Maenhaut, W., and Holben, B.N. (2009) Temporal trend in anthropogenic sulfur aerosol transport from central and eastern Europe to Israel. Journal of Geophysical Research-Atmospheres, 114.
Kendall, B., Anbar, A.D., Kappler, A., and Konhauser, K.O. (2012) The Global Iron Cycle, Fundamentals of Geobiology. John Wiley & Sons, Ltd, pp. 65-92.
King, P.L., and McLennan, S.M. (2010) Sulfur on Mars. Elements, 6 (2), 107-112.
Klingelhofer, G., Morris, R.V., Bernhardt, B., Schroder, C., Rodionov, D.S., de Souza, P.A., Yen, A., Gellert, R., Evlanov, E.N., Zubkov, B., Foh, J., Bonnes, U., Kankeleit, E., Gutlich, P., Ming, D.W., Renz, F., Wdowiak, T., Squyres, S.W., and Arvidson, R.E. (2004) Jarosite and hematite at Meridiani Planum from Opportunity's Mössbauer spectrometer. Science, 306 (5702), 1740-1745.
Konhauser, K., and Riding, R. (2012) Bacterial Biomineralization, Fundamentals of Geobiology. John Wiley & Sons, Ltd, pp. 105-130.
Krumbein, W., and Gorbushina, A. (2010) Global Relations Between the Redox Cycles of Carbon, Iron, and Sulfur, Handbook of Hydrocarbon and Lipid Microbiology. Springer, pp. 157-169.
Li, S., and Li, L. (2011) Radiative transfer modeling for quantifying lunar surface minerals, particle size, and submicroscopic metallic Fe. Journal of Geophysical Research-Planets, 116.
Lucey, P.G. (1998) Model near-infrared optical constants of olivine and pyroxene as a function of iron content. Journal of Geophysical Research-Planets, 103 (E1), 1703-1713.
Lueth, V.W., Rye, R.O., and Peters, L. (2005) "Sour gas" hydrothermal jarosite: ancient to modem acid-sulfate mineralization in the southern Rio Grande Rift. Chemical Geology, 215 (1-4), 339-360.
Madden, M.E.E., Madden, A.S., and Rimstidt, J.D. (2009) How long was Meridiani Planum wet? Applying a jarosite stopwatch to determine the duration of aqueous diagenesis. Geology, 37 (7), 635-638.
Martinez, G.M., and Renno, N.O. (2013) Water and brines on Mars: Current evidence and implications for MSL. Space Science Reviews, 175 (1-4), 29-51.

Masse, M., Beck, P., Schmitt, B., Pommerol, A., McEwen, A., Chevrier, V., Brissaud, O., and Sejourne, A. (2014) Spectroscopy and detectability of liquid brines on mars. Planetary and Space Science, 92, 136-149.

McAdam, A.C., Franz, H.B., Sutter, B., Archer, P.D., Freissinet, C., Eigenbrode, J.L., Ming, D.W., Atreya, S.K., Bish, D.L., Blake, D.F., Bower, H.E., Brunner, A., Buch, A., Glavin, D.P., Grotzinger, J.P., Mahaffy, P.R., McLennan, S.M., Morris, R.V., Navarro-González, R., Rampe, E.B., Squyres, S.W., Steele, A., Stern, J.C., Sumner, D.Y., and Wray, J.J. (2014) Sulfur-bearing phases detected by evolved gas analysis of the Rocknest aeolian deposit, Gale Crater, Mars. Journal of Geophysical Research: Planets, 2013JE004518.

McEwen, A.S., Ojha, L., Dundas, C.M., Mattson, S.S., Byrne, S., Wray, J.J., Cull, S.C., Murchie, S.L., Thomas, N., and Gulick, V.C. (2011) Seasonal Flows on Warm Martian Slopes. Science, 333 (6043), 740-743.

McLennan, S.M. (2001) Relationships between the trace element composition of sedimentary rocks and upper continental crust. Geochemistry Geophysics Geosystems, 2, art. no.-2000GC000109.

McLennan, S.M. (2012) Geochemistry of sedimentary processes on mars. In: J.P. Grotzinger, and R.E. Milliken (Eds.), Sedimentary Geology of Mars. Society for Sedimentary Geology Special Publication, pp. 119-138.

Mohan, K.K., Vaidya, R.N., Reed, M.G., and Fogler, H.S. (1993) Water sensitivity of sandstones containing swelling and non-swelling clays. Colloids and Surfaces a-Physicochemical and Engineering Aspects, 73, 237-254.

Morris, R.V., Ming, D.W., Blake, D.F., Vaniman, D.T., Bish, D.L., Chipera, S.J., Downs, R.T., Gellert, R., Treiman, A.H., Yen, A.S., Achilles, C.N., Anderson, R.C., Bristow, T.F., Crisp, J.A., Des Marais, D.J., Farmer, J.D., Grotzinger, J.P., Leshin, L.A., McAdam, A.C., Morookian, J.M., Morrison, S.M., Rampe, E.B., Sarrazin, P.C., Spanovich, N., and Stolper, E.M. (2013) The amorphous component in the Martian basaltic soil in global perspective from MSL and MER missions. Abstracts of Papers submitted to the Lunar and Planetary Science Conference XXXXIV (1653).

Morse, J.W., and Casey, W.H. (1988) Ostwald processes and mineral paragenesis in sediments. American Journal of Science, 288 (6), 537-560.

Murad, E., and Rojik, P. (2005) Iron mineralogy of mine-drainage precipitates as environmental indicators: review of current concepts and a case study from the Sokolov Basin, Czech Republic. Clay Minerals, 40 (4), 427-440.

Murchie, S.L., Mustard, J.F., Ehlmann, B.L., Milliken, R.E., Bishop, J.L., McKeown, N.K., Dobrea, E.Z.N., Seelos, F.P., Buczkowski, D.L., Wiseman, S.M., Arvidson, R.E., Wray, J.J., Swayze, G., Clark, R.N., Marais, D.J.D., McEwen, A.S., and Bibring, J.P. (2009) A synthesis of Martian aqueous mineralogy after 1 Mars year of observations from the Mars Reconnaissance Orbiter. Journal of Geophysical Research-Planets, 114.

Nielsen, A.E., and Sohnel, O. (1971) Interfacial tensions electrolyte crystal-aqueous solution, from nucleation data. Journal of Crystal Growth, 11 (3), 233-&.

Nordstrom, D.K., and Southam, G. (1997) Geomicrobiology of sulfide mineral oxidation. In: J.F. Banfield, and K.H. Nealson (Eds.), Geomicrobiology: Interactions between Microbes and Minerals. Reviews in Mineralogy, pp. 361-390.

Norlund, K.L.I., Baron, C., and Warren, L.A. (2010) Jarosite formation by an AMD sulphide-oxidizing environmental enrichment: Implications for biomarkers on Mars. Chemical Geology, 275 (3-4), 235-242.

Ober, J.A. (2002) Materials flow of sulfur. Open-file Report. U.S. Dept. of the Interior, U.S. Geological Survey 2-298, 56 pp. http://pubs.usgs.gov/of/2002/of02-298/of02-298.pdf

Papike, J.J., Karner, J.M., and Shearer, C.K. (2006) Comparative planetary mineralogy: Implications of martian and terrestrial jarosite. A crystal chemical perspective. Geochimica Et Cosmochimica Acta, 70 (5), 1309-1321.

Poulet, F., Bibring, J.P., Langevin, Y., Mustard, J.F., Mangold, N., Vincendon, M., Gondet, B., Pinet, P., Bardintzeff, J.M., and Platevoet, B. (2009a) Quantitative compositional analysis of martian mafic regions using the MEx/OMEGA reflectance data. Icarus, 201 (1), 69-83.

Poulet, F., Mangold, N., Platevoet, B., Bardintzeff, J.M., Sautter, V., Mustard, J.F., Bibring, J.P., Pinet, P., Langevin, Y., Gondet, B., and Aleon-Toppani, A. (2009b) Quantitative compositional analysis of martian mafic regions using the MEx/OMEGA reflectance data 2. Petrological implications. Icarus, 201 (1), 84-101.

Raiswell, R. (2011) Iron transport from the continents to the open ocean: The aging-rejuvenation cycle. Elements, 7 (2), 101-106.

Raiswell, R., and Canfield, D.E. (2012) The iron biogeochemical cycle past and present. Geochemical Perspectives, 1 (1), 1-220.

Rasch, P.J., Barth, M.C., Kiehl, J.T., Schwartz, S.E., and Benkovitz, C.M. (2000) A description of the global sulfur cycle and its controlling processes in the National Center for Atmospheric Research Community Climate Model, Version 3. Journal of Geophysical Research-Atmospheres, 105 (D1), 1367-1385.

Riaza, A., Garcia-Melendez, E., and Mueller, A. (2011) Spectral identification of pyrite mud weathering products: a field and laboratory evaluation. International Journal of Remote Sensing, 32 (1), 185-208.

Russell, M.J., Barge, L.M., Bhartia, R., Bocanegra, D., Bracher, P.J., Branscomb, E., Kidd, R., McGlynn, S., Meier, D.H., Nitschke, W., Shibuya, T., Vance, S., White, L., and Kanik, I. (2014) The Drive to Life on Wet and Icy Worlds. Astrobiology, 14 (4), 308-343.

Rye, R.O., and Stoffregen, R.E. (1995) Jarosite-water oxygen and hydrogen isotope fractionations: Preliminary experimental data. Economic Geology and the Bulletin of the Society of Economic Geologists, 90 (8), 2336-2342.

Savijarvi, H. (1995) Mars boundary-layer modeling - Diurnal moisture cycle and soil properties at the Viking-Lander-1 site. Icarus, 117 (1), 120-127.

Schoonen, M.A.A., Sklute, E.C., Dyar, M.D., and Strongin, D.R. (2012) Reactivity of sandstones under conditions relevant to geosequestration: 1. Hematite-bearing sandstone exposed to supercritical carbon dioxide commingled with aqueous sulfite or sulfide solutions. Chemical Geology, 296, 96-102.

Sievert, S.M., Kiene, R.P., and Schulz-Vogt, H.N. (2007) The sulfur cycle. Oceanography, 20 (2), 117-123.

Sklute, E.C., Schoonen, M.A.A., Dyar, M.D., and Strongin, D.R. (In Preparation-a) Reactivity of sandstones under conditions relevant to geosequestration: 2. Hematite-bearing sandstone exposed to supercritical carbon dioxide comingled with saline sulfite and/or sulfide solutions. Chemical Geology.

Sklute, E.C., Schoonen, M.A.A., Dyar, M.D., and Strongin, D.R. (In Preparation-b) Reactivity of sandstones under conditions relevant to geosequestration: 3. Gray sandstones exposed to supercritical carbon dioxide comingled with saline sulfite and/or sulfide solutions. Chemical Geology.

Smith, S.J., Pitcher, H., and Wigley, T.M.L. (2001) Global and regional anthropogenic sulfur dioxide emissions. Global and Planetary Change, 29 (1-2), 99-119.

Sowe, M., Wendt, L., McGuire, P.C., and Neukum, G. (2012) Hydrated minerals in the deposits of Aureum Chaos. Icarus, 218 (1), 406-419.

Stetter, K.O. (1996) Hyperthermophiles in the History of Life. In: J.A. Goode, G.R. Bock, and E. Symposium on Evolution of Hydrothermal Ecosystems on (Eds.), Evolution of hydrothermal ecosystems on Earth (and Mars?). Wiley, Chichester ; New York, pp. 1-10.

Swayze, G.A., Desborough, K.S., Smith, K.S., Lowers, H.A., Hammarstrom, J.M., Diehl, S.F., Leinz, R.W., and Driscoll, R.L. (2008) Understanding Jarosite -- from mine waste to Mars. Understanding Contaminants. U.S. Geological Survey Circular 1328, 8-13 pp.

Swayze, G.A., Smith, K.S., Clark, R.N., Sutley, S.J., Pearson, R.M., Vance, J.S., Hageman, P.L., Briggs, P.H., Meier, A.L., Singleton, M.J., and Roth, S. (2000) Using imaging spectroscopy to map acidic mine waste. Environmental Science & Technology, 34 (1), 47-54.

UNEP (2013) Environmental risks and challenges of anthropogenic metals flows and cycles, a report of the working group on the global metal flows to the international resource panel.

Wang, A., Feldman, W.C., Mellon, M.T., and Zheng, M.P. (2013) The preservation of subsurface sulfates with mid-to-high degree of hydration in equatorial regions on Mars. Icarus, 226 (1), 980-991.

Wang, A.A., Ling, Z.C., Freeman, J.J., and Kong, W.G. (2012) Stability field and phase transition pathways of hydrous ferric sulfates in the temperature range 50 degrees C to 5 degrees C: Implication for martian ferric sulfates. Icarus, 218 (1), 622-643.

Ward, N.J., Sullivan, L.A., Fyfe, D.M., Bush, R.T., and Ferguson, A.J.P. (2004) The process of sulfide oxidation in some acid sulfate soil materials. Australian Journal of Soil Research, 42 (4), 449-458.

Weitz, C.M., Dobrea, E.Z.N., Lane, M.D., and Knudson, A.T. (2012) Geologic relationships between gray hematite, sulfates, and clays in Capri Chasma. Journal of Geophysical Research-Planets, 117.

Xu, W.Q., Tosca, N.J., McLennan, S.M., and Parise, J.B. (2009) Humidity-induced phase transitions of ferric sulfate minerals studied by in situ and ex situ X-ray diffraction. American Mineralogist, 94 (11-12), 1629-1637.

Younger, P.L. (2002) Coalfield closure and the water environment in Europe. Transactions of the Institution of Mining and Metallurgy Section a-Mining Technology, 111, A201-A209.

Zhou, Y., and Wang, A. (2013) A comparison of dehydration processes of Al-, Fe^{2+}-, & Mg-sulfates under mars relevant pressures and three temperatures. Abstracts of Papers submitted to the Lunar and Planetary Science Conference XXXXIV (1797).

Chapter 2

Reactivity Of Sandstones Under Conditions Relevant To Geosequestration: 2. Hematite-Bearing Sandstone Exposed To Supercritical Carbon Dioxide Commingled with Saline Sulfite and/or Sulfide Solutions.

This chapter is being prepared for submission to Chemical Geology

Sklute, E. C., Schoonen, M. A. A., Dyar, M. D., Strongin, D. R. (In preparation) Reactivity Of Sandstones Under Conditions Relevant To Geosequestration: 2. Hematite-Bearing Sandstone Exposed To Supercritical Carbon Dioxide Commingled with Saline Sulfite and/or Sulfide Solutions.

2.1 Introduction

Carbon geosequestration, or geological carbon sequestration (GCS), in deep saline formations is one of the options for decreasing CO_2 emissions by large point sources (Wilson et al. 2003; Bradshaw and Dance 2005; Hepple and Benson 2005; IPCC 2005; White et al. 2005; Mazumder et al. 2006; Bachu 2008). Deep saline formations are attractive injection targets due to substantial storage capacity and widespread distribution (Dooley et al. 2005a; Flett et al. 2005; Damen et al. 2006; Bachu 2008). However, unlike injection for the purpose of enhanced oil and gas recovery, injecting into these formations does not provide economic return (Dooley et al. 2005a; Dooley et al. 2005b), so understanding the potential chemical reactions that could limit

the lifetime of such injection sites is an important step in assessing the feasibility of using deep saline formations as GCS targets.

Thermal power stations that use fossil fuel to generate steam are the largest sources of anthropogenic CO_2 (Chialvo et al. 2013) and thus are ideal systems for CO_2 capture and sequestration. The flue streams from these power plants, as well as many other point sources of CO_2, often contain co-contaminants like H_2S, SO_2, H_2O, NO_X, CO, CH_4, NH_3, N_2, H_2, O_2, and Ar depending on the fuel type, generator type, combustion conditions, and capture technique (Chialvo et al., 2013; Miller et al., 2004; Metz, 2005). Of these, H_2, N_2, O_2, and Ar are not adequately condensable and must be separated and released. The others, specifically H_2S, SO_2, and NO_X (the acid gases), could potentially be co-injected with CO_2. Co-injection of these gases would both sequester additional pollutants and mitigate gas purification costs (GHG 2003; Anheden et al. 2005; Chialvo et al. 2013). Co-injection of acid gases can also increase the reactivity of the system (DePaolo and Cole 2013), leading to beneficial increases in CO_2 mineralization; less desirable outcomes, like pore clogging at the injection site (Palandri et al. 2005) and cap rock dissolution, are also possible (Ellis et al. 2011). Therefore, research that enhances our ability to predict the geochemical interactions in these complex systems is an important endeavor.

There are three dominant reaction domains in the GCS process: near-field, where the system is dominated by supercritical CO_2 ($scCO_2$); far-field, where the system is dominated by the aqueous phase; and an interface region, where $scCO_2$ and fluid coexist. In our previous work, co-authors and I reported results of experiments simulating co-injection of $scCO_2$ into a "red" (hematite-bearing) sandstone with H_2S or SO_2 in both near-field and interfacial regimes (Schoonen et al. 2012). Here I examine the reactivity of the same "red" sandstone toward $scCO_2$

mixed with saline (NaCl) solutions of hydrogen sulfide and/or sulfite, simulating reactions in the far-field and interfacial regimes as a result of the co-injection of $scCO_2$ with H_2S or SO_2 into deep saline aquifers. Using water-rock ratios of 4.3:1 (rather than 1.4:1) and NaCl concentrations of 1.5, 3.0, and 6.0 molal (m), I examine the dependence of reactivity of the iron-bearing phases with respect to salinity in a simulated far-field regime. The experiments complement several modeling studies in which the interaction of H_2S and/or SO_2 co-injected along with CO_2 has been explored (Knauss et al. 2005; Xu et al. 2007; Ellis et al. 2010).

2.2 Methods

2.2.1 Batch Experiments

To simulate the far field effects of CO_2 injection into deep saline aquifers, small-scale batch experiments were conducted using 23 mL Parr™ bombs. These steel-encased, small Teflon™ beakers can withstand internal pressures of up to 125 bar. First, 0.70 g of crushed Moenkopi sandstone were transferred into Teflon™ beakers cooled down to ~ -5 ºC. Next, solid Na_2SO_3 salt, Na_2S nona-hydrate salt, or a combination these two sulfur salts was added to beakers containing enough NaCl to produce 1.5, 3.0, or 6.0 m solutions (see **Table 2-1** for details). Then, 3 mL of an argon-purged 5 mM Na_2SO_3 solution in water was added by pipet into the cold vessels. This dilute sulfite solution was used to ensure that dissolved oxygen in the fluid was minimized. Finally, dry ice chips (solid CO_2) were rapidly added to the vessels while on a high-capacity top-loading balance (Ohaus™). As soon as sufficient CO_2 ice had been added to create supercritical conditions on expansion, the vessels were rapidly closed, tightened, and weighed. Vessels were loaded sequentially and the entire loading process took less than 5

minutes per vessel. The vessels were then placed in a water bath at 75 °C and left to react for ten days, after which they were cooled and opened.

Final weights were within 0.25 grams of starting weights, and separate tests showed that although some CO_2 was expected to diffuse into the Teflon™, the amount of CO_2 lost to the Teflon™ had no material effect on the conditions in the aqueous fluid phase that is in direct contact with the mineral phase. At 75 °C and 75 bars, the calculated equilibrium fluid pH is 3.15, while at 70 bars P_{CO2}, the calculated equilibrium pH is 3.16. In addition, due to the decreased solubility of CO_2 with increased salinity (Takenouchi and Kennedy 1964; Duan and Sun 2003), the fluids were completely saturated with respect to CO_2 throughout the course of the experiments. Once opened, the fluids were rapidly extracted from the reaction vessels using syringes equipped with 0.45 μm filters. Solids were then removed using a membrane filter with pore size of 0.45 μm and dried under vacuum.

It should be noted that the addition of the sulfur source as a salt (Na_2S and Na_2SO_3) rather than a gas (H_2S, SO_2) is a compromise in experimental design for safety reasons. Modeling predicts that in the absence of hematite, overpressure of $scCO_2$ should drive the pH of a 3.0 m solution of NaCl to ~3.15. The addition of sulfur species as sodium salts leads to pH values of ~6.1 for experiments with Na_2S, ~5.8 for experiments with Na_2SO_3, and ~6.2 for a combination of the two. If the species were added as gases, however, the pH would be ~1.0 for H_2S, ~0.7 for SO_2, and ~0.7 for a combination of the two (calculated using Geochemist Workbench 9). This compromise is expected to influence results of these experiments because dissolution rates of carbonate (present in the new subsection of Moenkopi sandstone), along with many other minerals, is dependent primarily upon pH (DePaolo and Cole 2013; Kaszuba et al. 2013). However, it is reasonable to assume that dissolved sulfate species will be the driving force in co-

injection scenarios because sulfur-bearing gases are much more soluble than $scCO_2$ (Zhang et al. 2011). Hence, these experiments represent an important step in understanding the changes that occur in a mixed gas injection scenario, especially because most GCS targets are expected to quickly buffer the injection solutions (Palandri et al. 2005; Kharaka et al. 2013).

2.2.2 Characterization

Sandstone samples used for the batch experiments described in this study are both from the Triassic Moenkopi Formation in Arizona (Stewart et al. 1972). Two different subsamples of the Moenkopi sandstone were used. One was the same as used in the earlier study and is referred to as Moenkopi A (Schoonen et al. 2012). However, there was not enough Moenkopi A material remaining to conduct all experiments, so a second subsample was used for the study, and a round of experiments was performed to compare the reactivity of the two subsamples under identical conditions. This second subsample is referred to as Moenkopi B. As described in Schoonen et al. (2012), Moenkopi A contains 0.87 wt % Fe^{3+}, primarily as the mineral hematite. The sandstone further consists of quartz (45 mol%), K-feldspar (12 mol%), kaolinite (17 mol%), illite (6 mol%), calcite (10 mol%), dolomite (10 mol%), and trace amounts of plagioclase, and ilmenite (Walker et al. 1981). Both subsamples were analyzed by X-Ray Fluorescence (XRF) at the University of Washington's analytical lab (**Table 2-1**). XRF results showed Moenkopi B to be substantially lower in SiO_2 (63.77 wt % vs. 82.92 wt % for Moenkopi A) and FeO (1.68 wt % vs. 2.93 wt % for Moenkopi A). Moenkopi B was much higher in CaO (16.33 wt % vs. 0.28 wt % for Moenkopi A) and MgO (5.76 wt % vs. 0.60 wt % for Moenkopi A). These results, combined with a 4-fold increase in loss on ignition (LOI) for Moenkopi B with respect to Moenkopi A, along with Mössbauer and Raman analyses, confirmed that Moenkopi B has a much larger carbonate content than Moenkopi A. The difference between the two subsamples reflects the

natural variation in the Moenkopi Formation. For the experiments reported here, the sample was crushed and the <177 μm size fraction was used.

Table 2-1. Weights and volumes of the reagents used for the experiments in this study.

Experimental Details							
	Type	**Sandstone**	**Sulfite**	**Sulfide**	**CO_2**	**H_2O**	**NaCl**
PNF9_0	B	0.703g	-	-	3.47g	3mL	1.049g
PNF9_1	B	0.705g	-	0.183g	3.13g	3mL	0.262g
PNF9_2	B	0.704g	0.185g	-	3.55g	3mL	0.525g
PNF9_3	B	0.702g	0.185g	0.192g	3.38g	3mL	1.051g
PNF9_4	B	0.701g	0.184g	-	3.14g	3mL	0.240g
PNF9-5	B	0.702g	-	0.187	3.70g	3mL	0.525g
PNF9_6	B	0.701g	0.184g	-	3.44g	3mL	1.049g
PNF9_7	B	0.702g	0.185g	0.191g	3.24g	3mL	0.263g
PNF9_8	B	0.700g	0.185g	0.196g	3.13g	3mL	0.525g
PNF9_9	B	0.702g	-	0.189g	3.41g	3mL	1.050g
PNF5-4	A	0.705g	-	0.193g	3.40g	1mL	0.176g
PNF11-1	A	0.702g	-	0.185g	2.71g	3mL	0.526g
PNF11-2	A	0.704g	0.186g	0.182g	2.75g	3mL	0.526g
PNF11-3	A	0.705g	0.186g	0.189g	2.72g	3mL	1.051g
PNF11-4	B	0.703g	-	0.189g	3.69g	1mL	0.176g
PNF11-5	B	0.700g	0.188g	0.182g	3.63g	1mL	0.177g

Several complementary techniques were used to characterize the starting material and reacted materials, but Mössbauer spectroscopy proved to be the most useful technique in determining changes because they occurred primarily between iron-bearing phases. For those analyses, samples were deposited without packing into a holder backed by Kapton® polyimide film tape. Mössbauer spectra were collected for 12-48 hours at ambient temperature, pressure, and humidity on a WEB Research Co. model WT302 Mössbauer spectrometer with a 100-60mCi ^{57}Co source implanted in Rh. Measurements were conducted at the Mössbauer Spectroscopy Laboratory at Mount Holyoke College. Baseline corrections for Compton scattering of 122keV gamma rays were made by calculating $A/(1-b)$, where A is the raw absorption and b is the Compton fraction measured by blocking the 14.4 keV gamma rays with a 2 mm piece of Al foil.

All spectra were fit using Mexdisd, a program provided by DeGrave and van Alboom from the University of Gent, Belgium (De Grave and van Alboom 1991; Vandenberghe et al. 1994). The program uses a line-shape-independent model for fitting the spectra, and solves the full hyperfine-interaction Hamiltonian, producing a distribution of values for the hyperfine field and using quadrupole shift (QS), center shift (CS), and line width as adjustable parameters.

In addition to Mössbauer spectroscopy, the starting material and reacted materials were analyzed using Fourier Transform Infrared (FTIR) spectroscopy and Visible to Near Infrared (VNIR) spectroscopy. FTIR spectra were collected at Stony Brook University on a Nicolet Nexus 670 spectrometer equipped with a Diffuse Reflectance attachment and DGTS and MTC-A detectors. A small amount of the starting material was mixed with dry, IR-grade KBr and lightly ground in an agate mortar. A total of 256 spectra collected at a resolution of 4 nm^{-1} wavenumbers were summed. VNIR spectra were collected using an Analytic Spectral Devices, Inc. Fieldspec3 Max portable spectroradiometer in the Stony Brook University Vibrational Spectroscopy Laboratory. The spectrometer utilizes a quartz halogen illumination source and Si photodiode (0.35-1.0μm) and two InGaAs (1.0-2.5μm) detectors. Illumination and detector angles were set to 35º and 0º respectively and each spectrum was an average of 100 scans.

2.3 Results

Mössbauer spectra show that Moenkopi B differs from Moenkopi A in that iron is present in the carbonate phase as well as the hematite phase (**Figure 2-1**). In addition, FTIR spectra of the unreacted sandstone showed that the amount of carbonate in Moenkopi B is greater than that in Moenkopi A. Due to the presence of carbonate in the unreacted material, it was not possible to use FTIR to resolve minor mineralogical changes in the carbonate fraction of Moenkopi B. In the

previous work, it was also noted that XRD does not adequately show the mineralogical changes that occur in these experiments due to the small amount of material involved in the mineralogical reactions. Mössbauer spectroscopy, however, which derives its signal solely from the iron in the sample, provided valuable insights into the reactivity of this sandstone. In addition, bi-directional VNIR spectroscopy recorded subtle color changes noted in a previous paper (Schoonen et al. 2012) along with the carbonate features previously observed using FTIR.

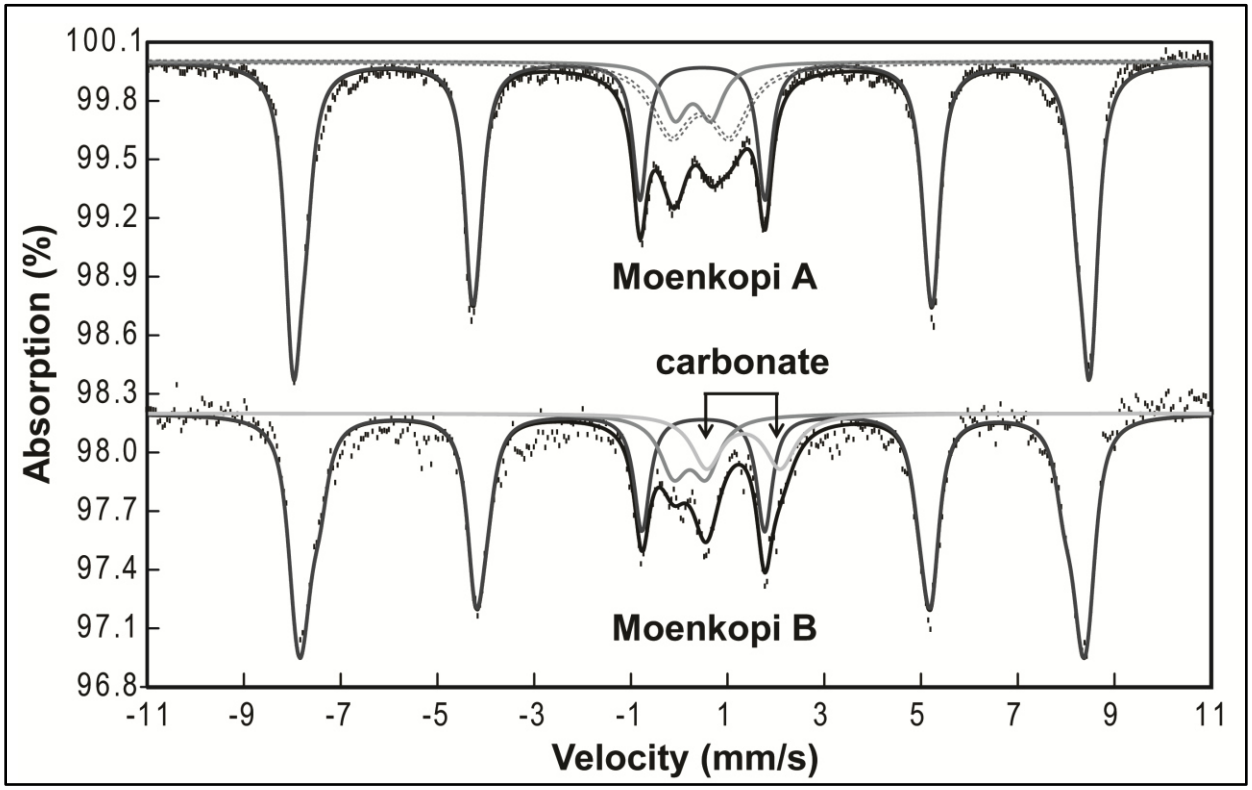

Figure 2-1. Mössbauer spectra of unreacted Moenkopi sandstones at 295K. Spectra are offset for clarity. In the fits, the light gray line is the carbonate doublet, the medium gray line is the low CS-low QS Fe^{3+} doublet, the dashed gray line is the low CS-high QS Fe^{3+} doublet, the dark gray line is the hematite sextet, and the black line is the sum of all the distributions.

The Mössbauer spectrum of the unreacted Moenkopi B sandstone was fit with a sextet with parameters corresponding to Fe^{3+} in hematite, a doublet associated with Fe^{3+} in octahedral

coordination, possibly in clay, and a doublet associated with Fe^{2+} in octahedral coordination, consistent with a carbonate (**Figure 2-1**). This sample has 78% of the spectral area in the hematite sextet, 11% in the carbonate doublet, and 11% in the Fe^{3+} doublet. Due to the low iron content in the sample and the similarity of Mössbauer parameters for carbonates, multiple doublet fits for carbonate were not attempted as they would have little interpretive value. Likewise, due to high overlap between 6-coordinated Fe^{3+} distributions for many materials and the Fe^{2+} distributions in pyrite (the unusual bonding environment in pyrite causes it to show up in the same spectral region), spectra are fit with a single low CS-low QS doublet and the results are reported as total iron in this CS-QS range. Changes in the spectral areas of these three components, however, indicate the mobility and reactivity of iron and can be used to effectively draw qualitative conclusions.

2.3.1 Reactions with $scCO_2$ alone in NaCl solutions

Moenkopi B showed minimal reactivity when exposed to only $scCO_2$ in a 6.0 m NaCl solution (**Figure 2-2; Table 2-2**). Mössbauer spectra showed a decrease in the spectral area of iron in carbonate by ~4% and an increase in spectral area for the low CS-low QS distribution of ~6%. In addition, the center-shift of the low CS-low QS doublet is increased by 0.03 mm/s. These changes are very close to the error in the technique for overlapped distributions (Dyar et al. 2008), but are consistent with observations that limestone undergoes some dissolution when exposed to $scCO_2$ (Rosenbauer et al. 2005). The subsequent increase in the spectral area of the low CS-low QS distribution is likely due to the precipitation of an additional phase that becomes supersaturated in solution upon carbonate dissolution, but the small amount of this new phase cannot be identified by any of the techniques used in this study.

2.3.2 Reactions with $scCO_2$ and sulfite in NaCl solutions

Moenkopi B reacted only slightly when exposed to $scCO_2$ and sulfite in 1.5, 3.0, and 6.0 m NaCl solutions (**Figure 2-2; Table 2-2**). Mössbauer experiments showed a ~4% spectral area loss in the hematite phase. There were no consistent changes in either the carbonate distribution or the low CS-low QS distribution with respect to salt concentration for these experiments (**Table 2-2**).

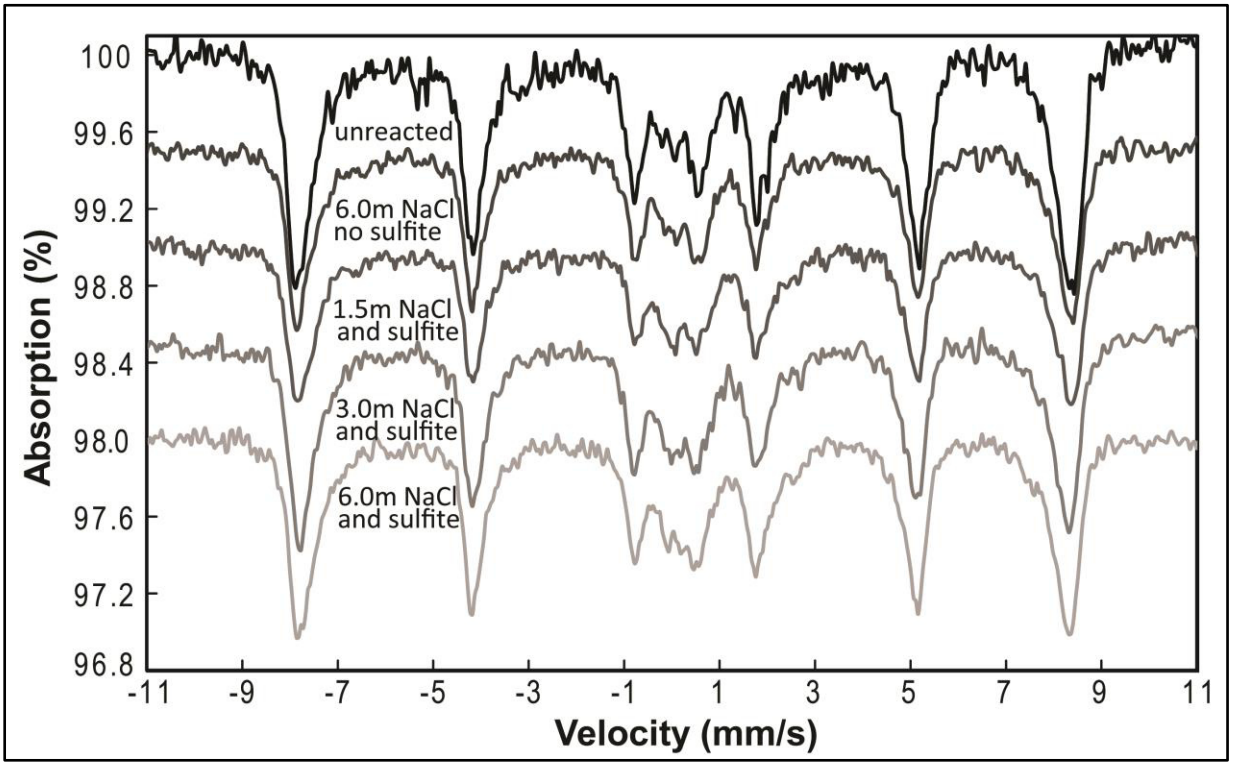

Figure 2-2. Mössbauer spectra at 295K of Moenkopi B reacted with $scCO_2$ or $scCO_2$, plus sulfite, in NaCl solutions. Spectra are offset for clarity.

The VNIR spectra of the three samples reacted with sulfite and $scCO_2$ at different salt concentrations are overlaid on the VNIR spectrum of Moenkopi B in **Figure 2-3** along with ratios of the starting material to the reacted material for all three samples. There is a clear absorption feature at ~1.98 μm in the reacted samples that is not present in the starting material.

The position of this feature is consistent with absorption band 5 of Gaffey et al., which is associated with siderite, dolomite, and calcite due to the vibration of the carbonate radical (Gaffey 1986; Gaffey 1987). The position of the water feature at 1.9 μm, however, can combine with this carbonate feature, altering its position and intensity, thus making it non-diagnostic (Gaffey 1986; Gaffey 1987). VNIR spectral changes only occur under these experimental conditions, hence, water-associated absorptions in these samples are unlikely. It is revealing that band 5 is deeper in the reacted samples, whereas the absorption consistent with absorption band 6 of Gaffey et al. is deeper in the unreacted sample. Band 5 will reflect changing iron content in a sample (Gaffey 1986), so these spectral differences indicate that the carbonate phase is involved in the uptake of iron that comes from hematite dissolution. The position of band 5 is consistent with siderite and dolomite, although the position of the absorption consistent with absorption band 2 of Gaffey et al. (~2.324 μm) is closer to that for siderite and appears at the same location for both the reacted and unreacted samples.

Table 2-2. Mössbauer parameters of Moenkopi B reacted with just $scCO_2$ in NaCl solutions and Moenkopi B reacted with $scCO_2$ 1.468 mol/L sulfite in NaCl solutions. Significant deviations from the starting materials are reflected in the use of bold type.*

Moenkopi B reacted with just $scCO_2$ and $scCO_2$ plus sulfite						
		unreacted	**6.0m NaCl**	**1.5m NaCl**	**3.0m NaCl**	**6.0m NaCl**
hematite	δ(mm/s)	0.38	0.38	0.38	0.37	0.37
	Δ (mm/s)	-0.24	-0.24	-0.22	-0.22	-0.22
	Field (KOe)	504.3	504.3	504.4	500.2	501.0
	Γ (mm/s)	0.38	0.34	0.37	0.39	0.37
	Area (%)	77.6	76.3	73.6	74.0	73.5
Fe^{2+} in carbonate	δ (mm/s)	1.33	1.31	1.21	1.21	1.27
	Δ (mm/s)	1.52	1.46	1.87	1.69	1.65
	Γ (mm/s)	0.75	0.51	0.98	0.90	0.87
	Area (%)	11.4	**6.7**	13.5	10.7	12.8
Fe^{3+}	δ (mm/s)	0.22	0.25	0.26	0.26	0.21
	Δ (mm/s)	0.67	0.62	0.65	0.64	0.61
	Γ (mm/s)	0.68	0.72	0.54	0.68	0.64
	Area (%)	11.0	**17.0**	12.9	15.3	13.5
	$\chi 2$	1.81	1.65	1.36	2.19	1.92

***Symbols in the table are as follows: δ is center shift, Δ is quadrupole splitting, Γ is line width, and $\chi 2$ is normalized chi squared. Errors on parameters are ±0.02 mm/s for δ, ±0.05 mm/s for δ, ±10-20% for overlapped doublet areas, and ±1-3% for ΣFe^{2+} vs. ΣFe^{3+} (Dyar et al. 2008).**

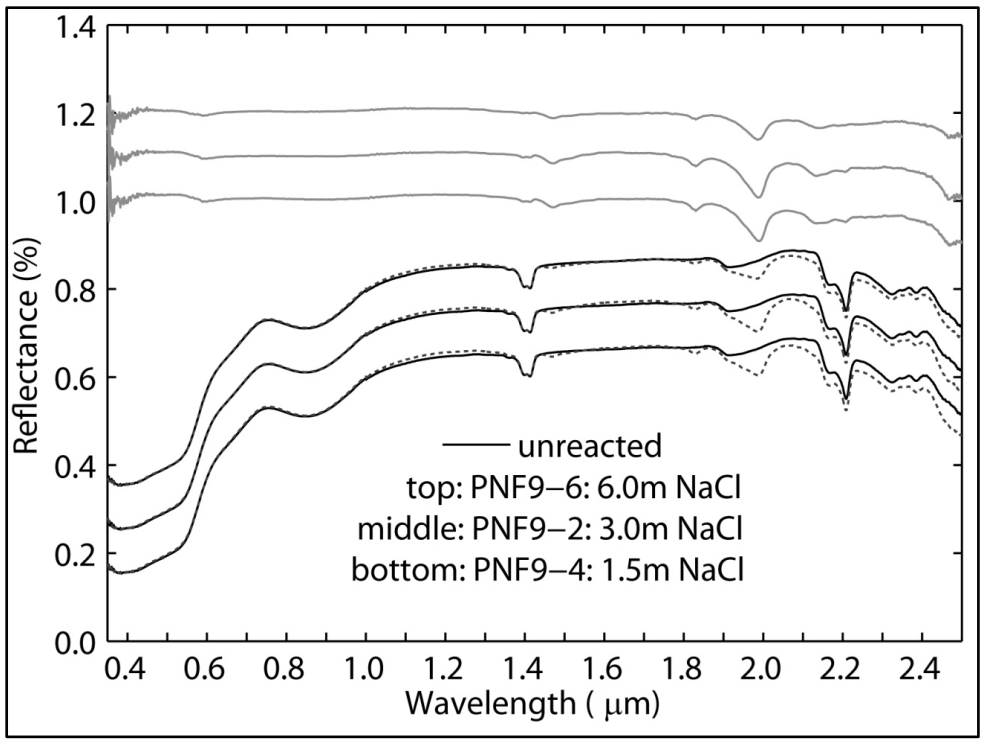

Figure 2-3. VNIR spectra of unreacted Moenkopi B (black) overlaid by reacted sandstone (dashed). Ratios of the unreacted to reacted spectra are shown above in gray.

2.3.3 Reactions with $scCO_2$ and sulfide in NaCl solutions

Mössbauer spectra demonstrate that all solutions where the sandstone was reacted with $scCO_2$, Na_2S, and NaCl undergo a complete loss of iron in the hematite phase consistent with dissolution (**Figure 2-4**; **Table 2-3**). The carbonate phase was minimally affected with a ~3% decrease in spectral area for all samples. The low CS-low QS component dominated the spectra of the reacted sandstones with > 90% of spectral area in that phase. The CS for that low CS-low QS phase increased from 0.22 to 0.32 mm/s and the parameters of the doublet in the reacted samples are consistent with Fe^{2+} in pyrite (**Figure 2-4**; **Table 2-3**).

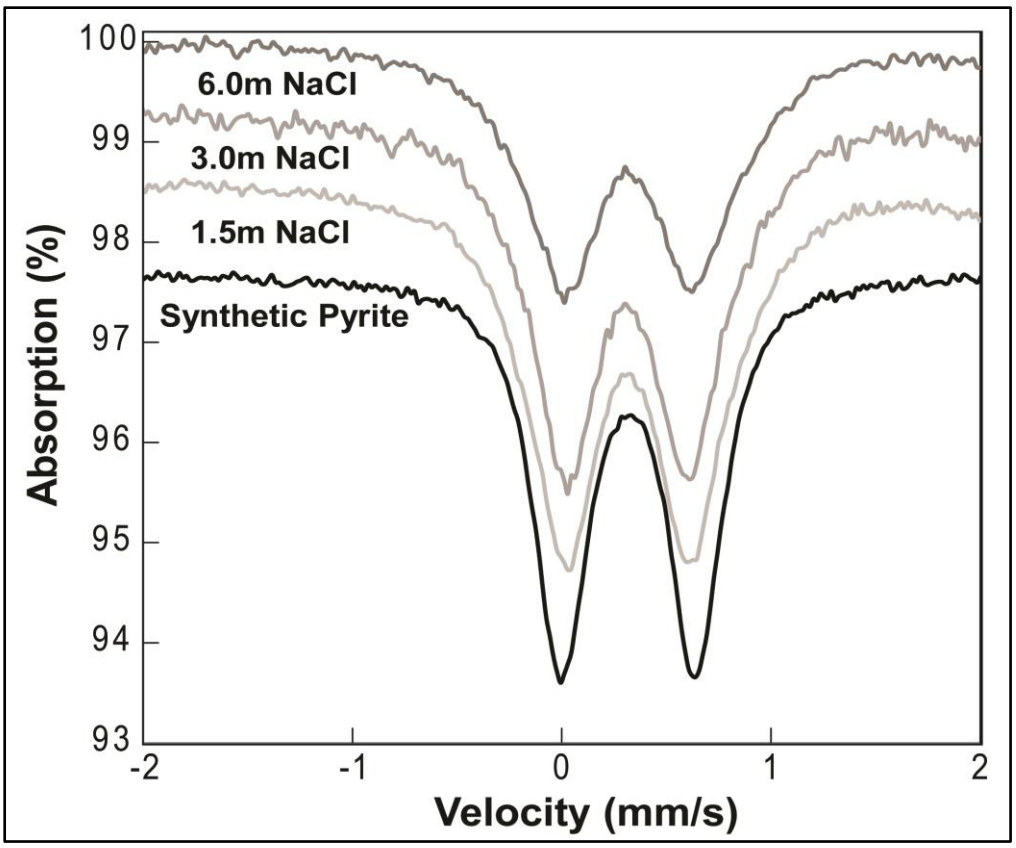

Figure 2-4. Mössbauer spectra at 295K of Moenkopi B reacted with $scCO_2$ and sulfide in NaCl solutions. Fits are not shown. Spectra are offset for clarity.

Visual inspection and the VNIR results also suggest that iron in hematite is converted to iron in pyrite. The blackening of the sample and the loss of most spectral features can be interpreted as pyrite coating the grains and, therefore, dominating the spectral signature in the VNIR where penetration depth of the light is minimal (**Figure 2-5**).

Table 2-3. Mössbauer parameters for Moenkopi B reacted with $scCO_2$ and 0.256 mol/L sulfide in NaCl solutions.

Moenkopi B reacted with $scCO_2$ and sulfide					
		unreacted	**1.5m NaCl**	**3.0m NaCl**	**6.0m NaCl**
hematite	δ (mm/s)	0.38			
	Δ (mm/s)	-0.24			
	Field (KOe)	504.3			
	Γ (mm/s)	0.38			
	Area (%)	77.6			
Fe^{2+} in carbonate	δ (mm/s)	1.33	1.20	1.20	1.20
	Δ (mm/s)	1.52	1.60	1.94	1.78
	Γ (mm/s)	0.75	0.88	0.56	0.95
	Area (%)	11.4	8.2	8.5	8.3
Fe^{3+} / Fe^{2+} in Pyrite (δ=0.32, Δ=0.64)	δ (mm/s)	0.22	0.31	0.32	0.32
	Δ (mm/s)	0.67	0.61	0.64	0.65
	Γ (mm/s)	0.68	0.41	0.41	0.45
	Area (%)	11.0	91.8	91.5	91.7
	$\chi 2$	1.81	1.10	0.85	2.12

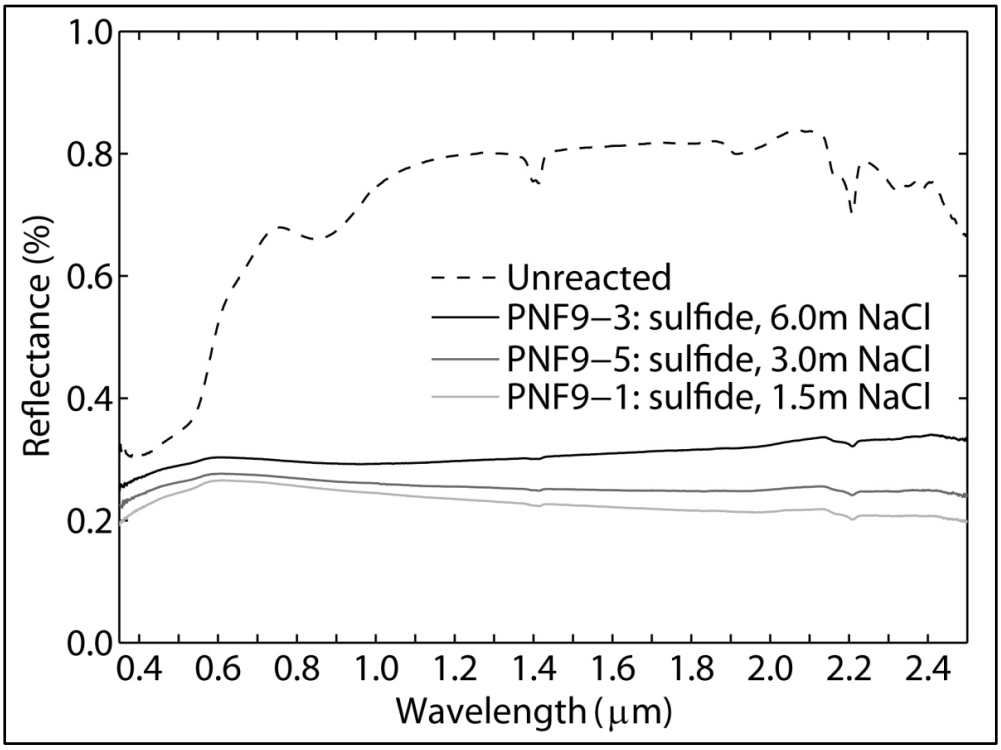

Figure 2-5. VNIR spectra of Moenkopi B reacted with $scCO_2$ and sulfide in NaCl solutions.

2.3.4 Reactions with $scCO_2$, sulfite, and sulfide in NaCl solutions

Iron in hematite. Mössbauer spectra confirm that all experiments where the sandstone was reacted with $scCO_2$, Na_2S, and Na_2SO_3 underwent significant mineralogical changes (**Figure 2-6**; **Table 2-4**). Successive decreases in the peak area of the hematite phase of 40%, 54.6%, and 23.7% were observed for the 1.5, 3.0, and 6.0 m NaCl concentrations, respectively.

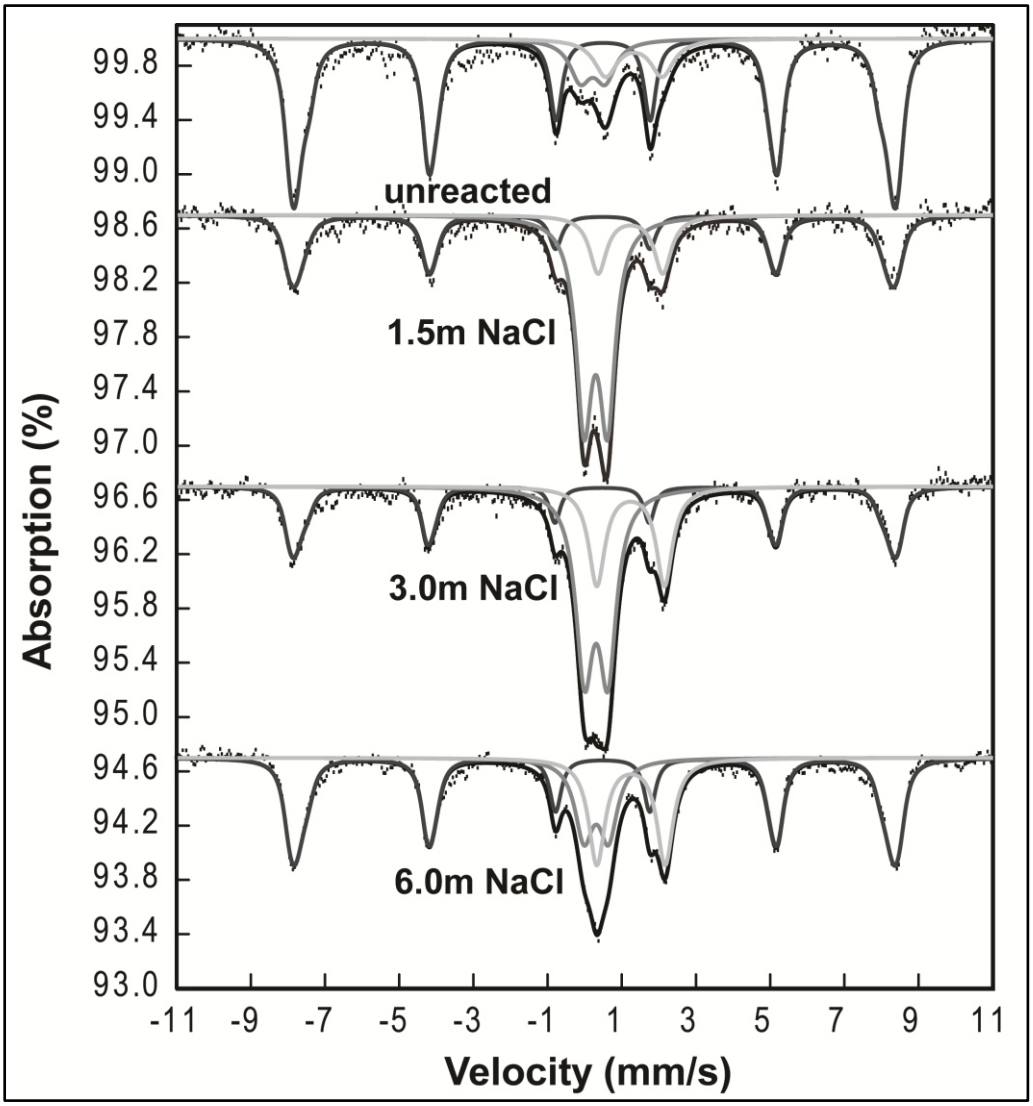

Figure 2-6. Mössbauer spectra at 295K of Moenkopi B reacted with $scCO_2$, sulfite, and sulfide in NaCl solutions. Spectra are offset for clarity. In the fits, the light gray line is the carbonate doublet, the medium gray line is the low CS-low QS Fe^{3+} doublet, the dark gray line is the hematite sextet, and the black line is the sum of all the distributions.

Table 2-4. Mössbauer parameters for Moenkopi B reacted with $scCO_2$, 1.468 mol/L sulfite, and 0.256 mol/L sulfide in NaCl solutions.

Moenkopi B reacted with $scCO_2$, sulfide, and sulfite					
		unreacted	**1.5m NaCl**	**3.0m NaCl**	**6.0m NaCl**
hematite	δ (mm/s)	0.38	0.36	0.36	0.37
	Δ (mm/s)	-0.24	-0.25	-0.21	-0.22
	Field (KOe)	504.3	502.5	504.3	504.0
	Γ (mm/s)	0.38	0.40	0.33	0.36
	Area (%)	77.6	37.6	32.9	53.9
Fe^{2+} in carbonate	δ (mm/s)	1.33	1.23	1.24	1.25
	Δ (mm/s)	1.52	1.74	1.82	1.84
	Γ (mm/s)	0.75	0.55	0.53	0.54
	Area (%)	11.4	14.8	23.0	25.8
Fe^{3+} / Fe^{2+} in Pyrite (δ=0.32, Δ=0.64)	δ (mm/s)	0.22	0.30	0.31	0.31
	Δ (mm/s)	0.67	0.63	0.63	0.66
	Γ (mm/s)	0.68	0.52	0.57	0.59
	Area (%)	11.0	47.6	44.1	20.3
	$\chi 2$	1.81	1.04	1.43	1.34

Iron in carbonate. Mössbauer spectra show that the iron-carbonate spectral component increased with increasing NaCl concentration. There is also a shift in the QS of this distribution to higher velocity and a shift in CS to lower velocity, indicating the formation of a new and distinct phase (**Figure 2-7**; **Table 2-4**). The shift in CS and QS values as the spectral area of this phase increases is most likely the result of mixing of overlapping spectral components as the existing carbonate spectral component is being overlaid by the spectral component from the new carbonate phase. Due to this high degree of overlap, the two distributions are fit with a single doublet. The parameters for this doublet are consistent with siderite. Visual inspection of **Figure 2-7**, however, shows that the match is not exact. Based on the Mössbauer data alone, iron existing in another carbonate phase cannot be ruled out.

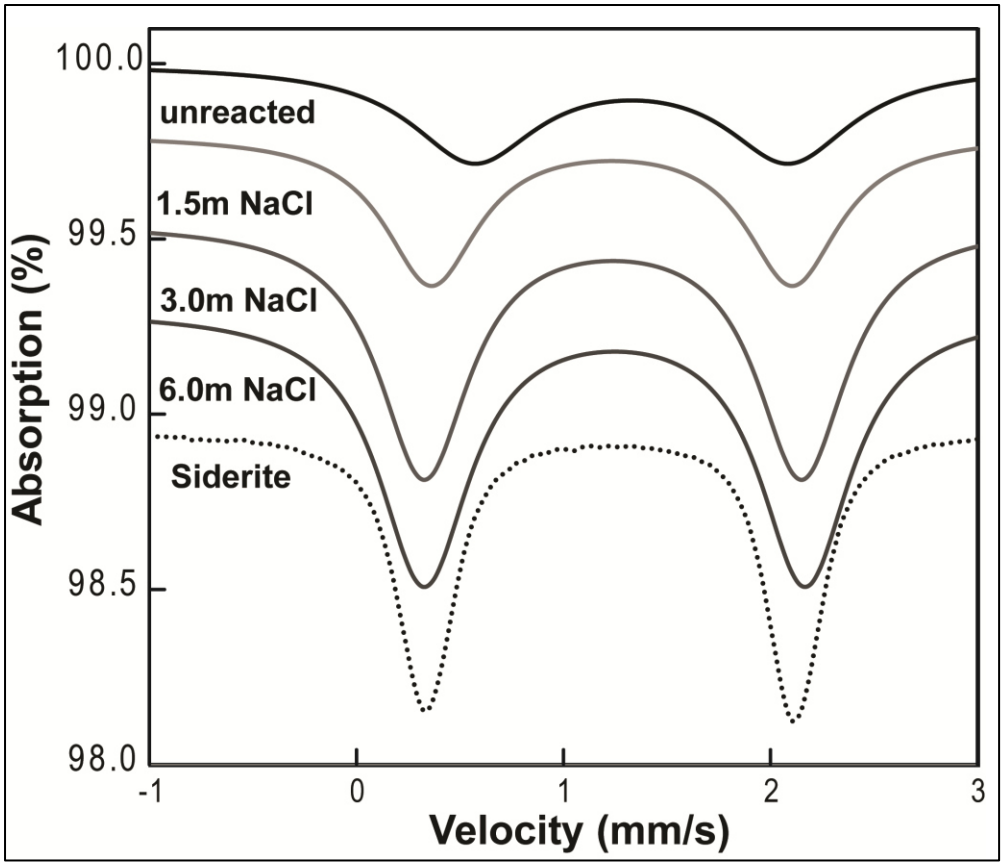

Figure 2-7. Ferrous component of Mössbauer fit from Figure 2-6 compared to siderite. The unreacted sandstone has lower QS and higher CS than the reacted sandstone, indicating the in-growth of a new phase.

Iron in pyrite/Fe^{3+}. Mössbauer spectra for reacted sandstone at all NaCl concentrations showed a marked increase in low CS-low QS spectral component. However, the largest increase in this spectral component was found in the sandstone subjected to the lowest salt concentration, opposite to the trend seen for carbonates. There is also a substantial change in the CS of the low CS-low QS doublet from 0.22 to 0.31 mm/s. The new parameters are consistent with pyrite, even though it is understood that this doublet is a combination of both the in-growing phase and the pre-existing phase (**Figure 2-8**; **Table 2-4**).

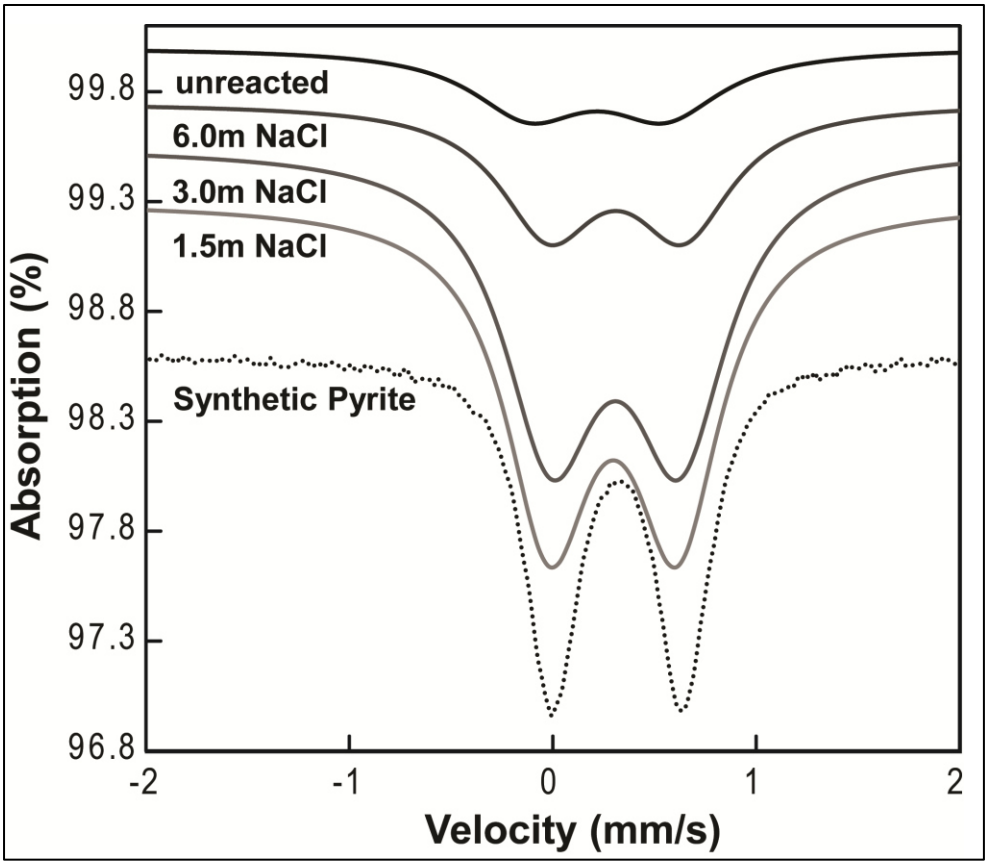

Figure 2-8. Low CS-low QS distribution from fits in Figure 2-6 compared to synthetic, acid-washed pyrite. The shift in both CS and QS of distribution indicates ingrowth of a new phase. The parameters of the new phase are consistent with pyrite.

VNIR results for Moenkopi B reacted with $scCO_2$, sulfite and sulfide in NaCl solutions mirror the Mössbauer results but also clarify the role of salt concentration on the mineralogical transformations (**Figure 2-9**). VNIR spectra of samples reacted in 1.5 and 3.0 m NaCl solutions show spectra dominated by the pyrite phase (a fairly featureless, low reflectance spectrum). The VNIR spectrum of PNF9-3 (6.0 m) appears unchanged from the unreacted sandstone, except in visible wavelengths, where the color change noted in the previous paper (Schoonen et al. 2012) is apparent. This shape change in the visible region of the spectrum is consistent with the growth of the surface carbonate phase. Where calcite and dolomite exhibit greater reflectance in low

wavelengths through the visible, the aragonite and siderite phases show a convex slope increasing from 0.3 to 0.6 μm (Clark et al. 2007; Cloutis et al. 2010).

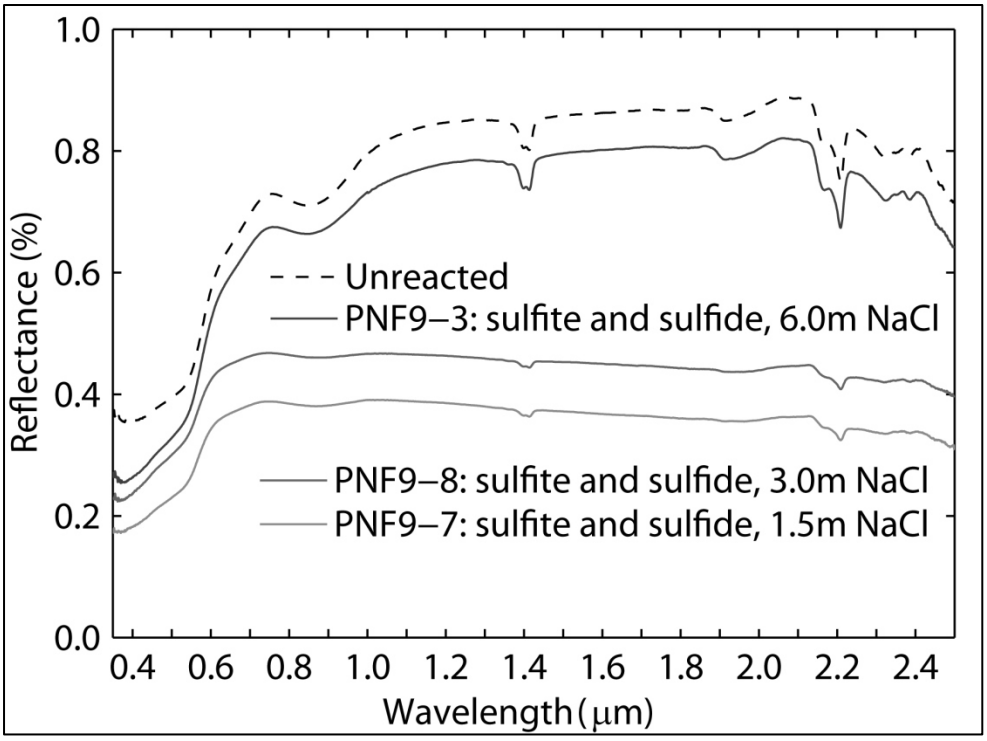

Figure 2-9. VNIR spectra of Moenkopi B reacted with $scCO_2$, sulfite and sulfide in NaCl solutions. Spectra are offset for clarity.

2.3.5 Fluid/Rock Ratio

To determine the role of the fluid:rock ratio on the reactivity of the sandstone, experiments were conducted under the two most reactive experimental regimes - $scCO_2$/sulfide and $scCO_2$/sulfite/sulfide - and at moderate salinity (3.0 m) using both a 1.4:1 and a 4.3:1 fluid rock ratio. All experiments are performed with the same amount of sulfite and sulfide, leading to a dilution effect in the higher fluid:rock ratio regime.

$scCO_2$ and sulfide. Moenkopi A and Moenkopi B were reacted with $scCO_2$ and sulfide in 3.0 m NaCl solutions in both 1.4:1 and 4.3:1 fluid:rock ratio experiments. For Moenkopi A,

Mössbauer spectra show that the hematite sextet goes from 75% to 34% spectral area in the low fluid:rock ratio experiments and to 30% spectral area in the high fluid:rock ratio experiments. (**Figure 2-10**; **Table 2-5**). For Moenkopi B, Mössbauer spectra show that the hematite sextet goes from 78% to 9% spectral area in the low fluid:rock ratio experiments and is completely lost in the high fluid:rock ratio experiments. (**Figure 2-10**; **Table 2-5**). However, noise in the latter spectrum makes it impossible to define a sextet of low spectral area, so the difference between the low and high fluid:rock ratio experiments may be smaller than it appears. The reaction product in all cases is pyrite. VNIR spectra of these samples showed no additional changes.

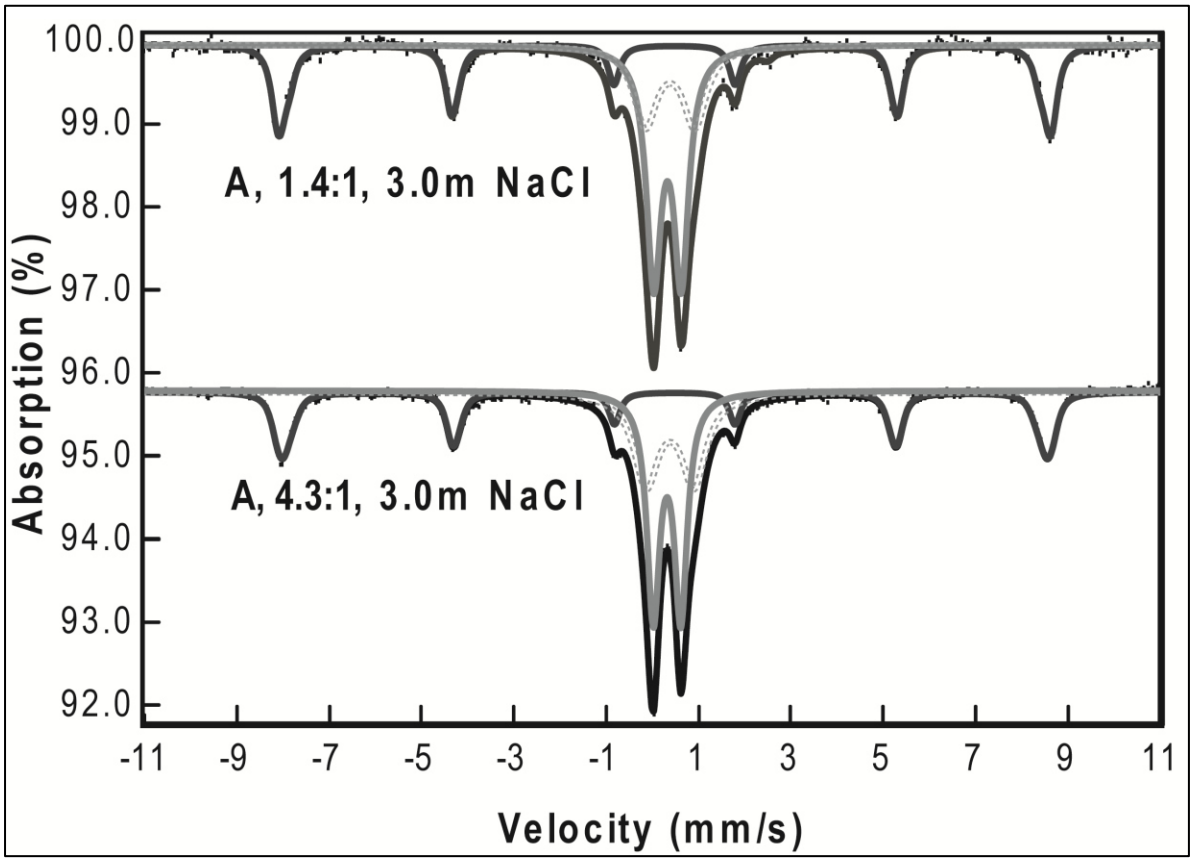

Figure 2-10. Mössbauer spectra at 295K of Moenkopi A reacted with $scCO_2$ and sulfide in 3.0m NaCl solutions for 1.4:1 (top) and 4.3:1 (bottom) fluid:rock ratio experiments. In the fits, the medium gray line is the low CS-low QS Fe^{3+} doublet, the dashed gray line is the low CS-high QS Fe^{3+} doublet, the dark gray line is the hematite sextet, and the black line is the sum of all the distributions.

Table 2-5. Mössbauer parameters for experiment examining effects of fluid:rock ratios.

Effects of Fluid:Rock Ratios									
		unreacted		**sulfide 3m NaCl Moenkopi A**		**sulfide 3m NaCl Moenkopi B**		**both 3m NaCl Moenkopi B**	
		Moen A	**Moen B**	**low f:r**	**high f:r**	**low f:r**	**high f:r**	**low f:r**	**high f:r**
hematite	δ (mm/s)	0.37	0.38	0.38	0.38	0.46		0.39	0.36
	Δ (mm/s)	-0.22	-0.24	-0.22	-0.22			-0.22	-0.21
	Field (KOe)	510.6	504.3	519.1	515.0	501.0		507.6	504.3
	Γ (mm/s)	0.35	0.38	0.29	0.28	0.27		0.34	0.33
	Area (%)	74.7	77.6	34.0	29.7	8.8		37.8	32.9
	Loss (%)			**40.7**	**45.0**	**68.8**	**77.6**	**39.8**	**44.8**
Fe^{2+} in carbonate	δ (mm/s)		1.33			1.10	1.20	1.24	1.24
	Δ (mm/s)		1.52			1.94	1.94	1.85	1.82
	Γ (mm/s)		0.75			0.72	0.56	0.45	0.53
	Area (%)		11.4			4.8	8.5	37.3	23.0
Fe^{3+} in oct. coord.	δ (mm/s)	0.44		0.39	0.38				
	Δ (mm/s)	1.21		1.06	1.03				
	Γ (mm/s)	0.97		0.61	0.64				
	Area (%)	17.1		23.8	30.8				
Fe^{3+} / Fe^{2+} in Pyrite	δ (mm/s)	0.28	0.22	0.33	0.32	0.34	0.32	0.32	0.31
	Δ (mm/s)	0.74	0.67	0.59	0.60	0.69	0.64	0.68	0.63
	Γ (mm/s)	0.61	0.68	0.39	0.34	0.47	0.41	0.59	0.57
	Area (%)	8.3	11.0	42.2	39.5	86.6	91.5	24.8	44.1
	$\chi 2$	3.62	1.81	2.02	3.62	1.67	0.85	1.42	1.43

$scCO_2$, sulfite, and sulfide. Moenkopi B was also reacted with $scCO_2$, sulfite and sulfide in 3.0 m NaCl solutions in both 1.4:1 and 4.3:1 fluid:rock ratio experiments (**Figure 2-12**; **Table 2-5**). Mössbauer spectra show a ~40% and ~45% spectral area decrease for the hematite phase in the low and high fluid:rock ratio experiments, respectively. The low fluid:rock ratio experiment, however, favored the formation of siderite, whereas the high fluid:rock ratio experiment favored the formation of pyrite. In fact, Mössbauer results imply that more iron ended up in the siderite phase (37.3% of the spectral area) for the 1.4:1 fluid:rock ratio experiment in a 3.0 m solution of NaCl than under any other experimental conditions explored in this or the previous paper. It is

interesting to note that Moenkopi A formed more siderite in low fluid:rock ratio experiments with no salt than in any experiment using saline fluids (**Figure 2-13**). It is unclear if the difference in that case was due to the fluid:rock ratio or fluid chemistry.

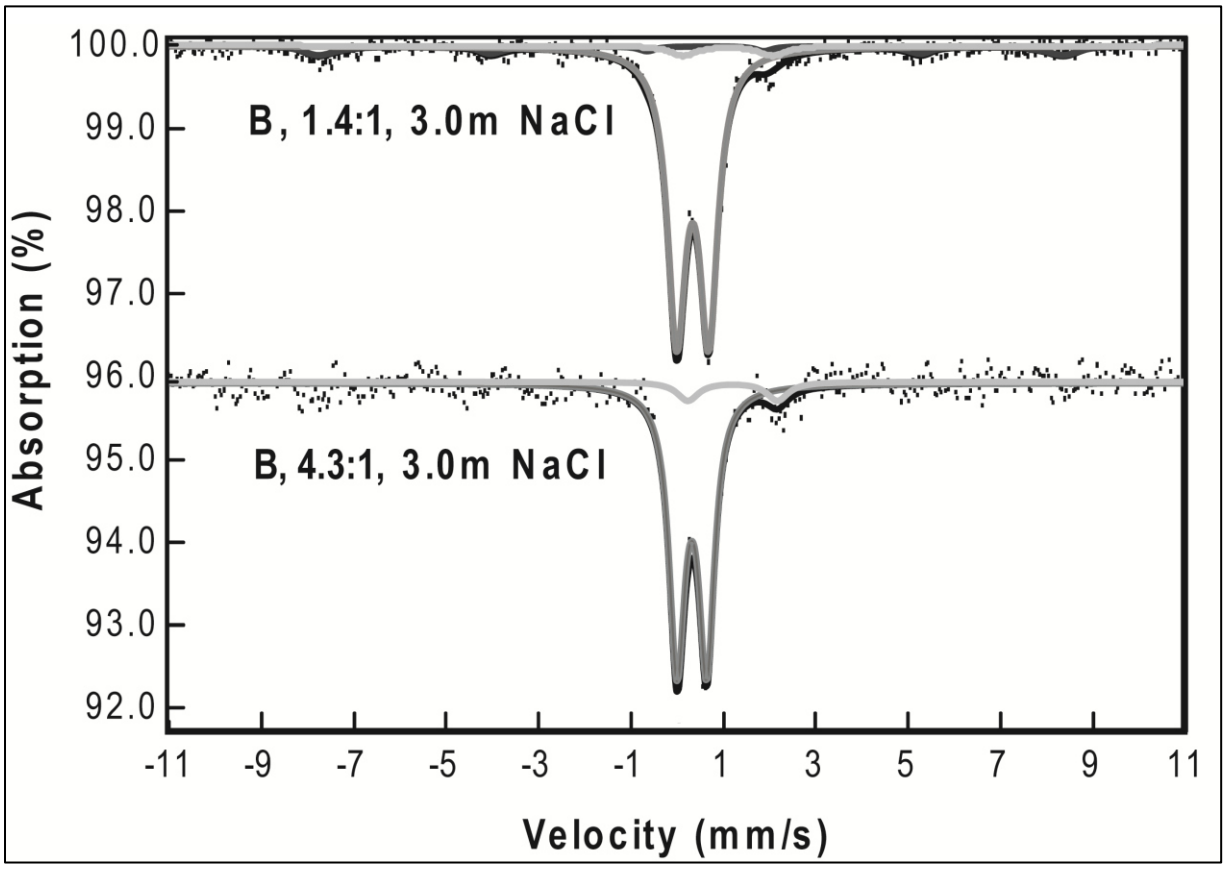

Figure 2-11. Mössbauer spectra at 295K of Moenkopi B reacted with $scCO_2$ and sulfide in 3.0m NaCl solutions for 1.4:1 (top) and 4.3:1 (bottom) fluid:rock ratio experiments. In the fits, the light gray line is the carbonate doublet, the medium gray line is the low CS-low QS Fe^{3+} doublet, the dark gray line is the hematite sextet, and the black line is the sum of all the distributions.

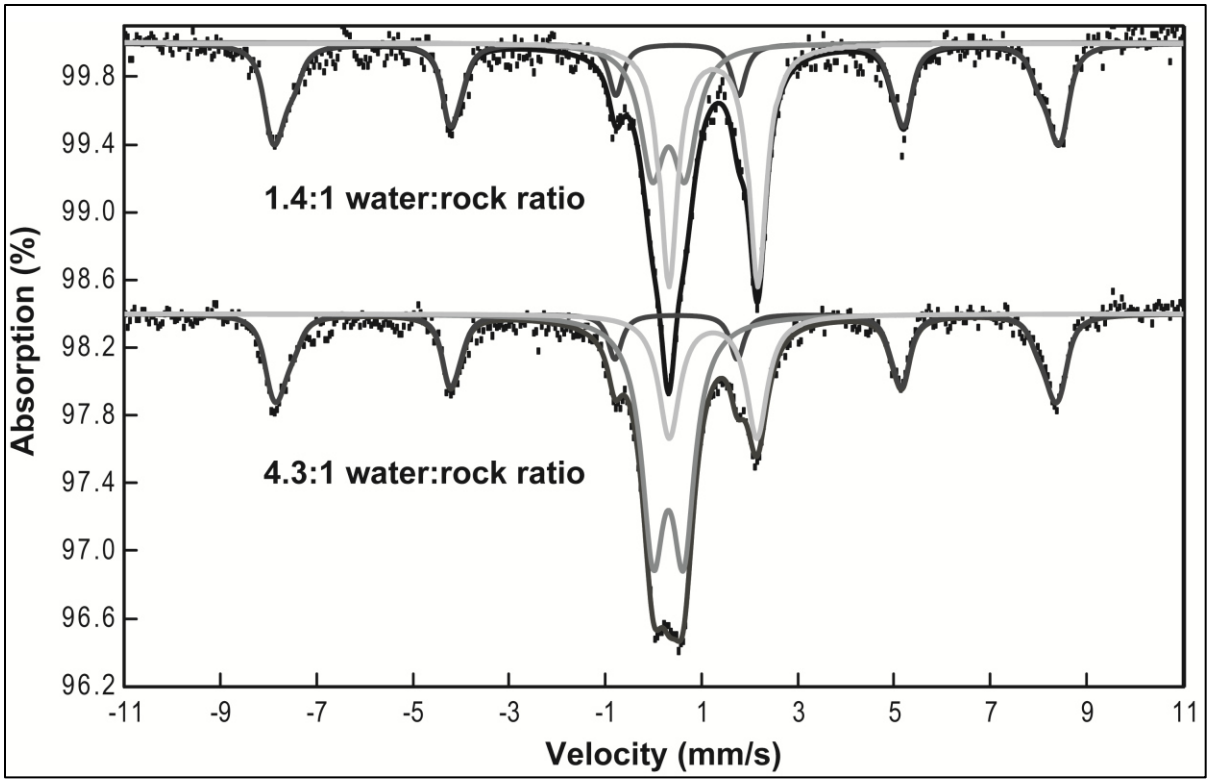

Figure 2-12. Mössbauer spectra at 295K of Moenkopi B reacted with $scCO_2$, sulfite and sulfide in a 3.0m NaCl solution. Spectra are offset for clarity. In the fits, the light gray line is the carbonate doublet, the medium gray line is the low CS-low QS Fe^{3+} doublet, the dark gray line is the hematite sextet, and the black line is the sum of all the distributions.

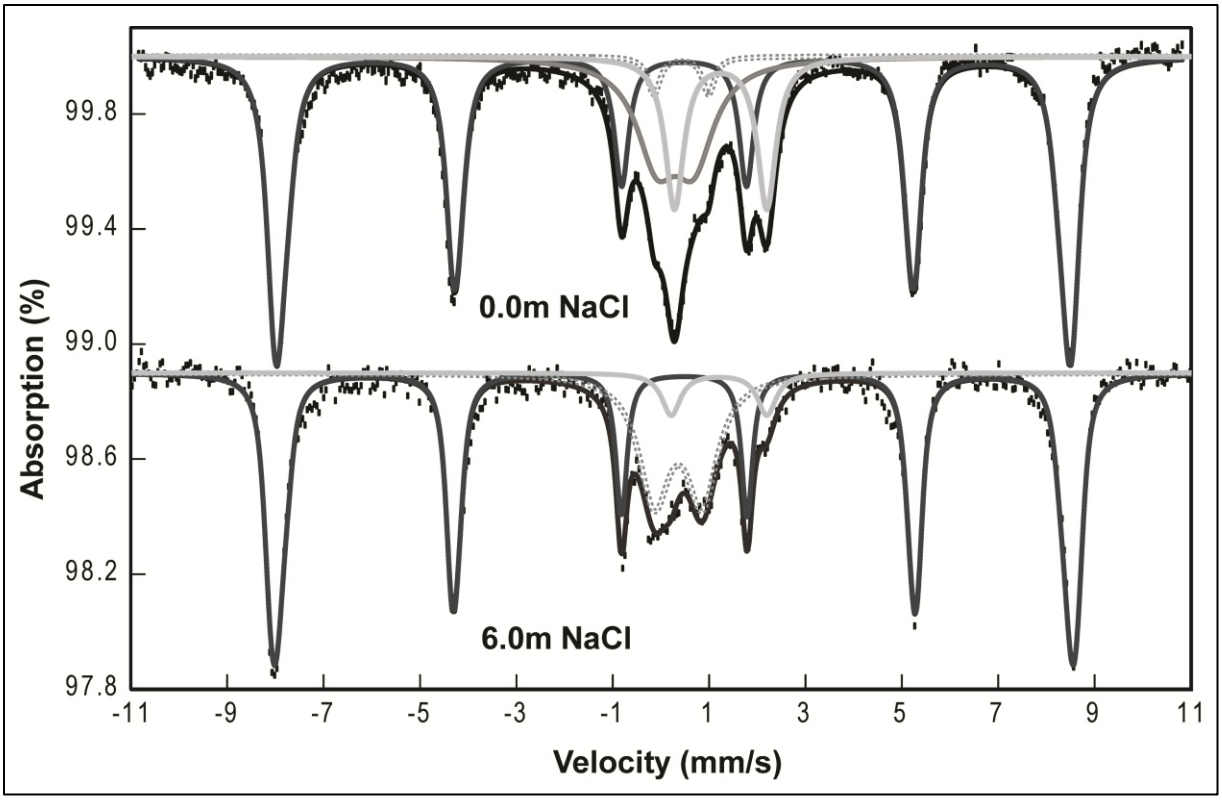

Figure 2-13. Mössbauer spectra at 295K for Moenkopi A reacted with $scCO_2$, sulfite, and sulfide in a 0m (top) and 6.0m (bottom) NaCl solution. The top spectrum is from a 1.4:1 fluid:rock ratio experiment and the bottom spectrum is from a 4.3:1 water:rock ratio experiment. Spectra are scaled and offset for clarity. In the fits, the light gray line is the carbonate doublet, the medium gray line is the low CS-low QS Fe^{3+} doublet, the dashed gray line is the low CS-high QS Fe^{3+} doublet, the dark gray line is the hematite sextet, and the black line is the sum of all the distributions.

2.3.6 Comparison with Moenkopi A

To determine if changes in mineralogy for experiments in this study were due to differences in experimental conditions or the different samples of sandstone, experiments were run to compare the reactivity of Moenkopi A and Moenkopi B. First, both Moenkopi A and Moenkopi B were reacted with sulfide and $scCO_2$ in 3.0 m NaCl solutions in 1.4:1 fluid:rock ratio experiments (**Figure 2-14**; **Table 2-6**). Mössbauer spectra show that the hematite phase of both Moenkopi A and Moenkopi B is primarily converted to pyrite. However, while the hematite

in Moenkopi A is only partially converted, the hematite in Moenkopi B is almost completely converted.

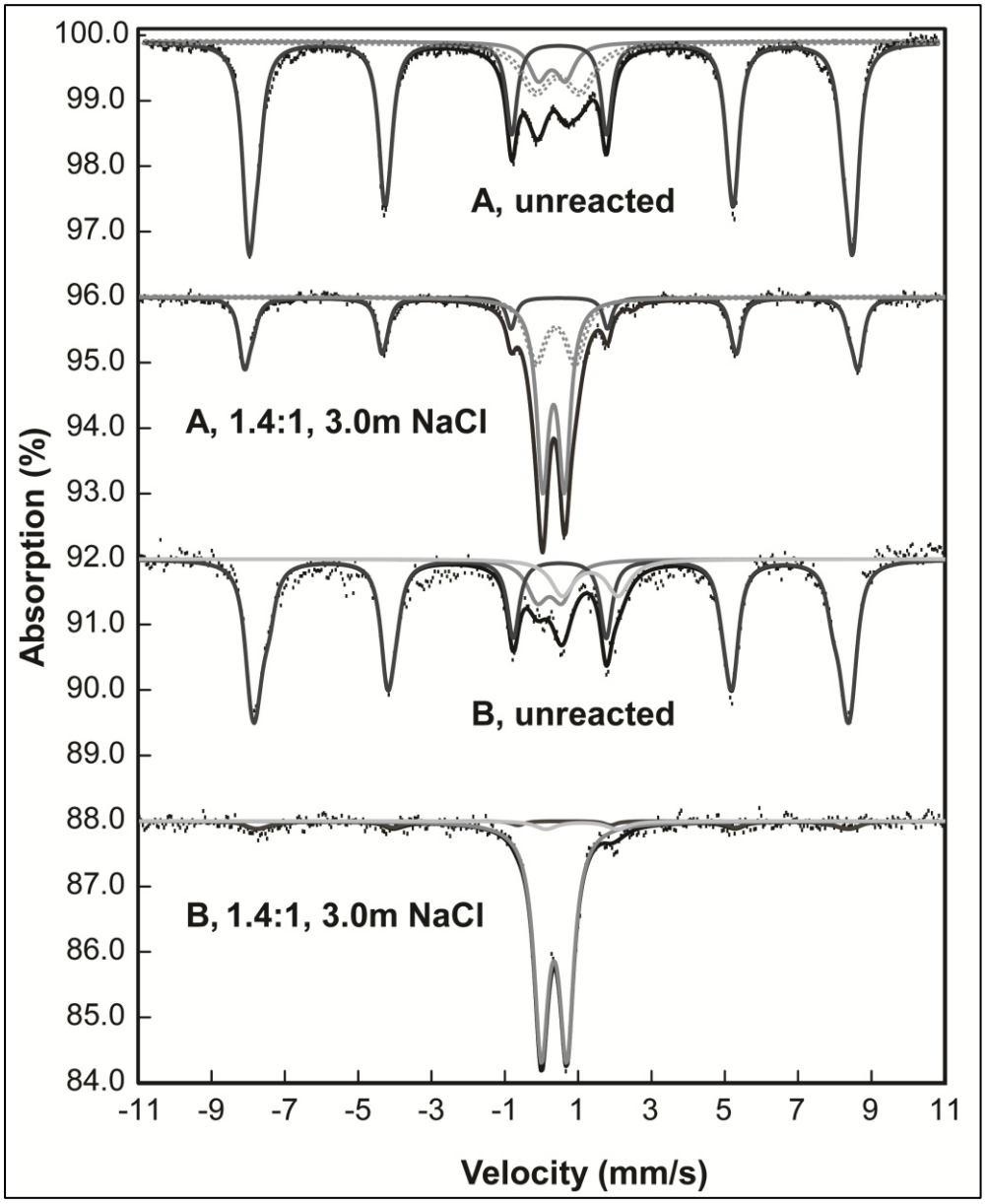

Figure 2-14. Mössbauer spectra at 295K comparing Moenkopi A and Moenkopi B, reacted with $scCO_2$ and sulfide in a 3.0m NaCl solution in 1.4:1 fluid:rock ratio experiments (1mL fluid). Unreacted samples are also shown for comparison. Spectra are offset for clarity. In the fits, the light gray line is the carbonate doublet, the medium gray line is the low CS-low QS Fe^{3+} doublet, the dashed gray line is the low CS-high QS Fe^{3+} doublet, the dark gray line is the hematite sextet, and the black line is the sum of all the distributions.

Table 2-6. Mössbauer parameters for experiment comparing Moenkopi A and Moenkopi B.

Comparison between Moenkopi A and Moenkopi B									
		unreacted		**sulfide 3m NaCl low fluid:rock**		**both 3m NaCl high fluid:rock**		**both 6m NaCl high fluid:rock**	
		Moen A	**Moen B**	**Moen A**	**Moen B**	**Moen A**	**Moen B**	**Moen A**	**Moen B**
hematite	δ (mm/s)	0.37	0.38	0.38	0.46	0.38	0.36	0.38	0.37
	Δ (mm/s)	-0.22	-0.24	-0.22	-0.32	-0.21	-0.21	-0.22	-0.22
	Field (KOe)	510.6	504.3	519.1	501.0	514.0	504.3	514.6	504.0
	Γ (mm/s)	0.35	0.38	0.29	0.40	0.27	0.33	0.27	0.36
	Area (%)	74.7	77.6	34.0	8.8	68.9	32.9	67.4	53.9
Fe^{2+} in carbonate	δ (mm/s)		1.33		1.10	1.20	1.24	1.21	1.25
	Δ (mm/s)		1.52		1.94	2.29	1.82	1.98	1.84
	Γ (mm/s)		0.75		0.72	0.52	0.53	0.47	0.54
	Area (%)		11.4		4.8	3.6	23.0	5.6	25.8
Fe^{3+} in oct. coord.	δ (mm/s)	0.44		0.39		0.38		0.36	
	Δ (mm/s)	1.21		1.06		1.00		1.00	
	Γ (mm/s)	0.97		0.61		0.88		0.78	
	Area (%)	17.1		23.8		27.6		27.0	
Fe^{3+} / Fe^{2+} in Pyrite	δ (mm/s)	0.28	0.22	0.33	0.34		0.31		0.31
	Δ (mm/s)	0.74	0.67	0.59	0.69		0.63		0.66
	Γ (mm/s)	0.61	0.68	0.39	0.47		0.57		0.59
	Area (%)	8.3	11.0	42.2	86.6		44.1		20.3
	$\chi 2$	3.62	1.81	2.02	1.67	1.78	1.43	2.26	1.34

Next, both Moenkopi A and Moenkopi B were reacted with sulfite, sulfide and $scCO_2$ in either a 3.0 or 6.0 m solution of NaCl in 4.3:1 fluid:rock ratio experiments (**Figure 2-15**; **Table 2-6**). In this high fluid:rock ratio regime, Mössbauer spectra indicate that higher salt concentrations favored the formation of siderite over pyrite in both Moenkopi A and Moenkopi B.

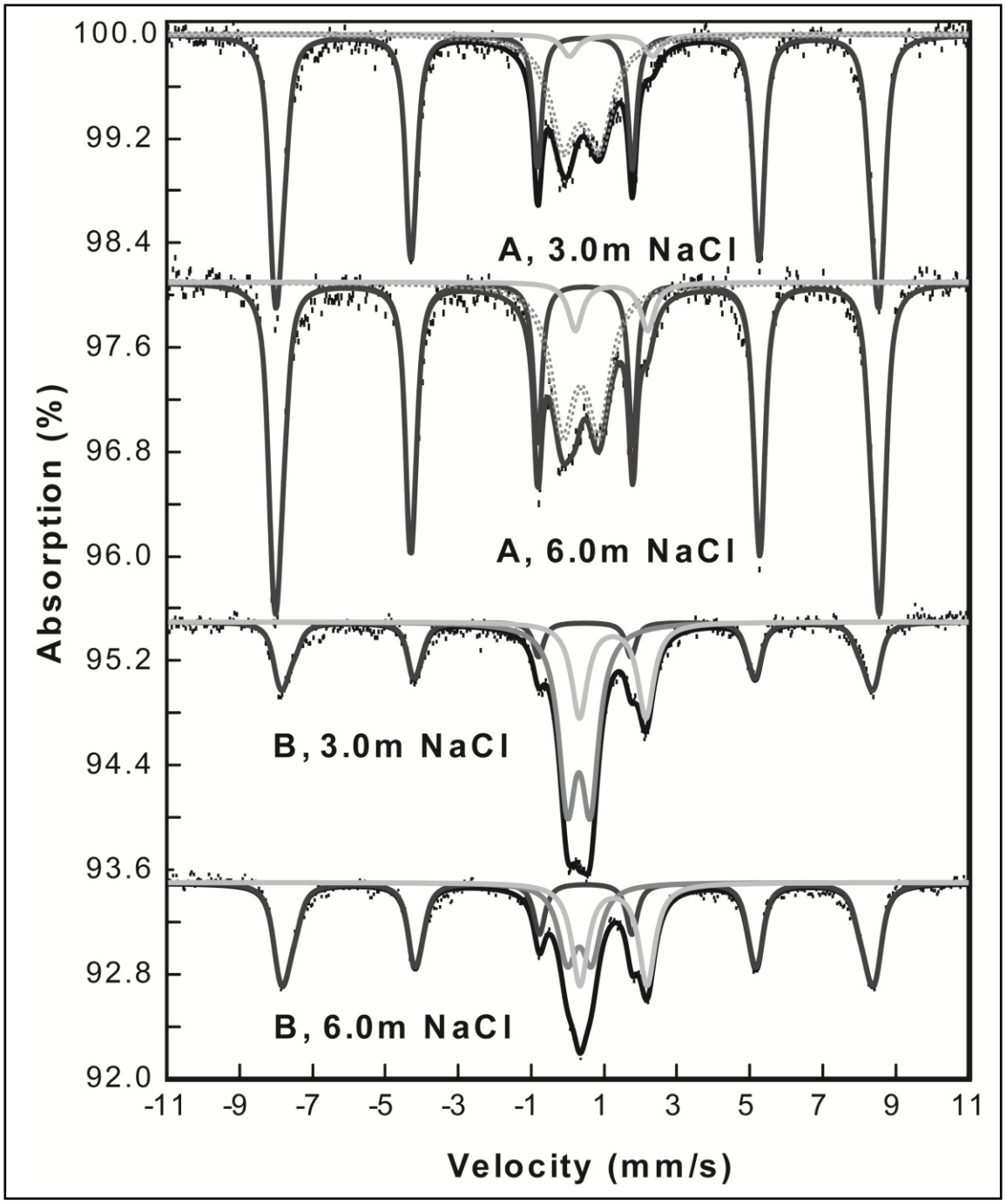

Figure 2-15. Mössbauer spectra at 295K of Moenkopi A (top) and Moenkopi B (bottom) reacted with $scCO_2$, sulfite, and sulfide in either 3.0m or 6.0m solutions of NaCl in a 4.3:1 fluid:rock ratio experiments. Spectra are offset for clarity. In the fits, the light gray line is the carbonate doublet, the medium gray line is the low CS-low QS Fe^{3+} doublet, the dashed gray line is the low CS-high QS Fe^{3+} doublet, the dark gray line is the hematite sextet, and the black line is the sum of all the distributions.

2.4 Discussion

The results of reacting Moenkopi A in simulated near-field (flow through) and interface region (batch; 1.4:1 fluid:rock ratio) regimes with $scCO_2$, sulfite and/or sulfide were previously reported (Schoonen et al. 2012). The near-field experiments produced no changes to the sample. This is not surprising because $scCO_2$ acts as a non-wetting, non-polar fluid that does not necessarily displace the layer of existing, polar fluid coating on the mineral grains as it flows through a system (Tokunaga 2012; Chialvo et al. 2013; DePaolo and Cole 2013). In the mid-field experiments, the 0.87 wt.% Fe^{3+}, primarily present in hematite, was partially reduced to form pyrite when the sandstone was reacted with $scCO_2$ and sulfide, and partially reduced to form siderite and pyrite when the sandstone was reacted with $scCO_2$, sulfite, and sulfide. Based on modeling results reported in that paper, pyrite and siderite will only coexist if sulfite is partially disproportionated to sulfide and sulfate; both full disproportionation and no disproportionation would favor other sets of stable phases (Schoonen et al. 2012).

In this study, Moenkopi B, was reacted in a simulated far-field (batch; 4.3:1 fluid:rock ratio) regime using saline fluids, $scCO_2$, sulfite, and/or sulfide. The results of these experiments are re-plotted as bar diagrams in **Figure 2-16** and **Figure 2-17** to clarify the trends in the experimental results. The major difference between the two sections of the Moenkopi sandstone is that Moenkopi B contains higher carbonate, some of which contains a small amount of Fe^{2+} (**Figure 2-1**; **Figure 2-17**), and has less total Fe. Similar to Moenkopi A, exposing Moenkopi B to pure $scCO_2$ or water and $scCO_2$ should not lead to any change in iron mineralogy due to a lack of any reductant; however, exposing this sandstone to a 6.0 m NaCl solution and $scCO_2$ does cause some dissolution of carbonate, liberating a small amount of Fe^{2+}, which is incorporated into another phase (**Figure 2-16**). Due to the small percentage of material that is transformed, the

new phase cannot be identified, but Mössbauer data indicate that an Fe^{3+} phase is formed because the only other spectral change is an increase in the spectral area of the doublet whose parameters are associated with Fe^{3+} in octahedral coordination (**Table 2-2**). Of course, the conversion of Fe^{2+} to Fe^{3+} requires an oxidant. There are a few possibilities as to how this may happen without an apparent oxidant in solution. For example, oxygen trapped in the Teflon™ may be responsible for the oxidation. However, dilute sulfite solutions are used to create anoxic conditions, thus this option seems unlikely. The other option is that iron is oxidized as CO_2 is reduced. Luquot et al. (2012) demonstrated that iron and carbon can form a redox couple leading to the precipitation of Fe^{3+} oxides and disordered graphite (Luquot et al. 2012).

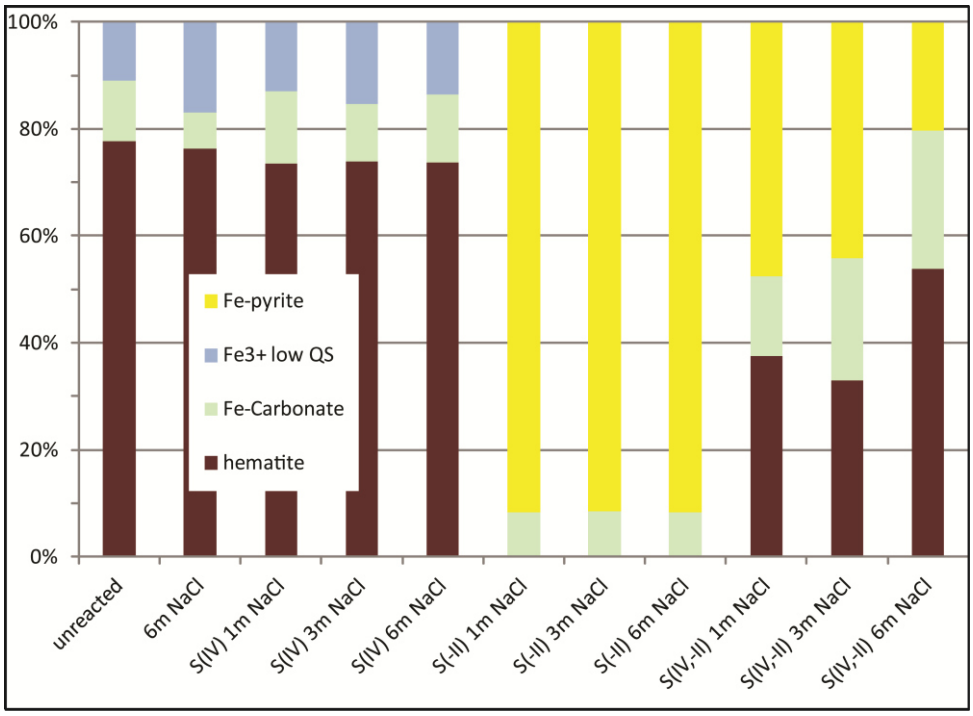

Figure 2-16. Bar graph of the Mössbauer results for Fe-bearing phases in Moenkopi B in the high fluid:rock ratio regime. Recall that Fe^{3+} in octahedral coordination (Fe^{3+} low QS) as well as Fe^{2+} in pyrite are highly overlapped doublets and the distributions are often a combination of phases but are represented as single colors (of the dominant phase) in this plot for simplicity and to clarify transformations. Hematite and carbonate spectral areas are more unique.

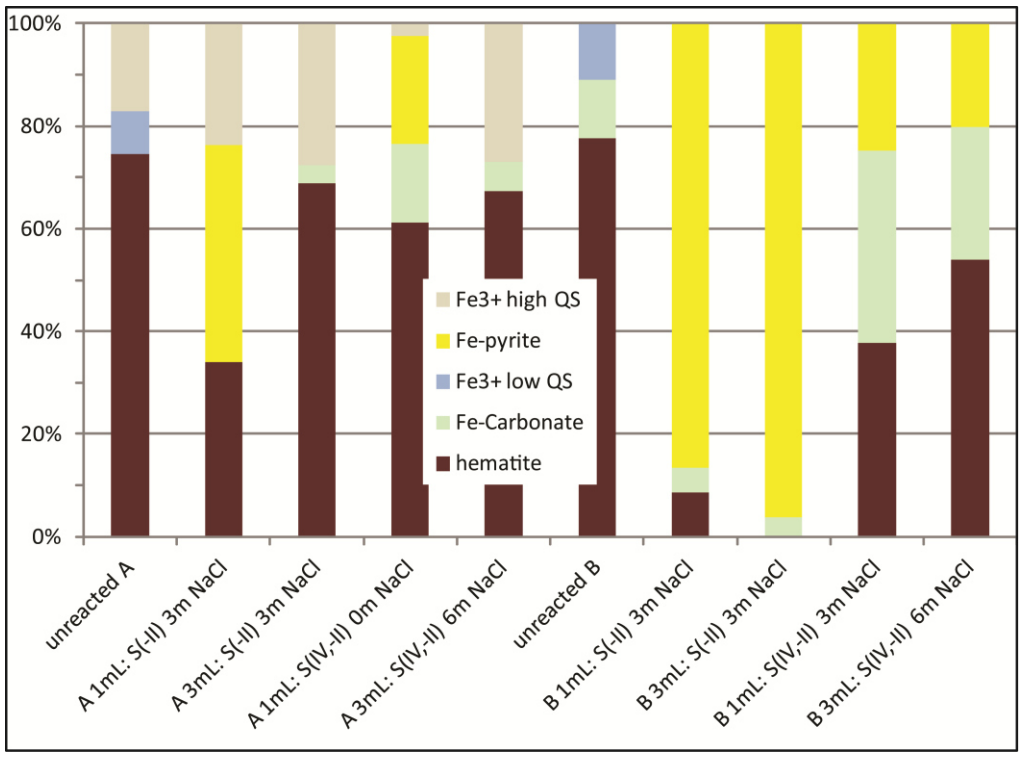

Figure 2-17. Bar graph of the Mössbauer results for comparing the reactivity of Moenkopi A and Moenkopi B in both low and high fluid:rock ratio regimes. Recall that Fe^{3+} in octahedral coordination (both Fe^{3+} phases) as well as Fe^{2+} in pyrite are highly overlapped doublets and the distributions are often a combination of phases but are represented as single colors (of the dominant phase) in this plot for simplicity and to clarify transformations. Hematite and carbonate spectral areas are more unique.

2.4.1 $scCO_2$ and sulfite

The far-field experiments showed that the Moenkopi sandstone is essentially non-reactive when exposed to only $scCO_2$ and sulfite, even in saline solutions (**Table 2-2**; **Figure 2-16**). There is a small but detectable change in the VNIR spectra of the reacted sandstones that shows an increase in the depth of one of the carbonate absorptions (**Figure 2-3**; band 5 from Gaffey (1986)). Due to the overlap in this band with the 1.9 μm water absorption, the absorption can change its depth and apparent position with changes in adsorbed or structural water. It is, therefore, not diagnostic of carbonate in the mixture. However, because this VNIR spectral

change only accompanies experiments with $scCO_2$ and sulfite, it is unlikely that the change in depth is due to water in the sample. This feature accompanies a 4% decrease in the spectral area of the Mössbauer hematite sextet, possibly indicating incorporation of iron into carbonate. The VNIR parameters are most consistent with siderite but confirmation could not be made by this or any other technique.

2.4.2 $scCO_2$ and sulfide.

Moenkopi B appeared to be much more reactive in these saline experiments when exposed to $scCO_2$ and sulfide. Mössbauer spectra demonstrated that the hematite phase was completely transformed into pyrite for all salt concentrations (**Table 2-3**; **Figure 2-16**). The iron in carbonate, however, appeared unreactive, except for the initial partial dissolution (4% spectral area loss for Fe in carbonate), where Moenkopi B was more reactive than Moenkopi A (**Figure 2-17**). Moenkopi A retained 33% spectral area of Fe in hematite in the previous study and 30% spectral area of Fe in hematite when reacted in a 3.0m NaCl solution. This reactivity difference appears to be due to the differences in composition between Moenkopi A and Moenkopi B, rather than to experimental conditions. Moenkopi B seems to have more accessible or reactive hematite than Moenkopi A. Mössbauer analysis showed that unreacted Moenkopi B has ~78% spectral area in the hematite phase. This iron phase is almost completely lost over the course of the reaction. Unreacted Moenkopi A has ~75% spectral area in the hematite phase, which is reduced to ~30% spectral area. The Mössbauer sextet for hematite has a larger hyperfine field value for Moenkopi A (514 KOe vs. 504 KOe), indicating that the grain size of Moenkopi B may be smaller, partially explaining the difference in reactivity, since smaller grains would have larger surface area. Also, the single distribution used to fit the hematite sextet is likely an average of multiple grain size distributions/hematite modes in both samples. Because Moenkopi

sandstone has hematite present both as coatings and as grains (Walker et al. 1981; Schoonen et al. 2012), it is likely that one of these modes is not as reactive, and one more prevalent, in Moenkopi A. Poulton et al. (2004) determined that the half-life for hematite reduction by sulfide is 182 days but others have found that, depending on the grain size, hematite dissolution can be completed in less than an hour (Murphy et al. 2011; Kaszuba et al. 2013). Based on the broad range of literature values, it appears that the kinetics for hematite dissolution are highly dependent on surface area/grain size and possibly other factors. Therefore it is likely that the percentage of iron in hematite in Moenkopi A remaining after 10 days of reaction is in the larger grains rather than the coatings. Given enough time, all the hematite may eventually dissolve.

2.4.3 $scCO_2$, sulfite, and sulfide

Reactions of the Moenkopi sandstone with sulfite, sulfide, and $scCO_2$ were highly sensitive to both salt concentration and fluid:rock ratio (**Figure 2-16** and **Figure 2-17**). Unlike the case with only sulfide, the Mössbauer data show that the hematite phase is preserved in all experiments, regardless of starting material. For experiments with Moenkopi B, the most hematite is lost in 3.0 m NaCl solutions (~45% spectral area) and the least hematite is lost in 6.0 m NaCl solutions (24% spectral area). The 1.5m NaCl solution falls in the middle with 40% spectral area lost. Moenkopi A lost 6 and 7% spectral area of Fe in hematite for 3.0 and 6.0 m NaCl solution experiments respectively as opposed to 14% for non-saline experiments. The highest ionic strength solution appears to inhibit the reactivity of the iron in hematite or prevent the iron from entering solution. For both sections of sandstone, higher salt concentrations favor the formation of siderite, and lower salt concentrations favor the formation of pyrite. However, Moenkopi A produced the most siderite in a salt-free, low water:rock ratio experiment. It is

unclear why this difference occurred, but lower fluid:rock ratios also favored the formation of siderite in Moenkopi B reacted in 3.0m saline fluids (**Figure 2-12**; **Figure 2-17**).

In the previous work, it was noted that siderite forms as euhedral grains, as identified by micro-Raman (Schoonen et al. 2012). Pyrite, on the other hand, forms as coatings. Because siderite is favored in lower fluid:rock ratio experiments, solutions that favor siderite formation have a higher likelihood of clogging pores closer to the injection site than solutions that favor the formation of pyrite.

2.4.4 Effects of fluid:rock ratios

Wetting of the surface appears to be a necessary factor in reacting the iron in the Moenkopi sandstone, as evidenced by the lack of reactivity observed in flow-through experiments (Schoonen et al. 2012). In that regime, CO_2 flushes the grains, causing evaporation of the fluid layer on the grain surface into the CO_2 over time (DePaolo and Cole 2013). The CO_2 then acts as a non-wetting fluid, inhibiting dissolution. Additional experiments performed to compare the reactivity of Moenkopi A and Moenkopi B support the importance of the role of fluid in these mineralogical changes. Both sections of sandstone were more reactive, i.e., more of the iron was transformed to another phase, in a higher fluid:rock ratio regime (**Figure 2-17**). For reactions with $scCO_2$ and sulfide in 3.0m NaCl fluids, Mössbauer spectra indicate that Moenkopi B lost ~69% and ~78% of the spectral area in hematite to other phases for low and high fluid:rock ratio experiments respectively (**Table 2-5**; **Figure 2-17**). For the same set of reactants, Moenkopi A lost ~41% and 45% spectral area for low and high fluid:rock ratio experiments respectively (**Table 2-5**; **Figure 2-17**). For reactions with $scCO_2$, sulfite, and sulfide, Mössbauer spectra show that Moenkopi B lost ~40% and ~45% of the spectral area in hematite to other phases for low and high fluid:rock ratios respectively (**Table 2-5**; **Figure 2-17**). In addition, both

sections of sandstone preferentially formed siderite at lower fluid:rock ratios (**Figure 2-12**, **Figure 2-15**, and **Figure 2-17**) when reacted with a fluid containing both sulfide and sulfite.

2.4.5 Comparison with previous work

Palandri and Kharaka (2005) and Palandri et al. (2005) investigated the reaction of hematite with CO_2, H_2S, and SO_2 in saline fluids to determine the thermodynamic and kinetic constraints on a simplified mixed gas sequestration system. Using idealized modeling and some experimentation, they found that siderite is the preferred precipitate unless all hematite is dissolved, at which point pyrite precipitates. However, Pruess et al. (2001) found that pyrite is favored in their simulations that included H_2S gas. Work by Garcia et al. (2012) on the reactivity of goethite towards CO_2 and SO_2 in brines and work by Murphy et al. (2010) on the reactivity of ferrihydrite towards $scCO_2$ and aqueous sulfide both found that siderite rather than pyrite precipitated. The later also saw the precipitation of elemental sulfur. Murphy et al. (2011), however, found that when nanohematite was reacted with $scCO_2$ and aqueous sulfide, siderite and pyrite precipitated. These results add to the variation in the literature but along the same theme. Pyrite and siderite are expected to form from the interaction of sulfur-bearing, saline fluids in contact with both $scCO_2$ and hematite-bearing rocks. Siderite formation is favored in the interface region simulations (lower fluid:rock ratios) and for higher salinities but only when both sulfite and sulfide are present in solution. Pyrite formation is favored for mid and low salinities and for higher fluid:rock ratios (far-field conditions) in fluids containing both sulfite and sulfide. Pyrite is the only phase formed in fluids containing only sulfide (**Figure 2-16** and **Figure 2-17**).

2.4.6 Geochemical considerations

Clearly this is a complicated system, and the precipitation products will change based on small variations in experimental conditions. The diffusion of $scCO_2$ into the saline fluid causes

an initial drop in pH. As a result, carbonates like calcite and dolomite present in the host rock will almost immediately dissolve, depending almost entirely on the pH of the fluid (Kaszuba et al. 2013). The carbonate dissolution reaction is fast compared to any other dissolution reactions expected for this system (Kaszuba et al. 2013). The presence of sulfur species in the gas will change the pH, making it more acidic (Chialvo et al. 2013). The extent of this pH change will depend on the species of gas (H_2S vs SO_2, where SO_2 is more soluble; Palandri and Kharaka (2005)), the extent to which that gas can diffuse into the fluid (Pruess et al. 2001), and the ability of the native minerals to buffer that acidity. The pH will then control which sulfur phases are stable in the solution, including the extent of SO_2 hydrolysis and disproportionation, thus regulating the relative amounts of soluble sulfide, sulfurous acid, and sulfuric acid. The species in solution then affect which phases will precipitate (based on supersaturation), while the pH helps dictate which phases are stable (Zhang et al. 2011).

When Fe^{2+} is present in solution, lower pH will favor the precipitation of pyrite over siderite and the precipitation of pyrite will inhibit the precipitation of siderite (Zhang et al. 2011), as seen in the sulfide-only experiments. Over time, dissolution of additional phases in the sandstone should raise the pH of the solution, destabilizing pyrite and leading to the precipitation of carbonates. However, over the timescale of these experiments, pyrite is favored.

Because low pH conditions lead to the dissolution of carbonates rather than the precipitation of carbonates, less CO_2 can dissolve from the gas phase because the solution is already saturated with respect to CO_2. However, when the salinity is raised, carbonate is "salted-out" of the fluid (Takenouchi and Kennedy 1965). Therefore, in the experiments with both sulfite and sulfide, some combination of the pH increase due to the presence of both species, and the decreased solubility of CO_2 with increasing salinity, are responsible for the formation of

carbonate (likely siderite) at the same time as pyrite. Because a fixed weight of CO_2 was used for all salt concentrations, the increase in salinity and resulting decrease in CO_2 solubility would have resulted in an effective increase in P_{CO2}, driving the precipitation of carbonate (likely siderite).

The favoring of carbonate (likely siderite) in the low fluid:rock ratio experiments can probably be attributed to hematite dissolution, which seems to proceed fairly rapidly in these experiments. Even though more hematite dissolves in high fluid:rock ratio experiments, the increase in dissolution (~5-9% Mössbauer spectral area) is small compared to the increase in fluid volume (1mL vs. 3mL). Because hematite dissolution consumes H^+ (Palandri et al. 2005), the pH of the low fluid:rock experiments is likely higher, thus favoring the precipitation of carbonate (likely siderite). Further experiments and modeling work are needed to further clarify the roles of pH and dissolved species in formation of minerals in this mixed gas system. For instance, similar batch experiments where pH is controlled by the titration of acid may provide a reasonable next step in separating contributions from pH and sulfur species. If experimental concentrations on sulfur species are informed by modeling like that done by Ellis et al. (2010), the predictive power of these experiments could be enhanced.

2.5 Conclusions

The reactivity of hematite-bearing sandstones under conditions relevant to GCS using sulfur-bearing gases is dependent upon the hematite phase. Based on the experiments reported here and in the previous work, the conclusions are as follows:

- Hematite in the “red” sandstone studied here is not reactive under conditions simulating the environment around the point of $scCO_2$ injection.

- Hematite is mildly reactive in water or brine containing sulfite and saturated with $scCO_2$, but the reaction is so incomplete that a reaction product could not be identified, although Fe-oxidation appears to occur.
- Hematite is completely converted to pyrite in $scCO_2$-saturated water or brine containing sulfide, regardless of NaCl content.
- Some hematite is converted to pyrite and siderite in $scCO_2$-saturated water or brine containing sulfide and sulfite.
- Reactivity of hematite decreases and siderite formation is favored with increasing NaCl content and decreasing water:rock ratios.

Although the reactive material in the Moenkopi sandstone only makes up < 1% of bulk composition, the substantial variability in reactivity and in products over the two sections of sandstone, over the range of salinities, and over the range of sulfur species that could be co-injected with $scCO_2$ indicates that hematite-bearing sandstones will not behave as inert repositories when subjected to $scCO_2$ with co-injected sulfur gases. In the absence of co-injected sulfur gases, some dissolution of carbonate phases is observed, which may enhance permeability. However, in the presence of co-injected sulfur gases, there is the potential for dissolution-re-precipitation reactions that lead to the formation of recalcitrant pyrite. Pyrite is expected to form closer to the injection site due the increased solubility of sulfur-bearing gases with respect to CO_2, which will cause zoning of the plume such that the leading edge is CO_2 rich and the lagging zone is S-rich. Therefore, pyrite precipitation may reduce permeability. However, pyrite forms generally as coatings whereas siderite, favored in low fluid:rock ratio experiments, forms as euhedral grains. On the other hand, if decreased permeability can be avoided, sulfides and iron carbonates may serve as excellent mineral traps for acid gases. Therefore, red sandstones, such

as the one tested here, require further evaluation before they are considered for the co-injection of $scCO_2$ and H_2S/SO_2.

Works Cited

Anheden, M., Andersson, A., Bernstone, C., Eriksson, S., Yan, J., Liljemark, S., and Wall, C. (2005) CO_2 quality requirement for a system with CO_2 capture, transport and storage. In: M. Wilson et al. (Eds.), Greenhouse Gas Control Technologies 7. Elsevier, pp. 2559-2564.

Bachu, S. (2008) CO_2 storage in geological media: Role, means, status and barriers to deployment. Progress in Energy and Combustion Science, 34 (2), 254-273.

Bradshaw, J., and Dance, T. (2005) Mapping geological storage prospectivity of CO_2 for the world's sedimentary basins and regional source to sink matching, Greenhouse Gas Control Technologies 7. Elsevier Science Ltd, Vancouver, Canada, pp. 583-591.

Chialvo, A.A., Vlcek, L., and Cole, D.R. (2013) Acid Gases in CO_2-rich Subsurface Geologic Environments. In: D.J. DePaolo, D.R. Cole, A. Navrotsky, and I.C. Bourg (Eds.), Geochemistry of Geologic CO_2 Sequestration. Reviews in Mineralogy & Geochemistry, pp. 361-398.

Clark, R.N., Swayze, G.A., Wise, R., Livio, E., Hoefen, T., Kokaly, R., and Sutley, S.J. (2007) USGS digital spectral library splib06a, U.S. Geological Survey: Digital Data Series 231.

Cloutis, E.A., Grasby, S.E., Last, W.M., Leveille, R., Osinski, G.R., and Sherriff, B.L. (2010) Spectral reflectance properties of carbonates from terrestrial analogue environments: Implications for Mars. Planetary and Space Science, 58 (4), 522-537.

Damen, K., Faaij, A., and Turkenburg, W. (2006) Health, safety and environmental risks of underground CO_2 storage - Overview of mechanisms and current knowledge. Climatic Change, 74 (1-3), 289-318.

De Grave, E., and van Alboom, A. (1991) Evaluation of ferrous and ferric Mössbauer fractions. Physics and Chemistry of Minerals, 18, 337-342.

DePaolo, D.J., and Cole, D.R. (2013) Geochemistry of geologic carbon sequestration: An overview. In: D.J. DePaolo, D.R. Cole, A. Navrotsky, and I.C. Bourg (Eds.), Geochemistry of Geologic CO_2 Sequestration. Reviews in Mineralogy & Geochemistry, pp. 1-14.

Dooley, J.J., Dahowski, R.T., Davidson, C.L., Bachu, S., Gupta, N., and Gale, J. (2005a) A CO_2-storage supply curve for North America and its implications for the deployment of carbon dioxide capture and storage systems, Greenhouse Gas Control Technologies 7. Elsevier Science Ltd, pp. 593-601.

Dooley, J.J., Kim, S.H., Edmonds, J.A., Friedman, S.J., and Wise, M.A. (2005b) A first-order global geological CO_2-storage potential supply curve and its application in a global integrated assessment model, Greenhouse Gas Control Technologies 7. Elsevier Science Ltd, pp. 573-581.

Duan, Z.H., and Sun, R. (2003) An improved model calculating CO_2 solubility in pure water and aqueous NaCl solutions from 273 to 533 K and from 0 to 2000 bar. Chemical Geology, 193 (3-4), 257-271.

Dyar, M.D., Schaefer, M.W., Sklute, E.C., and Bishop, J.L. (2008) Mössbauer spectroscopy of phyllosilicates: effects of fitting models on recoil-free fractions and redox ratios. Clay Minerals, 43 (1), 3-33.

Ellis, B.R., Crandell, L.E., and Peters, C.A. (2010) Limitations for brine acidification due to SO_2 co-injection in geologic carbon sequestration. International Journal of Greenhouse Gas Control, 4 (3), 575-582.

Ellis, B.R., Peters, C.A., Fitts, J., Bromhal, G., McIntyre, D., Warzinski, R., and Rosenbaum, E. (2011) Deterioration of a fractured carbonate caprock exposed to CO_2-acidified brine flow. Greenhouse Gases-Science and Technology, 1 (3), 248-260.

Flett, M.A., Gurton, R.M., and Taggart, I.J. (2005) Heterogeneous saline formations: Long-term benefits for geo-sequestration of greenhouse gases, Greenhouse Gas Control Technologies 7. Elsevier Science Ltd, pp. 501-509.

Gaffey, S.J. (1986) Spectral reflectance of carbonate minerals in the visible and near-infrared (0.35-2.55 microns) - calcite, aragonite, and dolomite. American Mineralogist, 71 (1-2), 151-162.

Gaffey, S.J. (1987) Spectral reflectance of carbonate minerals in the visible and near-infrared (0.35-2.55 μm) - anhydrous carbonate minerals. Journal of Geophysical Research-Solid Earth and Planets, 92 (B2), 1429-1440.

Garcia, S., Rosenbauer, R.J., Palandri, J., and Maroto-Valer, M.M. (2012) Sequestration of non-pure carbon dioxide streams in iron oxyhydroxide-containing saline repositories. International Journal of Greenhouse Gas Control, 7, 89-97.

GHG (2003) Potential for improvements in Gasification Combined Cycle Power Generation with CO_2 Capture. International Energy Agency Greenhouse Gas R&D program, IEA GHG, Chetenham, UK.

Hepple, R.P., and Benson, S.M. (2005) Geologic storage of carbon dioxide as a climate change mitigation strategy: performance requirements and the implications of surface seepage. Environmental Geology, 47 (4), 576-585.

IPCC (2005) IPCC special report on carbon dioxide capture and storage, Intergovernmental Pannel on Climate Change, New York, NY.

Kaszuba, J., Yardley, B., and Andreani, M. (2013) Experimental Perspectives of Mineral Dissolution and Precipitation due to Carbon Dioxide-Water-Rock Interactions. In: D.J. DePaolo, D.R. Cole, A. Navrotsky, and I.C. Bourg (Eds.), Geochemistry of Geologic CO_2 Sequestration. Reviews in Mineralogy & Geochemistry, pp. 153-188.

Kharaka, Y.K., Cole, D.R., Thordsen, J.J., Gans, K.D., and Thomas, R.B. (2013) Geochemical monitoring for potential environmental impacts of geologic sequestration of CO_2. In: D.J. DePaolo, D.R. Cole, A. Navrotsky, and I.C. Bourg (Eds.), Geochemistry of geologic CO_2 sequestration. Reviews in Mineralogy & Geochemistry, pp. 399-430.

Knauss, K.G., Johnson, J.W., and Steefel, C.I. (2005) Evaluation of the impact of CO_2, co-contaminant gas, aqueous fluid and reservoir rock interactions on the geologic sequestration of CO_2. Chemical Geology, 217 (3-4), 339-350.

Luquot, L., Andreani, M., Gouze, P., and Camps, P. (2012) CO_2 percolation experiment through chlorite/zeolite-rich sandstone (Pretty Hill Formation - Otway Basin-Australia). Chemical Geology, 294, 75-88.

Mazumder, S., van Hemert, P., Bruining, J., Wolf, K., and Drabe, K. (2006) In situ CO_2-coal reactions in view of carbon dioxide storage in deep unminable coal seams. Fuel, 85 (12-13), 1904-1912.

Murphy, R., Lammers, K., Smirnov, A., Schoonen, M.A.A., and Strongin, D.R. (2010) Ferrihydrite phase transformation in the presence of aqueous sulfide and supercritical CO_2. Chemical Geology, 271 (1-2), 26-30.

Murphy, R., Lammers, K., Smirnov, A., Schoonen, M.A.A., and Strongin, D.R. (2011) Hematite reactivity with supercritical CO_2 and aqueous sulfide. Chemical Geology, 283 (3-4), 210-217.

Palandri, J.L., and Kharaka, Y.K. (2005) Ferric iron-bearing sediments as a mineral trap for CO_2 sequestration: Iron reduction using sulfur-bearing waste gas. Chemical Geology, 217 (3-4), 351-364.

Palandri, J.L., Rosenbauer, R.J., and Kharaka, Y.K. (2005) Ferric iron in sediments as a novel CO_2 mineral trap: CO_2-SO_2 reaction with hematite. Applied Geochemistry, 20 (11), 2038-2048.

Poulton, S.W., Krom, M.D., and Raiswell, R. (2004) A revised scheme for the reactivity of iron (oxyhydr)oxide minerals towards dissolved sulfide. Geochimica Et Cosmochimica Acta, 68 (18), 3703-3715.

Pruess, K., Xu, T., Apps, J., and Garcia, J. (2001) Numerical Modeling of Aquifer Disposal of CO_2. Society of Petroleum Engineers.

Rosenbauer, R.J., Koksalan, T., and Palandri, J.L. (2005) Experimental investigation of CO_2-brine-rock interactions at elevated temperature and pressure: Implications for CO_2 sequestration in deep-saline aquifers. Fuel Processing Technology, 86 (14-15), 1581-1597.

Schoonen, M.A.A., Sklute, E.C., Dyar, M.D., and Strongin, D.R. (2012) Reactivity of sandstones under conditions relevant to geosequestration: 1. Hematite-bearing sandstone exposed to supercritical carbon dioxide commingled with aqueous sulfite or sulfide solutions. Chemical Geology, 296, 96-102.

Stewart, J.H., Poole, F.G., and Wilson, R.F. (1972) Stratigraphy and origin of the Triassic Moenkopi Formation and related strata in the Colorado Plateau region, with a section on sedimentary petrology.

Takenouchi, S., and Kennedy, G.C. (1964) Binary system H_2O-CO_2 at high temperatures + pressures. American Journal of Science, 262 (9), 1055-&.

Takenouchi, S., and Kennedy, G.C. (1965) Solubility of carbon dioxide in naci solutions at high temperatures and pressures. American Journal of Science, 263 (5), 445-&.

Tokunaga, T.K. (2012) DLVO-Based Estimates of adsorbed water Film thicknesses in geologic CO_2 reservoirs. Langmuir, 28 (21), 8001-8009.

Vandenberghe, R.E., De Grave, E., and de Bakker, P.M.A. (1994) On the methodology of the analysis of Mössbauer spectra. Hyperfine Interactions, 83 (1), 29-49.

Walker, T.R., Larson, E.E., and Hoblitt, R.P. (1981) Nature and origin of hematite in the Moenkopi formation (triassic), Colorado Plateau - a contribution to the origin of magnetism in red beds. Journal of Geophysical Research, 86 (NB1), 317-333.

White, C.M., Smith, D.H., Jones, K.L., Goodman, A.L., Jikich, S.A., LaCount, R.B., DuBose, S.B., Ozdemir, E., Morsi, B.I., and Schroeder, K.T. (2005) Sequestration of carbon dioxide in coal with enhanced coalbed methane recovery - A review. Energy & Fuels, 19 (3), 659-724.

Wilson, E.J., Johnson, T.L., and Keith, D.W. (2003) Regulating the ultimate sink: Managing the risks of geologic CO_2 storage. Environmental Science & Technology, 37 (16), 3476-3483.

Xu, T., Apps, J.A., Pruess, K., and Yamamoto, H. (2007) Numerical modeling of injection and mineral trapping Of CO_2 with H_2S and SO_2 in a sandstone formation. Chemical Geology, 242 (3-4), 319-346.

Zhang, W., Xu, T., and Li, Y. (2011) Modeling of fate and transport of coinjection of H_2S with CO_2 in deep saline formations. Journal of Geophysical Research-Solid Earth, 116.

Chapter 3

Reactivity Of Sandstones Under Conditions Relevant To Geosequestration: 3. Gray Sandstones Exposed To Supercritical Carbon Dioxide Commingled with Sulfite and/or Sulfide Solutions.

This chapter is being prepared for submission to Chemical Geology

Sklute, E. C., Schoonen, M. A. A., Dyar, M. D., Strongin, D. R. (In preparation) Reactivity Of Sandstones Under Conditions Relevant To Geosequestration: 3. Gray Sandstones Exposed To Supercritical Carbon Dioxide Commingled with Sulfite and/or Sulfide Solutions.

3.1 Introduction

Geological carbon sequestration (GCS) may become a crucial technology in the mitigation of global warming as we transition away from fossil fuels (DePaolo et al. 2013). Because up to 60% of global CO_2 emissions stem from point source electricity generation (IPCC 2005), developing a technology that could effectively capture emissions from major power plants, condense it into supercritical CO_2 ($scCO_2$), and sequester $scCO_2$ in deep geological formations, would have a significant impact. There is an additional economic (GHG 2003; Anheden et al. 2005; Chialvo et al. 2013) and environmental (Chestnut and Mills 2005; Ellis et al. 2010) incentive if CO_2 is co-sequestered with common flue gas contaminants like SO_2 and H_2S. However, these sulfur-bearing species can change the reactivity of the host rock (Chialvo et al. 2013; DePaolo and Cole 2013). Where increased reactivity could lead to more extensive

mineral trapping of CO_2, it also has the potential to shorten the lifetime of the injection site by reducing permeability (Kaszuba et al. 2005). Predicting the outcome of these co-injection scenarios relies, in part, on understanding the potential geochemical reactions in three distinct regimes: 1) the near-field or $scCO_2$-dominated regime, 2) the interfacial region where $scCO_2$ and aqueous fluid co-exist, and 3) the far-field or aqueous fluid-dominated regime. Clearly, increased mineralization in the near-field regime would lead to detrimental pore clogging, where increased mineralization in the far-field regime could be beneficial. Therefore, understanding the geochemical transformations of potential host-rock types exposed to simulated mixed gas systems in these three regimes is an important step in advancing GCS technology.

Deep saline formations are an attractive repository for sequestered CO_2 due to their widespread location and substantial storage capacity (Dooley et al. 2005; Flett et al. 2005; Damen et al. 2006; Bachu 2008). Therefore, in this and our previous work (Schoonen et al. 2012; Sklute et al. In Preparation), co-authors and I have focused on these types of formations for our geochemical experimentation. Four sandstones have been examined: 1) a hematite-bearing, "red" sandstone from the Moenkopi formation in Arizona, 2) a "gray" sandstone from Elk Hills petroleum reservoir in the San Joaquin Valley, California, 3) a "gray" sandstone from the South Timbalier Area in the Gulf of Mexico, and 4) a "gray" sandstone from the Provra section of the Emba field to the northeast of the Caspian Sea in Kazakhstan. Because sulfur-bearing gases are known to increase the reactivity of iron-oxide and –oxyhydroxide bearing sediments (Palandri and Kharaka 2005; Palandri et al. 2005; Murphy et al. 2010; Murphy et al. 2011; Garcia et al. 2012; DePaolo and Cole 2013), the first two papers focused on the Moenkopi sandstone (Schoonen et al. 2012; Sklute et al. In Preparation).

In those experiments, the Moenkopi sandstone was reacted with supercritical CO_2, equilibrated with either NaCl-bearing or NaCl-free solutions of sulfide and/or sulfite to simulate the co-injection of sulfur bearing gases during carbon sequestration. Those experiments were performed in a flow-through configuration to simulate the near-field regime, in 1.4:1 fluid:rock ratio batch experiments to simulate the interfacial region, and in 4.3:1 fluid:rock ratio batch experiments to simulate the far-field regime. For that sandstone, the < 1 wt % Fe, present mostly as hematite, was found to be reactive, converting either to pyrite, siderite, or a mixture of the two. The reactivity and conversion products depended on sulfur species, salinity, and water:rock ratio. Due to the complicated and conditional reactivity of that sandstone, it was concluded that the hematite-bearing sandstones require further investigation before being considered as potential GCS targets.

Here I report the results of similar experiments performed on three grey sandstones from The North Caspian Sea Basin in Kazakhstan, the Elk Hill oil field in California, and the South Timbalier oil field off the coast of Louisiana. Here, the iron is present mainly in clay and carbonate. Again, three primary interaction regimes are considered: near field, where the system is dominated by $scCO_2$, simulated by using flow through experiments; an interfacial region, where $scCO_2$ and the fluid coexist, simulated by low water:rock ratio batch experiments; and far field, where the fluid phase dominates, simulated by higher water:rock ratio batch experiments.

3.2 Methods

3.2.1 Sample Description

Three “gray” (or iron oxide and hydroxide free) sandstones were used in this study: Elk Hill, Caspian Sea, and South Timbalier. X-ray fluorescence (XRF) spectroscopy and Loss on

Ignition (LOI) compositional analyses for all samples, obtained by Washington State University's Geoanalytical Lab, are shown in **Table 3-1**. The Elk Hill sandstone is from the Elk Hill oil field in the San Joaquin Valley of California, USA (35º 10' 44.92" N, 119º, 27',7.19" W). Elk Hill is composed of 35% quartz, 18% K-feldspar, 34% plagioclase, ~1% calcite, ~1% dolomite, ~3% siderite, and 8% clays. The 8% clay is divided as 25% kaolinite, 30% illite, 29% smectite, 13% mixed layer, and 3% chlorite (Mohan et al. 1993). The Caspian Sea sandstone is from the Provra section of the Emba field in the North Caspian Basin in Kazakhstan (46º 16' 21.03" N, 53º 52' 31.80" E). It is expected to have similar mineralogy to the Tenzig field; it is primarily carbonate, quartz, and clay (Weber et al. 2003; Jones and Xiao 2006). The South Timbalier sandstone is from Block 17 in the South Timbalier area off the coast of Louisiana (approximately 28º 59' 43" N, 90º 15' 04" W). The South Timbalier area holds mainly quartz- and clay-rich deposits with combinations of illite, kaolinite and smectite clays that vary by depth (Totten et al. 2005).

Table 3-1. LOI and XRF major element analyses for the sandstones used in this study. LOI is given in weight percent. XRF analyses are given in wt% oxide and are normalized to 100% for the material left after LOI.

	South Timbalier	Elk Hill	Caspian Sea
LOI (%)	2.45	3.75	8.49
SiO_2	84.83	81.37	69.60
TiO_2	0.403	0.179	1.122
Al_2O_3	7.87	9.91	13.16
FeO*	**1.28**	**0.50**	**3.13**
MnO	0.014	0.008	0.199
MgO	0.64	0.41	3.12
CaO	0.97	1.90	5.42
Na_2O	1.84	2.61	1.76
K_2O	2.06	2.97	2.32
P_2O_5	0.100	0.138	0.171

3.2.2 Flow-through experiments

Flow-through experiments were used to simulate the near-field environment where $scCO_2$ dominates. Since it was previously noted that sandstones appear to be least reactive in this regime (Schoonen et al. 2012), flow-through experiments were only performed on one of the three sandstones. The specifications for the flow-through experiments are described in detail in that previous work (Schoonen et al. 2012). Briefly, ~ 3 g crushed South Timbalier sandstone was packed in a 4 mm diameter by 50 mm length PEEK chromatography column that was maintained in a 75 ºC water bath. The samples in the column were subjected to a constant flow of $scCO_2$ (liquid), $scCO_2$ mixed with an aqueous solution of Na_2SO_3 (5 mM; O_2-free), or $scCO_2$ mixed with an aqueous solution of Na_2S (5 mM; O_2-free). Flow rates were 0.2 mL/min for the $scCO_2$ and 0.02 mL/min for the aqueous solutions. Experiments were run for a total duration of 3 to 4 days.

3.2.3 Batch Experiments

The interfacial region where the fluid and $scCO_2$ co-exist and the far-field regime where the fluid phase dominates were simulated using small-scale batch experiments with fluid:rock ratios of 1.4:1 and 4.3:1 respectively. Batch experiments were carried out in 23 mL, Teflon™-lined, steel digestion bombs that can withstand internal pressure of 125 bar. For the low fluid:rock ratio experiments, ~0.7 g crushed sandstone, weighed by analytical balance, was added to pre-cooled (-5 ºC) Teflon beakers. Sulfur salts (Na_2SO_3, $Na_2S•9H_2O$, or both) were added next, followed by 1 mL of argon purged 5mM Na_2SO_3 (used to ensure O_2-free water) solution in water was added by pipet. CO_2 in the form of dry ice was quickly added last while the vessels were placed on a high-capacity, Ohaus™, top-loading balance, after which the

vessels were immediately closed, tightened, and re-weighed. Each vessel was loaded with enough CO_2 to create supercritical conditions upon expansion. The vessels were reacted for 10 days in a water bath maintained at 75 ºC. High fluid:rock ratio experiments were conducted as above with two changes. First, sufficient NaCl was added to each vessel directly after the sandstone to make 1.5, 3.0, or 6.0 molal (m) solutions upon the addition of water and that 3 mL of argon-purged 5mM Na_2SO_3 solutions were used instead of 1 mL. The reagent weights and volumes used in these experiments are listed in **Table 3-2**.

Table 3-2. Weights and volumes of the reagents used for the batch experiments in this study. The sandstones are abbreviated as ST for South Timbalier, EH for Elk Hill, and CS for Caspian Sea.

Experimental Details							
	Type	**Sandstone**	**Sulfite**	**Sulfide**	**CO_2**	**H_2O**	**NaCl**
PNF2-9	ST	0.701g	0.186g	-	3.55g	1mL	-
PNF2_10	ST	0.700g	-	0.185g	3.65g	1mL	-
PNF2-11	ST	0.702g	0.189g	0.183g	3.50g	1mL	-
PNF2_12	ST	0.700g	-	-	3.57g	1mL	-
PNF3_1	EH	0.704g	-	-	3.50g	1mL	-
PNF3_2	EH	0.703g	-	0.185g	3.50g	1mL	-
PNF3-3	EH	0.701g	0.184g	-	3.60g	1mL	-
PNF3_4	EH	0.700g	0.184g	0.183g	3.60g	1mL	-
PNF3_5	CS	0.701g	-	-	3.60g	1mL	-
PNF3_6	CS	0.702g	-	0.185g	3.40g	1mL	-
PNF3_7	CS	0.702g	0.184g	-	3.40g	1mL	-
PNF3_8	CS	0.700g	0.184g	0.184g	3.60g	1mL	-
PNF10_0	CS	0.703g	-	-	2.58g	3mL	1.06g
PNF10_1	CS	0.702g	0.184g	-	2.55g	3mL	0.26g
PNF10_2	CS	0.703g	-	0.186g	2.65g	3mL	0.26g
PNF10_3	CS	0.702g	0.185g	0.183g	2.64g	3mL	0.26g
PNF10_4	CS	0.700g	0.185g	-	2.47g	3mL	0.53g
PNF10_5	CS	0.703g	-	0.187g	2.56g	3mL	0.53g
PNF10_6	CS	0.699g	0.184g	0.187g	2.64g	3mL	0.53g
PNF10_7	CS	0.700g	0.186g	-	2.40g	3mL	1.05g
PNF10_8	CS	0.700g	-	0.187g	2.60g	3mL	1.05g
PNF10-9	CS	0.703g	0.186g	0.186g	2.63g	3mL	1.05g

In the previous work it was found that the carbonate and iron-bearing phases were the most reactive when the sandstones were exposed to $scCO_2$ and sulfur-bearing fluids (Schoonen et al. 2012; Sklute et al. In Preparation). Therefore, the majority of the batch experiments reported in this study are for the Caspian Sea sandstone, which contains the most iron (3.13 wt%) and lost the most on ignition (8.49 wt%; carbonate is lost on ignition but is not the only phase) since it represented the sandstone most likely to undergo mineralogical transformations over the course of the experiments.

3.2.4 Spectroscopic Analysis

In the previous work it was found that many of the standard techniques used to investigate changes in mineralogy like FTIR and XRD cannot resolve the subtle shifts observed in this type of experiment. Two complimentary techniques, however, Mössbauer spectroscopy and visible near infrared (VNIR) spectroscopy, are capable of recording subtle changes in the mineralogy of these samples. Mössbauer spectroscopy, which derives its entire signal from the iron in the sample, provides information about the oxidation state, coordination environment, and possible mineralogical associations of the iron. VNIR spectroscopy records absorptions from molecular vibrations, overtones, and combinations that occur in the VNIR wavelength range. These include H_2O, OH, and CO_2. Fe electronic transitions and metal-oxygen vibrations also can be seen in this wavelength range. Therefore, the two techniques together can be used to monitor the changes in iron-bearing, hydrated, and carbonate minerals.

Mössbauer spectra for PNF2, PNF3, and FTNF samples were taken on SEE Co Model MS4 Mössbauer Spectroscopy System, operated in the constant acceleration mode with a Ritverc MCo7 Series ^{57}Co source in Rh. Mössbauer spectra of PNF10 samples were conducted at Mount Holyoke College on a Web Research Co. (Now SEE Co.) WT302 Mössbauer spectrometer

equipped with a ~60 miCu ^{57}Co source in Rh. Spectra were referenced to α-Fe foil. All spectra were fit using Mexdisd, a program provided by Eddie DeGrave and Toon van Alboom at the University of Ghent, Belgium (De Grave and van Alboom 1991; Vandenberghe et al. 1994). The program uses a line-shapes independent fitting model and solves the full hyperfine-interaction Hamiltonian, using quadrupole splitting (QS), center shift (CS), and line width as adjustable parameters.

Throughout the course of these experiments, two spectra of the unreacted sandstone were taken on two different Mössbauer Spectrometers. The fits to these two spectra indicate the error associated with using two different spectrometers for one investigation. The parameters for those fits, listed in **Table 3-5** and **Table 3-6**, show that the same 5 distributions are identified and that the ferric/ferrous ratios are within 1 % spectral of each other. All major phases (> 10% spectral area) differ by a maximum of 0.01 mm/s and 3.8% spectral area, all minor phases differ by a maximum of 0.06 mm/s and 2.5% spectral area. The % spectral area differences are due to a high degree of overlap between distributions. Given these similarities, it is reasonable to assume that changes in Mössbauer parameters are due to geochemical alterations rather than the use of two different instruments.

VNIR spectra were acquired on an ASD Inc. Fieldspec3 Max UV-VIS-NIR portable bi-directional spectrometer with a quartz-halogen illumination source. The spectrometer has 3 detectors: an Si photodiode (0.35-1.0 μm) detector and two InGaAs (1.0-2.5 μm) detectors, producing spectral resolution of 0.001 μm. Illumination and viewing geometry were set to 35º and 0º respectively. All samples were referenced to Spectralon and each sample was an average of 100 scans.

3.3 Results

3.3.1 South Timbalier

Mössbauer spectroscopic observations. Mössbauer fits of the unreacted South Timbalier sandstone show that the sample's 1.25 wt% iron is contained in clay and carbonate phases (**Figure 3-1**; **Table 3-3**). All samples show one ferrous and three ferric distributions due to iron in octahedral coordination in clay and one ferrous distribution due to iron in octahedral coordination in carbonate. The parameters of the carbonate distribution are most consistent with siderite, which has a higher QS value than calcite, dolomite, or ankerite by ~ 0.3-0.5 mm/s. Due to the high degree of overlap between the distributions, individual ferric phase spectral areas are likely non-diagnostic of mineralogical changes. Similarly, the ferrous distributions in this sample are highly overlapped as well and small changes (< 5% spectral area) in individual ferrous distributions are not necessarily indicative of a mineralogical transformation. Changes in the total ferric/ferrous ratio, however, are indicative of changes in the oxidation state of iron over the course of the reactions.

The South Timbalier sandstones start with 55.5% of the Mössbauer spectral area in ferric phases. The low fluid:rock ratio batch experiment with $scCO_2$ and sulfide decreases that by 3.1%. This is near the error in the technique (~1-3% for well resolved distributions or sets of distributions; Dyar et al. (2008)) and may not indicate a significant mineralogical change. In addition, no significant deviations in the spectral area for any of the individual phases is noted. Surprisingly, the flow-through experiments, which elicited no significant changes in the previous work with "red" sandstones, show the most significant changes in these experiments. When reacted in a flow-through regime with just $scCO_2$, the South Timbalier sandstone loses 7.1% spectral area from the combined ferric phases. The iron appears to redistribute between both

ferrous phases but this is likely due to the degree of overlap. It is clear, however, that for these experimental conditions, some iron is reduced. In the flow-through experiments with $scCO_2$ and sulfite, the Mössbauer spectral area of the combined ferric phases increased by 5.3%. Again, the overlap between the various distributions cannot, with certainty, tell us from which phase the iron was lost or how it is re-precipitated, but for these experimental conditions some iron is oxidized. In the flow-through experiments with $scCO_2$ and sulfide, some of the iron also seems to oxidized (1.8 % spectral area change). Although this is within the error of the technique, the apparent oxidation is accompanied by a shape change in the spectrum at ~0 mm/s similar to that seen for the $scCO_2$ and sulfite experiments (**Figure 3-1**).

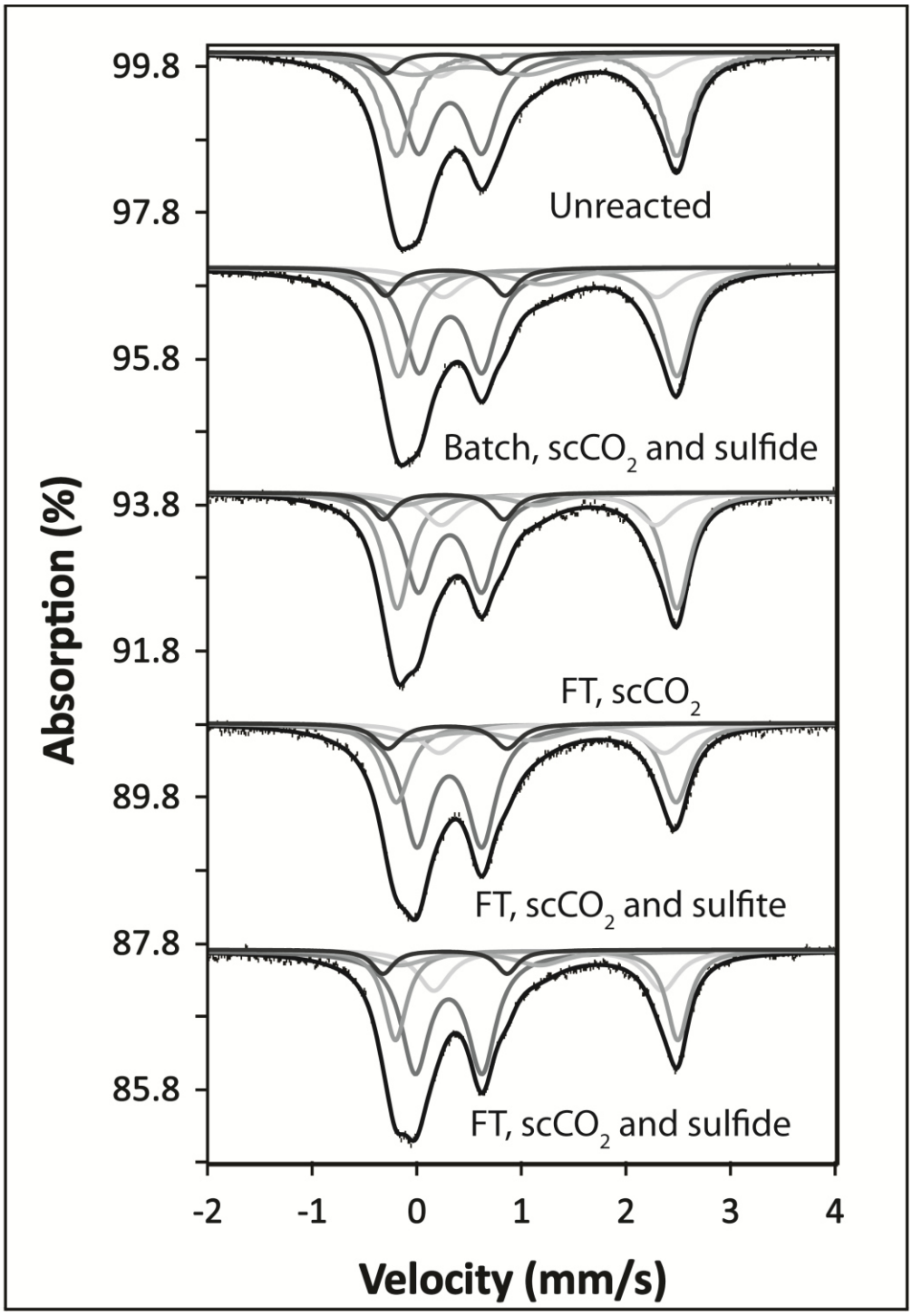

Figure 3-1. Mössbauer spectra of the South Timbalier sandstone reacted in flow-through or experiments with $scCO_2$, $scCO_2$ plus sulfite, $scCO_2$ plus sulfide, and low fluid:rock ratio batch experiments with $scCO_2$ plus sulfide. All spectra were acquired at 295K. Spectra are scaled and offset for clarity.

Table 3-3. Mössbauer parameters for the South Timbalier sandstone reacted in flow-through experiments with just $scCO_2$, $scCO_2$ plus sulfite, $scCO_2$ plus sulfide, and a low fluid:rock ratio batch experiments with $scCO_2$ plus sulfide in NaCl solutions. FT indicates flow-through experiments.*

South Timbalier Sandstone Mössbauer Fit Parameters						
		unreacted	**batch sulfide**	**FT $scCO_2$**	**FT $scCO_2$ + sulfite**	**FT $scCO_2$ + sulfide**
Fe^{3+} in octahedral coordination Clay #1	δ(mm/s)	0.31	0.32	0.31	0.31	0.30
	Δ (mm/s)	0.61	0.60	0.61	0.62	0.64
	Γ (mm/s)	0.37	0.35	0.33	0.34	0.33
	Area (%)	33.3	33.5	33.1	40.5	42.1
Fe^{3+} in octahedral coordination Clay #2	δ (mm/s)	0.25	0.27	0.25	0.29	0.27
	Δ (mm/s)	1.10	1.14	1.15	1.14	1.19
	Γ (mm/s)	0.27	0.28	0.27	0.31	0.25
	Area (%)	5.5	7.7	7.6	7.8	6.4
Fe^{3+} in octahedral coordination Clay #3	δ (mm/s)	0.50	0.50	0.50	0.50	0.50
	Δ (mm/s)	1.10	1.42	1.28	1.20	1.35
	Γ (mm/s)	0.85	0.71	0.56	0.79	0.61
	Area (%)	16.7	11.2	7.7	12.5	9.3
Total Ferric	**Area (%)**	**55.5**	**52.4**	**48.4**	**60.8**	**57.8**
Fe^{2+} in octahedral coordination Clay #4	δ (mm/s)	1.15	1.15	1.15	1.14	1.14
	Δ (mm/s)	2.68	2.67	2.67	2.68	2.70
	Γ(mm/s)	0.34	0.33	0.30	0.32	0.26
	Area (%)	34.0	35.0	37.3	26.1	25.7
Fe^{2+} in octahedral coordination Carbonate	δ (mm/s)	1.24	1.27	1.26	1.29	1.25
	Δ (mm/s)	2.06	2.05	2.05	2.16	2.19
	Γ (mm/s)	0.46	0.44	0.41	0.44	0.38
	Area (%)	10.5	12.5	14.4	13.1	16.6
	χ^2	1.54	1.38	0.47	0.69	0.61

***Symbols in the table are as follows: δ is center shift, Δ is quadrupole splitting, Γ is line width, and χ^2 is normalized chi squared. Errors on parameters are ±0.02 mm/s for δ, ±0.05 mm/s for δ, ±10-20% for overlapped doublet areas, and ±1-3% for ΣFe^{2+} vs. ΣFe^{3+} (Dyar et al. 2008).**

VNIR spectroscopic analyses. The VNIR spectra of unreacted and reacted South Timbalier sandstones are shown in **Figure 3-2**. All samples display absorptions associated with OH and H_2O in clay at ~1.41 μm, ~1.91 μm, and ~2.21 μm (Bishop et al. 2008), along with

weak carbonate features between 1.9 and 2.4 μm (Gaffey 1986). The positions and shapes of the clay absorption features are most consistent with iron-bearing smectites (Bishop et al. 2008). Only two samples displayed spectral variations from the unreacted starting material: PNF2_9, the batch experiment reacted with $scCO_2$ and sulfite; and PNF2_10, the batch experiment reacted with $scCO_2$ and sulfide. Each of these samples shows a slight shape change below 0.6 μm; PNF2_9 becomes more convex and PNF2_10 becomes more concave than the starting material. Because this wavelength region is dominated by electronic absorption from divalent cations and Fe^{3+} (Hunt 1977), changes in this region could indicate that cations have experienced a change in bonding environment consistent with dissolution and re-precipitation in new phases.

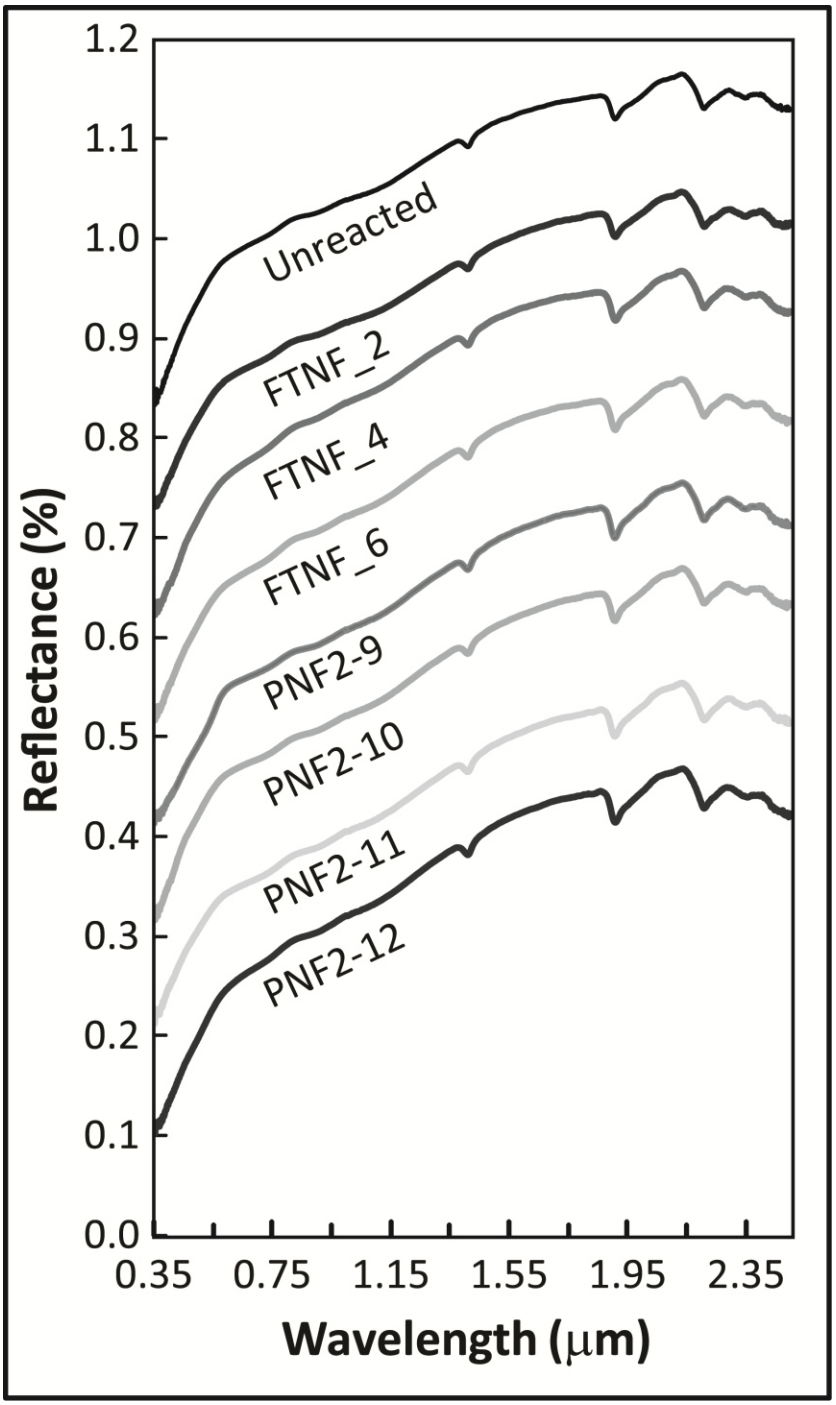

Figure 3-2. VNIR spectra of the South Timbalier sandstone reacted in flow-through or experiments with $scCO_2$, $scCO_2$ plus sulfite, $scCO_2$ plus sulfide, and low fluid:rock ratio batch experiments with $scCO_2$, $scCO_2$ plus sulfite, $scCO_2$ plus sulfide, and $scCO_2$ plus sulfite and sulfide. Spectra are offset in increments of 0.1% for clarity.

3.3.2 Elk Hill

Mössbauer spectroscopic observations. Mössbauer fits of the unreacted Elk Hill sandstone show that the sample's 0.50 wt% iron is contained in clay and carbonate phases (**Figure 3-3**; **Table 3-4**). All samples show one ferric and two ferrous distributions due to iron in octahedral coordination in clay and one ferrous distribution due to iron in octahedral coordination in carbonate. The parameters of the carbonate distribution are most consistent with dolomite or ankerite but the Mössbauer CS and QS ranges for the carbonates are quite close so calcite cannot be ruled out. The Mössbauer spectra of the Elk Hill sandstone display no significant mineralogical changes for the experimental conditions examined for this sample.

Table 3-4. Mössbauer parameters for Elk Hill sandstone reacted in low fluid:rock ratio batch experiments with $scCO_2$, $scCO_2$ plus sulfide, and $scCO_2$ plus sulfite and sulfide.

Elk Sandstone Mössbauer Fit Parameters					
		unreacted	**$scCO_2$ only**	**$scCO_2$ + sulfide**	**$scCO_2$ + sulfite + sulfide**
Fe^{3+} in octahedral coordination Clay #1	δ (mm/s)	0.31	0.31	0.29	0.28
	Δ (mm/s)	0.61	0.58	0.59	0.61
	Γ (mm/s)	0.32	0.30	0.28	0.32
	Area (%)	41.4	45.5	45.5	43.7
Fe^{2+} in octahedral coordination Clay #2	δ (mm/s)	1.11	1.11	1.10	1.14
	Δ (mm/s)	2.19	2.21	2.01	2.15
	Γ (mm/s)	0.42	0.32	0.32	0.33
	Area (%)	17.8	18.4	14.2	18.5
Fe^{2+} in octahedral coordination Clay #3	δ (mm/s)	1.12	1.10	1.08	1.06
	Δ (mm/s)	2.69	2.57	2.58	2.60
	Γ (mm/s)	0.32	0.27	0.30	0.30
	Area (%)	41.9	38.6	38.4	37.9
Fe^{2+} in octahedral coordination Carbonate	δ (mm/s)	1.24	1.21	1.19	1.19
	Δ (mm/s)	1.50	1.45	1.44	1.46
	Γ (mm/s)	0.26	0.26	0.26	0.26
	Area (%)	16.7	18.4	16.2	18.3
	$\chi 2$	0.54	0.46	0.52	0.75

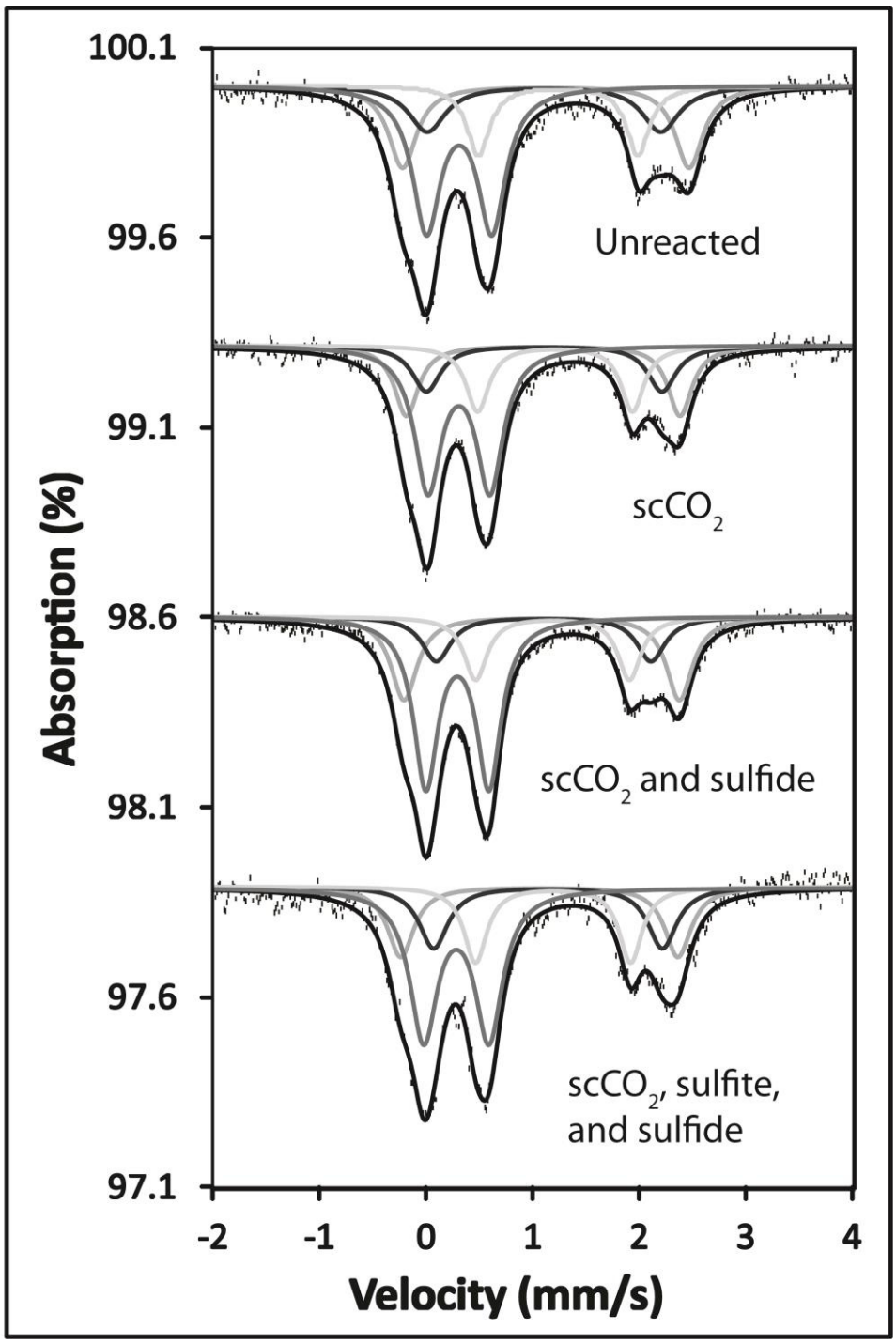

Figure 3-3. Mössbauer spectra of the Elk Hill sandstone in low fluid:rock ratio batch experiments with $scCO_2$, $scCO_2$ plus sulfide, and $scCO_2$ plus sulfite and sulfide. All spectra were acquired at 295K. Spectra are scaled and offset for clarity.

VNIR spectroscopic observations. The unreacted Elk Hill VNIR spectrum displays weak absorptions associated with clay and carbonate but since features in the VNIR do not correlate linearly with composition (Dalton et al. 2004), these features appear muted in an otherwise bland quartz/K-feldspar/plagioclase spectrum (**Figure 3-4**). VNIR spectra for the reacted Elk Hill samples show a continuum slope change along with the appearance of two absorption features at ~2.31 and 2.38 μm. These are consistent with bands 2 and 3 of dolomite (Gaffey 1986), and may indicate the mineralization of some of the CO_2. The addition of a new carbonate phase could lead to the apparent appearance of only two of the 7 carbonate bands when, in actuality, these two bands are simply increasing in relative depth due to differences in carbonate structure or composition (Gaffey 1986; Gaffey 1987). The VNIR data show no other significant mineralogical changes for the experimental conditions examined for this sample.

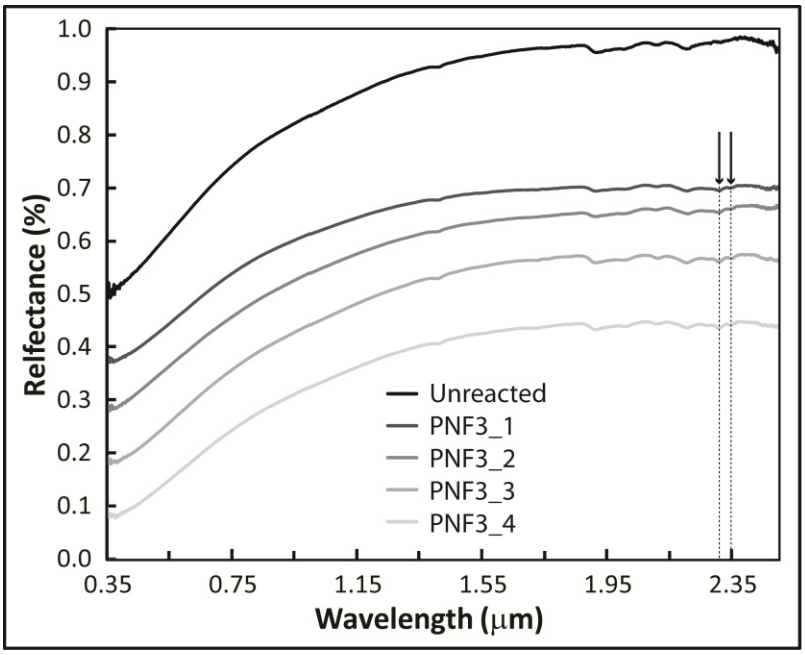

Figure 3-4. VNIR spectra of the Elk Hill sandstone reacted in low fluid:rock ratio batch experiments with $scCO_2$, $scCO_2$ plus sulfite, $scCO_2$ plus sulfide, and $scCO_2$ plus sulfite and sulfide. New spectral features are indicated with arrows. Spectra are offset in increments of 0.1% for clarity.

3.3.3 Caspian Sea

Mössbauer spectroscopic observations. Mössbauer fits of the unreacted Caspian Sea sandstone show that the sample's 3.13 wt% iron is contained in clay and carbonate phases (**Figure 3-5** and **Figure 3-6**; **Table 3-5** and **Table 3-6**). All samples show two ferric and two ferrous distributions due to iron in octahedral coordination in clay and one ferrous distribution due to iron in octahedral coordination in carbonate. The parameters of the carbonate distribution are most consistent with dolomite or ankerite but again, due to highly similar Mössbauer parameters, calcite cannot be ruled out. Several of the distributions in the Mössbauer fit seem minor, but multiple analyses of the individual and the full set of spectra indicate that they are real and differentiable phases and are required for complete and consistent fits.

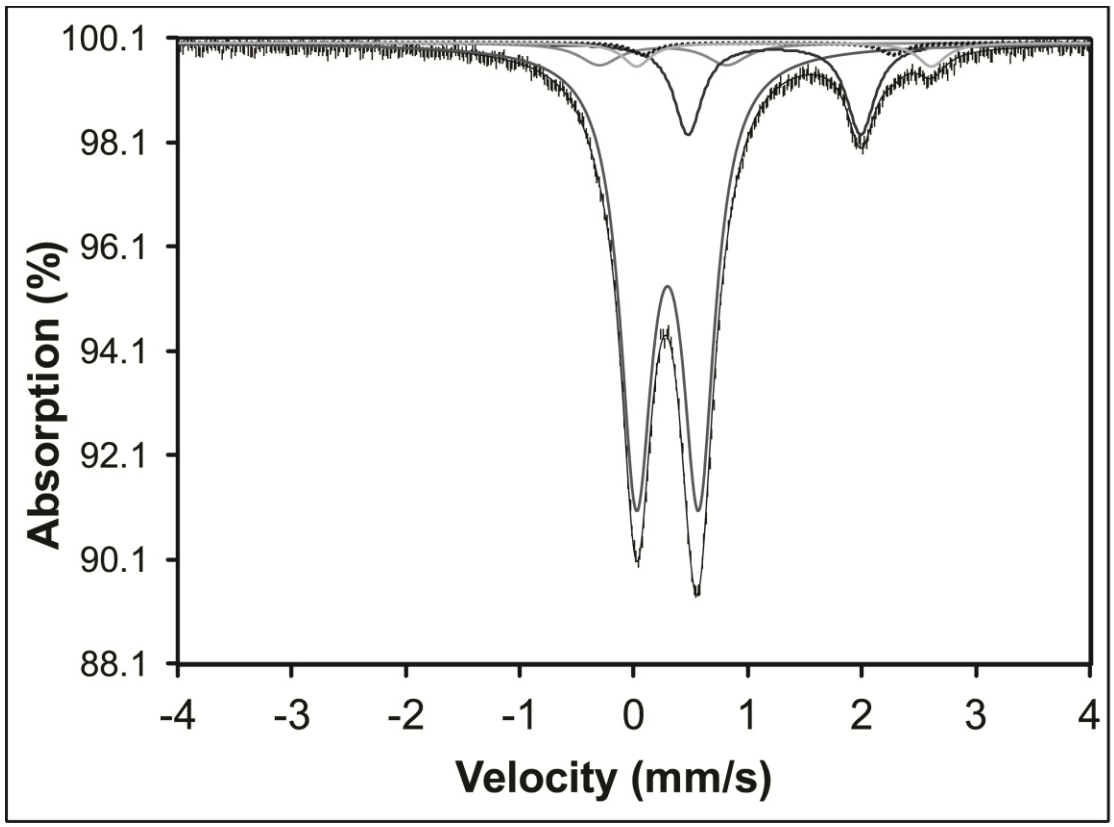

Figure 3-5. Mössbauer fit of unreacted Caspian Sea sandstone spectrum taken at 295K.

Table 3-5. Mössbauer parameters for Caspian Sea sandstone reacted in low fluid:rock ratio batch experiments with $scCO_2$, $scCO_2$ plus sulfide, and $scCO_2$ plus sulfite and sulfide.

Caspian Sea Mössbauer Fit Parameters: Low Fluid:Rock Ratio Experiments						
		unreacted	**$scCO_2$ only**	**$scCO_2$ + sulfite**	**$scCO_2$ + sulfide**	**$scCO_2$ + sulfite + sulfide**
Fe^{3+} in octahedral coordination Clay #1	δ (mm/s)	0.29	0.28	0.28	0.28	0.28
	Δ (mm/s)	0.54	0.51	0.51	0.51	0.52
	Γ (mm/s)	0.29	0.28	0.26	0.26	0.27
	Area (%)	72.80	74.5	68.2	73.9	73.3
Fe^{3+} in octahedral coordination Clay #2	δ (mm/s)	0.23	0.24	0.23	0.24	0.24
	Δ (mm/s)	1.10	1.06	1.03	1.06	1.05
	Γ (mm/s)	0.46	0.36	0.38	0.36	0.34
	Area (%)	7.2	6.1	4.6	6.2	5.5
Sum Ferric	Area (%)	**80.0**	**80.5**	**72.8**	**80.1**	**78.8**
Fe^{2+} in octahedral coordination Clay #3	δ (mm/s)	1.12	1.06	1.08	1.05	1.11
	Δ (mm/s)	2.20	2.08	2.09	2.10	2.15
	Γ (mm/s)	0.30	0.30	0.30	0.30	0.30
	Area (%)	2.7	2.0	4.0	2.1	2.3
Fe^{2+} in octahedral coordination Clay #4	δ (mm/s)	1.30	1.24	1.25	1.25	1.26
	Δ (mm/s)	2.58	2.43	2.46	2.44	2.47
	Γ (mm/s)	0.25	0.30	0.25	0.30	0.25
	Area (%)	3.8	4.1	3.6	3.8	3.7
Fe^{2+} in octahedral coordination Carbonate	δ (mm/s)	1.22	1.17	1.19	1.18	1.18
	Δ (mm/s)	1.50	1.43	1.48	1.44	1.45
	Γ (mm/s)	0.25	0.25	0.30	0.25	0.25
	Area (%)	13.6	13.4	**19.6**	14.1	15.3
	χ^2	0.73	0.87	0.99	0.94	1.31

In the low fluid:rock ratio regime, the Mössbauer spectra show that the Caspian Sea sandstone is most reactive when exposed to $scCO_2$ plus sulfite. This is in contrast to the work with "red" sandstones, where $scCO_2$ plus sulfide was the most reactive regime and $scCO_2$ plus sulfite was the least reactive. When reacted with $scCO_2$ plus sulfite, the Caspian Sea sandstone loses 7.2% spectral area from the ferric phase and gains 6% spectral area in the carbonate phase

(**Table 3-5**). Thus, for these experimental conditions, iron likely dissolved from clay, reduced, and re-precipitated as carbonate.

In the high fluid rock:ratio regime using saline fluids, the Mössbauer spectra show that the Caspian Sea sandstone undergoes carbonate dissolution when exposed to just $scCO_2$ in 6m NaCl solutions (**Table 3-6**). This carbonate dissolution in response to $scCO_2$, which is noted in a previous paper (Schoonen et al. 2012), and by others (Rosenbauer et al. 2005), results from the change in pH caused by the transformation of CO_2 into carbonic acid in solution (DePaolo and Cole 2013). With the addition of sulfur species, the carbonate dissolution is no longer apparent because the addition of sulfur as sulfur salts rather than sulfur-bearing gases effectively raises the pH of the solution from 3.15 for just $scCO_2$ to ~6.1 for Na_2S, ~5.8 for Na_2SO_3, and ~6.2 for a combination of the two (Sklute et al. In Preparation).

In contrast to the low fluid:rock ratio non-saline experiments, when the Caspian Sea sandstone was reacted in high fluid:rock ratio experiments with saline fluids, the Mössbauer spectra show that reactions with $scCO_2$ plus sulfite or $scCO_2$ plus sulfide resulted in almost no changes in iron mineralogy. Reactions with $scCO_2$ plus sulfite *and* sulfide, however, resulted in the loss of 3.4%, 3.4%, and 4.1% spectral area in the combined ferric phases and gains of 2.7%, 2.1%, and 2.4% spectral area in the carbonate phase for 1, 3, and 6 m NaCl solutions, respectively. When both sulfur salts are used, there appears to be slight clay dissolution, releasing Fe^{3+} into solution, followed by the reduction of Fe^{3+} to Fe^{2+}, and then precipitation of Fe^{2+} in carbonate. Although these changes are close to the error of the technique (1-3% area for well resolved distributions or ferric/ferrous ratios; Dyar et al. (2008)), their consistency between salt concentrations implies that they represent real, yet subtle, shifts in mineralogy.

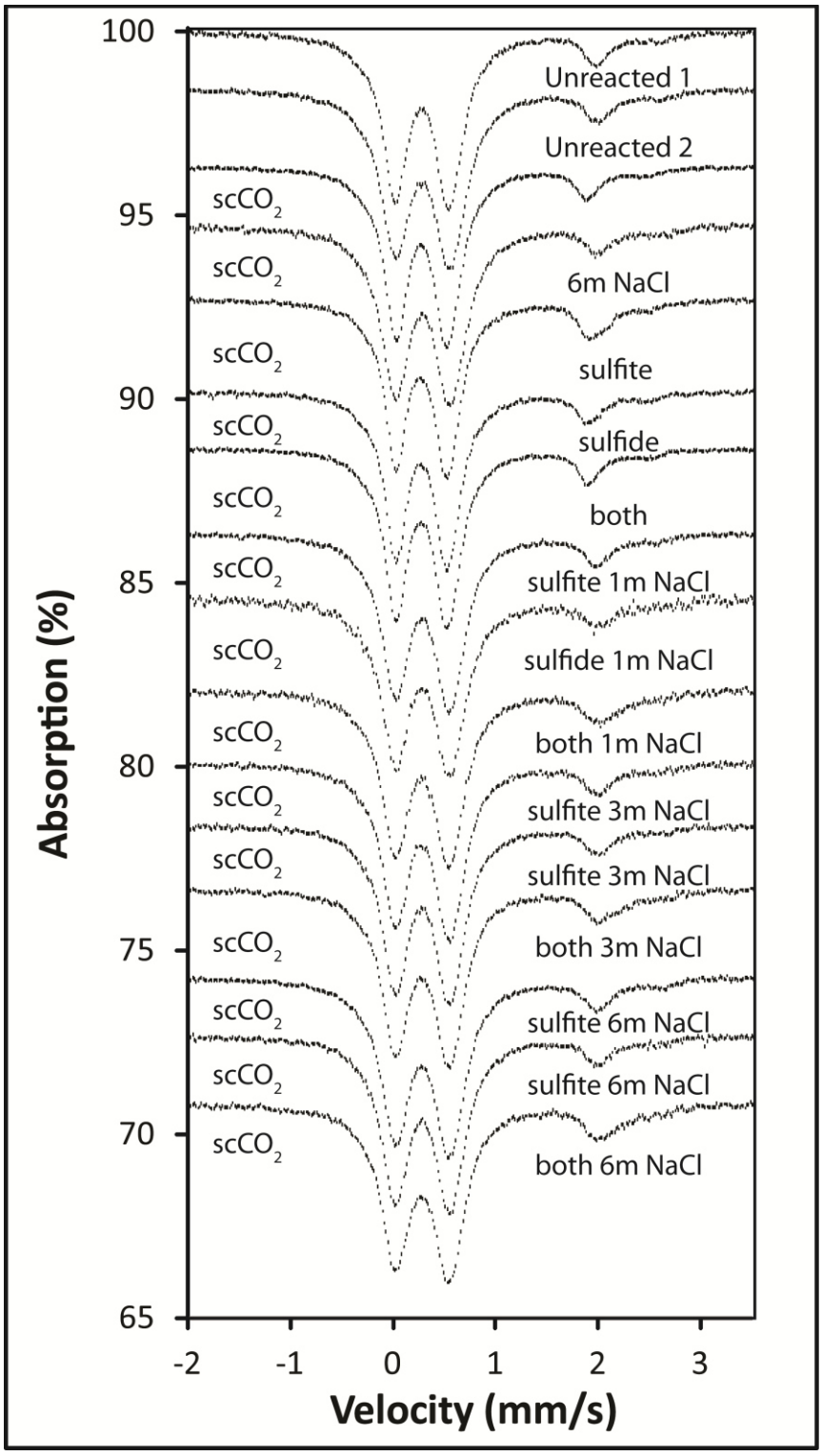

Figure 3-6. Mössbauer spectra of the Caspian Sea sandstone at 295K for all experimental conditions. Fits not shown. Spectra are offset for clarity.

Table 3-6. Mössbauer parameters for Caspian Sea sandstone reacted in high fluid:rock ratio batch experiments with $scCO_2$, $scCO_2$ plus sulfide, and $scCO_2$ plus sulfite and sulfide in 1m, 3m, and 6m NaCl solutions.

Caspian Sea Mössbauer Fit Parameters: High Fluid:Rock Ratio NaCl Solution Experiments												
NaCl concentration		**6m**		**1 molal**			**3 molal**			**6 molal**		
		unrctd	**$scCO_2$ only**	**$scCO_2$ sulfite**	**$scCO_2$ sulfide**	**$scCO_2$ sulfite sulfide**	**$scCO_2$ sulfite**	**$scCO_2$ sulfide**	**$scCO_2$ sulfite sulfide**	**$scCO_2$ sulfite**	**$scCO_2$ sulfide**	**$scCO_2$ sulfite sulfide**
Fe^{3+} in oct. coord. Clay #1	δ (mm/s)	0.29	0.30	0.29	0.29	0.28	0.29	0.29	0.29	0.29	0.29	0.29
	Δ (mm/s)	0.55	0.54	0.54	0.54	0.54	0.54	0.54	0.53	0.55	0.55	0.53
	Γ (mm/s)	0.34	0.33	0.32	0.33	0.33	0.31	0.31	0.33	0.4	0.33	0.34
	Area (%)	76.4	78.1	75.9	79.5	74.9	77.6	79.1	75.0	78.4	80.9	74.2
Fe^{3+} in oct. coord. Clay #2	δ (mm/s)	0.26	0.27	0.21	0.24	0.20	0.20	0.21	0.18	0.19	0.26	0.19
	Δ (mm/s)	1.12	0.98	0.99	1.09	1.09	1.04	1.04	1.04	1.06	1.12	0.98
	Γ (mm/s)	0.43	0.39	0.39	0.25	0.25	0.25	0.25	0.25	0.25	0.25	0.25
	Area (%)	4.7	7.0	5.1	3.3	2.7	3.7	1.7	2.6	3.0	2.3	2.6
Sum Fe^{3+}	Area (%)	**81.0**	**85.2**	**81.0**	**82.8**	**77.6**	**81.3**	**80.8**	**77.6**	**81.4**	**83.2**	**76.9**
Fe^{2+} in octa. coord. Clay #3	δ (mm/s)	1.18	1.11	1.13	1.10	1.15	1.16	1.15	1.14	1.14	1.17	1.13
	Δ (mm/s)	2.19	2.27	2.18	2.10	2.19	2.20	2.22	2.28	2.13	2.22	2.27
	Γ (mm/s)	0.26	0.25	0.32	0.25	0.25	0.25	0.25	0.25	0.25	0.25	0.25
	Area (%)	1.6	1.7	2.5	2.5	3.4	1.5	2.6	3.6	1.8	1.9	3.9
Fe^{2+} in octa. coord. Clay #4	δ (mm/s)	1.30	1.30	1.30	1.30	1.32	1.30	1.34	1.30	1.33	1.32	1.28
	Δ (mm/s)	2.59	2.60	2.49	2.51	2.53	2.50	2.57	2.63	2.56	2.54	2.60
	Γ (mm/s)	0.30	0.26	0.25	0.25	0.25	0.25	0.25	0.25	0.25	0.25	0.25
	Area (%)	3.6	2.8	2.8	2.5	2.6	3.3	2.6	2.9	3.1	2.8	2.9
Fe^{2+} in octa. coord. Carb.	δ (mm/s)	1.23	1.23	1.23	1.23	1.24	1.23	1.24	1.25	1.23	1.24	1.25
	Δ (mm/s)	1.51	1.52	1.50	1.49	1.51	1.51	1.51	1.52	1.50	1.51	1.51
	Γ (mm/s)	0.29	0.25	0.28	0.33	0.35	0.28	0.29	0.33	0.29	0.27	0.32
	Area (%)	13.8	**10.4**	13.8	13.0	**16.5**	14.1	13.2	**15.9**	13.7	12.1	**16.3**
	χ^2	1.29	1.05	1.13	0.92	0.87	1.02	0.92	1.00	1.38	0.90	0.92

VNIR spectroscopic observations. The VNIR spectroscopic data (**Figure 3-7**, **Figure 3-8**, and **Figure 3-9**) show different transformations than the Mössbauer data for the Caspian Sea sandstones. This could be due, in part, to the fact that VNIR spectra are only sensitive to changes in the first few microns of the sample, whereas Mössbauer data are only sensitive to the iron in the sample. The low fluid:rock ratio experiment with only $scCO_2$ and the high fluid:rock ratio experiment with $scCO_2$ in a 6 m NaCl solution are spectrally similar to each other and the unaltered sandstone (**Figure 3-7**, **Figure 3-8**, and **Figure 3-9**). There is a slight decrease in overall reflectance in the VNIR spectrum for the low fluid:rock ratio experiment that cannot be attributed to any particular mineralogical change. The iron-bearing carbonate dissolution seen in the high:fluid rock ratio Mössbauer data is not apparent in the VNIR data for that sample.

The VNIR data for the Caspian Sea sandstones reacted with $scCO_2$ and sulfite (**Figure 3-7**) are also in contrast with the Mössbauer data. The carbonate precipitation noted for the low fluid:rock ratio (0 m) experiment is not apparent in the VNIR spectrum. For the high fluid:rock ratio NaCl solution experiments, the VNIR spectra show distinct shape change between 0.3 and 0.6 μm. Where the concave shape in the unreacted sample spectrum is consistent with calcite or dolomite, the convex shape of the reacted sample spectra is consistent with aragonite or siderite (Clark et al. 2007; Cloutis et al. 2010). Given the Caspian Sea sandstone's MgO/CaO ratio (**Table 3-1**) and the pCO_2 for these experiments (~72-79 bar; Clifford (2007)), aragonite precipitation is possible (Lippmann 1973; Hill 1987). Since no siderite formation was detected in the Mössbauer data, aragonite seems the more likely reaction product. However, since absorptions in the visible wavelength range are due to electronic processes in divalent cations and Fe^{3+} (Hunt 1977), the spectral changes may indicate other mineralogical transformations that change the bonding environment around these cations.

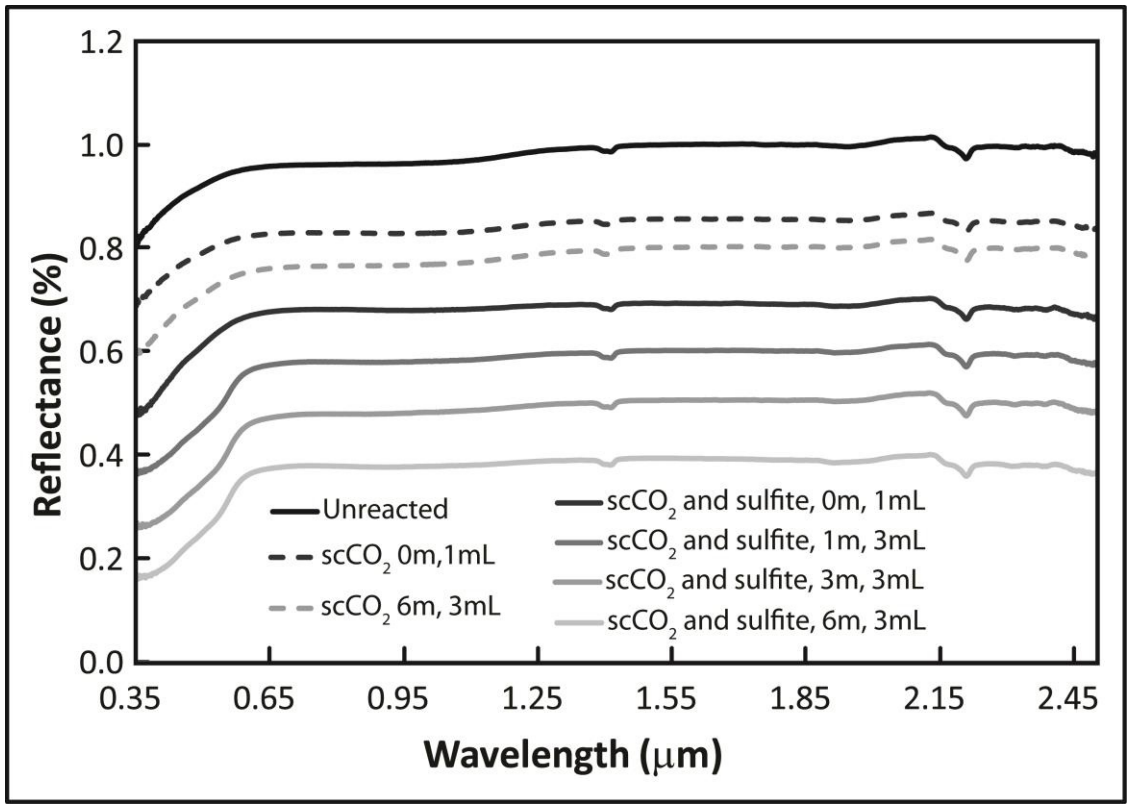

Figure 3-7. VNIR spectra of the Caspian Sea sandstone reacted with $scCO_2$, $scCO_2$ in 6 m NaCl solutions, and $scCO_2$ plus sulfite in 0m, 1, 3, and 6 m NaCl solutions. Low and high fluid:rock ratio experiments are indicated with 1 mL and 3 mL fluid volumes respectively. Spectra are offset in increments of 0.1% for clarity.

The VNIR data for the Caspian Sea sandstones reacted with $scCO_2$ and sulfide in low fluid:rock ratio experiments are spectrally similar to the unreacted sandstone (**Figure 3-8**). The high fluid:rock ratio saline experiments, however, have muted spectral features through the VNIR. This spectral transformation records a color change in these samples upon reaction. The unreacted starting material was a medium yellow gray but turned dark gray after reactions with $scCO_2$ and sulfide in saline fluids. It is unclear what mineralogical transformations, if any, are associated with the color change.

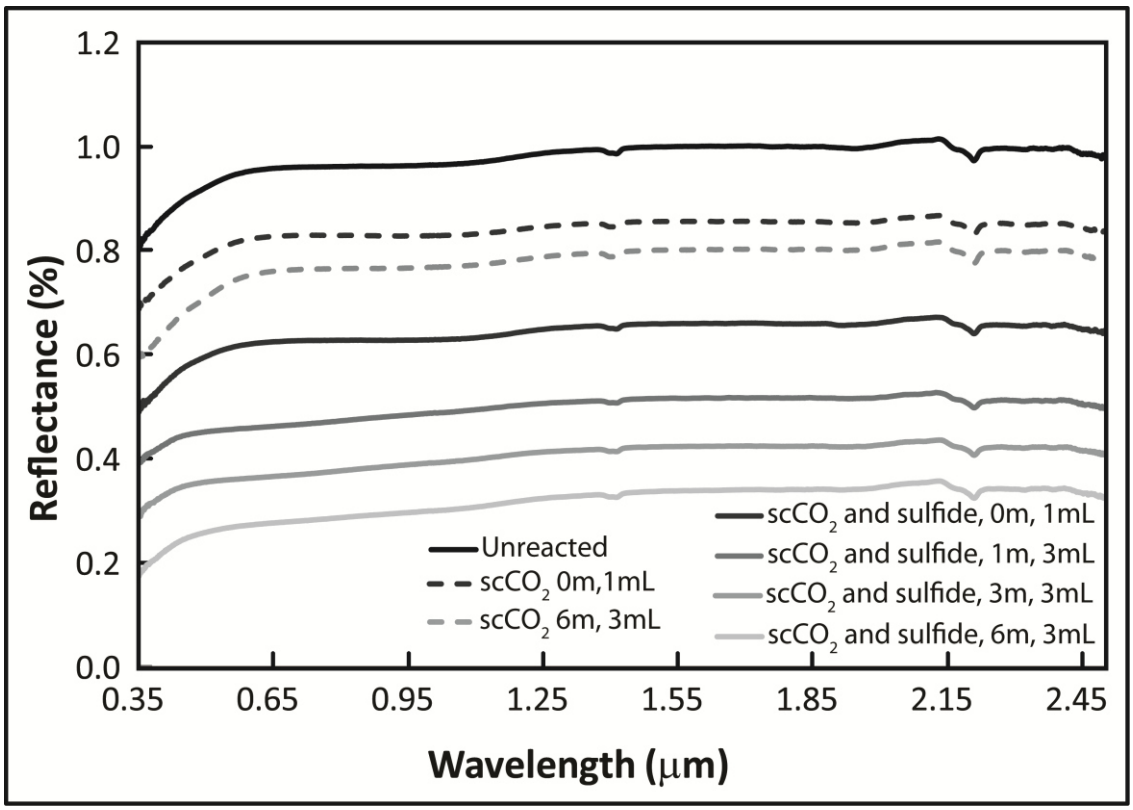

Figure 3-8. VNIR spectra of the Caspian Sea sandstone reacted with $scCO_2$, $scCO_2$ in 6m NaCl solutions, and scCO2 plus sulfide in 0, 1, 3, and 6 m NaCl solutions. Low and high fluid:rock ratio experiments are indicated with 1 mL and 3 mL fluid volumes respectively. Spectra are offset in increments of 0.1% for clarity.

The VNIR data for the Caspian Sea sandstones reacted with $scCO_2$, sulfite, and sulfide show an opposite trend to those reacted with just $scCO_2$ and sulfide. Here, the high fluid:rock ratio experiments appear spectrally similar to the unreacted sandstone where the low fluid:rock ratio spectrum appears distinct in the 0.3 to 0.6 μm range (**Figure 3-9**). Although the changes in the low fluid:rock ratio spectra are difficult to link to a specific mineralogical change, it is interesting that in all three experimental regimes, the low fluid:rock ratio spectra from non-saline experiments display different reactivity from the samples reacted in high fluid:rock ratios with saline fluids. The VNIR spectra of the high fluid:rock ratio experiments again fail to record changes in iron mineralogy observed in the Mössbauer spectra.

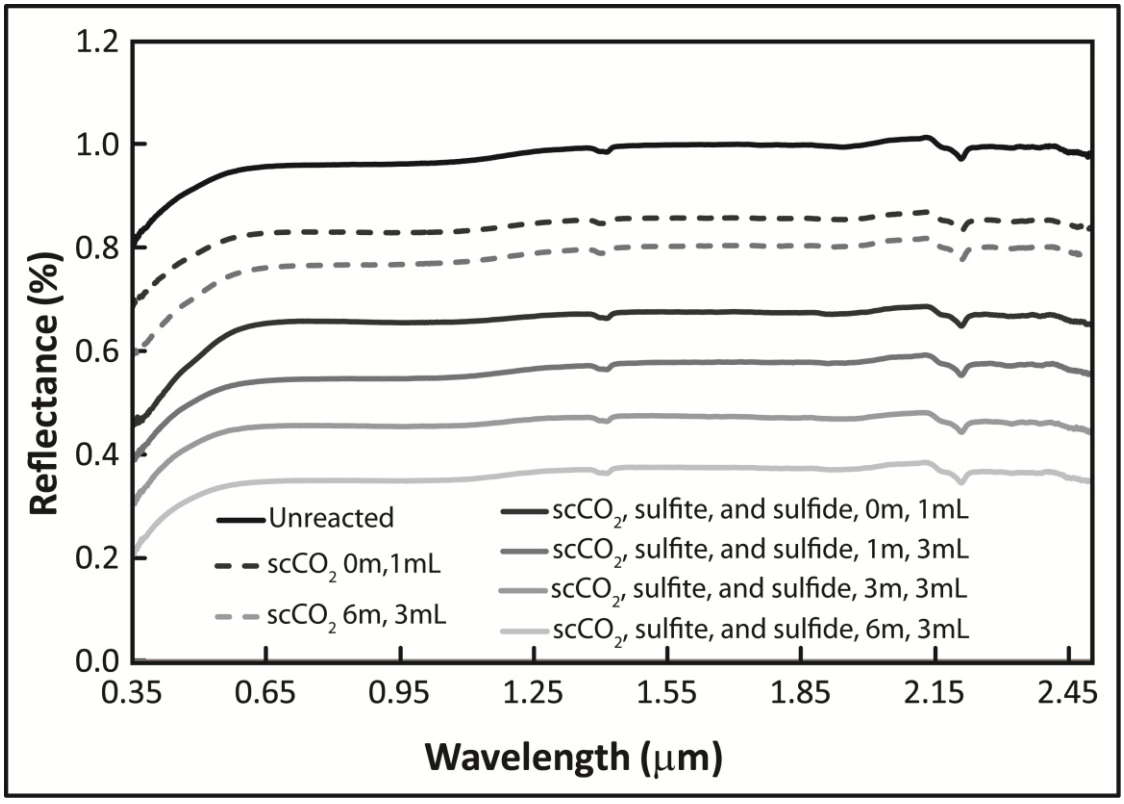

Figure 3-9. VNIR spectra of the Caspian Sea sandstone reacted with $scCO_2$, $scCO_2$ in 6m NaCl solutions, and scCO2 plus sulfite and sulfide in 0m, 1m, 3m, and 6m NaCl solutions. Low and high fluid:rock ratio experiments are indicated with 1mL and 3mL fluid volumes respectively. Spectra are offset in increments of 0.1% for clarity.

3.4 Discussion

Due to the complexity and variety of possible interactions when injecting CO_2 into deep geological formations, it is difficult to perform meaningful numerical simulations that can adequately describe the myriad potential interactions (Holloway 1997). This is due, in part, to the tendency for theoretical studies to assume chemical equilibrium (at least locally). However, kinetic effects seem to be more important in these systems (Kaszuba et al. 2013). Therefore, laboratory studies that focus on samples from representative rock types or target locations are particularly useful (Bertier et al. 2006). Since the utility of a carbon sequestration target lies in

the host rock's ability to withstand $scCO_2$ or mixed gas injection without significant reduction in permeability and still facilitate mineral trapping of CO_2, geochemical reactions that lead to dissolution and re-precipitation of minerals are the primary focus of these studies.

In two previous papers (Schoonen et al. 2012; Sklute et al. In Preparation), the reactivity of a "red", hematite-bearing sandstone from the Moenkopi formation in Arizona towards $scCO_2$ plus sulfite, sulfide, or a combination of the two was examined in experiments that simulated near-field, interfacial region, and far-field reaction scenarios. Here I have investigated the reactivity of three "gray", or clay and carbonate rich, sandstones under the same experimental conditions. Where the reactivity of "red" sandstones appeared to be primarily associated with transformations of the iron-bearing phases, Mössbauer spectra show the iron in the "gray" sandstones seems to be essentially non-reactive. The VNIR spectra, however, show possible transformations in the carbonate phases present in these samples.

Carbonate dissolution is one of the first and fastest processes expected in the carbon sequestration scenario (Bertier et al. 2006; Kaszuba et al. 2013), and carbonate dissolution is almost entirely dependent upon pH (Kaszuba et al. 2013). In this regard, the results from these experiments will differ from a true mixed gas injection scenario. In the interest of safety, these experiments used sulfur salts in place of sulfur bearing gases. Whereas the addition of sulfur salts raises the pH of the solution from 3.15 for just $scCO_2$ to ~6.1 for Na_2S, ~5.8 for Na_2SO_3, and ~6.2 for a combination of the two, the addition of these species as gases would have lowered the pH from 3.15 to ~1.0 for H_2S, ~0.7 for SO_2, and ~0.7 for a combination of the two (Sklute et al. In Preparation). Although these lower pH values would have produced a greater degree of carbonate dissolution, they would also have inhibited the precipitation of new carbonate species (Chialvo et al. 2013) until mineral buffering had raised the pH back to ~4.6-5 (Bickle et al. 2013;

DePaolo and Cole 2013; Kaszuba et al. 2013), a process that could have taken months (Bertier et al. 2006). Therefore, although these experiments are more indicative of later stage reactivity or reactions away from the leading edge of the plume, they provide useful information on longer term reactivity in a short amount of time. For these experiments, the effect of sulfur species seems to have very little effect on the reactivity of the sandstones other than the effect they have on the pH of the solution.

Experiments using the Caspian Sea sandstone show that although salt concentration is not important, either the presence of salt or the fluid rock ratio seems to change the reactivity of the sandstone. For all experimental conditions, the samples reacted in a simulated interfacial regime (low fluid:rock ratio) with non-saline fluids showed different reactivity from samples reacted in a simulated far-field scenario (high fluid:rock ratio) with saline fluids. In both cases, however, the reactivity was minimal over the time scale of these experiments.

3.5 Conclusion

Three "gray" sandstones from the Elk Hill oil field in California, the South Timbalier area in Louisiana, and the North Caspian Basin in Kazakhstan were subjected to $scCO_2$, $scCO_2$ plus sulfite, $scCO_2$ plus sulfide or $scCO_2$ plus sulfite and sulfide in flow-through, low fluid:rock ratio, and high fluid rock ration experiments. These variations were used to simulate the effect of co-injecting of SO_2 and H_2S with $scCO_2$ on the near-field, interfacial region, and far-field reactivity of sandstone types considered for geological sequestration of CO_2. Mineralogical changes were analyzed by Mössbauer and VNIR spectroscopy. All sandstones displayed minimal reactivity under the conditions used in this study. Since one major concern in GCS site assessment is potential for permeability reduction, "gray" sandstone formations may make

suitable GCS targets. Site specific experimental work using core samples is a logical next step to evaluate the changes in permeability over a range of conditions.

Works Cited

Anheden, M., Andersson, A., Bernstone, C., Eriksson, S., Yan, J., Liljemark, S., and Wall, C. (2005) CO_2 quality requirement for a system with CO_2 capture, transport and storage. In: M. Wilson et al. (Eds.), Greenhouse Gas Control Technologies 7. Elsevier, pp. 2559-2564.

Bachu, S. (2008) CO_2 storage in geological media: Role, means, status and barriers to deployment. Progress in Energy and Combustion Science, 34 (2), 254-273.

Bertier, P., Swennen, R., Laenen, B., Lagrou, D., and Dreesen, R. (2006) Experimental identification of CO_2-water-rock interactions caused by sequestration of CO_2 in Westphalian and Buntsandstein sandstones of the Campine Basin (NE-Belgium). Journal of Geochemical Exploration, 89 (1-3), 10-14.

Bickle, M., Kampman, N., and Wigley, M. (2013) Natural Analogues. In: D.J. DePaolo, D.R. Cole, A. Navrotsky, and I.C. Bourg (Eds.), Geochemistry of Geologic Co2 Sequestration. Reviews in Mineralogy & Geochemistry, pp. 15-71.

Bishop, J.L., Lane, M.D., Dyar, M.D., and Brown, A.J. (2008) Reflectance and emission spectroscopy study of four groups of phyllosilicates: smectites, kaolinite-serpentines, chlorites and micas. Clay Minerals, 43 (1), 35-54.

Chestnut, L.G., and Mills, D.M. (2005) A fresh look at the benefits and costs of the US Acid Rain Program. Journal of Environmental Management, 77 (3), 252-266.

Chialvo, A.A., Vlcek, L., and Cole, D.R. (2013) Acid Gases in CO_2-rich Subsurface Geologic Environments. In: D.J. DePaolo, D.R. Cole, A. Navrotsky, and I.C. Bourg (Eds.), Geochemistry of Geologic CO_2 Sequestration. Reviews in Mineralogy & Geochemistry, pp. 361-398.

Clark, R.N., Swayze, G.A., Wise, R., Livio, E., Hoefen, T., Kokaly, R., and Sutley, S.J. (2007) USGS digital spectral library splib06a, U.S. Geological Survey: Digital Data Series 231.

Clifford, A.A. (2007) Calculation of density, enthalpy and entropy for supercritical carbon dioxide. Critical Processes Ltd. http://www.criticalprocesses.com/Calculation%20of%20density,%20enthalpy%20and%20entropy%20of%20carbon%20dioxide.htm

Cloutis, E.A., Grasby, S.E., Last, W.M., Leveille, R., Osinski, G.R., and Sherriff, B.L. (2010) Spectral reflectance properties of carbonates from terrestrial analogue environments: Implications for Mars. Planetary and Space Science, 58 (4), 522-537.

Dalton, J.B., Bove, D.J., and Mladinich, C.S. (2004) Remote sensing charachterization of the Animas River watershed, southwest Colorado, by AVIRIS imaging spectroscopy. 2004-5203, USGS.

Damen, K., Faaij, A., and Turkenburg, W. (2006) Health, safety and environmental risks of underground CO_2 storage - Overview of mechanisms and current knowledge. Climatic Change, 74 (1-3), 289-318.

De Grave, E., and van Alboom, A. (1991) Evaluation of ferrous and ferric Mössbauer fractions. Physics and Chemistry of Minerals, 18, 337-342.

DePaolo, D.J., and Cole, D.R. (2013) Geochemistry of geologic carbon sequestration: An overview. In: D.J. DePaolo, D.R. Cole, A. Navrotsky, and I.C. Bourg (Eds.), Geochemistry of Geologic CO_2 Sequestration. Reviews in Mineralogy & Geochemistry, pp. 1-14.

DePaolo, D.J., Cole, D.R., Navrotsky, A., and Bourg, I.C. (2013) Geochemistry of Geologic CO_2 Sequestration, Geochemistry of Geologic CO_2 Sequestration. Reviews in Mineralogy & Geochemistry, pp. iii-iv.

Dooley, J.J., Dahowski, R.T., Davidson, C.L., Bachu, S., Gupta, N., and Gale, J. (2005) A CO_2-storage supply curve for North America and its implications for the deployment of carbon dioxide capture and storage systems, Greenhouse Gas Control Technologies 7. Elsevier Science Ltd, pp. 593-601.

Dyar, M.D., Schaefer, M.W., Sklute, E.C., and Bishop, J.L. (2008) Mössbauer spectroscopy of phyllosilicates: effects of fitting models on recoil-free fractions and redox ratios. Clay Minerals, 43 (1), 3-33.

Ellis, B.R., Crandell, L.E., and Peters, C.A. (2010) Limitations for brine acidification due to SO_2 co-injection in geologic carbon sequestration. International Journal of Greenhouse Gas Control, 4 (3), 575-582.

Flett, M.A., Gurton, R.M., and Taggart, I.J. (2005) Heterogeneous saline formations: Long-term benefits for geo-sequestration of greenhouse gases, Greenhouse Gas Control Technologies 7. Elsevier Science Ltd, pp. 501-509.

Gaffey, S.J. (1986) Spectral reflectance of carbonate minerals in the visible and near-infrared (0.35-2.55 microns) - calcite, aragonite, and dolomite. American Mineralogist, 71 (1-2), 151-162.

Gaffey, S.J. (1987) Spectral reflectance of carbonate minerals in the visible and near-infrared (0.35-2.55 μm) - anhydrous carbonate minerals. Journal of Geophysical Research-Solid Earth and Planets, 92 (B2), 1429-1440.

Garcia, S., Rosenbauer, R.J., Palandri, J., and Maroto-Valer, M.M. (2012) Sequestration of non-pure carbon dioxide streams in iron oxyhydroxide-containing saline repositories. International Journal of Greenhouse Gas Control, 7, 89-97.

GHG (2003) Potential for improvements in Gasification Combined Cycle Power Generation with CO_2 Capture. International Energy Agency Greenhouse Gas R&D program, IEA GHG, Chetenham, UK.

Hill, C.A. (1987) Geology of Carlsbad Cavern and other caves in the Guadalupe mountains, New Mexico and Texas. New Mexico Bureau Of Mines & Mineral Resources Bulletin 117 http://www.nps.gov/history/history/online_books/geology/publications/state/nm/1987-117/sec1-2.htm

Holloway, S. (1997) An overview of the underground disposal of carbon dioxide. Energy Conversion and Management, 38, S193-S198.

Hunt, G.R. (1977) Spectral signatures of particulate minerals in the visible and near IR. Geophysics, 42 (3), 501-513.

IPCC (2005) IPCC special report on carbon dioxide capture and storage, Intergovernmental Pannel on Climate Change, New York, NY.

Jones, G.D., and Xiao, Y.T. (2006) Geothermal convection in the Tengiz carbonate platform, Kazakhstan: Reactive transport models of diagenesis and reservoir quality. Aapg Bulletin, 90 (8), 1251-1272.

Kaszuba, J., Yardley, B., and Andreani, M. (2013) Experimental perspectives of mineral dissolution and precipitation due to carbon dioxide-water-rock interactions. In: D.J. DePaolo, D.R. Cole, A. Navrotsky, and I.C. Bourg (Eds.), Geochemistry of Geologic CO_2 Sequestration. Reviews in Mineralogy & Geochemistry, pp. 153-188.

Kaszuba, J.P., Janecky, D.R., and Snow, M.G. (2005) Experimental evaluation of mixed fluid reactions between supercritical carbon dioxide and NaCl brine: Relevance to the integrity of a geologic carbon repository. Chemical Geology, 217 (3-4), 277-293.

Lippmann, F. (1973) Sedimentary carbonate minerals. Springer-Verlag, New York, 228 pp.

Mohan, K.K., Vaidya, R.N., Reed, M.G., and Fogler, H.S. (1993) Water sensitivity of sandstones containing swelling and non-swelling clays. Colloids and Surfaces a-Physicochemical and Engineering Aspects, 73, 237-254.

Murphy, R., Lammers, K., Smirnov, A., Schoonen, M.A.A., and Strongin, D.R. (2010) Ferrihydrite phase transformation in the presence of aqueous sulfide and supercritical CO_2. Chemical Geology, 271 (1-2), 26-30.

Murphy, R., Lammers, K., Smirnov, A., Schoonen, M.A.A., and Strongin, D.R. (2011) Hematite reactivity with supercritical CO_2 and aqueous sulfide. Chemical Geology, 283 (3-4), 210-217.

Palandri, J.L., and Kharaka, Y.K. (2005) Ferric iron-bearing sediments as a mineral trap for CO_2 sequestration: Iron reduction using sulfur-bearing waste gas. Chemical Geology, 217 (3-4), 351-364.

Palandri, J.L., Rosenbauer, R.J., and Kharaka, Y.K. (2005) Ferric iron in sediments as a novel CO_2 mineral trap: CO_2-SO_2 reaction with hematite. Applied Geochemistry, 20 (11), 2038-2048.

Rosenbauer, R.J., Koksalan, T., and Palandri, J.L. (2005) Experimental investigation of CO_2-brine-rock interactions at elevated temperature and pressure: Implications for CO_2 sequestration in deep-saline aquifers. Fuel Processing Technology, 86 (14-15), 1581-1597.

Schoonen, M.A.A., Sklute, E.C., Dyar, M.D., and Strongin, D.R. (2012) Reactivity of sandstones under conditions relevant to geosequestration: 1. Hematite-bearing sandstone exposed to supercritical carbon dioxide commingled with aqueous sulfite or sulfide solutions. Chemical Geology, 296, 96-102.

Sklute, E.C., Schoonen, M.A.A., Dyar, M.D., and Strongin, D.R. (In Preparation) Reactivity of sandstones under conditions relevant to geosequestration: 2. Hematite-bearing sandstone exposed to supercritical carbon dioxide comingled with saline sulfite and/or sulfide solutions. Chemical Geology.

Totten, M.W., Dixon, M., and Hanan, M.A. (2005) Diagenesis of mixed-layer clay minerals in the South Timbalier area, Gulf of Mexico. Gulf Coast Association of Geological Societies Transactions, 55, 821-829.

Vandenberghe, R.E., De Grave, E., and de Bakker, P.M.A. (1994) On the methodology of the analysis of Mössbauer spectra. Hyperfine Interactions, 83 (1), 29-49.

Weber, J.L., Francis, B.P., Harris, P.M., and Clark, M. (2003) Stratigraphy, lithofacies and reservoir distribution, Tengiz field, Kazakhstan. In: W.M. Ahr, P.M. Harris, W.A. Morgan, and I.D. Sommerville (Eds.), Permo-Carboniferous carbonate platform and reefs: SEPM Special Publication 78 and AAPG Memoir 83, pp. 351-394.

Chapter 4

Optical Constants of Synthetic Potassium, Sodium, and Hydronium Jarosite

Submitted to American Mineralogist

Sklute, E. C., Glotch, T. D., Piatek, J. L., Woerner, W. R., Martone, A. A., Kraner, M. L. (In Review) - Optical Constants of Synthetic Potassium, Sodium, and Hydronium Jarosite. Am. Mineral.

4.1 Introduction

Jarosite has been the subject of a multitude of studies over the past decade (Bishop and Murad 2005; Frost et al. 2005; Navrotsky et al. 2005; Nomura et al. 2005; Barron et al. 2006; Papike et al. 2007; Cloutis et al. 2008; Madden et al. 2008; Bell et al. 2010; Norlund et al. 2010; Kula and Baldwin 2011; Madden et al. 2012; Pritchett et al. 2012; Zahrai et al. 2013) since its discovery on Mars in 2004 at the Mars Exploration Rover Opportunity landing site at Meridiani Planum (Klingelhofer et al. 2004). On Earth, this iron hydroxy sulfate [$(K,Na,H_3O)Fe_3(SO_4)_2(OH)_6$] occurs primarily as an oxidative weathering product of pyrite-rich sediments associated with acid mine drainage (AMD) (Navrotsky et al. 2005). Therefore, its discovery on Mars suggests a highly acidic formation environment (Bishop et al. 2004). On both Earth and Mars, jarosite's sensitivity to formation conditions makes it an important environmental indicator. It is, therefore, a key remote sensing target. Visible and near infrared (VNIR) remote sensing has been used to identify and map jarosite on both planets (Swayze et al.

2000; Farrand et al. 2009). However, quantitative abundance estimates cannot be extracted from these data because of a lack of optical constants (the real and imaginary indices of refraction, *n* and *k*). The absence of these optical constants from the literature is due, in part, to the inherent difficulty in obtaining such data for minerals that tend to crystallize naturally as fine grained (~10 μm) powders, like many sulfates including jarosite. Yet once optical constants have been determined, and quantitative mineral abundances obtained, it becomes possible to conduct a more in-depth evaluation of the target location.

As additional jarosite-bearing regions are discovered on Mars (Farrand et al. 2009; Roach et al. 2010; Wendt et al. 2011; Sefton-Nash et al. 2012; Sowe et al. 2012), there is a growing need for tools and data that can enhance our interpretations of past Martian environments. In the absence of targeted sample return, quantitatively modeled mineral abundances derived from remote sensing data can provide valuable constraints on past fluid compositions, atmospheric conditions, weathering timelines, and sub-surface processes. This will aid in developing a full picture of Martian history. To this end, jarosite is a particularly valuable environmental indicator mineral because it is extremely sensitive to environmental conditions. For example, terrestrial jarosite only precipitates under very specific Eh and pH conditions as a supergene deposit (Bigham et al. 1996a; Bigham et al. 1996b; Norlund et al. 2010). It also only remains stable under a narrow range of atmospheric and surface conditions (i.e. low surface moisture and low relative humidity (Madden et al. 2004; Papike et al. 2006)). This sensitivity has allowed it to be used as a 'stopwatch' for wetting processes on Mars (Madden et al. 2009). Jarosite can also crystallize from subsurface (volcanic) processes, and its ability to easily incorporate rare earth elements into its structure makes it a valuable geochronometer (Lueth et al. 2005; Papike et al. 2006). Jarosite can also be used as a geothermometer both through oxygen isotopes analysis

(Rye and Stoffregen 1995; Papike et al. 2006) and hydronium content (Swayze et al. 2008). In addition, because jarosite is a well-studied mineral, thermodynamic data are available to model its formation, stability, and partitioning behavior (Drouet and Navrotsky 2003; Navrotsky et al. 2005). For example, it is possible to determine the K/Na ratio of the fluid from which jarosite formed (Deyell and Dipple 2005; Papike et al. 2006).

On Earth, jarosite is quickly becoming a major environmental contaminant (Pappu et al. 2006). As one of the main byproducts of hydrometallurgical extraction of zinc (600,000 barrels of residue annually in the European Union), and as a precipitate linked to highly acidic AMD runoff (Swayze et al. 2000), it has the capacity to both store and release large quantities of heavy metals back into the environment (Papike et al. 2006; Swayze et al. 2008). In AMD regions, the most acidic runoffs are associated with iron (III) sulfates (Jerz and Rimstidt 2003). Among these, jarosite is often spectrally significant on remote sensing spatial scales. It indicates areas where neutral rain and snow-melt can be transformed into pH < 3 runoff (Swayze et al. 2000; Jerz and Rimstidt 2003). Swayze et al. (2000) showed that identifying jarosite in remote spectral analysis of AMD regions saved both time (2 years) and money ($2 million) in cleanup efforts at the California Gulch superfund site in Leadville, CO.

For single pass or targeted cleanup efforts, qualitative data may be sufficient. However, for monitoring, quantitatively determined abundances would greatly improve efficiency. As aeolian processes expose more pyrite to oxygen and water, jarosite concentrations increase, indicating an active area of contamination. If, however, an AMD region is no longer producing highly acidic waters, conditions will favor the formation of goethite and hematite, causing jarosite concentrations to diminish with time. Thus, by combining quantitative abundance analysis with the broad spatial coverage of remote sensing, detailed geochemical conditions on

the ground can be assessed in a manner that broadens scope and significantly reduces time and cost.

Jarosite is spectrally distinct in the VNIR (~0.35-2.5 μm) wavelength range from other hydrates, hydroxylates, and iron-bearing minerals (**Figure 4-1**) (Swayze et al. 2000). On a remote sensing platform, VNIR spectroscopy remains one of the most useful methods for identifying hydrated and hydroxylated minerals, like jarosite, over large spatial scales. This technique is, therefore, an indispensable tool for wide-scale monitoring and discovery missions. While VNIR spectroscopic identification of many minerals is straightforward (Clark et al. 2003), extracting quantitative abundances of single minerals from spectra of mineral mixtures can be quite difficult. In this wavelength region, multiple scattering is often the dominant process, in contrast to the mid-infrared (MIR), where absorption dominates (Clark 1999). The dominant scattering condition in the VNIR, which impacts the shape and depth of spectral features, depends on grain size, absorption coefficient, and internal and surface imperfections. In addition, light can be scattered multiple times in a regolith surface before being absorbed or reflected to a detector. This means that the contribution to a spectrum from a mineral in a mixture is not necessarily linearly correlated with its abundance in the sample (Hapke and Wells 1981). Therefore, a model is needed to relate the spectral abundance of a mineral with its abundance in a mineral mixture.

Fortunately, radiative transfer theory can be used to tackle the problem of nonlinear spectral mixing and to extract quantitative mineral abundance in the VNIR (Clark and Roush 1984; Mustard and Pieters 1987; Lucey 2004; Poulet and Erard 2004; Wilcox et al. 2006; Cahill and Lucey 2007; Lawrence and Lucey 2007; Denevi et al. 2008; Cahill et al. 2009; Poulet et al. 2009; Li and Li 2011). Quantitative abundances are obtainable because radiative transfer theory

explicitly models the interaction of light with particles, like atmospheric dust and aerosols, or soils and regoliths. Unmixing models based on radiative transfer theory use the fact that although reflectance is not linearly correlated with concentration in a mixed spectrum, the bulk single scattering albedo (SSA), or the probability that a photon will survive the interaction with a particle, is a linear combination of the SSA's of the minerals in the mixture. The SSA can be obtained from VNIR reflectance data, provided that the real and imaginary indices of refraction (optical constants n and k), of the minerals in the mixture are known. However, this method has seen limited use due to a distinct lack of optical constants for a wide variety of materials (Lucey 1998; Dalton et al. 2004; Cruikshank et al. 2005).

Optical constants can be determined by a variety of methods provided that large (mm) sized crystals of the pure material can be grown. For naturally fine-grained minerals (like many sulfates), which cannot be cast into thin films, optical constants can only be determined through inverting the theory of radiative transfer and applying it to spectra of pure minerals obtained in the lab. Although several treatments of radiative transfer theory, developed in the 1980s by Hapke (Hapke 1981; Hapke 1993), and later in the 1990s/2000's by Shkuratov et al. (Shkuratov et al. 1999), made this procedure more computationally straightforward, it remained, until recently, a lengthy and user intensive process. Recent increases in computing power have made the calculation of optical constants more robust and less time consuming. However, a general lack of detailed methodology in the literature for these more robust methods has hindered potential progress. Here I contribute to the library of optical constants in two ways: first, by providing robust n and k data for synthetic potassium, hydronium, and sodium jarosite; and second, by explicitly describing the calculation procedures, providing my Matlab computer code, and detailing how others may obtain optical constants of additional minerals.

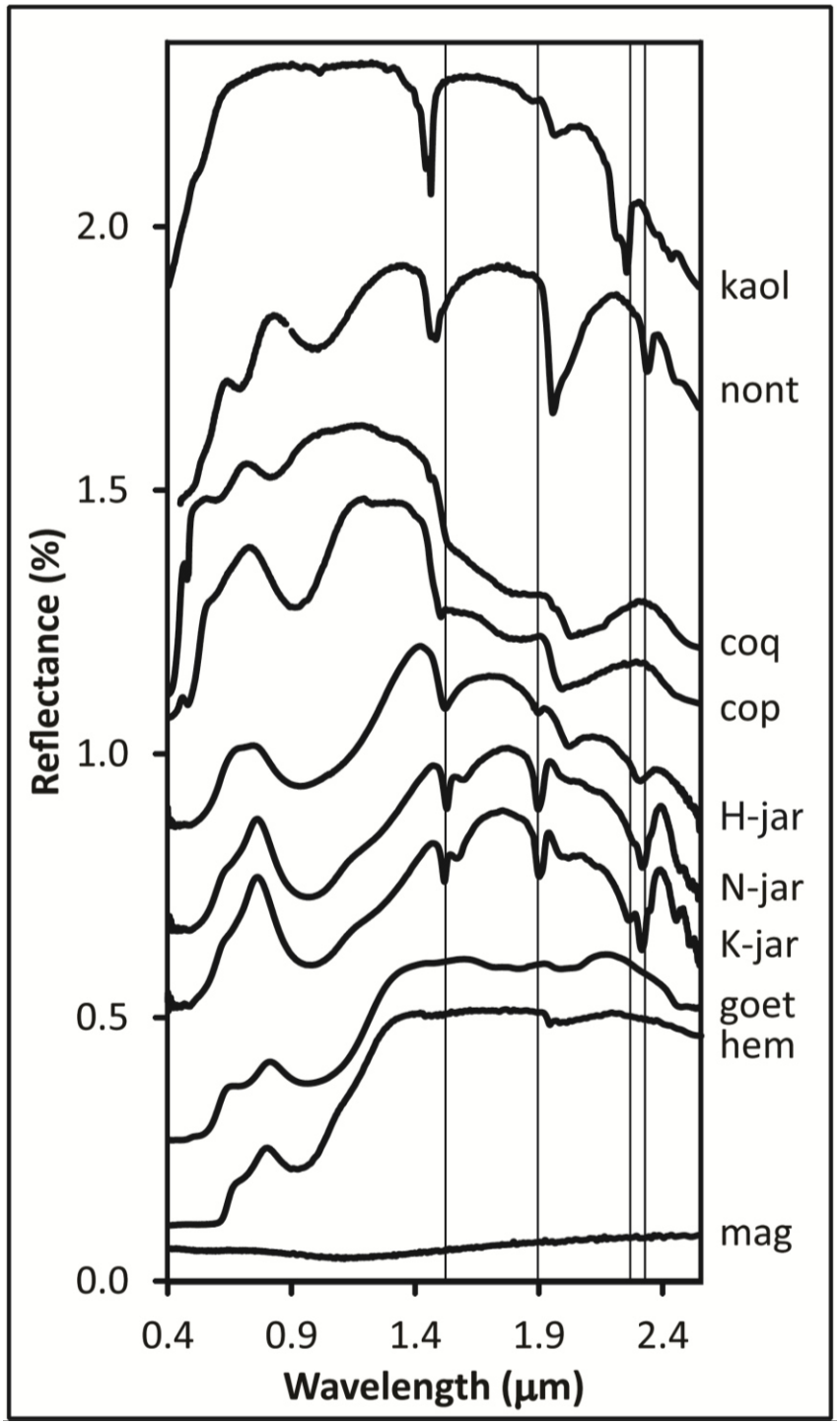

Figure 4-1. VNIR spectra of several common minerals (USGS Speclab) plotted with the jarosites used in this study. Abbreviations are as follows: kaolinite CM7 (kaol), nontronite NG-1.a (nont), coquimbite GDS22 (coq), copiapite GDS21 (cop), hydronium jarosite 63-90 μm (H-jar), sodium jarosite 63-90 μm (N-jar), potassium jarosite 63-90 μm (K-jar), goethite GDS134 (goet), hematite GDS27 (hem), magnetite HS195.3B (mag). Vertical lines mark the diagnostic jarosite spectral features.

4.2 Methods

4.2.1 Sample Synthesis

Hydronium jarosite was synthesized following a method modified from Majzlan et al. (2004). Hydrothermal reactions were carried out in 23 ml Teflon lined Parr pressure vessels. Each liner was filled with a mix of 12 mL of 18 mΩ millipore DI water and 3 g of $Fe_2(SO_4)_3 \cdot 5 H_2O$ and magnetically stirred for 30 minutes. The vessels were sealed and placed in a Fisher Isotemp forced-air circulation oven at 142 °C for 48 hours. After the reaction, the hydronium jarosite was washed with DI water and dried in an oven at 40 °C for 12 hours. The products of 16 reactions were combined for this study.

Potassium and sodium jarosite were synthesized following the redox-based hydrothermal method of Grohol et al. (2003). The 23 ml Teflon lined Parr pressure vessels were first loaded with 9.2 mL of 18 mΩ millipore DI water, 0.405 mL of H_2SO_4, and 0.9 g of K_2SO_4 for potassium jarosite or 0.626 g of Na_2SO_4 in the case of sodium jarosite. The solutions were magnetically stirred for 30 minutes, then placed in a glove bag with an O_2 atmosphere. A 0.103 g piece of 2 mm diameter iron wire (99.9% Aldrich), was added to the solution. The pressure vessels were sealed with an oxygen atmosphere. Prior to being added to the Teflon vessels, the iron wire was cleaned of any surface oxide residue by heating it to 800 ºC under an H_2 atmosphere for 1 hour. The pressure vessels were then placed in a Fisher Isotemp forced-air circulation oven at 201 °C for 4 days. After the reaction, the products were washed in DI water and dried in an oven at 40 °C for 12 hours. For potassium jarosite, the largest grain sizes were obtained when the Parr autoclaves were cooled at 0.1 ºC/min. For the sodium jarosites, large grain sizes required seeding from previous batches, and best results were obtained when the

autoclaves were pulled directly from the oven after 4 days. For potassium and sodium jarosite, the products of 32 and 16 reactions, respectively, were combined for this study.

4.2.2 Analysis

The synthesis products were dry-sieved into four size fractions: <45 μm, 45-63 μm, 63-90 μm, and 90-125 μm. Powder XRD patterns were collected using a Rigaku Ultima IV diffractometer (Cu Kα) in Bragg-Brentano reflection geometry with a D/teX Ultra high speed one-dimensional position sensitive detector. The patterns were collected from 10 to 159º at a rate of 0.5 º/min with a 0.01º step size for phase identification. Reflectance spectra of the three largest size fractions were collected by an 8° field of view foreoptic coupled via an optical fiber to an ASD Fieldspec3 Max UV-VIS-NIR spectrometer with a 512 element Si photodiode array detector for the 350-1000 nm interval and two TE cooled InGaAs photodiode detectors in the 1000-2500 nm interval, giving spectral resolution of 10 nm (at 1400 or 2100 nm). The incident light was provided by an Ocean Optics HL-2000-HP tungsten halogen light source directed down a 600 μm Ocean Optics optical fiber. Each size fraction of each sample was analyzed at 7 phase angles from 15 to 45˚ (spectra taken every 5˚). Incidence and emergence angles were obtained by using a custom-built goniometer (estimated error of < 2˚). All spectra were taken in the absence of ambient light and referenced to a calibrated Spectralon standard (Labsphere, Inc.), illuminated at the same angle as the sample. Since the intensity of the incident light varied with phase angle, the number of averaged scans was increased as phase angle increased to improve signal to noise. At incidence of 15˚, each spectrum is an average of 3000 scans. At 45˚, each spectrum is an average of 7500 scans. Due to the changing phase angle, the detector was optimized, and a new white reflectance baseline (500 scans dark current, 1000 scans white reflectance) was acquired before each measurement. Samples were mounted into an XRD sample

holder that had been spray painted flat black. Rather than packing the sample into the sample holder by compression, which can add preferential orientation and possibly introduce coherent effects, each sample was leveled by tapping the sides and underside of the sample plate. Repeat measurements from separate sample loadings of the same sample in the same configuration were compared, and errors are found to be ~0.01% reflectance.

The smallest size fraction of each sample was pressed into a compact pellet ~ 2 mm thickness and 13 mm diameter. Mid infrared (MIR) and far infrared (FIR) (for potassium jarosite only) specular reflectance spectra were collected for each pellet. MIR measurements were made on a Thermo Fisher Nicolet 6700 FTIR spectrometer with a DTGS detector (with a KBr window) and a CsI beamsplitter. FIR measurements were made on the same spectrometer equipped with a Nicolet Solid Substrate beamsplitter and a DTGS detector with a polyethylene window. MIR and FIR reflectance spectra were referenced to a gold mirror and each spectrum is an average of 256 scans.

4.2.3 Theory

The equation of radiative transfer (a form of the Boltzmann transfer equation; Hapke 2012), which explicitly models the interaction of light with a medium, has no analytic closed form solution (Hapke 2012). Therefore, use of the equation of radiative transfer varies based on the exact set of approximations or formulations used to obtain results. There are two primary modern formulations that have been applied to the modeling of planetary bodies: The Hapke model (Hapke 1981; Hapke 1996; Hapke 2012) and the Shkuratov model (Shkuratov et al. 1999). Although the Shkuratov model has the advantage of computational simplicity, it suffers from two drawbacks. First and foremost, we know that the imaginary index of refraction, *k,* is a fundamental property of a mineral and is, therefore, grain-size independent. However, the

computational simplicity of the Shkuratov model means that the same *k* cannot be obtained for two different size fractions of the same sample. Thus although a useable, and often useful quantity is obtained, it is not technically correct to call it *k*. Second, the Shkuratov model ignores illumination and viewing geometry, making it impossible to take factors like surface roughness into account (Li and Li 2011).

For these reasons, our model is based on the Hapke treatment of radiative transfer. The equations used in this work are slightly altered from those in the literature. Our equations follow directly from the theory as it is presented by Hapke. However, here fewer assumptions are made about the reflectance experiment, which cause the geometry (placement of μ and μ_0) in some of the expressions to differ from what is traditionally reported in the literature.

The Hapke treatment of radiative transfer requires three conditions be met: 1) the particle size has to be much larger than the wavelength of light; 2) the medium has to be continuous and closely packed such that the particles are touching; and 3) that particles are randomly oriented such that the multiply scattered light can be assumed isotropic (see Hapke 2012 for a full derivation and explanation). If these conditions are met, the bidirectional reflectance, or the ratio of the scattered radiance *I* to the source irradiance *J*, is

$$r(i,e,g) = K\frac{w}{4\pi}\frac{\mu_0}{\mu_0+\mu}\{[1+B(g)]p(g)+H(\mu_0/K)H(\mu/K)-1\}, \quad (4.1)$$

where μ and μ_0 are the cosine of the emission angle, *e*, and the incidence angle, *i*, respectively, and *g* is the phase angle. In Equation 4.1, $B(g)$ is the backscatter function, which can be set to zero if the phase angle is greater than 15˚ (Mustard and Pieters 1989). The phase angle dependence of singly scattered light is represented by $p(g)$, the phase function, and can be modeled with a two term Legendre polynomial, such that

$$p(g) = 1 + b\cos(g) + c(1.5\cos^2(g) - 0.5). \tag{4.2}$$

Multiply scattered light is described by Ambartsumian-Chandrasekhar's *H*-function (Ambartsumian 1958; Chandrasekhar 1960), which can be approximated by

$$H(\mathrm{x}) = \left\{1 - w\mathrm{x}\left[r_0 + \left(\frac{1 - 2r_0\mathrm{x}}{2}\right)\ln\left(\frac{1+\mathrm{x}}{\mathrm{x}}\right)\right]\right\}^{-1}. \tag{4.3}$$

Here r_0=(1-γ)/(1+γ) is the diffuse reflectance and $\gamma = \sqrt{1-w}$ is the albedo factor (Hapke 2002). The variable *w* is the single scattering albedo (SSA), and for a closely packed medium is

$$w = Q_s = S_e + (1 - S_e)\frac{(1 - S_i)}{1 - S_i\Theta}\Theta. \tag{4.4}$$

In Equation 4.4, Θ is the internal transmission factor, such that

$$\Theta = \frac{r_i + \exp\left(-\sqrt{\alpha(\alpha + \mathcal{s})}\langle D\rangle\right)}{1 + r_i\exp\left(-\sqrt{\alpha(\alpha + \mathcal{s})}\langle D\rangle\right)}, \tag{4.5}$$

$\langle D\rangle$ is the effective grain size, or the path length traveled by light through a particle, $\mathcal{s}$ is the internal scattering factor, and $\alpha = 4\pi k/\lambda$ is the absorption coefficient. In Equation 4.4, S_i and S_e are the Fresnel reflectance coefficients integrated over all angles and can be approximated by

$$S_i \approx 1.014 - \frac{4}{n(n+1)^2} \text{ and} \tag{4.7}$$

$$S_e \approx \frac{(n-1)^2 + k^2}{(n+1)^2 + k^2} + 0.05. \tag{4.8}$$

The constant, *K*, is the porosity factor (Hapke 2008). For equant particles,

$$K = -\ln\frac{\left(1 - 1.209\phi^{(2/3)}\right)}{1.209\phi^{(2/3)}}, \tag{4.9}$$

where $\phi = 1 - P$ is the filling factor, and *P* is the porosity. Due to a large degree of uncertainty in the value of ϕ, *K* it is initially set to 1 for the purpose of this work. However, porosity effects can significantly change the reflectance properties of a medium. If porosity effects are not accounted

for explicitly, the calculated value of k may be too small by as much as a factor of 2 (Hapke 2012). Therefore, this term is included in the equations and the errors associated with k are assumed to be overshadowed by the effect of the filling factor.

Strictly speaking, what is measured in a bidirectional reflectance experiment is not the ratio of the radiance to the irradiance, I/J, as is the definition of Equation 4.1, but the radiance I. The following derivation is adapted from Piatek (2003).

Let the area of the sample illuminated by the source be Ab. When the source is not normal to the sample, the illuminated area will be stretched by incidence angle μ_0, such that $I=J*Ab/\mu_0$. Similarly, if the detector, which can be assumed to be sensitive only to light from the source (even if it 'sees' a greater area of the sample) is not normal to the sample, it will 'see' an area that is stretched by emission angle μ, such that $I=J*r(i,e,g)*\mu$. Combining terms, you get

$$I(i,e,g) = J * \frac{Ab}{\mu_0} * \mu * r(i,e,g) = JAb * \frac{\mu}{\mu_0} * r(i,e,g). \tag{4.10}$$

The term JAb cannot be explicitly calculated. However, in a bidirectional reflectance experiment, each measurement is referenced to a standard. The same procedure would show that the radiance of the standard is

$$I(i',e',g') = JAb * \frac{\mu'}{\mu_0'} * r(i',e',g'). \tag{4.11}$$

The quantity actually recorded by the spectrometer is then

$$\frac{I(i,e,g)}{I(i',e',g')} = \frac{\frac{\mu}{\mu_0} * r(i,e,g)}{\frac{\mu'}{\mu_0'} * r(i',e',g')}. \tag{4.12}$$

Here we have to make a choice of how to deal with the standard. A primary assumption in the literature (Mustard and Pieters 1987; Lucey 2004; Dalton and Pitman 2012) is that commercially

available calibrated Spectralon standards are Lambertian scatterers. Although this may be true for hemispherical reflectance experiments (the calibration file for Spectralon is in hemispherical reflectance), it is not true for bidirectional reflectance (**Figure 4-2**; Piatek, 2003). Therefore, the standard is treated as an isotropic scatterer, i.e., setting $p(g)$=1. Now, substituting in values for r, and r', and still assuming that $B(g)$=0, we get

$$\frac{I(i,e,g)}{I(i',e',g')} = \frac{\frac{\mu}{\mu_0}\left[\frac{w}{4\pi}\frac{\mu_0}{\mu_0+\mu}(p(g)+H(\mu_0)H(\mu)-1)\right]}{\frac{\mu'}{\mu_0{}'}\left[\frac{w'}{4\pi}\frac{\mu_0{}'}{\mu_{0'}+\mu'}(H(\mu_0{}')H(\mu')-1)\right]} \tag{4.13}$$

$$= \frac{\left[\frac{w}{4\pi}\frac{\mu}{\mu_0+\mu}(p(g)+H(\mu_0)H(\mu)-1)\right]}{\left[\frac{w'}{4\pi}\frac{\mu'}{\mu_{0'}+\mu'}(H(\mu_0{}')H(\mu')-1)\right]}. \tag{4.14}$$

Because the sample was calibrated at each phase angle, i=i' and e=e' for our experiments. However, this is not required should a single calibration be used for multiple measurements.

The single scattering albedo for Spectralon can be quickly determined using the calibration data supplied by the manufacturer and a minimization code in Matlab, since the hemispherical reflectance is simply r_h=1-$\gamma H(\mu_0{}^*)$ (Hapke 2002; Piatek 2003). Equation 4.14 is the relationship used in all of our programs (thus assuming K =1). The above derivation assumes that ambient light does not contribute to light recorded by the detector. This is a valid assumption for our experiment since spectra are acquired in the absence of ambient light.

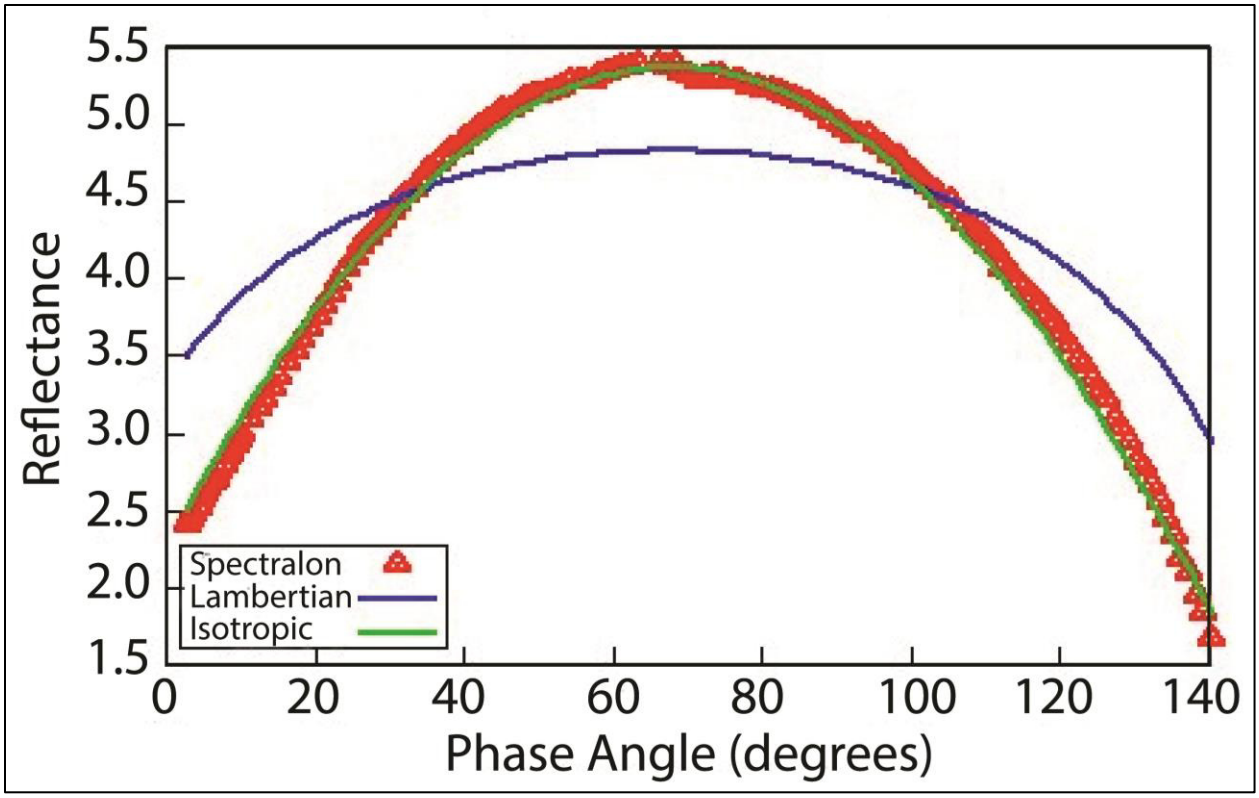

Figure 4-2. Phase curve for Spectralon reflectance standard, taken on a short arm goniometer with an incidence angle of 60º. Reference curves for a Lambertian and an isotropic scatterer show that Spectralon is an isotropic scatterer when used in a bidirectional reflectance experimental setup. Figure reproduced from Piatek (2003). Data are shown as absolute reflectance.

4.2.4 Program Description

The variable or unknown quantities in the above series of equations are the apparent grain size,$\langle D \rangle$, the internal scattering parameter, s, the phase function coefficients, b and c, and, of course, the wavelength dependent real and imaginary indices of refraction, n and k. When dealing with a single phase angle of a single grain-size, the radiative transfer problem is under-determined. However, solving simultaneously for multiple size fractions and/or multiple phase angles results in an over-determined problem, for which all variables can be calculated. The code is split into three routines, which are run iteratively (**Figure 4-3**)—one that determines k from

three mineral size fractions, one that determines n from k, and one that calculates appropriate phase function coefficients. The code is split in this way because a too highly over-determined problem can suffer from non-uniqueness of fit.

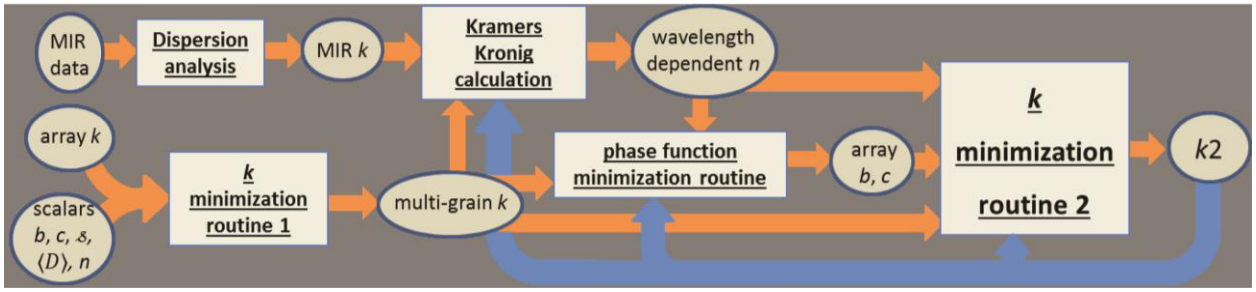

Figure 4-3. Flow chart of calculations performed by this suite of programs. The sequence starts after k has initially been determined by the lookup table program for individual grain sizes.

Each VNIR spectrum was smoothed once using a moving average low pass filter and then run through a Matlab encoded program following the method of previous workers (Lucey 1998; Quinn 2010; Quinn et al. 2010). This code first calculates the imaginary index of refraction, k, for each grain size individually, by assuming a constant real index of refraction, n, over the VNIR wavelength range, as well as fixed guesses for b, c,$\langle D \rangle$, and $\mathcal{s}$ (initial guesses for b and c were taken from Mustard and Pieters (1989),$\langle D \rangle$ was assumed to be the smallest size in the distribution, and $\mathcal{s}$ was initially set to zero). The code then matches the radiance coefficient at each wavelength to a value in a look-up table and delivers the associated k. This routine is used to get a reasonable first guess for k.

The second step uses Matlab's lsqcurvefit minimization routine with a multistart protocol (where the code randomly generates multiple start points for all variables) to find a single k for three grain-sizes simultaneously while also solving for b, c,$\langle D \rangle$, and $\mathcal{s}$ within user specified

bounds. Lsqcurvefit is a least squares minimization routine appropriate for use on non-linear equations (Coleman and Li 1994). The program finds the array of values, x, that minimizes the difference between the experimental data and the modeled data within user specified constraints. The multi-start protocol is used to ensure that global rather than local minima are obtained. Bounds for b and c were modified from Mustard and Pieters (1989),$\langle D \rangle$ was allowed to vary from 1/3 the smallest value of the grain size range to the highest value in the grain size range, s was allowed to vary between 0.0 and 0.08 μm^{-1}. Since k is, by definition, grain-size independent, this procedure provides better accuracy in solving for k than solving for each grain-size individually and then averaging them together. For this first pass, n, b, and c are considered scalars.

Once a multi grain-size k has been determined, it is used to determine a wavelength dependent n using a singly subtractive Kramers Kronig (SSKK) transformation (Lucarini et al. 2005). For a frequency v,

$$n(v) = n_1 + \frac{(v^2 - v_1^2)}{2\pi} P \int_0^\infty \frac{v' k(v')}{(v'^2 - v^2)(v'^2 - v_1^2)} dv'. \tag{4.15}$$

Here, n_1 is the real index of refraction at a known point, v_1, and v' is a dummy variable for integration. For n_1, average literature values of n in the visible (sodium D line: 0.16970 cm^{-1} or 0.58929 μm) are used. The P in front of the integral indicates that the Cauchy principle value of the integral must be taken. Where the integral is defined, the Cauchy principle value is simply the value of the integral. When the integral diverges (as is the case when either parenthetical expression in the denominator is zero), the Cauchy principle value defined as (Mauch 2004)

$$P \int_a^b f(x)dx = \lim_{\epsilon \to 0^+} \left(\int_a^{x_0 - \epsilon} f(x)dx + \int_{x_0 - \epsilon}^b f(x)dx \right). \tag{4.16}$$

Since measured spectra are not continuous, but rather a collection of values at closely spaced intervals, the data are integrated by section using a Simpson's rule approximation. The code first converts wavelength to frequency and re-interpolates to an equi-spaced array (5.913 cm^{-1} spacing). Each segment is assumed to have a constant k, and the bounds of integration are set so that the known k is at the midpoint of the range. The segments are subdivided 1000 times to produce a 0.0059 cm^{-1} mesh, and the Simpson's rule approximation is applied. Around the singularities, the spacing is 0.003 cm^{-1}. Integration done in this way avoids adding errors encountered from the singularities. An SSKK transformation ideally requires a much larger data set than is typically available. Therefore, MIR k values, which are estimated from Lorentz-Lorenz dispersion analysis (Glotch and Rossman 2009), are used to extend the range for a more convergent solution.

Once a wavelength-dependent n is determined, the spectra for all phase angles are run through a phase function program to determine wavelength dependent b, and c. This code also uses Matlab's lsqcurvefit program with a multi-start protocol to simultaneously minimize the difference between the modeled fit and the data for all phase angles of all grain sizes. The code first creates a coarse data set (0.05 μm) spacing, and then finds a single b and c for all grain sizes and all phase angles. All phase angles of each grain size are restricted to have a single $\langle D \rangle$ and s, which are also fit during this process.

Finally, n, b, and c are used as fixed arrays to minimize for a new k using the k minimization routine, followed by the SSKK routine, and then the phase function program, until values for k, n, b, and c do not vary. In practice, this takes an additional one to two iterations.

4.3 Results

The jarosites synthesized in this study are shown in **Figure 4-4**, and XRD analyses are shown in **Figure 4-5**. Hydronium jarosite grows as euhedral crystals with smooth faces but with deep cracks, which may propagate through the crystals. Sodium jarosite shows a great deal of pitting. Potassium jarosite seems to start as a finer-grained precipitate that then anneals to form larger grains, leading to surface roughness. Hydronium jarosite is the easiest of the three to synthesize as a coarse-grained sample whereas sodium jarosite is the most difficult and took many attempts. The VNIR spectra for hydronium, sodium, and potassium jarosite are shown in **Figure 4-6a**, **Figure 4-6b**, and **Figure 4-6c**, respectively. For each sample, the coarsest size fractions have the lowest overall albedos and the finest size fractions have the highest overall albedos. This trend is consistent with what is expected for VNIR spectra of powdered minerals of different size fractions. The MIR spectra of pressed pellets of the <45 μm size fraction of each jarosite are shown in **Figure 4-7**.

Figure 4-8a, **Figure 4-8b**, and **Figure 4-8c** show the final values of wavelength dependent variables for hydronium, sodium, and potassium jarosite, respectively. The grain-size independent imaginary index of refraction, k, for each sample is plotted at the top of each figure. The grain-size independent real index of refraction, n, is plotted in the middle of each figure. And the value of $p(g)$ vs. wavelength for g=30º is plotted at the bottom of each figure. The other minimized parameters (s and $\langle D \rangle$) are listed in Table 1.

Figure 4-9 shows the modeled spectra derived from using the grain-size independent values to produce grain-size specific VNIR spectra. The modeled results are overlaid on laboratory reflectance spectra.

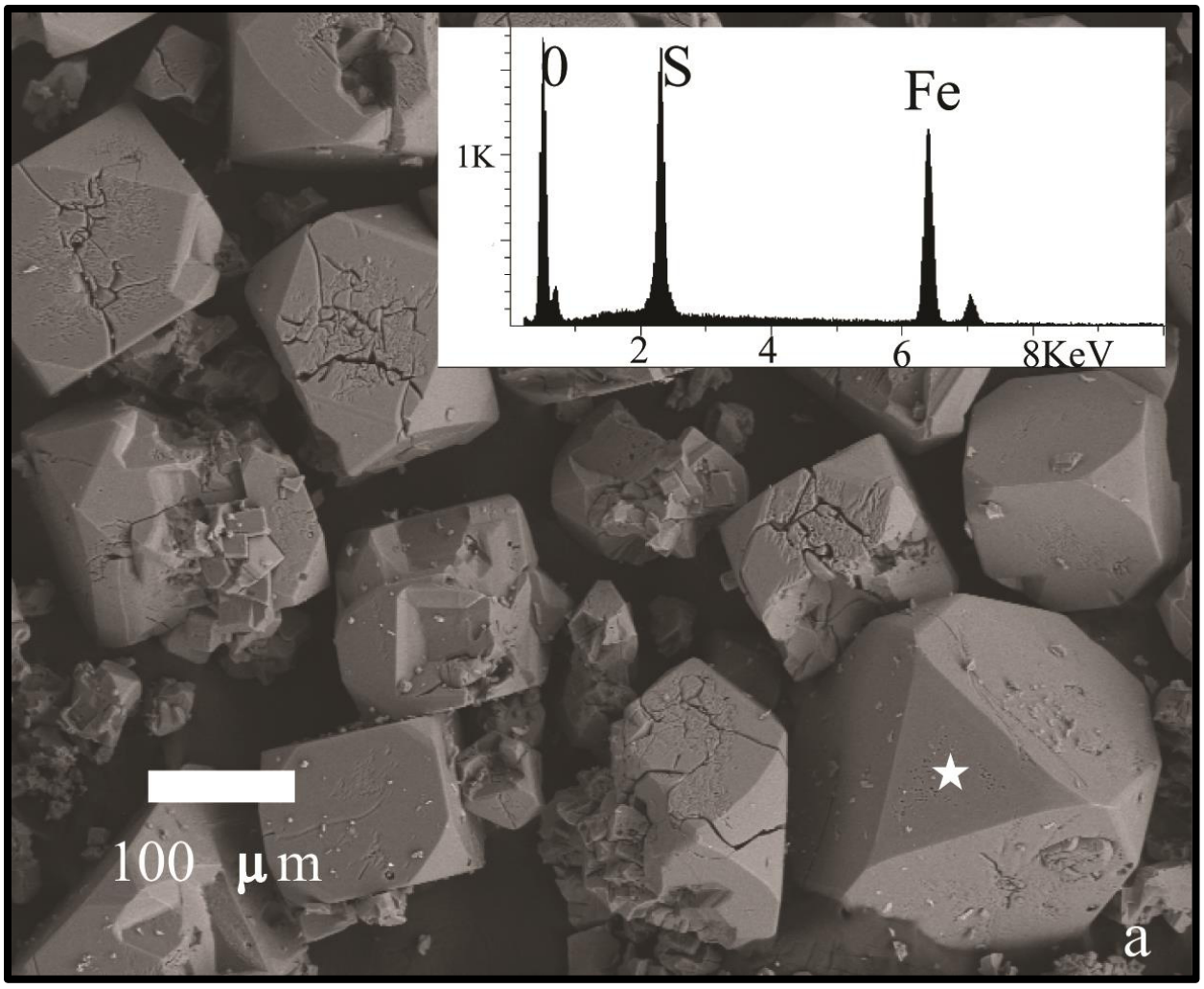

Figure 4-4a. SEM image of hydronium jarosite. EDS insets show the chemical composition of the point indicated.

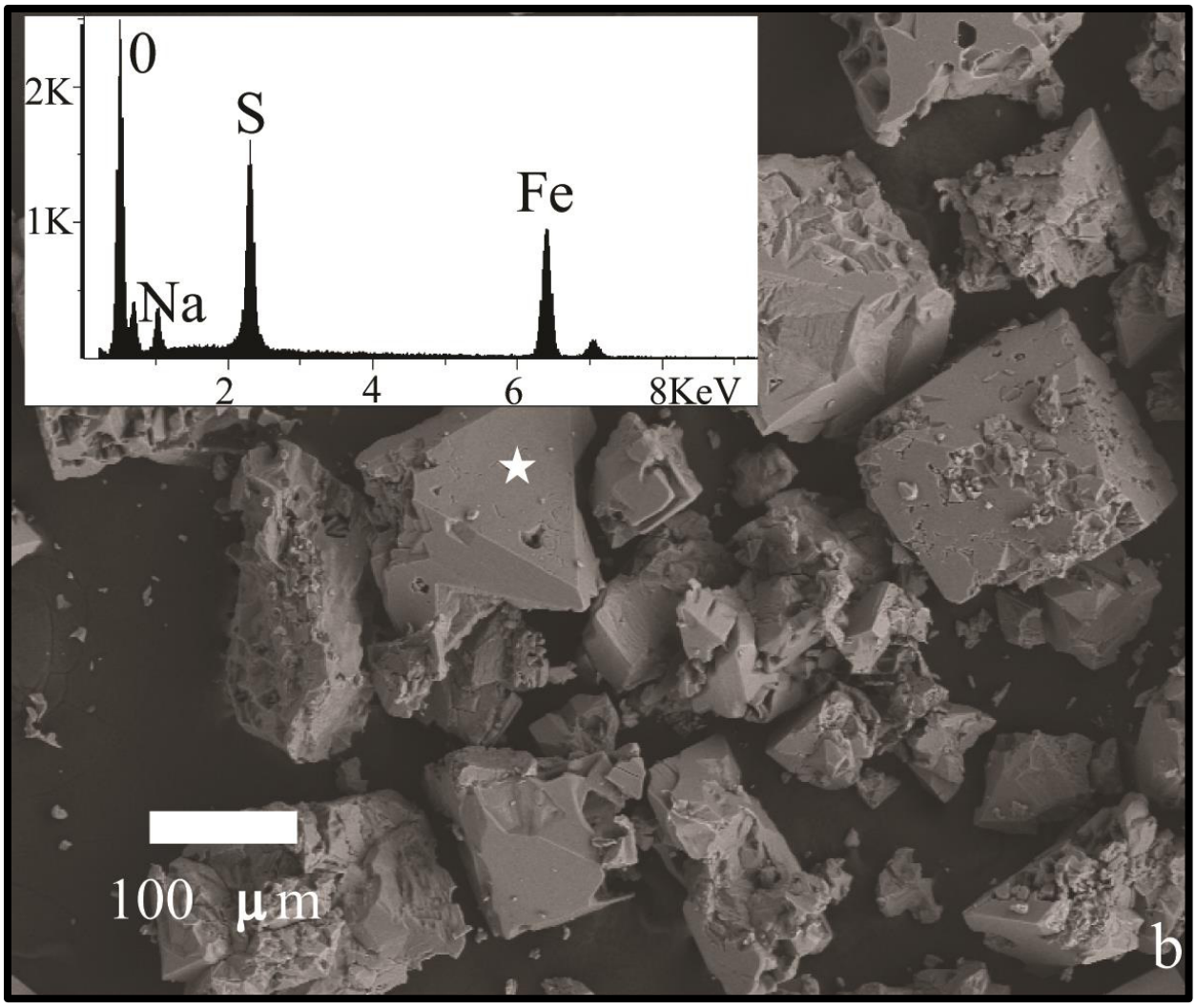

Figure 4-4b. SEM image of sodium jarosite. EDS insets show the chemical composition of the point indicated.

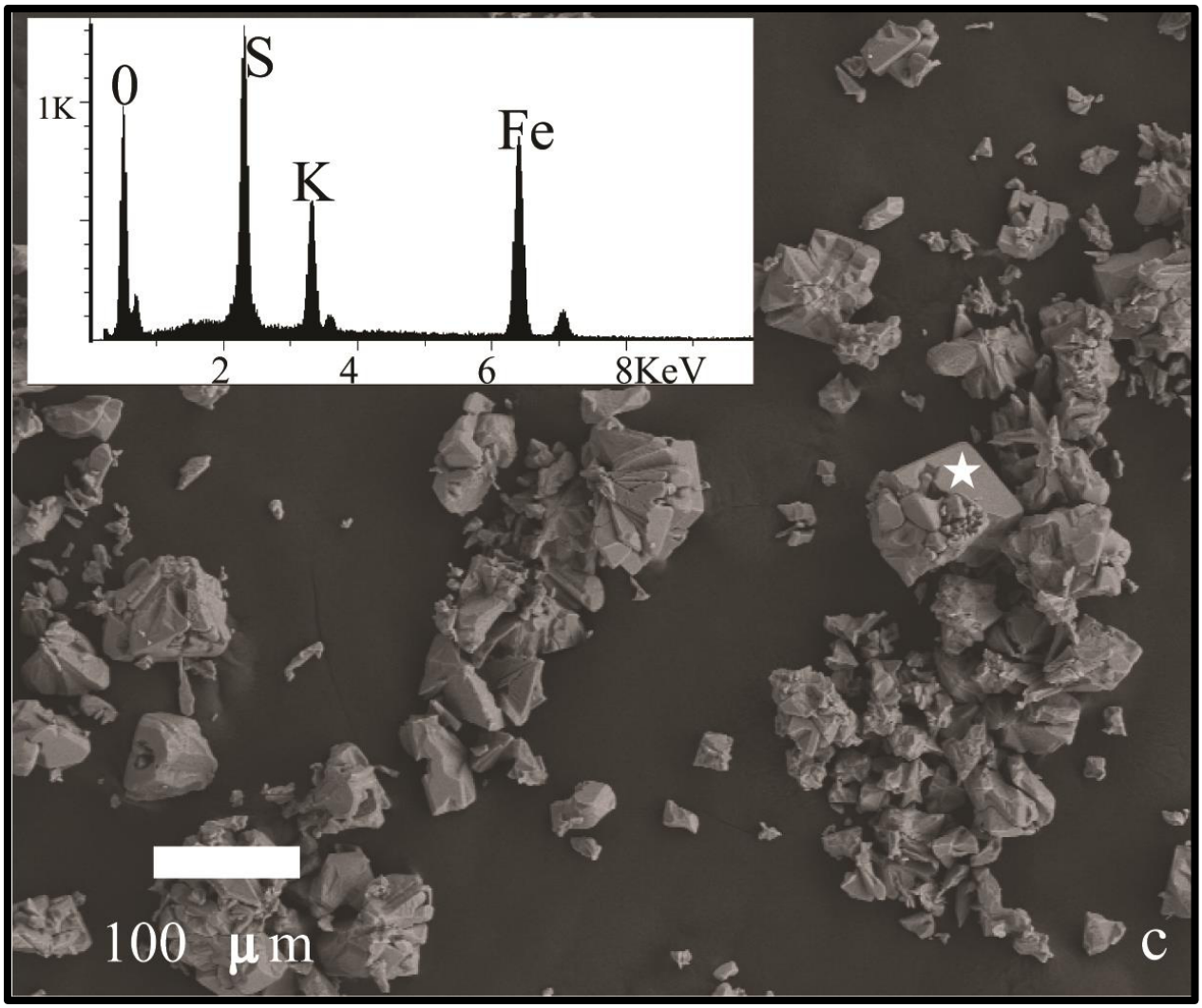

Figure 4-4c. SEM image of potassium jarosite. EDS insets show the chemical composition of the point indicated.

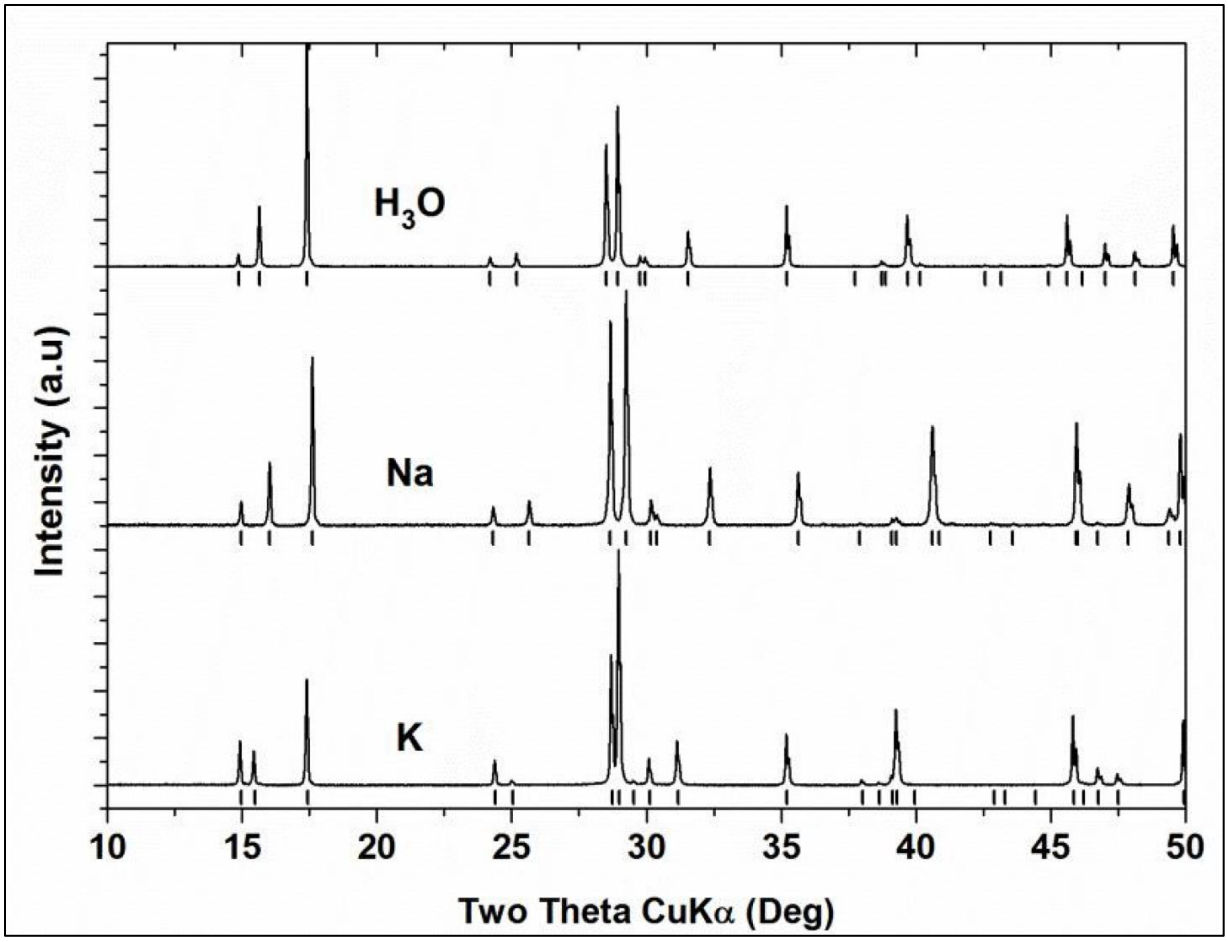

Figure 4-5. XRD patterns for hydronium (top), sodium (middle), and potassium (bottom) jarosite. Literature values are represented by ticks underneath each plot. All samples are phase pure.

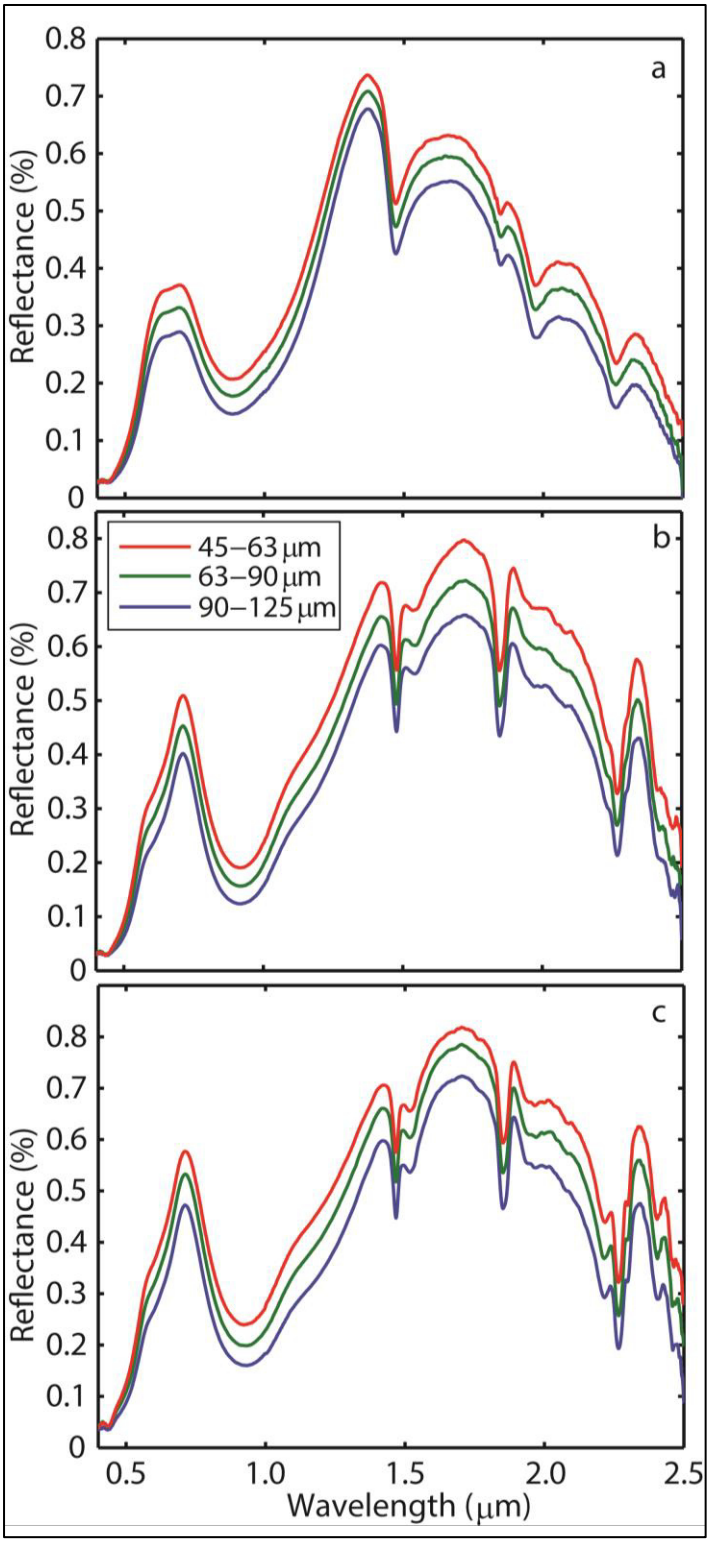

Figure 4-6. VNIR spectra of hydronium (a), sodium (b), and potassium (c) jarosite. Spectra for 45-63 μm, 63-90 μm, and 90-125 μm size fractions are shown for each sample.

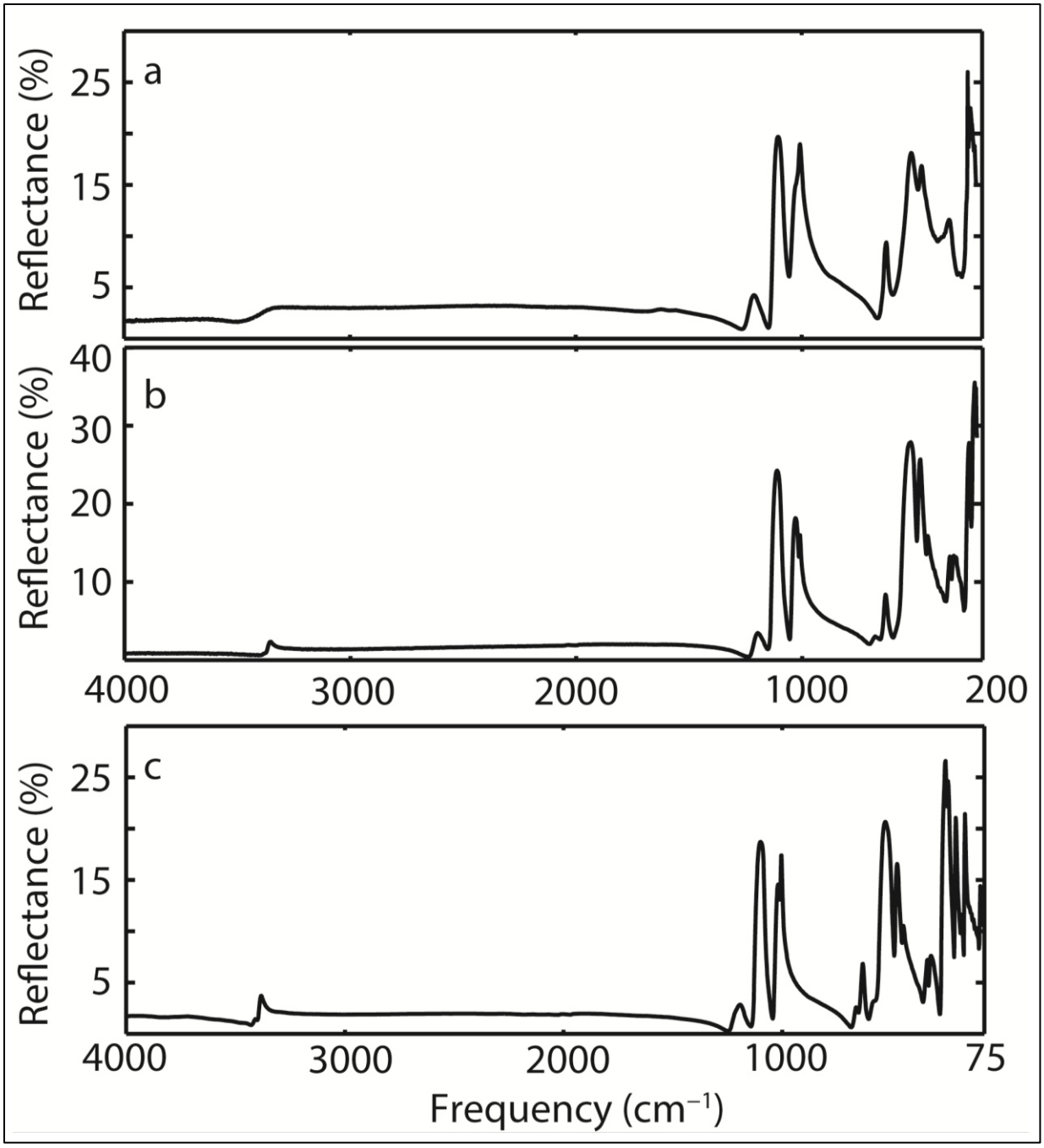

Figure 4-7. MIR data for hydronium jarosite (a) and sodium jarosite (b). MIR and FIR data for potassium jarosite (c).

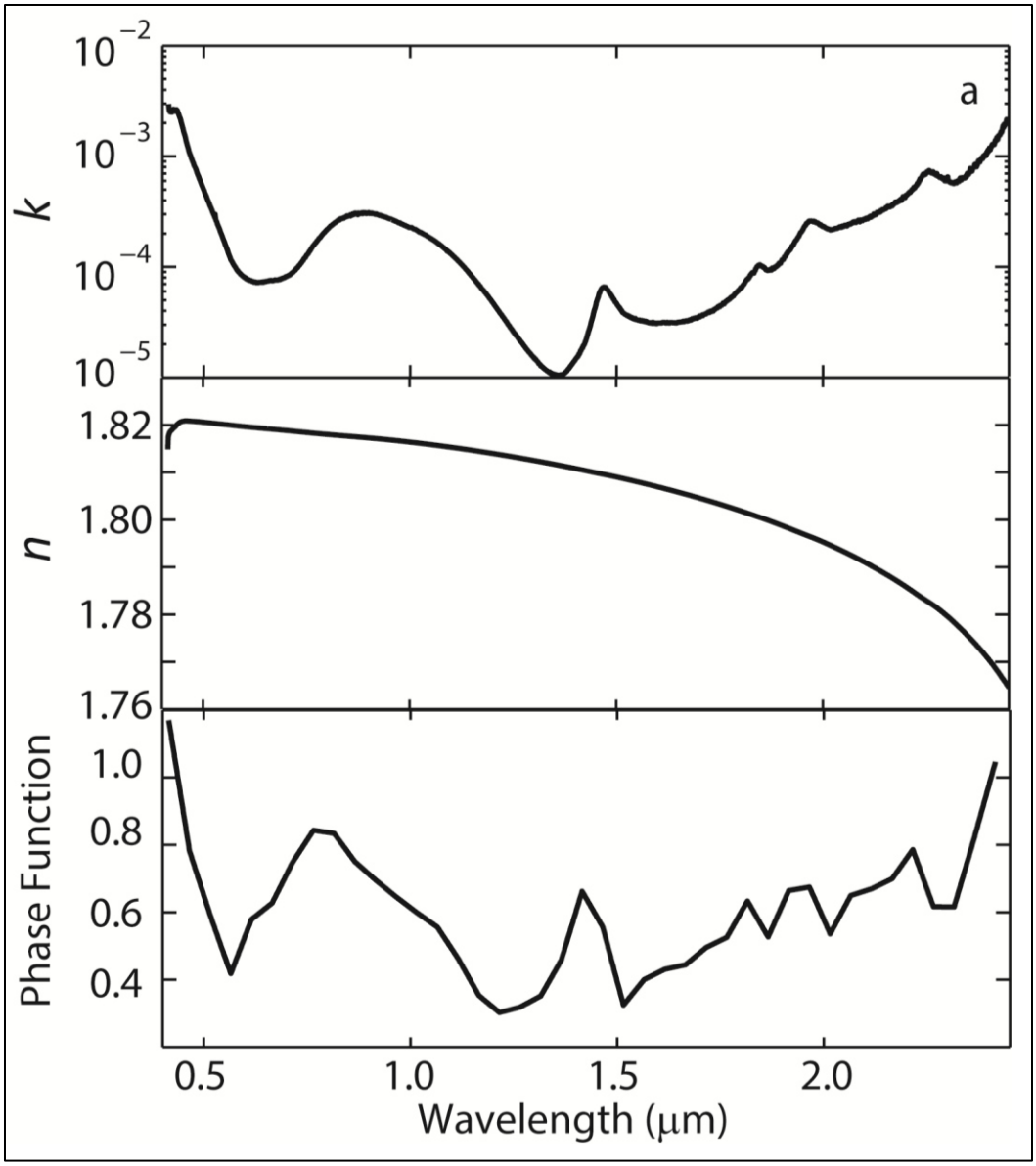

Figure 4-8a. Wavelength dependent variables for hydronium jarosite. The grain-size independent imaginary index of refraction, *k*, for each sample is plotted at the top, the grain-size independent real index of refraction, *n*, is plotted in the middle, and the value of *p*(*g*) vs. wavelength for *g*=30° is plotted at the bottom.

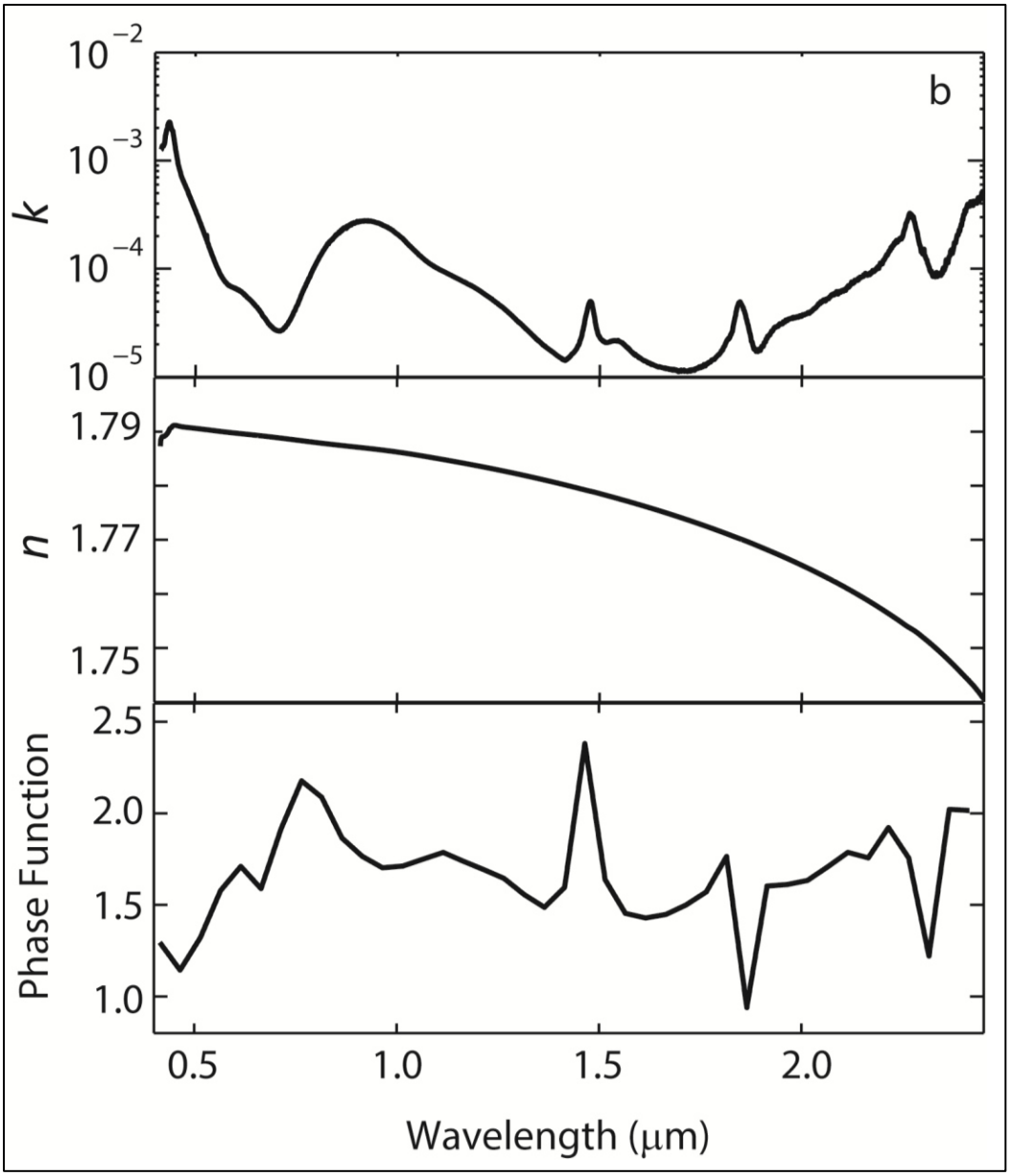

Figure 4-8b. Wavelength dependent variables for sodium jarosite. The grain-size independent imaginary index of refraction, *k*, for each sample is plotted at the top, the grain-size independent real index of refraction, *n*, is plotted in the middle, and the value of *p*(*g*) vs. wavelength for *g*=30° is plotted at the bottom.

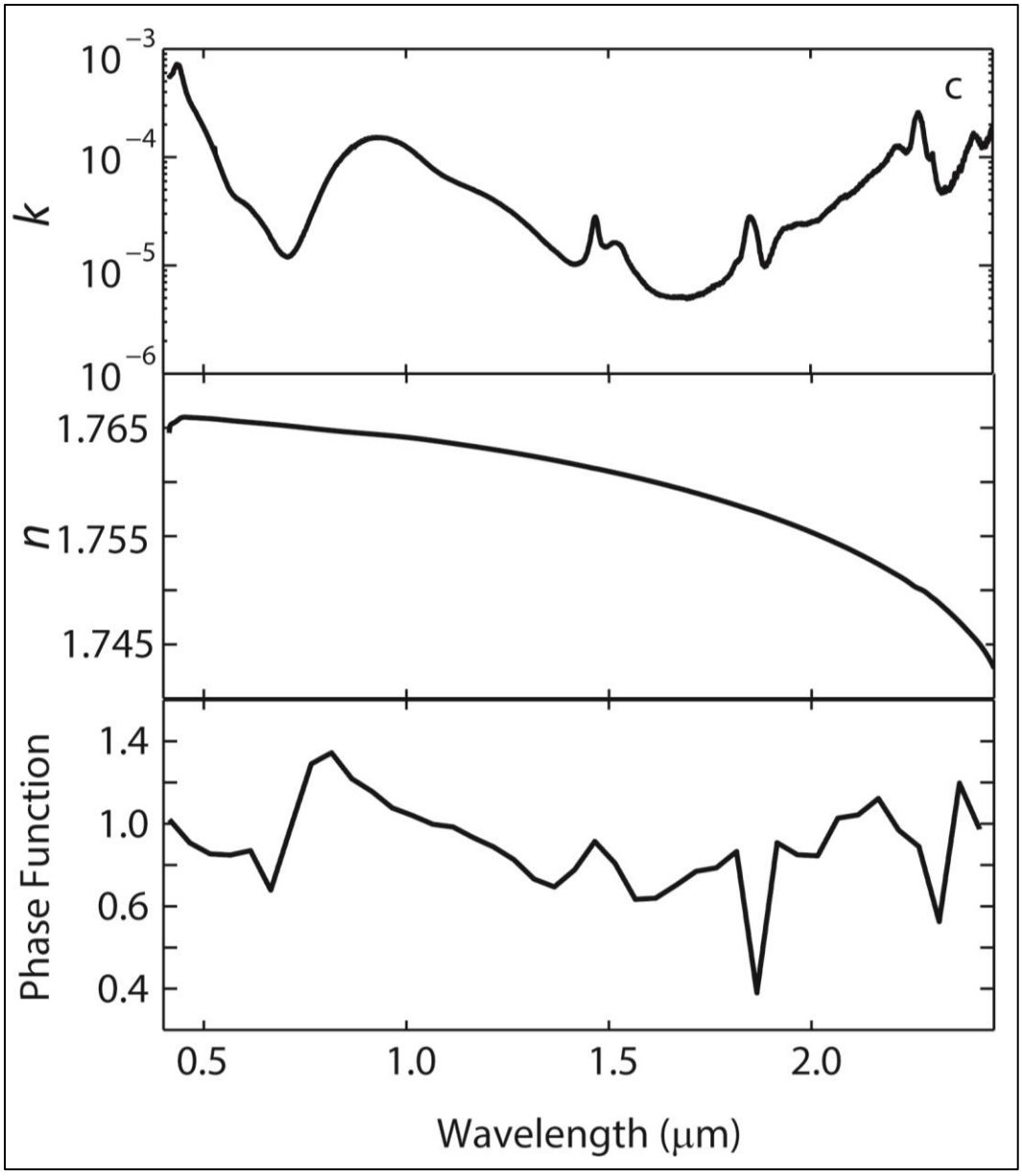

Figure 4-8c. Wavelength dependent variables for potassium jarosite. The grain-size independent imaginary index of refraction, *k*, for each sample is plotted at the top, the grain-size independent real index of refraction, *n*, is plotted in the middle, and the value of *p*(*g*) vs. wavelength for *g*=30° is plotted at the bottom.

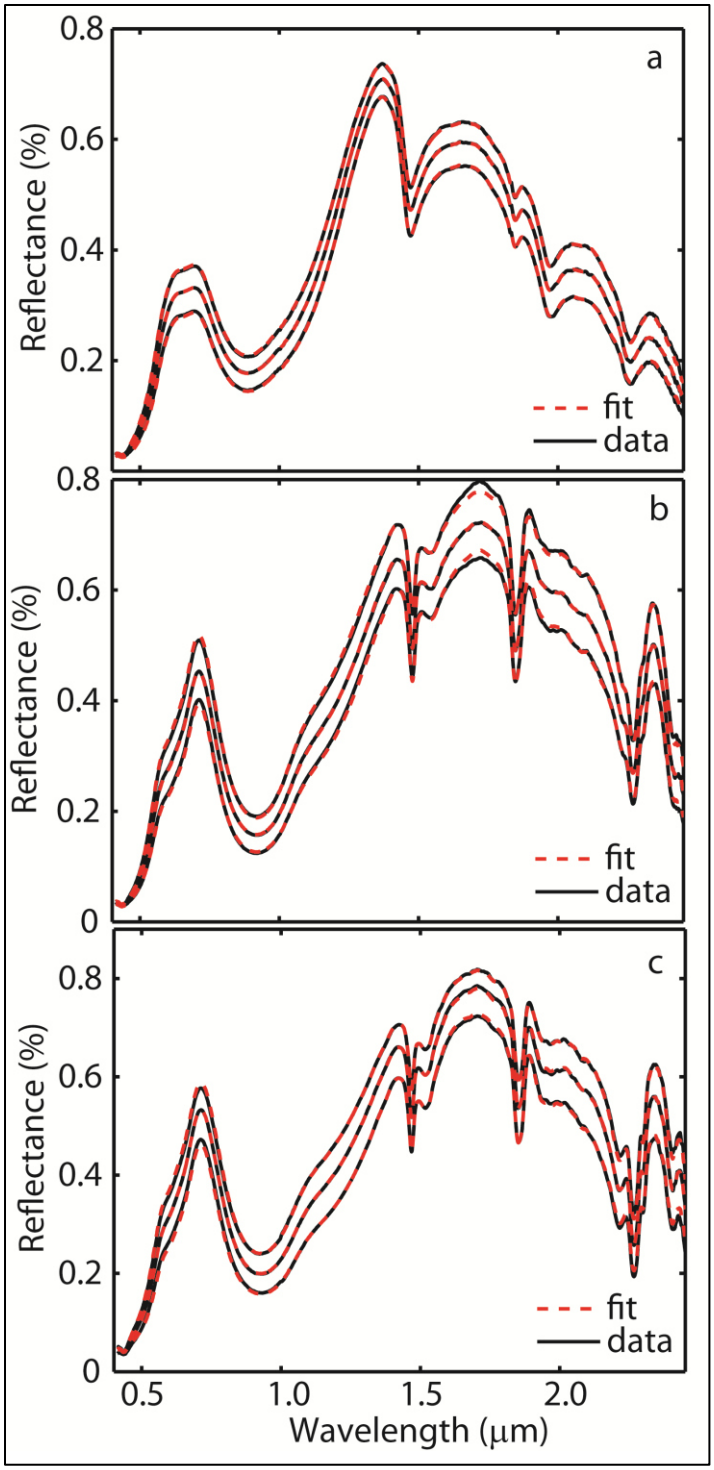

Figure 4-9. Modeled fits produced from multi gain-size *k* values for all three grain sizes of hydronium (a), sodium (b), and potassium (c) jarosite. For each sample, the 45-63 μm spectrum is on top, the 63-90 μm spectrum is in the middle, and 90-125 μm spectrum is on the bottom.

Table 4-1. Values of the near-surface scattering factor, s, and the apparent grain size, ⟨D⟩ delivered in the final minimiztion. All values are given in microns.

	H-Jar	Na-Jar	K-Jar
s 45-63	10^{-17}	0.04	10^{-14}
s 63-90	0.04	0.06	0.08
s 90-125	0.04	0.07	0.05
⟨D⟩ 45-63	20.5	59.8	51.0
⟨D⟩ 63-90	26.7	89.3	72.9
⟨D⟩ 90-125	35.6	125.9	112.8

The MIR indices of refraction derived from the application of a Lorentz-Lorentz dispersion analysis are shown in **Figure 4-10**. The top pane of each plot shows the fit overlaid on the laboratory spectrum. Recall that since the MIR data were acquired from powder pressed into pellets, these values are likely off by a factor of ~2 from those that would be modeled from polished single crystal specimens (Pecharroman et al. 1995).

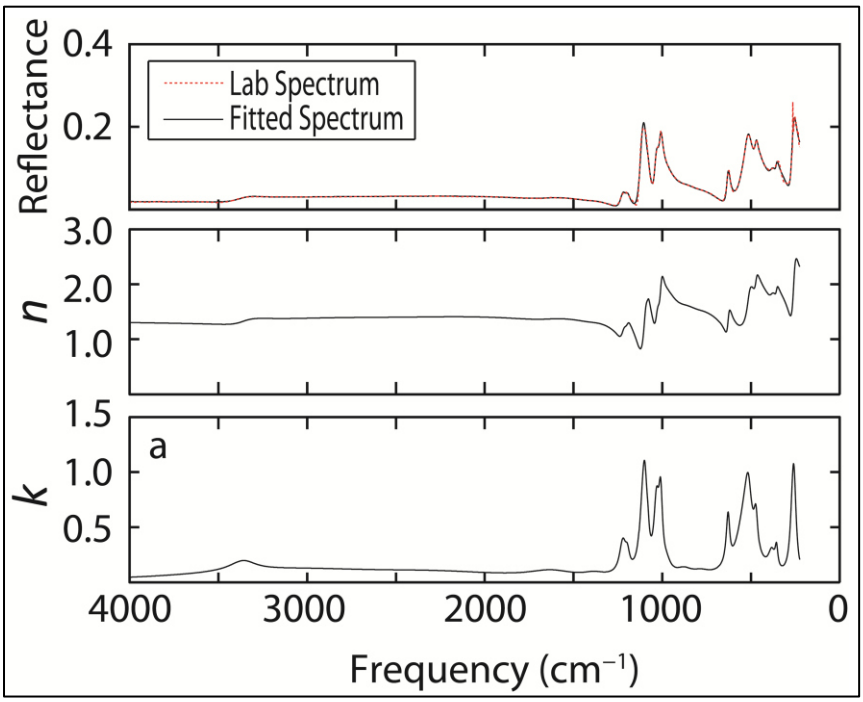

Figure 4-10a. MIR optical constants for hydronium jarosite. The modeled fit for each sample is shown in the top pane with the laboratory spectrum.

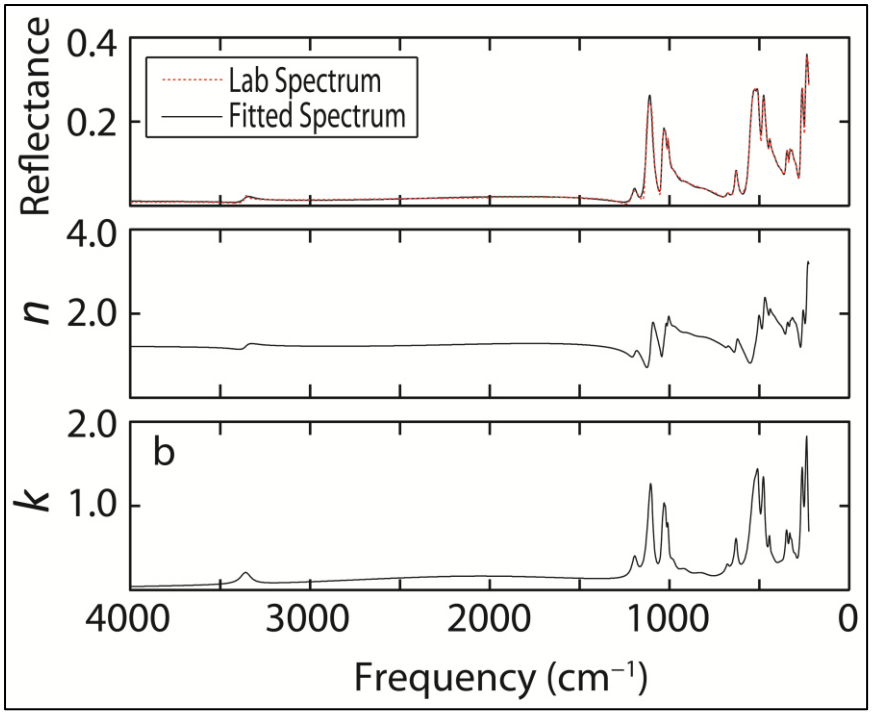

Figure 4-10b. MIR optical constants for sodium jarosite. The modeled fit for each sample is shown in the top pane with the laboratory spectrum.

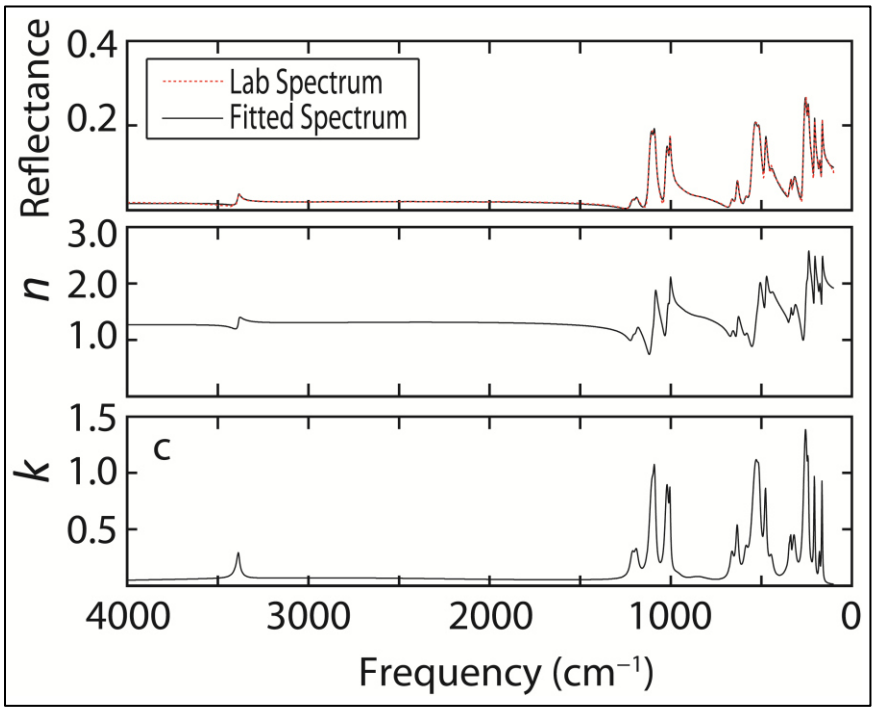

Figure 4-10c. MIR optical constants for potassium jarosite. The modeled fit for each sample is shown in the top pane with the laboratory spectrum.

4.4 Discussion

It must not be taken for granted that values obtained by this type of modeling are simply the number or numbers that create the closest numerical match between the modeled fit and the laboratory data. The goodness of fit between the model and the data is often, but not always, a sign of how well the theory represents the real system. In the case of optical constant determination, a perfect match between the model and the data can be obtained for a variety of solutions. This is because, depending on the configuration of the code, the problem is either under-determined (not enough constraints for the number of data points) or over-determined (more data points than parameters that constrain them). The seeming complexity of the procedure used for this study seeks to balance these two cases in order to maximize the probability of reaching a real and unique solution. Here, I discuss and justify these choices.

4.4.1 Lookup Table Approach

The under-determined case occurs when k is obtained from a single grain-size spectrum at a single phase angle. Here, b, c, s, and $\langle D \rangle$, along with the array, k, are variables. This creates a system of linear equations the length of the data set (N), but with N+4 unknowns. Historically, the most efficient method for dealing with this problem has been to make three simplifying assumptions. First, that the surface is made up of isotropic scatterers, thus removing the phase function coefficients b and c from consideration. Second, s is fixed at near zero. And third, $\langle D \rangle$ is specified based on prior knowledge or reasonable assumptions. In this case, a table can be created of modeled values calculated from a range of k values over the span of wavelengths. Each data point is matched to a value in the table, thus providing a specific k for each wavelength. If we assume knowledge of b and c, a similar table can be produced for the non-

isotropic case. This "lookup table" approach is, indeed, how the first approximation of k is derived.

Determining k in this fashion does not provide any means for verifying the solution. Since, however, k is a fundamental property of the material, it is, by definition, grain-size independent. Therefore, previous authors have constrained k either by averaging the k values for samples of multiple grain-sizes or by adjusting $\langle D \rangle$ so that k for multiple grain sizes fall closer to the mean (Lucey 1998; Roush et al. 2007). Minimization routines, like the one used in this study, allow for the simultaneous fitting of multiple data sets to determine a single array for k. **Figure 4-11** compares the "best fit" (minimum deviation between model and data) k obtained from the multi-minimization routine with k values obtained from "lookup tables" for both the isotropic case and the case where b and c are held fixed. Both "lookup table" k values shown are averages of the three grain sizes. **Figure 4-11** shows that the k curve produced in the multi-minimization routine is not the same as the average of the grain-size dependent k curves for the other cases. So, while both methods attempt to create a unique solution through the use of multiple grain sizes, the multi-minimization routine is more likely to converge more closely to the true unique solution because the grain-sizes constrain k during the fitting process.

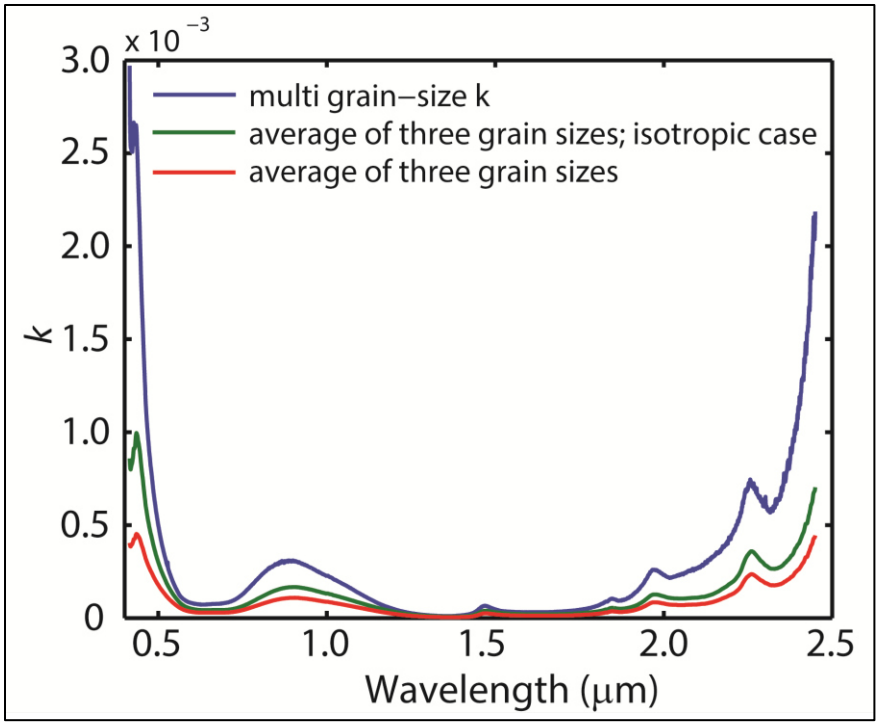

Figure 4-11. Imaginary index of refraction *k*, calculated for hydronium jarosite under three conditions: 1) simultaneous minimization to get a single *k* for three grain sizes, while solving for *b*, *c*, *s*, and ⟨D⟩ (blue); 2) assuming an isotropic phase function, then using a lookup table to find *k* for each grain size, assuming knowledge of *s* and ⟨D⟩, and then averaging the results (green); 3) the same as the isotropic case except assuming forward scattering phase function coefficients (Mustard and Pieters 1989) (red). The three cases do not produce equivalent results for this sample.

4.4.2 Shkuratov approach

Determining *k* using Shkuratov's formulation (Shkuratov et al. 1999) does not suffer from this non-uniqueness problem. Since the only free parameters for the Shkuratov method are the optical constants, *n* and *k*, the porosity *q* and the average path length of light before reflection, *S* (Shkuratov et al. 1999), there can be only one solution for *k* for a single *S* and *q*. Actually, Shkuratov et al. (1999) found that value of *k* is only mildly dependent upon *q*, so each *k* is primarily dependent on *S*. But the parameter *S* in the Shkuratov model is equivalent to ⟨*D*⟩ in the Hapke model. So, *k* in the Shkuratov model is necessarily grain size dependent. In other words, it

is mathematically impossible for *k* to be the same for multiple grain sizes using that model unless it is assumed that the path-length of light in all grain sizes is the same. While it is understood by users of this model that *k* is, by definition, grain size independent, final *k* values are typically determined by averaging multiple *k* values or adjusting other parameters so that *k* falls close to the mean (Roush et al. 2007). However, because I have found that the multi-grain-size *k* is not the average of *k* values determined for the three grain sizes independently, I argue that the optical constant values determined through the Shkuratov model are useful approximations (**Figure 4-12**), but are not the true optical constants of the material.

4.4.3 Phase function

Where the Shkuratov model simplifies calculations by removing dependence of *k* on viewing geometry, the Hapke method utilizes this dependence to further constrain the problem. Measuring each sample over a range of phase angles makes it possible to determine values for *b* and *c*. It is typical to determine a phase function at a single wavelength over a larger continuum of phase space. But since the goniometer and spectrometer used in this study produced full size data sets at each phase angle, and since Matlab's minimization routines can process large data sets, phase function coefficients were determined for the full wavelength range. Introducing an additional 3N variables, however, created a highly over-determined problem that suffered from non-uniqueness of fit.

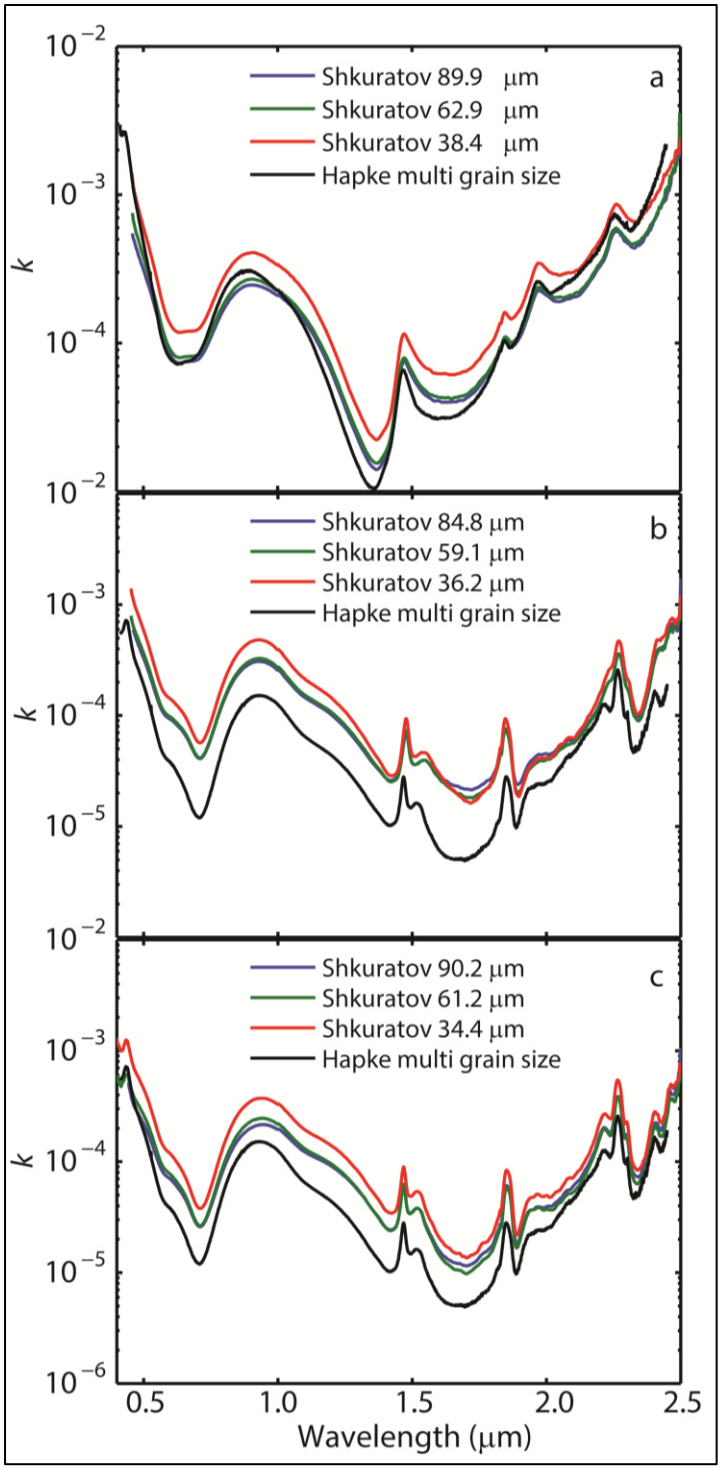

Figure 4-12. Imaginary index of refraction *k* determined using the Shkuratov method vs. the method described in this paper for hydronium (a), sodium (b), and potassium (c) jarosite. The grain size values that produced the best fits using the Shkuratov method are listed in the legends. The final grain sizes determined using this paper's method are listed in Table 4-1.

Our initial tests showed that the phase function does not vary systematically with grain size. Therefore, I made a simplifying assumption that the phase function is the same for all grain sizes. This leaves only s and $\langle D \rangle$ to account for spectral differences associated with grain size. This assumption also addresses the issue of over-determination. The phase function coefficients are optimized for 3 grain-sizes at 7 phase angles for a total of 27 spectra to be modeled from a single phase function coefficient curve. Interestingly, the grain sizes determined during this minimization step are very close to those determined during the k minimization step, demonstrating that a well constrained problem has been created. The measured and modeled spectra for one of these fits are shown in **Figure 4-13**.

The phase function chosen for this work was a two term Legendre polynomial. Although I also investigated the use of both two and three term double Heyney-Greenstein phase functions, the Legendre polynomial provided the only reasonable fits for this system. I recommend that other investigators determine which phase function is best for each individual system as the results may vary.

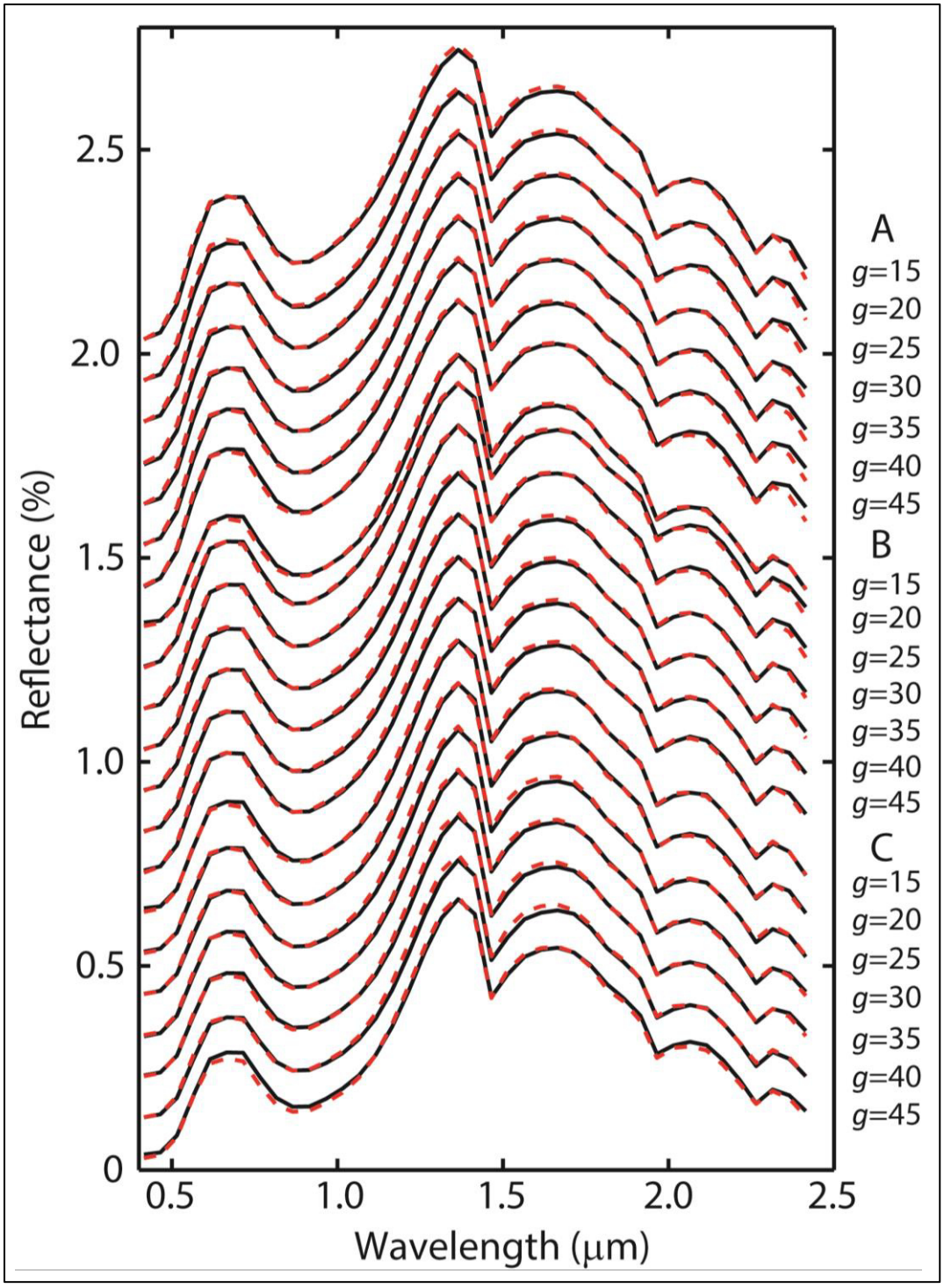

Figure 4-13. Modeled fits and laboratory spectra for hydronium jarosite's phase function minimization. Spectra are offset by 0.1% for clarity. Grain size ranges are grouped, such that 90-125 μm spectra are shown in group A, 63-90 μm in group B and 45-63 μm in group C.

Phase function data collection and the phase function minimization routine have the potential to consume large amounts of laboratory and computation time, respectively. Therefore, I tested several scaled-down procedures to test whether equivalent results could be obtained. An ideal data set for determining the actual phase function for a mineral would contain as wide a range of phase angles as possible. What is determined in this step, however, is probably a combination of phase effect, surface roughness, and shadow hiding. These effects can be explicitly accounted for using a more complicated version of Hapke's treatment (Hapke 2002). It has been shown, however, that these quantities, when solved for explicitly, do not correlate well with the physical property they are meant to describe (Shepard and Helfenstein 2007). Although a portion of the discrepancy experienced by Shepard and Helfenstein (2007) may have been due to the absence of a filling factor coefficient (Hapke, personal communication), it was the goal of this study to find the minimum number of phase angles that could reliably stabilize the results for *k*. A result was sought that accounted for phase, roughness, and shadow hiding, such that the value of *k* obtained in this study was as close to the imaginary index of refraction as possible, while still striving for the simplest experimental and theoretical configuration. I found that fewer phase angles could not produce equivalent results even when they were spaced over the same phase angle range (**Figure 4-14b**). I determined, however, that models utilizing a down-sampled data set ($\Delta\lambda$=0.05 μm) produced almost identical results to a full data set in a fraction of the computational time (**Figure 4-14a**). The derived *b* and *c* values are then re-interpolated to the fine wavelength spacing.

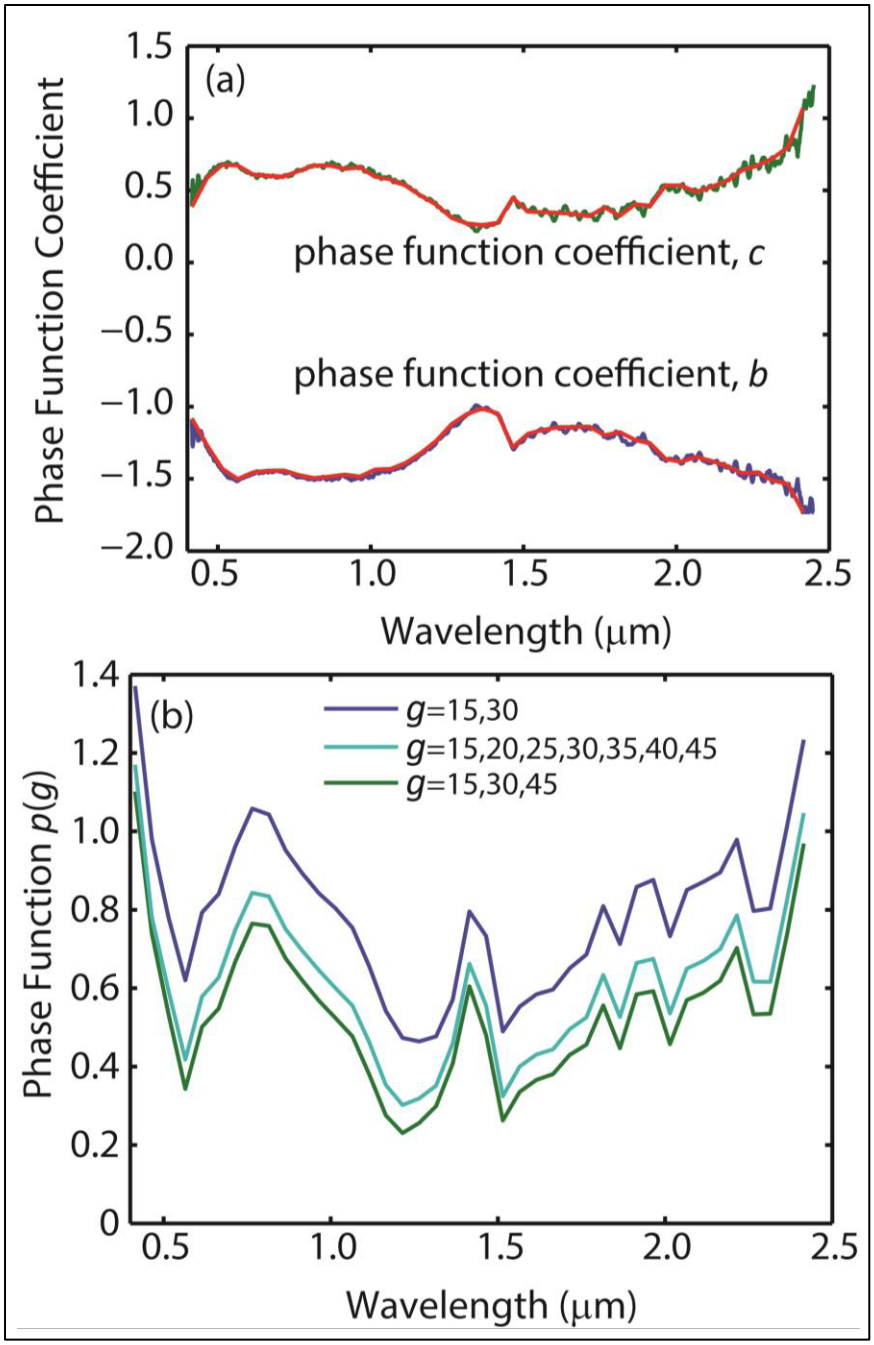

Figure 4-14. (a) P(g) vs. wavelength (calculated for g=30°) for down-sampled data sets (red) plotted with P(g) vs. wavelength (calculated for g=30°) full data set. Using the full data set introduces noise over the primary features. (b) P(g) vs. wavelength (calculated for g=30°) determined using spectra measured at g=15° and g=30° (blue); using spectra measured at g=15°, g=30°, and g=45° data (green); and using spectra measured at g=15°, g=20°, g=25°, g=30°, g=35°, g=40°, and g=45° (cyan). All grain sizes were used for all angles. The results are not equivalent. Spectral data are from hydronium jarosite.

4.4.4 Kramers-Kronig Transformation

The wavelength range of the data set used in this study was chosen based on results for the determination of *n* from *k* using the singly subtractive Kramers-Kronig (SSKK) approach. A Kramers-Kronig transformation ideally requires a data set that spans from 0 to infinity. Since this is not possible with laboratory data, I performed a series of experiments using VNIR data and varying amounts of MIR and FIR data (extending our data set to 25 μm, 50 μm, 75 μm, and 100 μm) to assess results from data sets with limited wavelength ranges. When *k* data for the VNIR and MIR are plotted together (**Figure 4-15**), the difference in magnitude of the two data sets is apparent (*k* in the MIR is orders of magnitude greater than *k* in the VNIR). Therefore, it is clear that including the MIR data in the integration will have a strong influence on the result.

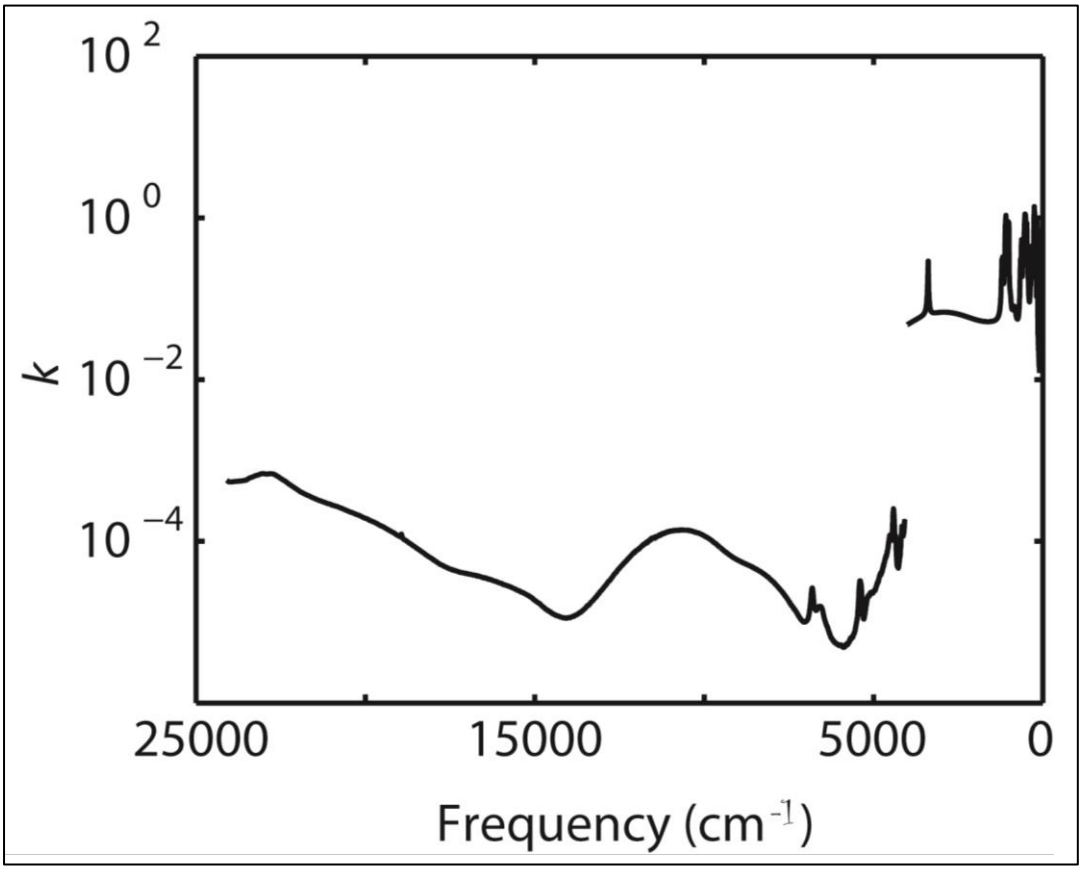

Figure 4-15. MIR and VNIR *k* data plotted for potassium jarosite.

Figure 4-15 shows that there is an offset between the VNIR data and the MIR data. The MIR data is adjusted to overlap with the VNIR data using a simple linear offset plus extrapolation. The result from that procedure is shown in **Figure 4-16**. The continuous slope of the data set supports this type of correction. The corrected and combined *k* values were then run through the SSKK conversion, using data sets ranging from 2.5 to 50 μm (**Figure 4-17**). The VNIR *n* values continue to change substantially for data sets that do not extend to at least 25 μm.

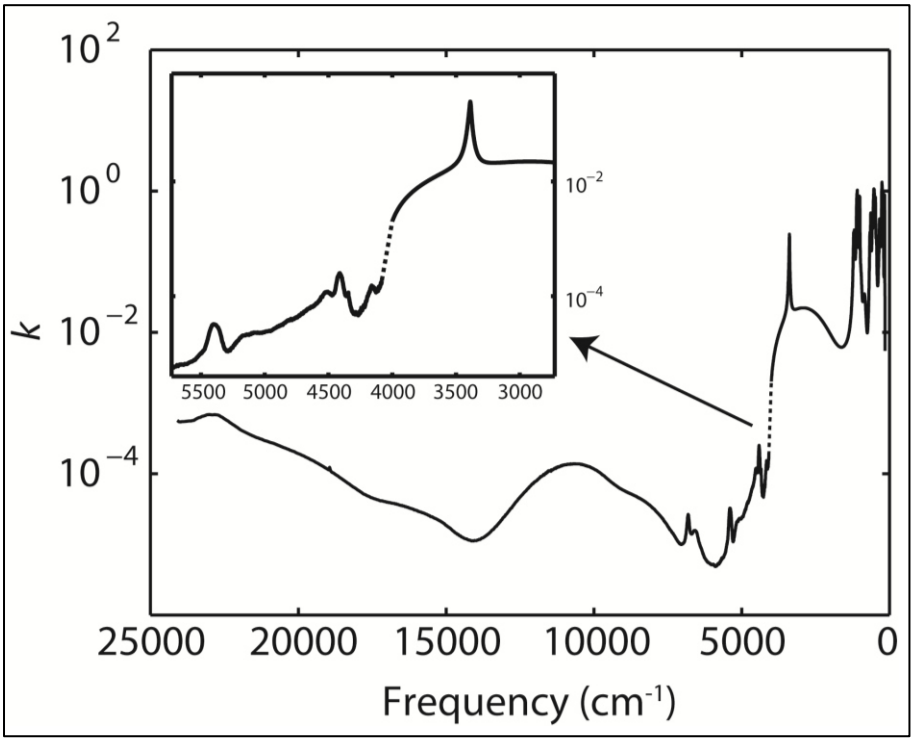

Figure 4-16. Adjusted and extrapolated *k* data for potassium jarosite. Note the continuity of the curve.

An interesting feature about the shape of *n* curve in the VNIR is that, when MIR data are included, the curve becomes fairly featureless and slopes down towards the MIR. This trend is identical for all samples with the differences arising from the value of *n* at the anchor point in the VNIR. Work from other authors shows the same trend (Roush et al. 2007). This characteristic

may serve as a way to approximate *n* in the VNIR without taking MIR data, if a predictable pattern can be determined.

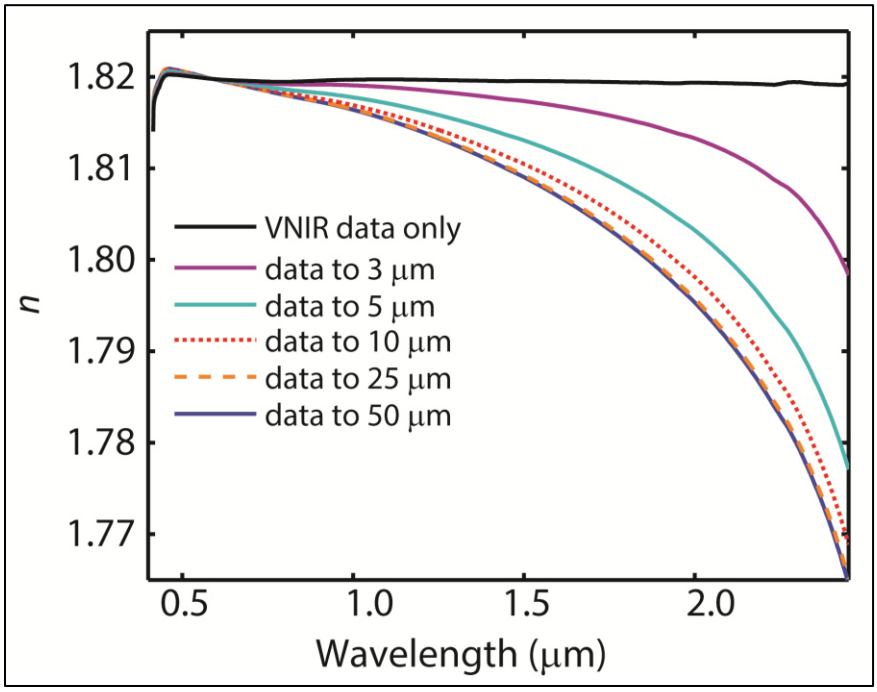

Figure 4-17. The real index of refraction *n* for hydronium jarosite calculated from *k* values that extend out to 2.5 μm, 3.0 μm, 5.0 μm, 10 μm, 25 μm, and 50 μm. VNIR data only become equivalent when MIR data out to at least 25 μm are used. These calculations, performed in frequency space, may be less sensitive to MIR data than those performed in wavelength space by the same method.

Table 1 shows that the apparent grain size, $\langle D \rangle$, for hydronium jarosite is small, about 1/3 of the median grain size in the range. The near-surface scattering coefficient, s, is also small, consistent with the smooth surfaces of the crystals. For the sodium and potassium jarosites, s is quite large (> 0.05 μm^{-1}) for both the medium and the large grained samples. This is consistent with the deep surface features apparent on both samples. For potassium jarosite, s for the smallest grain size is ~0, whereas that for sodium jarosite is 0.04 μm. These values are, again, consistent with observation as the potassium jarosite sample's larger grains are made from

smooth, smaller grains, where the sodium jarosite sample shows pitting that may affect even the smallest grains in the sample. The apparent grain size, $\langle D \rangle$, for both the potassium and the sodium jarosite are at the top edge of the grain size range. Since the values of $\langle D \rangle$ and s are related through the internal transmission factor (Equation 4.5), these values may have a mathematical influence on each other that is not fully related to the sample. However, repeated tapping of the sample cup to flatten the sample surface for analysis without introducing preferential orientation from pressing on the sample may have caused the smaller grains to sink. Since the penetration depth of VNIR light is quite shallow (~2*λ), it is possible that the spectra are, in fact, of some of the larger grains in the sample. Another explanation could be clumping; both the potassium and sodium samples clumped much more readily than the hydronium sample. This could lead to larger apparent grain sizes. For each iteration, though, the program never found the end grain size to be at a boundary, indicating that the values did still fall within the grain size ranges and that the boundary was not affecting the result. Whatever the explanation, the constraint that multiple grain sizes placed on the analysis to ensure k was as close to grain size independent as possible, still holds.

In the absence of large single crystals, the optical constants determined by our method are the closest approximation to the real optical constants of synthetic potassium, hydronium, and sodium jarosite that can be achieved. This leads to two questions: are synthetic samples appropriate proxies for natural samples? And are the end member optical constants sufficient to model jarosites within the solid solution? The most common deviation between synthetic and natural jarosites is metal site occupancy (Swayze et al. 2008). The synthesis method used in this study was specifically designed to eliminate metal vacancies in the lattice (Nocera et al. 2004). In addition, after studying the cell dimensions of a variety of both hydrothermal and low

temperature jarosites, Swayze et al. (2008) concluded that natural jarosites crystallize as mixtures of end members, not as intermediate compositions in the solid solution series. Thus, the optical constants determined in this study should be appropriate for modeling natural jarosites in all environments.

4.5 Implications

The use of modeling techniques that determine quantitative abundances from particulate surfaces in the VNIR has been hindered by the lack of available *n* and *k* data for many of the relevant minerals. The optical constants presented in this paper allow for the use of such modeling techniques to derive abundances of the mineral jarosite, on Earth and Mars, from mixed spectra. These abundances can be used on Mars to constrain surface processes that led to jarosite formation, and they can be used on Earth to monitor AMD and jarosite wastes.

The detailed description of the technique used in this paper, along with the availability of our Matlab code, has the potential to greatly expand this library of data in the near future. The process outlined in this study, although based on complicated theory, requires three simple inputs: a sample in three grain sizes that can be measured at several phase angles (10 hours of measurement time), MIR measurements of the same sample out to 50 μm, and a desktop computer capable of running Matlab (less than one week computation time on a single core). All data and programs used in this study are available at **http://aram.ess.sunysb.edu/tglotch/** and **Appendix A** and **B**.

Works Cited

Ambartsumian, V. (1958) The theory of radiative transfer in planetary atmospheres. In: V. Ambartsumian (Ed.), Theoretical Astrophysics. Pergamon, New York, pp. 550-564.

Barron, V., Torrent, J., and Greenwood, J.P. (2006) Transformation of jarosite to hematite in simulated Martian brines. Earth and Planetary Science Letters, 251 (3-4), 380-385.

Bell, J.H., Bowen, B.B., and Martini, B.A. (2010) Imaging spectroscopy of jarosite cement in the Jurassic Navajo Sandstone. Remote Sensing of Environment, 114 (10), 2259-2270.

Bigham, J.M., Schwertmann, U., and Pfab, G. (1996a) Influence of pH on mineral speciation in a bioreactor simulating acid mine drainage. Applied Geochemistry, 11 (6), 845-849.

Bigham, J.M., Schwertmann, U., Traina, S.J., Winland, R.L., and Wolf, M. (1996b) Schwertmannite and the chemical modeling of iron in acid sulfate waters. Geochimica Et Cosmochimica Acta, 60 (12), 2111-2121.

Bishop, J.L., Darby Dyar, M., Lane, M.D., and Banfield, J.F. (2004) Spectral identification of hydrated sulfates on Mars and comparison with acidic environments on Earth. International Journal of Astrobiology, 3 (04), 275-285.

Bishop, J.L., and Murad, E. (2005) The visible and infrared spectral properties of jarosite and alunite. American Mineralogist, 90 (7), 1100-1107.

Cahill, J.T., and Lucey, P.G. (2007) Radiative transfer modeling of lunar highlands spectral classes and relationship to lunar samples. Journal of Geophysical Research-Planets, 112 (E10).

Cahill, J.T.S., Lucey, P.G., and Wieczorek, M.A. (2009) Compositional variations of the lunar crust: Results from radiative transfer modeling of central peak spectra. Journal of Geophysical Research-Planets, 114.

Chandrasekhar, S. (1960) Radiative Transfer. Dover, New York.

Clark, R.N. (1999) Chapter 1: Spectroscopy of Rocks and Minerals, and Principles of Spectroscopy. In: A.N. Rencz (Ed.), Manual of Remote Sensing, Volume 3, Remote Sensing for the Earth Sciences. John Wiley and Sons, New York, pp. 3-58.

Clark, R.N., and Roush, T.L. (1984) Reflectance spectroscopy - quantitative-analysis techniques for remote-sensing applications. Journal of Geophysical Research, 89 (NB7), 6329-6340.

Clark, R.N., Swayze, G.A., Livo, K.E., Kokaly, R.F., Sutley, S.J., Dalton, J.B., McDougal, R.R., and Gent, C.A. (2003) Imaging spectroscopy: Earth and planetary remote sensing with the USGS Tetracorder and expert systems. Journal of Geophysical Research-Planets, 108 (E12).

Cloutis, E.A., Craig, M.A., Kruzelecky, R.V., Jamroz, W.R., Scott, A., Hawthorne, F.C., and Mertzman, S.A. (2008) Spectral reflectance properties of minerals exposed to simulated Mars surface conditions. Icarus, 195 (1), 140-168.

Coleman, T., and Li, Y. (1994) On the convergence of interior-reflective Newton methods for nonlinear minimization subject to bounds. Mathematical Programming, 67 (1-3), 189-224.

Cruikshank, D.P., Owen, T.C., Ore, C.D., Geballe, T.R., Roush, T.L., de Bergh, C., Sandford, S.A., Poulet, F., Benedix, G.K., and Emery, J.P. (2005) A spectroscopic study of the surfaces of Saturn's large satellites: H(2)O ice, tholins, and minor constituents. Icarus, 175 (1), 268-283.

Dalton, J.B., Bove, D.J., Mladinich, C.S., and Rockwell, B.W. (2004) Identification of spectrally similar materials using the USGS Tetracorder algorithm: the calcite-epidote- chlorite problem. Remote Sensing of Environment, 89 (4), 455-466.

Dalton, J.B., III, and Pitman, K.M. (2012) Low temperature optical constants of some hydrated sulfates relevant to planetary surfaces. Journal of Geophysical Research-Planets, 117.

Denevi, B.W., Lucey, P.G., and Sherman, S.B. (2008) Radiative transfer modeling of near-infrared spectra of lunar mare soils: Theory and measurement. Journal of Geophysical Research-Planets, 113 (E2).

Deyell, C.L., and Dipple, G.M. (2005) Equilibrium mineral-fluid calculations and their application to the solid solution between alunite and natroalunite in the El Indio-Pascua belt of Chile and Argentina. Chemical Geology, 215 (1-4), 219-234.

Drouet, C., and Navrotsky, A. (2003) Synthesis, characterization, and thermochemistry of K-Na-H3O jarosites. Geochimica Et Cosmochimica Acta, 67 (11), 2063-2076.

Farrand, W.H., Glotch, T.D., Rice, J.W., Hurowitz, J.A., and Swayze, G.A. (2009) Discovery of jarosite within the Mawrth Vallis region of Mars: Implications for the geologic history of the region. Icarus, 204 (2), 478-488.

Frost, R.L., Wills, R.A., Martens, W., and Weier, M. (2005) NIR spectroscopy of jarosites. Spectrochimica Acta Part a-Molecular and Biomolecular Spectroscopy, 62 (4-5), 869-874.

Glotch, T.D., and Rossman, G.R. (2009) Mid-infrared reflectance spectra and optical constants of six iron oxide/oxyhydroxide phases. Icarus, 204 (2), 663-671.

Grohol, D., Nocera, D.G., and Papoutsakis, D. (2003) Magnetism of pure iron jarosites. Physical Review B, 67 (6).

Hapke, B. (1981) Bidirectional reflectance spectroscopy 1. Theory. Journal of Geophysical Research, 86 (NB4), 3039-3054.

Hapke, B. (1993) Theory of Reflectance and Emittance Spectroscopy. Topics in Remote Sensing Cambridge University Press, New York, NY.

Hapke, B. (1996) A model of radiative and conductive energy transfer in planetary regoliths. Journal of Geophysical Research-Planets, 101 (E7), 16817-16831.

Hapke, B. (2002) Bidirectional reflectance spectroscopy 5. The coherent backscatter opposition effect and anisotropic scattering. Icarus, 157 (2), 523-534.

Hapke, B. (2008) Bidirectional reflectance spectroscopy - 6. Effects of porosity. Icarus, 195 (2), 918-926.

Hapke, B. (2012) Theory of Reflectance and Emittance Spectroscopy, 2nd edition. Cambridge University Press, New York.

Hapke, B., and Wells, E. (1981) Bidirectional reflectance spectroscopy 2. Experiments and observations. Journal of Geophysical Research, 86 (NB4), 3055-3060.

Jerz, J.K., and Rimstidt, J.D. (2003) Efflorescent iron sulfate minerals: Paragenesis, relative stability, and environmental impact. American Mineralogist, 88 (11-12), 1919-1932.

Klingelhofer, G., Morris, R.V., Bernhardt, B., Schroder, C., Rodionov, D.S., de Souza, P.A., Yen, A., Gellert, R., Evlanov, E.N., Zubkov, B., Foh, J., Bonnes, U., Kankeleit, E., Gutlich, P., Ming, D.W., Renz, F., Wdowiak, T., Squyres, S.W., and Arvidson, R.E. (2004) Jarosite and hematite at Meridiani Planum from Opportunity's Mossbauer spectrometer. Science, 306 (5702), 1740-1745.

Kula, J., and Baldwin, S.L. (2011) Jarosite, argon diffusion, and dating aqueous mineralization on Earth and Mars. Earth and Planetary Science Letters, 310 (3-4), 314-318.

Lawrence, S.J., and Lucey, P.G. (2007) Radiative transfer mixing models of meteoritic assemblages. Journal of Geophysical Research-Planets, 112 (E7).
Li, S., and Li, L. (2011) Radiative transfer modeling for quantifying lunar surface minerals, particle size, and submicroscopic metallic Fe. Journal of Geophysical Research-Planets, 116.
Lucarini, V., Saarinen, J.J., Peiponen, K.-E., and Vartiainen, E.M. (2005) Kramers-Kronig Relations in Optical Materials Research. Springer Series in Optical Sciences. Springer, New York, 162 pp.
Lucey, P.G. (1998) Model near-infrared optical constants of olivine and pyroxene as a function of iron content. Journal of Geophysical Research-Planets, 103 (E1), 1703-1713.
Lucey, P.G. (2004) Mineral maps of the Moon. Geophysical Research Letters, 31 (8).
Lueth, V.W., Rye, R.O., and Peters, L. (2005) "Sour gas" hydrothermal jarosite: ancient to modem acid-sulfate mineralization in the southern Rio Grande Rift. Chemical Geology, 215 (1-4), 339-360.
Madden, M.E.E., Bodnar, R.J., and Rimstidt, J.D. (2004) Jarosite as an indicator of water-limited chemical weathering on Mars. Nature, 431 (7010), 821-823.
Madden, M.E.E., Guess, J.R., Madden, A.S., and Rimstidt, J.D. (2008) Measuring jarosite dissolution rates to determine jarosite lifetimes on Earth and Mars. Geochimica Et Cosmochimica Acta, 72 (12), A243-A243.
Madden, M.E.E., Madden, A.S., and Rimstidt, J.D. (2009) How long was Meridiani Planum wet? Applying a jarosite stopwatch to determine the duration of aqueous diagenesis. Geology, 37 (7), 635-638.
Madden, M.E.E., Madden, A.S., Rimstidt, J.D., Zahrai, S., Kendall, M.R., and Miller, M.A. (2012) Jarosite dissolution rates and nanoscale mineralogy. Geochimica Et Cosmochimica Acta, 91, 306-321.
Majzlan, J., Stevens, R., Boerio-Goates, J., Woodfield, B.F., Navrotsky, A., Burns, P.C., Crawford, M.K., and Amos, T.G. (2004) Thermodynamic properties, low-temperature heat-capacity anomalies, and single-crystal X-ray refinement of hydronium jarosite, $(H_3O)Fe_3(SO_4)_2(OH)_6$. Physics and Chemistry of Minerals, 31 (8), 518-531.
Mauch, S. (2004) Introduction to Methods of Applied Mathematics or Advanced Mathematical Methods for Scientists and Engineers. http://www.its.caltech.edu/~sean
Mustard, J.F., and Pieters, C.M. (1987) Quantitative abundance estimates from bidirectional reflectance measurements. Journal of Geophysical Research-Solid Earth and Planets, 92 (B4), E617-E626.
Mustard, J.F., and Pieters, C.M. (1989) Photometric phase function of common geological minerals and applications to quantitative-analysis of mineral mixture reflectance spectra. Journal of Geophysical Research-Solid Earth and Planets, 94 (B10), 13619-13634.
Navrotsky, A., Forray, F.L., and Drouet, C. (2005) Jarosite stability on Mars. Icarus, 176 (1), 250-253.
Nocera, D.G., Bartlett, B.M., Grohol, D., Papoutsakis, D., and Shores, M.P. (2004) Spin frustration in 2D kagome lattices: A problem for inorganic synthetic chemistry. Chemistry-a European Journal, 10 (16), 3851-3859.
Nomura, K., Takeda, M., Iiyama, T., and Sakai, H. (2005) Mössbauer studies of Jarosite, Mikasaite and Yavapaiite, and implication to their Martian counterparts. Hyperfine Interactions, 166 (1-4), 657-664.

Norlund, K.L.I., Baron, C., and Warren, L.A. (2010) Jarosite formation by an AMD sulphide-oxidizing environmental enrichment: Implications for biomarkers on Mars. Chemical Geology, 275 (3-4), 235-242.

Papike, J.J., Burger, P.V., Karner, J.M., Shearer, C.K., and Lueth, V.W. (2007) Terrestrial analogs of martian jarosites: Major, minor element systematics and Na-K zoning in selected samples. American Mineralogist, 92 (2-3), 444-447.

Papike, J.J., Karner, J.M., and Shearer, C.K. (2006) Comparative planetary mineralogy: Implications of martian and terrestrial jarosite. A crystal chemical perspective. Geochimica Et Cosmochimica Acta, 70 (5), 1309-1321.

Pappu, A., Saxena, M., and Asolekar, S.R. (2006) Jarosite characteristics and its utilisation potentials. Science of the Total Environment, 359 (1-3), 232-243.

Pecharroman, C., Gonzalezcarreno, T., and Iglesias, J.E. (1995) The infrared dielectric-properties of maghemite, gamma-Fe203, from reflectance measurement on presses powders. Physics and Chemistry of Minerals, 22 (1), 21-29.

Piatek, J.L. (2003). Size-dependent scattering properties of planetary regolith analogs, 186 pp. Ph.D. Thesis, University of Pittsburgh, Pittsburgh.

Poulet, F., Bibring, J.P., Langevin, Y., Mustard, J.F., Mangold, N., Vincendon, M., Gondet, B., Pinet, P., Bardintzeff, J.M., and Platevoet, B. (2009) Quantitative compositional analysis of martian mafic regions using the MEx/OMEGA reflectance data. Icarus, 201 (1), 69-83.

Poulet, F., and Erard, S. (2004) Nonlinear spectral mixing: Quantitative analysis of laboratory mineral mixtures. Journal of Geophysical Research-Planets, 109 (E2).

Pritchett, B.N., Madden, M.E.E., and Madden, A.S. (2012) Jarosite dissolution rates and maximum lifetimes in high salinity brines: Implications for Earth and Mars. Earth and Planetary Science Letters, 357, 327-336.

Quinn, D. (2010) The Hapke Model in Excel. http://davenquinn.com/hapke/

Quinn, D.P., Gillis-Davis, J.J., and Lucey, P.G. (2010) Using Microsoft Excel for Hapke modeling: A technique to simplify calculations of optical constants and reflectance spectra. Abstracts of Papers Submitted to the Lunar and Planetary Science Conference XXXXI (2426).

Roach, L.H., Mustard, J.F., Swayze, G., Milliken, R.E., Bishop, J.L., Murchie, S.L., and Lichtenberg, K. (2010) Hydrated mineral stratigraphy of Ius Chasma, Valles Marineris. Icarus, 206 (1), 253-268.

Roush, T.L., Esposito, F., Rossman, G.R., and Colangeli, L. (2007) Estimated optical constants of gypsum in the regions of weak absorptions: Application of scattering theories and comparisons to independent measurements. Journal of Geophysical Research-Planets, 112.

Rye, R.O., and Stoffregen, R.E. (1995) Jarosite-water oxygen and hydrogen isotope fractionations: Preliminary experimental data. Economic Geology and the Bulletin of the Society of Economic Geologists, 90 (8), 2336-2342.

Sefton-Nash, E., Catling, D.C., Wood, S.E., Grindrod, P.M., and Teanby, N.A. (2012) Topographic, spectral and thermal inertia analysis of interior layered deposits in Iani Chaos, Mars. Icarus, 221 (1), 20-42.

Shepard, M.K., and Helfenstein, P. (2007) A test of the Hapke photometric model. Journal of Geophysical Research-Planets, 112 (E3).

Shkuratov, Y., Starukhina, L., Hoffmann, H., and Arnold, G. (1999) A model of spectral albedo of particulate surfaces: Implications for optical properties of the moon. Icarus, 137 (2), 235-246.

Sowe, M., Wendt, L., McGuire, P.C., and Neukum, G. (2012) Hydrated minerals in the deposits of Aureum Chaos. Icarus, 218 (1), 406-419.

Swayze, G.A., Desborough, K.S., Smith, K.S., Lowers, H.A., Hammarstrom, J.M., Diehl, S.F., Leinz, R.W., and Driscoll, R.L. (2008) Understanding Jarosite -- from mine waste to Mars. Understanding Contaminants. U.S. Geological Survey Circular 1328, 8-13 pp.

Swayze, G.A., Smith, K.S., Clark, R.N., Sutley, S.J., Pearson, R.M., Vance, J.S., Hageman, P.L., Briggs, P.H., Meier, A.L., Singleton, M.J., and Roth, S. (2000) Using imaging spectroscopy to map acidic mine waste. Environmental Science & Technology, 34 (1), 47-54.

Wendt, L., Gross, C., Kneissl, T., Sowe, M., Combe, J.-P., LeDeit, L., McGuire, P.C., and Neukum, G. (2011) Sulfates and iron oxides in Ophir Chasma, Mars, based on OMEGA and CRISM observations. Icarus, 213 (1), 86-103.

Wilcox, B.B., Lucey, P.G., and Hawke, B.R. (2006) Radiative transfer modeling of compositions of lunar pyroclastic deposits. Journal of Geophysical Research-Planets, 111 (E9).

Zahrai, S.K., Madden, M.E.E., Madden, A.S., and Rimstidt, J.D. (2013) Na-jarosite dissolution rates: The effect of mineral composition on jarosite lifetimes. Icarus, 223 (1), 438-443.

Chapter 5

Morphological, Structural, and Spectral Characteristics of Amorphous Iron Sulfates

This chapter is in being prepared for submission to Journal of Geophysical Research - Planets

Sklute, E. C., Jensen, H. B., Rogers, A. D., Reeder, R. J. (In Preparation) Morphological, Structural, and Spectral Characteristics of Amorphous Iron Sulfates.

5.1 Introduction

A preponderance of evidence from recent orbital and landed missions points to the existence of hydrated sulfate phases on the Martian surface (Milliken et al. 2009; Roach et al. 2009; Lichtenberg et al. 2010; Roach et al. 2010a; Roach et al. 2010b; Wang et al. 2013). Some of those phases are likely hydrated iron sulfates (Bishop et al. 2009; Lichtenberg et al. 2010; Milliken and Bish 2010; Roach et al. 2010a; Wiseman et al. 2010; Wray et al. 2011; Karunatillake et al. 2012). Because iron sulfate structure and stability (including amorphous phases) are path-dependent (Xu et al. 2009), identification of specific iron sulfate phases has important implications for both surficial and atmospheric processes on Mars. For example, the discovery of the iron sulfate mineral jarosite on Mars (Klingelhofer et al. 2004; Gendrin et al. 2005) suggests that ancient Mars experienced acidic fluid conditions near the surface (Bibring et

al. 2006; Hurowitz and McLennan 2007), similar to areas of acid mine drainage (AMD) on Earth (Tosca and McLennan 2009).

The phases that precipitate from sulfate-rich fluids such as AMD are dependent upon pH, relative humidity (RH), temperature, fluid composition, and redox conditions at the time of formation (Xu et al. 2009). These precipitates follow a predictable sequence on Earth, such that the first phases to form are ferrous sulfates, followed by mixed valence sulfates, then ferric sulfates, and finally iron hydroxides, and oxides (Jambor et al. 2000; Jerz and Rimstidt 2003). However, our current understanding of the progression of these systems may not directly apply to Mars due to fundamental differences in fluid composition, temperature, and partial pressure of H_2O between the two planets. For example, evaporation and modeling experiments that simulate Martian weathering and precipitation processes produce different sulfate assemblages than those that would be found on Earth, presumably due to the high ionic strength of the acidified fluids (Marion et al. 2008; Tosca and McLennan 2009). In addition, the stability of many common sulfates is significantly altered by the low temperatures and pressures of the Martian surface. For example, higher hydrates have expanded stability and meta-stability fields under Martian conditions (Vaniman et al. 2004; Ling and Wang 2010; Wang et al. 2013). And although Cloutis et al. (2008) showed that, once formed, many sulfates are stable under simulated Martian conditions, others have shown that when iron sulfate *fluids* are subjected to low relative humidities, as one would expect on Mars under certain conditions (Savijarvi 1995), amorphous phases, rather than crystalline phases, precipitate from the saturated fluids (Xu et al. 2009; Wang et al. 2012; Xu and Parise 2012). Therefore, as our Martian data set grows, it is important to reassess our understanding of integral geochemical systems and adjust our expectations based upon that new understanding.

For instance, hydrogen measurements from orbital neutron spectroscopy (Feldman et al. 2004; Boynton et al. 2007; Maurice et al. 2011) indicate that hydrated mineral phases constitute a portion of Martian soils. Furthermore, only hydrated sulfate phases can reasonably account for the amount of water suggested by these measurements (Wang et al. 2013). Strong correlations between H and S concentrations in the southern highlands, as measured by the Mars Odyssey Gamma Ray Spectrometer (GRS) instrument suite, indicate that hydrated iron sulfates are the most likely candidates for these hydrated sulfate phases (Karunatillake et al. 2012). Gale crater, the current location of the Curiosity rover, is located within the equatorial band of higher GRS-derived H_2O concentrations (5-6 wt%). Therefore, recent analyses of the Rocknest soil and mudstone performed at Gale crater could show some evidence of these hydrated sulfate phases. However, crystalline, highly hydrated sulfates were not detected by ChemMin in the Rocknest soils and Sheepbed mudstone (Bish et al. 2013; Vaniman et al. 2014), even though large amounts of water (2.00 and 2.03 wt % respectively), iron (18.58 and 21.71 wt% respectively), and sulfur (5.28 and 2.08 wt% as SO_3 respectively) were found to be present in these materials (Morris et al. 2014). Because a large portion of both the evolved H_2O and SO_2 gas (upon heating) seems to have originated from the XRD amorphous component of the soil (McAdam et al. 2014), I propose that amorphous iron sulfates are candidate phases in the soil, the mudstone, or both.

Amorphous iron sulfates have previously been shown to form via two broad mechanisms: 1) dehydration of crystalline hydrated sulfates (e.g. rozenite or melanterite will dehydrate to form amorphous ferrous sulfate) under Mars-relevant pressures and temperatures (Wang and Zhou 2014) and 2) dehydration of $Fe(III)_2(SO_4)_3$ saturated fluids at relative humidities (RH) < 11% (forming amorphous ferric sulfate) (Xu et al. 2009; Wang et al. 2012). Wang et al. (2012) also report a quasi-amorphous phase made through vacuum dehydration of ferricopiapite, but this

phase is not XRD amorphous. "Poorly crystalline sulfates" have also been observed in alteration assemblages during acid fog weathering of basalt (Tosca et al., 2004; Golden et al., 2005); and structurally "disordered" Mg sulfate was generated from flash-freezing Mg sulfate brines (McCord et al., 2002). Unfortunately, no precipitation experiments have been performed at Mars relevant atmospheric pressures, nor under conditions where both low RH (<30%) and low temperatures (<5 ºC) are present; thus, evaporation products in some Mars-relevant corners of the parameter space have not yet been reported.

The recent discovery of a phenomenon known as Recurring Slope Lineae (RSL) (McEwen et al. 2011) points to an active present day brine hydrologic cycle on Mars (Chevrier and Altheide 2008; Altheide et al. 2009; McEwen et al. 2011; Martinez and Renno 2013; Masse et al. 2014) that could create conditions appropriate for the formation of amorphous sulfates on the surface. Several salts that are present on Mars (Squyres et al. 2004; Gendrin et al. 2005; Wang et al. 2006b) create brines with eutectics below the freezing point of pure water (Brass 1980; Marion et al. 2003; Sears and Chittenden 2005; Chevrier and Altheide 2008; Altheide et al. 2009; Mohlmann and Thomsen 2011). Brines can form any time the relative humidity of the atmosphere is above the deliquescence relative humidity of the salt. However, these fluids will be subject to boiling if the atmospheric vapor pressure is below the saturation vapor pressure of the fluid and will be subject to evaporation any time the partial pressure of H_2O is below the saturation water vapor pressure for the fluid (Martinez and Renno 2013). These brines are more stable in the subsurface because the RH is likely higher (Wang et al. 2012; Wang et al. 2013) and the upper soil layer protects against evaporation (Chevrier et al. 2007; Chevrier and Altheide 2008). On the surface, they are stable for only short periods of time and would likely boil or

evaporate rapidly depending on latitude (Chevrier and Altheide 2008). Both of these phenomena could lead to amorphous sulfates.

A series of studies by A. Wang and collaborators and W. Xu and collaborators have investigated the phase transitions and stability of sulfates, including amorphous sulfates, at both standard temperature and pressure, and at Mars relevant temperatures and pressures. (Wang et al. 2006a; Wang et al. 2009; Ling and Wang 2010; Kong et al. 2011a; Kong et al. 2011b; Wang et al. 2011; Wang and Ling 2011; Wang et al. 2012; Chou et al. 2013; Wang et al. 2013). The stability of these amorphous phases, once formed, depends on RH and temperature conditions. For example, when solid amorphous ferric sulfates are kept at RH < 11% and 5 ºC, they will remain amorphous for at least four years (the length of the longest term experiments) (Wang et al. 2012). Increasing temperature to 21°C causes the stability field for the amorphous phase to shift to lower relative humidities (RH < 6%). Increasing relative humidity to 33% RH at 5 ºC causes the amorphous solid to increase its structural water content without immediately crystallizing, varying from 5 to 11 structural waters (Wang et al. 2012). *These studies imply that if amorphous ferric sulfates were to form on the surface of Mars, they may be able to persist as amorphous phases, enduring the diurnal RH fluctuations without crystallizing*.

Although several previous studies have established the stability fields of sulfate systems under terrestrial and Martian conditions (Vaniman et al. 2004; Vaniman and Chipera 2006; Wang et al. 2006a; Chipera and Vaniman 2007; Wang et al. 2009; Xu et al. 2009; Wang et al. 2011; Wang et al. 2012; Xu and Parise 2012; Wang et al. 2013), and the spectral characteristics of crystalline sulfates are well documented (Cloutis et al. 2006; Lane 2007), little work has been done to characterize the amorphous phases. Here I report the morphological and spectroscopic characteristics of amorphous ferric and ferrous iron sulfates so that these observations can be

added to spectral libraries to which we compare remotely acquired data. Accurate identification of these phases is critical for characterizing fluid compositions and conditions that produced hydrated phases on Mars, as well as the subsequent environmental conditions that may have modified crystalline sulfates.

5.2 Methods

For this work, amorphous ferric iron sulfates were synthesized from two starting materials: first using unaltered Acros Organics 97% $Fe(III)_2(SO_4)_3 \bullet 5H_2O$, identified by XRD to be the monoclinic phase lausenite ($Fe(III)_2(SO_4)_3 \bullet 6H_2O$); second by heating the Acros starting material for 2 h at 350 ºC to form the anhydrous trigonal phase mikasaite ($Fe(III)_2(SO_4)_3$) (Xu et al. 2009). Both powders were placed in enclosures maintained at 92% relative humidity (RH) at ambient temperature (confirmed by RH probe), using de-ionized water as a humidity buffer. Once deliquesced, the materials were dehydrated via two methods: either using low RH (11% by LiCl buffer) (Xu et al. 2009) or by vacuum ($3x10^{-2}$ mbar; Edwards E2M2 vacuum pump attached to an Applied Vacuum Engineering VF range bell jar). Both of these methods simulate the rapid loss of water that hydrated phases would likely experience once exposed on the Martian surface; dehydration in low RH simulates evaporation, whereas vacuum desiccation simulates boiling. These samples will be referred to as LV-amorphous, LH-amorphous, MV-amorphous, and MH-amorphous to reflect their starting materials of lausenite and mikasaite, as well as their dehydration method of vacuum or humidity buffer. Amorphous ferrous sulfate was prepared by vacuum dehydrating melanterite ($FeSO_4 \bullet 7H_2O$) for 3 days. This synthesis method was based on a published method for obtaining amorphous Mg sulfate from hexahydrate (Vaniman et al. 2004).

The materials were confirmed amorphous at the resolution of XRD using a Scintag PAD X powder diffractometer (Cu Kα radiation; 25mA; 45kV). Once created, the ferric sulfates were kept at low RH (less than 11%) except during spectral analyses (< 20 min). Lack of crystallinity was checked by XRD after each analysis. Because these phases lack long-term stability in Earth's atmosphere (Xu et al. 2009; Ling and Wang 2010), the reproducibility of the synthesis methods was confirmed through repeated synthesis and subsequent spectral analysis. This procedure allowed for a fresh sample to be produced for each measurement, rather than using the same sample after exposure to ambient and/or experimental conditions. Overlapping measurements were periodically taken to ensure that the above assumption remained valid.

Visible/near-infrared reflectance (VNIR) spectra were collected on an ASD Fieldspec3 Max UV-VIS-NIR bidirectional spectrometer (referenced to Spectralon, average of 300 scans) in the Vibrational Spectroscopy Laboratory (VSL) at Stony Brook University. When laboratory humidity exceeded 15% (monitored by RH probe), VNIR spectra were collected in an N_2 filled glove bag. Spectral emissivity measurements also taken at VSL, were acquired on a Nicolet 6700 FTIR instrument custom modified to collect emissivity data. Spectra were referenced to a custom-built blackbody calibration target heated to 68 and 98 ºC, and were acquired in a dry air purged chamber. Spectra were only collected when laboratory humidity was less than 15%. To avoid phase changes that could occur upon heating, the samples were cooled and held at 30° below the detector temperature (rather than heated above detector temperature) to achieve adequate signal to noise for spectral measurement (Baldridge and Christensen 2009). Spectral emissivity measurements were taken on both powders and pressed pellets. To ensure that the pressure (3.5 tonnes) did not introduce crystallinity, XRD patterns were collected from the pellets before and after emissivity measurements and compared to those for fresh, powdered

samples. Thermogravimetric analysis (TGA), using a Netzsch STA Jupiter simultaneous TG-DSC apparatus, was used to determine sample H_2O contents. Scanning Electron Microscopy (SEM) was used to image sample morphologies and confirm that the materials were not simply nanophase.

Synchrotron x-ray total scattering data were collected at beamline 11-ID-B at the Advanced Photon Source, Argonne National Laboratory, using a monochromatic x-ray beam (~58 keV, λ = 0.2127Å) of approximately 500 μm diameter. Samples were loaded into Kapton capillaries, approximately 1 mm in diameter. The total scattering experiment is well described by Billinge and Kanatzidis (2004) and Reeder and Michel (2013). Briefly, the total scattering experiment refers to the collection of both the elastic Bragg and the diffuse scattering components from a sample subjected to x-ray radiation. Total scattering experiments using conventional x-ray sources are of limited value for two reasons: first, the real space resolution is proportional to the range of angles over which data can be collected, which is, in turn, dependent upon the energy of the x-rays; and second, the intensity of the diffuse component is much less intense than the Bragg component, requiring higher photon fluxes for adequate signal. The high-energy synchrotron x-ray source allows measurements to be made to a much higher scattering angle and provides greatly increased flux, compared to a conventional source. After the scattering data are normalized and corrected for instrumental factors, the reduced structure function is Fourier transformed to give the pair distribution function (PDF), which is the distribution of inter-atomic distances of the material weighted by the scattering power of the atoms. The PDF provides direct structural information over a range of length scales, for crystalline and amorphous solids.

Mössbauer spectra were collected at Mount Holyoke College on a Web Research Co. (now See Co.) W100 spectrometer using a ~80 mCi 57Co source in Rhodium. Spectra were calibrated to α-Fe foil. Run times ranged from 2 to 12 hours. Mössbauer data were fit using Mexfieldd, a program provided by E. DeGrave at the University of Ghent, Belgium. The program solves the full hyperfine interaction Hamiltonian to fit Lorentzian doublets to the spectral data with isomer shift (δ), quadrupole splitting (Δ), and full width half maximum (Γ) as free parameters.

5.3. Results

5.3.1 General observations

When precipitated in low humidity or under vacuum, and processed in a low humidity environment after synthesis, amorphous ferric sulfates form as amber-colored, translucent solids that grind into fine, ocher-white powders (**Figure 5-1**). X-ray diffraction patterns of the solids and powders lack sharp peaks and display only a slight swell in the baseline centered around 26º 2θ (**Figure 5-2**). Therefore, both the solid and powdered forms can be designated XRD amorphous. Ferrous sulfates transform into a silky gray powder that maintains the shape of the crystals from which they formed (**Figure 5-3**). The ferrous sulfates display a similarly featureless XRD pattern with a swell centered around 29º 2θ (**Figure 5-2**). Therefore, they too can be designated XRD amorphous. Based on our experimental investigations and accounts in the literature, amorphous ferric sulfates seem to only form from saturated solutions whereas amorphous ferrous sulfates seem to only form from highly hydrated crystalline phases (Xu et al. 2009; Wang et al. 2012; Xu and Parise 2012; Wang and Zhou 2014). Although extensive stability studies have not been performed for the purpose of this work, as such studies have been

reported elsewhere (e.g. Wang et al. (2012)), a few general stability trends for the amorphous ferrous and ferric sulfates can be noted. The amorphous ferrous sulfates are less stable than the amorphous ferric sulfates under ambient conditions. Upon exposure to ambient winter lab conditions (~23 ºC, 14% RH), amorphous ferrous sulfates begin to turn from silver to gray over the course of 24 h and begin to show the emergence of sharp peaks in the XRD pattern after 48 h. The amorphous ferric sulfates, on the other hand, remain XRD amorphous for days, slowly taking on a surface coating of liquid water before finally beginning to crystallize. Under summer ambient lab conditions (~23 ºC, 35-55%RH), the amorphous ferrous sulfates begin to crystallize within minutes and the amorphous ferric sulfates within hours to a day, but amorphous ferric sulfates always form a surface coatings of liquid water before crystallizing.

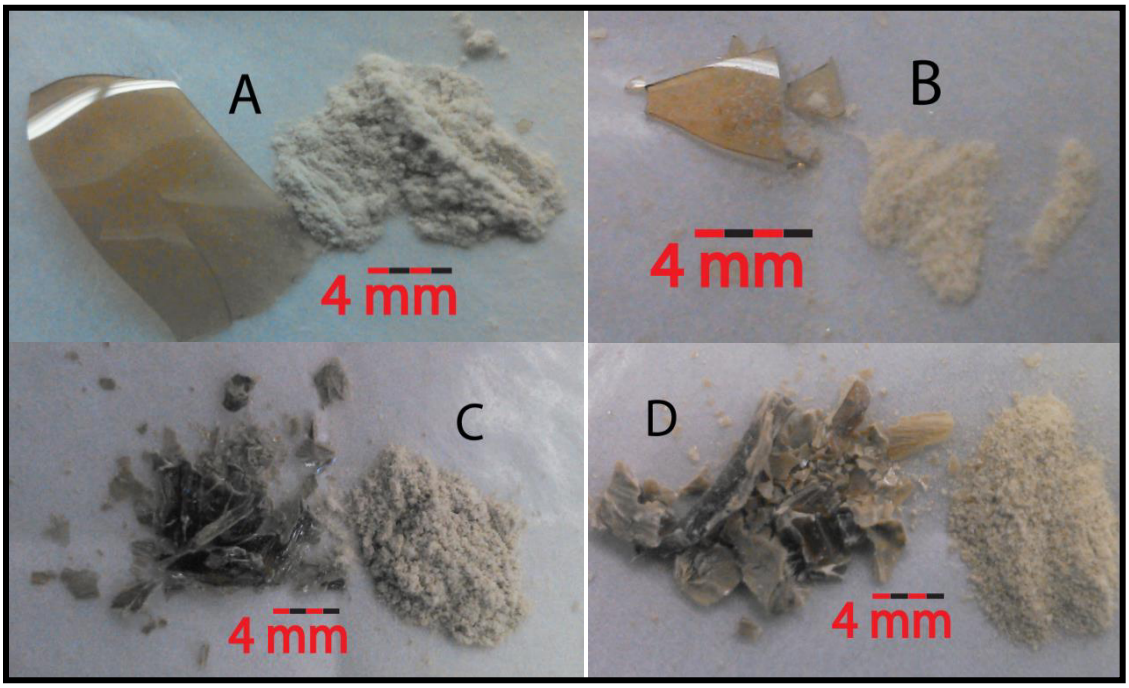

Figure 5-1. Image of partially ground, amorphous ferric sulfates: LH-amorphous (A), MH-amorphous (B), LV-amorphous (C), MV-amorphous (D).

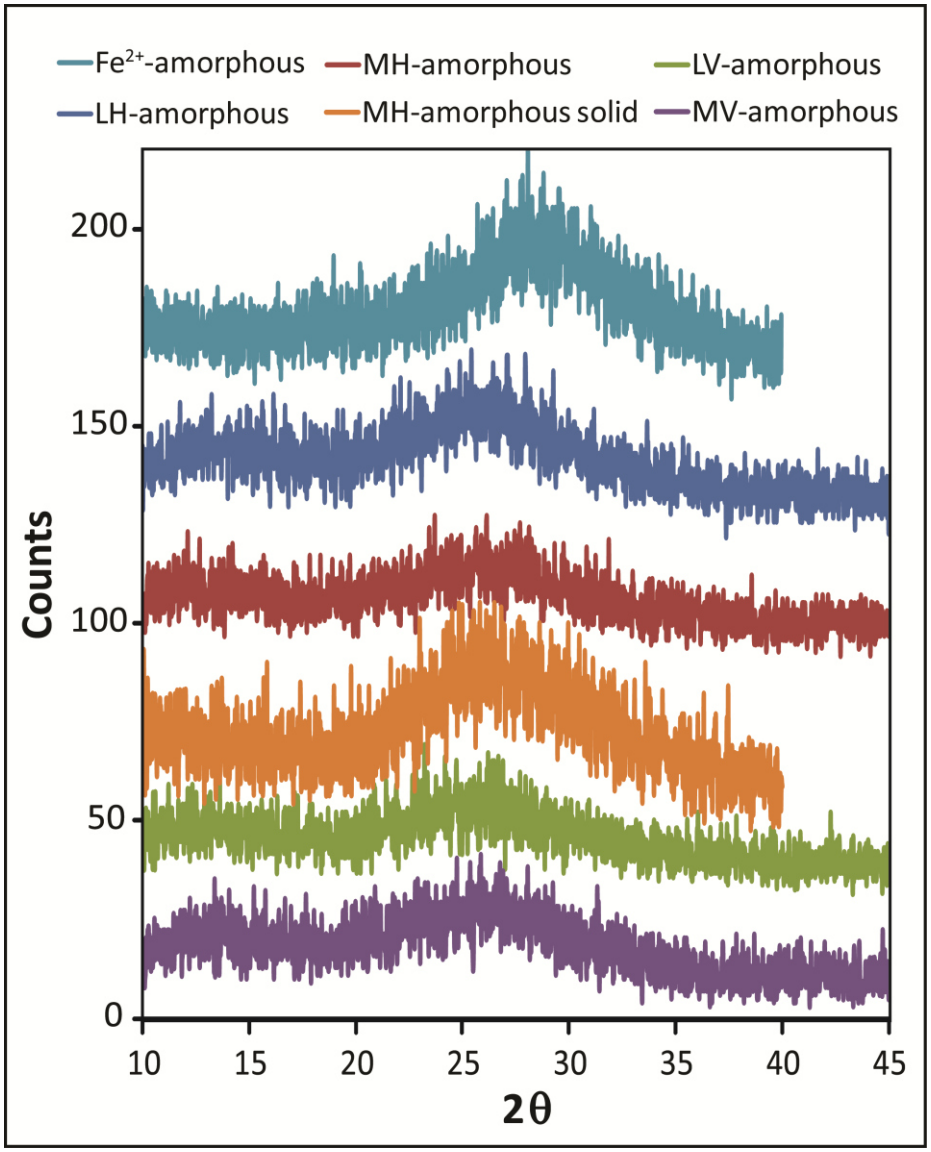

Figure 5-2. XRD patterns of amorphous ferric and ferrous sulfates. All XRD patterns are of powders except where indicated. All samples were run on a zero background plate.

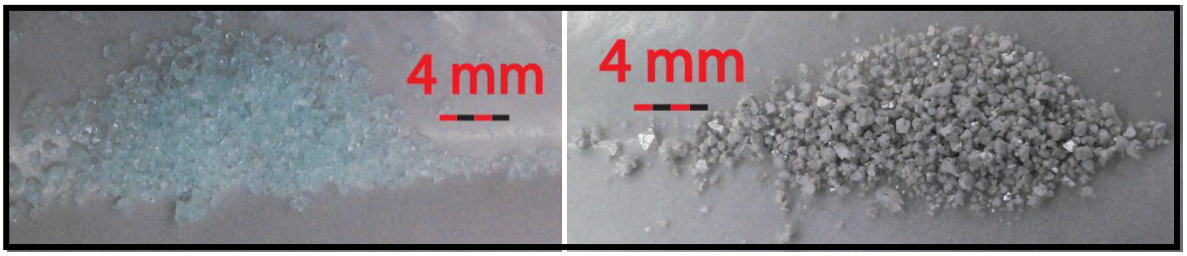

Figure 5-3. Image of starting melanterite (left) and vacuum dehydrated amorphous ferrous sulfate (right).

5.3.2 Morphology, hydration state, and range of structural order

SEM investigations show that the amorphous ferric sulfates display conchoidal fracture (**Figure 5-4**). SEM micrographs of the amorphous ferrous sulfate show that the crystals of melanterite have thin lamellar separation, yet they remain intact (**Figure 5-5**, left). This morphology is consistent with dehydration. Magnification shows that the microstructure appears to be sheets which, when ground (**Figure 5-5**, right) break into platelets. This fracture pattern is consistent with melanterite's structure, which consists of isolated octahedra and tetrahedra connected through hydrogen bonding to the structural waters in alternating layers. The rapid dehydration appears to separate some of the layers. SEM micrographs of the ground ferric and ferrous sulfates show that, although shards can be as small as 20 nm, the majority of the particles are large enough that, were they crystalline, they would be expected to produce sharp diffraction lines in the XRD patterns. Thus, the XRD amorphous nature of these samples may safely be attributed to lack of long-range structure rather than nanophase particles.

TGA data were acquired to determine the number of structural waters of the amorphous samples and to provide normalization for PDF analysis (**Section 5.2.0**). The TGA curves for the amorphous ferric sulfate samples show a gradual decrease to ~150 ºC followed by a steeper decrease to ~200 ºC. The slope of the TGA curves becomes gradual again by 250 ºC. This is interpreted as the loss of loosely bound and adsorbed water followed by the loss of structural water. The TGA curve for the amorphous ferrous sulfate sample is almost level to ~133 ºC followed by a steep decrease to ~250 ºC, after which the slope becomes gradual again. This is interpreted as the loss structural water from a single energetic environment. These TGA curves are typical for iron sulfates (McAdam et al. 2014). At 250 ºC, the amorphous ferric sulfates had transformed into mikasaite, and amorphous ferrous sulfate had transformed into anhydrous

ferrous sulfate (confirmed through XRD). LV-amorphous sulfate contained a total (structural and adsorbed) of 7.4 waters (per $Fe_2(SO_4)_3$ structural unit), where MV-amorphous sulfate contained only 6.3. LH-amorphous sulfate contained 8.5 waters and MH-amorphous contained 8.2. The ferrous sulfate sample contained 0.97 waters (per $FeSO_4$ structural unit).

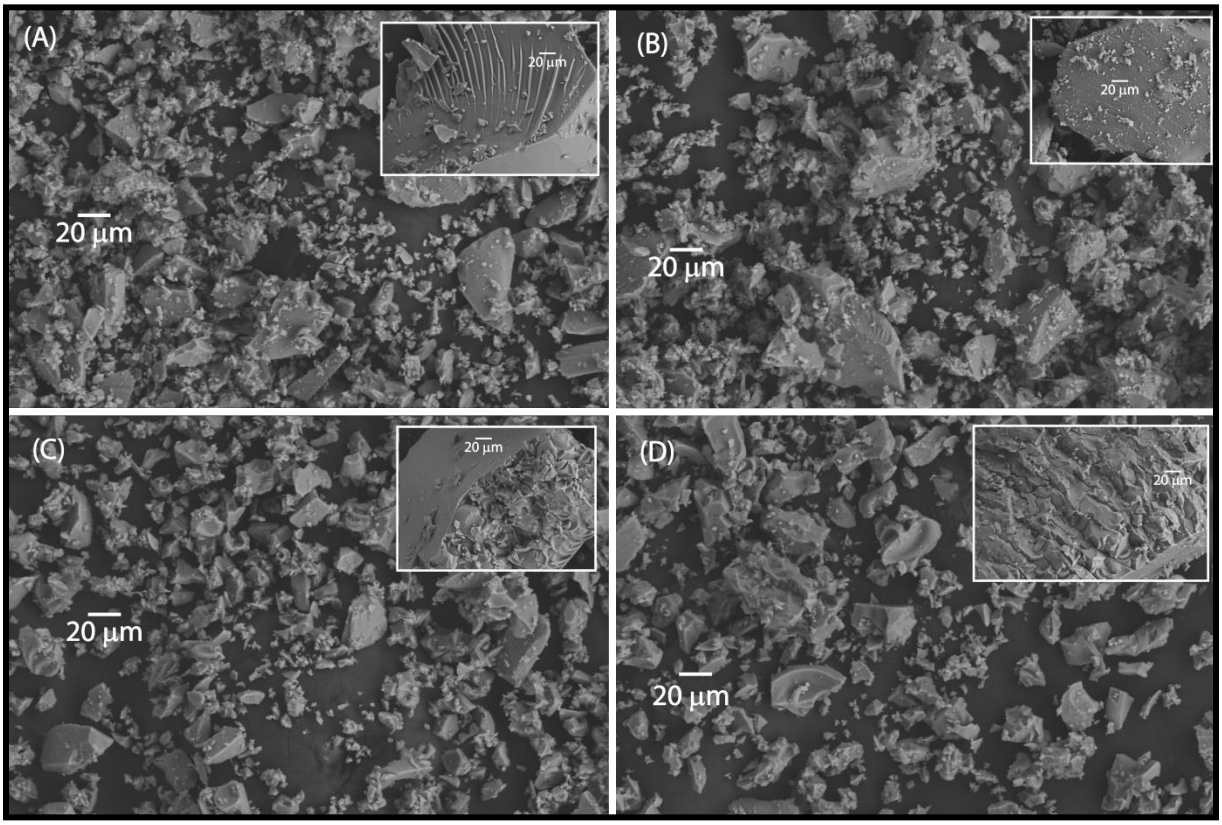

Figure 5-4. SEM images of A) the LH-amorphous sample, B) the MH-amorphous sample, C) the LV-amorphous sample, and D) the MV-amorphous sample. The main images are of the finest ground sections used for PDF. Insets are of minimally ground sections used for XRD.

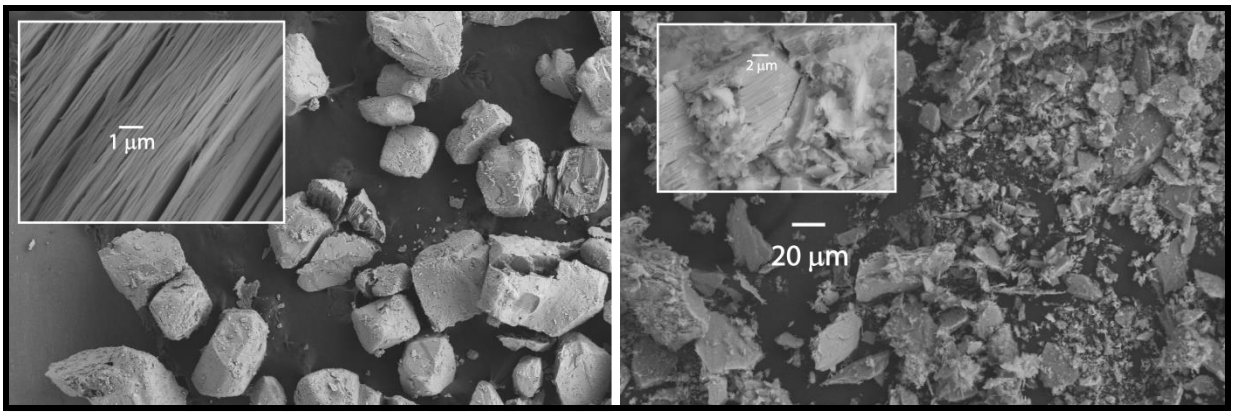

Figure 5-5. SEM images of unground (left) and ground (right) amorphous ferrous sulfate. Insets show layered structure likely resulting from rapid removal of interlayer water.

Figure 5-6 shows the PDF for MV-amorphous sulfate overlaid on those of ferricopiapite and mikasaite for reference. The top pane of **Figure 5-6** shows the full data range for the samples. The abundance of peaks for the crystalline phases reflects the large number of scattering pairs, or pairs of atoms, that are present at regular intervals in the sample. The overall decrease in G(r) with increasing r is due to the resolution of the analysis; the further the distance is between two pairs, the more energy it takes to probe the interaction. It is clear, however, that the fall off in G(r) is much faster for the amorphous sample than for the crystalline samples, indicating a general absence of structural order at high r. The bottom pane of **Figure 5-6** reveals that peaks for MV-amorphous sulfate are damped beyond ~ 10 Å, indicating that beyond ~10 Å, the structure has significant disorder. Although SEM cannot provide sufficient resolution to definitively state that particle zoning isn't on the order of 1 nm, the large smooth surfaces seen in the SEM images (**Figure 5-4**) strongly suggest that particle size is larger than 10 Å. Therefore, it can be concluded that this is a truly amorphous material with short- and medium range structure similar to ferricopiapite. **Figure 5-7** is a plot of all four amorphous ferric sulfate samples. The PDF for all four samples are similar, indicating that these samples share a basic short range bonding environment and that they are all amorphous.

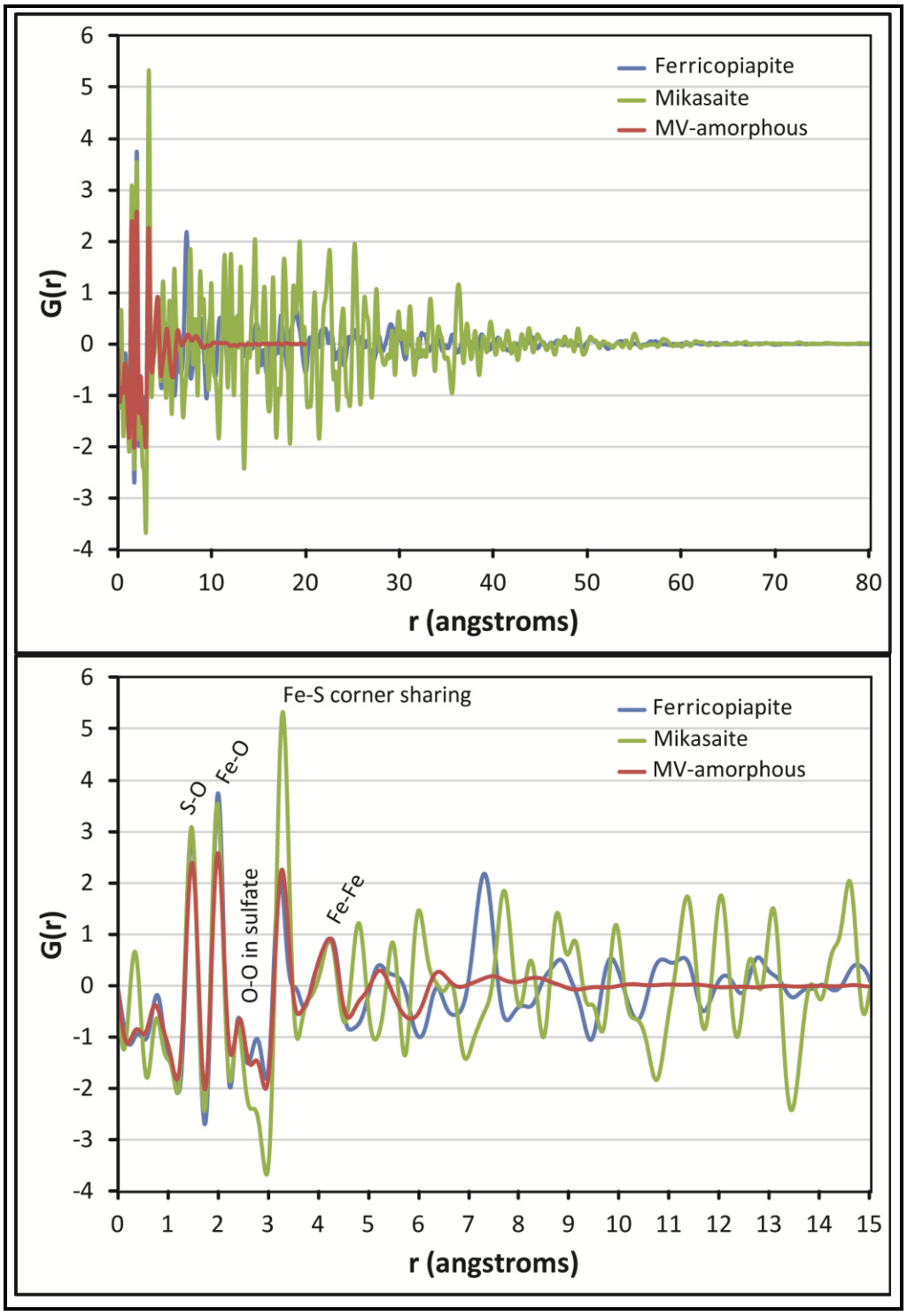

Figure 5-6. Pair distribution function of MV-amorphous ferric sulfate overlaid on the PDFs of crystalline ferricopiapite and mikasaite. The top pane shows the full data range and the bottom pane shows a close up at low r.

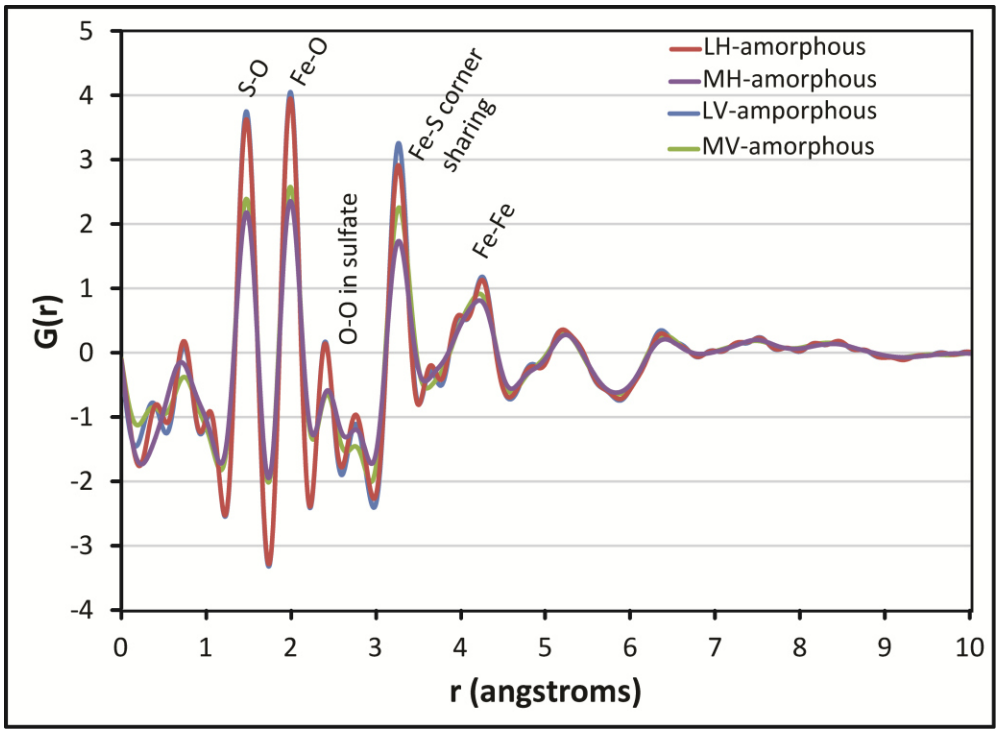

Figure 5-7. Pair distribution function of the amorphous ferric sulfate samples.

Figure 5-8 shows the PDF for the amorphous ferrous sulfate sample overlaid on those for szomolnokite and rozenite for reference. Again, the fall-off in G(r) is much faster for the crystalline samples than for the amorphous sample, indicating a general lack of long range structural order (**Figure 5-8** top). The amorphous ferrous sulfate appears to have short range order (< 4 Å) that is close to, yet distinct from, both szomolnokite and rozenite and displays lack of structural order past ~ 11 Å (**Figure 5-8** bottom). Since SEM imaging for this sample also suggests that the particle size seems larger than 11 Å, it can be concluded that this, too, is truly an amorphous material.

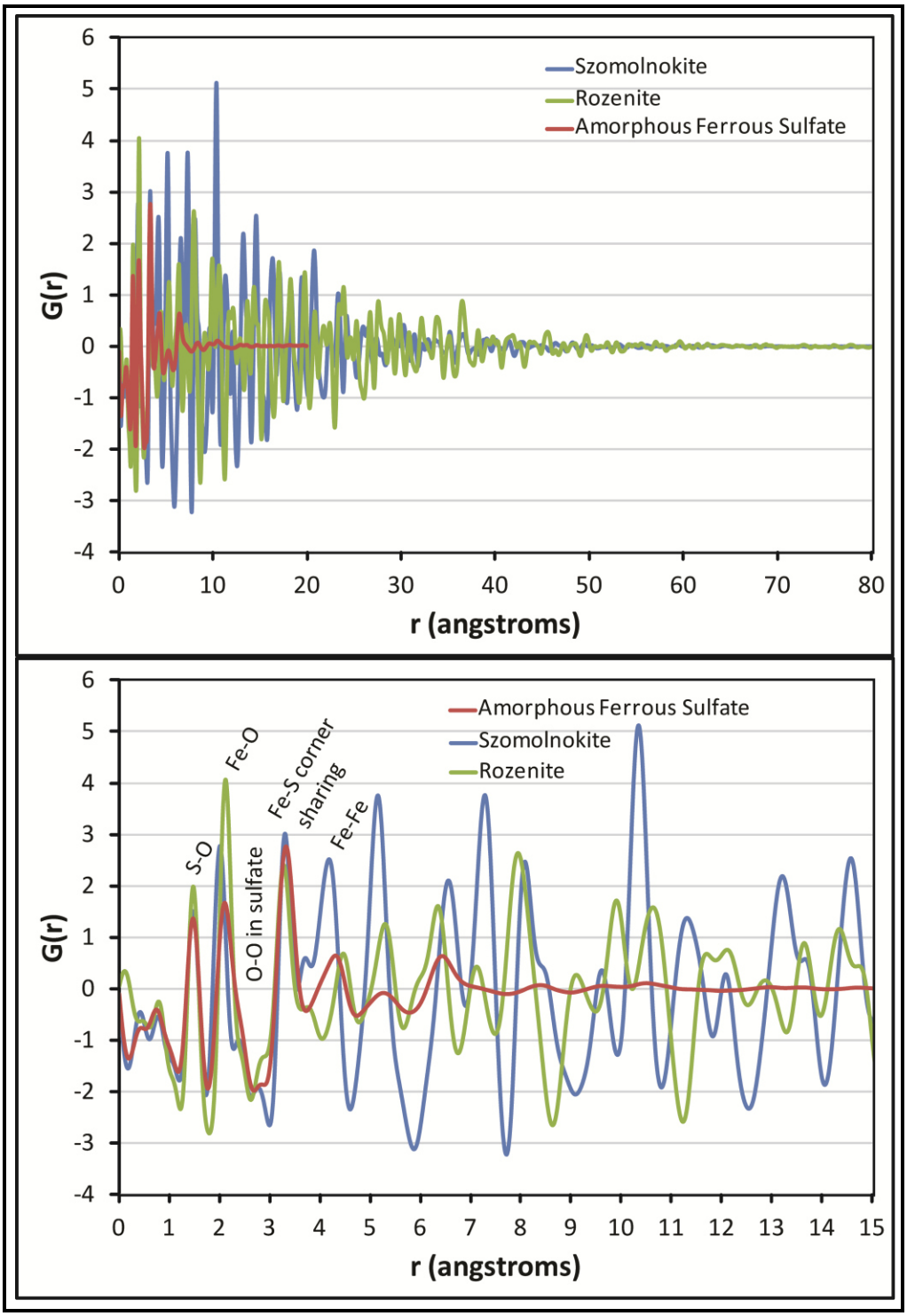

Figure 5-8. Pair distribution function of amorphous ferrous sulfate overlaid on the PDFs of crystalline szomolnokite and rozenite. The top pane shows the full data range and the bottom pane shows a close up at low r.

5.3.3 VNIR spectroscopic observations

VNIR spectra of amorphous sulfate samples are plotted along with several common sulfates in **Figure 5-9** and **Figure 5-11** through **5-13**. The reference samples are the same as those used by Cloutis et al. (2008). Also included are samples for which emissivity data have previously been acquired (Lane 2007). The VNIR range has been split into two regions based on the OMEGA (Observatoire pour la Minéralogie, l'Eau, les Glacesetl'Activité) channels for easier comparison with Mars data (VIS and SWIR). The OMEGA VIS sensor spans from 0.35 to 1.05 μm. Due to VIS calibration difficulties, data from this channel have not received a large amount of attention. However, a new radiometric calibration technique by Carrozzo et al. (2012) may provide a means to better utilize these data. Therefore, a detailed account of features in this region should prove useful. The OMEGA SWIR sensor covers the ~0.92 to 2.7 μm wavelength region; however, because the detector used for this study only measures reflectance out to 2.5 μm, data from 0.9 to 2.5 μm are presented.

Amorphous Fe^{3+} sulfates. In crystalline, Fe^{3+}-bearing minerals, absorptions due to spin-forbidden crystal field transitions of Fe^{3+} are observed between 0.3 and 1 μm (**Figure 5-9**). When Fe^{3+} is linked through an oxygen or hydroxyl group, spin polarization and magnetic coupling remove degeneracy, and lead to three common transitions: $^6A_{1g}$-($^4A_{1g}$,^4E_g), $^6A_{1g}$-$^4T_{2g}$, and $^6A_{1g}$-$^4T_{1g}$ (Rossman 1975; Cloutis et al. 2006). In iron-sulfates, these occur at ~0.43 μm, 0.5-0.6 μm, and 0.8-0.9 μm, respectively (Cloutis et al. 2006), where oxo-bridged iron leads to deeper features than hydroxo-bridged iron (Sherman and Waite 1985; Cloutis et al. 2006). The shape and position of these features relate to the distortion of the iron octahedra in the minerals (Burns 1993; Frost et al. 2005). Through this wavelength range, the amorphous ferric sulfate samples are distinct from the reference (crystalline sample) spectra. The absorptions due to Fe^{3+}

spin forbidden crystal field transitions are listed in **Table 5-1** along with those values for several common sulfates from Cloutis et al. (2006). Noting that the position of the ^6A1_g-($^4A_{1g}$,^4E_g) of all the ferric sulfates are similar, the $^6A_{1g}$-$^4T_{2g}$ and the $^6A_{1g}$-$^4T_{1g}$ absorptions can be plotted in two dimensions to clarify the distinction in amorphous vs. crystalline energies (**Figure 5-9**).

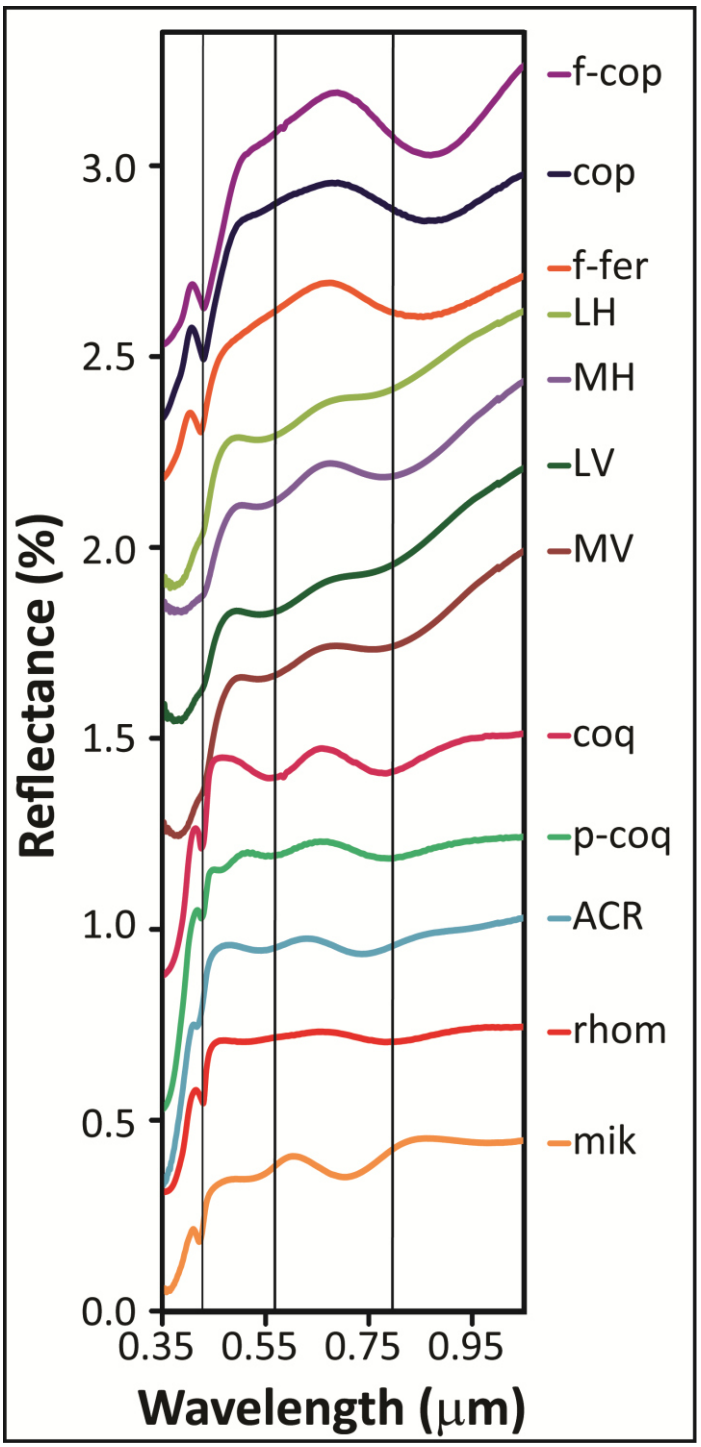

Figure 5-9. VIS spectra of (from the top) ferricopiapite S35 (<125 μm), copiapite spt117 (<45 μm), fibroferrite spt121 (<45 μm), LH-amorphous Fe^{3+} sulfate, MH-amorphous Fe^{3+} sulfate, LV-amorphous Fe^{3+} sulfate, MV-amorphous Fe^{3+} sulfate, coquimbite S40 (<125 μm), paracoquibite spt137 (<45 μm), Acros starting material (XRD match to lausenite), rhomboclase spt139 (<45 μm), and mikasaite. Reference samples are from the RELAB spectral library. Spectra are scaled and offset for clarity. Average positions of absorptions for the amorphous sulfates are shown with vertical lines.

Table 5-1. Positions of the ferric iron spin-forbidden crystal field transitions as seen in the VIS region of the VNIR spectrum. Exact positions were obtained for the amorphous samples by performing a continuum removal on the VNIR spectra. The comparison values are those provided by Cloutis et al. (2006). All values are reported in microns.

	^6A1_g-($^4A_{1g}$,^4E_g)	$^6A_{1g}$-$^4T_{2g}$	$^6A_{1g}$-$^4T_{1g}$
Ferricopiapite	0.431	0.550	0.860-0.873
Copiapite	0.430	0.550	0.855-866
Fibroferrite	0.427	0.550	0.844
LH-amorphous	0.430	0.565	0.789
MH-amorphous	0.429	0.558	0.812
LV-amorphous	0.428	0.579	0.776
MV-amorphous	0.429	0.570	0.808
Coquimbite	0.423-0.433	0.553-0.558	0.774-0.775
Acros (lausenite)	0.421	0.551	0.746
Rhomboclase	0.429	0.530	0.785
Mikasaite	0.424	0.535	0.709

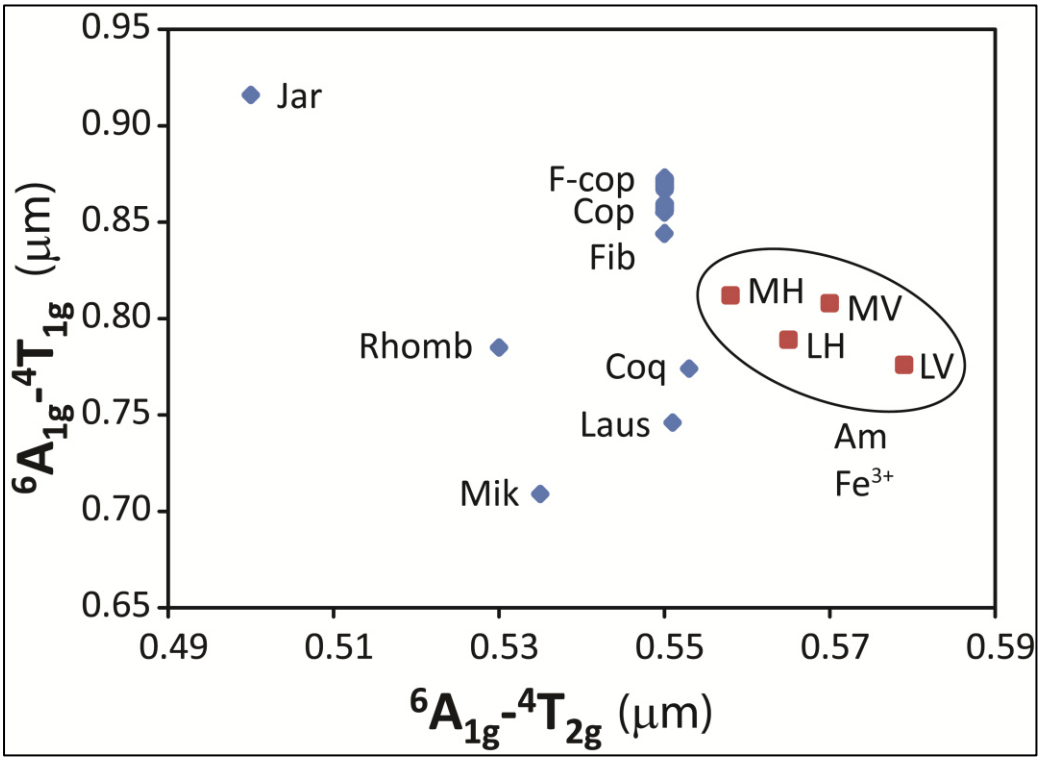

Figure 5-10. Plot of the VIS absorption positions for the $^6A_{1g}$-$^4T_{1g}$ vs. the $^6A_{1g}$-$^4T_{2g}$ spin forbidden crystal field transitions for the crystalline (blue) and amorphous (red) ferric sulfates.

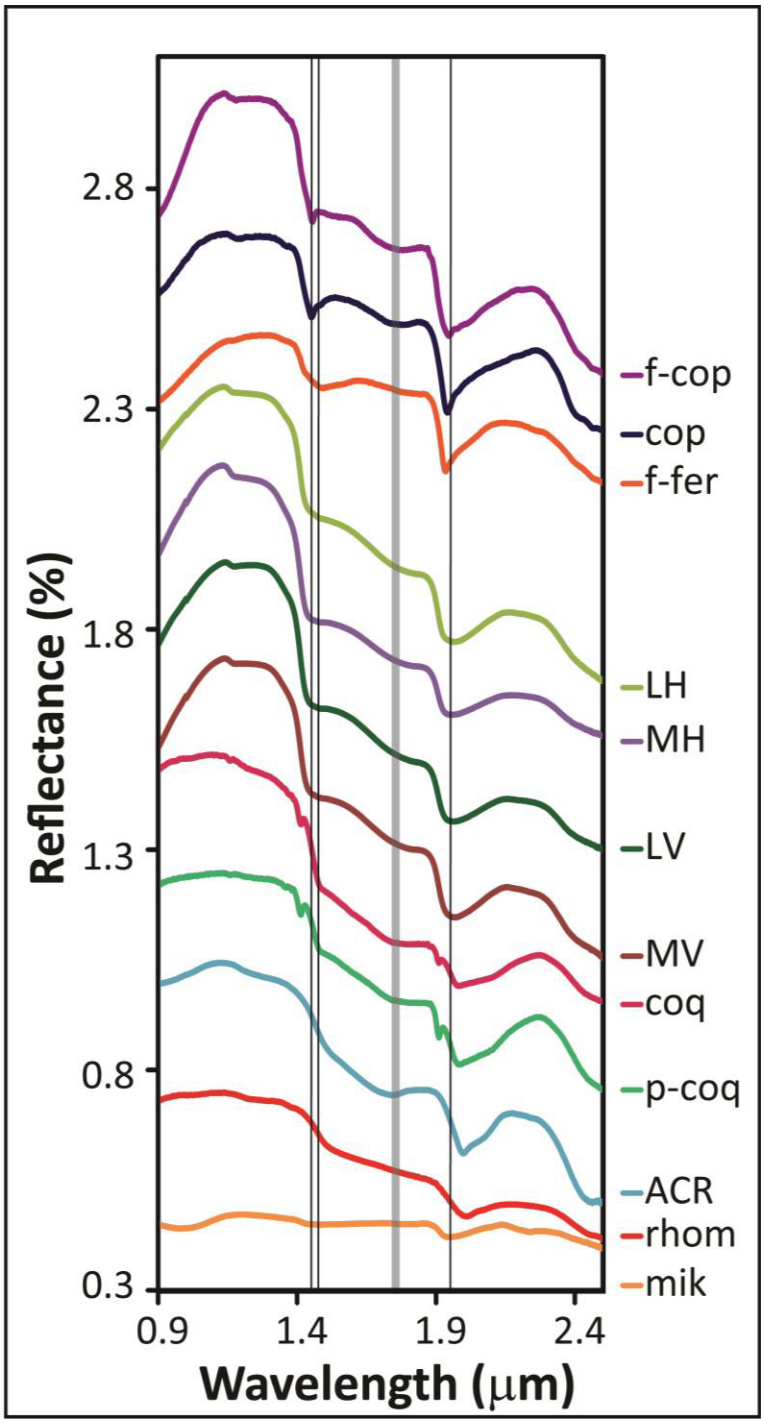

Figure 5-11. SWIR spectra of (from the top) ferricopiapite S35 (<125 μm), copiapite spt117 (<45 μm), fibroferrite spt121 (<45 μm), LH-amorphous Fe^{3+} sulfate, MH-amorphous Fe^{3+} sulfate, LV-amorphous Fe^{3+} sulfate, MV-amorphous Fe^{3+} sulfate, coquimbite S40 (<125 μm), paracoquibite spt137 (<45 μm), Acros starting material (XRD match to lausenite), rhomboclase spt139 (<45 μm), and mikasaite. Reference samples are from the RELAB spectral library. Spectra scaled are offset for clarity. Positions of absorptions for amorphous sulfates are shown with vertical lines.

In the SWIR wavelength region (**Figure 5-11**), H_2O-and OH-bearing sulfates show absorptions due to OH stretching overtones (~1.4 μm), overtones and combinations of structural H_2O (~1.4 μm), combinations of bending, stretching, and rotational features for OH and H_2O (~1.7-1.8 μm), H_2O combination modes (~1.9 μm), and combinations of bending, stretching, and rotational features for OH and H_2O along with S-O bending overtones (2.0-2.5 μm) (Cloutis et al. 2006).

Spectrally, the amorphous ferric sulfates appear similar to other polyhydrated sulfate species reported by Gendrin et al. (2005), with broad, muted absorptions related to H_2O vibrational combination and overtone modes and S-O vibrational overtones. They have broad reflectance maxima at 1.14 μm, similar to ferricopiapite, and they also display weak doublets at 1.45 and 1.47 μm, broad absorptions at 1.73-1.77 μm, and broad, asymmetrical and strong absorptions centered at 1.95 μm. These samples lack distinct absorptions in the 2.0-2.4 μm region. The amorphous ferric sulfate spectra also show decreasing reflectance towards longer wavelengths (blue slope) past ~1.43 μm. The broadening and smearing of H_2O and OH features in materials is often seen when there is structural disorder or where there are many non-equivalent water sites. In these cases, the sloping spectrum indicates the overlap of a large number of H_2O and OH features (Hunt 1977). Both the slopes and positions of the absorptions in the amorphous samples are most similar to ferricopiapite. Although all of the amorphous ferric sulfate samples share common features with many other sulfates, they do appear spectrally unique, specifically in the plateau-like right wing of the 1.9 μm feature.

Amorphous Fe^{2+} sulfate. The VIS and SWIR spectra of the amorphous ferrous sulfate sample are shown in **Figure 5-12** and **Figure 5-13**, respectively. Unlike the amorphous ferric sulfates, the amorphous ferrous sulfate is dissimilar from common crystalline phases to which it

is compared. It displays a reflectance maximum at 0.660 μm, a broad absorption at 1.076 μm due to Fe^{2+} spin allowed, crystal field transitions (Crowley et al. 2003), and water combination bands at 1.456 and 1.947 μm. Although the water features are similar in position to those in melanterite, the amorphous sample displays only one iron absorption, rather than the two seen in melanterite, rozenite, and szomolnokite. Because the presence of the second Fe^{2+} crystal field absorption is caused by a distortion in the symmetry of the iron octahedral site (Hunt 1977), the absence of a second absorption in the amorphous ferrous sulfate could indicate that the iron octahedra in the amorphous sulfate are less distorted than those in the crystalline sulfates.

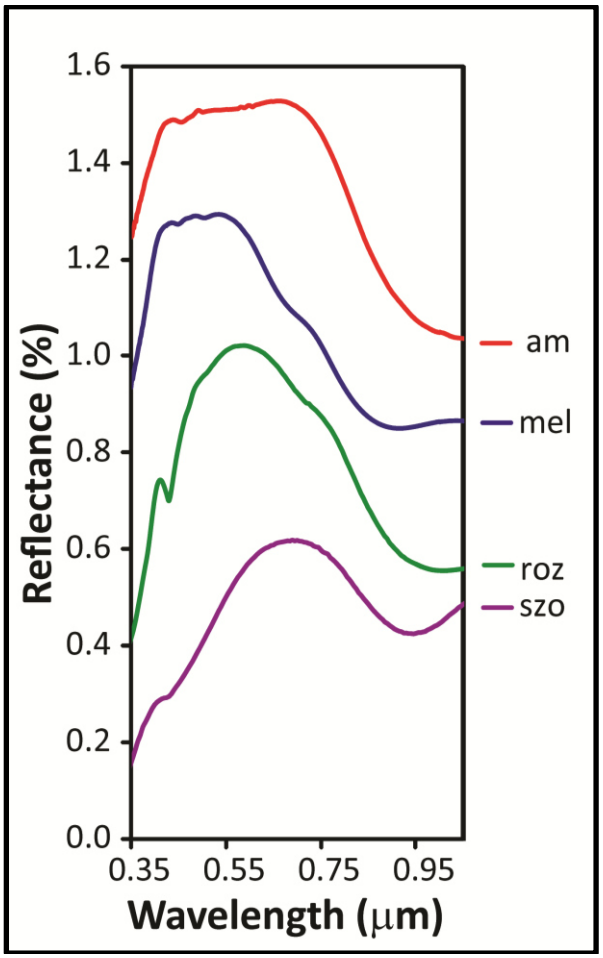

Figure 5-12. VIS spectrum of vacuum dehydrated, amorphous ferrous sulfate plotted with melanterite, rozenite JB626 (<125 μm), and szomolnokite S60 (<125 μm). Spectra are offset for clarity.

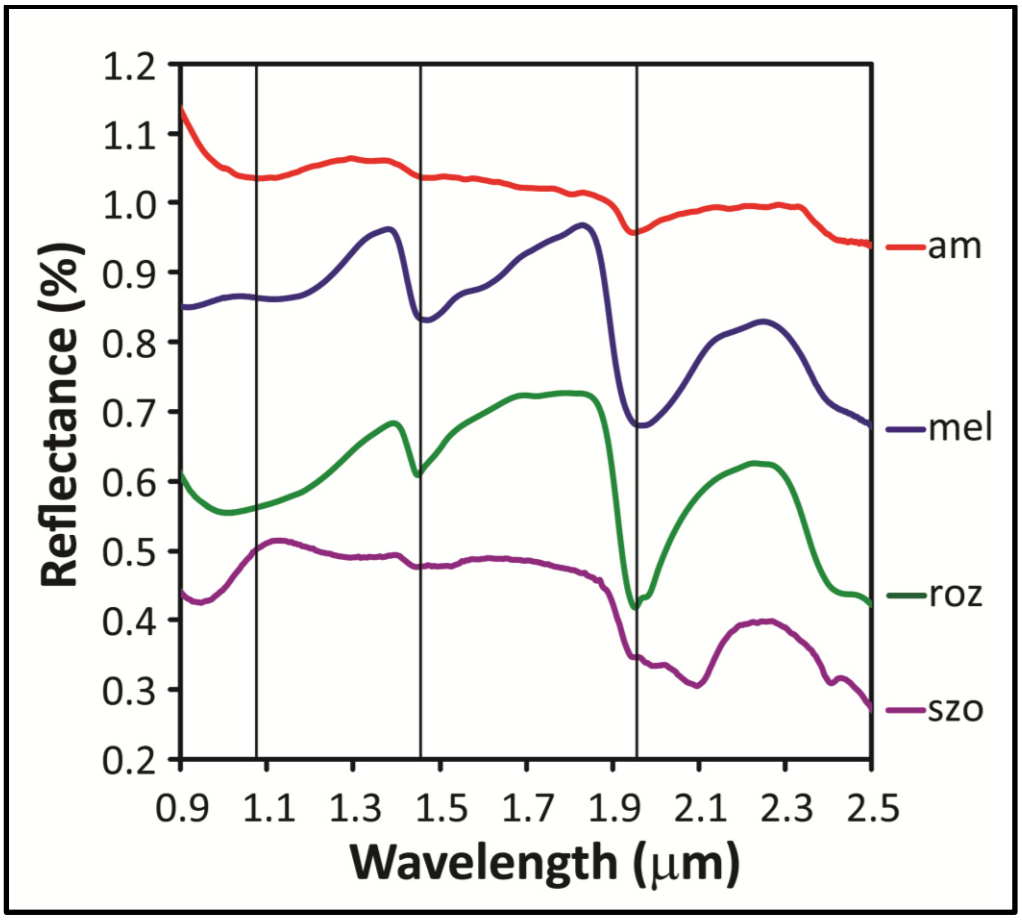

Figure 5-13. SWIR spectrum of vacuum dehydrated, amorphous ferrous sulfate plotted with melanterite, rozenite JB626 (<125 μm), and szomolnokite S60 (<125 μm). Spectra are offset for clarity. Positions of absorptions for amorphous sulfate are shown with vertical lines.

5.3.4 MIR emissivity spectroscopic observations

MIR emissivity spectra of iron sulfates are dominated by absorptions due to S-O vibrations in sulfate tetrahedra. The free sulfate anion has 4 vibrational modes: an asymmetric S-O stretch (ν_3; 1105 cm^{-1}), a symmetric S-O stretch (ν_1; 983 cm^{-1}), an asymmetric S-O-S bend (ν_4; 611 cm^{-1}), and a symmetric S-O-S bend (ν_2; 450 cm^{-1}) (Nakamoto 1986; Lane 2007). In a free or undistorted sulfate polyhedron, only ν_3 and ν_4 are IR active, but when the sulfate anion is in a structure, it often distorts such that absorptions due to ν_1 and ν_2 are also visible. These distortions

also affect the energy of the absorptions, making the MIR emissivity spectrum diagnostic (Lane 2007).

Amorphous Fe^{3+} sulfates. Emissivity spectra of pressed pellets of the amorphous ferric sulfates are plotted in **Figure 5-14** along with emissivity spectra of pressed pellets of the Acros starting material (XRD match to lausenite), the cooked starting material (mikasaite), and three ferric sulfates (ferricopiapite, coquimbite, and jarosite) for which there were emissivity data from Lane et al. (2007). The amorphous ferric sulfates are all very similar, displaying three overlapping ν_3 bands at approximately 1203, 1112, and 1025 cm^{-1}, one ν_1 band at 989 cm^{-1}, two ν_4 bands at 650 and 588 cm^{-1}, and a ν_2 absorption around 455 cm^{-1}. The low frequency ν_3 absorption and the ν_1 absorption are smoothed together in the vacuum dehydrated samples, whereas they are more distinct in the desiccated samples.

Based on the chemical formula and hydration state of the amorphous ferric samples (~6-8H_2O), the closest crystalline counterparts in **Figure 5-14** are the Acros starting material (lausenite, $Fe(III)_2(SO_4)_3 \bullet 6H_2O$, "ACR") and (para)coquimbite ($Fe(III)_2(SO_4)_3 \bullet 9H_2O$. However, the ν_1 and ν_3 band envelopes of the amorphous phases coincide more with those of ferricopiapite ($Fe(III)_{2/3}Fe(III)_4(SO_4)_6(OH)_2 \bullet 20H_2O$) than of lausenite or coquimbite. This observation is consistent with the total x-ray scattering data and Mössbauer data, which point to short- and medium-range (< 10Å) structure most similar to ferricopiapite (**Section 5.3.2**). Absorptions related to S-O-S bending and ferric sulfate lattice modes (< 650 cm^{-1}) are similar between the amorphous phases, ferricopiapite, lausenite, and coquimbite.

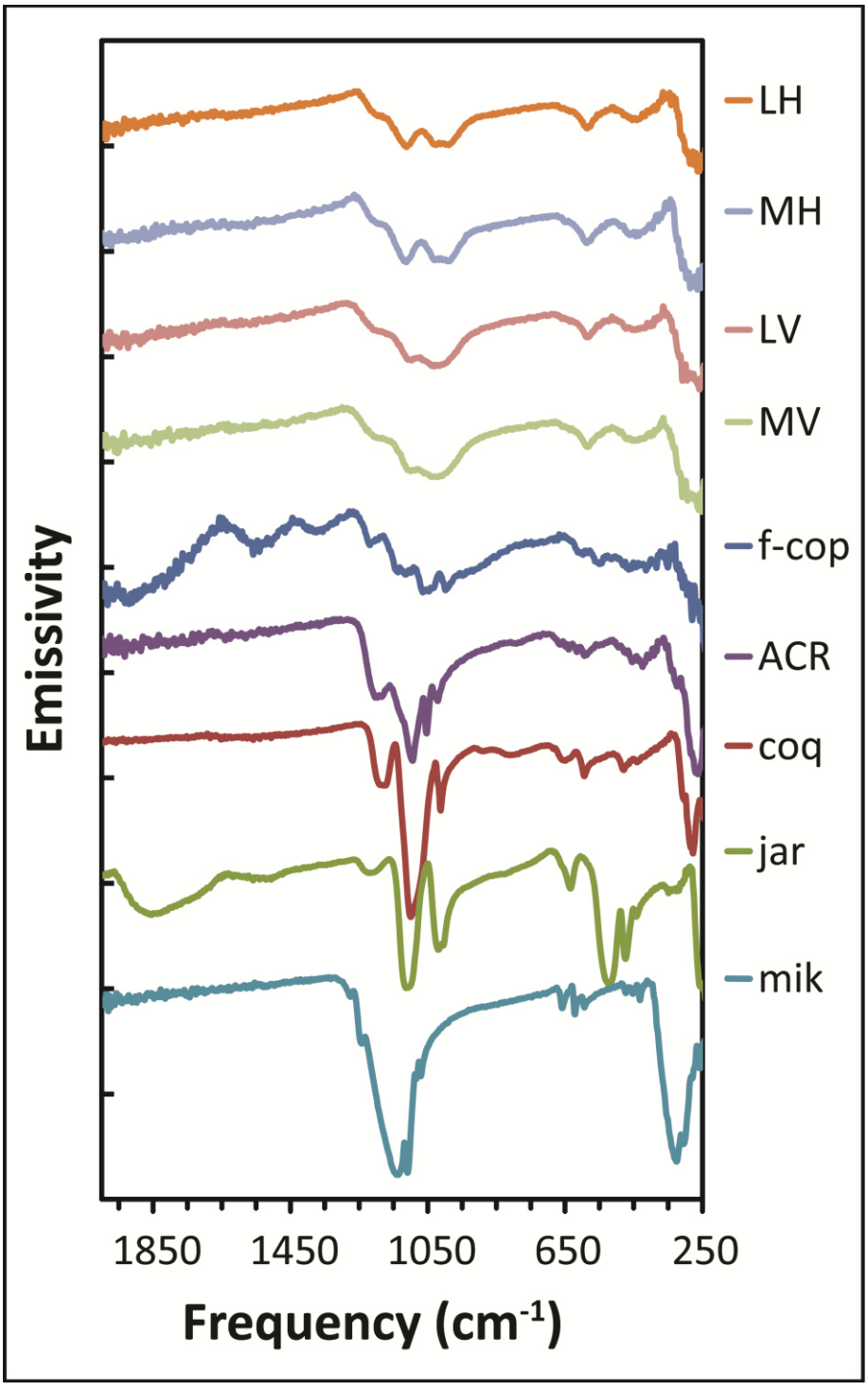

Figure 5-14. Emissivity spectra of (from the top) LH-amorphous ferric sulfate, MH-amorphous ferric sulfate, LV-amorphous ferric sulfate, MV-amorphous ferric sulfate, ferricopiapite S35, Acros starting material (XRD match to lausenite), coquimbite S46, jarosite S51, and mikasaite. Reference samples S35, S46, and S51 are from the ASU spectral library. All samples are in the form of pressed powder pellets. Spectra are scaled and offset for clarity.

Amorphous Fe^{2+} sulfates. An emissivity spectrum of a pressed-pellet of the amorphous ferrous sulfate is plotted in **Figure 5-15** along with emissivity spectra of pressed pellets of the melanterite starting material, rozenite, and szomolnokite. The amorphous ferrous sulfate displays two deep ν_3 bands at 1135 and ~1062 cm^{-1}, one ν_1 band at 970 cm^{-1}, one ν_4 band at 592 cm^{-1} with a shoulder at ~650 cm^{-1}, and two ν_2 bands at 455 and 441 cm^{-1}. These band positions are distinct from those of other ferrous sulfates. Based on chemical formula and hydration state, the closest crystalline counterpart to the amorphous ferrous sulfate is szomolnokite ($FeSO_4 \cdot H_2O$). Though the general ν_1 and ν_3 band envelope of the amorphous phase overlaps with szomolnokite, the specific band center positions are significantly shifted for all stretching and bending modes.

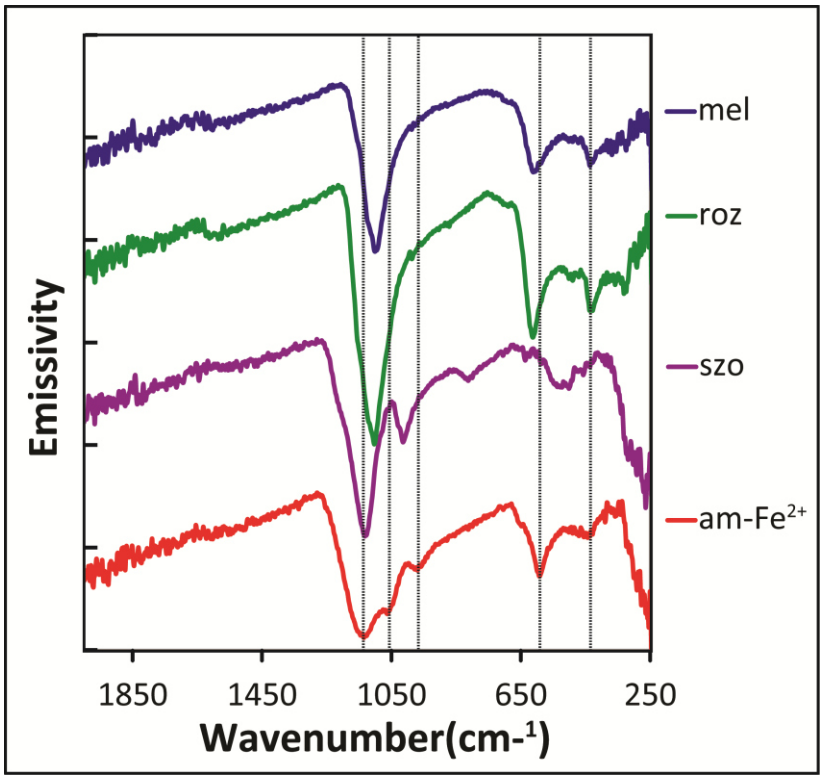

Figure 5-15. Emissivity spectra of (from the top) melanterite starting material, rozenite, szomolnokite, and vacuum dehydrated, amorphous ferrous sulfate. All samples were in the form of pressed powder pellets. Rozenite and szomolnokite were made from melanterite and all phases were confirmed by XRD. Spectra are scaled and offset for clarity.

5.3.5 Mössbauer spectroscopic observations

Amorphous Fe^{3+} sulfates. Mössbauer spectra of the amorphous ferric sulfates are shown in **Figure 5-16**, and the fit parameters are listed in **Table 5-2**. The spectra for the amorphous sulfates synthesized by all four formation pathways are similar. They can all be fit with a single ferric doublet with an isomer shift of 0.44-0.45 mm/s, typical for ferric sulfates (Dyar et al. (2013); **Table 5-2**). The quadrupole splitting (Δ) values show more variation with Δ for the hydration-dehydration samples of 0.33-0.34 mm/s and Δ for the hydration-vacuum samples of 0.39 mm/s. The increase in quadrupole splitting for the vacuum dehydrated samples indicates an increased distortion in the coordination polyhedron surrounding iron in those samples (Burns and Solberg 1990; Dyar et al. 2013). An extensive study of the Mössbauer parameters of sulfates by Dyar et al. (2013) allows for the comparison of these values to those for many common sulfates. The amorphous ferric sulfate doublet is most similar to a doublet in ferricopiapite, which represents one of two non-equivalent iron sites in that mineral.

Amorphous Fe^{2+} sulfates. The fitted Mössbauer spectrum for the amorphous ferrous sulfate is shown in **Figure 5-17**, and the fit parameters are listed in **Table 5-3**. The Mössbauer spectrum of the amorphous ferrous sulfate bears no similarity to any ferrous sulfate presented in the comprehensive study of iron sulfates by Dyar et al. (2013). It can be fit with three overlapping doublets, all with isomer shift of 1.28-1.29 mm/s and quadrupole splitting values of 1.62, 2.24, and 2.73 mm/s. A distribution of doublets like this can indicate a range of non-equivalent sites, and the exact position of each doublet may not be conclusive for identification purposes. However, it is worth noting that the doublet with the highest velocity Δ value is a close match for that of szomolnokite.

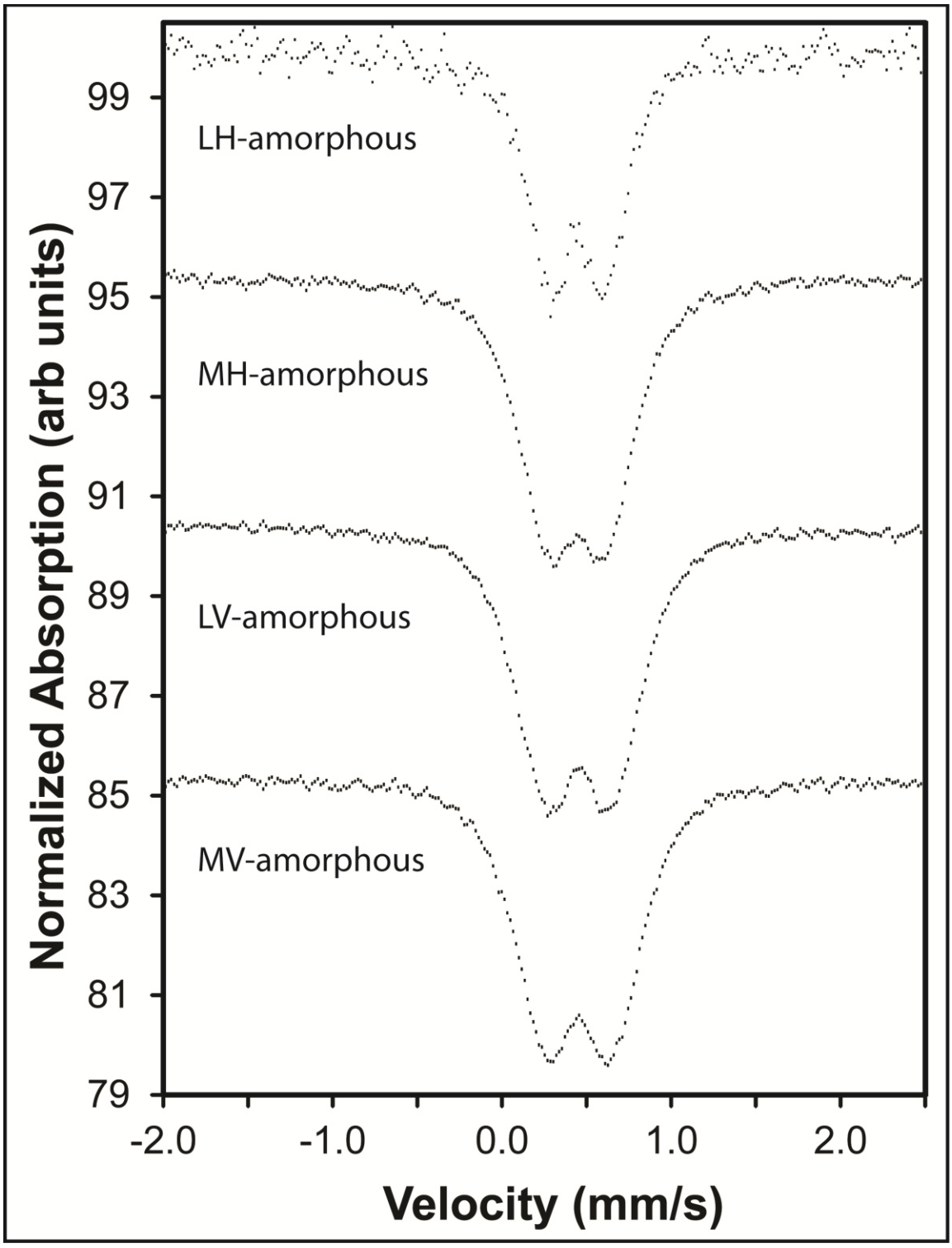

Figure 5-16. Mössbauer spectra of amorphous ferric sulfates taken at 295 K. Spectra are scaled and offset for clarity.

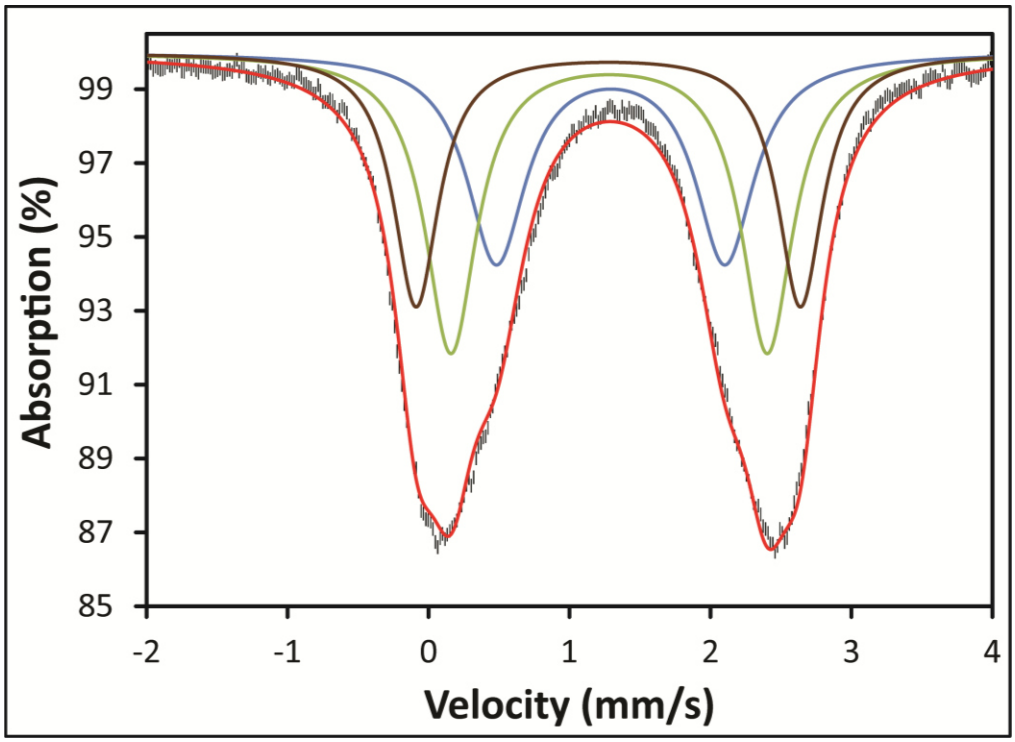

Figure 5017. Mössbuaer spectrum of amorphous ferrous sulfate taken at 295 K. Three distributions and total fit are overlayed on the spectrum.

Table 5-2. Mössbauer fit parameters for the amorphous ferric sulfates samples.

Sample	δ	Δ	Γ	χ^2
LH-amorph	0.445	0.328	0.293	1.31
MH-amorph	0.441	0.341	0.381	1.97
LV-amorph	0.453	0.393	0.399	3.56
MV-amorph	0.453	0.394	0.399	2.71

Table 5-3. Mössbauer fit parameters for the amorphous ferric sulfate.

Amorphous ferrous sulfate			
Dist.	**1**	**2**	**3**
δ	1.29	1.28	1.28
Δ	1.62	2.24	2.73
Γ	0.51	0.44	0.40
%Area	31.3	39.4	29.3
χ2	6.53		

5.3.6 VNIR and MIR characterization of basalt - amorphous ferric sulfate mixtures

Because the amorphous ferric sulfates are formed through the dehydration of solutions, it is possible for them to form as cementing coatings on grains and as alteration products of deliquesced surface material. Recently, Masse et al. (2014) investigated the spectral effects of coating basalts in brines at Mars relevant pressures and temperatures. Although they started with anhydrous ferric sulfate, after hydrating and then dehydrating they also had a hydrated ferric sulfate species spectrally mixed with their basalt. Several experiments were performed where ~0.38 g of amorphous ferric sulfate was precipitated onto 0.50 g of terrestrial flood basalt sands (63 μm grains). Optically, the amorphous ferric sulfates redden the surface of the basalt sands and grind into a fine powder, visually similar to the ground unaltered basalt (**Figure 5-18**). The spectra are dominated by the spectrally opaque basalt rather than the sulfate (**Figure 5-19** and **Figure 5-20**) and the VNIR spectrum bears a striking similarity to the end product observed by Masse et al. (2014). Although the detection of these sulfates is clearly possible in the VNIR range, the discrimination of them from other polyhydrated phases, especially without the visible wavelength range, may be challenging due to the spectral dominance of the basalt. In the MIR range, the presence of amorphous sulfate in a basalt mixture is limited to the presence of the ν4 absorption, making the emissivity spectrum of the coated material nearly identical to that for the unaltered basalt. Since the coated basalt was ground and then pressed into a pellet before the emissivity spectrum was obtained, it is unlikely that the MIR light simply passed through the coating to sample only the basalt.

Figure 5-18 Image of MH-amorphous precipitated onto <63 μm flood basalt unground (left) and ground (right). The inset on the right shows the ground, uncoated flood basalt.

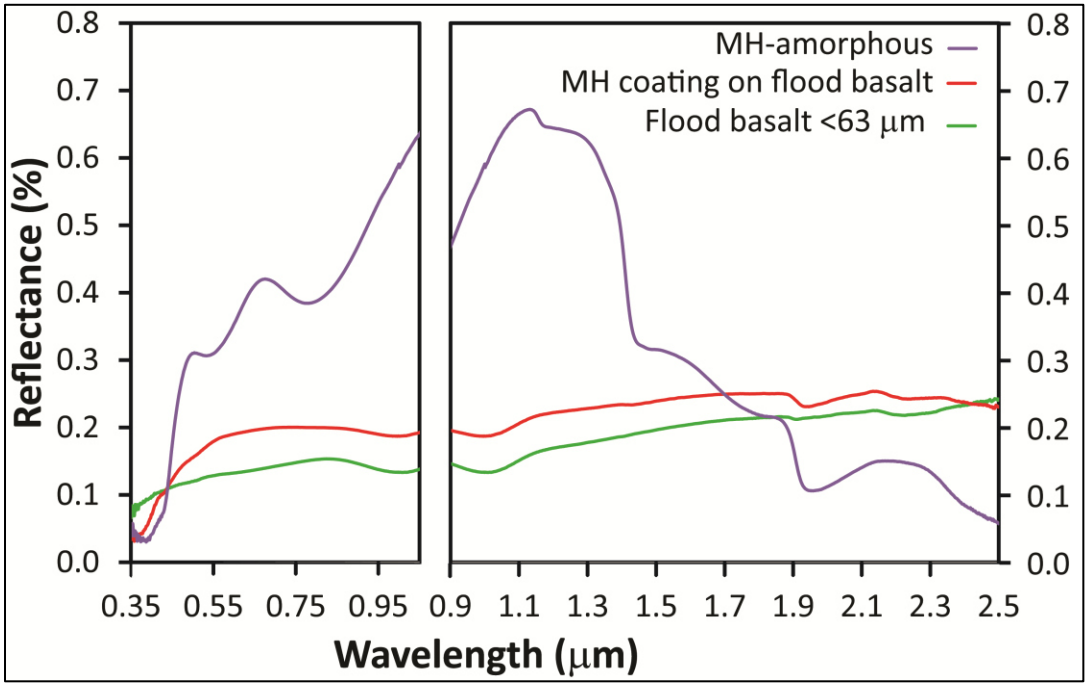

Figure 5-19. VIS (left) and SWIR (right) spectra of MH-amorphous ferric sulfate, MH-amorphous ferric sulfate precipitated onto <63 μm flood basalt, and <63 μm flood basalt.

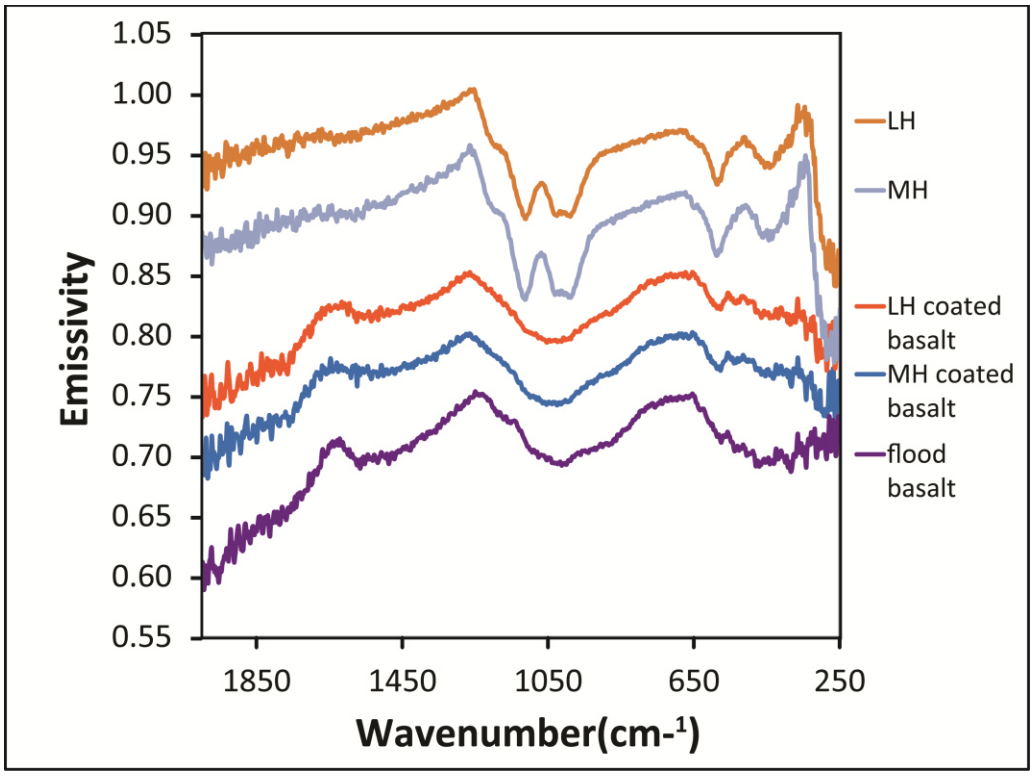

Figure 5-20. Emissivity spectra of (from the top) LH-amorphous ferric sulfate, MH-amorphous ferric sulfate, LH-amorphous ferric sulfate precipitated onto <63 μm basalt, MH-amorphous precipitated onto < 63 μm basalt, and < 63 μm flood basalt. All samples were measured as pressed powder pellets. Spectra are offset for clarity.

5.4 DISCUSSION

5.4.1 Structural and spectral comparison to crystalline iron sulfates

Each analysis technique used in this study provides different yet complementary information about the sample structures. Mössbauer data provides information about the number of non-equivalent iron sites in the structure, the valence state of iron in those sites, the coordination of iron in those sites (based on the value of the isomer shift), and information about the distortion of those sites (based on the quadrupole splitting value). PDF data provides short and medium range structural detail through mapping the bond lengths in the structure but requires myriad reference structures for complete structural determination. VIS data provides

information pertaining to the energy of the Fe^{3+} spin forbidden crystal field transitions (Hunt 1977), and because these transitions arise from the magnetic coupling of linked octahedral (Sherman et al. 1982), they are more sensitive to longer range structure, specifically along oxo- and hydroxo-bridged M-ligand units (Rossman 1975). Therefore, the VIS data may indicate structural differences not seen at the level of individual octahedra and, therefore, not as readily apparent from the Mössbauer data. Thermal infrared (TIR) absorptions arise from vibrational frequencies associated with molecular bending, stretching and translation, which are affected by bond lengths and angles. Thus the TIR data are sensitive to both short- and long-range structure.

Amorphous Fe^{3+} sulfates. The Mössbauer parameters for the amorphous ferric sulfates are very close to those for one doublet in ferricopiapite, indicating that the configuration of the coordination polyhedron in both the amorphous ferric sulfates and in ferricopiapite are likely similar. Likewise, in the MIR, despite the chemical and hydration state similarity to lausenite and (para)coquimbite, the band envelopes of the ν_3 and ν_1 absorptions most closely match ferricopiapite. PDF data (**Figure 5-6** and **Figure 5-7**) for the amorphous ferric sulfate samples mirror the conclusions from both Mössbauer and MIR data. Although the amorphous samples only possess structural order to about 10 Å, over that distance, their pair correlations are more similar to ferricopiapite, which is composed of finite clusters of $M_2(TO_4)_2O_7$ (Hawthorne et al. 2000), and less similar to mikasaite, which is composed of an infinite framework of "pinwheels" (Hawthorne et al. 2000). The greatest differences between the amorphous phases and ferricopiapite are observed at distances greater than 5 Å, or beyond the first octahedral unit. The position of the absorptions from the Fe^{3+} spin forbidden crystal field transitions (**Figure 5-10**) observed in the VIS data also indicate that the amorphous ferric sulfate samples show distinct longer range structure. Generally, the absorption from the Fe^{3+} $^6A_{1g}$-$^4T_{1g}$ spin-forbidden

transition (**Figure 5-10**, y-axis) is greater (in wavelength space) for hydroxo-bridged minerals than for oxo-bridged minerals, with the highest values corresponding to minerals with the most extensive networks of hydroxo-bridged octahedra (Rossman 1975; Rossman 1976). The opposite trend can be seen for the absorption from the Fe^{3+} $^6A_{1g}$-$^4T_{2g}$ spin-forbidden transition (**Figure 5-10**, x-axis); here, higher values (in wavelength space) correspond to minerals with less extensive octahedral linkages, such that absorption from the hydroxo-bridged dimers in copiapite is greater than that for the hydroxo-bridged chains of octahedra in botryogen or butlerite (Rossman 1975; Rossman 1976). Given these general trends, the amorphous ferric sulfates' VIS absorptions are most consistent with oxo-bridged, clusters – possibly dimers. PDF data on additional ferric sulfates of different base structural units are required for a more complete structural analysis.

Amorphous Fe^{2+} sulfates. The Mössbauer spectrum for the amorphous ferrous sulfate is unlike any crystalline ferrous sulfate reviewed by Dyar et al. (2013). However, the parameters of the doublet with the highest velocity Δ are a match to szomolnokite. The parameters with the lowest velocity Δ are closest, although not a match, to one doublet in voltaite. This similarity is worth noting simply because both the site in voltaite and the site in szomolnokite have Fe^{2+} coordinated by 4 oxygens from SO_4 groups and two from H_2O groups (Dyar et al. 2013). Mössbauer parameter similarities are not, however, unique enough to draw structural conclusions in the absence of other evidence (Dyar et al. 2013). Multiple overlapping doublets in the Mössbauer fit can indicate a range of non-equivalent sites for iron, rather than energetically similar but distinct sites. The MIR data support this conclusion showing broad, muted features.

The VNIR spectrum of the amorphous ferrous sulfate only displays a single absorption from the spin allowed $E_g \rightarrow T_{2g}$ Fe^{2+} crystal field transition. The crystalline ferrous sulfates display two absorptions, which is common for minerals where octahedral distortion has caused

further splitting of the energy levels (Hunt 1977). Cloutis et al. (2006) noted that ferrous iron-bearing sulfates display two absorptions from the Fe^{2+} crystal field transition when the iron is coordinated by only H_2O, as is the case for melanterite, but displays only one when the iron is coordinated by SO_4 and H_2O, as is the case for rozenite and szomolnokite. These findings are in contrast to those of Crowley et al. (2003), who found two Fe^{2+}-related absorptions for all three minerals. Sulfates are, however, challenging to analyze as they transform readily between phases, so it is unclear which of these analyses is correct. Crowley et al. (2003) did indicate that they performed their analyses at conditions intended to stabilize these phases, but my experience has been that phase transformations can occur very rapidly in ferrous sulfates based on ambient RH conditions, and VNIR analyses are more likely to sample these changes since the penetration depth of VNIR light is on the order of a few μm. In either case, the position of the absorption in this amorphous sample is shifted by ~0.10 μm to higher wavelengths, making it more similar to Fe^{2+} in silicates than in sulfates.

As with the Mössbauer and VNIR data, the MIR spectrum does not show any similarity to crystalline ferrous sulfates. The general ν_3 and ν_1 band envelope overlaps with szomolnokite (which has a similar hydration state to the amorphous phase), but features within that envelope are significantly shifted. Further work to characterize this structure is currently underway.

The PDF data (**Figure 5-8**) for the amorphous ferrous sulfates do show some short-range (< 6 Å) similarities with both szomolnokite and rozenite but also some differences. For instance, the peak attributed to the Fe-O distance is slightly different in all three samples as well as the O-O distances in sulfate and the Fe-Fe distance between adjacent units. These data, like the Mössbauer, VNIR, and MIR data, suggest that although the structure of the amorphous ferrous

sulfate is similar to the reference compounds, it is certainly not the same. More work is needed to determine the specific short and medium range structure for this sample

5.4.2 Effects of dehydration method and starting material on amorphous phase characteristics

Amorphous Fe^{3+}sulfates. Based on observations from the suite of techniques used in this study, it seems that the starting materials used for synthesis of the amorphous ferric sulfates have little effect on the structure of the amorphous phase. The observed structural similarities between amorphous samples synthesized from different starting materials are not unexpected because both starting materials deliquesce at 92% relative humidity, producing similar fluids. Although the starting material had little effect on the amorphous product, the method of dehydration did have a small influence on the Mössbauer quadrupole splitting parameter and the MIR emissivity spectra. The vacuum dehydrated samples have a higher quadrupole splitting (Δ) value than those dehydrated using buffering salts (**Section 5.3.5**). The increase in Δ indicates an increase in the distortion of the iron octahedron (Burns and Solberg 1990; Dyar et al. 2013). The MIR emissivity spectra also show slight differences due to the method of dehydration. The ν_3 and ν_1 absorptions are smoothed together in the vacuum dehydrated samples but are better defined in the samples dehydrated using RH buffering salts (Section 3.4). In the MIR, broadening features also indicate structural disorder, since a given absorption may occur over a greater range of energies, indicating a range of configurations and coordinations within the solid. The increased disorder for the vacuumed samples, observed in the MIR, SWIR, and Mössbauer data, is likely due to the relative rate of water loss; the vacuumed samples, which dehydrate more quickly, have a greater degree of disorder.

5.4.3 A case for amorphous iron sulfates on Mars

Recent results from the Mars Science Laboratory's (MSL) analysis of the Rocknest Soil at Gale Crater have added valuable information to our understanding of the Martian surface sediments. The soil at Rocknest was analyzed by ChemMin and SAM providing XRD and evolved gas analysis (EGA) data. Those analyses, reported in a series of papers by the science team (Bish et al. 2013; Archer et al. 2014; McAdam et al. 2014), estimated that 27 wt% of the Rocknest soil is XRD amorphous material and that material contains 21.01 wt% $FeO+Fe_2O_3$ and 5.18 wt% SO_3 (Morris et al. 2013). EGA results showed high levels of evolved H_2O and SO_2. The temperature at which some of the sulfate evolved is consistent with Fe sulfates (too low for Ca and Mg sulfates) (McAdam et al. 2014), yet no evidence for Fe sulfates, or any hydrated sulfate, was found by ChemMin in the crystalline portion of the Rocknest soil (Bish et al. 2013; McAdam et al. 2014). If the SO_2 attributed to sulfate was present as a crystalline sulfate phase, it should have been present above the ChemMin detection limit (McAdam et al. 2014). Therefore, the team has concluded that some percentage of the evolved SO_2 has come from the amorphous portion of the Rocknest soil. McAdam et al. (2014) interpret the iron in the amorphous portion to be likely present as nanophase iron oxide (XRD amorphous), as is consistent with Mössbauer findings at Meridiani Planum, and interpret the sulfate to be present as a sulfate anion adsorbed onto the surface of other XRD amorphous phases, like allophane or nanophase iron oxide.

An alternative explanation for the recent Rocknest findings could be that some of the evolved SO_2 and H_2O have come from amorphous Fe sulfates. Under conditions of high relative humidity (likely present in the shallow subsurface (Wang et al. 2013)), crystalline ferric sulfates would deliquesce. Then, once brought to low relative humidity (e.g. through excavation or brine flow), rapid dehydration would lead to structural disorder. Their ability to change hydration state

without crystallizing increases their potential longevity in the Martian climate. Under the ambient laboratory conditions in Stony Brook University's geology department (23 ºC, 14 %RH), the amorphous samples can remain XRD amorphous for several days. The low temperatures of the Martian surface and subsurface would retard the crystallization of these phases, because the activation energy may not be available for a change of structure. Therefore, it is likely that the daily Martian RH fluctuations would result in hydration and dehydration of the amorphous phase but not necessarily induce crystallization. And thus it would be possible for them to become incorporated into the regolith.

More broadly, evidence for a present-day brine hydrologic cycle suggests that amorphous sulfates could be present in soil as brine evaporative products in a more widespread fashion. Ferric sulfate brines have a eutectic temperature of 205 K, which would allow them to form anywhere on the Martian surface and over much of the Martian shallow subsurface (Chevrier and Altheide 2008). Because amorphous ferric sulfates are formed directly from the saturated fluid, evaporation or boiling of these brines has the potential to deposit amorphous ferric sulfates on the Martian surface. Ferrous sulfate brines, on the other hand, have a relatively high eutectic temperature of 267.2 K (Altheide et al. 2009). In addition, based on the similarity between Mg sulfates and ferrous sulfates, it is unlikely that ferrous sulfates would precipitate directly from a brine. Several studies have demonstrated that amorphous Mg sulfates can only be formed through a crystalline phase (Vaniman et al. 2004; Chipera and Vaniman 2007; Altheide et al. 2009) and these current experiments on ferrous sulfates, along with the experiments performed by Altheide et al. (2009), and Wang and Zhou (2014), indicate that there is no phase boundary between the saturated fluid and amorphous ferrous sulfate. In other words, despite current efforts from these experiments and those of other authors, (Wang and Zhou 2014), ferrous sulfates have

not been successfully precipitated from brines, and they go through other phases before deliquescence. Therefore, a brine dehydration scenario would not likely lead to amorphous ferrous sulfates. Wang and Zhou (2014) do show, however, that amorphous ferrous sulfate begins to form at Mars relevant pressures and relative humidities over the course of their 102 h experiment at 21 ºC. Their lower temperature experiments only lasted 174 h for 0 ºC and 238 h for -12 ºC, so it is likely that the amorphous phase did not have sufficient time to form. The implication is that, although amorphous ferrous sulfate is not likely to appear in an aqueous alteration region, it may form through the exposure of higher hydrates to lower RH conditions through processes that bring material from the subsurface to the surface. Although amorphous ferrous sulfates may form on Mars, it is unlikely that we will detect them since the amorphous ferrous sulfates are found to oxidize and/or recrystallize quite rapidly.

Globally, water-equivalent hydrogen (WEH) values as high as 15 wt % at the equator (Feldman et al. 2004; Maurice et al. 2011), have led authors to speculate how that water is stabilized in the shallow sub surface under present Martian conditions. Of the candidate mechanisms, which include subsurface H_2O ice, adsorbed water on dust, hydrous salts other than sulfates, and mid- to highly-hydrated sulfates, only the latter explanation meets the requirements for stability and realistic abundance in the shallow subsurface (Wang et al. 2013). In addition, the Mars Odyssey Gamma Ray Spectrometer (GRS) provided H:S ratios that are most consistent with hydrated iron sulfates with between ~2.5 and ~4 structural waters per sulfate (Karunatillake et al. 2012). Amorphous ferric sulfates remain consistent with GRS data, as these phases can hold between 1.7 and 3.7 structural waters per sulfate (5-11 waters per $Fe_2(SO_4)_3$; Wang et al. (2012)), although mixtures of higher and lower hydrates are possible.

The spectral characterizations reported in this study indicate that NIR absorptions associated with amorphous sulfates are weak compared to their crystalline counterparts, and thus could go undetected in remote measurements of intimate soil mixtures. If present in high concentrations in outcrops or mixed with spectrally transparent materials, however, the spectral details in the visible, NIR and MIR ranges should allow them to be distinguished from crystalline sulfates.

5.5 Summary and Conclusions

Our ability to accurately interpret the surface mineralogy of Mars is directly dependent upon the breadth of the library to which we compare Martian spectra. Here that library is expanded to include VNIR, MIR emissivity, and Mössbauer spectra of synthetic, amorphous ferric and ferrous sulfates. This is the first of two papers that will detail the structure and stability of these phases along with investigations into their presence in the Martian data set.

From this work, I have determined the following:

- Amorphous sulfates lack structural order beyond ~11 Å.

Amorphous ferrous sulfate

- Amorphous ferrous sulfate is spectrally distinct from all other ferrous sulfates available for comparison based on Mössbauer, VNIR, and MIR spectra.
- The Mössbauer parameters for two out of three doublets in amorphous ferrous sulfate are a fair match to sites in other minerals coordinated by four oxygens and two waters, indicating a possible structural similarity.
- However, the PDF data show that the amorphous ferrous sulfate has a similar but unique short-range bonding environment from szomolnokite and rozenite.

- The amorphous ferrous sulfate displays one, rather than two Fe^{2+} spin allowed crystal field transition absorptions in the VNIR and the position of that absorption is shifted to longer wavelengths than other ferrous sulfates that show a single absorption.
- The general MIR ν_3 and ν_1 band envelope overlaps with szomolnokite, but features within that envelope are significantly shifted, indicating that the sulfate tetrahedral environment is distinct from that of the reference compounds.

Amorphous ferric sulfates

- Amorphous ferric sulfates form spectrally similar products regardless of starting material; however, subtle spectral differences are observed with different formation pathways.
- Amorphous ferric sulfates only shows structural order to 10 Å with short range structure similar to ferricopiapite to ~ 8 Å.
- The vacuum dehydrated samples display greater iron site distortion (have a higher velocity Mössbauer Δ), along with a smoothing together of their MIR low frequency ν_3 absorption and their ν_1 absorption not seen in desiccated samples; this is likely due to the higher speed of water loss associated with the vacuum dehydration method.
- The amorphous ferric sulfates have Mössbauer parameters similar to one doublet of ferricopiapite, indicating similar iron octahedral distortion to one of the sites in ferricopiapite,

- Visible reflectance spectra show the amorphous ferric sulfates to be distinct from crystalline ferric sulfates based on the position of their spin-forbidden crystal field transition absorptions.
- The position of those absorptions may indicate that the basic structural units of the amorphous ferric sulfates are oxo-bridged iron octahedral clusters (possibly dimers).
- The amorphous ferric sulfates display broad, muted hydration features in SWIR reflectance spectra and broad, muted sulfate features in MIR emissivity spectra.
- As a class, the amorphous ferric sulfates should be spectrally distinct from other ferric sulfates in the spectral library.

One interesting aspect of amorphous ferric sulfates, and ferric sulfates in general, is the path dependent nature of their transformations. Whereas ferrous sulfates can reversibly change hydration states, as well as crystallinity, while remaining solid, amorphous ferric sulfates seem only to result from the rapid dehydration of a fully deliquesced crystalline sulfate or an iron and sulfate saturated fluid. This implies that the discovery of amorphous ferric sulfates on Mars would indicate that they are the result of substantial hydration as well as rapid dehydration. We thus may be able to use them to place constraints on not only the fluids from which they formed, and surface conditions on Mars at the time of formation, but also atmospheric conditions at the time of formation.

Works Cited

Altheide, T., Chevrier, V., Nicholson, C., and Denson, J. (2009) Experimental investigation of the stability and evaporation of sulfate and chloride brines on Mars. Earth and Planetary Science Letters, 282 (1-4), 69-78.

Archer, P.D., Franz, H.B., Sutter, B., Arevalo, R.D., Coll, P., Eigenbrode, J.L., Glavin, D.P., Jones, J.J., Leshin, L.A., Mahaffy, P.R., McAdam, A.C., McKay, C.P., Ming, D.W., Morris, R.V., Navarro-González, R., Niles, P.B., Pavlov, A., Squyres, S.W., Stern, J.C., Steele, A., and Wray, J.J. (2014) Abundances and implications of volatile-bearing species from evolved gas analysis of the Rocknest aeolian deposit, Gale Crater, Mars. Journal of Geophysical Research: Planets, 119 (1), 2013JE004493.

Baldridge, A.M., and Christensen, P.R. (2009) A laboratory technique for thermal emission measurement of hydrated minerals. Applied Spectroscopy, 63 (6), 678-688.

Bibring, J.P., Langevin, Y., Mustard, J.F., Poulet, F., Arvidson, R., Gendrin, A., Gondet, B., Mangold, N., Pinet, P., Forget, F., and team, O. (2006) Global mineralogical and aqueous mars history derived from OMEGA/Mars express data. Science, 312 (5772), 400-404.

Billinge, S.L., and Kanatzidis, M.G. (2004) Beyond crystallography: the study of disorder, nanocrystallinity and crystallographically challenged materials with pair distribution functions. Chemical Communications (7), 749-760.

Bish, D.L., Blake, D.F., Vaniman, D.T., Chipera, S.J., Morris, R.V., Ming, D.W., Treiman, A.H., Sarrazin, P., Morrison, S.M., Downs, R.T., Achilles, C.N., Yen, A.S., Bristow, T.F., Crisp, J.A., Morookian, J.M., Farmer, J.D., Rampe, E.B., Stolper, E.M., Spanovich, N., and Team, M.S.L.S. (2013) X-ray diffraction results from Mars Science Laboratory: Mineralogy of Rocknest at Gale Crater. Science, 341 (6153).

Bishop, J.L., Parente, M., Weitz, C.M., Dobrea, E.Z.N., Roach, L.H., Murchie, S.L., McGuire, P.C., McKeown, N.K., Rossi, C.M., Brown, A.J., Calvin, W.M., Milliken, R., and Mustard, J.F. (2009) Mineralogy of Juventae Chasma: Sulfates in the light-toned mounds, mafic minerals in the bedrock, and hydrated silica and hydroxylated ferric sulfate on the plateau. Journal of Geophysical Research-Planets, 114.

Boynton, W.V., Taylor, G.J., Evans, L.G., Reedy, R.C., Starr, R., Janes, D.M., Kerry, K.E., Drake, D.M., Kim, K.J., Williams, R.M.S., Crombie, M.K., Dohm, J.M., Baker, V., Metzger, A.E., Karunatillake, S., Keller, J.M., Newsom, H.E., Arnold, J.R., Bruckner, J., Englert, P.A.J., Gasnault, O., Sprague, A.L., Mitrofanov, I., Squyres, S.W., Trombka, J.I., d'Uston, L., Wanke, H., and Hamara, D.K. (2007) Concentration of H, Si, Cl, K, Fe, and Th in the low- and mid-latitude regions of Mars. Journal of Geophysical Research-Planets, 112 (E12).

Brass, G.W. (1980) Stability of brines on Mars. Icarus, 42 (1), 20-28.

Burns, R.G. (1993) Origin of electronic spectra of minerals in the visible-near infrared region. In: C.M. Pieters, and P.A.J. Englert (Eds.), Remote Geochemical Analysis: Elemental and Mineralogical Composition. Cambridge University Press, Cambridge, pp. 3-29.

Burns, R.G., and Solberg, T.C. (1990) ^{57}Fe-bearing oxide, silicate, and aluminosilicate minerals, crystal structure trends in Mossbauer spectra, in Spectroscopic characterization of minerals and their surfaces, 415. American Chemical Society Symposium Series, Washington, DC, pp. 262-283.

Carrozzo, F.G., Altieri, F., Bellucci, G., Poulet, F., D'Aversa, E., and Bibring, J.P. (2012) Iron mineralogy of the surface of Mars from the 1μm band spectral properties. Journal of Geophysical Research-Planets, 117.

Chevrier, V., Sears, D.W.G., Chittenden, J.D., Roe, L.A., Ulrich, R., Bryson, K., Billingsley, L., and Hanley, J. (2007) Sublimation rate of ice under simulated Mars conditions and the effect of layers of mock regolith JSC Mars-1. Geophysical Research Letters, 34 (2).

Chevrier, V.F., and Altheide, T.S. (2008) Low temperature aqueous ferric sulfate solutions on the surface of Mars. Geophysical Research Letters, 35 (22).

Chipera, S.J., and Vaniman, D.T. (2007) Experimental stability of magnesium sulfate hydrates that may be present on Mars. Geochimica Et Cosmochimica Acta, 71 (1), 241-250.

Chou, I.M., Seal, R.R., II, and Wang, A. (2013) The stability of sulfate and hydrated sulfate minerals near ambient conditions and their significance in environmental and planetary sciences. Journal of Asian Earth Sciences, 62, 734-758.

Cloutis, E.A., Craig, M.A., Kruzelecky, R.V., Jamroz, W.R., Scott, A., Hawthorne, F.C., and Mertzman, S.A. (2008) Spectral reflectance properties of minerals exposed to simulated Mars surface conditions. Icarus, 195 (1), 140-168.

Cloutis, E.A., Hawthorne, F.C., Mertzman, S.A., Krenn, K., Craig, M.A., Marcino, D., Methot, M., Strong, J., Mustard, J.F., Blaney, D.L., Bell, J.F., and Vilas, F. (2006) Detection and discrimination of sulfate minerals using reflectance spectroscopy. Icarus, 184 (1), 121-157.

Crowley, J.K., Williams, D.E., Hammarstrom, J.M., Piatak, N., Chou, I.M., and Mars, J.C. (2003) Spectral reflectance properties (0.4-2.5 μm) of secondary Fe-oxide, Fe-hydroxide, and Fe-sulfate-hydrate minerals associated with sulphide-bearing mine wastes. Geochemistry: Exploration, Environment, Analysis, 3 (3), 219-228.

Dyar, M.D., Breves, E., Jawin, E., Marchand, G., Nelms, M., O'Connor, V., Peel, S., Rothstein, Y., Sklute, E.C., Lane, M.D., Bishop, J.L., and Mertzman, S.A. (2013) Mossbauer parameters of iron in sulfate minerals. American Mineralogist, 98 (11-12), 1943-1965.

Feldman, W.C., Prettyman, T.H., Maurice, S., Plaut, J.J., Bish, D.L., Vaniman, D.T., Mellon, M.T., Metzger, A.E., Squyres, S.W., Karunatillake, S., Boynton, W.V., Elphic, R.C., Funsten, H.O., Lawrence, D.J., and Tokar, R.L. (2004) Global distribution of near-surface hydrogen on Mars. Journal of Geophysical Research-Planets, 109 (E9).

Frost, R.L., Wills, R.A., Martens, W., Weier, M., and Reddy, B.J. (2005) NIR spectroscopy of selected iron(II) and iron(III) sulphates. Spectrochimica Acta Part a-Molecular and Biomolecular Spectroscopy, 62 (1-3), 42-50.

Gendrin, A., Mangold, N., Bibring, J.P., Langevin, Y., Gondet, B., Poulet, F., Bonello, G., Quantin, C., Mustard, J., Arvidson, R., and LeMouelic, S. (2005) Sulfates in Martian layered terrains: the OMEGA/Mars Express view. Science, 307 (5715), 1587-1591.

Hawthorne, F.C., Krivovichev, S.V., and Burns, P.C. (2000) The crystal chemistry of sulfate minerals. Sulfate Minerals - Crystallography, Geochemistry and Environmental Significance, 40, 1-112.

Hunt, G.R. (1977) Spectral signatures of particulate minerals in the visible and near IR. Geophysics, 42 (3), 501-513.

Hurowitz, J.A., and McLennan, S.M. (2007) A similar to 3.5 Ga record of water-limited, acidic weathering conditions on Mars. Earth and Planetary Science Letters, 260 (3-4), 432-443.

Jambor, J.I., Nordstrom, D.K., and Alpers, C.N. (2000) Metal-sulfate salts from sulfide mineral oxidation. Sulfate Minerals - Crystallography, Geochemistry and Environmental Significance, 40, 303-350.

Jerz, J.K., and Rimstidt, J.D. (2003) Efflorescent iron sulfate minerals: Paragenesis, relative stability, and environmental impact. American Mineralogist, 88 (11-12), 1919-1932.

Karunatillake, S., Gasnault, O., McLennan, S.M., Rogers, D.A., Wray, J.J., Squyres, S.W., and Boynton, W.V. (2012) The Hydration State of Sulfates on Mars. Abstracts of Papers submitted to the Lunar and Planetary Science Conference XXXXIII (2940).

Klingelhofer, G., Morris, R.V., Bernhardt, B., Schroder, C., Rodionov, D.S., de Souza, P.A., Yen, A., Gellert, R., Evlanov, E.N., Zubkov, B., Foh, J., Bonnes, U., Kankeleit, E., Gutlich, P., Ming, D.W., Renz, F., Wdowiak, T., Squyres, S.W., and Arvidson, R.E. (2004) Jarosite and hematite at Meridiani Planum from Opportunity's Mossbauer spectrometer. Science, 306 (5702), 1740-1745.

Kong, W.G., Wang, A., and Chou, I.M. (2011a) Experimental determination of the phase boundary between kornelite and pentahydrated ferric sulfate at 0.1 MPa. Chemical Geology, 284 (3-4), 333-338.

Kong, W.G., Wang, A., Freeman, J.J., and Sobron, P. (2011b) A comprehensive spectroscopic study of synthetic Fe^{2+}, Fe^{3+}, Mg^{2+} and Al^{3+} copiapite by Raman, XRD, LIBS, MIR and vis-NIR. Journal of Raman Spectroscopy, 42 (5), 1120-1129.

Lane, M.D. (2007) Mid-infrared emission spectroscopy of sulfate and sulfate-bearing minerals. American Mineralogist, 92 (1), 1-18.

Lichtenberg, K.A., Arvidson, R.E., Morris, R.V., Murchie, S.L., Bishop, J.L., Fernandez Remolar, D., Glotch, T.D., Dobrea, E.N., Mustard, J.F., Andrews-Hanna, J., and Roach, L.H. (2010) Stratigraphy of hydrated sulfates in the sedimentary deposits of Aram Chaos, Mars. Journal of Geophysical Research-Planets, 115.

Ling, Z.C., and Wang, A. (2010) A systematic spectroscopic study of eight hydrous ferric sulfates relevant to Mars. Icarus, 209 (2), 422-433.

Marion, G.M., Catling, D.C., and Kargel, J.S. (2003) Modeling aqueous ferrous iron chemistry at low temperatures with application to Mars. Geochimica Et Cosmochimica Acta, 67 (22), 4251-4266.

Marion, G.M., Kargel, J.S., and Catling, D.C. (2008) Modeling ferrous-ferric iron chemistry with application to martian surface geochemistry. Geochimica Et Cosmochimica Acta, 72 (1), 242-266.

Martinez, G.M., and Renno, N.O. (2013) Water and brines on Mars: Current evidence and implications for MSL. Space Science Reviews, 175 (1-4), 29-51.

Masse, M., Beck, P., Schmitt, B., Pommerol, A., McEwen, A., Chevrier, V., Brissaud, O., and Sejourne, A. (2014) Spectroscopy and detectability of liquid brines on mars. Planetary and Space Science, 92, 136-149.

Maurice, S., Feldman, W., Diez, B., Gasnault, O., Lawrence, D.J., Pathare, A., and Prettyman, T. (2011) Mars Odyssey neutron data: 1. Data processing and models of water-equivalent-hydrogen distribution. Journal of Geophysical Research-Planets, 116.

McAdam, A.C., Franz, H.B., Sutter, B., Archer, P.D., Freissinet, C., Eigenbrode, J.L., Ming, D.W., Atreya, S.K., Bish, D.L., Blake, D.F., Bower, H.E., Brunner, A., Buch, A., Glavin, D.P., Grotzinger, J.P., Mahaffy, P.R., McLennan, S.M., Morris, R.V., Navarro-González, R., Rampe, E.B., Squyres, S.W., Steele, A., Stern, J.C., Sumner, D.Y., and Wray, J.J.

(2014) Sulfur-bearing phases detected by evolved gas analysis of the Rocknest aeolian deposit, Gale Crater, Mars. Journal of Geophysical Research: Planets, 2013JE004518.
McEwen, A.S., Ojha, L., Dundas, C.M., Mattson, S.S., Byrne, S., Wray, J.J., Cull, S.C., Murchie, S.L., Thomas, N., and Gulick, V.C. (2011) Seasonal Flows on Warm Martian Slopes. Science, 333 (6043), 740-743.
Milliken, R.E., and Bish, D.L. (2010) Sources and sinks of clay minerals on Mars. Philosophical Magazine, 90 (17-18), 2293-2308.
Milliken, R.E., Fischer, W.W., and Hurowitz, J.A. (2009) Missing salts on early Mars. Geophysical Research Letters, 36.
Mohlmann, D., and Thomsen, K. (2011) Properties of cryobrines on Mars. Icarus, 212 (1), 123-130.
Morris, R.V., Ming, D.W., Blake, D.F., Vaniman, D.T., Bish, D.L., Chipera, S.J., Downs, R.T., Gellert, R., Treiman, A.H., Yen, A.S., Achilles, C.N., Anderson, R.C., Bristow, T.F., Crisp, J.A., Des Marais, D.J., Farmer, J.D., Grotzinger, J.P., Leshin, L.A., McAdam, A.C., Morookian, J.M., Morrison, S.M., Rampe, E.B., Sarrazin, P.C., Spanovich, N., and Stolper, E.M. (2013) The amorphous component in the Martian basaltic soil in global perspective from MSL and MER missions. Abstracts of Papers submitted to the Lunar and Planetary Science Conference XXXXIV (1653).
Morris, R.V., Ming, D.W., Gellert, R., Vaniman, D.T., Bish, D.L., Blake, D.F., Chipera, S.J., Downs, R.T., Treiman, A.H., Yen, A.S., Achilles, C.N., Archer, P.D., Bristow, T.F., Crisp, J.A., Des Marais, D.J., Farmer, J.D., Grotzinger, J.P., Mahaffy, P.R., McAdam, A.C., Morookian, J.M., Morrison, S.M., and Rampe, E.B. (2014) Chemical composition fo crystalline, smectite, and amorphous components for Rocknest soil and John Klein and Cumberland mudstone drill fines using APXS, CHEMIN, and SAM datasets from Gale Crater, Mars. Abstracts of Papers submitted to the Lunar and Planetary Science Conference XXXXV (1319).
Nakamoto, K. (1986) Infrared and raman spectra of inorganic and coordinated compounds. Wiley and Sons, New York.
Reeder, R.J., and Michel, F.M. (2013) Application of Total X-Ray Scattering Methods and Pair Distribution Function Analysis for Study of Structure of Biominerals. In: J.J.D. Yoreo (Ed.), Research Methods in Biomineralization Science. Methods in Enzymology, pp. 477-500.
Roach, L.H., Mustard, J.F., Lane, M.D., Bishop, J.L., and Murchie, S.L. (2010a) Diagenetic haematite and sulfate assemblages in Valles Marineris. Icarus, 207 (2), 659-674.
Roach, L.H., Mustard, J.F., Murchie, S.L., Bibring, J.P., Forget, F., Lewis, K.W., Aharonson, O., Vincendon, M., and Bishop, J.L. (2009) Testing evidence of recent hydration state change in sulfates on Mars. Journal of Geophysical Research-Planets, 114.
Roach, L.H., Mustard, J.F., Swayze, G., Milliken, R.E., Bishop, J.L., Murchie, S.L., and Lichtenberg, K. (2010b) Hydrated mineral stratigraphy of Ius Chasma, Valles Marineris. Icarus, 206 (1), 253-268.
Rossman, G.R. (1975) Spectroscopic and magnetic studies of ferric iron hydroxy sulfates-intesification of color in ferric iron clusters bridged by a single hydroxide ion. American Mineralogist, 60 (7-8), 698-704.
Rossman, G.R. (1976) Spectroscopic and magnetic studies of ferric iron hydroxy sulfates-series $Fe(OH)SO_4 \bullet nH_2O$ and jarosites. American Mineralogist, 61 (5-6), 398-404.

Ruff, S.W., Christensen, P.R., Barbera, P.W., and Anderson, D.L. (1997) Quantitative thermal emission spectroscopy of minerals: A laboratory technique for measurement and calibration. Journal of Geophysical Research-Solid Earth, 102 (B7), 14899-14913.

Savijarvi, H. (1995) Mars boundary-layer modeling - Diurnal moisture cycle and soil properties at the Viking-Lander-1 site. Icarus, 117 (1), 120-127.

Sears, D.W.G., and Chittenden, J.D. (2005) On laboratory simulation and the temperature dependence of the evaporation rate of brine on Mars. Geophysical Research Letters, 32 (23).

Sherman, D.M., Burns, R.G., and Burns, V.M. (1982) Spectral characteristics of the iron-oxides with application to the Martian bright region mineralogy. Journal of Geophysical Research, 87 (NB12), 169-180.

Sherman, D.M., and Waite, T.D. (1985) Electronic-spectra of Fe^{3+} oxides and oxide hydroxides in the near IR to near UV. American Mineralogist, 70 (11-12), 1262-1269.

Squyres, S.W., Grotzinger, J.P., Arvidson, R.E., Bell, J.F., Calvin, W., Christensen, P.R., Clark, B.C., Crisp, J.A., Farrand, W.H., Herkenhoff, K.E., Johnson, J.R., Klingelhofer, G., Knoll, A.H., McLennan, S.M., McSween, H.Y., Morris, R.V., Rice, J.W., Rieder, R., and Soderblom, L.A. (2004) In situ evidence for an ancient aqueous environment at Meridiani Planum, Mars. Science, 306 (5702), 1709-1714.

Tosca, N.J., and McLennan, S.M. (2009) Experimental constraints on the evaporation of partially oxidized acid-sulfate waters at the martian surface. Geochimica Et Cosmochimica Acta, 73 (4), 1205-1222.

Vaniman, D.T., Bish, D.L., Chipera, S.J., Fialips, C.I., Carey, J.W., and Feldman, W.C. (2004) Magnesium sulphate salts and the history of water on Mars. Nature, 431 (7009), 663-665.

Vaniman, D.T., Bish, D.L., Ming, D.W., Bristow, T.F., Morris, R.V., Blake, D.F., Chipera, S.J., Morrison, S.M., Treiman, A.H., Rampe, E.B., Rice, M., Achilles, C.N., Grotzinger, J.P., McLennan, S.M., Williams, J., Bell, J.F., Newsom, H.E., Downs, R.T., Maurice, S., Sarrazin, P., Yen, A.S., Morookian, J.M., Farmer, J.D., Stack, K., Milliken, R.E., Ehlmann, B.L., Sumner, D.Y., Berger, G., Crisp, J.A., Hurowitz, J.A., Anderson, R., Des Marais, D.J., Stolper, E.M., Edgett, K.S., Gupta, S., Spanovich, N., and Team, M.S.L.S. (2014) Mineralogy of a Mudstone at Yellowknife Bay, Gale Crater, Mars. Science, 343 (6169).

Vaniman, D.T., and Chipera, S.J. (2006) Transformations of Mg- and Ca-sulfate hydrates in Mars regolith. American Mineralogist, 91 (10), 1628-1642.

Wang, A., Feldman, W.C., Mellon, M.T., and Zheng, M.P. (2013) The preservation of subsurface sulfates with mid-to-high degree of hydration in equatorial regions on Mars. Icarus, 226 (1), 980-991.

Wang, A., Freeman, J.J., Chou, I.M., and Jolliff, B.L. (2011) Stability of Mg-sulfates at-10 degrees C and the rates of dehydration/rehydration processes under conditions relevant to Mars. Journal of Geophysical Research-Planets, 116.

Wang, A., Freeman, J.J., and Jolliff, B.L. (2009) Phase transition pathways of the hydrates of magnesium sulfate in the temperature range 50 degrees C to 5 degrees C: Implication for sulfates on Mars. Journal of Geophysical Research-Planets, 114.

Wang, A., Freeman, J.J., Jolliff, B.L., and Chou, I.M. (2006a) Sulfates on Mars: A systematic Raman spectroscopic study of hydration states of magnesium sulfates. Geochimica Et Cosmochimica Acta, 70 (24), 6118-6135.

Wang, A., Haskin, L.A., Squyres, S.W., Jolliff, B.L., Crumpler, L., Gellert, R., Schroder, C., Herkenhoff, K., Hurowitz, J., Tosca, N.J., Farrand, W.H., Anderson, R., and Knudson, A.T. (2006b) Sulfate deposition in subsurface regolith in Gusev crater, Mars. Journal of Geophysical Research-Planets, 111 (E2).

Wang, A., and Ling, Z.C. (2011) Ferric sulfates on Mars: A combined mission data analysis of salty soils at Gusev crater and laboratory experimental investigations. Journal of Geophysical Research-Planets, 116.

Wang, A.A., Ling, Z.C., Freeman, J.J., and Kong, W.G. (2012) Stability field and phase transition pathways of hydrous ferric sulfates in the temperature range 50 degrees C to 5 degrees C: Implication for martian ferric sulfates. Icarus, 218 (1), 622-643.

Wang, A.A., and Zhou, Y.H. (2014) Experimental comparison of the pathways and rates of the dehydration of Al-, Fe-, Mg- and Ca-sulfates under Mars relevant conditions. Icarus, 234, 162-173.

Wiseman, S.M., Arvidson, R.E., Morris, R.V., Poulet, F., Andrews-Hanna, J.C., Bishop, J.L., Murchie, S.L., Seelos, F.P., Des Marais, D., and Griffes, J.L. (2010) Spectral and stratigraphic mapping of hydrated sulfate and phyllosilicate-bearing deposits in northern Sinus Meridiani, Mars. Journal of Geophysical Research-Planets, 115.

Wray, J.J., Milliken, R.E., Dundas, C.M., Swayze, G.A., Andrews-Hanna, J.C., Baldridge, A.M., Chojnacki, M., Bishop, J.L., Ehlmann, B.L., Murchie, S.L., Clark, R.N., Seelos, F.P., Tornabene, L.L., and Squyres, S.W. (2011) Columbus crater and other possible groundwater-fed paleolakes of Terra Sirenum, Mars. Journal of Geophysical Research-Planets, 116.

Xu, W., and Parise, J.B. (2012) Temperature and humidity effects on ferric sulfate stability and phase transformation. American Mineralogist, 97 (2-3), 378-383.

Xu, W.Q., Tosca, N.J., McLennan, S.M., and Parise, J.B. (2009) Humidity-induced phase transitions of ferric sulfate minerals studied by in situ and ex situ X-ray diffraction. American Mineralogist, 94 (11-12), 1629-1637.

Chapter 6

Concluding Remarks

Investigations into the reactions of simulated carbon sequestration systems, remote analysis of acid mine drainage precipitates and the Martian surface, and synthesizing phases that may be present on Mars do not, at first, seem to share common themes. Yet the systems studied here are, in fact, quite similar. Each depends on the reactions between iron and sulfur in acidic fluids. Both the carbon sequestration system and Mars have an overpressure of primarily CO_2. As we consider co-injecting SO_2 and H_2S with CO_2 into deep saline aquifers, we can also consider an ancient Mars that experienced significant volcanic degassing in a CO_2 atmosphere. The acidic sulfate-rich effluents that flow from mining sites may be quite similar to those that flow(ed) on the surface of Mars. We mine sulfides for valuable metals and may form sulfides in the sequestering of SO_2 and H_2S with CO_2. The central theme, however, and the driving force behind much of geoscience, is that we must be able to simulate and analyze the transformations between mineral phases in a way that provides the most information possible.

This dissertation has reported the results of experiments on the interactions between iron and sulfur in extreme environments but has also detailed methodology for the analyses of such phases. Determining mineralogy is not completely straightforward. XRF can provide chemical composition, and we can model the likely minerals from these values, but many systems will not

lend themselves to this type of analysis. XRD has historically been used for mineralogical identification, but cannot be used remotely and fails to provide detailed information about nanoscopic and amorphous phases, both of which may be indicators of microbial activity, and both of which may be important phases on other planets. VNIR and MIR spectroscopy provide valuable information about the vibrational energies of elements and groups within a structure, but neither can be used directly to determine quantitative abundances, and both sample mineral surfaces, not bulk mineralogy. Mössbauer only samples the iron in minerals and cannot always produce unique identifications. So determining a compatible set of techniques is central to understanding the interactions of the system in question. Indeed, choosing complementary instrument suites has been one of the more powerful tools in planetary science.

For systems containing iron and sulfur, the combination of Mössbauer, VNIR, and MIR spectroscopy delivers information on structure, composition, and mineralogy. PDF, although quite an undertaking, provides insight into the angstrom scale bonding environment of materials. Although we cannot take this technique to other planets, finding the relationship between spectroscopic and structural characteristics allows us to significantly extend our interpretations using other techniques. Although work of this type has been done (e.g. Cloutis et al. (2006); Lane (2007); Dyar et al. (2013)), there is still a great deal more to do. Similarly fundamental parameters of minerals, like optical constants, can facilitate more in-depth analyses. These fundamental undertakings that do not lose sight of the bigger picture are paramount to advancements in our field.

In addition, recognizing the crossover between seemingly unrelated systems provides access to the insights amassed in other fields. There is a large body of literature on each of the

subjects studied here that may be relevant to the others. It is my sincere hope that researchers will take greater advantage of the crossover between such systems.

Finally, the geology of Earth is inextricably linked to the biology of Earth (Hazen et al. 2008). Or, perhaps, it is the biology which is linked to the geology. Russell et al. (2014) writes: "The [submarine alkaline hydrothermal] theory views life, like other self-organizing systems in the Universe, as an inevitable outcome of particular disequilibria." These acidic, saline systems that contain multivalent elements are areas of such disequilibria. On Earth, areas of AMD systems have disequilibrium caused by redox states of iron and sulfur exposed to an oxygenated atmosphere, and these systems are exploited by a host of bacteria and archaea (Johnson 1998). In the deep oceans, similar disequilibria are the sustaining source for a world that we thought shouldn't be there (Kelley et al. 2002). Deep gold mines (Baker et al. 2003), deep saline formations (Haveman and Pedersen 2002; Baker et al. 2003), and oil and gas reservoirs (Orphan et al. 2000) all hold life. Even sediments almost a kilometer below the floor of the ocean hold microbial communities (Parkes et al. 2000). We continue to find life in places we did not think possible, and most of these places contain sulfur. Thus, albeit a bit of a challenge (Squyres and Knoll 2005; Tosca et al. 2008; Norlund et al. 2010), life could be possible on Mars.

Works Cited

Baker, B.J., Moser, D.P., MacGregor, B.J., Fishbain, S., Wagner, M., Fry, N.K., Jackson, B., Speolstra, N., Loos, S., Takai, K., Lollar, B.S., Fredrickson, J., Balkwill, D., Onstott, T.C., Wimpee, C.F., and Stahl, D.A. (2003) Related assemblages of sulphate-reducing bacteria associated with ultradeep gold mines of South Africa and deep basalt aquifers of Washington State. Environmental Microbiology, 5, 267-277.

Cloutis, E.A., Hawthorne, F.C., Mertzman, S.A., Krenn, K., Craig, M.A., Marcino, D., Methot, M., Strong, J., Mustard, J.F., Blaney, D.L., Bell, J.F., and Vilas, F. (2006) Detection and discrimination of sulfate minerals using reflectance spectroscopy. Icarus, 184, 121-157.

Dyar, M.D., Breves, E., Jawin, E., Marchand, G., Nelms, M., O'Connor, V., Peel, S., Rothstein, Y., Sklute, E.C., Lane, M.D., Bishop, J.L., and Mertzman, S.A. (2013) Mossbauer parameters of iron in sulfate minerals. American Mineralogist, 98, 1943-1965.

Haveman, S.A., and Pedersen, K. (2002) Distribution of culturable microorganisms in Fennoscandian Shield groundwater. Fems Microbiology Ecology, 39, 129-137.

Hazen, R.M., Papineau, D., Leeker, W.B., Downs, R.T., Ferry, J.M., McCoy, T.J., Sverjensky, D.A., and Yang, H.X. (2008) Mineral evolution. American Mineralogist, 93, 1693-1720.

Johnson, D.B. (1998) Biodiversity and ecology of acidophilic microorganisms. Fems Microbiology Ecology, 27, 307-317.

Kelley, D.S., Baross, J.A., and Delaney, J.R. (2002) Volcanoes, fluids, and life at mid-ocean ridge spreading centers. Annual Review of Earth and Planetary Sciences, 30, 385-491.

Lane, M.D. (2007) Mid-infrared emission spectroscopy of sulfate and sulfate-bearing minerals. American Mineralogist, 92, 1-18.

Norlund, K.L.I., Baron, C., and Warren, L.A. (2010) Jarosite formation by an AMD sulphide-oxidizing environmental enrichment: Implications for biomarkers on Mars. Chemical Geology, 275, 235-242.

Orphan, V.J., Taylor, L.T., Hafenbradl, D., and Delong, E.F. (2000) Culture-dependent and culture-independent characterization of microbial assemblages associated with high-temperature petroleum reservoirs. Applied and Environmental Microbiology, 66, 700-711.

Parkes, R.J., Cragg, B.A., and Wellsbury, P. (2000) Recent studies on bacterial populations and processes in subseafloor sediments: A review. Hydrogeology Journal, 8, 11-28.

Russell, M.J., Barge, L.M., Bhartia, R., Bocanegra, D., Bracher, P.J., Branscomb, E., Kidd, R., McGlynn, S., Meier, D.H., Nitschke, W., Shibuya, T., Vance, S., White, L., and Kanik, I. (2014) The Drive to Life on Wet and Icy Worlds. Astrobiology, 14, 308-343.

Squyres, S.W., and Knoll, A.H. (2005) Sedimentary rocks at Meridiani Planum: Origin, diagetiesis, and implications for life on Mars. Earth and Planetary Science Letters, 240, 1-10.

Tosca, N.J., Knoll, A.H., and McLennan, S.M. (2008) Water activity and the challenge for life on early Mars. Science, 320, 1204-1207.

Complete List of Citations

Altheide, T., Chevrier, V., Nicholson, C., and Denson, J. (2009) Experimental investigation of the stability and evaporation of sulfate and chloride brines on Mars. Earth and Planetary Science Letters, 282 (1-4), 69-78.

Ambartsumian, V. (1958) The Theory of Radiative Transfer in Planetary Atmospheres. In: V. Ambartsumian (Ed.), Theoretical Astrophysics. Pergamon, New York, pp. 550-564.

Anheden, M., Andersson, A., Bernstone, C., Eriksson, S., Yan, J., Liljemark, S., and Wall, C. (2005) CO_2 quality requirement for a system with CO_2 capture, transport and storage. In: M. Wilson et al. (Eds.), Greenhouse Gas Control Technologies 7. Elsevier, pp. 2559-2564.

Archer, P.D., Franz, H.B., Sutter, B., Arevalo, R.D., Coll, P., Eigenbrode, J.L., Glavin, D.P., Jones, J.J., Leshin, L.A., Mahaffy, P.R., McAdam, A.C., McKay, C.P., Ming, D.W., Morris, R.V., Navarro-González, R., Niles, P.B., Pavlov, A., Squyres, S.W., Stern, J.C., Steele, A., and Wray, J.J. (2014) Abundances and implications of volatile-bearing species from evolved gas analysis of the Rocknest aeolian deposit, Gale Crater, Mars. Journal of Geophysical Research: Planets, 119 (1), 2013JE004493.

Bachu, S. (2008) CO_2 storage in geological media: Role, means, status and barriers to deployment. Progress in Energy and Combustion Science, 34 (2), 254-273.

Baker, B.J., Moser, D.P., MacGregor, B.J., Fishbain, S., Wagner, M., Fry, N.K., Jackson, B., Speolstra, N., Loos, S., Takai, K., Lollar, B.S., Fredrickson, J., Balkwill, D., Onstott, T.C., Wimpee, C.F., and Stahl, D.A. (2003) Related assemblages of sulphate-reducing bacteria associated with ultradeep gold mines of South Africa and deep basalt aquifers of Washington State. Environmental Microbiology, 5 (4), 267-277.

Baldridge, A.M., and Christensen, P.R. (2009) A laboratory technique for thermal emission measurement of hydrated minerals. Applied Spectroscopy, 63 (6), 678-688.

Barron, V., Torrent, J., and Greenwood, J.P. (2006) Transformation of jarosite to hematite in simulated Martian brines. Earth and Planetary Science Letters, 251 (3-4), 380-385.

Bell, J.H., Bowen, B.B., and Martini, B.A. (2010) Imaging spectroscopy of jarosite cement in the Jurassic Navajo Sandstone. Remote Sensing of Environment, 114 (10), 2259-2270.

Bennett, S.A., Achterberg, E.P., Connelly, D.P., Statham, P.J., Fones, G.R., and German, C.R. (2008) The distribution and stabilisation of dissolved Fe in deep-sea hydrothermal plumes. Earth and Planetary Science Letters, 270 (3-4), 157-167.

Bertier, P., Swennen, R., Laenen, B., Lagrou, D., and Dreesen, R. (2006) Experimental identification of CO_2-water-rock interactions caused by sequestration of CO_2 in

Westphalian and Buntsandstein sandstones of the Campine Basin (NE-Belgium). Journal of Geochemical Exploration, 89 (1-3), 10-14.

Bibring, J.P., Langevin, Y., Gendrin, A., Gondet, B., Poulet, F., Berthe, M., Soufflot, A., Arvidson, R., Mangold, N., Mustard, J., Drossart, P., and Team, O. (2005) Mars surface diversity as revealed by the OMEGA/Mars Express observations. Science, 307 (5715), 1576-1581.

Bibring, J.P., Langevin, Y., Mustard, J.F., Poulet, F., Arvidson, R., Gendrin, A., Gondet, B., Mangold, N., Pinet, P., Forget, F., and team, O. (2006) Global mineralogical and aqueous mars history derived from OMEGA/Mars express data. Science, 312 (5772), 400-404.

Bickle, M., Kampman, N., and Wigley, M. (2013) Natural Analogues. In: D.J. DePaolo, D.R. Cole, A. Navrotsky, and I.C. Bourg (Eds.), Geochemistry of Geologic CO_2 Sequestration. Reviews in Mineralogy & Geochemistry, pp. 15-71.

Bigham, J.M., Schwertmann, U., and Pfab, G. (1996a) Influence of pH on mineral speciation in a bioreactor simulating acid mine drainage. Applied Geochemistry, 11 (6), 845-849.

Bigham, J.M., Schwertmann, U., Traina, S.J., Winland, R.L., and Wolf, M. (1996b) Schwertmannite and the chemical modeling of iron in acid sulfate waters. Geochimica Et Cosmochimica Acta, 60 (12), 2111-2121.

Bigham, J.M., and Nordstrom, D.K. (2000) Iron and aluminum hydroxysulfates from acid sulfate waters. Sulfate Minerals - Crystallography, Geochemistry and Environmental Significance, 40, 351-403.

Billinge, S.L., and Kanatzidis, M.G. (2004) Beyond crystallography: the study of disorder, nanocrystallinity and crystallographically challenged materials with pair distribution functions. Chemical Communications (7), 749-760.

Bish, D.L., Blake, D.F., Vaniman, D.T., Chipera, S.J., Morris, R.V., Ming, D.W., Treiman, A.H., Sarrazin, P., Morrison, S.M., Downs, R.T., Achilles, C.N., Yen, A.S., Bristow, T.F., Crisp, J.A., Morookian, J.M., Farmer, J.D., Rampe, E.B., Stolper, E.M., Spanovich, N., and Team, M.S.L.S. (2013) X-ray diffraction results from Mars Science Laboratory: Mineralogy of Rocknest at Gale Crater. Science, 341 (6153).

Bishop, J.L., Darby Dyar, M., Lane, M.D., and Banfield, J.F. (2004) Spectral identification of hydrated sulfates on Mars and comparison with acidic environments on Earth. International Journal of Astrobiology, 3 (04), 275-285.

Bishop, J.L., and Murad, E. (2005) The visible and infrared spectral properties of jarosite and alunite. American Mineralogist, 90 (7), 1100-1107.

Bishop, J.L., Lane, M.D., Dyar, M.D., and Brown, A.J. (2008) Reflectance and emission spectroscopy study of four groups of phyllosilicates: smectites, kaolinite-serpentines, chlorites and micas. Clay Minerals, 43 (1), 35-54.

Bishop, J.L., Parente, M., Weitz, C.M., Dobrea, E.Z.N., Roach, L.H., Murchie, S.L., McGuire, P.C., McKeown, N.K., Rossi, C.M., Brown, A.J., Calvin, W.M., Milliken, R., and Mustard, J.F. (2009) Mineralogy of Juventae Chasma: Sulfates in the light-toned mounds, mafic minerals in the bedrock, and hydrated silica and hydroxylated ferric sulfate on the plateau. Journal of Geophysical Research-Planets, 114.

Boucher, O., and Anderson, T.L. (1995) General circulation model assessment of the sensitivity of direct climate forcing by anthropogenic sulfate aerosols to aerosol size and chemistry. Journal of Geophysical Research-Atmospheres, 100 (D12), 26117-26134.

Boynton, W.V., Taylor, G.J., Evans, L.G., Reedy, R.C., Starr, R., Janes, D.M., Kerry, K.E., Drake, D.M., Kim, K.J., Williams, R.M.S., Crombie, M.K., Dohm, J.M., Baker, V., Metzger, A.E., Karunatillake, S., Keller, J.M., Newsom, H.E., Arnold, J.R., Bruckner, J., Englert, P.A.J., Gasnault, O., Sprague, A.L., Mitrofanov, I., Squyres, S.W., Trombka, J.I., d'Uston, L., Wanke, H., and Hamara, D.K. (2007) Concentration of H, Si, Cl, K, Fe, and Th in the low- and mid-latitude regions of Mars. Journal of Geophysical Research-Planets, 112 (E12).

Bradshaw, J., and Dance, T. (2005) Mapping geological storage prospectivity of CO_2 for the world's sedimentary basins and regional source to sink matching, Greenhouse Gas Control Technologies 7. Elsevier Science Ltd, Vancouver, Canada, pp. 583-591.

Brass, G.W. (1980) Stability of brines on Mars. Icarus, 42 (1), 20-28.

Brimblecombe, P., Hammer, C., Henning, R., Ryaboshapko, A., and Boutron, C.F. (1989) Human influence on the sulfur cycle. In: A.Y. Lein, P. Brimblecombe, and U. International Council of Scientific (Eds.), Evolution of the global biogeochemical sulphur cycle. Wiley, Chichester, West Sussex, England ; New York, pp. 77-121.

Burns, R.G. (1993) Origin of electronic spectra of minerals in the visible-near infrared region. In: C.M. Pieters, and P.A.J. Englert (Eds.), Remote Geochemical Analysis: Elemental and Mineralogical Composition. Cambridge University Press, Cambridge, pp. 3-29.

Burns, R.G., and Solberg, T.C. (1990) ^{57}Fe-bearing oxide, silicate, and aluminosilicate minerals, crystal structure trends in Mössbauer spectra, in Spectroscopic characterization of minerals and their surfaces, 415. American Chemical Society Symposium Series, Washington, DC, pp. 262-283.

Cahill, J.T., and Lucey, P.G. (2007) Radiative transfer modeling of lunar highlands spectral classes and relationship to lunar samples. Journal of Geophysical Research-Planets, 112 (E10).

Cahill, J.T.S., Lucey, P.G., and Wieczorek, M.A. (2009) Compositional variations of the lunar crust: Results from radiative transfer modeling of central peak spectra. Journal of Geophysical Research-Planets, 114.

Canfield, D.E. (2004) The evolution of the Earth surface sulfur reservoir. American Journal of Science, 304 (10), 839-861.

Canfield, D.E., and Farquhar, J. (2012) The Global Sulfur Cycle, Fundamentals of Geobiology. John Wiley & Sons, Ltd, pp. 49-64.

Canfield, D.E., and Raiswell, R. (1999) The evolution of the sulfur cycle. American Journal of Science, 299 (7-9), 697-723.

Carrozzo, F.G., Altieri, F., Bellucci, G., Poulet, F., D'Aversa, E., and Bibring, J.P. (2012) Iron mineralogy of the surface of Mars from the 1 μm band spectral properties. Journal of Geophysical Research-Planets, 117.

Chandrasekhar, S. (1960) Radiative Transfer. Dover, New York.

Chestnut, L.G., and Mills, D.M. (2005) A fresh look at the benefits and costs of the US Acid Rain Program. Journal of Environmental Management, 77 (3), 252-266.

Chevrier, V., Sears, D.W.G., Chittenden, J.D., Roe, L.A., Ulrich, R., Bryson, K., Billingsley, L., and Hanley, J. (2007) Sublimation rate of ice under simulated Mars conditions and the effect of layers of mock regolith JSC Mars-1. Geophysical Research Letters, 34 (2).

Chevrier, V.F., and Altheide, T.S. (2008) Low temperature aqueous ferric sulfate solutions on the surface of Mars. Geophysical Research Letters, 35 (22).

Chevrier, V.F., and Rivera-Valentin, E.G. (2012) Formation of recurring slope lineae by liquid brines on present-day Mars. Geophysical Research Letters, 39.

Chialvo, A.A., Vlcek, L., and Cole, D.R. (2013) Acid gases in CO_2-rich subsurface geologic environments. In: D.J. DePaolo, D.R. Cole, A. Navrotsky, and I.C. Bourg (Eds.), Geochemistry of Geologic CO_2 Sequestration. Reviews in Mineralogy & Geochemistry, pp. 361-398.

Chipera, S.J., and Vaniman, D.T. (2007) Experimental stability of magnesium sulfate hydrates that may be present on Mars. Geochimica Et Cosmochimica Acta, 71 (1), 241-250.

Chou, I.M., Seal, R.R., II, and Wang, A. (2013) The stability of sulfate and hydrated sulfate minerals near ambient conditions and their significance in environmental and planetary sciences. Journal of Asian Earth Sciences, 62, 734-758.

Christensen, B., Laake, M., and Lien, T. (1996) Treatment of acid mine water by sulfate-reducing bacteria; Results from a bench scale experiment. Water Research, 30 (7), 1617-1624.

Christensen, P.R., Morris, R.V., Lane, M.D., Bandfield, J.L., and Malin, M.C. (2001) Global mapping of Martian hematite mineral deposits: Remnants of water-driven processes on early Mars. Journal of Geophysical Research-Planets, 106 (E10), 23873-23885.

Chu, N.C., Johnson, C.M., Beard, B.L., German, C.R., Nesbitt, R.W., Frank, M., Bohn, M., Kubik, P.W., Usui, A., and Graham, I. (2006) Evidence for hydrothermal venting in Fe isotope compositions of the deep Pacific Ocean through time. Earth and Planetary Science Letters, 245 (1-2), 202-217.

Clark, R.N. (1999) Chapter 1: Spectroscopy of Rocks and Minerals, and Principles of Spectroscopy. In: A.N. Rencz (Ed.), Manual of Remote Sensing, Volume 3, Remote Sensing for the Earth Sciences. John Wiley and Sons, New York, pp. 3-58.

Clark, R.N., and Roush, T.L. (1984) Reflectance spectroscopy - quantitative-analysis techniques for remote-sensing applications. Journal of Geophysical Research, 89 (NB7), 6329-6340.

Clark, R.N., Vance, J.S., Livo, K.E., and Green, R.O. (1998) Mineral mapping with imaging spectroscopy: the Ray Mine, AZ. In: R.O. Green (Editor), 7th annual JPL Airborne Earth Science Workshop. JPL Publication, pp. 67-76.

Clark, R.N., Swayze, G.A., Livo, K.E., Kokaly, R.F., Sutley, S.J., Dalton, J.B., McDougal, R.R., and Gent, C.A. (2003) Imaging spectroscopy: Earth and planetary remote sensing with the USGS Tetracorder and expert systems. Journal of Geophysical Research-Planets, 108 (E12).

Clark, R.N., Swayze, G.A., Wise, R., Livio, E., Hoefen, T., Kokaly, R., and Sutley, S.J. (2007) USGS digital spectral library splib06a, U.S. Geological Survey: Digital Data Series 231.

Clifford, A.A. (2007) Calculation of density, enthalpy and entropy for supercritical carbon dioxide. Critical Processes Ltd. http://www.criticalprocesses.com/Calculation%20of%20density,%20enthalpy%20and%20entropy%20of%20carbon%20dioxide.htm

Cloutis, E.A., Hawthorne, F.C., Mertzman, S.A., Krenn, K., Craig, M.A., Marcino, D., Methot, M., Strong, J., Mustard, J.F., Blaney, D.L., Bell, J.F., and Vilas, F. (2006) Detection and discrimination of sulfate minerals using reflectance spectroscopy. Icarus, 184 (1), 121-157.

Cloutis, E.A., Craig, M.A., Kruzelecky, R.V., Jamroz, W.R., Scott, A., Hawthorne, F.C., and Mertzman, S.A. (2008) Spectral reflectance properties of minerals exposed to simulated Mars surface conditions. Icarus, 195 (1), 140-168.

Cloutis, E.A., Grasby, S.E., Last, W.M., Leveille, R., Osinski, G.R., and Sherriff, B.L. (2010) Spectral reflectance properties of carbonates from terrestrial analogue environments: Implications for Mars. Planetary and Space Science, 58 (4), 522-537.

Coleman, T., and Li, Y. (1994) On the convergence of interior-reflective Newton methods for nonlinear minimization subject to bounds. Mathematical Programming, 67 (1-3), 189-224.

Crowley, J.K., Williams, D.E., Hammarstrom, J.M., Piatak, N., Chou, I.M., and Mars, J.C. (2003) Spectral reflectance properties (0.4-2.5 μm) of secondary Fe-oxide, Fe-hydroxide, and Fe-sulfate-hydrate minerals associated with sulphide-bearing mine wastes. Geochemistry: Exploration, Environment, Analysis, 3 (3), 219-228.

Cruikshank, D.P., Owen, T.C., Ore, C.D., Geballe, T.R., Roush, T.L., de Bergh, C., Sandford, S.A., Poulet, F., Benedix, G.K., and Emery, J.P. (2005) A spectroscopic study of the surfaces of Saturn's large satellites: H_2O ice, tholins, and minor constituents. Icarus, 175 (1), 268-283.

Cruikshank, D.P., Dalton, J.B., Ore, C.M.D., Bauer, J., Stephan, K., Filacchione, G., Hendrix, A.R., Hansen, C.J., Coradini, A., Cerroni, P., Tosi, F., Capaccioni, F., Jaumann, R., Buratti, B.J., Clark, R.N., Brown, R.H., Nelson, R.M., McCord, T.B., Baines, K.H., Nicholson, P.D., Sotin, C., Meyer, A.W., Bellucci, G., Combes, M., Bibring, J.P., Langevin, Y., Sicardy, B., Matson, D.L., Formisano, V., Drossart, P., and Mennella, V. (2007) Surface composition of Hyperion. Nature, 448 (7149), 54-56.

Dalton, J.B. (2010) Spectroscopy of Icy Moon Surface Materials. Space Science Reviews, 153 (1-4), 219-247.

Dalton, J.B., Bove, D.J., and Mladinich, C.S. (2004a) Remote sensing charachterization of the Animas River watershed, southwest Colorado, by AVIRIS imaging spectroscopy. 2004-5203, USGS.

Dalton, J.B., Bove, D.J., Mladinich, C.S., and Rockwell, B.W. (2004b) Identification of spectrally similar materials using the USGS Tetracorder algorithm: the calcite-epidote-chlorite problem. Remote Sensing of Environment, 89 (4), 455-466.

Dalton, J.B., Cruikshank, D.P., Stephan, K., McCord, T.B., Coustenis, A., Carlson, R.W., and Coradini, A. (2010) Chemical composition of icy satellite surfaces. Space Science Reviews, 153 (1-4), 113-154.

Dalton, J.B., III, and Pitman, K.M. (2012) Low temperature optical constants of some hydrated sulfates relevant to planetary surfaces. Journal of Geophysical Research-Planets, 117.

Damen, K., Faaij, A., and Turkenburg, W. (2006) Health, safety and environmental risks of underground CO_2 storage - Overview of mechanisms and current knowledge. Climatic Change, 74 (1-3), 289-318.

De Grave, E., and van Alboom, A. (1991) Evaluation of ferrous and ferric Mössbauer fractions. Physics and Chemistry of Minerals, 18, 337-342.

Denevi, B.W., Lucey, P.G., and Sherman, S.B. (2008) Radiative transfer modeling of near-infrared spectra of lunar mare soils: Theory and measurement. Journal of Geophysical Research-Planets, 113 (E2).

DePaolo, D.J., Cole, D.R., Navrotsky, A., and Bourg, I.C. (2013a) Geochemistry of Geologic CO_2 Sequestration, Geochemistry of Geologic CO_2 Sequestration. Reviews in Mineralogy & Geochemistry, pp. iii-iv.

DePaolo, D.J., and Cole, D.R. (2013b) Geochemistry of geologic carbon sequestration: An overview. In: D.J. DePaolo, D.R. Cole, A. Navrotsky, and I.C. Bourg (Eds.), Geochemistry of Geologic CO_2 Sequestration. Reviews in Mineralogy & Geochemistry, pp. 1-14.

Deyell, C.L., and Dipple, G.M. (2005) Equilibrium mineral-fluid calculations and their application to the solid solution between alunite and natroalunite in the El Indio-Pascua belt of Chile and Argentina. Chemical Geology, 215 (1-4), 219-234.

Dooley, J.J., Dahowski, R.T., Davidson, C.L., Bachu, S., Gupta, N., and Gale, J. (2005a) A CO_2-storage supply curve for North America and its implications for the deployment of carbon dioxide capture and storage systems, Greenhouse Gas Control Technologies 7. Elsevier Science Ltd, pp. 593-601.

Dooley, J.J., Kim, S.H., Edmonds, J.A., Friedman, S.J., and Wise, M.A. (2005b) A first-order global geological CO_2-storage potential supply curve and its application in a global integrated assessment model, Greenhouse Gas Control Technologies 7. Elsevier Science Ltd, pp. 573-581.

Drouet, C., and Navrotsky, A. (2003) Synthesis, characterization, and thermochemistry of K-Na-H3O jarosites. Geochimica Et Cosmochimica Acta, 67 (11), 2063-2076.

Duan, Z.H., and Sun, R. (2003) An improved model calculating CO_2 solubility in pure water and aqueous NaCl solutions from 273 to 533 K and from 0 to 2000 bar. Chemical Geology, 193 (3-4), 257-271.

Dyar, M.D., Schaefer, M.W., Sklute, E.C., and Bishop, J.L. (2008) Mössbauer spectroscopy of phyllosilicates: effects of fitting models on recoil-free fractions and redox ratios. Clay Minerals, 43 (1), 3-33.

Dyar, M.D., Breves, E., Jawin, E., Marchand, G., Nelms, M., O'Connor, V., Peel, S., Rothstein, Y., Sklute, E.C., Lane, M.D., Bishop, J.L., and Mertzman, S.A. (2013) Mössbauer parameters of iron in sulfate minerals. American Mineralogist, 98 (11-12), 1943-1965.

Ellis, B.R., Crandell, L.E., and Peters, C.A. (2010) Limitations for brine acidification due to SO_2 co-injection in geologic carbon sequestration. International Journal of Greenhouse Gas Control, 4 (3), 575-582.

Ellis, B.R., Peters, C.A., Fitts, J., Bromhal, G., McIntyre, D., Warzinski, R., and Rosenbaum, E. (2011) Deterioration of a fractured carbonate caprock exposed to CO_2-acidified brine flow. Greenhouse Gases-Science and Technology, 1 (3), 248-260.

Eriksson, E. (1963) Yearly circulation of sulfur in nature. Journal of Geophysical Research, 68 (13), 4001-&.

Fairen, A.G., Davila, A.F., Gago-Duport, L., Amils, R., and McKay, C.P. (2009) Stability against freezing of aqueous solutions on early Mars. Nature, 459 (7245), 401-404.

Farrand, W.H., Glotch, T.D., Rice, J.W., Hurowitz, J.A., and Swayze, G.A. (2009) Discovery of jarosite within the Mawrth Vallis region of Mars: Implications for the geologic history of the region. Icarus, 204 (2), 478-488.

Feldman, W.C., Prettyman, T.H., Maurice, S., Plaut, J.J., Bish, D.L., Vaniman, D.T., Mellon, M.T., Metzger, A.E., Squyres, S.W., Karunatillake, S., Boynton, W.V., Elphic, R.C., Funsten, H.O., Lawrence, D.J., and Tokar, R.L. (2004) Global distribution of near-surface hydrogen on Mars. Journal of Geophysical Research-Planets, 109 (E9).

Flett, M.A., Gurton, R.M., and Taggart, I.J. (2005) Heterogeneous saline formations: Long-term benefits for geo-sequestration of greenhouse gases, Greenhouse Gas Control Technologies 7. Elsevier Science Ltd, pp. 501-509.

Frost, R.L., Wills, R.A., Martens, W., and Weier, M. (2005a) NIR spectroscopy of jarosites. Spectrochimica Acta Part a-Molecular and Biomolecular Spectroscopy, 62 (4-5), 869-874.

Frost, R.L., Wills, R.A., Martens, W., Weier, M., and Reddy, B.J. (2005b) NIR spectroscopy of selected iron(II) and iron(III) sulphates. Spectrochimica Acta Part a-Molecular and Biomolecular Spectroscopy, 62 (1-3), 42-50.

Gaffey, S.J. (1986) Spectral reflectance of carbonate minerals in the visible and near-infrared (0.35-2.55 microns) - calcite, aragonite, and dolomite. American Mineralogist, 71 (1-2), 151-162.

Gaffey, S.J. (1987) Spectral reflectance of carbonate minerals in the visible and near-infrared (0.35-2.55 μm) - anhydrous carbonate minerals. Journal of Geophysical Research-Solid Earth and Planets, 92 (B2), 1429-1440.

Gaillard, F., Michalski, J., Berger, G., McLennan, S.M., and Scaillet, B. (2013) Geochemical reservoirs and timing of sulfur cycling on Mars. Space Science Reviews, 174 (1-4), 251-300.

Galloway, J.N. (2001) Acidification of the world - Natural and anthropogenic. Water Air and Soil Pollution, 130 (1-4), 17-24.

Garcia, S., Rosenbauer, R.J., Palandri, J., and Maroto-Valer, M.M. (2012) Sequestration of non-pure carbon dioxide streams in iron oxyhydroxide-containing saline repositories. International Journal of Greenhouse Gas Control, 7, 89-97.

Gendrin, A., Mangold, N., Bibring, J.P., Langevin, Y., Gondet, B., Poulet, F., Bonello, G., Quantin, C., Mustard, J., Arvidson, R., and LeMouelic, S. (2005) Sulfates in Martian layered terrains: the OMEGA/Mars Express view. Science, 307 (5715), 1587-1591.

GHG (2003) Potential for improvements in Gasification Combined Cycle Power Generation with CO_2 Capture. International Energy Agency Greenhouse Gas R&D program, IEA GHG, Chetenham, UK.

Glotch, T.D., and Rogers, A.D. (2007) Evidence for aqueous deposition of hematite- and sulfate-rich light-toned layered deposits in Aureum and Iani Chaos, Mars. Journal of Geophysical Research-Planets, 112 (E6).

Glotch, T.D., and Rossman, G.R. (2009) Mid-infrared reflectance spectra and optical constants of six iron oxide/oxyhydroxide phases. Icarus, 204 (2), 663-671.

Grohol, D., Nocera, D.G., and Papoutsakis, D. (2003) Magnetism of pure iron jarosites. Physical Review B, 67 (6).

Hapke, B. (1981) Bidirectional reflectance spectroscopy 1. Theory. Journal of Geophysical Research, 86 (NB4), 3039-3054.

Hapke, B. (1993) Theory of Reflectance and Emittance Spectroscopy. Topics in Remote Sensing Cambridge University Press, New York, NY.

Hapke, B. (1996) A model of radiative and conductive energy transfer in planetary regoliths. Journal of Geophysical Research-Planets, 101 (E7), 16817-16831.

Hapke, B. (2002) Bidirectional reflectance spectroscopy 5. The coherent backscatter opposition effect and anisotropic scattering. Icarus, 157 (2), 523-534.

Hapke, B. (2008) Bidirectional reflectance spectroscopy - 6. Effects of porosity. Icarus, 195 (2), 918-926.

Hapke, B. (2012) Theory of Reflectance and Emittance Spectroscopy, 2nd edition. Cambridge University Press, New York.

Hapke, B., and Wells, E. (1981) Bidirectional reflectance spectroscopy 2. Experiments and observations. Journal of Geophysical Research, 86 (NB4), 3055-3060.

Haveman, S.A., and Pedersen, K. (2002) Distribution of culturable microorganisms in Fennoscandian Shield groundwater. Fems Microbiology Ecology, 39 (2), 129-137.

Hawthorne, F.C., Krivovichev, S.V., and Burns, P.C. (2000) The crystal chemistry of sulfate minerals. Sulfate Minerals - Crystallography, Geochemistry and Environmental Significance, 40, 1-112.

Hazen, R.M., Papineau, D., Leeker, W.B., Downs, R.T., Ferry, J.M., McCoy, T.J., Sverjensky, D.A., and Yang, H.X. (2008) Mineral evolution. American Mineralogist, 93 (11-12), 1693-1720.

Hepple, R.P., and Benson, S.M. (2005) Geologic storage of carbon dioxide as a climate change mitigation strategy: performance requirements and the implications of surface seepage. Environmental Geology, 47 (4), 576-585.

Hill, C.A. (1987) Geology of Carlsbad Cavern and other caves in the Guadalupe mountains, New Mexico and Texas. New Mexico Bureau Of Mines & Mineral Resources Bulletin 117
http://www.nps.gov/history/history/online_books/geology/publications/state/nm/1987-117/sec1-2.htm

Holloway, S. (1997) An overview of the underground disposal of carbon dioxide. Energy Conversion and Management, 38, S193-S198.

Hunt, G.R. (1977) Spectral signatures of particulate minerals in the visible and near IR. Geophysics, 42 (3), 501-513.

Hurowitz, J.A., and McLennan, S.M. (2007) A similar to 3.5 Ga record of water-limited, acidic weathering conditions on Mars. Earth and Planetary Science Letters, 260 (3-4), 432-443.

Huston, D.L., Pehrsson, S., Eglington, B.M., and Zaw, K. (2010) The geology and metallogeny of volcanic-hosted massive sulfide deposits: Variations through geologic time and with tectonic setting. Economic Geology, 105 (3), 571-591.

IPCC (2005) IPCC special report on carbon dioxide capture and storage, Intergovernmental Pannel on Climate Change, New York, NY.

IPCC (2014) IPCC, 2014: Summary for policymakers., IPCC, Cabridge, United Kingdom and New York, NY, USA.

Ivanov, M.V. (1983) The Global biogeochemical sulphur cycle. In: J.R. Freney, M.V. Ivanov, U. International Council of Scientific, and S.U.W.o.t.G.B.S. Cycle (Eds.), SCOPE ;19. Published on behalf of the Scientific Committee on Problems of the Environment of the International Council of Scientific Union by Wiley, Chichester [Sussex] ; New York, pp. 61-78.

Jambor, J.L., and Blowes, D.W. (1994) Short course handbook on environmental geochemistry of sulfide mine wastes, 22. Mineralogical Association of Canada, Waterloo, Ontario, 438 pp.

Jambor, J.I., Nordstrom, D.K., and Alpers, C.N. (2000) Metal-sulfate salts from sulfide mineral oxidation. Sulfate Minerals - Crystallography, Geochemistry and Environmental Significance, 40, 303-350.

Jerz, J.K., and Rimstidt, J.D. (2003) Efflorescent iron sulfate minerals: Paragenesis, relative stability, and environmental impact. American Mineralogist, 88 (11-12), 1919-1932.

Johnson, D.B. (1998) Biodiversity and ecology of acidophilic microorganisms. Fems Microbiology Ecology, 27 (4), 307-317.

Johnson, D.B. (2003) Chemical and microbiological characteristics of mineral spoils and drainage waters at abandoned coal and metal mines. Water, Air and Soil Pollution: Focus, 3 (1), 47-66.

Johnson, D.B., and Hallberg, K.B. (2005) Acid mine drainage remediation options: a review. Science of the Total Environment, 338 (1-2), 3-14.

Jones, G.D., and Xiao, Y.T. (2006) Geothermal convection in the Tengiz carbonate platform, Kazakhstan: Reactive transport models of diagenesis and reservoir quality. Aapg Bulletin, 90 (8), 1251-1272.

Karnieli, A., Derimian, Y., Indoitu, R., Panov, N., Levy, R.C., Remer, L.A., Maenhaut, W., and Holben, B.N. (2009) Temporal trend in anthropogenic sulfur aerosol transport from central and eastern Europe to Israel. Journal of Geophysical Research-Atmospheres, 114.

Karunatillake, S., Gasnault, O., McLennan, S.M., Rogers, D.A., Wray, J.J., Squyres, S.W., and Boynton, W.V. (2012) The hydration state of sulfates on Mars. Abstracts of Papers submitted to the Lunar and Planetary Science Conference XXXXIII (2940).

Kaszuba, J.P., Janecky, D.R., and Snow, M.G. (2005) Experimental evaluation of mixed fluid reactions between supercritical carbon dioxide and NaCl brine: Relevance to the integrity of a geologic carbon repository. Chemical Geology, 217 (3-4), 277-293.

Kaszuba, J., Yardley, B., and Andreani, M. (2013) Experimental perspectives of mineral dissolution and precipitation due to carbon dioxide-water-rock interactions. In: D.J.

DePaolo, D.R. Cole, A. Navrotsky, and I.C. Bourg (Eds.), Geochemistry of Geologic CO_2 Sequestration. Reviews in Mineralogy & Geochemistry, pp. 153-188.

Kelley, D.S., Baross, J.A., and Delaney, J.R. (2002) Volcanoes, fluids, and life at mid-ocean ridge spreading centers. Annual Review of Earth and Planetary Sciences, 30, 385-491.

Kendall, B., Anbar, A.D., Kappler, A., and Konhauser, K.O. (2012) The Global Iron Cycle, Fundamentals of Geobiology. John Wiley & Sons, Ltd, pp. 65-92.

Kharaka, Y.K., Cole, D.R., Thordsen, J.J., Gans, K.D., and Thomas, R.B. (2013) Geochemical monitoring for potential environmental impacts of geologic sequestration of CO_2. In: D.J. DePaolo, D.R. Cole, A. Navrotsky, and I.C. Bourg (Eds.), Geochemistry of Geologic CO_2 Sequestration. Reviews in Mineralogy & Geochemistry, pp. 399-430.

King, P.L., and McLennan, S.M. (2010) Sulfur on Mars. Elements, 6 (2), 107-112.

Klingelhofer, G., Morris, R.V., Bernhardt, B., Schroder, C., Rodionov, D.S., de Souza, P.A., Yen, A., Gellert, R., Evlanov, E.N., Zubkov, B., Foh, J., Bonnes, U., Kankeleit, E., Gutlich, P., Ming, D.W., Renz, F., Wdowiak, T., Squyres, S.W., and Arvidson, R.E. (2004) Jarosite and hematite at Meridiani Planum from Opportunity's Mössbauer spectrometer. Science, 306 (5702), 1740-1745.

Knauss, K.G., Johnson, J.W., and Steefel, C.I. (2005) Evaluation of the impact of CO_2, co-contaminant gas, aqueous fluid and reservoir rock interactions on the geologic sequestration of CO_2. Chemical Geology, 217 (3-4), 339-350.

Kong, W.G., Wang, A., and Chou, I.M. (2011)a Experimental determination of the phase boundary between kornelite and pentahydrated ferric sulfate at 0.1 MPa. Chemical Geology, 284 (3-4), 333-338.

Kong, W.G., Wang, A., Freeman, J.J., and Sobron, P. (2011b) A comprehensive spectroscopic study of synthetic Fe^{2+}, Fe^{3+}, Mg^{2+} and Al^{3+} copiapite by Raman, XRD, LIBS, MIR and vis-NIR. Journal of Raman Spectroscopy, 42 (5), 1120-1129.

Konhauser, K., and Riding, R. (2012) Bacterial Biomineralization, Fundamentals of Geobiology. John Wiley & Sons, Ltd, pp. 105-130.

Krumbein, W., and Gorbushina, A. (2010) Global Relations Between the Redox Cycles of Carbon, Iron, and Sulfur, Handbook of Hydrocarbon and Lipid Microbiology. Springer, pp. 157-169.

Kula, J., and Baldwin, S.L. (2011) Jarosite, argon diffusion, and dating aqueous mineralization on Earth and Mars. Earth and Planetary Science Letters, 310 (3-4), 314-318.

Lane, M.D. (2007) Mid-infrared emission spectroscopy of sulfate and sulfate-bearing minerals. American Mineralogist, 92 (1), 1-18.

Lawrence, S.J., and Lucey, P.G. (2007) Radiative transfer mixing models of meteoritic assemblages. Journal of Geophysical Research-Planets, 112 (E7).

Li, S., and Li, L. (2011) Radiative transfer modeling for quantifying lunar surface minerals, particle size, and submicroscopic metallic Fe. Journal of Geophysical Research-Planets, 116.

Lichtenberg, K.A., Arvidson, R.E., Morris, R.V., Murchie, S.L., Bishop, J.L., Fernandez Remolar, D., Glotch, T.D., Dobrea, E.N., Mustard, J.F., Andrews-Hanna, J., and Roach, L.H. (2010) Stratigraphy of hydrated sulfates in the sedimentary deposits of Aram Chaos, Mars. Journal of Geophysical Research-Planets, 115.

Ling, Z.C., and Wang, A. (2010) A systematic spectroscopic study of eight hydrous ferric sulfates relevant to Mars. Icarus, 209 (2), 422-433.

Lippmann, F. (1973) Sedimentary Carbonate Minerals. Springer-Verlag, New York, 228 pp.

Lucarini, V., Saarinen, J.J., Peiponen, K.-E., and Vartiainen, E.M. (2005) Kramers-Kronig Relations in Optical Materials Research. Springer Series in Optical Sciences. Springer, New York, 162 pp.

Lucey, P.G. (1998) Model near-infrared optical constants of olivine and pyroxene as a function of iron content. Journal of Geophysical Research-Planets, 103 (E1), 1703-1713.

Lucey, P.G. (2004) Mineral maps of the Moon. Geophysical Research Letters, 31 (8).

Lueth, V.W., Rye, R.O., and Peters, L. (2005) "Sour gas" hydrothermal jarosite: ancient to modem acid-sulfate mineralization in the southern Rio Grande Rift. Chemical Geology, 215 (1-4), 339-360.

Luquot, L., Andreani, M., Gouze, P., and Camps, P. (2012) CO_2 percolation experiment through chlorite/zeolite-rich sandstone (Pretty Hill Formation - Otway Basin-Australia). Chemical Geology, 294, 75-88.

Madden, M.E.E., Bodnar, R.J., and Rimstidt, J.D. (2004) Jarosite as an indicator of water-limited chemical weathering on Mars. Nature, 431 (7010), 821-823.

Madden, M.E.E., Guess, J.R., Madden, A.S., and Rimstidt, J.D. (2008) Measuring jarosite dissolution rates to determine jarosite lifetimes on Earth and Mars. Geochimica Et Cosmochimica Acta, 72 (12), A243-A243.

Madden, M.E.E., Madden, A.S., and Rimstidt, J.D. (2009) How long was Meridiani Planum wet? Applying a jarosite stopwatch to determine the duration of aqueous diagenesis. Geology, 37 (7), 635-638.

Madden, M.E.E., Madden, A.S., Rimstidt, J.D., Zahrai, S., Kendall, M.R., and Miller, M.A. (2012) Jarosite dissolution rates and nanoscale mineralogy. Geochimica Et Cosmochimica Acta, 91, 306-321.

Majzlan, J., Stevens, R., Boerio-Goates, J., Woodfield, B.F., Navrotsky, A., Burns, P.C., Crawford, M.K., and Amos, T.G. (2004) Thermodynamic properties, low-temperature heat-capacity anomalies, and single-crystal X-ray refinement of hydronium jarosite, (H3O)Fe3(SO4)2(OH)6. Physics and Chemistry of Minerals, 31 (8), 518-531.

Marion, G.M., Catling, D.C., and Kargel, J.S. (2003) Modeling aqueous ferrous iron chemistry at low temperatures with application to Mars. Geochimica Et Cosmochimica Acta, 67 (22), 4251-4266.

Marion, G.M., Kargel, J.S., and Catling, D.C. (2008) Modeling ferrous-ferric iron chemistry with application to martian surface geochemistry. Geochimica Et Cosmochimica Acta, 72 (1), 242-266.

Martinez, G.M., and Renno, N.O. (2013) Water and brines on Mars: Current evidence and implications for MSL. Space Science Reviews, 175 (1-4), 29-51.

Masse, M., Beck, P., Schmitt, B., Pommerol, A., McEwen, A., Chevrier, V., Brissaud, O., and Sejourne, A. (2014) Spectroscopy and detectability of liquid brines on mars. Planetary and Space Science, 92, 136-149.

Mauch, S. (2004) Introduction to Methods of Applied Mathematics or Advanced Mathematical Methods for Scientists and Engineers. http://www.its.caltech.edu/˜sean

Maurice, S., Feldman, W., Diez, B., Gasnault, O., Lawrence, D.J., Pathare, A., and Prettyman, T. (2011) Mars Odyssey neutron data: 1. Data processing and models of water-equivalent-hydrogen distribution. Journal of Geophysical Research-Planets, 116.

Mazumder, S., van Hemert, P., Bruining, J., Wolf, K., and Drabe, K. (2006) In situ CO_2-coal reactions in view of carbon dioxide storage in deep unminable coal seams. Fuel, 85 (12-13), 1904-1912.

McAdam, A.C., Franz, H.B., Sutter, B., Archer, P.D., Freissinet, C., Eigenbrode, J.L., Ming, D.W., Atreya, S.K., Bish, D.L., Blake, D.F., Bower, H.E., Brunner, A., Buch, A., Glavin, D.P., Grotzinger, J.P., Mahaffy, P.R., McLennan, S.M., Morris, R.V., Navarro-González, R., Rampe, E.B., Squyres, S.W., Steele, A., Stern, J.C., Sumner, D.Y., and Wray, J.J. (2014) Sulfur-bearing phases detected by evolved gas analysis of the Rocknest aeolian deposit, Gale Crater, Mars. Journal of Geophysical Research: Planets, 2013JE004518.

McEwen, A.S., Ojha, L., Dundas, C.M., Mattson, S.S., Byrne, S., Wray, J.J., Cull, S.C., Murchie, S.L., Thomas, N., and Gulick, V.C. (2011) Seasonal flows on warm Martian slopes. Science, 333 (6043), 740-743.

McLennan, S.M. (2001) Relationships between the trace element composition of sedimentary rocks and upper continental crust. Geochemistry Geophysics Geosystems, 2, art. no.-2000GC000109.

McLennan, S.M. (2012) Geochemistry of sedimentary processes on mars. In: J.P. Grotzinger, and R.E. Milliken (Eds.), Sedimentary geology of Mars. Society for Sedimentary Geology Special Publication, pp. 119-138.

Milliken, R.E., Fischer, W.W., and Hurowitz, J.A. (2009) Missing salts on early Mars. Geophysical Research Letters, 36.

Milliken, R.E., and Bish, D.L. (2010) Sources and sinks of clay minerals on Mars. Philosophical Magazine, 90 (17-18), 2293-2308.

Mohan, K.K., Vaidya, R.N., Reed, M.G., and Fogler, H.S. (1993) Water sensitivity of sandstones containing swelling and non-swelling clays. Colloids and Surfaces a-Physicochemical and Engineering Aspects, 73, 237-254.

Mohlmann, D., and Thomsen, K. (2011) Properties of cryobrines on Mars. Icarus, 212 (1), 123-130.

Morris, R.V., Ming, D.W., Blake, D.F., Vaniman, D.T., Bish, D.L., Chipera, S.J., Downs, R.T., Gellert, R., Treiman, A.H., Yen, A.S., Achilles, C.N., Anderson, R.C., Bristow, T.F., Crisp, J.A., Des Marais, D.J., Farmer, J.D., Grotzinger, J.P., Leshin, L.A., McAdam, A.C., Morookian, J.M., Morrison, S.M., Rampe, E.B., Sarrazin, P.C., Spanovich, N., and Stolper, E.M. (2013) The amorphous component in the Martian basaltic soil in global perspective from MSL and MER missions. Abstracts of Papers submitted to the Lunar and Planetary Science Conference XXXXIV (1653).

Morris, R.V., Ming, D.W., Gellert, R., Vaniman, D.T., Bish, D.L., Blake, D.F., Chipera, S.J., Downs, R.T., Treiman, A.H., Yen, A.S., Achilles, C.N., Archer, P.D., Bristow, T.F., Crisp, J.A., Des Marais, D.J., Farmer, J.D., Grotzinger, J.P., Mahaffy, P.R., McAdam, A.C., Morookian, J.M., Morrison, S.M., and Rampe, E.B. (2014) Chemical composition fo crystalline, smectite, and amorphous components for Rocknest soil and John Klein and Cumberland mudstone drill fines using APXS, CHEMIN, and SAM datasets from Gale Crater, Mars. Abstracts of Papers submitted to the Lunar and Planetary Science Conference XXXXV (1319).

Morse, J.W., and Casey, W.H. (1988) Ostwald processes and mineral paragenesis in sediments. American Journal of Science, 288 (6), 537-560.

Murad, E., and Rojik, P. (2005) Iron mineralogy of mine-drainage precipitates as environmental indicators: review of current concepts and a case study from the Sokolov Basin, Czech Republic. Clay Minerals, 40 (4), 427-440.

Murchie, S.L., Mustard, J.F., Ehlmann, B.L., Milliken, R.E., Bishop, J.L., McKeown, N.K., Dobrea, E.Z.N., Seelos, F.P., Buczkowski, D.L., Wiseman, S.M., Arvidson, R.E., Wray, J.J., Swayze, G., Clark, R.N., Marais, D.J.D., McEwen, A.S., and Bibring, J.P. (2009) A synthesis of Martian aqueous mineralogy after 1 Mars year of observations from the Mars Reconnaissance Orbiter. Journal of Geophysical Research-Planets, 114.

Murphy, R., Lammers, K., Smirnov, A., Schoonen, M.A.A., and Strongin, D.R. (2010) Ferrihydrite phase transformation in the presence of aqueous sulfide and supercritical CO_2. Chemical Geology, 271 (1-2), 26-30.

Murphy, R., Lammers, K., Smirnov, A., Schoonen, M.A.A., and Strongin, D.R. (2011) Hematite reactivity with supercritical CO_2 and aqueous sulfide. Chemical Geology, 283 (3-4), 210-217.

Mustard, J.F., and Pieters, C.M. (1987) Quantitative abundance estimates from bidirectional reflectance measurements. Journal of Geophysical Research-Solid Earth and Planets, 92 (B4), E617-E626.

Mustard, J.F., and Pieters, C.M. (1989) Photometric phase function of common geological minerals and applications to quantitative-analysis of mineral mixture reflectance spectra. Journal of Geophysical Research-Solid Earth and Planets, 94 (B10), 13619-13634.

Nakamoto, K. (1986) Infrared and raman spectra of inorganic and coordinated compounds. Wiley and Sons, New York.

Navrotsky, A., Forray, F.L., and Drouet, C. (2005) Jarosite stability on Mars. Icarus, 176 (1), 250-253.

Nielsen, A.E., and Sohnel, O. (1971) Interfacial tensions electrolyte crystal-aqueous solution, from nucleation data. Journal of Crystal Growth, 11 (3), 233-&.

Nocera, D.G., Bartlett, B.M., Grohol, D., Papoutsakis, D., and Shores, M.P. (2004) Spin frustration in 2D kagome lattices: A problem for inorganic synthetic chemistry. Chemistry-a European Journal, 10 (16), 3851-3859.

Nomura, K., Takeda, M., Iiyama, T., and Sakai, H. (2005) Mössbauer studies of jarosite, mikasaite and yavapaiite, and implication to their Martian counterparts. Hyperfine Interactions, 166 (1-4), 657-664.

Nordstrom, D.K., and Southam, G. (1997) Geomicrobiology of sulfide mineral oxidation. In: J.F. Banfield, and K.H. Nealson (Eds.), Geomicrobiology: Interactions between Microbes and Minerals. Reviews in Mineralogy, pp. 361-390.

Norlund, K.L.I., Baron, C., and Warren, L.A. (2010) Jarosite formation by an AMD sulphide-oxidizing environmental enrichment: Implications for biomarkers on Mars. Chemical Geology, 275 (3-4), 235-242.

Ober, J.A. (2002) Materials flow of sulfur. Open-file Report. U.S. Dept. of the Interior, U.S. Geological Survey 2-298, 56 pp. http://pubs.usgs.gov/of/2002/of02-298/of02-298.pdf

Orphan, V.J., Taylor, L.T., Hafenbradl, D., and Delong, E.F. (2000) Culture-dependent and culture-independent characterization of microbial assemblages associated with high-temperature petroleum reservoirs. Applied and Environmental Microbiology, 66 (2), 700-711.

Palandri, J.L., and Kharaka, Y.K. (2005a) Ferric iron-bearing sediments as a mineral trap for CO_2 sequestration: Iron reduction using sulfur-bearing waste gas. Chemical Geology, 217 (3-4), 351-364.

Palandri, J.L., Rosenbauer, R.J., and Kharaka, Y.K. (2005b) Ferric iron in sediments as a novel CO_2 mineral trap: CO_2-SO_2 reaction with hematite. Applied Geochemistry, 20 (11), 2038-2048.

Papike, J.J., Karner, J.M., and Shearer, C.K. (2006) Comparative planetary mineralogy: Implications of martian and terrestrial jarosite. A crystal chemical perspective. Geochimica Et Cosmochimica Acta, 70 (5), 1309-1321.

Papike, J.J., Burger, P.V., Karner, J.M., Shearer, C.K., and Lueth, V.W. (2007) Terrestrial analogs of martian jarosites: Major, minor element systematics and Na-K zoning in selected samples. American Mineralogist, 92 (2-3), 444-447.

Pappu, A., Saxena, M., and Asolekar, S.R. (2006) Jarosite characteristics and its utilisation potentials. Science of the Total Environment, 359 (1-3), 232-243.

Parkes, R.J., Cragg, B.A., and Wellsbury, P. (2000) Recent studies on bacterial populations and processes in subseafloor sediments: A review. Hydrogeology Journal, 8 (1), 11-28.

Pecharroman, C., Gonzalezcarreno, T., and Iglesias, J.E. (1995) The infrared dielectric-properties of maghemite, gamma-Fe_20_3, from reflectance measurement on presses powders. Physics and Chemistry of Minerals, 22 (1), 21-29.

Piatek, J.L. (2003). Size-dependent scattering properties of planetary regolith analogs, 186 pp. Ph.D. Thesis, University of Pittsburgh, Pittsburgh.

Poulet, F., and Erard, S. (2004) Nonlinear spectral mixing: Quantitative analysis of laboratory mineral mixtures. Journal of Geophysical Research-Planets, 109 (E2).

Poulet, F., Mangold, N., Platevoet, B., Bardintzeff, J.M., Sautter, V., Mustard, J.F., Bibring, J.P., Pinet, P., Langevin, Y., Gondet, B., and Aleon-Toppani, A. (2009a) Quantitative compositional analysis of martian mafic regions using the MEx/OMEGA reflectance data 2. Petrological implications. Icarus, 201 (1), 84-101.

Poulet, F., Bibring, J.P., Langevin, Y., Mustard, J.F., Mangold, N., Vincendon, M., Gondet, B., Pinet, P., Bardintzeff, J.M., and Platevoet, B. (2009b) Quantitative compositional analysis of martian mafic regions using the MEx/OMEGA reflectance data. Icarus, 201 (1), 69-83.

Poulton, S.W., Krom, M.D., and Raiswell, R. (2004) A revised scheme for the reactivity of iron (oxyhydr)oxide minerals towards dissolved sulfide. Geochimica Et Cosmochimica Acta, 68 (18), 3703-3715.

Pritchett, B.N., Madden, M.E.E., and Madden, A.S. (2012) Jarosite dissolution rates and maximum lifetimes in high salinity brines: Implications for Earth and Mars. Earth and Planetary Science Letters, 357, 327-336.

Pruess, K., Xu, T., Apps, J., and Garcia, J. (2001) Numerical Modeling of Aquifer Disposal of CO_2.

Quinn, D. (2010) The Hapke Model in Excel. http://davenquinn.com/hapke/

Quinn, D.P., Gillis-Davis, J.J., and Lucey, P.G. (2010) Using Microsoft Excel for Hapke modeling: A technique to simplify calculations of optical constants and reflectance spectra. Abstracts of Papers Submitted to the Lunar and Planetary Science Conference XXXXI (2426).

Raiswell, R. (2011) Iron transport from the continents to the open ocean: The aging-rejuvenation cycle. Elements, 7 (2), 101-106.

Raiswell, R., and Canfield, D.E. (2012) The iron biogeochemical cycle past and present. Geochemical Perspectives, 1 (1), 1-220.

Rasch, P.J., Barth, M.C., Kiehl, J.T., Schwartz, S.E., and Benkovitz, C.M. (2000) A description of the global sulfur cycle and its controlling processes in the National Center for Atmospheric Research Community Climate Model, Version 3. Journal of Geophysical Research-Atmospheres, 105 (D1), 1367-1385.

Reeder, R.J., and Michel, F.M. (2013) Application of Total X-Ray Scattering Methods and Pair Distribution Function Analysis for Study of Structure of Biominerals. In: J.J.D. Yoreo (Ed.), Research Methods in Biomineralization Science. Methods in Enzymology, pp. 477-500.

Riaza, A., Garcia-Melendez, E., and Mueller, A. (2011) Spectral identification of pyrite mud weathering products: a field and laboratory evaluation. International Journal of Remote Sensing, 32 (1), 185-208.

Roach, L.H., Mustard, J.F., Murchie, S.L., Bibring, J.P., Forget, F., Lewis, K.W., Aharonson, O., Vincendon, M., and Bishop, J.L. (2009) Testing evidence of recent hydration state change in sulfates on Mars. Journal of Geophysical Research-Planets, 114.

Roach, L.H., Mustard, J.F., Lane, M.D., Bishop, J.L., and Murchie, S.L. (2010a) Diagenetic haematite and sulfate assemblages in Valles Marineris. Icarus, 207 (2), 659-674.

Roach, L.H., Mustard, J.F., Swayze, G., Milliken, R.E., Bishop, J.L., Murchie, S.L., and Lichtenberg, K. (2010b) Hydrated mineral stratigraphy of Ius Chasma, Valles Marineris. Icarus, 206 (1), 253-268.

Rosenbauer, R.J., Koksalan, T., and Palandri, J.L. (2005) Experimental investigation of CO_2-brine-rock interactions at elevated temperature and pressure: Implications for CO_2 sequestration in deep-saline aquifers. Fuel Processing Technology, 86 (14-15), 1581-1597.

Rossman, G.R. (1975) Spectroscopic and magnetic studies of ferric iron hydroxy sulfates-intesification of color in ferric iron clusters bridged by a single hydroxide ion. American Mineralogist, 60 (7-8), 698-704.

Rossman, G.R. (1976) Spectroscopic and magnetic studies of ferric iron hydroxy sulfates-series Fe(OH)SO4.nH2O and jarosites. American Mineralogist, 61 (5-6), 398-404.

Roush, T.L., Esposito, F., Rossman, G.R., and Colangeli, L. (2007) Estimated optical constants of gypsum in the regions of weak absorptions: Application of scattering theories and comparisons to independent measurements. Journal of Geophysical Research-Planets, 112.

Russell, M.J., Barge, L.M., Bhartia, R., Bocanegra, D., Bracher, P.J., Branscomb, E., Kidd, R., McGlynn, S., Meier, D.H., Nitschke, W., Shibuya, T., Vance, S., White, L., and Kanik, I. (2014) The drive to life on wet and icy worlds. Astrobiology, 14 (4), 308-343.

Rye, R.O., and Stoffregen, R.E. (1995) Jarosite-water oxygen and hydrogen isotope fractionations: Preliminary experimental data. Economic Geology and the Bulletin of the Society of Economic Geologists, 90 (8), 2336-2342.

Savijarvi, H. (1995) Mars boundary-layer modeling - Diurnal moisture cycle and soil properties at the Viking-Lander-1 site. Icarus, 117 (1), 120-127.

Schoonen, M.A.A., Sklute, E.C., Dyar, M.D., and Strongin, D.R. (2012) Reactivity of sandstones under conditions relevant to geosequestration: 1. Hematite-bearing sandstone exposed to supercritical carbon dioxide commingled with aqueous sulfite or sulfide solutions. Chemical Geology, 296, 96-102.

Sears, D.W.G., and Chittenden, J.D. (2005) On laboratory simulation and the temperature dependence of the evaporation rate of brine on Mars. Geophysical Research Letters, 32 (23).

Sefton-Nash, E., Catling, D.C., Wood, S.E., Grindrod, P.M., and Teanby, N.A. (2012) Topographic, spectral and thermal inertia analysis of interior layered deposits in Iani Chaos, Mars. Icarus, 221 (1), 20-42.

Shepard, M.K., and Helfenstein, P. (2007) A test of the Hapke photometric model. Journal of Geophysical Research-Planets, 112 (E3).

Sherman, D.M., Burns, R.G., and Burns, V.M. (1982) Spectral characteristics of the iron-oxides with application to the Martian bright region mineralogy. Journal of Geophysical Research, 87 (NB12), 169-180.

Sherman, D.M., and Waite, T.D. (1985) Electronic-spectra of Fe^{3+} oxides and oxide hydroxides in the near IR to near UV. American Mineralogist, 70 (11-12), 1262-1269.

Shkuratov, Y., Starukhina, L., Hoffmann, H., and Arnold, G. (1999) A model of spectral albedo of particulate surfaces: Implications for optical properties of the moon. Icarus, 137 (2), 235-246.

Sievert, S.M., Kiene, R.P., and Schulz-Vogt, H.N. (2007) The sulfur cycle. Oceanography, 20 (2), 117-123.

Sklute, E.C., Schoonen, M.A.A., Dyar, M.D., and Strongin, D.R. (In Preparation) Reactivity of sandstones under conditions relevant to geosequestration: 2. Hematite-bearing sandstone exposed to supercritical carbon dioxide comingled with saline sulfite and/or sulfide solutions. Chemical Geology.

Sklute, E.C., Schoonen, M.A.A., Dyar, M.D., and Strongin, D.R. (In Preparation) Reactivity of sandstones under conditions relevant to geosequestration: 3. Gray sandstones exposed to supercritical carbon dioxide comingled with saline sulfite and/or sulfide solutions. Chemical Geology.

Smith, S.J., Pitcher, H., and Wigley, T.M.L. (2001) Global and regional anthropogenic sulfur dioxide emissions. Global and Planetary Change, 29 (1-2), 99-119.

Sowe, M., Wendt, L., McGuire, P.C., and Neukum, G. (2012) Hydrated minerals in the deposits of Aureum Chaos. Icarus, 218 (1), 406-419.

Squyres, S.W., Grotzinger, J.P., Arvidson, R.E., Bell, J.F., Calvin, W., Christensen, P.R., Clark, B.C., Crisp, J.A., Farrand, W.H., Herkenhoff, K.E., Johnson, J.R., Klingelhofer, G., Knoll, A.H., McLennan, S.M., McSween, H.Y., Morris, R.V., Rice, J.W., Rieder, R., and Soderblom, L.A. (2004) In situ evidence for an ancient aqueous environment at Meridiani Planum, Mars. Science, 306 (5702), 1709-1714.

Squyres, S.W., and Knoll, A.H. (2005) Sedimentary rocks at Meridiani Planum: Origin, diagetiesis, and implications for life on Mars. Earth and Planetary Science Letters, 240 (1), 1-10.

Stetter, K.O. (1996) Hyperthermophiles in the History of Life. In: J.A. Goode, G.R. Bock, and E. Symposium on Evolution of Hydrothermal Ecosystems on (Eds.), Evolution of hydrothermal ecosystems on Earth (and Mars?). Wiley, Chichester ; New York, pp. 1-10.

Stewart, J.H., Poole, F.G., and Wilson, R.F. (1972) Stratigraphy and origin of the Triassic Moenkopi Formation and related strata in the Colorado Plateau region, with a section on sedimentary petrology.

Swayze, G.A., Smith, K.S., Clark, R.N., Sutley, S.J., Pearson, R.M., Vance, J.S., Hageman, P.L., Briggs, P.H., Meier, A.L., Singleton, M.J., and Roth, S. (2000) Using imaging spectroscopy to map acidic mine waste. Environmental Science & Technology, 34 (1), 47-54.

Swayze, G.A., Desborough, K.S., Smith, K.S., Lowers, H.A., Hammarstrom, J.M., Diehl, S.F., Leinz, R.W., and Driscoll, R.L. (2008) Understanding jarosite -- from mine waste to Mars. Understanding Contaminants. U.S. Geological Survey Circular 1328, 8-13 pp.

Takenouchi, S., and Kennedy, G.C. (1964) Binary system H_2O-CO_2 at high temperatures + pressures. American Journal of Science, 262 (9), 1055-&.

Takenouchi, S., and Kennedy, G.C. (1965) Solubility of carbon dioxide in naci solutions at high temperatures and pressures. American Journal of Science, 263 (5), 445-&.

Tokunaga, T.K. (2012) DLVO-based estimates of adsorbed water film thicknesses in geologic CO_2 reservoirs. Langmuir, 28 (21), 8001-8009.

Tosca, N.J., Knoll, A.H., and McLennan, S.M. (2008) Water activity and the challenge for life on early Mars. Science, 320 (5880), 1204-1207.

Tosca, N.J., and McLennan, S.M. (2009) Experimental constraints on the evaporation of partially oxidized acid-sulfate waters at the Martian surface. Geochimica Et Cosmochimica Acta, 73 (4), 1205-1222.

Totten, M.W., Dixon, M., and Hanan, M.A. (2005) Diagenesis of mixed-layer clay minerals in the South Timbalier area, Gulf of Mexico. Gulf Coast Association of Geological Societies Transactions, 55, 821-829.

UNEP (2013) Environmental risks and challenges of anthropogenic metals flows and cycles, a report of the working group on the global metal flows to the international resource panel.

Vandenberghe, R.E., De Grave, E., and de Bakker, P.M.A. (1994) On the methodology of the analysis of Mössbauer spectra. Hyperfine Interactions, 83 (1), 29-49.

Vaniman, D.T., Bish, D.L., Chipera, S.J., Fialips, C.I., Carey, J.W., and Feldman, W.C. (2004) Magnesium sulphate salts and the history of water on Mars. Nature, 431 (7009), 663-665.

Vaniman, D.T., and Chipera, S.J. (2006) Transformations of Mg- and Ca-sulfate hydrates in Mars regolith. American Mineralogist, 91 (10), 1628-1642.

Vaniman, D.T., Bish, D.L., Ming, D.W., Bristow, T.F., Morris, R.V., Blake, D.F., Chipera, S.J., Morrison, S.M., Treiman, A.H., Rampe, E.B., Rice, M., Achilles, C.N., Grotzinger, J.P., McLennan, S.M., Williams, J., Bell, J.F., Newsom, H.E., Downs, R.T., Maurice, S., Sarrazin, P., Yen, A.S., Morookian, J.M., Farmer, J.D., Stack, K., Milliken, R.E., Ehlmann, B.L., Sumner, D.Y., Berger, G., Crisp, J.A., Hurowitz, J.A., Anderson, R., Des Marais, D.J., Stolper, E.M., Edgett, K.S., Gupta, S., Spanovich, N., and Team, M.S.L.S. (2014) Mineralogy of a Mudstone at Yellowknife Bay, Gale Crater, Mars. Science, 343 (6169).

Walker, T.R., Larson, E.E., and Hoblitt, R.P. (1981) Nature and origin of hematite in the Moenkopi formation (triassic), Colorado Plateau - a contribution to the origin of magnetism in red beds. Journal of Geophysical Research, 86 (NB1), 317-333.

Wang, A., Freeman, J.J., Jolliff, B.L., and Chou, I.M. (2006a) Sulfates on Mars: A systematic Raman spectroscopic study of hydration states of magnesium sulfates. Geochimica Et Cosmochimica Acta, 70 (24), 6118-6135.

Wang, A., Haskin, L.A., Squyres, S.W., Jolliff, B.L., Crumpler, L., Gellert, R., Schroder, C., Herkenhoff, K., Hurowitz, J., Tosca, N.J., Farrand, W.H., Anderson, R., and Knudson, A.T. (2006b) Sulfate deposition in subsurface regolith in Gusev crater, Mars. Journal of Geophysical Research-Planets, 111 (E2).

Wang, A., Freeman, J.J., and Jolliff, B.L. (2009) Phase transition pathways of the hydrates of magnesium sulfate in the temperature range 50 degrees C to 5 degrees C: Implication for sulfates on Mars. Journal of Geophysical Research-Planets, 114.

Wang, A., Freeman, J.J., Chou, I.M., and Jolliff, B.L. (2011a) Stability of Mg-sulfates at-10 degrees C and the rates of dehydration/rehydration processes under conditions relevant to Mars. Journal of Geophysical Research-Planets, 116.

Wang, A., and Ling, Z.C. (2011b) Ferric sulfates on Mars: A combined mission data analysis of salty soils at Gusev crater and laboratory experimental investigations. Journal of Geophysical Research-Planets, 116.

Wang, A.A., Ling, Z.C., Freeman, J.J., and Kong, W.G. (2012) Stability field and phase transition pathways of hydrous ferric sulfates in the temperature range 50 degrees C to 5 degrees C: Implication for martian ferric sulfates. Icarus, 218 (1), 622-643.

Wang, A., Feldman, W.C., Mellon, M.T., and Zheng, M.P. (2013) The preservation of subsurface sulfates with mid-to-high degree of hydration in equatorial regions on Mars. Icarus, 226 (1), 980-991.

Wang, A.A., and Zhou, Y.H. (2014) Experimental comparison of the pathways and rates of the dehydration of Al-, Fe-, Mg- and Ca-sulfates under Mars relevant conditions. Icarus, 234, 162-173.

Ward, N.J., Sullivan, L.A., Fyfe, D.M., Bush, R.T., and Ferguson, A.J.P. (2004) The process of sulfide oxidation in some acid sulfate soil materials. Australian Journal of Soil Research, 42 (4), 449-458.

Weber, J.L., Francis, B.P., Harris, P.M., and Clark, M. (2003) Stratigraphy, lithofacies and reservoir distribution, Tengiz field, Kazakhstan. In: W.M. Ahr, P.M. Harris, W.A. Morgan, and I.D. Sommerville (Eds.), Permo-Carboniferous carbonate platform and reefs: SEPM Special Publication 78 and AAPG Memoir 83, pp. 351-394.

Weitz, C.M., Dobrea, E.Z.N., Lane, M.D., and Knudson, A.T. (2012) Geologic relationships between gray hematite, sulfates, and clays in Capri Chasma. Journal of Geophysical Research-Planets, 117.

Wendt, L., Gross, C., Kneissl, T., Sowe, M., Combe, J.-P., LeDeit, L., McGuire, P.C., and Neukum, G. (2011) Sulfates and iron oxides in Ophir Chasma, Mars, based on OMEGA and CRISM observations. Icarus, 213 (1), 86-103.

White, C.M., Smith, D.H., Jones, K.L., Goodman, A.L., Jikich, S.A., LaCount, R.B., DuBose, S.B., Ozdemir, E., Morsi, B.I., and Schroeder, K.T. (2005) Sequestration of carbon dioxide in coal with enhanced coalbed methane recovery - A review. Energy & Fuels, 19 (3), 659-724.

Wilcox, B.B., Lucey, P.G., and Hawke, B.R. (2006) Radiative transfer modeling of compositions of lunar pyroclastic deposits. Journal of Geophysical Research-Planets, 111 (E9).

Wilson, E.J., Johnson, T.L., and Keith, D.W. (2003) Regulating the ultimate sink: Managing the risks of geologic CO_2 storage. Environmental Science & Technology, 37 (16), 3476-3483.

Wiseman, S.M., Arvidson, R.E., Morris, R.V., Poulet, F., Andrews-Hanna, J.C., Bishop, J.L., Murchie, S.L., Seelos, F.P., Des Marais, D., and Griffes, J.L. (2010) Spectral and stratigraphic mapping of hydrated sulfate and phyllosilicate-bearing deposits in northern Sinus Meridiani, Mars. Journal of Geophysical Research-Planets, 115.

Wray, J.J., Milliken, R.E., Dundas, C.M., Swayze, G.A., Andrews-Hanna, J.C., Baldridge, A.M., Chojnacki, M., Bishop, J.L., Ehlmann, B.L., Murchie, S.L., Clark, R.N., Seelos, F.P., Tornabene, L.L., and Squyres, S.W. (2011) Columbus crater and other possible groundwater-fed paleolakes of Terra Sirenum, Mars. Journal of Geophysical Research-Planets, 116.

Xu, T., Apps, J.A., Pruess, K., and Yamamoto, H. (2007) Numerical modeling of injection and mineral trapping Of CO_2 with H_2S and SO_2 in a sandstone formation. Chemical Geology, 242 (3-4), 319-346.

Xu, W.Q., Tosca, N.J., McLennan, S.M., and Parise, J.B. (2009) Humidity-induced phase transitions of ferric sulfate minerals studied by in situ and ex situ X-ray diffraction. American Mineralogist, 94 (11-12), 1629-1637.

Xu, W., and Parise, J.B. (2012) Temperature and humidity effects on ferric sulfate stability and phase transformation. American Mineralogist, 97 (2-3), 378-383.

Younger, P.L. (2002) Coalfield closure and the water environment in Europe. Transactions of the Institution of Mining and Metallurgy Section a-Mining Technology, 111, A201-A209.

Zahrai, S.K., Madden, M.E.E., Madden, A.S., and Rimstidt, J.D. (2013) Na-jarosite dissolution rates: The effect of mineral composition on jarosite lifetimes. Icarus, 223 (1), 438-443.

Zhang, W., Xu, T., and Li, Y. (2011) Modeling of fate and transport of coinjection of H2S with CO_2 in deep saline formations. Journal of Geophysical Research-Solid Earth, 116.

Zhou, Y., and Wang, A. (2013) A comparison of dehydration processes of Al-, Fe^{2+}-, & Mg-sulfates under mars relevant pressures and three temperatures. Abstracts of Papers submitted to the Lunar and Planetary Science Conference XXXXIV (1797).

Appendix A

Matlab Computer program used for the determination of optical constants

Outline of Program Structure

The program is run from the file MASTERPROGRAM_PP.m

- Indicates the programs that are called.

Section 1: Data import – UV data is approximated and added

Section 2: Small grain size initial k - lookup table program

- MasterHapke1_PP.m

Section 3: Medium grain size initial k - lookup table program

- MasterHapke1_PP.m

Section 4: Large grain size initial k - lookup table program

- MasterHapke1_PP.m

Section 5: Data check – choose wavelength range

Section 6: First iterative minimization: determine k_1

- MasterHapke2_PP.m
    - MASTERWRAPPER_PP.m

- MasterHapke3_PP.m

Section 7: k_1 input parameter evaluation (not required)

- HapkeEval1_PP.m

Section 8: k_1 output parameter evaluation

- HapkeEval2_PP.m
    - HapkeEval3_PP.m
        - MasterHapke3_PP.m

Section 9: First k combination: k_1 + MIR dispersion k (MIR dispersion k determined separately)

- MasterKcombine.m

Section 10: First Kramers-Kronig transformation: determine n_1

- MasterSSKK.m

Section 11: First phase function minimization: determine $P(g)_1$

- MasterPhase1_PP.m
    - MasterPhaseWrapper.m
        - MasterPhase2_PP.m

Section 12: $P(g)_1$ output evaluation

- MasterPhaseEval1_PP.m
    - MasterPhaseWrapper.m
        - MasterPhase2_PP.m

Section 13: Second iterative minimization: determine k_2

- MasterHapke4_PP.m
    - MASTERWRAPPER2_PP.m
        - MasterHapke5_PP.m

Section 14: k_2 input parameter evaluation (not required)

- HapkeEval4_PP.m

Section 15: k_2 output parameter evaluation

- HapkeEval5_PP.m
    - HapkeEval6_PP.m
        - MasterHapke5_PP.m

Section 16: Second k combination: k_2 + MIR dispersion k

- MasterKcombine.m

Section 17: Second Kramers-Kronig transformation: determine n_2

- MasterSSKK.m

Section 18: Second phase function minimization: determine $P(g)_2$

- MasterPhase1_PP.m
    - MasterPhaseWrapper.m
        - MasterPhase2_PP.m

Section 19: $P(g)_2$ output evaluation

- MasterPhaseEval1_PP.m
    - MasterPhaseWrapper.m
        - MasterPhase2_PP.m

Section 20: Third iterative minimization: determine k_3

- MasterHapke4_PP.m
    - MASTERWRAPPER2_PP.m
        - MasterHapke5_PP.m

Section 21: k_3 input parameter evaluation (not required)

- HapkeEval4_PP.m

Section 22: k_3 output parameter evaluation

- HapkeEval5_PP.m
    - HapkeEval6_PP.m
        - MasterHapke5_PP.m

Section 23: Third k combination: k_3 + MIR dispersion k

- MasterKcombine.m

Section 24: Third Kramers-Kronig transformation: determine n_3

- MasterSSKK.m

Section 25: Third phase function minimization: determine $P(g)_3$

- MasterPhase1_PP.m
    - MasterPhaseWrapper.m
        - MasterPhase2_PP.m

Section 26: $P(g)_3$ output evaluation

- MasterPhaseEval1_PP.m
    - MasterPhaseWrapper.m
        - MasterPhase2_PP.m

Section 27: Fourth iterative minimization: determine k_4

- MasterHapke4_PP.m
    - MASTERWRAPPER2_PP.m
        - MasterHapke5_PP.m

Section 28: k_4 input parameter evaluation (not required)

- HapkeEval4_PP.m

Section 29: k_4 output parameter evaluation

- HapkeEval5_PP.m
    - HapkeEval6_PP.m
        - MasterHapke5_PP.m

Section 30: Fourth k combination: k_4 + MIR dispersion k

- MasterKcombine.m

Section 31: Fourth Kramers-Kronig transformation: determine n_4

- MasterSSKK.m

Section 32: Check Results

Section 33: Instructions on how to extend analysis

A permalink to current versions of these and other programs can be found at: http://aram.ess.sunysb.edu/tools.html.

MASTERPROGRAM_PP.m

```
%************************************************************************
%************************MASTER PROGRAM**********************************
%************************************************************************
%This file allows you to define starting values, name input and output
%files, and either run by section or run and advance
%*************************important information**************************
%************************************************************************
%This program runs a Hapke radiative transfer model to derive optical
%constants n and k from reflectance data. This version of the program
%assumes that you have used a calibrated spectralon standard
% IF YOU HAVE NOT USED A CALIBRATED SPECTRALON STANDARD
% YOU MUST USE A DIFFERENT VERSION OF THE PROGRAM
% IF YOU HAVE USED A CALIBRATED SPECTRALON STANDARD
% MAKE SURE THAT THE FILES calspec2.mat and specwave2.mat
% ARE DOWNLOADED WITH THE PROGRAM AND IN YOUR WORKING DIRECTORY
%*****************************Let's Begin*********************************
%moves to correct directory (programs and data must be in this directory)
%cd Desktop/ASD/sulfates/data/MASTERPROGRAM;
%define FILE NAMES for your three grain sizes (VNIR spectral names)
%data should be 2 column (wavelength, data) with no header. Can be in nm or
%microns but not wavenumbers.
   loadfile1=('kjs.mat');%small grain size
   loadfile2=('kjm.mat');%medium grain size
   loadfile3=('kjb.mat');%large grain size
%Define your useable range (in microns) - if you have bad data in the file,
%it will make the slope and intercept calculations wonky
%LOW MUST BE AT LEAST ONE POINT IN FROM END OF DATA
   low=0.405;
   high=2.451;
%Define angles
   thetai=-30;%incident
   thetae=0;%emission
%Define average n (usually at sodium D line)
   n1=(1.714+1.8175)/2;
%Define opposition surge (can be set to zero if |thetai-thetae|>15)
   Bg=0;
%Define extinction efficiency (set to 1 for closely spaced particles)
   QE=1;
%************************************************************************
%*******NEED TO EXTEND DATA INTO UV FOR ACCURATE KRAMERS KRONIG***********
%************************************************************************
%if you have knowledge of the UV behavior of your sample, change code to
%cat in data - sorry folks, this part can't be fool proofed but some short
%cuts are provided below ---------------------------------------
%************************************************************************
%***********DATA LINEAR INTO UV AT VALUE OF ENDPOINT*********************
%************************************************************************
%Define UV wavelength point for extrapolation We really only need about 10
%points but more is always better
   UV=0.301;
%<<<<<<<<<<<<<<<<<<<<HIT THE RUN SECTION BUTTON>>>>>>>>>>>>>>>>>>>>>>>>>>
%-------------------CHANGE WITH CARE BELOW LINE----------------------------
% add a %{ here if you are not using a straight endpoint extrapolation
```

```
   sml=importdata(loadfile1);
   med=importdata(loadfile2);
   big=importdata(loadfile3);
   lambda=sml(:,1);
%make sure wavelength is in microns
   if lambda(1,1)>100
      lambda=lambda./1000;
   end
   sml=sml(:,2);
   med=med(:,2);
   big=big(:,2);
   lamdiff=lambda(2)-lambda(1);
   ind1=find(abs(lambda-low)<=eps);
   ind2=find(abs(lambda-high)<=eps);
%extract useable data
   sml=sml(ind1:ind2);
   med=med(ind1:ind2);
   big=big(ind1:ind2);
%Wavelength range must go one point farther than data to make up for
%loss in slope and icept calculations
   wavelength=lambda(ind1:ind2);
%extrapolate left side of k to 0.2 using Ahrekiel's constant method
%Cloutis 2008b shows that jarsotie is essentially flat from 200-400nm
   leftw=[UV:lamdiff:wavelength(1)];
   head=length(leftw);
   leftds=linspace(sml(1),sml(1),head); %these are now going to overlap by 1
   leftdm=linspace(med(1),med(1),head); %these are now going to overlap by 1
   leftdb=linspace(big(1),big(1),head); %these are now going to overlap by 1
%change orientation of arrays to match wavelength and k arrays
   leftw=leftw';
   leftds=leftds';
   leftdm=leftdm';
   leftdb=leftdb';
%now can the head pieces to the wavelength and data arrays
   wavelength=cat(1,leftw,wavelength(2:end));
   sml=cat(1,leftds,sml(2:end));
   med=cat(1,leftdm,med(2:end));
   big=cat(1,leftdb,big(2:end));
%visualize data to make sure it didn't get all mucked up
   figure(1)
   plot(wavelength,sml,wavelength,med+.1,wavelength,big+0.2)
   xlim([UV high])
   xlabel('Wavelength (um)')
   ylabel('Reflectance (%)')
   legend('sml','med','big','location','south')
   figure(1)
   smllong=cat(2,wavelength,sml);
   medlong=cat(2,wavelength,med);
   biglong=cat(2,wavelength,big);
   save('kjsmllong.mat','smllong');
   save('kjmedlong.mat','medlong');
   save('kjbiglong.mat','biglong');
   smldat='kjsmllong.mat';
   meddat='kjmedlong.mat';
   bigdat='kjbiglong.mat';
   save('variables.mat','lamdiff','smldat','meddat','bigdat','low','high',...
         'UV','thetai','thetae','Bg','QE','n1')
```

```
%}
%HERE IS SOME CODE FOR FUNCTION FITTING IF YOU HAVE A NON_LINEAR END
%REPLACES FROM-------------------------------------------------------
% The %{ at the top and %} at the bottom comment out the section
%{
   sml=importdata(loadfile1);
   med=importdata(loadfile2);
   big=importdata(loadfile3);
   lambda=sml(:,1);
%make sure wavelength is in microns
   if lambda(1,1)>100
      lambda=lambda./1000;
   end
   sml=sml(:,2);
   med=med(:,2);
   big=big(:,2);
   lamdiff=lambda(2)-lambda(1);
   ind1=find(abs(lambda-low)<=eps);
   ind2=find(abs(lambda-high)<=eps);
%extract useable data
   sml=sml(ind1:ind2);
   med=med(ind1:ind2);
   big=big(ind1:ind2);
%Wavelength range must go one point farther than data to make up for
%loss in slope and icept calculations
   wavelength=lambda(ind1:ind2);
%extrapolate left side of k to 0.2 using ahrekiel's constant method
%Cloutis 2008b shows that jarsotie is essentially flat from 200-400nm
   leftw=[UV:lamdiff:wavelength(1)];%row
   leftw=leftw';%column
   head=length(leftw);
%now extend wavelength
   longwave=cat(1,leftw,wavelength(2:end));
%fit the end of the data
%%REQUIRES DIFFERENT FUCNTION SOMETIMES, TRY 'poly3' and 'poly4'
%'linearinterp' works better than 'poly1'
%type help curvefit or doc fit to bring up more info
%define end of curve to fit (must be column vectors)
%upper end of fittable range or feature
   sp=1;
%change ep to end of useable feature (index not wavelength)
   ep=sp+100;
   shortlam=wavelength(sp:ep);
   features=sml(sp:ep);
   featurem=med(sp:ep);
   featureb=big(sp:ep);
%fit curve
   fs=fit(shortlam,features,'poly3');
   fm=fit(shortlam,featurem,'poly3');
   fb=fit(shortlam,featureb,'poly3');
%extract fit coefficients
   fcoefs=coeffvalues(fs);
   fcoefm=coeffvalues(fm);
   fcoefb=coeffvalues(fb);
%evaluate the function over the new range
   UVdatas=feval(fs,leftw);
   UVdatam=feval(fm,leftw);
```

```
   UVdatab=feval(fb,leftw);
%plot it to see how we did
   figure(1)
   plot(shortlam,features,leftw,UVdatas,shortlam,features+0.1,leftw,...
         UVdatam+0.1,shortlam,featureb+0.2,leftw,UVdatab+0.2)
   legend('sml data','sml fit','med data','med fit','big data','big fit')
   figure(1)
%now can the head pieces to the wavelength and data arrays
   wavelength=cat(1,leftw,wavelength(2:end));
   sml=cat(1,UVdatas,sml(2:end));
   med=cat(1,UVdatam,med(2:end));
   big=cat(1,UVdatab,big(2:end));
%save new data
   smllong=cat(2,wavelength,sml);
   medlong=cat(2,wavelength,med);
   biglong=cat(2,wavelength,big);
   save('smllong.mat','smllong');
   save('medlong.mat','medlong');
   save('biglong.mat','biglong');
   smldat='smllong.mat';
   meddat='medlong.mat';
   bigdat='biglong.mat';
   save('variables.mat','lamdiff','smldat','meddat','bigdat','low','high',...
         'UV','thetai','thetae','Bg','QE','n1')
%}
%--------------------------------------------------------------------------
%##############################---SECTION TWO---##############################
   clear
%INITIAL GUESSES (program will iteratively extract found values)
%SMALL
%grainsize
   D1=45;
%phase function coefficients for Legendre Polynomial (-1.7<b<1.7, -1<c<2)
%the above is a theoretical range. This program works better if b>-0.5,
%c>-0.1 but since this just provides a guess k for minimization, the
%values are not that important
   b1=0.1;
   c1=0.3;
%internal scattering parameter (initially set to zero)
   s1=0;
%define filling factor (ff). If you cannot define it, set it to
%0.00000000000000001 but according to Hapke 2008, absence of a good estimate
%this term can result in k being off by as much as a factor of 2
   ff=0.46;
%calculate the porosity constant for equant particles (K in Hapke 2008)
   PoreK1=(-log(1-1.209*ff^(2/3)))/(1.209*ff^(2/3));
% define SAVE FILE NAMES
   output='kjs_ppout';
   fig1='kjs_ppfig1';
   fig2='kjs_ppfig2';
   fig3='kjs_ppfig3';
   fig4='kjs_ppfig4';
   fig5='kjs_ppfig5';
   fig6='kjs_ppfig6';
   fig7='kjs_ppfig7';
%<<<<<<<<<<<<<<<<<<<<<<<now run this section>>>>>>>>>>>>>>>>>>>>>>>>>
%DO NOT CHANGE BETWEEN LINES
```

```
%-------------------------------------------------------------------------
   load('variables.mat','lamdiff','smldat','low','high','UV'...
         ,'thetai','thetae','Bg','QE','n1')
   data=smldat;
   kname='smlk.mat';
   D=D1;
   b=b1;
   c=c1;
   s=s1;%INITIAL GUESSES (program will iteratively extract found values)
   PoreK=PoreK1;
%save variables
   save('variables.mat','-append','D1','b1','c1','s1','PoreK1')
%CALL PROGRAM
%the most common error should involve k values larger than range of
%table. To fix this, go to line 76 of MasterHapke1. If you increase max
%k in table, decrease spacing or else MATLAB will be cranky
   run MasterHapke1_PP.m
%-------------------------------------------------------------------------
%############################---SECTION THREE--##############################
   clear
%MEDIUM
%grainsize
   D2=63;
%phase function coefficients for Legendre Polynomial (-1.7<b<1.7, -1<c<2)
   b2=0.1;
   c2=0.3;
%internal scattering parameter (initially set to zero)
   s2=0;
%define filling factor (ff). If you cannot define it, set it to
%0.00000000000000001 but according to Hapke 2008, absence of a good estimate
%this term can result in k being off by as much as a factor of 2
   ff=0.46;
%calculate the porosity constant for equant particles (K in Hapke 2008)
   PoreK2=(-log(1-1.209*ff^(2/3)))/(1.209*ff^(2/3));
% define SAVE FILE NAMES
   output='kjm_ppout';
   fig1='kjm_ppfig1';
   fig2='kjm_ppfig2';
   fig3='kjm_ppfig3';
   fig4='kjm_ppfig4';
   fig5='kjm_ppfig5';
   fig6='kjm_ppfig6';
   fig7='kjm_ppfig7';
%<<<<<<<<<<<<<<<<<<<<<<now run this section>>>>>>>>>>>>>>>>>>>>>>>>>
%DO NOT CHANGE THIS SECTION
%-------------------------------------------------------------------------
   load('variables.mat','lamdiff','meddat','low','high','UV'...
         ,'thetai','thetae','Bg','QE','n1')
   data=meddat;
   kname='medk.mat';
   D=D2;
   b=b2;
   c=c2;
   s=s2;
   PoreK=PoreK2;
%save variables
   save('variables.mat','-append','D2','b2','c2','s2','PoreK2')
```

```
%CALL PROGRAM
%the most common error should involve k values larger than range of
%table. To fix this, go to line 76 of MasterHapke1. If you increase max
%k in table, decrease spacing or else MATLAB will be cranky
   run MasterHapke1_PP.m
%-------------------------------------------------------------------------
%############################---SECTION FOUR---############################
   clear
%LARGE
%grainsize
   D3=90;
%phase function coefficients for Legendre Polynomial (-1.7<b<1.7, -1<c<2)
   b3=-0.1;
   c3=0.3;
%internal scattering parameter (initially set to zero)
   s3=0;
%define filling factor (ff). If you cannot define it, set it to
%0.00000000000000001 but according to Hapke 2008, absence of a good estimate
%this term can result in k being off by as much as a factor of 2
   ff=0.46;
%calculate the porosity constant for equant particles (K in Hapke 2008)
   PoreK3=(-log(1-1.209*ff^(2/3)))/(1.209*ff^(2/3));
% define SAVE FILE NAMES
   output='kjb_ppout';
   fig1='kjb_ppfig1';
   fig2='kjb_ppfig2';
   fig3='kjb_ppfig3';
   fig4='kjb_ppfig4';
   fig5='kjb_ppfig5';
   fig6='kjb_ppfig6';
   fig7='kjb_ppfig7';
%<<<<<<<<<<<<<<<<<<<<<<now run this section>>>>>>>>>>>>>>>>>>>>>>>>>
%DO NOT CHANGE THIS SECTION
%-------------------------------------------------------------------------
   load('variables.mat','lamdiff','bigdat','low','high','UV'...
         ,'thetai','thetae','Bg','QE','n1')
   data=bigdat;
   kname='bigk.mat';
   D=D3;
   b=b3;
   c=c3;
   s=s3;
   PoreK=PoreK3;
%save variables
   save('variables.mat','-append','D3','b3','c3','s3','PoreK3')
%CALL PROGRAM
%the most common error should involve k values larger than range of
%table. To fix this, go to line 76 of MasterHapke1. If you increase max
%k in table, decrease spacing or else MATLAB will be cranky
   run MasterHapke1_PP.m
%-------------------------------------------------------------------------
%############################---SECTION FIVE---############################
   clear
   close all
%plot data to let you choose useable range
%this is a good time to cut out noise
   load('variables.mat','smldat','meddat','bigdat');
```

```
   SML=importdata(smldat);
   MED=importdata(meddat);
   BIG=importdata(bigdat);
   plot(SML(:,1),SML(:,2),MED(:,1),MED(:,2),BIG(:,1),BIG(:,2))
   set(gca,'FontSize',16);
   xlabel('Wavelength');
   ylabel('Reflectance');
   legend('small grain','medium grain','large grain','location','south');
   hgsave('VNIR_data');
   clear('BIG','MED','SML')
%use ginput(1) in command line to get a cursor on the plot
%-------------------------------------------------------------------------
%############################---SECTION SIX---##############################
   clear
   close
%RUN FIRST ITERATIVE MINIMIZATION
   load('variables.mat','UV','high','n1','smldat','meddat','bigdat')
%This section takes a good long while to run (days)
%guess k (med k from initial runs)
   kstart='medk.mat';
%Define start and end points (in microns=nm/1000)
%if you cut the range above enough, let lstart=UV and lend=high-1
   lstart=UV;
   lend=high;
%define lower and upper bounds for parameters
%b
   lowb1=-1.7;
   lowb2=-1.7;
   lowb3=-1.7;
   upb1=1.7;
   upb2=1.7;
   upb3=1.7;
%c
   lowc1=-1;
   lowc2=-1;
   lowc3=-1;
   upc1=2;
   upc2=2;
   upc3=2;
%s (in microns; 0.06um-1=600cm-1; micron=10000/wavenumber)
   lows1=0;
   lows2=0;
   lows3=0;
   ups1=0.06;
   ups2=0.06;
   ups3=0.06;
%D (in microns) this is path length of light which can be as small
%as 1/3 grain size. Upper bound determined by sieve.
   lowD1=30/3;
   lowD2=63/3;
   lowD3=90/3;
   upD1=63;
   upD2=90;
   upD3=125;
%k (min k set to zero)
   upk=0.04;
%n
```

```
   n=n1;
%save required variables to be extracted by program
   save('variables.mat','-append','lstart','lend')
%DEFINE MINIMIZATION PARAMETERS
%Maximum function evaluations
   maxfun=1000000000000000; %search MaxFunEvals for more info
%Function Tolerance (smaller is closer match)
   funtol=0.000000000000001; %search FunTol for more info
   xtol=0.0000000000000000001; %search XTol for more info
%Maximum iterations
   maxit=2000;
%number of start points
   spts=10;
%Define savefile
   k1save=('071414kj_pp_k1.mat');
   save('variables','-append','k1save');
   ksave=k1save;
%run program
   run MasterHapke2_PP.m
   clear
%-------------------------------------------------------------------------
%############################---SECTION SEVEN---############################
%This section evaluates and graphs the INPUT guesses from the previous
section
%If you are not interested in this, you can skip to the next section
%All input information is saved in 'solutions' (in k1save file)
%This program also appends all guesses to k1save file in a more user
%friendly format
%WARNING: This program does not save plots, if you want to save the plots,
%do so manually. Also, this program only plots, at most, guesses for the best
8
%solutions and gives an error if there are fewer than 6 convergent start
%points
   load('variables.mat','k1save')
   ksave=k1save;
   run HapkeEval1_PP.m
%-------------------------------------------------------------------------
%############################---SECTION EIGHT---############################
   clear
   close all
%This section evaluates and graphs the OUTPUT guesses from the previous
section
%You MUST RUN this section for the program to continue
%This program also appends all outputs to k1save file in a more user
%friendly format
%WARNING: This program does not save plots, if you want to save the plots,
%do so manually. Also, this program only plots, at most, the best 8
%solutions and gives an error if there are fewer than 6 convergent start
%points
   load('variables.mat','k1save')
   ksave=k1save;
   run HapkeEval2_PP.m
%-------------------------------------------------------------------------
%############################---SECTION NINE---############################
   clear
   close all
%**********************TIME TO ADD IN YOUR MIR DATA************************
```

```
%If you do not have MIR data (which is not recommended), the next program
%will run and you can skip this step
%If you do have MIR data, use the DISPERSION programs on the website to get
%k data for your sample through the MIR
%filenames (currently requires k and wavenumbers to be in separate files)
   loadfile4=('kjar_110813_disp_k.mat');
   loadfile5=('kjar_110813_disp_v.mat');
%savefile names
   k1fullsave=('testk1disp.mat');
   kfullsave=k1fullsave;
   load('variables.mat','k1save');
   ksave=k1save;
   save('variables.mat','-append','k1fullsave')
%run the program
   run MasterKcombine.m
%------------------------------------------------------------------------
%############################---SECTION TEN---#############################
   clear
   close all
%This section determined the real index of refraction, n, from k, using a
%singly subtractive Kramers Kronig calculation. For this lamdiff, you will
%need MIR data of your sample and should obtain n and k for those data
%using a dispersion analysis (see other material).
%leave this line alone
   fullk=0;
%if you did not have dispersion data, add this line:
%load('variables.mat','k1save');fullk=k1save;
%Define savefile for used data
   n1save=('testn1.mat');
%define savefile for all data
   n1savelong=('testn1long.mat');
   load('variables.mat','k1fullsave');
   kfullsave=k1fullsave;
   nsave=n1save;
   nsave2=n1savelong;
   save('variables.mat','-append','n1save','n1savelong')
%Select anchor wavelength (this is usually sodium D line of 0.58929um)
%this is the wavelength at which n1 was determined
   anchor=0.58929;
%Run Program
   run MasterSSKK.m
%------------------------------------------------------------------------
%############################---SECTION ELEVEN---############################
   close all
   clear
%RUN PHASE FUNCTION PROGRAM
%again, there is no real good way to make this fool proof.
%If you use more or fewer phase angles, you will have to edit the code.
%It is set up for 7 phase angles from 15 to 45 degrees
%hopefully you will find it easy enough to expand
%ALSO this program EXTENDS DATA INTO UV AS in SECTION 1
%if you need to fit a curve, you will have to copy and paste that commented
%out code into MasterPhase1_PP for each wavelength. . . :(
%Import sample data - if your data is in a different form, edit here
%the program needs in15b etc to be arrays of just data, wavelength separate
%BIG
   in15b=importdata('smKJBi15e0b.mat');
```

```
   in20b=importdata('smKJBi20e0b.mat');
   in25b=importdata('smKJBi25e0b.mat');
   in30b=importdata('smKJBi30e0b.mat');
   in35b=importdata('smKJBi35e0b.mat');
   in40b=importdata('smKJBi40e0b.mat');
   in45b=importdata('smKJBi45e0b.mat');
%MED
   in15m=importdata('smKJMi15e0b.mat');
   in20m=importdata('smKJMi20e0b.mat');
   in25m=importdata('smKJMi25e0b.mat');
   in30m=importdata('smKJMi30e0b.mat');
   in35m=importdata('smKJMi35e0b.mat');
   in40m=importdata('smKJMi40e0b.mat');
   in45m=importdata('smKJMi45e0b.mat');
%SML
   in15s=importdata('smKJSi15e0b.mat');
   in20s=importdata('smKJSi20e0b.mat');
   in25s=importdata('smKJSi25e0b.mat');
   in30s=importdata('smKJSi30e0b.mat');
   in35s=importdata('smKJSi35e0b.mat');
   in40s=importdata('smKJSi40e0b.mat');
   in45s=importdata('smKJSi45e0b.mat');
%load the associated wavelength file
   wave=importdata('KJMwaveb.mat');
%assign save file name
   phase1save=('testp1.mat');
   save('variables.mat','-append','phase1save');
   phasesave=phase1save;
%upper bound for scaling k
   scale=10; %setting this number to 1 will keep the program from scaling k
%define lower and upper bounds for parameters
%b
   lowb=-1.7;
   upb=1.7;
%c
   lowc=-1;
   upc=2;
%s (in microns; 0.06um-1=600cm-1; micron=10000/wavenumber)
   lows1=0;
   lows2=0;
   lows3=0;
   ups1=0.06;
   ups2=0.06;
   ups3=0.06;
%D (in microns) this is path length of light which can be as small
%as 1/3 grain size. Upper bound determined by sieve.
   lowD1=30/3;
   lowD2=63/3;
   lowD3=90/3;
   upD1=63;
   upD2=90;
   upD3=125;
%Starting guesses
   bguess=-1.4;
   cguess=0.3;
%guess for D
   D1=75;
```

```
   D2=40;
   D3=30;
%guess for s
   s1=0.06;
   s2=0.04;
   s3=0.02;
%file names from the last iteration
   load('variables.mat','k1save','n1save')
   ksave=k1save;
   nsave=n1save;
%DEFINE MINIMIZATION PARAMETERS
%Maximum function evaluations
   maxfun=1000000000000000; %search MaxFunEvals for more info
%Function Tolerance (smaller is closer match)
   funtol=0.00000000000000000001; %search FunTol for more info
   xtol=0.00000000000000000001; %search XTol for more info
%Maximum iterations
   maxit=2000;
%number of start points
   spts=20;
%Run Program
   run MasterPhase1_PP
%-----------------------------------------------------------------------
%##########################---SECTION TWELVE---############################
%This section evaluates the results of the phase function program
%I often used the phase function program to test new minimization
%procedures since it runs quickly
   load('variables.mat','phase1save','n1save','k1save')
   phasesave=phase1save;
   nsave=n1save;
   ksave=k1save;
%run the program
   run MasterPhaseEval1_PP.m
%-----------------------------------------------------------------------
%##########################---SECTION THIRTEEN---############################
   clear
   close all
%RUN SECOND ITERATIVE MINIMIZATION
   load('variables.mat','UV','high','n1','smldat','meddat','bigdat',...
         'k1save','n1save','phase1save')
%This section takes a good long while to run (days)
%loadfiles leave alone
   phasesave=phase1save;
   nsave=n1save;
   ksave=k1save;
%define lower and upper bounds for parameters
%s (in microns; 0.06um-1=600cm-1; micron=10000/wavenumber)
   lows1=0;
   lows2=0;
   lows3=0;
   ups1=0.06;
   ups2=0.06;
   ups3=0.06;
%D (in microns) this is path length of light which can be as small
%as 1/3 grain size. Upper bound determined by sieve.
   lowD1=30/3;
   lowD2=63/3;
```

```
   lowD3=90/3;
   upD1=63;
   upD2=90;
   upD3=125;
%k (min k set to zero)
   upk=0.04;
%DEFINE MINIMIZATION PARAMETERS
%Maximum function evaluations
   maxfun=1000000000000000; %search MaxFunEvals for more info
%Function Tolerance (smaller is closer match)
   funtol=0.000000000000001; %search FunTol for more info
   xtol=0.0000000000000000001; %search XTol for more info
%Maximum iterations
   maxit=2000;
%number of start points
   spts=10;
%Define savefile - fill in - should have different name from above
   k2save=('testk2.mat');
   save('variables','-append','k2save');
   ksave2=k2save;
%run program
   run MasterHapke4_PP.m
%-------------------------------------------------------------------------
%#########################---SECTION FOURTEEN---############################
   clear
%This section evaluates and graphs the INPUT guesses from the previous
section
%If you are not interested in this, you can skip to the next section
%All input information is saved in 'solutions' (in k1save file)
%This program also appends all guesses to k1save file in a more user
%friendly format
%WARNING: This program does not save plots, if you want to save the plots,
%do so manually. Also, this program only plots, at most, guesses for the best
8
%solutions and gives an error if there are fewer than 6 convergent start
%points
   load('variables.mat','k2save')
   ksave=k2save;
   run HapkeEval4_PP.m
%-------------------------------------------------------------------------
%############################---SECTION FIFTEEN---############################
   clear
   close all
%This section evaluates and graphs the OUTPUT guesses from the previous
section
%You MUST RUN this section for the program to continue
%This program also appends all outputs to k1save file in a more user
%friendly format
%WARNING: This program does not save plots, if you want to save the plots,
%do so manually. Also, this program only plots, at most, the best 8
%solutions and gives an error if there are fewer than 6 convergent start
%points
   load('variables.mat','k2save')
   ksave=k2save;
   run HapkeEval5_PP.m
%-------------------------------------------------------------------------
%############################---SECTION SIXTEEN---############################
```

```
   clear
   close all
%**********************TIME TO ADD IN YOUR MIR DATA************************
%If you do not have MIR data (which is not recommended), the next program
%will run and you can skip this step
%If you do have MIR data, use the DISPERSION programs on the website to get
%k data for your sample through the MIR
%filenames (currently requires k and wavenumbers to be in separate files)
   loadfile4=('kjar_110813_disp_k.mat');
   loadfile5=('kjar_110813_disp_v.mat');
%savefile names
   k2fullsave=('testk2disp.mat');
   load('variables.mat','k2save');
   save('variables.mat','-append','k2fullsave')
   kfullsave=k2fullsave;
   ksave=k2save;
%run the program
   run MasterKcombine.m
%-------------------------------------------------------------------------
%##########################---SECTION SEVENTEEN---############################
   clear
   close all
%This section determined the real index of refraction, n, from k, using a
%singly subtractive Kramers Kronig calculation. For this lamdiff, you will
%need MIR data of your sample and should obtain n and k for those data
%using a dispersion analysis (see other material).
%leave this line alone
   fullk=0;
%if you did not have dispersion data, add this line:
%load('variables.mat','k1save');fullk=k1save;
%Define savefile for used data
   n2save=('testn2.mat');
%define savefile for all data
   n2savelong=('testn2long.mat');
   load('variables.mat','k2fullsave');
   kfullsave=k2fullsave;
   nsave=n2save;
   nsave2=n2savelong;
   save('variables.mat','-append','n2save','n2savelong')
%Select anchor wavelength (this is usually sodium D line of 0.58929um)
%this is the wavelength at which n1 was determined
   anchor=0.58929;
%Run Program
   run MasterSSKK.m
%-------------------------------------------------------------------------
%##########################---SECTION EIGHTEEN---############################
   close all
   clear
%RUN PHASE FUNCTION PROGRAM
%again, there is no real good way to make this fool proof.
%If you use more or fewer phase angles, you will have to edit the code.
%It is set up for 7 phase angles from 15 to 45 degrees
%hopefully you will find it easy enough to expand
%ALSO this program EXTENDS DATA INTO UV AS in SECTION 1
%if you need to fit a curve, you will have to copy and paste that commented
%out code into MasterPhase1_PP for each wavelength. . . :(
%Import sample data - if your data is in a different form, edit here
```

```
%the program needs in15b etc to be arrays of just data, wavelength separate
%BIG
   in15b=importdata('smKJBi15e0b.mat');
   in20b=importdata('smKJBi20e0b.mat');
   in25b=importdata('smKJBi25e0b.mat');
   in30b=importdata('smKJBi30e0b.mat');
   in35b=importdata('smKJBi35e0b.mat');
   in40b=importdata('smKJBi40e0b.mat');
   in45b=importdata('smKJBi45e0b.mat');
%MED
   in15m=importdata('smKJMi15e0b.mat');
   in20m=importdata('smKJMi20e0b.mat');
   in25m=importdata('smKJMi25e0b.mat');
   in30m=importdata('smKJMi30e0b.mat');
   in35m=importdata('smKJMi35e0b.mat');
   in40m=importdata('smKJMi40e0b.mat');
   in45m=importdata('smKJMi45e0b.mat');
%SML
   in15s=importdata('smKJSi15e0b.mat');
   in20s=importdata('smKJSi20e0b.mat');
   in25s=importdata('smKJSi25e0b.mat');
   in30s=importdata('smKJSi30e0b.mat');
   in35s=importdata('smKJSi35e0b.mat');
   in40s=importdata('smKJSi40e0b.mat');
   in45s=importdata('smKJSi45e0b.mat');
%load the associated wavelength file
   wave=importdata('KJMwaveb.mat');
%assign save file name
   phase2save=('testp2.mat');
   save('variables.mat','-append','phase2save');
   phasesave=phase2save;
%upper bound for scaling k
   scale=10; %setting this number to 1 will keep the program from scaling k
%define lower and upper bounds for parameters
%b
   lowb=-1.7;
   upb=1.7;
%c
   lowc=-1;
   upc=2;
%s (in microns; 0.06um-1=600cm-1; micron=10000/wavenumber)
   lows1=0;
   lows2=0;
   lows3=0;
   ups1=0.06;
   ups2=0.06;
   ups3=0.06;
%D (in microns) this is path length of light which can be as small
%as 1/3 grain size. Upper bound determined by sieve.
   lowD1=30/3;
   lowD2=63/3;
   lowD3=90/3;
   upD1=63;
   upD2=90;
   upD3=125;
%Starting guesses
   bguess=-1.4;
```

```
   cguess=0.3;
%guess for D
   D1=75;
   D2=40;
   D3=30;
%guess for s
   s1=0.06;
   s2=0.04;
   s3=0.02;
%file names from the last iteration
   load('variables.mat','k2save','n2save')
   ksave=k2save;
   nsave=n2save;
%DEFINE MINIMIZATION PARAMETERS
%Maximum function evaluations
   maxfun=1000000000000000; %search MaxFunEvals for more info
%Function Tolerance (smaller is closer match)
   funtol=0.00000000000000000001; %search FunTol for more info
   xtol=0.000000000000000000001; %search XTol for more info
%Maximum iterations
   maxit=2000;
%number of start points
   spts=20;
%Run Program
   run MasterPhase1_PP.m
%-------------------------------------------------------------------------
%#########################---SECTION NINETEEN---############################
%This section evaluates the results of the phase function program
%I often used the phase function program to test new minimization
%procedured since it runs quickly
   load('variables.mat','phase2save','n2save','k2save')
   phasesave=phase2save;
   nsave=n2save;
   ksave=k2save;
%run the program
   run MasterPhaseEval1_PP.m
%-------------------------------------------------------------------------
%#########################---SECTION TWENTY---############################
   clear
   close all
%RUN THIRD ITERATIVE MINIMIZATION
   load('variables.mat','UV','high','n1','smldat','meddat','bigdat',...
         'k2save','n2save','phase2save')
%This section takes a good long while to run (days)
%loadfiles, leave alone
   phasesave=phase2save;
   nsave=n2save;
   ksave=k2save;
%define lower and upper bounds for parameters
%s (in microns; 0.06um-1=600cm-1; micron=10000/wavenumber)
   lows1=0;
   lows2=0;
   lows3=0;
   ups1=0.06;
   ups2=0.06;
   ups3=0.06;
%D (in microns) this is path length of light which can be as small
```

```
%as 1/3 grain size. Upper bound determined by sieve.
   lowD1=30/3;
   lowD2=63/3;
   lowD3=90/3;
   upD1=63;
   upD2=90;
   upD3=125;
%k (min k set to zero)
   upk=0.04;
%DEFINE MINIMIZATION PARAMETERS
%Maximum function evaluations
   maxfun=1000000000000000; %search MaxFunEvals for more info
%Function Tolerance (smaller is closer match)
   funtol=0.000000000000001; %search FunTol for more info
   xtol=0.0000000000000000001; %search XTol for more info
%Maximum iterations
   maxit=2000;
%number of start points
   spts=10;
%Define savefile - should be different from above
   k3save=('testk3.mat');
   save('variables','-append','k3save');
   ksave2=k3save;
%run program
   run MasterHapke4_PP.m
%-------------------------------------------------------------------------
%##########################---SECTION TWENTYONE---##########################
   clear
%This section evaluates and graphs the INPUT guesses from the previous
section
%If you are not interested in this, you can skip to the next section
%All input information is saved in 'solutions' (in k1save file)
%This program also appends all guesses to k1save file in a more user
%friendly format
%WARNING: This program does not save plots, if you want to save the plots,
%do so manually. Also, this program only plots, at most, guesses for the best
8
%solutions and gives an error if there are fewer than 6 convergent start
%points
   load('variables.mat','k3save')
   ksave=k3save;
   run HapkeEval4_PP.m
%-------------------------------------------------------------------------
%##########################---SECTION TWENTYTWO---##########################
   clear
   close all
%This section evaluates and graphs the OUTPUT guesses from the previous
section
%You MUST RUN this section for the program to continue
%This program also appends all outputs to k1save file in a more user
%friendly format
%WARNING: This program does not save plots, if you want to save the plots,
%do so manually. Also, this program only plots, at most, the best 8
%solutions and gives an error if there are fewer than 6 convergent start
%points
   load('variables.mat','k3save')
   ksave=k3save;
```

```
   run HapkeEval5_PP.m
%-------------------------------------------------------------------------
%########################---SECTION TWENTYTHREE---#########################
   clear
   close all
%**********************TIME TO ADD IN YOUR MIR DATA************************
%If you do not have MIR data (which is not recommended), the next program
%will run and you can skip this step
%If you do have MIR data, use the DISPERSION programs on the website to get
%k data for your sample through the MIR
%filenames (currently requires k and wavenumbers to be in separate files)
   loadfile4=('kjar_110813_disp_k.mat');
   loadfile5=('kjar_110813_disp_v.mat');
%savefile names
   k3fullsave=('testk3disp.mat');
   load('variables.mat','k3save');
   save('variables.mat','-append','k3fullsave')
   kfullsave=k3fullsave;
   ksave=k3save;
%run the program
   run MasterKcombine.m
%-------------------------------------------------------------------------
%########################---SECTION TWENTYFOUR---##########################
   close all
%This section determined the real index of refraction, n, from k, using a
%singly subtractive Kramers Kronig calculation. For this lamdiff, you will
%need MIR data of your sample and should obtain n and k for those data
%using a dispersion analysis (see other material).
%leave this line alone
   fullk=0;
%if you did not have dispersion data, add this line:
%load('variables.mat','k1save');fullk=k1save;
%Define savefile for used data
   n3save=('testn3.mat');
%define savefile for all data
   n3savelong=('testn3long.mat');
   load('variables.mat','k3fullsave');
   kfullsave=k3fullsave;
   nsave=n3save;
   nsave2=n3savelong;
   save('variables.mat','-append','n3save','n3savelong')
%Select anchor wavelength (this is usually sodium D line of 0.58929um)
%this is the wavelength at which n1 was determined
   anchor=0.58929;
%Run Program
   run MasterSSKK.m
%-------------------------------------------------------------------------
%########################---SECTION TWENTYFIVE---##########################
   close all
   clear
%RUN PHASE FUNCTION PROGRAM
%again, there is no real good way to make this fool proof.
%If you use more or fewer phase angles, you will have to edit the code.
%It is set up for 7 phase angles from 15 to 45 degrees
%hopefully you will find it easy enough to expand
%ALSO this program EXTENDS DATA INTO UV AS in SECTION 1
%if you need to fit a curve, you will have to copy and paste that commented
```

```
%out code into MasterPhase1_PP for each wavelength. . . :(
%Import sample data - if your data is in a different form, edit here
%the program needs in15b etc to be arrays of just data, wavelength separate
%BIG
   in15b=importdata('smKJBi15e0b.mat');
   in20b=importdata('smKJBi20e0b.mat');
   in25b=importdata('smKJBi25e0b.mat');
   in30b=importdata('smKJBi30e0b.mat');
   in35b=importdata('smKJBi35e0b.mat');
   in40b=importdata('smKJBi40e0b.mat');
   in45b=importdata('smKJBi45e0b.mat');
%MED
   in15m=importdata('smKJMi15e0b.mat');
   in20m=importdata('smKJMi20e0b.mat');
   in25m=importdata('smKJMi25e0b.mat');
   in30m=importdata('smKJMi30e0b.mat');
   in35m=importdata('smKJMi35e0b.mat');
   in40m=importdata('smKJMi40e0b.mat');
   in45m=importdata('smKJMi45e0b.mat');
%SML
   in15s=importdata('smKJSi15e0b.mat');
   in20s=importdata('smKJSi20e0b.mat');
   in25s=importdata('smKJSi25e0b.mat');
   in30s=importdata('smKJSi30e0b.mat');
   in35s=importdata('smKJSi35e0b.mat');
   in40s=importdata('smKJSi40e0b.mat');
   in45s=importdata('smKJSi45e0b.mat');
%load the associated wavelength file
   wave=importdata('KJMwaveb.mat');
%assign save file name
   phase3save=('testp3.mat');
   save('variables.mat','-append','phase3save');
   phasesave=phase3save;
%upper bound for scaling k
   scale=10; %setting this number to 1 will keep the program from scaling k
%define lower and upper bounds for parameters
%b
   lowb=-1.7;
   upb=1.7;
%c
   lowc=-1;
   upc=2;
%s (in microns; 0.06um-1=600cm-1; micron=10000/wavenumber)
   lows1=0;
   lows2=0;
   lows3=0;
   ups1=0.06;
   ups2=0.06;
   ups3=0.06;
%D (in microns) this is path length of light which can be as small
%as 1/3 grain size. Upper bound determined by sieve.
   lowD1=30/3;
   lowD2=63/3;
   lowD3=90/3;
   upD1=63;
   upD2=90;
   upD3=125;
```

```
%Starting guesses
   bguess=-1.4;
   cguess=0.3;
%guess for D
   D1=75;
   D2=40;
   D3=30;
%guess for s
   s1=0.06;
   s2=0.04;
   s3=0.02;
%file names from the last iteration
   load('variables.mat','k3save','n3save')
   ksave=k3save;
   nsave=n3save;
%DEFINE MINIMIZATION PARAMETERS
%Maximum function evaluations
   maxfun=10000000000000000; %search MaxFunEvals for more info
%Function Tolerance (smaller is closer match)
   funtol=0.00000000000000000001; %search FunTol for more info
   xtol=0.00000000000000000001; %search XTol for more info
%Maximum iterations
   maxit=2000;
%number of start points
   spts=20;
%Run Program
   run MasterPhase1_PP.m
%-------------------------------------------------------------------------
%########################---SECTION TWENTYSIX---############################
%This section evaluates the results of the phase function program
%I often used the phase function program to test new minimization
%procedures since it runs quickly
   load('variables.mat','phase3save','n3save','k3save')
   phasesave=phase3save;
   nsave=n3save;
   ksave=k3save;
%run the program
   run MasterPhaseEval1_PP.m
%-------------------------------------------------------------------------
%########################---SECTION TWENTYSEVEN---##########################
   close all
%RUN FOURTH ITERATIVE MINIMIZATION
   load('variables.mat','UV','high','n1','smldat','meddat','bigdat',...
         'k3save','n3save','phase3save')
%This section takes a good long while to run (days)
%loadfiles - leave alone
   phasesave=phase3save;
   nsave=n3save;
   ksave=k3save;
%define lower and upper bounds for parameters
%s (in microns; 0.06um-1=600cm-1; micron=10000/wavenumber)
   lows1=0;
   lows2=0;
   lows3=0;
   ups1=0.06;
   ups2=0.06;
   ups3=0.06;
```

```
%D (in microns) this is path length of light which can be as small
%as 1/3 grain size. Upper bound determined by sieve.
   lowD1=30/3;
   lowD2=63/3;
   lowD3=90/3;
   upD1=63;
   upD2=90;
   upD3=125;
%k (min k set to zero)
   upk=0.04;
%DEFINE MINIMIZATION PARAMETERS
%Maximum function evaluations
   maxfun=1000000000000000; %search MaxFunEvals for more info
%Function Tolerance (smaller is closer match)
   funtol=0.000000000000001; %search FunTol for more info
   xtol=0.0000000000000000001; %search XTol for more info
%Maximum iterations
   maxit=2000;
%number of start points
   spts=10;
%Define savefile - should be different from above
   k4save=('testk4.mat');
   save('variables','-append','k4save');
   ksave2=k4save;
%run program
   run MasterHapke4_PP.m
%-------------------------------------------------------------------------
%##########################---SECTION TWENTYEIGHT---##########################
   clear
%This section evaluates and graphs the INPUT guesses from the previous
section
%If you are not interested in this, you can skip to the next section
%All input information is saved in 'solutions' (in k1save file)
%This program also appends all guesses to k1save file in a more user
%friendly format
%WARNING: This program does not save plots, if you want to save the plots,
%do so manually. Also, this program only plots, at most, guesses for the best
8
%solutions and gives an error if there are fewer than 6 convergent start
%points
   load('variables.mat','k4save')
   ksave=k4save;
   run HapkeEval4_PP.m
%-------------------------------------------------------------------------
%##########################---SECTION TWENTYNINE---##########################
   clear
   close all
%This section evaluates and graphs the OUTPUT guesses from the previous
section
%You MUST RUN this section for the program to continue
%This program also appends all outputs to k1save file in a more user
%friendly format
%WARNING: This program does not save plots, if you want to save the plots,
%do so manually. Also, this program only plots, at most, the best 8
%solutions and gives an error if there are fewer than 6 convergent start
%points
   load('variables.mat','k4save')
```

```
   ksave=k4save;
   run HapkeEval5_PP.m
%-------------------------------------------------------------------------
%############################---SECTION THIRTY---############################
   clear
   close all
%**********************TIME TO ADD IN YOUR MIR DATA************************
%If you do not have MIR data (which is not recommended), the next program
%will run and you can skip this step
%If you do have MIR data, use the DISPERSION programs on the website to get
%k data for your sample through the MIR
%filenames (currently requires k and wavenumbers to be in separate files)
   loadfile4=('kjar_110813_disp_k.mat');
   loadfile5=('kjar_110813_disp_v.mat');
%savefile names
   k3fullsave=('testk4disp.mat');
   load('variables.mat','k4save');
   save('variables.mat','-append','k4fullsave')
   kfullsave=k4fullsave;
   ksave=k4save;
%run the program
   run MasterKcombine.m
%-------------------------------------------------------------------------
%#########################---SECTION THIRTYONE---############################
   clear
   close all
%This section determined the real index of refraction, n, from k, using a
%singly subtractive Kramers Kronig calculation. For this lamdiff, you will
%need MIR data of your sample and should obtain n and k for those data
%using a dispersion analysis (see other material).
%leave this line alone
   fullk=0;
%if you did not have dispersion data, add this line:
%load('variables.mat','k1save');fullk=k1save;
%Define savefile for used data
   n4save=('testn4.mat');
%define savefile for all data
   n4savelong=('testn4long.mat');
   load('variables.mat','k4fullsave');
   kfullsave=k4fullsave;
   nsave=n4save;
   nsave2=n4savelong;
   save('variables.mat','-append','n4save','n4savelong')
%Select anchor wavelength (this is usually sodium D line of 0.58929um)
%this is the wavelength at which n1 was determined
   anchor=0.58929;
%Run Program
   run MasterSSKK.m
%-------------------------------------------------------------------------
%#########################---SECTION THIRTYTWO---##########################
%HERE IS A GOOD TIME TO SEE IF YOU HAVE CONVERGED
  load('variables.mat','n1save','n2save','n3save','k1save','k2save',...
      'k3save','ksize)
   n1=importdata(n1save);
   n1lam=n1.vislam;
   n1=n1.visn;
   n2=importdata(n2save);
```

```
    n2lam=n2.vislam;
    n2=n2.visn;
    n3=importdata(n3save);
    n3lam=n3.vislam;
    n3=n3.visn;
    n4=importdata(n4save);
    n4lam=n4.vislam;
    n4=n4.visn;
    k1=importdata(k1save);
    kwave1=k1.wavelength(1:ksize);
    k1=k1.Kout(1:ksize);
    k2=load(k2save);
    kwave2=k2.wavelength(1:ksize);
    k2=k2.Kout(1:ksize);
    k3=load(k3save);
    kwave3=k3.wavelength(1:ksize);
    k3=k3.Kout(1:ksize);
    k4=load(k4save);
    kwave4=k4.wavelength(1:ksize);
    k4=k4.Kout(1:ksize);
    plot(n1lam,n1,n2lam,n2,n3lam,n3,n4lam,n4)
    xlabel('Wavelength (um)')
    ylabel('n')
    legend('n1','n2','n3','n4')
    figure(2)
    semilogy(k1wave,k1,k2wave,k2,k3wave,k3,k4wave,k4)
    xlabel('Wavelength (um)')
    ylabel('k')
    legend('k1','k2','k3','k4')
%The end point motion is a result of the Kramers Kronig being applied
%to less than an infinite range and we are working on a solution to make
%everything infinite.
%-------------------------------------------------------------------------
%##########################---SECTION THIRTYTHREE---########################
%COPY AND PASTE SECTIONS 25-31 and change save and load names for another
%round
```

MasterHapke1_PP.m

```
%define B(g)+1
   Bgplus1=Bg+1;
%Phase angle (g)
   g=d2r(abs(thetae-thetai));
%cos(g)
   cosg=cos(g);
%u_0
   u0=cos(d2r(thetai));
%u
   u=cos(d2r(thetae));
%u_0 + u
   sumu=u0+u;
%single particle phase function P(g)
   Pg=1+b*cosg+c*(1.5*(cosg^2)-0.5);
%approximate surface reflection coefficient S_E
   Se=((n1-1)^2)/((n1+1)^2)+0.05;
%approximate internal scattering coefficient S_I
   Si=1.014-4/(n1*((n1+1)^2));
%import data
   sample=importdata(data);
%make sure wavelength is in microns
   if sample(1,1)>100
      lambda=sample(:,1)./1000;
   else
      lambda=sample(:,1);
   end
   sample=sample(:,2);
   ind1=find(abs(lambda-UV)<=eps);
   ind2=find(abs(lambda-high)<=eps);
%longer reflectance range will be needed for slope and icept calculation
   reflect=sample(ind1:ind2);
%Wavelength range must go one point farther than data to make up for
%loss in slope and icept calculations
   wavelength=lambda(ind1:ind2);
   size=length(reflect)-1;
   size1=size+1;
   size2=size+2;
%create table of values of sequentially increasing w (single scattering
%albedo)
%must be 2 points longer than data file to make up for loss in slope and
%icept calculations
   w=linspace(0,0.9999,size2);
%transpose to column vector
   w=w';
%calculate Hu and Hu0
   gamma1=sqrt(1-w);
   r01=(1-gamma1)./(1+gamma1);
%perform the change of variables to account for porosity outside of H(u)
%and H(u0) equations for simplicity, i.e. H(u) will become H(u/PoreK) see
%Hapke 2012b (the book) for details.
   uK=u/PoreK;
   u0K=u0/PoreK;
   Hu0=(1-w.*u0K.*(r01+((1-2.*r01.*u0K)./2).*log((1+u0K)./u0K))).^(-1);
```

```
   Hu=(1-w.*uK.*(r01+((1-2.*r01.*uK)./2).*log((1+uK)./uK))).^(-1);
%calculate Hu and Hu0 for isotropic case
%import spectralon w data
   specwave=importdata('specwave2.mat');
   calspec=importdata('calspecw2.mat');
   isoind1=find(specwave==0.5);
   isoind2=find(specwave==1.25);
   isow=mean(calspec(isoind1:isoind2));
   isow=linspace(isow,isow,size2);
   isow=isow';
   gammai1=sqrt(1-isow);
   r0i1=(1-gammai1)./(1+gammai1);
   isoHu0=(1-isow.*u0.*(r0i1+((1-2.*r0i1.*u0)./2).*log((1+u0)./u0))).^(-1);
   isoHu=(1-isow.*u.*(r0i1+((1-2.*r0i1.*u)./2).*log((1+u)./u))).^(-1);
%calculate radiance coefficient
rc=PoreK*((w./(4*pi))*(u/(u+u0)).*((Bgplus1*Pg)+(Hu0.*Hu)-1))./...
      ((isow./(4*pi))*(u/(u+u0)).*((1)+(isoHu0.*isoHu)-1));
   save(output,'rc');
   clear('r01','Hu0','Hu');
%Calculate slope and intercept of each delta w (size of vectors data+1)
   slope=zeros(size1,1);
   icept=zeros(size1,1);
   for i=1:1:size1
      slope(i)=(w(i+1)-w(i))/(rc(i+1)-rc(i));
      icept(i)=(w(i)-slope(i)*rc(i));
   end
   figure(1)
   plot(w(1:size1),slope,w(1:size1),icept,w,rc)
   set(gca,'Fontsize',16);
   xlabel('w');
   legend('slope of w and r_c vs. w','intercept of w and r_c vs. ...
            w','r_c vs.w','location','northeast')
%save figure
   hgsave(fig1);
%create table of values of sequentially increasing k by lambda
   k=0.0000001:0.000002:0.0800;
   sizek=length(k);
%make sure that wavelength is a column vector so the matrix populates
%correctly
   if length(wavelength(:,1))<length(wavelength(1,:))
      wavelength=wavelength';
   end
   invwave=1./wavelength;
%calculate scattering efficiency for each (k,lambda)
   Alpha=invwave*(4*pi*k);
   ri=(1-sqrt(Alpha./(Alpha+s)))./(1+sqrt(Alpha./(Alpha+s)));
   THETA=(ri+exp(-sqrt(Alpha.*(Alpha+s))*D))./...
         (1+ri.*exp(-sqrt(Alpha.*(Alpha+s))*D));
   ScatEf=Se+(1-Se).*(((1-Si).*THETA)./(1-Si.*THETA));
%make table of values to search
   rc=rc(1:size1);
   table=[rc,slope,icept];
   save(output,'-append','table','wavelength');
   clear('slope','icept','i','lamdiff','lamend');
%Value matching by finding the 1st calculated rc value that matches the
%reflectance value and then delivers the associated slope
   findslope=zeros(size1,1);
```

```
   for j=1:1:size1
      findslope(j)=fcm(table,reflect(j));
   end
%Value matching by finding the 1st calculated rc value that matches the
%reflectance value and then delivers the associated intercept
   findicept=zeros(size1,1);
   for l=1:1:size1
      findicept(l)=fcm2(table,reflect(l));
   end
%calculate new rc using the equation of a line with the real reflectance
%value and the solved for/found slope and intercept values
   w2=reflect.*findslope+findicept;
%Calculate H(u_0) again from new w value
%calculate Hu and Hu0
   gamma2=sqrt(1-w2);
   r02=(1-gamma2)./(1+gamma2);
   Hu02=(1-w2.*u0K.*(r02+((1-2.*r02.*u0K)./2).*log((1+u0K)./u0K))).^(-1);
   Hu2=(1-w2.*uK.*(r02+((1-2.*r02.*uK)./2).*log((1+uK)./uK))).^(-1);
   isow=isow(1:size1);
   isoHu0=isoHu0(1:size1);
   isoHu=isoHu(1:size1);
%calculate radiance coefficient
rc2=PoreK*(w2./(4*pi))*(u/(u+u0)).*((Bgplus1*Pg)+(Hu02.*Hu2)-1)./...
      ((isow./(4*pi))*(u/(u+u0)).*((1)+(isoHu0.*isoHu)-1));
   save(output,'-append','findslope','findicept','w2','rc2');
   clear('r02','j','l');
%Calculate first error
   error1=rc2-reflect;
%plot reflectance data ans rc2 for comparison
   wave=wavelength';
   figure(2)
   plot(wave(1:size1),reflect(1:size1),wave(1:size1),rc2)
   set(gca,'Fontsize',16);
   set(gca,'XLim',[0.35 2.5]);
   set(gca,'YLim',[0 0.9]);
   xlabel('Wavelength (\mum)');
   ylabel('Refelctance (%)');
   legend('data','radiance coefficient','location','southeast');
%save figure
   hgsave(fig2);
%plot error1
   figure(3)
   plot(wave(1:size1),error1)
   set(gca,'Fontsize',16);
   set(gca,'XLim',[0.35 2.5]);
   set(gca,'YLim',[-0.0001 0.0001]);
   xlabel('Wavelength (\mum)');
   ylabel('Error');
%save figure
   hgsave(fig3);
   save(output,'-append','error1');
   clear error1;
%Next we match w2 (solved w) to a scatterind efficiencey value
%this is where you plug in for finer k
   dist2=zeros(size1,sizek);
   for ii=1:1:size1
      dist2(ii,:)=abs(ScatEf(ii,:)-w2(ii));
```

```
   end
%create tables of the minimum value and minimum location found in last
%lamdiff
   minval=zeros(size1,1);
   minloc=zeros(size1,1);
   for jj=1:1:size1
      [minval(jj),minloc(jj)]=min(dist2(jj,:));
   end
%make arrays useable for fact checking
   min1=[minval, minloc];
%output corresponding k value
   mink=k(minloc);
   offsety=k(minloc+1);
%find corresponding Scatering Efficiency Values
   minx=zeros(1,size1);
   for kk=1:1:size1
      minx(kk)=ScatEf(kk,minloc(kk));
   end
   offsetx=zeros(1,size);
   for ll=1:1:size
      offsetx(ll)=ScatEf(ll,minloc(ll)+1);
   end
%calculate slope of found k values and found scattering efficiency values
   mink=mink';
   offsety=offsety';
   minx=minx';
   offsetx=offsetx';
   slopetable=[mink(1:size),offsety(1:size),minx(1:size),offsetx];
   slope2=zeros(size,1);
   icept2=zeros(size,1);
   for mm=1:1:size
      slope2(mm)=(offsety(mm)-mink(mm))/(offsetx(mm)-minx(mm));
      icept2(mm)=mink(mm)-slope2(mm)*minx(mm);
   end
%solve for k
   k2=slope2.*w2(1:size)+icept2;
   save(output,'-append','min1','slopetable','icept2','slope2','k2');
   clear('dist2','ii','minval','minloc','min1','mink','offsety','offsetx'...
         ,'minx','jj','kk','ll','mm');
%calculate scattering efficiency for each solved k
   Alpha2=(4*pi*k2)./wavelength(1:size);
   ri2=(1-sqrt(Alpha2./(Alpha2+s)))./(1+sqrt(Alpha2./(Alpha2+s)));
   THETA2=(ri2+exp(-sqrt(Alpha2.*(Alpha2+s))*D))./...
            (1+ri2.*exp(-sqrt(Alpha2.*(Alpha2+s))*D));
   ScatAlb=Se+(1-Se).*(((1-Si).*THETA2)./(1-Si.*THETA2));
   save(output,'-append','ScatAlb')
   clear('slope2','icept2');
%Calculate second error
   error2=w2(1:size)-ScatAlb;
   save(output,'-append','error2');
%plot w2 and single scattering albedo
   figure(4)
   plot(wave(1:size),w2(1:size),wave(1:size),ScatAlb)
   set(gca,'Fontsize',16);
   set(gca,'XLim',[0.35 2.5]);
   xlabel('Wavelength (\mum)');
   ylabel('Single Scattering Albedo');
```

```
   legend('Single Scattering Albedo1','Single Scattering Albedo2 ',...
         'location','southeast');
%save figure
   hgsave(fig4);
%plot error2
   figure(5)
   plot(wave(1:size),error2)
   set(gca,'Fontsize',16);
   set(gca,'XLim',[0.35 2.5]);
   set(gca,'YLim',[-0.0001 0.0001]);
   xlabel('Wavelength (\mum)');
   ylabel('Error');
%save figure
   hgsave(fig5);
%plot k2
   figure(6)
   semilogy(wave(1:size),k2)
   set(gca,'Fontsize',16);
   set(gca,'XLim',[0.35 2.5]);
   xlabel('Wavelength (\mum)');
   ylabel('k');
%save figure
   hgsave(fig6)
%Calculate H(u_0) again from new w value
   gamma3=sqrt(1-ScatAlb);
   r03=(1-gamma3)./(1+gamma3);
   Hu03=(1-ScatAlb.*u0K.*(r03+((1-2.*r03.*u0K)./2).*log...
         ((1+u0K)./u0K))).^(-1);
   Hu3=(1-ScatAlb.*uK.*(r03+((1-2.*r03.*uK)./2).*log((1+uK)./uK))).^(-1);
%scale iso values again
   isow=isow(1:size);
   isoHu0=isoHu0(1:size);
   isoHu=isoHu(1:size);
%calculate radiance coefficient
   rc3=PoreK*(ScatAlb./(4*pi))*(u/(u+u0)).*((Bgplus1*Pg)+(Hu03.*Hu3)-1)./...
      ((isow./(4*pi))*(u/(u+u0)).*((1)+(isoHu0.*isoHu)-1));
   save(output,'-append','r03','Hu03','Hu3','rc3','ff','PoreK');
%plot it
   figure(7)
   plot(wavelength(1:size),reflect(1:size),wavelength(1:size), ...
         rc3(1:size),'--r')
   set(gca,'Fontsize',16);
   set(gca,'XLim',[0.35 2.5]);
   xlabel('Wavelength (\mum)');
   ylabel('Reflectance (%)');
   legend('Data','Model ','location','southeast');
%save figure
   hgsave(fig7);
%get a wavelength vector to cat with data so that it is not just numbers
   kwave=wavelength(1:end-1);
%save k for next lamdiffs
   save(kname,'k2','kwave');
%clear all unneeded variables
   clear('Alpha','Alpha2','Bgplus1','D','Hu02','Hu03','Hu2','Hu3', ...
      'Pg','ScatAlb','ScatEf','Se','Si','THETA','THETA2','cosg','error2'...
      ,'findslope','findicept','g','invwave','k','lambda','r03','rc', ...
      'rc2','reflect','ri','ri2','sample','size','size1','size2'...
```

```
   ,'slopetable','sumu','table','u','u0','w','w2','wave')
clear('fig1','fig2','fig3','fig4','fig5','fig6','fig7','output', ...
   'kname','b','c','D',''gamma1','gamma2','gamma3','gammai1','isoHu', ...
   'isoHu0','isoind1','isoind2','ind1',','r0i1','rc3','specwave', ...
   'calspec','isow','k2','PoreK','ff','wavelength')
```

MasterHapke2_PP.m

```
%This program performs an iterative minimization using Hapke's radiative
%transfer theory to find a global and grain-size independent value of
%imaginary index of refraction, k.
%import starting k curve
   K=importdata(kstart);
   K=K.k2;
   load('variables.mat','lamdiff');
%k will always be one point shorter UV after last step.
%so cut a point off the end
   SML=importdata(smldat);
   if SML(end,1)==lend;
      lend=lend-lamdiff;
   end
%make sure it is in the correct configuration
   if length(SML(:,1))<length(SML(1,:))
      SML=SML'; %make column
   end
   startindex=find(abs(SML(:,1)-lstart)<=eps);
   endindex=find(abs(SML(:,1)-lend)<=eps);
%make wavelength vector 4 points longer (in short wavelength direction)
%than k vector to fool program into thinking it has the same number of
%equations as unknowns
   foolsindex=startindex+4;
   lambda=SML(:,1);
   wavelength=lambda(startindex:endindex);
   wavelength=wavelength';
   wavelength=cat(2,wavelength,wavelength,wavelength);
%extract useable k range but keep the 4 points for later
   kone=K(1);
   ktwo=K(2);
   kthree=K(3);
   kfour=K(4);
   K=K(foolsindex:endindex);
%make an array as long as the full data set
   if length(K(:,1))>length(K(1,:))
      K=K'; %row (must be for program to work)
   end
   k=cat(2,K,K,K);
   realsize=length(k);
   fakesize=length(k)+4;
   ksize=length(K);
   save('variables.mat','-append','ksize','startindex','endindex',...
         'foolsindex','kone','ktwo','kthree','kfour')
%make DATA array
   sml=importdata(smldat);
   sml=sml(:,2);
   sml=sml(startindex:endindex);
   if length(sml(:,1))>length(sml(1,:))
      sml=sml'; %row (must be for program to work)
   end
   med=importdata(meddat);
   med=med(:,2);
   med=med(startindex:endindex);
```

```
   if length(med(:,1))>length(med(1,:))
      med=med'; %row (must be for program to work)
   end
   big=importdata(bigdat);
   big=big(:,2);
   big=big(startindex:endindex);
   if length(big(:,1))>length(big(1,:))
      big=big'; %row (must be for program to work)
   end
   DATA=cat(2,sml,med,big);
%load variables
   load('variables.mat','b1','b2','b3','c1','c2','c3','s1','s2','s3', ...
         'D1','D2','D3','thetai','thetae','PoreK1','PoreK2','PoreK3');
%make coefficient guess matrix from user supplied values in MASTER PROGRAM
   coefg=[b1,b2,b3,c1,c2,c3,s1,s2,s3,D1,D2,D3,k];
   extra1=length(coefg)-length(k);
   save('variables.mat','-append','extra1');
   lbk=zeros(1,realsize);
   lb=[lowb1,lowb2,lowb3,lowc1,lowc2,lowc3,lows1,lows2,lows3,lowD1, ...
      lowD2,lowD3,lbk];
   ubk=linspace(upk,upk,realsize);
   ub=[upb1,upb2,upb3,upc1,upc2,upc3,ups1,ups2,ups3,upD1,upD2,upD3,ubk];
%define size variable (needed later)
%Phase angle (g)
   g=d2r(abs(thetae-thetai));
%cos(g)
   cosg=cos(g);
%u_0
   u0=cos(d2r(thetai));
%change of variables that makes H function easier
   u0K1=u0/PoreK1;
   u0K2=u0/PoreK2;
   u0K3=u0/PoreK3;
%u
   u=cos(d2r(thetae));
%change of variables that makes H function easier
   uK1=u/PoreK1;
   uK2=u/PoreK2;
   uK3=u/PoreK3;
%load the data for the calibrated spectralon standard
   load('calspecw2.mat');
   calspecw=best;
%load its wavelength vector
   load('specwave2.mat');
%make these coarse and shorter like the other spectral data
   lowind2=find(abs(specwave-lstart)<=eps);
   highind2=find(abs(specwave-lend)<=eps);
%recreate the wavelength vectorwho
   isowave=specwave(lowind2:highind2);
   isow=calspecw(lowind2:highind2);
%make sure it is a column vector
   if length(isow(:,1))>length(isow(1,:))
      isow=isow';
   end
save('variables.mat','-append','u0K1','u0K2','u0K3','uK1','uK2','uK3', ...
      'isow','cosg','u','u0')
%create abstract function to pass through variables
```

```
myObjFcn = @(coefg,wavelength)MASTERWRAPPER_PP(coefg,wavelength,kone, ...
            ktwo,kthree,kfour,n,u0,u,u0K1,u0K2,u0K3,uK1,uK2,uK3,cosg, ...
            ksize,isow,PoreK1,PoreK2,PoreK3);
%USE LSQCURVEFIT TO PERFORM LEAST SQUARES MINIMIZATION between data and
%model. Levenberg-Marquardt',... 'ScaleProblem','Jacobian'
%Format is [output]=lsqcurvefit(function,x0,xdata,ydata,lb,ub)
   options=optimoptions(@lsqcurvefit,'Algorithm',...
      'trust-region-reflective','Display','iter','MaxIter',maxit, ...
      'FinDiffType','central','MaxFunEvals',maxfun,'TolFun',funtol,...
      'TolX', xtol);
   problem = createOptimProblem('lsqcurvefit','x0',coefg, ...
         'objective',myObjFcn,'xdata',wavelength,'ydata',DATA,'lb',...
         lb,'ub',ub,'options',options);
   ms = MultiStart('UseParallel','always');
   [coef,fval,exitflag,output,solutions] = run(ms,problem,spts);
   save(ksave,'solutions','wavelength');
   save('variables.mat','-append','coefg','lb','ub')
   clear('D1','D2','D3','b1','b2','b3','c1','c2','c3','s1','s2','s3', ...
         'thetai','thetae',',','lowc2','lowc3','lowD1','lowD2','lowD3', ...
         'lows1','lows2','lows3','lbk','ubk','sml',',','upc2','upc3', ...
         'upD1','upD2','upD3','ups1','ups2','ups3','DATA','K','coefg', ...
         'endindex',',','krange','kstart','lambda','lb','lend','lstart', ...
         'maxfun','maxit','realsize','spts',',','solutions','ksize', ...
         'problem','outpt','options','ms','fval','flag','coef')
```

MASTERWRAPPER_PP.m

```
function[rc]=MASTERWRAPPER_PP(coefg,wavelength,kone,ktwo,kthree,kfour,...
      n,u0,u,u0K1,u0K2,u0K3,uK1,uK2,uK3,cosg,ksize,isow,PoreK1,PoreK2,PoreK3)
%wrapper function
%UNPACK VARIABLES
   b1=coefg(1);
   b2=coefg(2);
   b3=coefg(3);
   c1=coefg(4);
   c2=coefg(5);
   c3=coefg(6);
   s1=coefg(7);
   s2=coefg(8);
   s3=coefg(9);
   D1=coefg(10);
   D2=coefg(11);
   D3=coefg(12);
   kend=ksize+12;
   k=coefg(13:kend); %row
   waveend=ksize+4;
   wavelength=wavelength(1:waveend); %row
   k=cat(2,kone,ktwo,kthree,kfour,k);

[rc]=MasterHapke3_PP(b1,b2,b3,c1,c2,c3,s1,s2,s3,k,D1,D2,D3,wavelength,n,...
      u0,u,u0K1,u0K2,u0K3,uK1,uK2,uK3,cosg,isow,PoreK1,PoreK2,PoreK3);
```

MasterHapke3_PP.m

```
%the guts of the Hapke calculation
function [rc]=MasterHapke3_PP(b1,b2,b3,c1,c2,c3,s1,s2,s3,k,D1,D2,D3, ...
      wavelength,n,u0,u,u0K1,u0K2,u0K3,uK1,uK2,uK3,cosg,isow,PoreK1, ...
      PoreK2,PoreK3)
%DEFINE RELATIONS
%single particle phase function P(g)
   Pg1=1+b1.*cosg+c1.*(1.5.*(cosg.^2)-0.5);
   Pg2=1+b2.*cosg+c2.*(1.5.*(cosg.^2)-0.5);
   Pg3=1+b3.*cosg+c3.*(1.5.*(cosg.^2)-0.5);
%calculate variables for isotropic standard
   gammai1=sqrt(1-isow);
   r0i1=(1-gammai1)./(1+gammai1);
   isoHu0=(1-isow.*u0.*(r0i1+((1-2.*r0i1.*u0)./2).*log((1+u0)./u0))).^(-1);
   isoHu=(1-isow.*u.*(r0i1+((1-2.*r0i1.*u)./2).*log((1+u)./u))).^(-1);
%FIRST GRAINSIZE
%initial alpha and k
   Alpha=((4*pi).*k)./wavelength;
%internal transmission factor
   ri1=(1-sqrt(Alpha./(Alpha+s1)))./(1+sqrt(Alpha./(Alpha+s1)));
   THETA1=(ri1+exp(-sqrt(Alpha.*(Alpha+s1)).*D1))./ ...
         (1+ri1.*exp(-sqrt(Alpha.*(Alpha+s1)).*D1));
%approximate surface reflection coefficient S_E
   Se=((n-1).^2+k.^2)./((n+1).^2+k.^2)+0.05;
%approximate internal scattering coefficient S_I
   Si=1.014-4./(n.*((n+1).^2));
%single scattering albedo
   w1=Se+(1-Se).*(((1-Si).*THETA1)./(1-Si.*THETA1));
%H function
   gamma1=sqrt(1-w1);
   r01=(1-gamma1)./(1+gamma1);
   Hu01=(1-w1.*u0K1.*(r01+((1-2.*r01.*u0K1)./2).*log((1+u0K1)./u0K1))).^(-1);
   Hu1=(1-w1.*uK1.*(r01+((1-2.*r01.*uK1)./2).*log((1+uK1)./uK1))).^(-1);
%radiance coefficient
   rc1=PoreK1*((w1./(4*pi))*(u/(u+u0)).*((Pg1)+(Hu01.*Hu1)-1))./ ...
      ((isow./(4*pi))*(u/(u+u0)).*((1)+(isoHu0.*isoHu)-1));
%SECOND GRAINSIZE
%internal transmission factor
   ri2=(1-sqrt(Alpha./(Alpha+s2)))./(1+sqrt(Alpha./(Alpha+s2)));
   THETA2=(ri2+exp(-sqrt(Alpha.*(Alpha+s2)).*D2))./ ...
         (1+ri2.*exp(-sqrt(Alpha.*(Alpha+s2)).*D2));
%single scattering albedo
   w2=Se+(1-Se).*(((1-Si).*THETA2)./(1-Si.*THETA2));
%H function
   gamma2=sqrt(1-w2);
   r02=(1-gamma2)./(1+gamma2);
   Hu02=(1-w2.*u0K2.*(r02+((1-2.*r02.*u0K2)./2).*log((1+u0K2)./u0K2))).^(-1);
   Hu2=(1-w2.*uK2.*(r02+((1-2.*r02.*uK2)./2).*log((1+uK2)./uK2))).^(-1);
%radiance coefficient
   rc2=PoreK2*((w2./(4*pi))*(u/(u+u0)).*((Pg2)+(Hu02.*Hu2)-1))./ ...
      ((isow./(4*pi))*(u/(u+u0)).*((1)+(isoHu0.*isoHu)-1));
%THIRD GRAINSIZE
%internal transmission factor
   ri3=(1-sqrt(Alpha./(Alpha+s3)))./(1+sqrt(Alpha./(Alpha+s3)));
```

```
   THETA3=(ri3+exp(-sqrt(Alpha.*(Alpha+s3)).*D3))./ ...
         (1+ri3.*exp(-sqrt(Alpha.*(Alpha+s3)).*D3));
%single scattering albedo
   w3=Se+(1-Se).*(((1-Si).*THETA3)./(1-Si.*THETA3));
%H function
   gamma3=sqrt(1-w3);
   r03=(1-gamma3)./(1+gamma3);
   Hu03=(1-w3.*u0K3.*(r03+((1-2.*r03.*u0K3)./2).*log((1+u0K3)./u0K3))).^(-1);
   Hu3=(1-w3.*uK3.*(r03+((1-2.*r03.*uK3)./2).*log((1+uK3)./uK3))).^(-1);
%radiance coefficient
   rc3=PoreK3*((w3./(4*pi))*(u/(u+u0)).*((Pg3)+(Hu03.*Hu3)-1))./ ...
      ((isow./(4*pi))*(u/(u+u0)).*((1)+(isoHu0.*isoHu)-1));

   rc=cat(2,rc1,rc2,rc3);
end
```

HapkeEval1_PP.m

```
%This program evaluates the input guesses for the minimization program and
%appends them to the save file in a user friendly format
%load solution set
   load(ksave,'solutions','wavelength');
%extract sizes for general plotting
   ksize=load('variables.mat','ksize');
   ksize=ksize.ksize;
   krange=ksize+12;
%extract input guesses
%warning for too few convergent solutions
   if length(solutions)<6;
      error('program converged on less than 6 start points, ...
            try changing maxit, maxfun,
   elseif length(solutions)<7
      onein=solutions (1,1);
      twoin=solutions (1,2);
      threein=solutions (1,3);
      fourin=solutions (1,4);
      fivein=solutions (1,5);
      sixin=solutions (1,6);
      onein=onein(1).X0;
      twoin=twoin(1).X0;
      threein=threein(1).X0;
      fourin=fourin(1).X0;
      fivein=fivein(1).X0;
      sixin=sixin(1).X0;
      onein=onein{1,1};
      twoin=twoin{1,1};
      threein=threein{1,1};
      fourin=fourin{1,1};
      fivein=fivein{1,1};
      sixin=sixin{1,1};
      count=[1 2 3 4 5 6];
      b11=onein(1);
      b12=onein(2);
      b13=onein(3);
      b21=twoin(1);
      b22=twoin(2);
      b23=twoin(3);
      b31=threein(1);
      b32=threein(2);
      b33=threein(3);
      b41=fourin(1);
      b42=fourin(2);
      b43=fourin(3);
      b51=fivein(1);
      b52=fivein(2);
      b53=fivein(3);
      b61=sixin(1);
      b62=sixin(2);
      b63=sixin(3);
      B1in=[b11 b21 b31 b41 b51 b61];
      B2in=[b12 b22 b32 b42 b52 b62];
```

```
B3in=[b13 b23 b33 b43 b53 b63];
figure(1)
plot(count,B1in,'r+',count,B2in,'g+',count,B3in,'b+')
c11=onein(4);
c12=onein(5);
c13=onein(6);
c21=twoin(4);
c22=twoin(5);
c23=twoin(6);
c31=threein(4);
c32=threein(5);
c33=threein(6);
c41=fourin(4);
c42=fourin(5);
c43=fourin(6);
c51=fivein(4);
c52=fivein(5);
c53=fivein(6);
c61=sixin(4);
c62=sixin(5);
c63=sixin(6);
C1in=[c11 c21 c31 c41 c51 c61];
C2in=[c12 c22 c32 c42 c52 c62];
C3in=[c13 c23 c33 c43 c53 c63];
figure(2)
plot(count,C1in,'r+',count,C2in,'g+',count,C3in,'b+')
s11=onein(7);
s12=onein(8);
s13=onein(9);
s21=twoin(7);
s22=twoin(8);
s23=twoin(9);
s31=threein(7);
s32=threein(8);
s33=threein(9);
s41=fourin(7);
s42=fourin(8);
s43=fourin(9);
s51=fivein(7);
s52=fivein(8);
s53=fivein(9);
s61=sixin(7);
s62=sixin(8);
s63=sixin(9);
S1in=[s11 s21 s31 s41 s51 s61];
S2in=[s12 s22 s32 s42 s52 s62];
S3in=[s13 s23 s33 s43 s53 s63];
figure(3)
semilogy(count,S1in,'r+',count,S2in,'g+',count,S3in,'b+')
d11=onein(10);
d12=onein(11);
d13=onein(12);
d21=twoin(10);
d22=twoin(11);
d23=twoin(12);
d31=threein(10);
d32=threein(11);
```

```
    d33=threein(12);
    d41=fourin(10);
    d42=fourin(11);
    d43=fourin(12);
    d51=fivein(10);
    d52=fivein(11);
    d53=fivein(12);
    d61=sixin(10);
    d62=sixin(11);
    d63=sixin(12);
    D1in=[d11 d21 d31 d41 d51 d61];
    D2in=[d12 d22 d32 d42 d52 d62];
    D3in=[d13 d23 d33 d43 d53 d63];
    figure(4)
    plot(count,D1in,'r+',count,D2in,'g+',count,D3in,'b+')
    k1=onein(13:krange);
    k2=twoin(13:krange);
    k3=threein(13:krange);
    k4=fourin(13:krange);
    k5=fivein(13:krange);
    k6=sixin(13:krange);
    Kin=[k1 k2 k3 k4 k5 k6];
    wave=wavelength(1:ksize);
    figure(5)
    semilogy(wave,k1,wave,k2,wave,k3,wave,k4,wave,k5,wave,k6)
    legend('one','two','three','four','five','six','location','southeast')
    save(ksave,'-append','B1in','B2in','C1in','C2in','S1in','S2in', ...
       'D1in','D2in','Kin','onein')
elseif length(solutions)<8
    onein=solutions (1,1);
    twoin=solutions (1,2);
    threein=solutions (1,3);
    fourin=solutions (1,4);
    fivein=solutions (1,5);
    sixin=solutions (1,6);
    sevin=solutions (1,7);
    onein=onein(1).X0;
    twoin=twoin(1).X0;
    threein=threein(1).X0;
    fourin=fourin(1).X0;
    fivein=fivein(1).X0;
    sixin=sixin(1).X0;
    sevin=sevin(1).X0;
    onein=onein{1,1};
    twoin=twoin{1,1};
    threein=threein{1,1};
    fourin=fourin{1,1};
    fivein=fivein{1,1};
    sixin=sixin{1,1};
    sevin=sevin{1,1};
    count=[1 2 3 4 5 6 7];
    b11=onein(1);
    b12=onein(2);
    b13=onein(3);
    b21=twoin(1);
    b22=twoin(2);
    b23=twoin(3);
```

```
b31=threein(1);
b32=threein(2);
b33=threein(3);
b41=fourin(1);
b42=fourin(2);
b43=fourin(3);
b51=fivein(1);
b52=fivein(2);
b53=fivein(3);
b61=sixin(1);
b62=sixin(2);
b63=sixin(3);
b71=sevin(1);
b72=sevin(2);
b73=sevin(3);
B1in=[b11 b21 b31 b41 b51 b61 b71];
B2in=[b12 b22 b32 b42 b52 b62 b72];
B3in=[b13 b23 b33 b43 b53 b63 b73];
figure(1)
plot(count,B1in,'r+',count,B2in,'g+',count,B3in,'b+')
c11=onein(4);
c12=onein(5);
c13=onein(6);
c21=twoin(4);
c22=twoin(5);
c23=twoin(6);
c31=threein(4);
c32=threein(5);
c33=threein(6);
c41=fourin(4);
c42=fourin(5);
c43=fourin(6);
c51=fivein(4);
c52=fivein(5);
c53=fivein(6);
c61=sixin(4);
c62=sixin(5);
c63=sixin(6);
c71=sevin(4);
c72=sevin(5);
c73=sevin(6);
C1in=[c11 c21 c31 c41 c51 c61 c71];
C2in=[c12 c22 c32 c42 c52 c62 c72];
C3in=[c13 c23 c33 c43 c53 c63 c73];
figure(2)
plot(count,C1in,'r+',count,C2in,'g+',count,C3in,'b+')
s11=onein(7);
s12=onein(8);
s13=onein(9);
s21=twoin(7);
s22=twoin(8);
s23=twoin(9);
s31=threein(7);
s32=threein(8);
s33=threein(9);
s41=fourin(7);
s42=fourin(8);
```

```
    s43=fourin(9);
    s51=fivein(7);
    s52=fivein(8);
    s53=fivein(9);
    s61=sixin(7);
    s62=sixin(8);
    s63=sixin(9);
    s71=sevin(7);
    s72=sevin(8);
    s73=sevin(9);
    S1in=[s11 s21 s31 s41 s51 s61 s71];
    S2in=[s12 s22 s32 s42 s52 s62 s72];
    S3in=[s13 s23 s33 s43 s53 s63 s73];
    figure(3)
    semilogy(count,S1in,'r+',count,S2in,'g+',count,S3in,'b+')
    d11=onein(10);
    d12=onein(11);
    d13=onein(12);
    d21=twoin(10);
    d22=twoin(11);
    d23=twoin(12);
    d31=threein(10);
    d32=threein(11);
    d33=threein(12);
    d41=fourin(10);
    d42=fourin(11);
    d43=fourin(12);
    d51=fivein(10);
    d52=fivein(11);
    d53=fivein(12);
    d61=sixin(10);
    d62=sixin(11);
    d63=sixin(12);
    d71=sevin(10);
    d72=sevin(11);
    d73=sevin(12);
    D1in=[d11 d21 d31 d41 d51 d61 d71];
    D2in=[d12 d22 d32 d42 d52 d62 d72];
    D3in=[d13 d23 d33 d43 d53 d63 d73];
    figure(4)
    plot(count,D1in,'r+',count,D2in,'g+',count,D3in,'b+')
    k1=onein(13:krange);
    k2=twoin(13:krange);
    k3=threein(13:krange);
    k4=fourin(13:krange);
    k5=fivein(13:krange);
    k6=sixin(13:krange);
    k7=sevin(13:krange);
    Kin=[k1 k2 k3 k4 k5 k6 k7];
    wave=wavelength(1:ksize);
    figure(5)
    semilogy(wave,k1,wave,k2,wave,k3,wave,k4,wave,k5,wave,k6,wave,k7)
    legend('one','two','three','four','five','six','seven','location', ...
       'southeast')
    save(ksave,'-append','B1in','B2in','C1in','C2in','S1in','S2in', ...
          'D1in','D2in','Kin','onein')
elseif length(solutions)>7
```

```
onein=solutions (1,1);
twoin=solutions (1,2);
threein=solutions (1,3);
fourin=solutions (1,4);
fivein=solutions (1,5);
sixin=solutions (1,6);
sevin=solutions (1,7);
eightin=solutions (1,8);
onein=onein(1).X0;
twoin=twoin(1).X0;
threein=threein(1).X0;
fourin=fourin(1).X0;
fivein=fivein(1).X0;
sixin=sixin(1).X0;
sevin=sevin(1).X0;
eightin=eightin(1).X0;
onein=onein{1,1};
twoin=twoin{1,1};
threein=threein{1,1};
fourin=fourin{1,1};
fivein=fivein{1,1};
sixin=sixin{1,1};
sevin=sevin{1,1};
eightin=eightin{1,1};
count=[1 2 3 4 5 6 7 8];
b11=onein(1);
b12=onein(2);
b13=onein(3);
b21=twoin(1);
b22=twoin(2);
b23=twoin(3);
b31=threein(1);
b32=threein(2);
b33=threein(3);
b41=fourin(1);
b42=fourin(2);
b43=fourin(3);
b51=fivein(1);
b52=fivein(2);
b53=fivein(3);
b61=sixin(1);
b62=sixin(2);
b63=sixin(3);
b71=sevin(1);
b72=sevin(2);
b73=sevin(3);
b81=eightin(1);
b82=eightin(2);
b83=eightin(3);
B1in=[b11 b21 b31 b41 b51 b61 b71 b81];
B2in=[b12 b22 b32 b42 b52 b62 b72 b82];
B3in=[b13 b23 b33 b43 b53 b63 b73 b83];
figure(1)
plot(count,B1in,'r+',count,B2in,'g+',count,B3in,'b+')
c11=onein(4);
c12=onein(5);
c13=onein(6);
```

```
c21=twoin(4);
c22=twoin(5);
c23=twoin(6);
c31=threein(4);
c32=threein(5);
c33=threein(6);
c41=fourin(4);
c42=fourin(5);
c43=fourin(6);
c51=fivein(4);
c52=fivein(5);
c53=fivein(6);
c61=sixin(4);
c62=sixin(5);
c63=sixin(6);
c71=sevin(4);
c72=sevin(5);
c73=sevin(6);
c81=eightin(4);
c82=eightin(5);
c83=eightin(6);
C1in=[c11 c21 c31 c41 c51 c61 c71 c81];
C2in=[c12 c22 c32 c42 c52 c62 c72 c82];
C3in=[c13 c23 c33 c43 c53 c63 c73 c83];
figure(2)
plot(count,C1in,'r+',count,C2in,'g+',count,C3in,'b+')
s11=onein(7);
s12=onein(8);
s13=onein(9);
s21=twoin(7);
s22=twoin(8);
s23=twoin(9);
s31=threein(7);
s32=threein(8);
s33=threein(9);
s41=fourin(7);
s42=fourin(8);
s43=fourin(9);
s51=fivein(7);
s52=fivein(8);
s53=fivein(9);
s61=sixin(7);
s62=sixin(8);
s63=sixin(9);
s71=sevin(7);
s72=sevin(8);
s73=sevin(9);
s81=eightin(7);
s82=eightin(8);
s83=eightin(9);
S1in=[s11 s21 s31 s41 s51 s61 s71 s81];
S2in=[s12 s22 s32 s42 s52 s62 s72 s82];
S3in=[s13 s23 s33 s43 s53 s63 s73 s83];
figure(3)
semilogy(count,S1in,'r+',count,S2in,'g+',count,S3in,'b+')
d11=onein(10);
d12=onein(11);
```

```
    d13=onein(12);
    d21=twoin(10);
    d22=twoin(11);
    d23=twoin(12);
    d31=threein(10);
    d32=threein(11);
    d33=threein(12);
    d41=fourin(10);
    d42=fourin(11);
    d43=fourin(12);
    d51=fivein(10);
    d52=fivein(11);
    d53=fivein(12);
    d61=sixin(10);
    d62=sixin(11);
    d63=sixin(12);
    d71=sevin(10);
    d72=sevin(11);
    d73=sevin(12);
    d81=eightin(10);
    d82=eightin(11);
    d83=eightin(12);
    D1in=[d11 d21 d31 d41 d51 d61 d71 d81];
    D2in=[d12 d22 d32 d42 d52 d62 d72 d82];
    D3in=[d13 d23 d33 d43 d53 d63 d73 d83];
    figure(4)
    plot(count,D1in,'r+',count,D2in,'g+',count,D3in,'b+')
    k1=onein(13:krange);
    k2=twoin(13:krange);
    k3=threein(13:krange);
    k4=fourin(13:krange);
    k5=fivein(13:krange);
    k6=sixin(13:krange);
    k7=sevin(13:krange);
    k8=sevin(13:krange);
    Kin=[k1 k2 k3 k4 k5 k6 k7 k8];
    wave=wavelength(1:ksize);
    figure(5)
    semilogy(wave,k1,wave,k2,wave,k3,wave,k4,wave,k5,wave,k6,wave,k7, ...
             wave,k8)
    legend('one','two','three','four','five','six','seven', ...
          'eight','location','southeast')
    save(ksave,'-append','B1in','B2in','C1in','C2in','S1in','S2in', ...
          'D1in','D2in','Kin','onein')
end
clear
```

HapkeEval2_PP.m

```
%This program evaluates the output guesses for the minimization program and
%appends them to the save file out a user friendly format
%load solution set
   load(ksave,'solutions','wavelength');
%extract sizes for general plotting
   ksize=load('variables.mat','ksize');
   load('variables.mat','extra1')
   ksize=ksize.ksize;
   krange=ksize+extra1;
   wavelength=wavelength(1:krange);
%extract output guesses
%warnoutg for too few convergent solutions
   if length(solutions)<6;
      error('program converged on less than 6 start points, try ...
            changing maxit, maxfun, or bounds and start again.')
   elseif length(solutions)<7
      oneout=solutions (1,1);
      twoout=solutions (1,2);
      threeout=solutions (1,3);
      fourout=solutions (1,4);
      fiveout=solutions (1,5);
      sixout=solutions (1,6);
      oneout=oneout(1).X;
      twoout=twoout(1).X;
      threeout=threeout(1).X;
      fourout=fourout(1).X;
      fiveout=fiveout(1).X;
      sixout=sixout(1).X;
      count=[1 2 3 4 5 6];
      b11=oneout(1);
      b12=oneout(2);
      b13=oneout(3);
      b21=twoout(1);
      b22=twoout(2);
      b23=twoout(3);
      b31=threeout(1);
      b32=threeout(2);
      b33=threeout(3);
      b41=fourout(1);
      b42=fourout(2);
      b43=fourout(3);
      b51=fiveout(1);
      b52=fiveout(2);
      b53=fiveout(3);
      b61=sixout(1);
      b62=sixout(2);
      b63=sixout(3);
      B1out=[b11 b21 b31 b41 b51 b61];
      B2out=[b12 b22 b32 b42 b52 b62];
      B3out=[b13 b23 b33 b43 b53 b63];
      figure(1)
      plot(count,B1out,'r+',count,B2out,'g+',count,B3out,'b+')
      c11=oneout(4);
```

```
c12=oneout(5);
c13=oneout(6);
c21=twoout(4);
c22=twoout(5);
c23=twoout(6);
c31=threeout(4);
c32=threeout(5);
c33=threeout(6);
c41=fourout(4);
c42=fourout(5);
c43=fourout(6);
c51=fiveout(4);
c52=fiveout(5);
c53=fiveout(6);
c61=sixout(4);
c62=sixout(5);
c63=sixout(6);
C1out=[c11 c21 c31 c41 c51 c61];
C2out=[c12 c22 c32 c42 c52 c62];
C3out=[c13 c23 c33 c43 c53 c63];
figure(2)
plot(count,C1out,'r+',count,C2out,'g+',count,C3out,'b+')
s11=oneout(7);
s12=oneout(8);
s13=oneout(9);
s21=twoout(7);
s22=twoout(8);
s23=twoout(9);
s31=threeout(7);
s32=threeout(8);
s33=threeout(9);
s41=fourout(7);
s42=fourout(8);
s43=fourout(9);
s51=fiveout(7);
s52=fiveout(8);
s53=fiveout(9);
s61=sixout(7);
s62=sixout(8);
s63=sixout(9);
S1out=[s11 s21 s31 s41 s51 s61];
S2out=[s12 s22 s32 s42 s52 s62];
S3out=[s13 s23 s33 s43 s53 s63];
figure(3)
semilogy(count,S1out,'r+',count,S2out,'g+',count,S3out,'b+')
d11=oneout(10);
d12=oneout(11);
d13=oneout(12);
d21=twoout(10);
d22=twoout(11);
d23=twoout(12);
d31=threeout(10);
d32=threeout(11);
d33=threeout(12);
d41=fourout(10);
d42=fourout(11);
d43=fourout(12);
```

```
        d51=fiveout(10);
        d52=fiveout(11);
        d53=fiveout(12);
        d61=sixout(10);
        d62=sixout(11);
        d63=sixout(12);
        D1out=[d11 d21 d31 d41 d51 d61];
        D2out=[d12 d22 d32 d42 d52 d62];
        D3out=[d13 d23 d33 d43 d53 d63];
        figure(4)
        plot(count,D1out,'r+',count,D2out,'g+',count,D3out,'b+')
        k1=oneout(13:krange);
        k2=twoout(13:krange);
        k3=threeout(13:krange);
        k4=fourout(13:krange);
        k5=fiveout(13:krange);
        k6=sixout(13:krange);
        Kout=[k1 k2 k3 k4 k5 k6];
        wave=wavelength(1:ksize);
        figure(5)
        semilogy(wave,k1,wave,k2,wave,k3,wave,k4,wave,k5,wave,k6)
        legend('one','two','three','four','five','six','location','southeast')
save(ksave,'-append','B1out','B2out','C1out','C2out','S1out','S2out', ...
        'D1out','D2out','Kout','oneout')
    elseif length(solutions)<8
        oneout=solutions (1,1);
        twoout=solutions (1,2);
        threeout=solutions (1,3);
        fourout=solutions (1,4);
        fiveout=solutions (1,5);
        sixout=solutions (1,6);
        sevout=solutions (1,7);
        oneout=oneout(1).X;
        twoout=twoout(1).X;
        threeout=threeout(1).X;
        fourout=fourout(1).X;
        fiveout=fiveout(1).X;
        sixout=sixout(1).X;
        sevout=sevout(1).X;
        count=[1 2 3 4 5 6 7];
        b11=oneout(1);
        b12=oneout(2);
        b13=oneout(3);
        b21=twoout(1);
        b22=twoout(2);
        b23=twoout(3);
        b31=threeout(1);
        b32=threeout(2);
        b33=threeout(3);
        b41=fourout(1);
        b42=fourout(2);
        b43=fourout(3);
        b51=fiveout(1);
        b52=fiveout(2);
        b53=fiveout(3);
        b61=sixout(1);
        b62=sixout(2);
```

```
b63=sixout(3);
b71=sevout(1);
b72=sevout(2);
b73=sevout(3);
B1out=[b11 b21 b31 b41 b51 b61 b71];
B2out=[b12 b22 b32 b42 b52 b62 b72];
B3out=[b13 b23 b33 b43 b53 b63 b73];
figure(1)
plot(count,B1out,'r+',count,B2out,'g+',count,B3out,'b+')
c11=oneout(4);
c12=oneout(5);
c13=oneout(6);
c21=twoout(4);
c22=twoout(5);
c23=twoout(6);
c31=threeout(4);
c32=threeout(5);
c33=threeout(6);
c41=fourout(4);
c42=fourout(5);
c43=fourout(6);
c51=fiveout(4);
c52=fiveout(5);
c53=fiveout(6);
c61=sixout(4);
c62=sixout(5);
c63=sixout(6);
c71=sevout(4);
c72=sevout(5);
c73=sevout(6);
C1out=[c11 c21 c31 c41 c51 c61 c71];
C2out=[c12 c22 c32 c42 c52 c62 c72];
C3out=[c13 c23 c33 c43 c53 c63 c73];
figure(2)
plot(count,C1out,'r+',count,C2out,'g+',count,C3out,'b+')
s11=oneout(7);
s12=oneout(8);
s13=oneout(9);
s21=twoout(7);
s22=twoout(8);
s23=twoout(9);
s31=threeout(7);
s32=threeout(8);
s33=threeout(9);
s41=fourout(7);
s42=fourout(8);
s43=fourout(9);
s51=fiveout(7);
s52=fiveout(8);
s53=fiveout(9);
s61=sixout(7);
s62=sixout(8);
s63=sixout(9);
s71=sevout(7);
s72=sevout(8);
s73=sevout(9);
S1out=[s11 s21 s31 s41 s51 s61 s71];
```

```
    S2out=[s12 s22 s32 s42 s52 s62 s72];
    S3out=[s13 s23 s33 s43 s53 s63 s73];
    figure(3)
    semilogy(count,S1out,'r+',count,S2out,'g+',count,S3out,'b+')
    d11=oneout(10);
    d12=oneout(11);
    d13=oneout(12);
    d21=twoout(10);
    d22=twoout(11);
    d23=twoout(12);
    d31=threeout(10);
    d32=threeout(11);
    d33=threeout(12);
    d41=fourout(10);
    d42=fourout(11);
    d43=fourout(12);
    d51=fiveout(10);
    d52=fiveout(11);
    d53=fiveout(12);
    d61=sixout(10);
    d62=sixout(11);
    d63=sixout(12);
    d71=sevout(10);
    d72=sevout(11);
    d73=sevout(12);
    D1out=[d11 d21 d31 d41 d51 d61 d71];
    D2out=[d12 d22 d32 d42 d52 d62 d72];
    D3out=[d13 d23 d33 d43 d53 d63 d73];
    figure(4)
    plot(count,D1out,'r+',count,D2out,'g+',count,D3out,'b+')
    k1=oneout(13:krange);
    k2=twoout(13:krange);
    k3=threeout(13:krange);
    k4=fourout(13:krange);
    k5=fiveout(13:krange);
    k6=sixout(13:krange);
    k7=sevout(13:krange);
    Kout=[k1 k2 k3 k4 k5 k6 k7];
    wave=wavelength(1:ksize);
    figure(5)
    semilogy(wave,k1,wave,k2,wave,k3,wave,k4,wave,k5,wave,k6,wave,k7)
    legend('one','two','three','four','five','six','seven', ...
          'location','southeast')
    save(ksave,'-append','B1out','B2out','C1out','C2out','S1out', ...
          'S2out','D1out','D2out','Kout','oneout')
elseif length(solutions)>7
    oneout=solutions (1,1);
    twoout=solutions (1,2);
    threeout=solutions (1,3);
    fourout=solutions (1,4);
    fiveout=solutions (1,5);
    sixout=solutions (1,6);
    sevout=solutions (1,7);
    eightout=solutions (1,8);
    oneout=oneout(1).X;
    twoout=twoout(1).X;
    threeout=threeout(1).X;
```

```
fourout=fourout(1).X;
fiveout=fiveout(1).X;
sixout=sixout(1).X;
sevout=sevout(1).X;
eightout=eightout(1).X;
count=[1 2 3 4 5 6 7 8];
b11=oneout(1);
b12=oneout(2);
b13=oneout(3);
b21=twoout(1);
b22=twoout(2);
b23=twoout(3);
b31=threeout(1);
b32=threeout(2);
b33=threeout(3);
b41=fourout(1);
b42=fourout(2);
b43=fourout(3);
b51=fiveout(1);
b52=fiveout(2);
b53=fiveout(3);
b61=sixout(1);
b62=sixout(2);
b63=sixout(3);
b71=sevout(1);
b72=sevout(2);
b73=sevout(3);
b81=eightout(1);
b82=eightout(2);
b83=eightout(3);
B1out=[b11 b21 b31 b41 b51 b61 b71 b81];
B2out=[b12 b22 b32 b42 b52 b62 b72 b82];
B3out=[b13 b23 b33 b43 b53 b63 b73 b83];
figure(1)
plot(count,B1out,'r+',count,B2out,'g+',count,B3out,'b+')
c11=oneout(4);
c12=oneout(5);
c13=oneout(6);
c21=twoout(4);
c22=twoout(5);
c23=twoout(6);
c31=threeout(4);
c32=threeout(5);
c33=threeout(6);
c41=fourout(4);
c42=fourout(5);
c43=fourout(6);
c51=fiveout(4);
c52=fiveout(5);
c53=fiveout(6);
c61=sixout(4);
c62=sixout(5);
c63=sixout(6);
c71=sevout(4);
c72=sevout(5);
c73=sevout(6);
c81=eightout(4);
```

```
c82=eightout(5);
c83=eightout(6);
C1out=[c11 c21 c31 c41 c51 c61 c71 c81];
C2out=[c12 c22 c32 c42 c52 c62 c72 c82];
C3out=[c13 c23 c33 c43 c53 c63 c73 c83];
figure(2)
plot(count,C1out,'r+',count,C2out,'g+',count,C3out,'b+')
s11=oneout(7);
s12=oneout(8);
s13=oneout(9);
s21=twoout(7);
s22=twoout(8);
s23=twoout(9);
s31=threeout(7);
s32=threeout(8);
s33=threeout(9);
s41=fourout(7);
s42=fourout(8);
s43=fourout(9);
s51=fiveout(7);
s52=fiveout(8);
s53=fiveout(9);
s61=sixout(7);
s62=sixout(8);
s63=sixout(9);
s71=sevout(7);
s72=sevout(8);
s73=sevout(9);
s81=eightout(7);
s82=eightout(8);
s83=eightout(9);
S1out=[s11 s21 s31 s41 s51 s61 s71 s81];
S2out=[s12 s22 s32 s42 s52 s62 s72 s82];
S3out=[s13 s23 s33 s43 s53 s63 s73 s83];
figure(3)
semilogy(count,S1out,'r+',count,S2out,'g+',count,S3out,'b+')
d11=oneout(10);
d12=oneout(11);
d13=oneout(12);
d21=twoout(10);
d22=twoout(11);
d23=twoout(12);
d31=threeout(10);
d32=threeout(11);
d33=threeout(12);
d41=fourout(10);
d42=fourout(11);
d43=fourout(12);
d51=fiveout(10);
d52=fiveout(11);
d53=fiveout(12);
d61=sixout(10);
d62=sixout(11);
d63=sixout(12);
d71=sevout(10);
d72=sevout(11);
d73=sevout(12);
```

```
        d81=eightout(10);
        d82=eightout(11);
        d83=eightout(12);
        D1out=[d11 d21 d31 d41 d51 d61 d71 d81];
        D2out=[d12 d22 d32 d42 d52 d62 d72 d82];
        D3out=[d13 d23 d33 d43 d53 d63 d73 d83];
        figure(4)
        plot(count,D1out,'r+',count,D2out,'g+',count,D3out,'b+')
        k1=oneout(extra1:krange);
        k2=twoout(extra1:krange);
        k3=threeout(extra1:krange);
        k4=fourout(extra1:krange);
        k5=fiveout(extra1:krange);
        k6=sixout(extra1:krange);
        k7=sevout(extra1:krange);
        k8=sevout(extra1:krange);
        Kout=[k1 k2 k3 k4 k5 k6 k7 k8];
        wave=wavelength(1:ksize);
        figure(5)
        semilogy(wave,k1,wave,k2,wave,k3,wave,k4,wave,k5,wave,k6,wave,k7, ...
                 wave,k8)
        legend('one','two','three','four','five','six','seven','eight', ...
               'location','southeast')
        save(ksave,'-append','B1out','B2out','C1out','C2out','S1out', ...
        'S2out','D1out','D2out','Kout','oneout')
    end
        load('variables.mat','smldat','meddat','bigdat')

[rc]=HapkeEval3_PP(oneout,ksize,krange,smldat,meddat,bigdat,wavelength);

clear
```

HapkeEval3_PP.m

```
%This program evaluates and plots outputs from the minimization routine.
%This is not a standalone program, it must be run from HapkeEval2
function[rc]=HapkeEval3_PP(oneout,ksize,krange,smldat,meddat,bigdat, ...
            wavelength)
%IMPORT DATA FILE to which minimization is performed
%extract sizes for general plotting
   load('variables.mat','endindex');
   load('variables.mat','startindex');
   load('variables.mat','kone','ktwo','kthree','kfour')
%load variables
   load('variables.mat','thetai','thetae','PoreK1','PoreK2','PoreK3', ...
         'u0K1','u0K2','u0K3','uK1','uK2','uK3','isow','cosg','u0','u','n1');
   n=n1;
%import data for plotting
   sml=importdata(smldat);
   sml=sml(:,2);
   sml=sml(startindex:endindex);
   med=importdata(meddat);
   med=med(:,2);
   med=med(startindex:endindex);
   big=importdata(bigdat);
   big=big(:,2);
   big=big(startindex:endindex);
%UNPACK VARIABLES
   b1=oneout(1);
   b2=oneout(2);
   b3=oneout(3);
   c1=oneout(4);
   c2=oneout(5);
   c3=oneout(6);
   s1=oneout(7);
   s2=oneout(8);
   s3=oneout(9);
   D1=oneout(10);
   D2=oneout(11);
   D3=oneout(12);
   k=oneout(13:krange);
   k=cat(2,kone,ktwo,kthree,kfour,k);
   waverange=ksize+4;
   wavelength=wavelength(1:waverange); %row
   save('variables.mat','-append','waverange');
%run though to get rc
[rc]=MasterHapke3_PP(b1,b2,b3,c1,c2,c3,s1,s2,s3,k,D1,D2,D3,wavelength,n,...
      u0,u,u0K1,u0K2,u0K3,uK1,uK2,uK3,cosg,isow,PoreK1,PoreK2,PoreK3);
%import grain size dependent ks
   kb=importdata('bigk.mat');
   kb=kb.k2;
   kb=kb(startindex:endindex);
   km=importdata('medk.mat');
   km=km.k2;
   km=km(startindex:endindex);
   ks=importdata('smlk.mat');
   ks=ks.k2;
```

```
    ks=ks(startindex:endindex);
    waverange21=waverange+1;
    waverange22=waverange*2;
    waverange31=waverange22+1;
    waverange32=waverange*3;
    figure(6)
    plot(wavelength,rc(1:waverange),wavelength,sml)
    set(gca,'Fontsize',16);
    set(gca,'XLim',[0.35 2.5]);
    xlabel('Wavelength (\mum)');
    ylabel('Radiance (%)');
    legend('fit','data ','location','southeast');
    figure(7)
    plot(wavelength,rc(waverange21:waverange22),wavelength,med)
    set(gca,'Fontsize',16);
    set(gca,'XLim',[0.35 2.5]);
    xlabel('Wavelength (\mum)');
    ylabel('Radiance (%)');
    legend('fit','data ','location','southeast');
    figure(8)
    plot(wavelength,rc(waverange31:waverange32),wavelength,big)
    set(gca,'Fontsize',16);
    set(gca,'XLim',[0.35 2.5]);
    xlabel('Wavelength (\mum)');
    ylabel('Radiance (%)');
    legend('fit','data ','location','southeast');
    figure(9)
    semilogy(wavelength,kb,wavelength,km,wavelength,ks,wavelength,k)
    set(gca,'Fontsize',16);
    set(gca,'XLim',[0.35 2.5]);
    xlabel('Wavelength (\mum)');
    ylabel('k');
    legend('big k','med k','small k','multi grain-size k','location','north');
end
```

MasterKcombine.m

```
%This script takes data from vnir k and dispersion k and turns it into a
%single adjusted vector with help from the user
%load dispersion data
   load(loadfile4)
   load(loadfile5)
%plot k vs. frequency
   figure(1)
   plot(v,k)
   xlabel('Wavenumber (cm-1)')
   ylabel('k')
   title('MIR k')
%load vnir data
   load(ksave,'Kout','wavelength');
   load('variables.mat','endindex');
   load('variables.mat','foolsindex');
   load('variables.mat','lamdiff');
   load('variables.mat','ksize');
   lam=wavelength(1:ksize);%vnir wavelength
   vnirk=K(1:ksize);%K data
%work in column vectors
   if size(lam,2)>size(lam,1)
      lam=lam';
   end
   if size(vnirk,2)>size(vnirk,1)
      vnirk=vnirk';
   end
   if size(k,2)>size(k,1)
      k=k';
   end
   if size(v,2)>size(v,1)
      v=v';
   end
%plot vnir data
   figure(2)
   plot(lam,vnirk)
   xlabel('Wavelength (um)')
   ylabel('k')
   title('VNIR k')
%here is where we do a little modelling magic to make the arrays meet
%in case you cut off some noise at the end
%first, get a frequency space vector for vnirk
   vnirv=10000./lam;
%find the low end of vnirv
   if vnirv(1)>vnirv(end);
      vnirvend=vnirv(end);
   else
      vnirvend=vnirv(1);
      end
%find high end of v
   if v(1)>v(end);
      vend=v(1);
   else
      vend=v(end);
```

```
   end
%next, check to make sure we need to do this modelling
   if vend<vnirvend
      newend=10000/vend-lamdiff;
      %fit the end of the data so that it will meet the MIR data
      %REQUIRES DIFFERENT FUCNTION SOMETIMES, TRY POLY3 and POLY4
      %define end of curve to fit (must be column vectors)
      ep=length(lam);
      sp=ep-50;
      shortlam=lam(sp:ep);
      shortvnirk=vnirk(sp:ep);
      %fit curve
      f=fit(shortlam,shortvnirk,'poly3');
      %extract fit coefficients
      fcoef=coeffvalues(f);
      %extrapolate the end of lam
      lamend=lam(end):lamdiff:newend;
      lamend=lamend';
      %evaluate the function over the new range
      extrak=feval(f,lamend);
      %plot it to see how we did
      figure(3)
      plot(lam,vnirk,lamend,extrak,'r')
      legend('VNIRk','extended fit','location','north')
      xlabel('Wavelength (um)')
      ylabel('k')
      title('extended VNIR k')
   else
      fvnirk=vnirk;
      flam=lam;
   end
%HERE IS WHERE WE ADJUST THE MIR DATA DOWN TO THE VNIR DATA (n would go up
%based on epsilon infinity values so k goes down)
%combine fit end with data (for this step only)
   fvnirk=cat(1,vnirk,extrak);
   flam=cat(1,lam,lamend);
%make sure we are picking the right end by checking frequency space
   if 10000/flam(1)>10000/flam(end) %picks the low frequency end
      low=fvnirk(end);
   else
      low=fvnirk(1);
   end
%next make sure we are picking right end of MIR data
   if v(1)>v(end) % picks the high frequency end
      hi=k(1);
   else
      hi=k(end);
   end
%find difference between the two k values
   offset=hi-low;
%correct for offset in MIR data
   adjk=k-offset;
%plot it to make sure it worked
   figure(4)
   plot(v,k,v,adjk)
   xlabel('Wavenumber (cm-1)')
   ylabel('k')
```

```
   legend('MIRk','adjusted MIRk','location','northeast')
   title('MIR k adjustment')
%make column vectors
   if size(adjk,2)>size(adjk,1)
      adjk=adjk';
   end
   if size(vnirv,2)>size(vnirv,1)
      vnirv=vnirv';
   end
%plot to make sure it worked
   figure(5)
   plot(vnirv,vnirk)
%make sure frequency is ascending
   if vnirv(1)>vnirv(end)
      vnirv=flipdim(vnirv,1);
      vnirk=flipdim(vnirk,1);
   end
   if v(1)>v(end)
      v=flipdim(v,1);
      adjk=flipdim(adjk,1);
   end
%we don't like negative data, we are positive people
   negind=find(adjk<0);
   newstart=max(negind)+1;
   v=v(newstart:end);
   adjk=adjk(newstart:end);
%cat them together (mid ir will always be first in frequency space)
   fullv=cat(1,v,vnirv);
   fullk=cat(1,adjk,vnirk);
   figure(6)
   semilogy(fullv,fullk,v,adjk,vnirv,vnirk)
   xlabel('Wavenumber (cm-1)')
   ylabel('k')
   legend('combined k','adjusted MIRk','VNIR k','location','northeast')
   title('combined k')
%get info on first and last element to re interpolate
   first=fullv(1);
   last=fullv(end);
   sizev=length(fullv);
%reinterpolate so vector is evenly spaced
   evenfullv=linspace(first,last,sizev);
   evenfullk=interp1(fullv,fullk,evenfullv);
   figure(7)
   semilogy(fullv,fullk,'r',evenfullv,evenfullk)
   xlabel('Wavenumber (cm-1)')
   ylabel('k')
   legend('k','evenly spaced k','location','northeast')
%save to a .mat file
   save(kfullsave,'evenfullv','evenfullk')
```

MasterSSKK.m

```
%*********************************************************
%******************SSKKconversion*************************
%*********************************************************
%This program performs a subtractive kramers kronig to get the
% real index of refraction, n, from the imaginary index of
%refraction, k.
%figure out if there is MIR data
   if fullk==0 %this will only happen if fullk was not redefined in
               MASTERPROGRAM
      %import k data in INCREASING FREQUENCY (use kcombine.m to make this)
      load(kfullsave);
   else
      load('variables.mat','waverange','startindex','endindex');
      vnirk=load(k1save,'K');
      vnirk=K(1:waverange);
      load(k1save','wavelength');
      wavelength=wavelength(startindex:endindex);
      vnirv=10000./wavelength;
      %make sure frequency is ascending
         if vnirv(1)>vnirv(end)
            vnirv=flipdim(vnirv,1);
            vnirk=flipdim(vnirk,1);
         end
      %get info on first and last element to re interpolate
      first=vnirv(1);
      last=vnirv(end);
      sizev=length(vnirv);
      %reinterpolate so vector is evenly spaced
      evenfullv=linspace(first,last,sizev);
      evenfullk=interp1(vnirv,vnirk,evenfullv);
   end
%kap=k;
%simplify names
   kap=evenfullk; clear evenfullk;
   v=evenfullv; clear evenfullv;
%define size of data set
   sizev=length(v);
%define the real index of refraction and the anchor point
   load('variables','n1')
   lam1=anchor; %average of sodium D doublet
   v1=10000/lam1; %converted to frequency
%define del which allows for calculation at asymptotes
   del=0.000001;
   delsml=0.001;
   intnb=1000; %specifies the number of intervals to run approximation
   halfv=(v(2)-v(1))/2;
%make start point and end point values for integration that place k at the
%center of each range
   for l=1:1:sizev
      sp(l)=v(l)-halfv; %start point of matrix value
      ep(l)=v(l)+halfv; %end point of matrix value
   end
%create dummy array to speed up computation
```

```
   Q=zeros(sizev,1);
   sumX=0;
   sumX2=0;
   sumW=0;
   sumW2=0;
   sumM=0;
%find asymptote #2=>Specifies the EXACT location of the asymptote
   dist1=abs(sp-v1);
   [min_val1,min_loc1]=min(dist1); %find what sp it is closest to
   v1a=v1+halfv;
   dist2=abs(sp-v1a);
   [min_val2,min_loc2]=min(dist2); %if you subtract a half step or add half a
step
   v1b=v1-halfv; %is it still closest to that point?
   dist3=abs(sp-v1b); %this lets you know if it is in between
   [min_val3,min_loc3]=min(dist3); %sp(i) and sp(i+1) or sp(i) and sp(i-1)
   if min_loc1==min_loc3 %define the second asymptote based on results
      bad=min_loc1;
   elseif min_loc1==min_loc2
      bad=min_loc1-1;
   end
%Set up loop in v0 (the wavelength at which we are getting a single value
%of n
   for j=1:1:sizev
      q=zeros(sizev,1);
      %make a counter for progress
      D=j
      %define value of v_0 for each itereation
      v0=v(j);
      %set up loop where each step, i, is an integral of the small space
      %between two frequencies sp(i) and ep(i) (half way between v(i)s) where
      kap can %assumed constant
      %fi=f at ith point in loop
      %fip1=f at f(ith+1)th point in loop
      %fm=f lying halfway between fi and fip1 in loop
      %loops were converted into a series of matrices and summing functions
      %to make an approximation of the integral using Simpson's Rule
      for i=1:1:sizev
         %account for singularities (determine principal value of function)
         if i==j %this takes care of the case where v_0=v
            x1=v(i)-del;
            h1=abs(x1-sp(i))/intnb; %width of each interval
            x1=sp(i):h1:x1; %fine mesh for calculation
            y1=(x1.*kap(i))./((x1.^2-v0^2).*(x1.^2-v1^2)); %evaluate f at x1
            X1 = x1(2:end)-x1(1:end-1); %vectorized form of dx
            Y1 = y1(2:end)+y1(1:end-1) +4.0.*((y1(2:end)+y1(1:end-
            1))./2.0); %vectorized f1 = (1/6)*sum(X1.*Y1); %vectorized
            version of loop
            x2=v(i)+del;
            h2=abs(ep(i)-x2)/intnb; %width of each interval
            x2=x2:h2:ep(i); %fine mesh for calculation
            y2=(x2.*kap(i))./((x2.^2-v0^2).*(x2.^2-v1^2)); %evaluate f at x2
            X2 = x2(2:end)-x2(1:end-1); %vectorized form of dx
            Y2 = y2(2:end)+y2(1:end-1)+4.0.*((y2(2:end)+y2(1:end-
            1))./2.0); %vectorized f2 = (1/6)*sum(X2.*Y2); %vectorized
            version of loop
            q(i)=f1+f2; %sum the two halves
```

```
        elseif i==bad %this takes care of the case where v_1=v
            w1=v1-delsml;
            h1=abs(w1-sp(i))/intnb; %width of each interval
            w1=sp(i):h1:w1; %fine mesh for calculation
            z1=(w1.*kap(i))./((w1.^2-v0^2).*(w1.^2-v1^2)); %evaluate f at z1
            W1 = w1(2:end)-w1(1:end-1); %vectorized form of dx
            Z1 = z1(2:end)+z1(1:end-1)+4.0.*((z1(2:end)+z1(1:end-
            1))./2.0); %vectorized f1 = (1/6)*sum(W1.*Z1); %vectorized
            version of loop
            w2=v1+delsml;
            h2=abs(ep(i)-w2)/intnb; %width of each interval
            w2=w2:h2:ep(i); %fine mesh for calculation
            z2=(w2.*kap(i))./((w2.^2-v0^2).*(w2.^2-v1^2)); %evaluate f at z2
            W2 = w2(2:end)-w2(1:end-1); %vectorized form of dx
            Z2 = z2(2:end)+z2(1:end-1)+4.0.*((z2(2:end)+z2(1:end-
            1))./2.0); %vectorized f2 = (1/6)*sum(W2.*Z2); %vectorized
            version of loop
            q(i)=f1+f2; %sum the two halves
        else %integrate the main part of the function
            x=v(i);
            h=abs(ep(i)-sp(i))/intnb; %width of each interval
            x=sp(i):h:ep(i); %fine mesh for calculation
            y=(x.*kap(i))./((x.^2-v0^2).*(x.^2-v1^2));
            X = x(2:end)-x(1:end-1); %vectorized form of dx
            Y = y(2:end)+y(1:end-1)+4.0.*((y(2:end)+y(1:end-
            1))./2.0); %vectorized f = (1/6)*sum(X.*Y); %vectorized version
            of loop
            q(i)=f;
        end
      end
      %sum all the values of integration for final solution and arrange
      %into a vector by value of omega used for integration
      Q(j)=sum(q);
      %calculate the real index of refraction for each j
      n(j)=n1+((2/pi)*(v0^2-v1^2))*Q(j);
   end
   save(nsave2,'v','n','v1','n1')
%extract VNIR n and save to different file for later
   vlam=10000./v;
%make sure in same order as k will be
   if vlam(1)>vlam(end)
      vlam=flipdim(vlam,2);
      n=flipdim(n,2);
   end
   load('variables.mat','lend','lstart','lamdiff')
%find the end point of n to match k
%having trouble with end points right now so just cutting them for now
   lstart=lstart+5*lamdiff;
   dist=abs(vlam-lend);
   [minval,minloc]=min(dist);
   upend=minloc;
   dist=abs(vlam-lstart);
   [minval,minloc]=min(dist);
   downend=minloc;
%plot to make sure it is ok
   figure(1)
   plot(vlam(1:upend),n(1:upend),'r',vlam(downend:upend),n(downend:upend))
```

```
   legend('n cropped at high wavelengths','n cropped at low wavelengths'...
         ,'location','south')
%reinterpolate to same spacing as k
   visvlam=vlam(downend:upend);
   vnirn=n(downend:upend);
   vislam=lstart:lamdiff:lend;
   visn=interp1(visvlam,vnirn,vislam,'linear','extrap');
   figure(2)
   plot(visvlam,vnirn,vislam,visn)
   legend('n','reinterpolated n','location','south')
   xlabel('Wavelength (um)')
   ylabel('n')
   title('VNIR n')
   save(nsave,'vislam','visn')
%save some stuff for later
   lstart2=lstart;
   lend2=lend;
   save('variables.mat','-append','lstart2','lend2')
```

MasterPhase1_PP.m

```
%This program will use data from multiple viewing geometries to calculate
%phase function parameters for a sample where k and n for i=30, e=0 is
% already known.
%This program downsamples the data and then uses a
%minimization routine to find the best wavelength dependent b and c
%coefficients for the phase function by minimizing the difference between
%the calculated and observed data for multiple viewing geometries and
%multiple grain sizes simultaneously.
%define upper and lower wavelength bounds for good data
   load('variables','lstart2','lend2','low','lamdiff');
%find indices of those values in the wavelength vector
   lowind=find(abs(wave-low)<=eps);
   highind=find(abs(wave-lend2)<=eps);
%recreate the wavelength vector
   wave=wave(lowind:highind);
%make sure data is column
   if length(in15b(1,:))>length(in15b(:,1));
      in15b=in15b';
      in20b=in20b';
      in25b=in25b';
      in30b=in30b';
      in35b=in35b';
      in40b=in40b';
      in45b=in45b';
      in15b=in15m';
      in20b=in20m';
      in25b=in25m';
      in30b=in30m';
      in35b=in35m';
      in40b=in40m';
      in45b=in45m';
      in15b=in15s';
      in20b=in20s';
      in25b=in25s';
      in30b=in30s';
      in35b=in35s';
      in40b=in40s';
      in45b=in45s';
   end
%extract reflectance data over new, smaller range
   i15e0a=in15b(lowind:highind);
   i20e0a=in20b(lowind:highind);
   i25e0a=in25b(lowind:highind);
   i30e0a=in30b(lowind:highind);
   i35e0a=in35b(lowind:highind);
   i40e0a=in40b(lowind:highind);
   i45e0a=in45b(lowind:highind);
   i15e0b=in15m(lowind:highind);
   i20e0b=in20m(lowind:highind);
   i25e0b=in25m(lowind:highind);
   i30e0b=in30m(lowind:highind);
   i35e0b=in35m(lowind:highind);
   i40e0b=in40m(lowind:highind);
```

```
    i45e0b=in45m(lowind:highind);
    i15e0c=in15s(lowind:highind);
    i20e0c=in20s(lowind:highind);
    i25e0c=in25s(lowind:highind);
    i30e0c=in30s(lowind:highind);
    i35e0c=in35s(lowind:highind);
    i40e0c=in40s(lowind:highind);
    i45e0c=in45s(lowind:highind);
%extend data into UV based on assumptions
%extrapolate left side of k to 0.2 using ahrekiel's constant method
%Cloutis 2008b shows that jarsotie is essentially flat from 200-400nm
    leftw=[lstart2:lamdiff:wave(1)];
    head=length(leftw);
    UV15a=linspace(i15e0a(1),i15e0a(1),head); %these are going to overlap by 1
    UV20a=linspace(i20e0a(1),i20e0a(1),head);
    UV25a=linspace(i25e0a(1),i25e0a(1),head);
    UV30a=linspace(i30e0a(1),i30e0a(1),head);
    UV35a=linspace(i35e0a(1),i35e0a(1),head);
    UV40a=linspace(i40e0a(1),i40e0a(1),head);
    UV45a=linspace(i45e0a(1),i45e0a(1),head);
    UV15b=linspace(i15e0b(1),i15e0b(1),head);
    UV20b=linspace(i20e0b(1),i20e0b(1),head);
    UV25b=linspace(i25e0b(1),i25e0b(1),head);
    UV30b=linspace(i30e0b(1),i30e0b(1),head);
    UV35b=linspace(i35e0b(1),i35e0b(1),head);
    UV40b=linspace(i40e0b(1),i40e0b(1),head);
    UV45b=linspace(i45e0b(1),i45e0b(1),head);
    UV15c=linspace(i15e0c(1),i15e0c(1),head);
    UV20c=linspace(i20e0c(1),i20e0c(1),head);
    UV25c=linspace(i25e0c(1),i25e0c(1),head);
    UV30c=linspace(i30e0c(1),i30e0c(1),head);
    UV35c=linspace(i35e0c(1),i35e0c(1),head);
    UV40c=linspace(i40e0c(1),i40e0c(1),head);
    UV45c=linspace(i45e0c(1),i45e0c(1),head);
%change orientation of arrays
    UV15a=UV15a';
    UV20a=UV20a';
    UV25a=UV25a';
    UV30a=UV30a';
    UV35a=UV35a';
    UV40a=UV40a';
    UV45a=UV45a';
    UV15b=UV15b';
    UV20b=UV20b';
    UV25b=UV25b';
    UV30b=UV30b';
    UV35b=UV35b';
    UV40b=UV40b';
    UV45b=UV45b';
    UV15c=UV15c';
    UV20c=UV20c';
    UV25c=UV25c';
    UV30c=UV30c';
    UV35c=UV35c';
    UV40c=UV40c';
    UV45c=UV45c';
    leftw=leftw';
```

```
%cat the data together
   i15e0a=cat(1,UV15a,i15e0a(2:end));
   i20e0a=cat(1,UV20a,i20e0a(2:end));
   i25e0a=cat(1,UV25a,i25e0a(2:end));
   i30e0a=cat(1,UV30a,i30e0a(2:end));
   i35e0a=cat(1,UV35a,i35e0a(2:end));
   i40e0a=cat(1,UV40a,i40e0a(2:end));
   i45e0a=cat(1,UV45a,i45e0a(2:end));
   i15e0b=cat(1,UV15b,i15e0b(2:end));
   i20e0b=cat(1,UV20b,i20e0b(2:end));
   i25e0b=cat(1,UV25b,i25e0b(2:end));
   i30e0b=cat(1,UV30b,i30e0b(2:end));
   i35e0b=cat(1,UV35b,i35e0b(2:end));
   i40e0b=cat(1,UV40b,i40e0b(2:end));
   i45e0b=cat(1,UV45b,i45e0b(2:end));
   i15e0c=cat(1,UV15c,i15e0c(2:end));
   i20e0c=cat(1,UV20c,i20e0c(2:end));
   i25e0c=cat(1,UV25c,i25e0c(2:end));
   i30e0c=cat(1,UV30c,i30e0c(2:end));
   i35e0c=cat(1,UV35c,i35e0c(2:end));
   i40e0c=cat(1,UV40c,i40e0c(2:end));
   i45e0c=cat(1,UV45c,i45e0c(2:end));
   wave=cat(1,leftw,wave(2:end));
   waveend=wave(end);
%make a coarse wavelength vector to speed up fitting (0.05 for coarse,
%0.001 for normal)
   coarsewave=wave(1):0.05:waveend;
%create a variable describing the length of that vector
   sizep=length(coarsewave);
%extract data for coarser wavelength vector
   g15a=interp1(wave,i15e0a,coarsewave);
   g20a=interp1(wave,i20e0a,coarsewave);
   g25a=interp1(wave,i25e0a,coarsewave);
   g30a=interp1(wave,i30e0a,coarsewave);
   g35a=interp1(wave,i35e0a,coarsewave);
   g40a=interp1(wave,i40e0a,coarsewave);
   g45a=interp1(wave,i45e0a,coarsewave);
   g15b=interp1(wave,i15e0b,coarsewave);
   g20b=interp1(wave,i20e0b,coarsewave);
   g25b=interp1(wave,i25e0b,coarsewave);
   g30b=interp1(wave,i30e0b,coarsewave);
   g35b=interp1(wave,i35e0b,coarsewave);
   g40b=interp1(wave,i40e0b,coarsewave);
   g45b=interp1(wave,i45e0b,coarsewave);
   g15c=interp1(wave,i15e0c,coarsewave);
   g20c=interp1(wave,i20e0c,coarsewave);
   g25c=interp1(wave,i25e0c,coarsewave);
   g30c=interp1(wave,i30e0c,coarsewave);
   g35c=interp1(wave,i35e0c,coarsewave);
   g40c=interp1(wave,i40e0c,coarsewave);
   g45c=interp1(wave,i45e0c,coarsewave);
%cat together data vectors for fitting
   DATA=cat(2,g15a,g20a,g25a,g30a,g35a,g40a,g45a,g15b,g20b,g25b,g30b,...
         g35b,g40b,g45b,g15c,g20c,g25c,g30c,g35c,g40c,g45c);
%create wavelength vector for fitting
   X=cat(2,coarsewave,coarsewave,coarsewave,coarsewave,coarsewave,...
      coarsewave,coarsewave);
```

```
%create coefficient array - this is what the program is solving for
%lower limit for b
   lowbv1=linspace(lowb,lowb,sizep);
%lower limit for c
   lowcv=linspace(lowc,lowc,sizep);
%lower bound;
   lb=cat(2,lowbv1,lowcv,90/3,63/3,45/3,0.00,0,0,1);
%upper limit for b
   upbv1=linspace(upb,upb,sizep);
%upper limit for c
   upcv=linspace(upc,upc,sizep);
%upper bound
   ub=cat(2,upbv1,upcv,125,90,63,.06,.06,.06,10);
%starting values for b
   b1=linspace(bguess,bguess,sizep);
%starting values for c
   c=linspace(cguess,cguess,sizep);
%guess for a k scale factor
   scale=1;
%coefficient guess array
   coefg=cat(2,b1,c,D1,D2,D3,s1,s2,s3,scale);
% save('variables.mat','coarsewave','size');
% Import data for K and N matrices
   load(ksave,'oneout','wavelength');
   load('variables.mat','extra1','ksize')
   ksize2=ksize+extra1;
   wavesize=length(wavelength)/3;
   extra=wavesize-ksize;
   kwave=wavelength(extra+1:wavesize);
   K=oneout(extra1+1:ksize2);
   N=importdata(nsave,'visn','vislam');
   v=N.vislam;
   N=N.visn;
   nsize=length(N);
%make sure the arrays are all the same length
   if v(1)>kwave(1)
      offset=v(1)-kwave(1);
      indexoff=offset/lamdiff;
      newstart=indexoff+1;
      kwave=kwave(newstart:end);
      K=K(newstart:end);
   end
%find k for wavelengths in coarsewave
   k=interp1(kwave,K,coarsewave);
   n=interp1(v,N,coarsewave);
%make sure they are column vectors
   if length(k(1,:))>length(k(:,1))
      k=k';
   end
   if length(n(1,:))>length(n(:,1))
      n=n';
   end
%expand n to match b and c - must expand k in wrapper to add in scale
%factor
   n=cat(1,n,n,n,n,n,n,n);
%define thetai and thetae (as many angles as sets of angle data)
   thetai=[-15 -20 -25 -30 -35 -40 -45];
```

```
   thetae=[0 0 0 0 0 0 0];
   thetai=thetai;
%expand thetas so there is one thetai and one thetae for each set of
%wavelengths (ex: there is a set of 41 thetais of 15 degrees if there are
%41 wavelengths per spectrum)
   ti1=linspace(thetai(1),thetai(1),sizep);
   ti2=linspace(thetai(2),thetai(2),sizep);
   ti3=linspace(thetai(3),thetai(3),sizep);
   ti4=linspace(thetai(4),thetai(4),sizep);
   ti5=linspace(thetai(5),thetai(5),sizep);
   ti6=linspace(thetai(6),thetai(6),sizep);
   ti7=linspace(thetai(7),thetai(7),sizep);
   te1=linspace(thetae(1),thetae(1),sizep);
   te2=linspace(thetae(2),thetae(2),sizep);
   te3=linspace(thetae(3),thetae(3),sizep);
   te4=linspace(thetae(4),thetae(4),sizep);
   te5=linspace(thetae(5),thetae(5),sizep);
   te6=linspace(thetae(6),thetae(6),sizep);
   te7=linspace(thetae(7),thetae(7),sizep);
   thetai=[ti1 ti2 ti3 ti4 ti5 ti6 ti7];
   thetai=thetai';
   thetae=[te1 te2 te3 te4 te5 te6 te7];
   thetae=thetae';
%PERFORM OTHER TIME CONSUMING CALCULATIONS
   load('variables.mat','Bg');
   Bgplus1=Bg+1;
%Phase angle (g)
   g=d2r(abs(thetae-thetai));
%cos(g)
   cosg=cos(g);
%u_0
   u0=cos(d2r(thetai));
%u
   u=cos(d2r(thetae));
   load('variables.mat','PoreK1','PoreK2','PoreK3');
   u0K1=u0/PoreK1;
   u0K2=u0/PoreK2;
   u0K3=u0/PoreK3;
   uK1=u/PoreK1;
   uK2=u/PoreK2;
   uK3=u/PoreK3;
%load the data for the calibrated spectralon standard
   load('calspecw2.mat');
   calspecw=best;
%load its wavelength vector
   load('specwave2.mat');
%define extended start point
   lowlam2=wave(1);
%make these coarse and shorter like the other spectral data
   lowind2=find(abs(specwave-lowlam2)<=eps);
   highind2=find(abs(specwave-waveend)<=eps);
%recreate the wavelength vector
   isowave=specwave(lowind2:highind2);
   shortspecw=calspecw(lowind2:highind2);
   isow=interp1(isowave,shortspecw,coarsewave);
%make sure it is a column vector
   if length(isow(1,:))>length(isow(:,1))
```

```
      isow=isow';
   end
%expand to match b and c
   isow=cat(1,isow,isow,isow,isow,isow,isow,isow);
%create size variable for later calculation
   sizeb=length(DATA)/3;
%Create an anonymous function in order to pass coarsewave, size, K and N
% as extra parameters to the objective function.
   myObjFcn = @(coefg,X)MasterPhaseWrapper(coefg,X,k,n,cosg,u0,u,u0K1,...
         u0K2,u0K3,uK1,uK2,uK3,isow,sizep,sizeb,PoreK1',PoreK2,PoreK3);
%USE LSQCURVEFIT TO PERFORM LEAST SQUARES MINIMIZATION between data and
%model. Format is [output]=lsqcurvefit(function,x0,xdata,ydata,lb,ub)
   options=optimoptions(@lsqcurvefit,'Algorithm', ...
         'trust-region-reflective','Display','iter','MaxIter',maxit, ...
         'FinDiffType','central','MaxFunEvals',maxfun, 'TolFun', ...
         funtol,'TolX', xtol);
   problem = createOptimProblem('lsqcurvefit','x0',coefg, ...
         'objective',myObjFcn,'xdata',X,'ydata',DATA,'lb',lb,'ub',ub, ...
         'options',options);
   ms = MultiStart('UseParallel','always');
   [coef,fval,flag,outpt,solutions] = run(ms,problem,spts);
   save(phasesave,'solutions','X','DATA','coarsewave','sizep','isow', ...
      'u0','u','cosg');
```

MasterPhaseWrapper.m

```
function[rc]=MasterPhaseWrapper(coefg,X,k,n,cosg,u0,u,u0K1,...
         u0K2,u0K3,uK1,uK2,uK3,isow,sizep,sizeb,PoreK1,PoreK2,PoreK3)
%wrapper function
%UNPACK VARIABLES
   b1=coefg(1:sizep);
%b2=coefg(40:78);
   size2=sizep+1;
   size3=sizep*2;
   size4=size3+1;
   size5=size3+2;
   size6=size3+3;
   size7=size3+4;
   size8=size3+5;
   size9=size3+6;
   size10=size3+7;
   c=coefg(size2:size3);
   D1=coefg(size4);
   D2=coefg(size5);
   D3=coefg(size6);
   s1=coefg(size7);
   s2=coefg(size8);
   s3=coefg(size9);
   scale=coefg(size10);
%scale k and expand to match length of b and c
   k=scale*k;
   k=cat(1,k,k,k,k,k,k,k);
%expand them to make a single b or c for each set of wavelengths, i.e.,
%each 710nm point has a single b or c but that can be differenct for each
%wavelength
   bs1=cat(2,b1,b1,b1,b1,b1,b1,b1);
%bs2=cat(2,b2,b2,b2,b2,b2,b2,b2,b2,b2
   cs=cat(2,c,c,c,c,c,c,c);
%make sure they are column vectors for program
   if length(bs1(1,:))>length(bs1(:,1))
      bs1=bs1';
   end
   if length(cs(1,:))>length(cs(:,1))
      cs=cs';
   end
   if length(X(1,:))>length(X(:,1))
      X=X';
   end
[rc]=MasterPhase2_PP(bs1,cs,D1,D2,D3,s1,s2,s3,X,k,n,cosg,u0,u,...
         u0K1,u0K2,u0K3,uK1,uK2,uK3,isow,sizeb,PoreK1,PoreK2,PoreK3);
```

MasterPhase2_PP.m

```
%This program performs an iterative minimization using Hapke's radiative
%transfer theory to find the phase function coefficients b and c.
%the guts of the Hapke calculation
function [rc]=MasterPhase2_PP(bs1,cs,D1,D2,D3,s1,s2,s3,X,k,n,cosg,u0,u,...
            u0K1,u0K2,u0K3,uK1,uK2,uK3,isow,sizeb,PoreK1,PoreK2,PoreK3)
%load variables
   sizeb2=sizeb+1;
   sizec=2*sizeb;
   sizec2=sizec+1;
   sized=3*sizeb;
%CALCULATIONS ARE PERFORMED BY GRAIN SIZE
%That means that each set of 7 phase angle spectra are in a row and those
%three rows are end to end by grain size. Here they get separated.
%Currently, the phase function coefficients are not grain size dependent
%but they could be altered pretty easily to be so
%DEFINE RELATIONS
%single particle phase function P(g)
   Pg=1+bs1.*cosg+cs.*(1.5.*(cosg.^2)-0.5);
%initial alpha and k
   Alpha=((4*pi).*k)./X;
%k=(Alpha.*wavelength)/(4*pi*n);
%internal transmission factor
   ri1=(1-sqrt(Alpha./(Alpha+s1)))./(1+sqrt(Alpha./(Alpha+s1)));
   ri2=(1-sqrt(Alpha./(Alpha+s2)))./(1+sqrt(Alpha./(Alpha+s2)));
   ri3=(1-sqrt(Alpha./(Alpha+s3)))./(1+sqrt(Alpha./(Alpha+s3)));
   THETA1=(ri1+exp(-sqrt(Alpha.*(Alpha+s1)).*D1))./ ...
         (1+ri1.*exp(-sqrt(Alpha.*(Alpha+s1)).*D1));
   THETA2=(ri2+exp(-sqrt(Alpha.*(Alpha+s2)).*D2))./ ...
         (1+ri2.*exp(-sqrt(Alpha.*(Alpha+s2)).*D2));
   THETA3=(ri3+exp(-sqrt(Alpha.*(Alpha+s3)).*D3))./ ...
         (1+ri3.*exp(-sqrt(Alpha.*(Alpha+s3)).*D3));
approximate surface reflection coefficient S_E
   Se=((n-1).^2+k.^2)./((n+1).^2+k.^2)+0.05;
%approximate internal scattering coefficient S_I
   Si=1.014-4./(n.*((n+1).^2));
%single scattering albedo
   SSA1=Se+(1-Se).*(((1-Si).*THETA1)./(1-Si.*THETA1));
   SSA2=Se+(1-Se).*(((1-Si).*THETA2)./(1-Si.*THETA2));
   SSA3=Se+(1-Se).*(((1-Si).*THETA3)./(1-Si.*THETA3));
%H function
   gamma1=sqrt(1-SSA1);
   gamma2=sqrt(1-SSA2);
   gamma3=sqrt(1-SSA3);
   r01=(1-gamma1)./(1+gamma1);
   r02=(1-gamma2)./(1+gamma2);
   r03=(1-gamma3)./(1+gamma3);
   Hu01=(1-(1-gamma1).*u0K1.*(r01+(1-0.5.*r01-r01.*u0K1).*log((1+u0K1)./ ...
         u0K1))).^(-1);
   Hu02=(1-(1-gamma2).*u0K2.*(r02+(1-0.5.*r02-r02.*u0K2).*log((1+u0K2)./ ...
         u0K2))).^(-1);
   Hu03=(1-(1-gamma3).*u0K3.*(r03+(1-0.5.*r03-r03.*u0K3).*log((1+u0K3)./ ...
         u0K3))).^(-1);
   Hu1=(1-(1-gamma1).*uK1.*(r01+(1-0.5.*r01-r01.*uK1).*log((1+uK1)./ ...
```

```
        uK1))).^(-1);
   Hu2=(1-(1-gamma2).*uK2.*(r02+(1-0.5.*r02-r02.*uK2).*log((1+uK2)./ ...
        uK2))).^(-1);
   Hu3=(1-(1-gamma3).*uK3.*(r03+(1-0.5.*r03-r03.*uK3).*log((1+uK3)./ ...
        uK3))).^(-1);
%isometric spectralon standard
   isogam=sqrt(1-isow);
   isor0=(1-isogam)./(1+isogam);
   isoHu0=(1-(1-isogam).*u0.*(isor0+(1-0.5.*isor0-isor0.*u0).*log...
        ((1+u0)./u0))).^(-1);
   isoHu=(1-(1-isogam).*u.*(isor0+(1-0.5.*isor0-isor0.*u).*log((1+u)./ ...
        u))).^(-1);
%radiance coefficient
%rc=(SSA./4).*(1./(u+u0)).*((Pg)+(Hu0.*Hu)-1);
   rc1=PoreK1*((SSA1./(4*pi)).*(u./(u+u0)).*((Pg)+(Hu01.*Hu1)-1))./...
        ((isow./(4*pi)).*(u./(u+u0)).*((1)+(isoHu0.*isoHu)-1));
   rc2=PoreK2*((SSA2./(4*pi)).*(u./(u+u0)).*((Pg)+(Hu02.*Hu2)-1))./...
        ((isow./(4*pi)).*(u./(u+u0)).*((1)+(isoHu0.*isoHu)-1));
   rc3=PoreK3*((SSA3./(4*pi)).*(u./(u+u0)).*((Pg)+(Hu03.*Hu3)-1))./...
        ((isow./(4*pi)).*(u./(u+u0)).*((1)+(isoHu0.*isoHu)-1));
%make sure rc is a row vetor to make the fitter happy
   if length(rc1(:,1))>length(rc1(1,:))
      rc1=rc1';
   end
   if length(rc2(:,1))>length(rc2(1,:))
      rc2=rc2';
   end
   if length(rc3(:,1))>length(rc3(1,:))
      rc3=rc3';
   end
%cat them together
   rc=cat(2,rc1,rc2,rc3);
```

MasterPhaseEval1_PP.m

```
%This program evaluates the input and output values of the phase function
%program
%THIS PROGRAM MUST BE RUN BEFORE YOU CLEAR VARABLES
   load(phasesave,'solutions','X','DATA','sizep','isow','coarsewave');
   load('variables.mat','extra1','ksize')
   onein=solutions(1,1).X0;
   onein=onein{1,1};
   oneout=solutions(1,1).X;
   coefg=oneout;
% Import data for K and N matrices here instead of inside the objective
% function.
%K=importdata('011513_synj_k3.mat','K');
   load(ksave,'solutions','wavelength');
   K=solutions(1,1);
   K=K.X;
   kend=ksize+extra1;
   wavesize=length(wavelength)/3;
   extra=wavesize-ksize;
   kwave=wavelength(extra+1:wavesize);
   K=K(extra1+1:kend);
   N=importdata(nsave,'visn','vislam');
   v=N.vislam;
   N=N.visn;
%find k for wavelengths in coarsewave
   k=interp1(kwave,K,coarsewave);
   n=interp1(v,N,coarsewave);
%make sure they are column vectors
   if length(k(1,:))>length(k(:,1))
      k=k';
   end
   if length(n(1,:))>length(n(:,1))
      n=n';
   end
%expand n to match b and c - k is expanded in wrapper to add scale factor
   n=cat(1,n,n,n,n,n,n,n);
%define thetai and thetae (as many angles as sets of angle data)
   thetai=[-15 -20 -25 -30 -35 -40 -45];
   thetae=[0 0 0 0 0 0 0];
%expand thetas so there is one thetai and one thetae for each set of
%wavelengths (ex: there is a set of 41 thetais of 15 degrees if there are
%41 wavelengths per spectrum)
   ti1=linspace(thetai(1),thetai(1),sizep);
   ti2=linspace(thetai(2),thetai(2),sizep);
   ti3=linspace(thetai(3),thetai(3),sizep);
   ti4=linspace(thetai(4),thetai(4),sizep);
   ti5=linspace(thetai(5),thetai(5),sizep);
   ti6=linspace(thetai(6),thetai(6),sizep);
   ti7=linspace(thetai(7),thetai(7),sizep);
   te1=linspace(thetae(1),thetae(1),sizep);
   te2=linspace(thetae(2),thetae(2),sizep);
   te3=linspace(thetae(3),thetae(3),sizep);
   te4=linspace(thetae(4),thetae(4),sizep);
   te5=linspace(thetae(5),thetae(5),sizep);
```

```
   te6=linspace(thetae(6),thetae(6),sizep);
   te7=linspace(thetae(7),thetae(7),sizep);
   thetai=[ti1 ti2 ti3 ti4 ti5 ti6 ti7];
   thetai=thetai';
   thetae=[te1 te2 te3 te4 te5 te6 te7];
   thetae=thetae';
%PERFORM OTHER TIME CONSUMING CALCULATIONS OUT OF LOOP AND FEED THROUGH IN
%IN ANONYMOUS FUNCTION
   load('variables.mat','Bg');
   Bgplus1=Bg+1;
%Phase angle (g)
   g=d2r(abs(thetae-thetai));
%cos(g)
   cosg=cos(g);
%u_0
   u0=cos(d2r(thetai));
%u
   u=cos(d2r(thetae));
   load('variables.mat','PoreK1','PoreK2','PoreK3');
   u0K1=u0/PoreK1;
   u0K2=u0/PoreK2;
   u0K3=u0/PoreK3;
   uK1=u/PoreK1;
   uK2=u/PoreK2;
   uK3=u/PoreK3;
%create size variable for later calculation
   sizeb=length(DATA)/3;
[rc]=MasterPhaseWrapper(coefg,X,k,n,cosg,u0,u,u0K1,...
         u0K2,u0K3,uK1,uK2,uK3,isow,sizep,sizeb,PoreK1,PoreK2,PoreK3);
   a=sizep;
   a2=a+1;
   b=a*2;
   b2=b+1;
   c=a*3;
   c2=c+1;
   d=a*4;
   d2=d+1;
   e=a*5;
   e2=e+1;
   f=a*6;
   f2=f+1;
   g=a*7;
   g2=g+1;
   h=a*8;
   h2=h+1;
   i=a*9;
   i2=i+1;
   j=a*10;
   j2=j+1;
   k=a*11;
   k2=k+1;
   l=a*12;
   l2=l+1;
   m=a*13;
   m2=m+1;
   n=a*14;
   n2=n+1;
```

```
o=a*15;
o2=o+1;
p=a*16;
p2=p+1;
q=a*17;
q2=q+1;
r=a*18;
r2=r+1;
s=a*19;
s2=s+1;
t=a*20;
t2=t+1;
v=a*21;
X=cat(2,X,X,X);
figure(25)
plot(X(1:a),DATA(1:a),'k',X(1:a),rc(1:a),'--r',X(a2:b), ...
   DATA(a2:b)+0.1,'k',X(a2:b),rc(X(b2:c),DATA(b2:c)+0.2,'k', ...
   X(b2:c),rc(b2:c)+0.2,'--r',X(c2:d),DATA(c2:d)+0.3,'k',X(d2:e), ...
   DATA(d2:e)+0.4,'k',X(d2:e),rc(d2:e)+0.4,'--r',X(e2:f), ...
   DATA(e2:f)+0.5,'k',X(f2:g),DATA(f2:g)+0.6,'k',X(f2:g), ...
   rc(f2:g)+0.6,'--r',X(g2:h),DATA(g2:h)+0.7,'k',X(h2:i), ...
   DATA(h2:i)+0.8,'k',X(h2:i),rc(h2:i)+0.8,'--r',X(i2:j), ...
   DATA(i2:j)+0.9,'k',X(j2:k),DATA(j2:k)+1.0,'k',X(j2:k), ...
   rc(j2:k)+1.0,'--r',X(k2:l),DATA(k2:l)+1.1,'k',X(l2:m), ...
   DATA(l2:m)+1.2,'k',X(l2:m),rc(l2:m)+1.2,'--r',X(f2:g), ...
   DATA(f2:g)+1.3,'k',X(n2:o),DATA(n2:o)+1.4,'k',X(n2:o), ...
   rc(n2:o)+1.4,'--r',X(o2:p),DATA(o2:p)+1.5,'k',X(p2:q), ...
   DATA(p2:q)+1.6,'k',X(p2:q),rc(p2:q)+1.6,'--r',X(q2:r), ...
   DATA(q2:r)+1.7,'k',X(r2:s),DATA(r2:s)+1.8,'k',X(r2:s), ...
   rc(r2:s)+1.8,'--r',X(s2:t),DATA(s2:t)+1.9,'k',X(t2:v), ...
   DATA(t2:v)+2.0,'k',X(t2:v),rc(t2:v)+2.0,'--r')
legend('90-125 \mum g=15','g=20','g=25','g=30','g=35','g=40','g=45',...
      '63-90 \mum g=15','g=20','g=25','g=30','g=35','g=40','g=45',...
      '45-63 \mum g=15','g=20','g=25','g=30','g=35','g=40','g=45')
figure(1)
plot(X(1:a),DATA(1:a),X(1:a),rc(1:a))
legend('DATA','i=-15,e=0')
figure(2)
plot(X(a2:b),DATA(a2:b),X(a2:b),rc(a2:b))
legend('DATA','i=-20,e=0')
figure(3)
plot(X(b2:c),DATA(b2:c),X(b2:c),rc(b2:c))
legend('DATA','i=-25,e=0')
figure(4)
plot(X(c2:d),DATA(c2:d),X(c2:d),rc(c2:d))
legend('DATA','i=-30,e=0')
figure(5)
plot(X(d2:e),DATA(d2:e),X(d2:e),rc(d2:e))
legend('DATA','i=-35,e=0')
figure(6)
plot(X(e2:f),DATA(e2:f),X(e2:f),rc(e2:f))
legend('DATA','i=-40,e=0')
figure(7)
plot(X(f2:g),DATA(f2:g),X(f2:g),rc(f2:g))
legend('DATA','i=-45,e=0')
figure(8)
plot(X(g2:h),DATA(g2:h),X(g2:h),rc(g2:h))
```

```
legend('DATA','i=-15,e=0')
figure(9)
plot(X(h2:i),DATA(h2:i),X(h2:i),rc(h2:i))
legend('DATA','i=-20,e=0')
figure(10)
plot(X(i2:j),DATA(i2:j),X(i2:j),rc(i2:j))
legend('DATA','i=-25,e=0')
figure(11)
plot(X(j2:k),DATA(j2:k),X(j2:k),rc(j2:k))
legend('DATA','i=-30,e=0')
figure(12)
plot(X(k2:l),DATA(k2:l),X(k2:l),rc(k2:l))
legend('DATA','i=-35,e=0')
figure(13)
plot(X(l2:m),DATA(l2:m),X(l2:m),rc(l2:m))
legend('DATA','i=-40,e=0')
figure(14)
plot(X(m2:n),DATA(m2:n),X(m2:n),rc(m2:n))
legend('DATA','i=-45,e=0')
figure(15)
plot(X(n2:o),DATA(n2:o),X(n2:o),rc(n2:o))
legend('DATA','i=-15,e=0')
figure(16)
plot(X(o2:p),DATA(o2:p),X(o2:p),rc(o2:p))
legend('DATA','i=-20,e=0')
figure(17)
plot(X(p2:q),DATA(p2:q),X(p2:q),rc(p2:q))
legend('DATA','i=-25,e=0')
figure(18)
plot(X(q2:r),DATA(q2:r),X(q2:r),rc(q2:r))
legend('DATA','i=-30,e=0')
figure(19)
plot(X(r2:s),DATA(r2:s),X(r2:s),rc(r2:s))
legend('DATA','i=-35,e=0')
figure(20)
plot(X(s2:t),DATA(s2:t),X(s2:t),rc(s2:t))
legend('DATA','i=-40,e=0')
figure(21)
plot(X(t2:v),DATA(t2:v),X(t2:v),rc(t2:v))
legend('DATA','i=-45,e=0')
figure(23)
bs1=coefg(1:a);
cs=coefg(a2:b);
plot(coarsewave,coefg(1:a),coarsewave,coefg(a2:b))
figure(24)
longb=cat(2,bs1,bs1,bs1,bs1,bs1,bs1,bs1);
longc=cat(2,cs,cs,cs,cs,cs,cs,cs);
cosg=cosg';
Pg=1+longb.*cosg+longc.*(1.5.*(cosg.^2)-0.5);
plot(X(1:length(X)/3),Pg)
```

MasterHapke4_PP.m

```
%This program performs an iterative minimization using Hapke's radiative
%transfer theory to find a global and grain-size independent value of
%imaginary index of refraction, k using a wavelength dependend n and
%phase function
   load(ksave,'oneout','wavelength');
   load('variables.mat','extra1','lamdiff','ksize','isow')
   ksize2=ksize+extra1;
   wavesize=length(wavelength)/3;
   extra=wavesize-ksize;
   kwave=wavelength(extra+1:wavesize);
   k=oneout(extra1+1:ksize2);
   N=importdata(nsave,'visn','vislam');
   v=N.vislam;
   n=N.visn;
   nsize=length(n);
%make sure the arrays are all the same length
   if v(1)>kwave(1)
      offset=v(1)-kwave(1);
      indexoff=offset/lamdiff;
      newstart=indexoff+1;
      kwave=kwave(newstart:end);
      k=k(newstart:end);
   end
%make sure isow is right length
   if length(isow)>nsize
      indexoff2=length(isow)-nsize+1;
      isow=isow(indexoff2:end);
   end
%load data
   sml=importdata(smldat);
   med=importdata(meddat);
   big=importdata(bigdat);
%make sure column
   if length(sml(:,1))<length(sml(1,:))
      sml=sml';
      med=med';
      big=big';
   end
   wave=sml(:,1);
   sml=sml(:,2);
   med=med(:,2);
   big=big(:,2);
%scale data
   lowind=find(abs(wave-v(1))<=eps);
   highind=find(abs(wave-v(end))<lamdiff/2);%bandaid
%recreate the wavelength vector
   wave=wave(lowind:highind);
%scale the data vectors to the same length
   sml=sml(lowind:highind);
   med=med(lowind:highind);
   big=big(lowind:highind);
%make sure all of these are row vectors
   if length(n(:,1))>length(n(1,:))
```

```
      n=n';
   end
   if length(k(:,1))>length(k(1,:))
      k=k';
   end
   if length(wave(:,1))>length(wave(1,:))
      wave=wave';
   end
   if length(sml(:,1))>length(sml(1,:))
      sml=sml';
   end
   if length(med(:,1))>length(med(1,:))
      med=med';
   end
   if length(big(:,1))>length(big(1,:))
      big=big';
   end
%make vectors for minimization routing
%k
   kone2=k(1);
   ktwo2=k(2);
   k=k(3:end);
   K=cat(2,k,k,k);
%wavelength
   wavelength=cat(2,wave,wave,wave);
%data
   DATA=cat(2,sml,med,big);
   realsize2=length(k);
   fakesize=length(k)+2;
   ksize2=length(K);
%import phase function coefficients
   phase=importdata(phasesave);
   coarsewave=phase.coarsewave;
   phase=phase.solutions.X; %extract solution data
   psize=length(phase)-7; %this accounts for s and D and sk parameters
   phsize=psize/2;
   b=phase(1:phsize);
   c=phase(phsize+1:psize);
%pull out scale factor and s and D as guesses
   s1=phase(end-1);
   s2=phase(end-2);
   s3=phase(end-3);
   D1=phase(end-4);
   D2=phase(end-5);
   D3=phase(end-6);
   scale=phase(end);
%reinterpolate them to full length
   b1=interp1(coarsewave,b,wave,'linear','extrap');
   c1=interp1(coarsewave,c,wave,'linear','extrap');
   save('variables.mat','-append','ksize2','fakesize','realsize2','nsize'...
         ,'kone2','ktwo2')
%load variables
   load('variables.mat','thetai','thetae','PoreK1','PoreK2','PoreK3');
%CREATE A COEFFICIENT GUESS MATRIX to feed to program
   coefg=[s1,s2,s3,D1,D2,D3,K];
%set lower and upper bounds
   lbk=zeros(1,ksize2);
```

```
   extra2=length(coefg)-length(k);
   save('variables.mat','-append','extra2');
   lb=[lows1,lows2,lows3,lowD1,lowD2,lowD3,lbk];
   ubk=linspace(upk,upk,ksize2);
   ub=[ups1,ups2,ups3,upD1,upD2,upD3,ubk];
%DEFINE PHASE RELATION
   g=d2r(abs(thetae-thetai)); %Phase angle (g)
   cosg=cos(g); %cos(g)
   u0=cos(d2r(thetai)); %u_0
   u=cos(d2r(thetae)); %u
%calculate phase function
   Pg=1+b1.*cosg+c1.*(1.5.*(cosg.^2)-0.5);
%change of variables that makes H function easier
   u0K1=u0/PoreK1;
   u0K2=u0/PoreK2;
   u0K3=u0/PoreK3;
%change of variables that makes H function easier
   uK1=u/PoreK1;
   uK2=u/PoreK2;
   uK3=u/PoreK3;
%make sure it is a column vector
   if length(isow(:,1))>length(isow(1,:))
      isow=isow';
   end
%create abstract function to pass through variables
   myObjFcn = @(coefg,wavelength)MASTERWRAPPER2_PP(coefg,wavelength, ...
            kone2,ktwo2,n,u0,u,u0K1,u0K2,u0K3,uK1,uK2,uK3,Pg, ...
            realsize2,fakesize,isow,PoreK1,PoreK2,PoreK3);
%USE LSQCURVEFIT TO PERFORM LEAST SQUARES MINIMIZATION between data and
%model. Levenberg-Marquardt',... 'ScaleProblem','Jacobian'
%Format is [output]=lsqcurvefit(function,x0,xdata,ydata,lb,ub)
   options=optimoptions(@lsqcurvefit,'Algorithm', ...
         'trust-region-reflective','Display','iter','MaxIter',maxit, ...
         'FinDiffType','central','MaxFunEvals',maxfun, 'TolFun', ...
         funtol,'TolX', xtol);
   problem = createOptimProblem('lsqcurvefit','x0',coefg, ...
         'objective',myObjFcn,'xdata',wavelength,'ydata',DATA,'lb', ...
         lb,'ub',ub,'options',options);
   ms = MultiStart('UseParallel','always');
   [coef,fval,exitflag,output,solutions] = run(ms,problem,spts);
   save(ksave2,'solutions','wavelength','kone2','ktwo2','DATA','isow'...
         ,'realsize2','Pg','n','u','u0')
   save('variables.mat','-append','coefg','lb','ub')

Clear
```

MASTERWRAPPER2_PP.m

```
function[rc]=MASTERWRAPPER2_PP(coefg,wavelength,kone2,ktwo2,...
         n,u0,u,u0K1,u0K2,u0K3,uK1,uK2,uK3,Pg,realsize2,fakesize, ...
         isow,PoreK1,PoreK2,PoreK3)
%wrapper function
%UNPACK VARIABLES
   s1=coefg(1);
   s2=coefg(2);
   s3=coefg(3);
   D1=coefg(4);
   D2=coefg(5);
   D3=coefg(6);
   kend=realsize2+6;% +6 (scalars)
   k=coefg(7:kend); %row
   wavelength=wavelength(1:fakesize); %row
%re-extend k
   k=cat(2,kone2,ktwo2,k);
[rc]=MasterHapke5_PP(Pg,s1,s2,s3,k,D1,D2,D3,wavelength,n,...
      u0,u,u0K1,u0K2,u0K3,uK1,uK2,uK3,isow,PoreK1,PoreK2,PoreK3);
```

MasterHapke5_PP.m

```
%the guts of the Hapke calculation
function [rc]=MasterHapke5_PP(Pg,s1,s2,s3,k,D1,D2,D3,wavelength,n,...
         u0,u,u0K1,u0K2,u0K3,uK1,uK2,uK3,isow,PoreK1,PoreK2,PoreK3)
%calculate variables for isotropic standard
   gammai1=sqrt(1-isow);
   r0i1=(1-gammai1)./(1+gammai1);
   isoHu0=(1-isow.*u0.*(r0i1+((1-2.*r0i1.*u0)./2).*log((1+u0)./u0))).^(-1);
   isoHu=(1-isow.*u.*(r0i1+((1-2.*r0i1.*u)./2).*log((1+u)./u))).^(-1);
%FIRST GRAINSIZE
%initial alpha and k
   Alpha=((4*pi).*k)./wavelength;
%k=(Alpha.*wavelength)/(4*pi*n);
%internal transmission factor
   ri1=(1-sqrt(Alpha./(Alpha+s1)))./(1+sqrt(Alpha./(Alpha+s1)));
   THETA1=(ri1+exp(-sqrt(Alpha.*(Alpha+s1)).*D1))./ ...
         (1+ri1.*exp(-sqrt(Alpha.*(Alpha+s1)).*D1));
%approximate surface reflection coefficient S_E
   Se=((n-1).^2+k.^2)./((n+1).^2+k.^2)+0.05;
%approximate internal scattering coefficient S_I
   Si=1.014-4./(n.*((n+1).^2));
%single scattering albedo
   w1=Se+(1-Se).*(((1-Si).*THETA1)./(1-Si.*THETA1));
%H function
   gamma1=sqrt(1-w1);
   r01=(1-gamma1)./(1+gamma1);
   Hu01=(1-w1.*u0K1.*(r01+((1-2.*r01.*u0K1)./2).*log((1+u0K1)./u0K1))).^(-1);
   Hu1=(1-w1.*uK1.*(r01+((1-2.*r01.*uK1)./2).*log((1+uK1)./uK1))).^(-1);
%radiance coefficient
   rc1=PoreK1*((w1./(4*pi))*(u/(u+u0)).*((Pg)+(Hu01.*Hu1)-1))./ ...
      ((isow./(4*pi))*(u/(u+u0)).*((1)+(isoHu0.*isoHu)-1));
%SECOND GRAINSIZE
%internal transmission factor
   ri2=(1-sqrt(Alpha./(Alpha+s2)))./(1+sqrt(Alpha./(Alpha+s2)));
   THETA2=(ri2+exp(-sqrt(Alpha.*(Alpha+s2)).*D2))./ ...
         (1+ri2.*exp(-sqrt(Alpha.*(Alpha+s2)).*D2));
%single scattering albedo
   w2=Se+(1-Se).*(((1-Si).*THETA2)./(1-Si.*THETA2));
%H function
   gamma2=sqrt(1-w2);
   r02=(1-gamma2)./(1+gamma2);
   Hu02=(1-w2.*u0K2.*(r02+((1-2.*r02.*u0K2)./2).*log((1+u0K2)./u0K2))).^(-1);
   Hu2=(1-w2.*uK2.*(r02+((1-2.*r02.*uK2)./2).*log((1+uK2)./uK2))).^(-1);
%radiance coefficient
   rc2=PoreK2*((w2./(4*pi))*(u/(u+u0)).*((Pg)+(Hu02.*Hu2)-1))./ ...
      ((isow./(4*pi))*(u/(u+u0)).*((1)+(isoHu0.*isoHu)-1));
%internal transmission factor
   ri3=(1-sqrt(Alpha./(Alpha+s3)))./(1+sqrt(Alpha./(Alpha+s3)));
   THETA3=(ri3+exp(-sqrt(Alpha.*(Alpha+s3)).*D3))./(1+ri3.*exp(-
         sqrt(Alpha.*(Alpha+s3)).*D3));
%single scattering albedo
   w3=Se+(1-Se).*(((1-Si).*THETA3)./(1-Si.*THETA3));
%H function
   gamma3=sqrt(1-w3);
```

```
   r03=(1-gamma3)./(1+gamma3);
   Hu03=(1-w3.*u0K3.*(r03+((1-2.*r03.*u0K3)./2).*log((1+u0K3)./u0K3))).^(-1);
   Hu3=(1-w3.*uK3.*(r03+((1-2.*r03.*uK3)./2).*log((1+uK3)./uK3))).^(-1);
%radiance coefficient
   rc3=PoreK3*((w3./(4*pi))*(u/(u+u0)).*((Pg)+(Hu03.*Hu3)-1))./ ...
      ((isow./(4*pi))*(u/(u+u0)).*((1)+(isoHu0.*isoHu)-1));
      rc=cat(2,rc1,rc2,rc3);
end
```

HapkeEval4_PP.m

```
%This program evaluates the input guesses for the minimization program and
%appends them to the save file in a user friendly format
%load solution set
   load(ksave,'solutions','wavelength');
%extract sizes for general plotting
   load('variables.mat','fakesize');
   krange=fakesize+6;
%extract input guesses
%warning for too few convergent solutions
   if length(solutions)<6;
      error('program converged on less than 6 start points, ...
            try changing maxit, maxfun,or bounds and start again.')
   elseif length(solutions)<7
      onein=solutions (1,1);
      twoin=solutions (1,2);
      threein=solutions (1,3);
      fourin=solutions (1,4);
      fivein=solutions (1,5);
      sixin=solutions (1,6);
      onein=onein(1).X0;
      twoin=twoin(1).X0;
      threein=threein(1).X0;
      fourin=fourin(1).X0;
      fivein=fivein(1).X0;
      sixin=sixin(1).X0;
      onein=onein{1,1};
      twoin=twoin{1,1};
      threein=threein{1,1};
      fourin=fourin{1,1};
      fivein=fivein{1,1};
      sixin=sixin{1,1};
      count=[1 2 3 4 5 6];
      s11=onein(1);
      s12=onein(2);
      s13=onein(3);
      s21=twoin(1);
      s22=twoin(2);
      s23=twoin(3);
      s31=threein(1);
      s32=threein(2);
      s33=threein(3);
      s41=fourin(1);
      s42=fourin(2);
      s43=fourin(3);
      s51=fivein(1);
      s52=fivein(2);
      s53=fivein(3);
      s61=sixin(1);
      s62=sixin(2);
      s63=sixin(3);
      S1in=[s11 s21 s31 s41 s51 s61];
      S2in=[s12 s22 s32 s42 s52 s62];
      S3in=[s13 s23 s33 s43 s53 s63];
```

```
    figure(1)
    semilogy(count,S1in,'r+',count,S2in,'g+',count,S3in,'b+')
    d11=onein(4);
    d12=onein(5);
    d13=onein(6);
    d21=twoin(4);
    d22=twoin(5);
    d23=twoin(6);
    d31=threein(4);
    d32=threein(5);
    d33=threein(6);
    d41=fourin(4);
    d42=fourin(5);
    d43=fourin(6);
    d51=fivein(4);
    d52=fivein(5);
    d53=fivein(6);
    d61=sixin(4);
    d62=sixin(5);
    d63=sixin(6);
    D1in=[d11 d21 d31 d41 d51 d61];
    D2in=[d12 d22 d32 d42 d52 d62];
    D3in=[d13 d23 d33 d43 d53 d63];
    figure(2)
    plot(count,D1in,'r+',count,D2in,'g+',count,D3in,'b+')
    k1=onein(7:krange);
    k2=twoin(7:krange);
    k3=threein(7:krange);
    k4=fourin(7:krange);
    k5=fivein(7:krange);
    k6=sixin(7:krange);
    Kin=[k1 k2 k3 k4 k5 k6];
    wave=wavelength(1:fakesize);
    figure(3)
    semilogy(wave,k1,wave,k2,wave,k3,wave,k4,wave,k5,wave,k6)
    legend('one','two','three','four','five','six','location','southeast')
    save(ksave,'-append','S1in','S2in','D1in','D2in','Kin','onein')
elseif length(solutions)<8
    onein=solutions (1,1);
    twoin=solutions (1,2);
    threein=solutions (1,3);
    fourin=solutions (1,4);
    fivein=solutions (1,5);
    sixin=solutions (1,6);
    sevin=solutions (1,7);
    onein=onein(1).X0;
    twoin=twoin(1).X0;
    threein=threein(1).X0;
    fourin=fourin(1).X0;
    fivein=fivein(1).X0;
    sixin=sixin(1).X0;
    sevin=sevin(1).X0;
    onein=onein{1,1};
    twoin=twoin{1,1};
    threein=threein{1,1};
    fourin=fourin{1,1};
    fivein=fivein{1,1};
```

```
sixin=sixin{1,1};
sevin=sevin{1,1};
count=[1 2 3 4 5 6 7];
s11=onein(1);
s12=onein(2);
s13=onein(3);
s21=twoin(1);
s22=twoin(2);
s23=twoin(3);
s31=threein(1);
s32=threein(2);
s33=threein(3);
s41=fourin(1);
s42=fourin(2);
s43=fourin(3);
s51=fivein(1);
s52=fivein(2);
s53=fivein(3);
s61=sixin(1);
s62=sixin(2);
s63=sixin(3);
s71=sevin(1);
s72=sevin(2);
s73=sevin(3);
S1in=[s11 s21 s31 s41 s51 s61 s71];
S2in=[s12 s22 s32 s42 s52 s62 s72];
S3in=[s13 s23 s33 s43 s53 s63 s73];
figure(1)
semilogy(count,S1in,'r+',count,S2in,'g+',count,S3in,'b+')
d11=onein(4);
d12=onein(5);
d13=onein(6);
d21=twoin(4);
d22=twoin(5);
d23=twoin(6);
d31=threein(4);
d32=threein(5);
d33=threein(6);
d41=fourin(4);
d42=fourin(5);
d43=fourin(6);
d51=fivein(4);
d52=fivein(5);
d53=fivein(6);
d61=sixin(4);
d62=sixin(5);
d63=sixin(6);
d71=sevin(4);
d72=sevin(5);
d73=sevin(6);
D1in=[d11 d21 d31 d41 d51 d61 d71];
D2in=[d12 d22 d32 d42 d52 d62 d72];
D3in=[d13 d23 d33 d43 d53 d63 d73];
figure(2)
plot(count,D1in,'r+',count,D2in,'g+',count,D3in,'b+')
k1=onein(7:krange);
k2=twoin(7:krange);
```

```
    k3=threein(7:krange);
    k4=fourin(7:krange);
    k5=fivein(7:krange);
    k6=sixin(7:krange);
    k7=sevin(7:krange);
    Kin=[k1 k2 k3 k4 k5 k6 k7];
    wave=wavelength(1:fakesize);
    figure(3)
    semilogy(wave,k1,wave,k2,wave,k3,wave,k4,wave,k5,wave,k6,wave,k7)
    legend('one','two','three','four','five','six','seven','location', ...
          'southeast')
    save(ksave,'-append','S1in','S2in','D1in','D2in','Kin','onein')
elseif length(solutions)>7
    onein=solutions (1,1);
    twoin=solutions (1,2);
    threein=solutions (1,3);
    fourin=solutions (1,4);
    fivein=solutions (1,5);
    sixin=solutions (1,6);
    sevin=solutions (1,7);
    eightin=solutions (1,8);
    onein=onein(1).X0;
    twoin=twoin(1).X0;
    threein=threein(1).X0;
    fourin=fourin(1).X0;
    fivein=fivein(1).X0;
    sixin=sixin(1).X0;
    sevin=sevin(1).X0;
    eightin=eightin(1).X0;
    onein=onein{1,1};
    twoin=twoin{1,1};
    threein=threein{1,1};
    fourin=fourin{1,1};
    fivein=fivein{1,1};
    sixin=sixin{1,1};
    sevin=sevin{1,1};
    eightin=eightin{1,1};
    count=[1 2 3 4 5 6 7 8];
    s11=onein(1);
    s12=onein(2);
    s13=onein(3);
    s21=twoin(1);
    s22=twoin(2);
    s23=twoin(3);
    s31=threein(1);
    s32=threein(2);
    s33=threein(3);
    s41=fourin(1);
    s42=fourin(2);
    s43=fourin(3);
    s51=fivein(1);
    s52=fivein(2);
    s53=fivein(3);
    s61=sixin(1);
    s62=sixin(2);
    s63=sixin(3);
    s71=sevin(1);
```

```
    s72=sevin(2);
    s73=sevin(3);
    s81=eightin(1);
    s82=eightin(2);
    s83=eightin(3);
    S1in=[s11 s21 s31 s41 s51 s61 s71 s81];
    S2in=[s12 s22 s32 s42 s52 s62 s72 s82];
    S3in=[s13 s23 s33 s43 s53 s63 s73 s83];
    figure(1)
    semilogy(count,S1in,'r+',count,S2in,'g+',count,S3in,'b+')
    d11=onein(4);
    d12=onein(5);
    d13=onein(6);
    d21=twoin(4);
    d22=twoin(5);
    d23=twoin(6);
    d31=threein(4);
    d32=threein(5);
    d33=threein(6);
    d41=fourin(4);
    d42=fourin(5);
    d43=fourin(6);
    d51=fivein(4);
    d52=fivein(5);
    d53=fivein(6);
    d61=sixin(4);
    d62=sixin(5);
    d63=sixin(6);
    d71=sevin(4);
    d72=sevin(5);
    d73=sevin(6);
    d81=eightin(4);
    d82=eightin(5);
    d83=eightin(6);
    D1in=[d11 d21 d31 d41 d51 d61 d71 d81];
    D2in=[d12 d22 d32 d42 d52 d62 d72 d82];
    D3in=[d13 d23 d33 d43 d53 d63 d73 d83];
    figure(2)
    plot(count,D1in,'r+',count,D2in,'g+',count,D3in,'b+')
    k1=onein(7:krange);
    k2=twoin(7:krange);
    k3=threein(7:krange);
    k4=fourin(7:krange);
    k5=fivein(7:krange);
    k6=sixin(7:krange);
    k7=sevin(7:krange);
    k8=sevin(7:krange);
    Kin=[k1 k2 k3 k4 k5 k6 k7 k8];
    wave=wavelength(1:fakesize);
    figure(3)
    semilogy(wave,k1,wave,k2,wave,k3,wave,k4,wave,k5,wave,k6,wave,k7, ...
             wave,k8)
    legend('one','two','three','four','five','six','seven','eight', ...
          'location','southeast')
    save(ksave,'-append','S1in','S2in','D1in','D2in','Kin','onein')
end
clear
```

HapkeEval5_PP.m

```
%This program evaluates the output guesses for the minimization program and
%appends them to the save file out a user friendly format
%load solution set
   load(ksave,'solutions','wavelength','realsize2');
%extract sizes for general plotting
   load('variables.mat','fakesize','extra1')
   extra2=extra1/2;
   krange=fakesize+extra2;
   wavelength=wavelength(1:krange);
%extract output guesses
%warnoutg for too few convergent solutions
   if length(solutions)<6;
      error('program converged on less than 6 start points, ...
            try changing maxit, maxfun,or bounds and start again.')
   elseif length(solutions)<7
      oneout=solutions (1,1);
      twoout=solutions (1,2);
      threeout=solutions (1,3);
      fourout=solutions (1,4);
      fiveout=solutions (1,5);
      sixout=solutions (1,6);
      oneout=oneout(1).X;
      twoout=twoout(1).X;
      threeout=threeout(1).X;
      fourout=fourout(1).X;
      fiveout=fiveout(1).X;
      sixout=sixout(1).X;
      count=[1 2 3 4 5 6];
      s11=oneout(1);
      s12=oneout(2);
      s13=oneout(3);
      s21=twoout(1);
      s22=twoout(2);
      s23=twoout(3);
      s31=threeout(1);
      s32=threeout(2);
      s33=threeout(3);
      s41=fourout(1);
      s42=fourout(2);
      s43=fourout(3);
      s51=fiveout(1);
      s52=fiveout(2);
      s53=fiveout(3);
      s61=sixout(1);
      s62=sixout(2);
      s63=sixout(3);
      S1out=[s11 s21 s31 s41 s51 s61];
      S2out=[s12 s22 s32 s42 s52 s62];
      S3out=[s13 s23 s33 s43 s53 s63];
      figure(3)
      semilogy(count,S1out,'r+',count,S2out,'g+',count,S3out,'b+')
      d11=oneout(4);
      d12=oneout(5);
```

```
    d13=oneout(6);
    d21=twoout(4);
    d22=twoout(5);
    d23=twoout(6);
    d31=threeout(4);
    d32=threeout(5);
    d33=threeout(6);
    d41=fourout(4);
    d42=fourout(5);
    d43=fourout(6);
    d51=fiveout(4);
    d52=fiveout(5);
    d53=fiveout(6);
    d61=sixout(4);
    d62=sixout(5);
    d63=sixout(6);
    D1out=[d11 d21 d31 d41 d51 d61];
    D2out=[d12 d22 d32 d42 d52 d62];
    D3out=[d13 d23 d33 d43 d53 d63];
    figure(4)
    plot(count,D1out,'r+',count,D2out,'g+',count,D3out,'b+')
    k1=oneout(7:krange);
    k2=twoout(7:krange);
    k3=threeout(7:krange);
    k4=fourout(7:krange);
    k5=fiveout(7:krange);
    k6=sixout(7:krange);
    Kout=[k1 k2 k3 k4 k5 k6];
    wave=wavelength(1:fakesize);
    figure(5)
    semilogy(wave,k1,wave,k2,wave,k3,wave,k4,wave,k5,wave,k6)
    legend('one','two','three','four','five','six','location','southeast')
    save(ksave,'-append','S1out','S2out','D1out','D2out','Kout','oneout')
elseif length(solutions)<8
    oneout=solutions (1,1);
    twoout=solutions (1,2);
    threeout=solutions (1,3);
    fourout=solutions (1,4);
    fiveout=solutions (1,5);
    sixout=solutions (1,6);
    sevout=solutions (1,7);
    oneout=oneout(1).X;
    twoout=twoout(1).X;
    threeout=threeout(1).X;
    fourout=fourout(1).X;
    fiveout=fiveout(1).X;
    sixout=sixout(1).X;
    sevout=sevout(1).X;
    count=[1 2 3 4 5 6 7];
    s11=oneout(1);
    s12=oneout(2);
    s13=oneout(3);
    s21=twoout(1);
    s22=twoout(2);
    s23=twoout(3);
    s31=threeout(1);
    s32=threeout(2);
```

```
s33=threeout(3);
s41=fourout(1);
s42=fourout(2);
s43=fourout(3);
s51=fiveout(1);
s52=fiveout(2);
s53=fiveout(3);
s61=sixout(1);
s62=sixout(2);
s63=sixout(3);
s71=sevout(1);
s72=sevout(2);
s73=sevout(3);
S1out=[s11 s21 s31 s41 s51 s61 s71];
S2out=[s12 s22 s32 s42 s52 s62 s72];
S3out=[s13 s23 s33 s43 s53 s63 s73];
figure(3)
semilogy(count,S1out,'r+',count,S2out,'g+',count,S3out,'b+')
d11=oneout(4);
d12=oneout(5);
d13=oneout(6);
d21=twoout(4);
d22=twoout(5);
d23=twoout(6);
d31=threeout(4);
d32=threeout(5);
d33=threeout(6);
d41=fourout(4);
d42=fourout(5);
d43=fourout(6);
d51=fiveout(4);
d52=fiveout(5);
d53=fiveout(6);
d61=sixout(4);
d62=sixout(5);
d63=sixout(6);
d71=sevout(4);
d72=sevout(5);
d73=sevout(6);
D1out=[d11 d21 d31 d41 d51 d61 d71];
D2out=[d12 d22 d32 d42 d52 d62 d72];
D3out=[d13 d23 d33 d43 d53 d63 d73];
figure(4)
plot(count,D1out,'r+',count,D2out,'g+',count,D3out,'b+')
k1=oneout(7:krange);
k2=twoout(7:krange);
k3=threeout(7:krange);
k4=fourout(7:krange);
k5=fiveout(7:krange);
k6=sixout(7:krange);
k7=sevout(7:krange);
Kout=[k1 k2 k3 k4 k5 k6 k7];
wave=wavelength(1:ksize);
figure(5)
semilogy(wave,k1,wave,k2,wave,k3,wave,k4,wave,k5,wave,k6,wave,k7)
legend('one','two','three','four','five','six','seven','location', ...
      'southeast')
```

```
    save(ksave,'-append','S1out','S2out','D1out','D2out','Kout','oneout')
elseif length(solutions)>7
    oneout=solutions (1,1);
    twoout=solutions (1,2);
    threeout=solutions (1,3);
    fourout=solutions (1,4);
    fiveout=solutions (1,5);
    sixout=solutions (1,6);
    sevout=solutions (1,7);
    eightout=solutions (1,8);
    oneout=oneout(1).X;
    twoout=twoout(1).X;
    threeout=threeout(1).X;
    fourout=fourout(1).X;
    fiveout=fiveout(1).X;
    sixout=sixout(1).X;
    sevout=sevout(1).X;
    eightout=eightout(1).X;
    count=[1 2 3 4 5 6 7 8];
    s11=oneout(1);
    s12=oneout(2);
    s13=oneout(3);
    s21=twoout(1);
    s22=twoout(2);
    s23=twoout(3);
    s31=threeout(1);
    s32=threeout(2);
    s33=threeout(3);
    s41=fourout(1);
    s42=fourout(2);
    s43=fourout(3);
    s51=fiveout(1);
    s52=fiveout(2);
    s53=fiveout(3);
    s61=sixout(1);
    s62=sixout(2);
    s63=sixout(3);
    s71=sevout(1);
    s72=sevout(2);
    s73=sevout(3);
    s81=eightout(1);
    s82=eightout(2);
    s83=eightout(3);
    S1out=[s11 s21 s31 s41 s51 s61 s71 s81];
    S2out=[s12 s22 s32 s42 s52 s62 s72 s82];
    S3out=[s13 s23 s33 s43 s53 s63 s73 s83];
    figure(3)
    semilogy(count,S1out,'r+',count,S2out,'g+',count,S3out,'b+')
    d11=oneout(4);
    d12=oneout(5);
    d13=oneout(6);
    d21=twoout(4);
    d22=twoout(5);
    d23=twoout(6);
    d31=threeout(4);
    d32=threeout(5);
    d33=threeout(6);
```

```
      d41=fourout(4);
      d42=fourout(5);
      d43=fourout(6);
      d51=fiveout(4);
      d52=fiveout(5);
      d53=fiveout(6);
      d61=sixout(4);
      d62=sixout(5);
      d63=sixout(6);
      d71=sevout(4);
      d72=sevout(5);
      d73=sevout(6);
      d81=eightout(4);
      d82=eightout(5);
      d83=eightout(6);
      D1out=[d11 d21 d31 d41 d51 d61 d71 d81];
      D2out=[d12 d22 d32 d42 d52 d62 d72 d82];
      D3out=[d13 d23 d33 d43 d53 d63 d73 d83];
      figure(4)
      plot(count,D1out,'r+',count,D2out,'g+',count,D3out,'b+')
      k1=oneout(7:krange);
      k2=twoout(7:krange);
      k3=threeout(7:krange);
      k4=fourout(7:krange);
      k5=fiveout(7:krange);
      k6=sixout(7:krange);
      k7=sevout(7:krange);
      k8=sevout(7:krange);
      Kout=[k1 k2 k3 k4 k5 k6 k7 k8];
      wave=wavelength(1:fakesize);
      figure(5)
      semilogy(wave,k1,wave,k2,wave,k3,wave,k4,wave,k5,wave,k6,wave,k7, ...
               wave,k8)
      legend('one','two','three','four','five','six','seven','eight', ...
            'location','southeast')
      save(ksave,'-append','S1out','S2out','D1out','D2out','Kout','oneout')
   end
   load('variables.mat','PoreK1','PoreK2','PoreK3')
   load(ksave,'kone2','ktwo2','DATA','isow','realsize2','Pg','n','u','u0')
   u0K1=u0/PoreK1;
   u0K2=u0/PoreK2;
   u0K3=u0/PoreK3;
   uK1=u/PoreK1;
   uK2=u/PoreK2;
   uK3=u/PoreK3;
[rc]=HapkeEval6_PP(oneout,DATA,kone2,ktwo2,fakesize,realsize2,wavelength,n...
            ,u0,u,u0K1,u0K2,u0K3,uK1,uK2,uK3,isow,PoreK1,PoreK2,PoreK3,Pg);

clear
```

HapkeEval6_PP.m

```
%This program evaluates and plots outputs from the minimization routine.
%This is not a standalone program, it must be run from HapkeEval2
function[rc]=HapkeEval6_PP(oneout,DATA,kone2,ktwo2,fakesize,realsize2, ...
                  wavelength,n,u0K1,u0K2,u0K3,uK1,uK2,uK3,isow,PoreK1, ...
                  PoreK2,PoreK3,Pg)
%IMPORT DATA FILE to which minimization is performed
%extract sizes for general plotting
%UNPACK VARIABLES
   s1=oneout(1);
   s2=oneout(2);
   s3=oneout(3);
   D1=oneout(4);
   D2=oneout(5);
   D3=oneout(6);
   krange=realsize2+6;
   k=oneout(7:krange);
   k=cat(2,kone2,ktwo2,k);
   wavelength=wavelength(1:fakesize); %row
%run though to get rc
[rc]=MasterHapke5_PP(Pg,s1,s2,s3,k,D1,D2,D3,wavelength,n,...
            u0,u,u0K1,u0K2,u0K3,uK1,uK2,uK3,isow,PoreK1,PoreK2,PoreK3);
%import grain size dependent ks
   Load('variables.mat','startindex','endindex');
   kb=importdata('bigk.mat');
   kb=kb.k2;
   kb=kb(startindex:endindex);
   km=importdata('medk.mat');
   km=km.k2;
   km=km(startindex:endindex);
   ks=importdata('smlk.mat');
   kwave=ks.kwave;
   kwave=kwave(startindex:endindex);
   ks=ks.k2;
   ks=ks(startindex:endindex);
   waverange21=fakesize+1;
   waverange22=fakesize*2;
   waverange31=waverange22+1;
   waverange32=fakesize*3;
   figure(6)
   plot(wavelength,rc(1:fakesize),wavelength,DATA(1:fakesize))
   set(gca,'Fontsize',16);
   set(gca,'XLim',[0.35 2.5]);
   xlabel('Wavelength (\mum)');
   ylabel('Radiance (%)');
   legend('fit','data ','location','southeast');
   figure(7)
   plot(wavelength,rc(waverange21:waverange22),wavelength,DATA(waverange21:wa
   verange22))
   set(gca,'Fontsize',16);
   set(gca,'XLim',[0.35 2.5]);
   xlabel('Wavelength (\mum)');
   ylabel('Radiance (%)');
   legend('fit','data ','location','southeast');
```

```
    figure(8)
    plot(wavelength,rc(waverange31:waverange32),wavelength,DATA(waverange31:wa
    verange32))
    set(gca,'Fontsize',16);
    set(gca,'XLim',[0.35 2.5]);
    xlabel('Wavelength (\mum)');
    ylabel('Radiance (%)');
    legend('fit','data ','location','southeast');
    figure(9)
    semilogy(kwave,kb,kwave,km,kwave,ks,wavelength,k)
    set(gca,'Fontsize',16);
    set(gca,'XLim',[0.35 2.5]);
    xlabel('Wavelength (\mum)');
    ylabel('k');
    legend('big k','med k','small k','multi grain-size k','location','north');
end
```

Appendix B

Optical Constants for synthetic hydronium, sodium, and potassium jarosite

Wavelength (μm)	Hydronium jarosite		Sodium Jarosite		Potassium jarosite	
	k	*n*	*k*	*n*	*k*	*n*
0.4130	0.0025898	1.8149	0.0012609	1.7873	0.0005758	1.7888
0.4140	0.0023970	1.8174	0.0012704	1.7885	0.0005563	1.7893
0.4150	0.0023088	1.8179	0.0013326	1.7887	0.0005544	1.7894
0.4160	0.0022796	1.8182	0.0013691	1.7889	0.0005627	1.7895
0.4170	0.0022807	1.8183	0.0013429	1.7890	0.0005674	1.7896
0.4180	0.0022862	1.8185	0.0013518	1.7891	0.0005725	1.7896
0.4190	0.0022842	1.8186	0.0013621	1.7891	0.0005768	1.7896
0.4200	0.0022913	1.8187	0.0014080	1.7891	0.0005851	1.7896
0.4210	0.0022949	1.8188	0.0014157	1.7891	0.0005873	1.7897
0.4220	0.0023265	1.8189	0.0014839	1.7891	0.0005962	1.7897
0.4230	0.0023423	1.8190	0.0016139	1.7891	0.0006053	1.7897
0.4240	0.0024067	1.8191	0.0017046	1.7892	0.0006240	1.7897
0.4250	0.0024514	1.8192	0.0017529	1.7893	0.0006441	1.7897
0.4260	0.0024213	1.8193	0.0018460	1.7893	0.0006557	1.7898
0.4270	0.0024111	1.8194	0.0019280	1.7894	0.0006659	1.7898
0.4280	0.0024174	1.8195	0.0019484	1.7895	0.0006816	1.7898
0.4290	0.0023910	1.8195	0.0020220	1.7896	0.0006910	1.7898
0.4300	0.0024326	1.8196	0.0021255	1.7897	0.0007032	1.7899
0.4310	0.0024956	1.8197	0.0021868	1.7898	0.0007154	1.7899
0.4320	0.0025049	1.8198	0.0022289	1.7899	0.0007210	1.7899
0.4330	0.0024986	1.8199	0.0022629	1.7900	0.0007186	1.7899
0.4340	0.0024699	1.8200	0.0022679	1.7902	0.0007121	1.7900
0.4350	0.0024241	1.8201	0.0022433	1.7903	0.0007105	1.7900
0.4360	0.0023964	1.8202	0.0021958	1.7905	0.0007120	1.7900
0.4370	0.0023501	1.8203	0.0020976	1.7906	0.0007082	1.7901
0.4380	0.0022975	1.8203	0.0020238	1.7907	0.0007018	1.7901
0.4390	0.0022500	1.8204	0.0019710	1.7907	0.0006866	1.7901
0.4400	0.0022001	1.8205	0.0019095	1.7908	0.0006624	1.7901
0.4410	0.0021669	1.8205	0.0019020	1.7908	0.0006443	1.7902

0.4420	0.0021179	1.8206	0.0018770	1.7909	0.0006216	1.7902
0.4430	0.0020622	1.8206	0.0017984	1.7910	0.0005979	1.7902
0.4440	0.0020017	1.8207	0.0016957	1.7911	0.0005792	1.7902
0.4450	0.0019481	1.8207	0.0016057	1.7911	0.0005629	1.7902
0.4460	0.0018850	1.8207	0.0015044	1.7912	0.0005413	1.7902
0.4470	0.0018295	1.8208	0.0014121	1.7912	0.0005229	1.7902
0.4480	0.0017758	1.8208	0.0013324	1.7912	0.0005057	1.7902
0.4490	0.0017267	1.8208	0.0012693	1.7912	0.0004891	1.7902
0.4500	0.0016804	1.8208	0.0012182	1.7912	0.0004730	1.7902
0.4510	0.0016382	1.8208	0.0011564	1.7912	0.0004578	1.7902
0.4520	0.0015957	1.8209	0.0010884	1.7912	0.0004426	1.7902
0.4530	0.0015473	1.8209	0.0010372	1.7911	0.0004278	1.7902
0.4540	0.0014982	1.8209	0.0009907	1.7911	0.0004146	1.7902
0.4550	0.0014530	1.8209	0.0009438	1.7911	0.0004030	1.7902
0.4560	0.0014093	1.8209	0.0009066	1.7911	0.0003928	1.7902
0.4570	0.0013679	1.8209	0.0008833	1.7911	0.0003844	1.7902
0.4580	0.0013232	1.8209	0.0008468	1.7910	0.0003743	1.7902
0.4590	0.0012862	1.8209	0.0008184	1.7910	0.0003661	1.7902
0.4600	0.0012486	1.8209	0.0007953	1.7910	0.0003574	1.7902
0.4610	0.0012130	1.8209	0.0007725	1.7910	0.0003490	1.7902
0.4620	0.0011831	1.8209	0.0007491	1.7910	0.0003415	1.7902
0.4630	0.0011538	1.8209	0.0007252	1.7910	0.0003342	1.7902
0.4640	0.0011247	1.8209	0.0007057	1.7909	0.0003275	1.7902
0.4650	0.0010988	1.8209	0.0006882	1.7909	0.0003219	1.7902
0.4660	0.0010746	1.8208	0.0006736	1.7909	0.0003164	1.7902
0.4670	0.0010511	1.8208	0.0006623	1.7909	0.0003118	1.7902
0.4680	0.0010232	1.8208	0.0006481	1.7909	0.0003058	1.7902
0.4690	0.0010063	1.8208	0.0006397	1.7909	0.0003021	1.7902
0.4700	0.0009819	1.8208	0.0006222	1.7909	0.0002962	1.7902
0.4710	0.0009564	1.8208	0.0006094	1.7909	0.0002911	1.7902
0.4720	0.0009375	1.8208	0.0005976	1.7908	0.0002868	1.7902
0.4730	0.0009224	1.8208	0.0005870	1.7908	0.0002835	1.7902
0.4740	0.0009005	1.8208	0.0005761	1.7908	0.0002793	1.7902
0.4750	0.0008766	1.8208	0.0005641	1.7908	0.0002741	1.7902
0.4760	0.0008644	1.8208	0.0005545	1.7908	0.0002711	1.7902
0.4770	0.0008485	1.8208	0.0005426	1.7908	0.0002671	1.7902
0.4780	0.0008322	1.8208	0.0005330	1.7908	0.0002642	1.7902
0.4790	0.0008152	1.8208	0.0005201	1.7908	0.0002600	1.7902
0.4800	0.0007962	1.8208	0.0005056	1.7908	0.0002550	1.7902
0.4810	0.0007780	1.8208	0.0004946	1.7908	0.0002510	1.7902
0.4820	0.0007589	1.8207	0.0004845	1.7908	0.0002467	1.7902
0.4830	0.0007415	1.8207	0.0004747	1.7908	0.0002422	1.7902
0.4840	0.0007233	1.8207	0.0004634	1.7907	0.0002373	1.7902

0.4850	0.0007108	1.8207	0.0004562	1.7907	0.0002338	1.7902
0.4860	0.0006952	1.8207	0.0004461	1.7907	0.0002298	1.7902
0.4870	0.0006799	1.8207	0.0004362	1.7907	0.0002262	1.7902
0.4880	0.0006680	1.8207	0.0004287	1.7907	0.0002233	1.7902
0.4890	0.0006541	1.8207	0.0004193	1.7907	0.0002194	1.7902
0.4900	0.0006386	1.8207	0.0004099	1.7907	0.0002161	1.7902
0.4910	0.0006230	1.8207	0.0003998	1.7907	0.0002121	1.7902
0.4920	0.0006111	1.8207	0.0003915	1.7907	0.0002086	1.7902
0.4930	0.0005998	1.8207	0.0003848	1.7907	0.0002059	1.7902
0.4940	0.0005866	1.8206	0.0003769	1.7907	0.0002026	1.7902
0.4950	0.0005748	1.8206	0.0003691	1.7907	0.0001993	1.7902
0.4960	0.0005616	1.8206	0.0003598	1.7906	0.0001950	1.7902
0.4970	0.0005491	1.8206	0.0003519	1.7906	0.0001917	1.7901
0.4980	0.0005377	1.8206	0.0003445	1.7906	0.0001885	1.7901
0.4990	0.0005285	1.8206	0.0003389	1.7906	0.0001859	1.7901
0.5000	0.0005172	1.8206	0.0003313	1.7906	0.0001826	1.7901
0.5010	0.0005046	1.8206	0.0003230	1.7906	0.0001787	1.7901
0.5020	0.0004956	1.8206	0.0003176	1.7906	0.0001762	1.7901
0.5030	0.0004849	1.8206	0.0003105	1.7906	0.0001731	1.7901
0.5040	0.0004745	1.8206	0.0003033	1.7906	0.0001700	1.7901
0.5050	0.0004649	1.8205	0.0002969	1.7906	0.0001669	1.7901
0.5060	0.0004553	1.8205	0.0002904	1.7906	0.0001640	1.7901
0.5070	0.0004459	1.8205	0.0002839	1.7905	0.0001610	1.7901
0.5080	0.0004357	1.8205	0.0002767	1.7905	0.0001574	1.7901
0.5090	0.0004269	1.8205	0.0002706	1.7905	0.0001545	1.7901
0.5100	0.0004182	1.8205	0.0002644	1.7905	0.0001516	1.7901
0.5110	0.0004110	1.8205	0.0002596	1.7905	0.0001491	1.7901
0.5120	0.0004040	1.8205	0.0002549	1.7905	0.0001467	1.7901
0.5130	0.0003933	1.8205	0.0002472	1.7905	0.0001428	1.7901
0.5140	0.0003864	1.8205	0.0002424	1.7905	0.0001404	1.7901
0.5150	0.0003786	1.8205	0.0002369	1.7905	0.0001377	1.7901
0.5160	0.0003697	1.8204	0.0002305	1.7905	0.0001345	1.7901
0.5170	0.0003619	1.8204	0.0002251	1.7905	0.0001317	1.7901
0.5180	0.0003553	1.8204	0.0002207	1.7905	0.0001295	1.7901
0.5190	0.0003479	1.8204	0.0002155	1.7904	0.0001268	1.7901
0.5200	0.0003406	1.8204	0.0002106	1.7904	0.0001242	1.7901
0.5210	0.0003336	1.8204	0.0002059	1.7904	0.0001216	1.7901
0.5220	0.0003257	1.8204	0.0002003	1.7904	0.0001186	1.7901
0.5230	0.0003200	1.8204	0.0001965	1.7904	0.0001165	1.7901
0.5240	0.0003135	1.8204	0.0001920	1.7904	0.0001141	1.7901
0.5250	0.0003071	1.8204	0.0001875	1.7904	0.0001117	1.7901
0.5260	0.0003274	1.8204	0.0002037	1.7904	0.0001211	1.7901
0.5270	0.0002962	1.8204	0.0001802	1.7904	0.0001077	1.7901

0.5280	0.0002872	1.8203	0.0001738	1.7904	0.0001040	1.7901
0.5290	0.0002820	1.8203	0.0001704	1.7904	0.0001021	1.7901
0.5300	0.0002768	1.8203	0.0001671	1.7903	0.0001001	1.7901
0.5310	0.0002700	1.8203	0.0001624	1.7903	0.0000975	1.7901
0.5320	0.0002642	1.8203	0.0001585	1.7903	0.0000952	1.7901
0.5330	0.0002586	1.8203	0.0001548	1.7903	0.0000931	1.7900
0.5340	0.0002540	1.8203	0.0001517	1.7903	0.0000913	1.7900
0.5350	0.0002478	1.8203	0.0001475	1.7903	0.0000889	1.7900
0.5360	0.0002424	1.8203	0.0001441	1.7903	0.0000869	1.7900
0.5370	0.0002371	1.8203	0.0001408	1.7903	0.0000850	1.7900
0.5380	0.0002319	1.8202	0.0001376	1.7903	0.0000831	1.7900
0.5390	0.0002266	1.8202	0.0001346	1.7903	0.0000812	1.7900
0.5400	0.0002216	1.8202	0.0001316	1.7902	0.0000793	1.7900
0.5410	0.0002167	1.8202	0.0001287	1.7902	0.0000776	1.7900
0.5420	0.0002119	1.8202	0.0001259	1.7902	0.0000759	1.7900
0.5430	0.0002072	1.8202	0.0001231	1.7902	0.0000742	1.7900
0.5440	0.0002027	1.8202	0.0001205	1.7902	0.0000726	1.7900
0.5450	0.0001988	1.8202	0.0001184	1.7902	0.0000712	1.7900
0.5460	0.0001937	1.8202	0.0001153	1.7902	0.0000693	1.7900
0.5470	0.0001894	1.8202	0.0001129	1.7902	0.0000678	1.7900
0.5480	0.0001851	1.8201	0.0001105	1.7902	0.0000663	1.7900
0.5490	0.0001802	1.8201	0.0001078	1.7902	0.0000646	1.7900
0.5500	0.0001768	1.8201	0.0001060	1.7902	0.0000635	1.7900
0.5510	0.0001734	1.8201	0.0001044	1.7901	0.0000624	1.7900
0.5520	0.0001693	1.8201	0.0001024	1.7901	0.0000611	1.7900
0.5530	0.0001654	1.8201	0.0001004	1.7901	0.0000599	1.7900
0.5540	0.0001610	1.8201	0.0000981	1.7901	0.0000584	1.7900
0.5550	0.0001578	1.8201	0.0000967	1.7901	0.0000575	1.7900
0.5560	0.0001534	1.8201	0.0000945	1.7901	0.0000561	1.7900
0.5570	0.0001503	1.8201	0.0000932	1.7901	0.0000552	1.7900
0.5580	0.0001462	1.8200	0.0000911	1.7901	0.0000539	1.7900
0.5590	0.0001427	1.8200	0.0000895	1.7901	0.0000529	1.7899
0.5600	0.0001388	1.8200	0.0000877	1.7901	0.0000517	1.7899
0.5610	0.0001361	1.8200	0.0000867	1.7901	0.0000511	1.7899
0.5620	0.0001335	1.8200	0.0000859	1.7900	0.0000505	1.7899
0.5630	0.0001305	1.8200	0.0000847	1.7900	0.0000497	1.7899
0.5640	0.0001275	1.8200	0.0000830	1.7900	0.0000487	1.7899
0.5650	0.0001257	1.8200	0.0000822	1.7900	0.0000483	1.7899
0.5660	0.0001235	1.8200	0.0000811	1.7900	0.0000477	1.7899
0.5670	0.0001213	1.8200	0.0000800	1.7900	0.0000471	1.7899
0.5680	0.0001188	1.8199	0.0000786	1.7900	0.0000463	1.7899
0.5690	0.0001172	1.8199	0.0000780	1.7900	0.0000459	1.7899
0.5700	0.0001153	1.8199	0.0000772	1.7900	0.0000454	1.7899

0.5710	0.0001135	1.8199	0.0000764	1.7900	0.0000450	1.7899
0.5720	0.0001112	1.8199	0.0000752	1.7900	0.0000443	1.7899
0.5730	0.0001099	1.8199	0.0000748	1.7899	0.0000441	1.7899
0.5740	0.0001083	1.8199	0.0000741	1.7899	0.0000437	1.7899
0.5750	0.0001067	1.8199	0.0000734	1.7899	0.0000433	1.7899
0.5760	0.0001051	1.8199	0.0000728	1.7899	0.0000429	1.7899
0.5770	0.0001037	1.8199	0.0000722	1.7899	0.0000426	1.7899
0.5780	0.0001018	1.8199	0.0000713	1.7899	0.0000421	1.7899
0.5790	0.0001000	1.8198	0.0000704	1.7899	0.0000416	1.7899
0.5800	0.0000995	1.8198	0.0000706	1.7899	0.0000417	1.7899
0.5810	0.0000983	1.8198	0.0000702	1.7899	0.0000415	1.7899
0.5820	0.0000966	1.8198	0.0000695	1.7899	0.0000410	1.7899
0.5830	0.0000959	1.8198	0.0000694	1.7899	0.0000410	1.7899
0.5840	0.0000948	1.8198	0.0000691	1.7899	0.0000408	1.7899
0.5850	0.0000938	1.8198	0.0000688	1.7898	0.0000405	1.7899
0.5860	0.0000924	1.8198	0.0000681	1.7898	0.0000401	1.7898
0.5870	0.0000918	1.8198	0.0000682	1.7898	0.0000401	1.7898
0.5880	0.0000905	1.8198	0.0000676	1.7898	0.0000396	1.7898
0.5890	0.0000900	1.8198	0.0000677	1.7898	0.0000396	1.7898
0.5900	0.0000892	1.8197	0.0000674	1.7898	0.0000394	1.7898
0.5910	0.0000884	1.8197	0.0000671	1.7898	0.0000392	1.7898
0.5920	0.0000872	1.8197	0.0000665	1.7898	0.0000388	1.7898
0.5930	0.0000868	1.8197	0.0000666	1.7898	0.0000388	1.7898
0.5940	0.0000861	1.8197	0.0000664	1.7898	0.0000386	1.7898
0.5950	0.0000858	1.8197	0.0000664	1.7898	0.0000386	1.7898
0.5960	0.0000843	1.8197	0.0000655	1.7898	0.0000380	1.7898
0.5970	0.0000845	1.8197	0.0000659	1.7897	0.0000382	1.7898
0.5980	0.0000831	1.8197	0.0000650	1.7897	0.0000375	1.7898
0.5990	0.0000833	1.8197	0.0000653	1.7897	0.0000377	1.7898
0.6000	0.0000823	1.8197	0.0000647	1.7897	0.0000372	1.7898
0.6010	0.0000813	1.8196	0.0000641	1.7897	0.0000368	1.7898
0.6020	0.0000811	1.8196	0.0000642	1.7897	0.0000367	1.7898
0.6030	0.0000802	1.8196	0.0000636	1.7897	0.0000362	1.7898
0.6040	0.0000804	1.8196	0.0000639	1.7897	0.0000364	1.7898
0.6050	0.0000791	1.8196	0.0000630	1.7897	0.0000357	1.7898
0.6060	0.0000795	1.8196	0.0000634	1.7897	0.0000359	1.7898
0.6070	0.0000790	1.8196	0.0000631	1.7897	0.0000356	1.7898
0.6080	0.0000778	1.8196	0.0000621	1.7897	0.0000350	1.7898
0.6090	0.0000782	1.8196	0.0000624	1.7897	0.0000351	1.7898
0.6100	0.0000775	1.8196	0.0000617	1.7896	0.0000346	1.7898
0.6110	0.0000771	1.8196	0.0000613	1.7896	0.0000343	1.7898
0.6120	0.0000771	1.8196	0.0000613	1.7896	0.0000342	1.7898
0.6130	0.0000764	1.8195	0.0000606	1.7896	0.0000337	1.7898

0.6140	0.0000761	1.8195	0.0000601	1.7896	0.0000334	1.7898
0.6150	0.0000757	1.8195	0.0000596	1.7896	0.0000330	1.7898
0.6160	0.0000754	1.8195	0.0000591	1.7896	0.0000327	1.7898
0.6170	0.0000755	1.8195	0.0000590	1.7896	0.0000326	1.7897
0.6180	0.0000753	1.8195	0.0000585	1.7896	0.0000322	1.7897
0.6190	0.0000751	1.8195	0.0000580	1.7896	0.0000319	1.7897
0.6200	0.0000741	1.8195	0.0000569	1.7896	0.0000312	1.7897
0.6210	0.0000743	1.8195	0.0000567	1.7896	0.0000310	1.7897
0.6220	0.0000745	1.8195	0.0000566	1.7896	0.0000309	1.7897
0.6230	0.0000744	1.8195	0.0000561	1.7895	0.0000305	1.7897
0.6240	0.0000742	1.8195	0.0000557	1.7895	0.0000302	1.7897
0.6250	0.0000733	1.8194	0.0000546	1.7895	0.0000296	1.7897
0.6260	0.0000735	1.8194	0.0000545	1.7895	0.0000294	1.7897
0.6270	0.0000734	1.8194	0.0000540	1.7895	0.0000291	1.7897
0.6280	0.0000733	1.8194	0.0000536	1.7895	0.0000288	1.7897
0.6290	0.0000736	1.8194	0.0000534	1.7895	0.0000287	1.7897
0.6300	0.0000732	1.8194	0.0000526	1.7895	0.0000282	1.7897
0.6310	0.0000736	1.8194	0.0000525	1.7895	0.0000281	1.7897
0.6320	0.0000736	1.8194	0.0000520	1.7895	0.0000278	1.7897
0.6330	0.0000736	1.8194	0.0000516	1.7895	0.0000275	1.7897
0.6340	0.0000736	1.8194	0.0000512	1.7895	0.0000272	1.7897
0.6350	0.0000736	1.8194	0.0000508	1.7895	0.0000269	1.7897
0.6360	0.0000737	1.8194	0.0000504	1.7894	0.0000266	1.7897
0.6370	0.0000737	1.8193	0.0000499	1.7894	0.0000263	1.7897
0.6380	0.0000734	1.8193	0.0000492	1.7894	0.0000258	1.7897
0.6390	0.0000734	1.8193	0.0000488	1.7894	0.0000255	1.7897
0.6400	0.0000739	1.8193	0.0000486	1.7894	0.0000254	1.7897
0.6410	0.0000739	1.8193	0.0000482	1.7894	0.0000251	1.7897
0.6420	0.0000732	1.8193	0.0000472	1.7894	0.0000245	1.7897
0.6430	0.0000737	1.8193	0.0000470	1.7894	0.0000243	1.7897
0.6440	0.0000742	1.8193	0.0000468	1.7894	0.0000242	1.7897
0.6450	0.0000742	1.8193	0.0000463	1.7894	0.0000239	1.7897
0.6460	0.0000739	1.8193	0.0000456	1.7894	0.0000234	1.7897
0.6470	0.0000740	1.8193	0.0000452	1.7894	0.0000231	1.7897
0.6480	0.0000741	1.8193	0.0000447	1.7893	0.0000228	1.7896
0.6490	0.0000746	1.8192	0.0000445	1.7893	0.0000227	1.7896
0.6500	0.0000746	1.8192	0.0000441	1.7893	0.0000224	1.7896
0.6510	0.0000747	1.8192	0.0000436	1.7893	0.0000221	1.7896
0.6520	0.0000748	1.8192	0.0000431	1.7893	0.0000218	1.7896
0.6530	0.0000748	1.8192	0.0000427	1.7893	0.0000215	1.7896
0.6540	0.0000749	1.8192	0.0000422	1.7893	0.0000212	1.7896
0.6550	0.0000750	1.8192	0.0000417	1.7893	0.0000209	1.7896
0.6560	0.0000755	1.8192	0.0000414	1.7893	0.0000207	1.7896

0.6570	0.0000751	1.8192	0.0000407	1.7893	0.0000203	1.7896
0.6580	0.0000752	1.8192	0.0000402	1.7893	0.0000199	1.7896
0.6590	0.0000756	1.8192	0.0000399	1.7893	0.0000198	1.7896
0.6600	0.0000756	1.8192	0.0000394	1.7893	0.0000194	1.7896
0.6610	0.0000757	1.8192	0.0000389	1.7892	0.0000191	1.7896
0.6620	0.0000757	1.8191	0.0000384	1.7892	0.0000188	1.7896
0.6630	0.0000749	1.8191	0.0000374	1.7892	0.0000183	1.7896
0.6640	0.0000750	1.8191	0.0000370	1.7892	0.0000180	1.7896
0.6650	0.0000751	1.8191	0.0000366	1.7892	0.0000178	1.7896
0.6660	0.0000748	1.8191	0.0000360	1.7892	0.0000174	1.7896
0.6670	0.0000752	1.8191	0.0000358	1.7892	0.0000173	1.7896
0.6680	0.0000753	1.8191	0.0000354	1.7892	0.0000171	1.7896
0.6690	0.0000754	1.8191	0.0000351	1.7892	0.0000169	1.7896
0.6700	0.0000755	1.8191	0.0000347	1.7892	0.0000166	1.7896
0.6710	0.0000759	1.8191	0.0000345	1.7892	0.0000165	1.7896
0.6720	0.0000756	1.8191	0.0000339	1.7892	0.0000162	1.7896
0.6730	0.0000756	1.8191	0.0000335	1.7891	0.0000159	1.7896
0.6740	0.0000753	1.8191	0.0000329	1.7891	0.0000156	1.7896
0.6750	0.0000754	1.8190	0.0000325	1.7891	0.0000154	1.7896
0.6760	0.0000754	1.8190	0.0000322	1.7891	0.0000152	1.7896
0.6770	0.0000755	1.8190	0.0000318	1.7891	0.0000150	1.7895
0.6780	0.0000752	1.8190	0.0000312	1.7891	0.0000147	1.7895
0.6790	0.0000753	1.8190	0.0000309	1.7891	0.0000145	1.7895
0.6800	0.0000758	1.8190	0.0000308	1.7891	0.0000144	1.7895
0.6810	0.0000758	1.8190	0.0000305	1.7891	0.0000142	1.7895
0.6820	0.0000755	1.8190	0.0000300	1.7891	0.0000139	1.7895
0.6830	0.0000763	1.8190	0.0000300	1.7891	0.0000139	1.7895
0.6840	0.0000764	1.8190	0.0000297	1.7891	0.0000138	1.7895
0.6850	0.0000761	1.8190	0.0000292	1.7890	0.0000135	1.7895
0.6860	0.0000766	1.8190	0.0000291	1.7890	0.0000134	1.7895
0.6870	0.0000771	1.8189	0.0000290	1.7890	0.0000134	1.7895
0.6880	0.0000768	1.8189	0.0000286	1.7890	0.0000131	1.7895
0.6890	0.0000770	1.8189	0.0000283	1.7890	0.0000130	1.7895
0.6900	0.0000772	1.8189	0.0000281	1.7890	0.0000129	1.7895
0.6910	0.0000777	1.8189	0.0000281	1.7890	0.0000128	1.7895
0.6920	0.0000779	1.8189	0.0000278	1.7890	0.0000127	1.7895
0.6930	0.0000776	1.8189	0.0000275	1.7890	0.0000125	1.7895
0.6940	0.0000782	1.8189	0.0000275	1.7890	0.0000125	1.7895
0.6950	0.0000784	1.8189	0.0000273	1.7890	0.0000125	1.7895
0.6960	0.0000786	1.8189	0.0000272	1.7889	0.0000124	1.7895
0.6970	0.0000793	1.8189	0.0000272	1.7889	0.0000124	1.7895
0.6980	0.0000791	1.8189	0.0000269	1.7889	0.0000122	1.7895
0.6990	0.0000794	1.8188	0.0000268	1.7889	0.0000122	1.7895

0.7000	0.0000797	1.8188	0.0000267	1.7889	0.0000121	1.7895
0.7010	0.0000800	1.8188	0.0000267	1.7889	0.0000121	1.7895
0.7020	0.0000803	1.8188	0.0000267	1.7889	0.0000121	1.7895
0.7030	0.0000806	1.8188	0.0000266	1.7889	0.0000120	1.7894
0.7040	0.0000810	1.8188	0.0000266	1.7889	0.0000120	1.7894
0.7050	0.0000809	1.8188	0.0000265	1.7889	0.0000119	1.7894
0.7060	0.0000813	1.8188	0.0000265	1.7889	0.0000119	1.7894
0.7070	0.0000821	1.8188	0.0000267	1.7888	0.0000120	1.7894
0.7080	0.0000821	1.8188	0.0000265	1.7888	0.0000120	1.7894
0.7090	0.0000826	1.8188	0.0000266	1.7888	0.0000120	1.7894
0.7100	0.0000835	1.8188	0.0000269	1.7888	0.0000121	1.7894
0.7110	0.0000840	1.8187	0.0000270	1.7888	0.0000122	1.7894
0.7120	0.0000846	1.8187	0.0000271	1.7888	0.0000122	1.7894
0.7130	0.0000847	1.8187	0.0000271	1.7888	0.0000122	1.7894
0.7140	0.0000852	1.8187	0.0000272	1.7888	0.0000123	1.7894
0.7150	0.0000862	1.8187	0.0000276	1.7888	0.0000125	1.7894
0.7160	0.0000868	1.8187	0.0000278	1.7888	0.0000126	1.7894
0.7170	0.0000875	1.8187	0.0000281	1.7888	0.0000126	1.7894
0.7180	0.0000886	1.8187	0.0000285	1.7887	0.0000129	1.7894
0.7190	0.0000889	1.8187	0.0000286	1.7887	0.0000129	1.7894
0.7200	0.0000892	1.8187	0.0000286	1.7887	0.0000129	1.7894
0.7210	0.0000904	1.8187	0.0000291	1.7887	0.0000131	1.7894
0.7220	0.0000912	1.8186	0.0000294	1.7887	0.0000133	1.7894
0.7230	0.0000925	1.8186	0.0000299	1.7887	0.0000136	1.7894
0.7240	0.0000928	1.8186	0.0000301	1.7887	0.0000136	1.7894
0.7250	0.0000937	1.8186	0.0000304	1.7887	0.0000138	1.7894
0.7260	0.0000945	1.8186	0.0000308	1.7887	0.0000139	1.7894
0.7270	0.0000954	1.8186	0.0000312	1.7887	0.0000141	1.7894
0.7280	0.0000968	1.8186	0.0000318	1.7887	0.0000144	1.7894
0.7290	0.0000978	1.8186	0.0000323	1.7886	0.0000146	1.7893
0.7300	0.0000982	1.8186	0.0000325	1.7886	0.0000147	1.7893
0.7310	0.0000993	1.8186	0.0000330	1.7886	0.0000150	1.7893
0.7320	0.0001008	1.8186	0.0000338	1.7886	0.0000153	1.7893
0.7330	0.0001014	1.8186	0.0000341	1.7886	0.0000155	1.7893
0.7340	0.0001025	1.8185	0.0000346	1.7886	0.0000157	1.7893
0.7350	0.0001036	1.8185	0.0000352	1.7886	0.0000160	1.7893
0.7360	0.0001048	1.8185	0.0000357	1.7886	0.0000163	1.7893
0.7370	0.0001065	1.8185	0.0000366	1.7886	0.0000167	1.7893
0.7380	0.0001076	1.8185	0.0000372	1.7886	0.0000170	1.7893
0.7390	0.0001083	1.8185	0.0000376	1.7885	0.0000172	1.7893
0.7400	0.0001101	1.8185	0.0000385	1.7885	0.0000177	1.7893
0.7410	0.0001119	1.8185	0.0000395	1.7885	0.0000181	1.7893
0.7420	0.0001127	1.8185	0.0000400	1.7885	0.0000183	1.7893

0.7430	0.0001140	1.8185	0.0000407	1.7885	0.0000187	1.7893
0.7440	0.0001142	1.8185	0.0000410	1.7885	0.0000188	1.7893
0.7450	0.0001161	1.8184	0.0000420	1.7885	0.0000193	1.7893
0.7460	0.0001175	1.8184	0.0000428	1.7885	0.0000197	1.7893
0.7470	0.0001195	1.8184	0.0000439	1.7885	0.0000202	1.7893
0.7480	0.0001210	1.8184	0.0000448	1.7885	0.0000206	1.7893
0.7490	0.0001219	1.8184	0.0000454	1.7885	0.0000209	1.7893
0.7500	0.0001228	1.8184	0.0000460	1.7884	0.0000212	1.7893
0.7510	0.0001243	1.8184	0.0000469	1.7884	0.0000216	1.7893
0.7520	0.0001264	1.8184	0.0000482	1.7884	0.0000222	1.7893
0.7530	0.0001273	1.8184	0.0000489	1.7884	0.0000225	1.7893
0.7540	0.0001295	1.8184	0.0000502	1.7884	0.0000232	1.7892
0.7550	0.0001304	1.8184	0.0000510	1.7884	0.0000235	1.7892
0.7560	0.0001327	1.8184	0.0000524	1.7884	0.0000242	1.7892
0.7570	0.0001337	1.8183	0.0000531	1.7884	0.0000245	1.7892
0.7580	0.0001366	1.8183	0.0000549	1.7884	0.0000254	1.7892
0.7590	0.0001383	1.8183	0.0000560	1.7884	0.0000259	1.7892
0.7600	0.0001393	1.8183	0.0000569	1.7883	0.0000263	1.7892
0.7610	0.0001410	1.8183	0.0000581	1.7883	0.0000269	1.7892
0.7620	0.0001433	1.8183	0.0000597	1.7883	0.0000276	1.7892
0.7630	0.0001450	1.8183	0.0000610	1.7883	0.0000282	1.7892
0.7640	0.0001467	1.8183	0.0000621	1.7883	0.0000288	1.7892
0.7650	0.0001476	1.8183	0.0000629	1.7883	0.0000292	1.7892
0.7660	0.0001492	1.8183	0.0000641	1.7883	0.0000298	1.7892
0.7670	0.0001509	1.8183	0.0000654	1.7883	0.0000304	1.7892
0.7680	0.0001532	1.8183	0.0000670	1.7883	0.0000312	1.7892
0.7690	0.0001542	1.8182	0.0000679	1.7883	0.0000316	1.7892
0.7700	0.0001559	1.8182	0.0000692	1.7883	0.0000323	1.7892
0.7710	0.0001576	1.8182	0.0000705	1.7882	0.0000329	1.7892
0.7720	0.0001601	1.8182	0.0000722	1.7882	0.0000338	1.7892
0.7730	0.0001612	1.8182	0.0000732	1.7882	0.0000343	1.7892
0.7740	0.0001631	1.8182	0.0000745	1.7882	0.0000350	1.7892
0.7750	0.0001650	1.8182	0.0000759	1.7882	0.0000357	1.7892
0.7760	0.0001675	1.8182	0.0000777	1.7882	0.0000367	1.7892
0.7770	0.0001694	1.8182	0.0000792	1.7882	0.0000374	1.7892
0.7780	0.0001712	1.8182	0.0000807	1.7882	0.0000382	1.7892
0.7790	0.0001723	1.8182	0.0000817	1.7882	0.0000387	1.7891
0.7800	0.0001726	1.8182	0.0000824	1.7882	0.0000390	1.7891
0.7810	0.0001751	1.8181	0.0000844	1.7881	0.0000400	1.7891
0.7820	0.0001769	1.8181	0.0000859	1.7881	0.0000408	1.7891
0.7830	0.0001801	1.8181	0.0000884	1.7881	0.0000420	1.7891
0.7840	0.0001812	1.8181	0.0000896	1.7881	0.0000426	1.7891
0.7850	0.0001830	1.8181	0.0000912	1.7881	0.0000434	1.7891

0.7860	0.0001856	1.8181	0.0000933	1.7881	0.0000445	1.7891
0.7870	0.0001874	1.8181	0.0000950	1.7881	0.0000454	1.7891
0.7880	0.0001900	1.8181	0.0000972	1.7881	0.0000465	1.7891
0.7890	0.0001918	1.8181	0.0000989	1.7881	0.0000474	1.7891
0.7900	0.0001928	1.8181	0.0001002	1.7881	0.0000480	1.7891
0.7910	0.0001947	1.8181	0.0001020	1.7881	0.0000489	1.7891
0.7920	0.0001958	1.8181	0.0001032	1.7880	0.0000496	1.7891
0.7930	0.0001984	1.8181	0.0001055	1.7880	0.0000508	1.7891
0.7940	0.0002003	1.8180	0.0001072	1.7880	0.0000518	1.7891
0.7950	0.0002029	1.8180	0.0001095	1.7880	0.0000530	1.7891
0.7960	0.0002039	1.8180	0.0001108	1.7880	0.0000537	1.7891
0.7970	0.0002057	1.8180	0.0001127	1.7880	0.0000547	1.7891
0.7980	0.0002075	1.8180	0.0001145	1.7880	0.0000557	1.7891
0.7990	0.0002093	1.8180	0.0001165	1.7880	0.0000567	1.7891
0.8000	0.0002112	1.8180	0.0001184	1.7880	0.0000576	1.7891
0.8010	0.0002131	1.8180	0.0001203	1.7880	0.0000586	1.7891
0.8020	0.0002149	1.8180	0.0001223	1.7880	0.0000596	1.7891
0.8030	0.0002159	1.8180	0.0001237	1.7879	0.0000604	1.7891
0.8040	0.0002178	1.8180	0.0001257	1.7879	0.0000614	1.7890
0.8050	0.0002214	1.8180	0.0001288	1.7879	0.0000631	1.7890
0.8060	0.0002223	1.8180	0.0001302	1.7879	0.0000638	1.7890
0.8070	0.0002241	1.8179	0.0001322	1.7879	0.0000648	1.7890
0.8080	0.0002250	1.8179	0.0001336	1.7879	0.0000656	1.7890
0.8090	0.0002276	1.8179	0.0001363	1.7879	0.0000670	1.7890
0.8100	0.0002284	1.8179	0.0001377	1.7879	0.0000677	1.7890
0.8110	0.0002292	1.8179	0.0001392	1.7879	0.0000684	1.7890
0.8120	0.0002318	1.8179	0.0001419	1.7879	0.0000699	1.7890
0.8130	0.0002336	1.8179	0.0001439	1.7879	0.0000710	1.7890
0.8140	0.0002361	1.8179	0.0001465	1.7878	0.0000724	1.7890
0.8150	0.0002376	1.8179	0.0001483	1.7878	0.0000734	1.7890
0.8160	0.0002382	1.8179	0.0001495	1.7878	0.0000741	1.7890
0.8170	0.0002388	1.8179	0.0001508	1.7878	0.0000748	1.7890
0.8180	0.0002421	1.8179	0.0001541	1.7878	0.0000766	1.7890
0.8190	0.0002436	1.8179	0.0001560	1.7878	0.0000776	1.7890
0.8200	0.0002451	1.8178	0.0001579	1.7878	0.0000786	1.7890
0.8210	0.0002466	1.8178	0.0001599	1.7878	0.0000796	1.7890
0.8220	0.0002481	1.8178	0.0001617	1.7878	0.0000807	1.7890
0.8230	0.0002507	1.8178	0.0001644	1.7878	0.0000821	1.7890
0.8240	0.0002522	1.8178	0.0001663	1.7878	0.0000831	1.7890
0.8250	0.0002557	1.8178	0.0001697	1.7877	0.0000850	1.7890
0.8260	0.0002553	1.8178	0.0001701	1.7877	0.0000852	1.7890
0.8270	0.0002538	1.8178	0.0001697	1.7877	0.0000850	1.7890
0.8280	0.0002572	1.8178	0.0001731	1.7877	0.0000868	1.7890

0.8290	0.0002607	1.8178	0.0001765	1.7877	0.0000886	1.7890
0.8300	0.0002602	1.8178	0.0001768	1.7877	0.0000888	1.7890
0.8310	0.0002626	1.8178	0.0001795	1.7877	0.0000902	1.7889
0.8320	0.0002628	1.8178	0.0001806	1.7877	0.0000908	1.7889
0.8330	0.0002630	1.8178	0.0001816	1.7877	0.0000914	1.7889
0.8340	0.0002633	1.8177	0.0001826	1.7877	0.0000920	1.7889
0.8350	0.0002645	1.8177	0.0001843	1.7877	0.0000931	1.7889
0.8360	0.0002668	1.8177	0.0001869	1.7877	0.0000946	1.7889
0.8370	0.0002651	1.8177	0.0001862	1.7876	0.0000943	1.7889
0.8380	0.0002695	1.8177	0.0001905	1.7876	0.0000967	1.7889
0.8390	0.0002698	1.8177	0.0001915	1.7876	0.0000973	1.7889
0.8400	0.0002710	1.8177	0.0001933	1.7876	0.0000983	1.7889
0.8410	0.0002721	1.8177	0.0001950	1.7876	0.0000993	1.7889
0.8420	0.0002743	1.8177	0.0001977	1.7876	0.0001008	1.7889
0.8430	0.0002754	1.8177	0.0001994	1.7876	0.0001018	1.7889
0.8440	0.0002754	1.8177	0.0002001	1.7876	0.0001023	1.7889
0.8450	0.0002806	1.8177	0.0002054	1.7876	0.0001051	1.7889
0.8460	0.0002785	1.8177	0.0002044	1.7876	0.0001046	1.7889
0.8470	0.0002784	1.8177	0.0002052	1.7876	0.0001051	1.7889
0.8480	0.0002815	1.8176	0.0002087	1.7876	0.0001070	1.7889
0.8490	0.0002804	1.8176	0.0002086	1.7875	0.0001069	1.7889
0.8500	0.0002814	1.8176	0.0002101	1.7875	0.0001079	1.7889
0.8510	0.0002845	1.8176	0.0002135	1.7875	0.0001098	1.7889
0.8520	0.0002854	1.8176	0.0002150	1.7875	0.0001107	1.7889
0.8530	0.0002885	1.8176	0.0002185	1.7875	0.0001126	1.7889
0.8540	0.0002820	1.8176	0.0002135	1.7875	0.0001101	1.7889
0.8550	0.0002872	1.8176	0.0002188	1.7875	0.0001130	1.7889
0.8560	0.0002871	1.8176	0.0002194	1.7875	0.0001133	1.7889
0.8570	0.0002914	1.8176	0.0002236	1.7875	0.0001157	1.7889
0.8580	0.0002945	1.8176	0.0002270	1.7875	0.0001177	1.7889
0.8590	0.0002888	1.8176	0.0002226	1.7875	0.0001155	1.7889
0.8600	0.0002929	1.8176	0.0002268	1.7875	0.0001179	1.7888
0.8610	0.0002970	1.8176	0.0002312	1.7874	0.0001204	1.7888
0.8620	0.0002922	1.8175	0.0002278	1.7874	0.0001186	1.7888
0.8630	0.0002995	1.8175	0.0002349	1.7874	0.0001227	1.7888
0.8640	0.0002980	1.8175	0.0002345	1.7874	0.0001225	1.7888
0.8650	0.0003020	1.8175	0.0002390	1.7874	0.0001250	1.7888
0.8660	0.0002970	1.8175	0.0002355	1.7874	0.0001231	1.7888
0.8670	0.0002998	1.8175	0.0002390	1.7874	0.0001250	1.7888
0.8680	0.0002981	1.8175	0.0002385	1.7874	0.0001246	1.7888
0.8690	0.0002996	1.8175	0.0002409	1.7874	0.0001259	1.7888
0.8700	0.0002979	1.8175	0.0002403	1.7874	0.0001255	1.7888
0.8710	0.0002919	1.8175	0.0002357	1.7874	0.0001231	1.7888

0.8720	0.0003024	1.8175	0.0002464	1.7874	0.0001288	1.7888
0.8730	0.0003019	1.8175	0.0002468	1.7873	0.0001290	1.7888
0.8740	0.0003024	1.8175	0.0002481	1.7873	0.0001297	1.7888
0.8750	0.0002974	1.8175	0.0002442	1.7873	0.0001278	1.7888
0.8760	0.0003011	1.8174	0.0002485	1.7873	0.0001302	1.7888
0.8770	0.0002992	1.8174	0.0002475	1.7873	0.0001298	1.7888
0.8780	0.0003006	1.8174	0.0002497	1.7873	0.0001311	1.7888
0.8790	0.0003032	1.8174	0.0002530	1.7873	0.0001331	1.7888
0.8800	0.0003046	1.8174	0.0002552	1.7873	0.0001344	1.7888
0.8810	0.0003048	1.8174	0.0002564	1.7873	0.0001351	1.7888
0.8820	0.0003039	1.8174	0.0002566	1.7873	0.0001352	1.7888
0.8830	0.0002998	1.8174	0.0002535	1.7873	0.0001336	1.7888
0.8840	0.0003056	1.8174	0.0002601	1.7873	0.0001372	1.7888
0.8850	0.0003071	1.8174	0.0002624	1.7873	0.0001384	1.7888
0.8860	0.0003051	1.8174	0.0002612	1.7872	0.0001378	1.7888
0.8870	0.0003029	1.8174	0.0002599	1.7872	0.0001373	1.7888
0.8880	0.0003051	1.8174	0.0002630	1.7872	0.0001391	1.7888
0.8890	0.0003038	1.8173	0.0002627	1.7872	0.0001392	1.7888
0.8900	0.0003070	1.8173	0.0002668	1.7872	0.0001416	1.7888
0.8910	0.0003024	1.8173	0.0002633	1.7872	0.0001398	1.7888
0.8920	0.0003013	1.8173	0.0002631	1.7872	0.0001397	1.7887
0.8930	0.0003037	1.8173	0.0002662	1.7872	0.0001415	1.7887
0.8940	0.0003039	1.8173	0.0002669	1.7872	0.0001420	1.7887
0.8950	0.0003030	1.8173	0.0002664	1.7872	0.0001418	1.7887
0.8960	0.0003054	1.8173	0.0002692	1.7872	0.0001435	1.7887
0.8970	0.0003044	1.8173	0.0002686	1.7872	0.0001434	1.7887
0.8980	0.0003088	1.8173	0.0002736	1.7871	0.0001463	1.7887
0.8990	0.0003054	1.8173	0.0002708	1.7871	0.0001449	1.7887
0.9000	0.0003031	1.8173	0.0002691	1.7871	0.0001442	1.7887
0.9010	0.0003053	1.8173	0.0002718	1.7871	0.0001460	1.7887
0.9020	0.0003053	1.8172	0.0002724	1.7871	0.0001466	1.7887
0.9030	0.0003064	1.8172	0.0002740	1.7871	0.0001477	1.7887
0.9040	0.0003041	1.8172	0.0002722	1.7871	0.0001470	1.7887
0.9050	0.0003027	1.8172	0.0002715	1.7871	0.0001468	1.7887
0.9060	0.0003057	1.8172	0.0002754	1.7871	0.0001491	1.7887
0.9070	0.0003031	1.8172	0.0002735	1.7871	0.0001482	1.7887
0.9080	0.0003039	1.8172	0.0002750	1.7871	0.0001490	1.7887
0.9090	0.0003035	1.8172	0.0002755	1.7871	0.0001493	1.7887
0.9100	0.0003019	1.8172	0.0002746	1.7870	0.0001489	1.7887
0.9110	0.0003025	1.8172	0.0002759	1.7870	0.0001498	1.7887
0.9120	0.0003010	1.8172	0.0002749	1.7870	0.0001494	1.7887
0.9130	0.0003018	1.8172	0.0002761	1.7870	0.0001503	1.7887
0.9140	0.0002991	1.8172	0.0002739	1.7870	0.0001493	1.7887

0.9150	0.0002998	1.8171	0.0002754	1.7870	0.0001501	1.7887
0.9160	0.0003016	1.8171	0.0002780	1.7870	0.0001515	1.7887
0.9170	0.0002998	1.8171	0.0002771	1.7870	0.0001511	1.7887
0.9180	0.0002979	1.8171	0.0002763	1.7870	0.0001506	1.7887
0.9190	0.0002971	1.8171	0.0002764	1.7870	0.0001508	1.7887
0.9200	0.0002964	1.8171	0.0002764	1.7870	0.0001510	1.7887
0.9210	0.0002968	1.8171	0.0002775	1.7870	0.0001517	1.7887
0.9220	0.0002950	1.8171	0.0002762	1.7870	0.0001511	1.7887
0.9230	0.0002944	1.8171	0.0002760	1.7869	0.0001511	1.7887
0.9240	0.0002927	1.8171	0.0002747	1.7869	0.0001504	1.7886
0.9250	0.0002953	1.8171	0.0002781	1.7869	0.0001524	1.7886
0.9260	0.0002934	1.8171	0.0002768	1.7869	0.0001518	1.7886
0.9270	0.0002929	1.8171	0.0002767	1.7869	0.0001519	1.7886
0.9280	0.0002913	1.8170	0.0002755	1.7869	0.0001514	1.7886
0.9290	0.0002897	1.8170	0.0002742	1.7869	0.0001509	1.7886
0.9300	0.0002891	1.8170	0.0002741	1.7869	0.0001509	1.7886
0.9310	0.0002883	1.8170	0.0002740	1.7869	0.0001509	1.7886
0.9320	0.0002898	1.8170	0.0002760	1.7869	0.0001521	1.7886
0.9330	0.0002890	1.8170	0.0002755	1.7869	0.0001519	1.7886
0.9340	0.0002871	1.8170	0.0002739	1.7868	0.0001512	1.7886
0.9350	0.0002864	1.8170	0.0002734	1.7868	0.0001511	1.7886
0.9360	0.0002859	1.8170	0.0002728	1.7868	0.0001511	1.7886
0.9370	0.0002852	1.8170	0.0002722	1.7868	0.0001510	1.7886
0.9380	0.0002846	1.8170	0.0002715	1.7868	0.0001509	1.7886
0.9390	0.0002849	1.8170	0.0002721	1.7868	0.0001514	1.7886
0.9400	0.0002830	1.8169	0.0002704	1.7868	0.0001506	1.7886
0.9410	0.0002820	1.8169	0.0002697	1.7868	0.0001504	1.7886
0.9420	0.0002811	1.8169	0.0002690	1.7868	0.0001503	1.7886
0.9430	0.0002802	1.8169	0.0002684	1.7868	0.0001502	1.7886
0.9440	0.0002793	1.8169	0.0002676	1.7868	0.0001501	1.7886
0.9450	0.0002783	1.8169	0.0002667	1.7868	0.0001500	1.7886
0.9460	0.0002774	1.8169	0.0002660	1.7867	0.0001498	1.7886
0.9470	0.0002765	1.8169	0.0002655	1.7867	0.0001496	1.7886
0.9480	0.0002757	1.8169	0.0002650	1.7867	0.0001494	1.7886
0.9490	0.0002761	1.8169	0.0002654	1.7867	0.0001499	1.7886
0.9500	0.0002743	1.8169	0.0002638	1.7867	0.0001490	1.7886
0.9510	0.0002746	1.8168	0.0002641	1.7867	0.0001494	1.7886
0.9520	0.0002737	1.8168	0.0002631	1.7867	0.0001490	1.7886
0.9530	0.0002718	1.8168	0.0002609	1.7867	0.0001480	1.7886
0.9540	0.0002720	1.8168	0.0002610	1.7867	0.0001481	1.7885
0.9550	0.0002711	1.8168	0.0002600	1.7867	0.0001477	1.7885
0.9560	0.0002691	1.8168	0.0002578	1.7867	0.0001467	1.7885
0.9570	0.0002682	1.8168	0.0002569	1.7866	0.0001465	1.7885

0.9580	0.0002683	1.8168	0.0002572	1.7866	0.0001468	1.7885
0.9590	0.0002674	1.8168	0.0002561	1.7866	0.0001466	1.7885
0.9600	0.0002655	1.8168	0.0002539	1.7866	0.0001457	1.7885
0.9610	0.0002646	1.8168	0.0002528	1.7866	0.0001452	1.7885
0.9620	0.0002637	1.8167	0.0002515	1.7866	0.0001447	1.7885
0.9630	0.0002637	1.8167	0.0002512	1.7866	0.0001447	1.7885
0.9640	0.0002625	1.8167	0.0002500	1.7866	0.0001441	1.7885
0.9650	0.0002614	1.8167	0.0002489	1.7866	0.0001436	1.7885
0.9660	0.0002601	1.8167	0.0002480	1.7866	0.0001431	1.7885
0.9670	0.0002589	1.8167	0.0002472	1.7866	0.0001426	1.7885
0.9680	0.0002581	1.8167	0.0002465	1.7865	0.0001422	1.7885
0.9690	0.0002573	1.8167	0.0002456	1.7865	0.0001418	1.7885
0.9700	0.0002556	1.8167	0.0002439	1.7865	0.0001408	1.7885
0.9710	0.0002549	1.8167	0.0002429	1.7865	0.0001405	1.7885
0.9720	0.0002541	1.8167	0.0002416	1.7865	0.0001400	1.7885
0.9730	0.0002549	1.8166	0.0002426	1.7865	0.0001409	1.7885
0.9740	0.0002531	1.8166	0.0002405	1.7865	0.0001399	1.7885
0.9750	0.0002512	1.8166	0.0002381	1.7865	0.0001388	1.7885
0.9760	0.0002502	1.8166	0.0002369	1.7865	0.0001382	1.7885
0.9770	0.0002493	1.8166	0.0002359	1.7865	0.0001377	1.7885
0.9780	0.0002496	1.8166	0.0002356	1.7864	0.0001377	1.7885
0.9790	0.0002487	1.8166	0.0002343	1.7864	0.0001372	1.7885
0.9800	0.0002476	1.8166	0.0002332	1.7864	0.0001368	1.7885
0.9810	0.0002464	1.8166	0.0002320	1.7864	0.0001364	1.7885
0.9820	0.0002455	1.8166	0.0002304	1.7864	0.0001360	1.7884
0.9830	0.0002443	1.8165	0.0002292	1.7864	0.0001354	1.7884
0.9840	0.0002432	1.8165	0.0002280	1.7864	0.0001348	1.7884
0.9850	0.0002425	1.8165	0.0002264	1.7864	0.0001341	1.7884
0.9860	0.0002425	1.8165	0.0002259	1.7864	0.0001340	1.7884
0.9870	0.0002407	1.8165	0.0002236	1.7864	0.0001329	1.7884
0.9880	0.0002401	1.8165	0.0002219	1.7863	0.0001322	1.7884
0.9890	0.0002392	1.8165	0.0002202	1.7863	0.0001314	1.7884
0.9900	0.0002382	1.8165	0.0002188	1.7863	0.0001310	1.7884
0.9910	0.0002375	1.8165	0.0002173	1.7863	0.0001305	1.7884
0.9920	0.0002366	1.8165	0.0002159	1.7863	0.0001298	1.7884
0.9930	0.0002356	1.8164	0.0002143	1.7863	0.0001292	1.7884
0.9940	0.0002348	1.8164	0.0002129	1.7863	0.0001286	1.7884
0.9950	0.0002339	1.8164	0.0002114	1.7863	0.0001279	1.7884
0.9960	0.0002327	1.8164	0.0002098	1.7863	0.0001271	1.7884
0.9970	0.0002328	1.8164	0.0002088	1.7863	0.0001262	1.7884
0.9980	0.0002331	1.8164	0.0002078	1.7862	0.0001255	1.7884
0.9990	0.0002332	1.8164	0.0002066	1.7862	0.0001247	1.7884
1.0000	0.0002333	1.8164	0.0002053	1.7862	0.0001239	1.7884

1.0010	0.0002335	1.8164	0.0002038	1.7862	0.0001231	1.7884
1.0020	0.0002322	1.8164	0.0002019	1.7862	0.0001223	1.7884
1.0030	0.0002307	1.8164	0.0002001	1.7862	0.0001217	1.7884
1.0040	0.0002293	1.8163	0.0001986	1.7862	0.0001211	1.7884
1.0050	0.0002281	1.8163	0.0001972	1.7862	0.0001205	1.7884
1.0060	0.0002270	1.8163	0.0001960	1.7862	0.0001199	1.7884
1.0070	0.0002263	1.8163	0.0001949	1.7861	0.0001192	1.7883
1.0080	0.0002257	1.8163	0.0001937	1.7861	0.0001185	1.7883
1.0090	0.0002252	1.8163	0.0001924	1.7861	0.0001177	1.7883
1.0100	0.0002247	1.8163	0.0001910	1.7861	0.0001170	1.7883
1.0110	0.0002240	1.8163	0.0001895	1.7861	0.0001162	1.7883
1.0120	0.0002231	1.8163	0.0001878	1.7861	0.0001154	1.7883
1.0130	0.0002220	1.8163	0.0001861	1.7861	0.0001147	1.7883
1.0140	0.0002207	1.8162	0.0001844	1.7861	0.0001139	1.7883
1.0150	0.0002194	1.8162	0.0001827	1.7861	0.0001132	1.7883
1.0160	0.0002180	1.8162	0.0001811	1.7860	0.0001124	1.7883
1.0170	0.0002167	1.8162	0.0001795	1.7860	0.0001118	1.7883
1.0180	0.0002156	1.8162	0.0001779	1.7860	0.0001111	1.7883
1.0190	0.0002145	1.8162	0.0001763	1.7860	0.0001104	1.7883
1.0200	0.0002127	1.8162	0.0001740	1.7860	0.0001092	1.7883
1.0210	0.0002120	1.8162	0.0001724	1.7860	0.0001084	1.7883
1.0220	0.0002121	1.8162	0.0001715	1.7860	0.0001079	1.7883
1.0230	0.0002114	1.8161	0.0001699	1.7860	0.0001070	1.7883
1.0240	0.0002107	1.8161	0.0001683	1.7860	0.0001060	1.7883
1.0250	0.0002099	1.8161	0.0001668	1.7859	0.0001051	1.7883
1.0260	0.0002090	1.8161	0.0001653	1.7859	0.0001042	1.7883
1.0270	0.0002071	1.8161	0.0001632	1.7859	0.0001029	1.7883
1.0280	0.0002070	1.8161	0.0001627	1.7859	0.0001027	1.7883
1.0290	0.0002059	1.8161	0.0001614	1.7859	0.0001020	1.7883
1.0300	0.0002048	1.8161	0.0001602	1.7859	0.0001014	1.7882
1.0310	0.0002038	1.8161	0.0001589	1.7859	0.0001008	1.7882
1.0320	0.0002029	1.8161	0.0001576	1.7859	0.0001002	1.7882
1.0330	0.0002021	1.8160	0.0001563	1.7859	0.0000995	1.7882
1.0340	0.0002013	1.8160	0.0001549	1.7858	0.0000988	1.7882
1.0350	0.0002004	1.8160	0.0001534	1.7858	0.0000980	1.7882
1.0360	0.0001995	1.8160	0.0001520	1.7858	0.0000972	1.7882
1.0370	0.0001985	1.8160	0.0001508	1.7858	0.0000964	1.7882
1.0380	0.0001973	1.8160	0.0001496	1.7858	0.0000956	1.7882
1.0390	0.0001962	1.8160	0.0001485	1.7858	0.0000948	1.7882
1.0400	0.0001950	1.8160	0.0001473	1.7858	0.0000941	1.7882
1.0410	0.0001939	1.8160	0.0001461	1.7858	0.0000933	1.7882
1.0420	0.0001929	1.8159	0.0001448	1.7857	0.0000926	1.7882
1.0430	0.0001920	1.8159	0.0001435	1.7857	0.0000919	1.7882

1.0440	0.0001910	1.8159	0.0001423	1.7857	0.0000912	1.7882
1.0450	0.0001901	1.8159	0.0001412	1.7857	0.0000906	1.7882
1.0460	0.0001892	1.8159	0.0001402	1.7857	0.0000899	1.7882
1.0470	0.0001883	1.8159	0.0001392	1.7857	0.0000893	1.7882
1.0480	0.0001873	1.8159	0.0001378	1.7857	0.0000886	1.7882
1.0490	0.0001863	1.8159	0.0001365	1.7857	0.0000880	1.7882
1.0500	0.0001854	1.8159	0.0001352	1.7856	0.0000873	1.7882
1.0510	0.0001845	1.8158	0.0001339	1.7856	0.0000866	1.7881
1.0520	0.0001835	1.8158	0.0001330	1.7856	0.0000859	1.7881
1.0530	0.0001825	1.8158	0.0001322	1.7856	0.0000853	1.7881
1.0540	0.0001815	1.8158	0.0001314	1.7856	0.0000846	1.7881
1.0550	0.0001806	1.8158	0.0001304	1.7856	0.0000840	1.7881
1.0560	0.0001796	1.8158	0.0001294	1.7856	0.0000834	1.7881
1.0570	0.0001786	1.8158	0.0001283	1.7856	0.0000828	1.7881
1.0580	0.0001776	1.8158	0.0001272	1.7855	0.0000821	1.7881
1.0590	0.0001766	1.8158	0.0001263	1.7855	0.0000816	1.7881
1.0600	0.0001755	1.8157	0.0001254	1.7855	0.0000810	1.7881
1.0610	0.0001743	1.8157	0.0001245	1.7855	0.0000804	1.7881
1.0620	0.0001732	1.8157	0.0001237	1.7855	0.0000798	1.7881
1.0630	0.0001721	1.8157	0.0001228	1.7855	0.0000793	1.7881
1.0640	0.0001710	1.8157	0.0001218	1.7855	0.0000788	1.7881
1.0650	0.0001700	1.8157	0.0001209	1.7855	0.0000784	1.7881
1.0660	0.0001692	1.8157	0.0001201	1.7854	0.0000779	1.7881
1.0670	0.0001675	1.8157	0.0001186	1.7854	0.0000769	1.7881
1.0680	0.0001674	1.8157	0.0001184	1.7854	0.0000768	1.7881
1.0690	0.0001671	1.8156	0.0001182	1.7854	0.0000766	1.7881
1.0700	0.0001653	1.8156	0.0001168	1.7854	0.0000757	1.7880
1.0710	0.0001642	1.8156	0.0001161	1.7854	0.0000752	1.7880
1.0720	0.0001631	1.8156	0.0001153	1.7854	0.0000748	1.7880
1.0730	0.0001621	1.8156	0.0001145	1.7854	0.0000744	1.7880
1.0740	0.0001611	1.8156	0.0001138	1.7853	0.0000740	1.7880
1.0750	0.0001601	1.8156	0.0001131	1.7853	0.0000736	1.7880
1.0760	0.0001591	1.8156	0.0001124	1.7853	0.0000731	1.7880
1.0770	0.0001581	1.8156	0.0001117	1.7853	0.0000727	1.7880
1.0780	0.0001571	1.8155	0.0001111	1.7853	0.0000722	1.7880
1.0790	0.0001560	1.8155	0.0001104	1.7853	0.0000717	1.7880
1.0800	0.0001551	1.8155	0.0001098	1.7853	0.0000713	1.7880
1.0810	0.0001541	1.8155	0.0001091	1.7853	0.0000709	1.7880
1.0820	0.0001530	1.8155	0.0001085	1.7852	0.0000706	1.7880
1.0830	0.0001519	1.8155	0.0001079	1.7852	0.0000702	1.7880
1.0840	0.0001508	1.8155	0.0001074	1.7852	0.0000698	1.7880
1.0850	0.0001495	1.8155	0.0001069	1.7852	0.0000694	1.7880
1.0860	0.0001484	1.8155	0.0001064	1.7852	0.0000689	1.7880

1.0870	0.0001473	1.8154	0.0001059	1.7852	0.0000685	1.7880
1.0880	0.0001457	1.8154	0.0001048	1.7852	0.0000677	1.7880
1.0890	0.0001456	1.8154	0.0001047	1.7852	0.0000677	1.7879
1.0900	0.0001448	1.8154	0.0001041	1.7851	0.0000674	1.7879
1.0910	0.0001439	1.8154	0.0001035	1.7851	0.0000671	1.7879
1.0920	0.0001429	1.8154	0.0001029	1.7851	0.0000668	1.7879
1.0930	0.0001420	1.8154	0.0001024	1.7851	0.0000665	1.7879
1.0940	0.0001409	1.8154	0.0001020	1.7851	0.0000661	1.7879
1.0950	0.0001398	1.8153	0.0001015	1.7851	0.0000658	1.7879
1.0960	0.0001388	1.8153	0.0001011	1.7851	0.0000654	1.7879
1.0970	0.0001378	1.8153	0.0001006	1.7850	0.0000651	1.7879
1.0980	0.0001367	1.8153	0.0001001	1.7850	0.0000649	1.7879
1.0990	0.0001356	1.8153	0.0000995	1.7850	0.0000646	1.7879
1.1000	0.0001346	1.8153	0.0000990	1.7850	0.0000643	1.7879
1.1010	0.0001337	1.8153	0.0000986	1.7850	0.0000641	1.7879
1.1020	0.0001327	1.8153	0.0000982	1.7850	0.0000638	1.7879
1.1030	0.0001318	1.8153	0.0000977	1.7850	0.0000635	1.7879
1.1040	0.0001308	1.8152	0.0000973	1.7850	0.0000631	1.7879
1.1050	0.0001297	1.8152	0.0000969	1.7849	0.0000628	1.7879
1.1060	0.0001288	1.8152	0.0000965	1.7849	0.0000626	1.7879
1.1070	0.0001278	1.8152	0.0000960	1.7849	0.0000623	1.7879
1.1080	0.0001268	1.8152	0.0000957	1.7849	0.0000621	1.7878
1.1090	0.0001259	1.8152	0.0000953	1.7849	0.0000619	1.7878
1.1100	0.0001249	1.8152	0.0000949	1.7849	0.0000617	1.7878
1.1110	0.0001239	1.8152	0.0000945	1.7849	0.0000614	1.7878
1.1120	0.0001229	1.8151	0.0000942	1.7849	0.0000612	1.7878
1.1130	0.0001219	1.8151	0.0000938	1.7848	0.0000609	1.7878
1.1140	0.0001209	1.8151	0.0000934	1.7848	0.0000606	1.7878
1.1150	0.0001199	1.8151	0.0000930	1.7848	0.0000603	1.7878
1.1160	0.0001189	1.8151	0.0000926	1.7848	0.0000601	1.7878
1.1170	0.0001179	1.8151	0.0000921	1.7848	0.0000599	1.7878
1.1180	0.0001169	1.8151	0.0000917	1.7848	0.0000596	1.7878
1.1190	0.0001159	1.8151	0.0000913	1.7848	0.0000594	1.7878
1.1200	0.0001149	1.8150	0.0000908	1.7847	0.0000591	1.7878
1.1210	0.0001140	1.8150	0.0000904	1.7847	0.0000589	1.7878
1.1220	0.0001130	1.8150	0.0000900	1.7847	0.0000586	1.7878
1.1230	0.0001120	1.8150	0.0000896	1.7847	0.0000584	1.7878
1.1240	0.0001111	1.8150	0.0000893	1.7847	0.0000582	1.7878
1.1250	0.0001102	1.8150	0.0000889	1.7847	0.0000579	1.7878
1.1260	0.0001093	1.8150	0.0000885	1.7847	0.0000577	1.7877
1.1270	0.0001083	1.8150	0.0000881	1.7847	0.0000575	1.7877
1.1280	0.0001074	1.8149	0.0000878	1.7846	0.0000572	1.7877
1.1290	0.0001064	1.8149	0.0000874	1.7846	0.0000570	1.7877

1.1300	0.0001054	1.8149	0.0000870	1.7846	0.0000568	1.7877
1.1310	0.0001044	1.8149	0.0000867	1.7846	0.0000566	1.7877
1.1320	0.0001035	1.8149	0.0000863	1.7846	0.0000564	1.7877
1.1330	0.0001025	1.8149	0.0000859	1.7846	0.0000562	1.7877
1.1340	0.0001016	1.8149	0.0000855	1.7846	0.0000560	1.7877
1.1350	0.0001007	1.8149	0.0000851	1.7845	0.0000558	1.7877
1.1360	0.0000998	1.8148	0.0000847	1.7845	0.0000556	1.7877
1.1370	0.0000988	1.8148	0.0000843	1.7845	0.0000554	1.7877
1.1380	0.0000978	1.8148	0.0000839	1.7845	0.0000552	1.7877
1.1390	0.0000968	1.8148	0.0000835	1.7845	0.0000550	1.7877
1.1400	0.0000959	1.8148	0.0000832	1.7845	0.0000548	1.7877
1.1410	0.0000950	1.8148	0.0000828	1.7845	0.0000546	1.7877
1.1420	0.0000940	1.8148	0.0000824	1.7844	0.0000544	1.7877
1.1430	0.0000931	1.8148	0.0000821	1.7844	0.0000542	1.7877
1.1440	0.0000922	1.8147	0.0000817	1.7844	0.0000540	1.7876
1.1450	0.0000913	1.8147	0.0000814	1.7844	0.0000538	1.7876
1.1460	0.0000904	1.8147	0.0000810	1.7844	0.0000536	1.7876
1.1470	0.0000896	1.8147	0.0000807	1.7844	0.0000534	1.7876
1.1480	0.0000887	1.8147	0.0000804	1.7844	0.0000532	1.7876
1.1490	0.0000879	1.8147	0.0000800	1.7844	0.0000530	1.7876
1.1500	0.0000871	1.8147	0.0000797	1.7843	0.0000528	1.7876
1.1510	0.0000862	1.8146	0.0000793	1.7843	0.0000526	1.7876
1.1520	0.0000854	1.8146	0.0000790	1.7843	0.0000525	1.7876
1.1530	0.0000846	1.8146	0.0000786	1.7843	0.0000523	1.7876
1.1540	0.0000837	1.8146	0.0000782	1.7843	0.0000521	1.7876
1.1550	0.0000829	1.8146	0.0000779	1.7843	0.0000519	1.7876
1.1560	0.0000820	1.8146	0.0000775	1.7843	0.0000517	1.7876
1.1570	0.0000812	1.8146	0.0000772	1.7842	0.0000515	1.7876
1.1580	0.0000804	1.8146	0.0000768	1.7842	0.0000513	1.7876
1.1590	0.0000796	1.8145	0.0000765	1.7842	0.0000511	1.7876
1.1600	0.0000788	1.8145	0.0000761	1.7842	0.0000509	1.7876
1.1610	0.0000780	1.8145	0.0000758	1.7842	0.0000506	1.7876
1.1620	0.0000772	1.8145	0.0000754	1.7842	0.0000504	1.7875
1.1630	0.0000769	1.8145	0.0000755	1.7842	0.0000505	1.7875
1.1640	0.0000756	1.8145	0.0000748	1.7841	0.0000500	1.7875
1.1650	0.0000753	1.8145	0.0000749	1.7841	0.0000501	1.7875
1.1660	0.0000746	1.8144	0.0000745	1.7841	0.0000499	1.7875
1.1670	0.0000734	1.8144	0.0000738	1.7841	0.0000494	1.7875
1.1680	0.0000731	1.8144	0.0000738	1.7841	0.0000496	1.7875
1.1690	0.0000719	1.8144	0.0000731	1.7841	0.0000491	1.7875
1.1700	0.0000711	1.8144	0.0000727	1.7841	0.0000489	1.7875
1.1710	0.0000704	1.8144	0.0000724	1.7840	0.0000487	1.7875
1.1720	0.0000697	1.8144	0.0000720	1.7840	0.0000485	1.7875

1.1730	0.0000689	1.8144	0.0000717	1.7840	0.0000482	1.7875
1.1740	0.0000682	1.8143	0.0000714	1.7840	0.0000480	1.7875
1.1750	0.0000675	1.8143	0.0000710	1.7840	0.0000478	1.7875
1.1760	0.0000673	1.8143	0.0000711	1.7840	0.0000479	1.7875
1.1770	0.0000666	1.8143	0.0000708	1.7840	0.0000477	1.7875
1.1780	0.0000659	1.8143	0.0000705	1.7840	0.0000475	1.7875
1.1790	0.0000648	1.8143	0.0000698	1.7839	0.0000471	1.7875
1.1800	0.0000646	1.8143	0.0000698	1.7839	0.0000472	1.7874
1.1810	0.0000638	1.8142	0.0000695	1.7839	0.0000470	1.7874
1.1820	0.0000632	1.8142	0.0000692	1.7839	0.0000468	1.7874
1.1830	0.0000625	1.8142	0.0000688	1.7839	0.0000466	1.7874
1.1840	0.0000618	1.8142	0.0000685	1.7839	0.0000464	1.7874
1.1850	0.0000611	1.8142	0.0000681	1.7839	0.0000462	1.7874
1.1860	0.0000605	1.8142	0.0000678	1.7838	0.0000460	1.7874
1.1870	0.0000598	1.8142	0.0000674	1.7838	0.0000458	1.7874
1.1880	0.0000591	1.8141	0.0000671	1.7838	0.0000456	1.7874
1.1890	0.0000584	1.8141	0.0000668	1.7838	0.0000454	1.7874
1.1900	0.0000578	1.8141	0.0000664	1.7838	0.0000452	1.7874
1.1910	0.0000572	1.8141	0.0000661	1.7838	0.0000450	1.7874
1.1920	0.0000565	1.8141	0.0000657	1.7838	0.0000448	1.7874
1.1930	0.0000559	1.8141	0.0000654	1.7837	0.0000446	1.7874
1.1940	0.0000552	1.8141	0.0000650	1.7837	0.0000444	1.7874
1.1950	0.0000546	1.8141	0.0000646	1.7837	0.0000442	1.7874
1.1960	0.0000540	1.8140	0.0000643	1.7837	0.0000440	1.7874
1.1970	0.0000534	1.8140	0.0000640	1.7837	0.0000438	1.7873
1.1980	0.0000528	1.8140	0.0000636	1.7837	0.0000436	1.7873
1.1990	0.0000522	1.8140	0.0000633	1.7837	0.0000434	1.7873
1.2000	0.0000516	1.8140	0.0000629	1.7836	0.0000433	1.7873
1.2010	0.0000510	1.8140	0.0000626	1.7836	0.0000431	1.7873
1.2020	0.0000504	1.8140	0.0000623	1.7836	0.0000429	1.7873
1.2030	0.0000498	1.8139	0.0000619	1.7836	0.0000427	1.7873
1.2040	0.0000492	1.8139	0.0000615	1.7836	0.0000425	1.7873
1.2050	0.0000486	1.8139	0.0000612	1.7836	0.0000423	1.7873
1.2060	0.0000480	1.8139	0.0000608	1.7836	0.0000420	1.7873
1.2070	0.0000475	1.8139	0.0000604	1.7835	0.0000418	1.7873
1.2080	0.0000469	1.8139	0.0000600	1.7835	0.0000417	1.7873
1.2090	0.0000464	1.8139	0.0000597	1.7835	0.0000415	1.7873
1.2100	0.0000458	1.8138	0.0000593	1.7835	0.0000413	1.7873
1.2110	0.0000453	1.8138	0.0000589	1.7835	0.0000411	1.7873
1.2120	0.0000447	1.8138	0.0000586	1.7835	0.0000409	1.7873
1.2130	0.0000442	1.8138	0.0000582	1.7834	0.0000407	1.7873
1.2140	0.0000437	1.8138	0.0000579	1.7834	0.0000404	1.7872
1.2150	0.0000431	1.8138	0.0000575	1.7834	0.0000402	1.7872

1.2160	0.0000426	1.8138	0.0000572	1.7834	0.0000400	1.7872
1.2170	0.0000422	1.8137	0.0000568	1.7834	0.0000398	1.7872
1.2180	0.0000417	1.8137	0.0000565	1.7834	0.0000396	1.7872
1.2190	0.0000412	1.8137	0.0000562	1.7834	0.0000393	1.7872
1.2200	0.0000408	1.8137	0.0000558	1.7833	0.0000391	1.7872
1.2210	0.0000403	1.8137	0.0000555	1.7833	0.0000389	1.7872
1.2220	0.0000398	1.8137	0.0000552	1.7833	0.0000387	1.7872
1.2230	0.0000393	1.8137	0.0000548	1.7833	0.0000385	1.7872
1.2240	0.0000388	1.8136	0.0000545	1.7833	0.0000383	1.7872
1.2250	0.0000384	1.8136	0.0000542	1.7833	0.0000381	1.7872
1.2260	0.0000379	1.8136	0.0000539	1.7833	0.0000379	1.7872
1.2270	0.0000375	1.8136	0.0000536	1.7832	0.0000377	1.7872
1.2280	0.0000370	1.8136	0.0000533	1.7832	0.0000375	1.7872
1.2290	0.0000365	1.8136	0.0000529	1.7832	0.0000373	1.7872
1.2300	0.0000361	1.8136	0.0000526	1.7832	0.0000370	1.7871
1.2310	0.0000359	1.8135	0.0000526	1.7832	0.0000371	1.7871
1.2320	0.0000352	1.8135	0.0000519	1.7832	0.0000366	1.7871
1.2330	0.0000347	1.8135	0.0000515	1.7832	0.0000364	1.7871
1.2340	0.0000343	1.8135	0.0000512	1.7831	0.0000362	1.7871
1.2350	0.0000339	1.8135	0.0000508	1.7831	0.0000360	1.7871
1.2360	0.0000335	1.8135	0.0000505	1.7831	0.0000358	1.7871
1.2370	0.0000331	1.8134	0.0000502	1.7831	0.0000356	1.7871
1.2380	0.0000327	1.8134	0.0000499	1.7831	0.0000354	1.7871
1.2390	0.0000323	1.8134	0.0000496	1.7831	0.0000351	1.7871
1.2400	0.0000319	1.8134	0.0000492	1.7830	0.0000349	1.7871
1.2410	0.0000315	1.8134	0.0000489	1.7830	0.0000347	1.7871
1.2420	0.0000312	1.8134	0.0000486	1.7830	0.0000345	1.7871
1.2430	0.0000308	1.8134	0.0000483	1.7830	0.0000343	1.7871
1.2440	0.0000304	1.8133	0.0000480	1.7830	0.0000341	1.7871
1.2450	0.0000301	1.8133	0.0000476	1.7830	0.0000338	1.7871
1.2460	0.0000300	1.8133	0.0000476	1.7830	0.0000339	1.7871
1.2470	0.0000293	1.8133	0.0000470	1.7829	0.0000335	1.7870
1.2480	0.0000289	1.8133	0.0000467	1.7829	0.0000333	1.7870
1.2490	0.0000286	1.8133	0.0000464	1.7829	0.0000331	1.7870
1.2500	0.0000283	1.8133	0.0000460	1.7829	0.0000329	1.7870
1.2510	0.0000279	1.8132	0.0000457	1.7829	0.0000327	1.7870
1.2520	0.0000276	1.8132	0.0000454	1.7829	0.0000325	1.7870
1.2530	0.0000275	1.8132	0.0000454	1.7828	0.0000325	1.7870
1.2540	0.0000269	1.8132	0.0000448	1.7828	0.0000321	1.7870
1.2550	0.0000269	1.8132	0.0000448	1.7828	0.0000321	1.7870
1.2560	0.0000266	1.8132	0.0000444	1.7828	0.0000319	1.7870
1.2570	0.0000263	1.8131	0.0000441	1.7828	0.0000317	1.7870
1.2580	0.0000260	1.8131	0.0000438	1.7828	0.0000315	1.7870

1.2590	0.0000257	1.8131	0.0000435	1.7828	0.0000312	1.7870
1.2600	0.0000254	1.8131	0.0000432	1.7827	0.0000310	1.7870
1.2610	0.0000251	1.8131	0.0000429	1.7827	0.0000308	1.7870
1.2620	0.0000248	1.8131	0.0000426	1.7827	0.0000306	1.7869
1.2630	0.0000243	1.8131	0.0000420	1.7827	0.0000302	1.7869
1.2640	0.0000243	1.8130	0.0000419	1.7827	0.0000302	1.7869
1.2650	0.0000240	1.8130	0.0000416	1.7827	0.0000299	1.7869
1.2660	0.0000237	1.8130	0.0000413	1.7826	0.0000297	1.7869
1.2670	0.0000235	1.8130	0.0000410	1.7826	0.0000295	1.7869
1.2680	0.0000232	1.8130	0.0000407	1.7826	0.0000293	1.7869
1.2690	0.0000229	1.8130	0.0000403	1.7826	0.0000291	1.7869
1.2700	0.0000227	1.8130	0.0000400	1.7826	0.0000289	1.7869
1.2710	0.0000224	1.8129	0.0000397	1.7826	0.0000287	1.7869
1.2720	0.0000222	1.8129	0.0000394	1.7826	0.0000285	1.7869
1.2730	0.0000219	1.8129	0.0000391	1.7825	0.0000283	1.7869
1.2740	0.0000217	1.8129	0.0000388	1.7825	0.0000281	1.7869
1.2750	0.0000214	1.8129	0.0000385	1.7825	0.0000279	1.7869
1.2760	0.0000212	1.8129	0.0000382	1.7825	0.0000277	1.7869
1.2770	0.0000209	1.8128	0.0000380	1.7825	0.0000275	1.7869
1.2780	0.0000207	1.8128	0.0000377	1.7825	0.0000273	1.7868
1.2790	0.0000205	1.8128	0.0000374	1.7824	0.0000271	1.7868
1.2800	0.0000203	1.8128	0.0000371	1.7824	0.0000269	1.7868
1.2810	0.0000200	1.8128	0.0000368	1.7824	0.0000267	1.7868
1.2820	0.0000198	1.8128	0.0000365	1.7824	0.0000265	1.7868
1.2830	0.0000196	1.8128	0.0000361	1.7824	0.0000263	1.7868
1.2840	0.0000194	1.8127	0.0000358	1.7824	0.0000261	1.7868
1.2850	0.0000192	1.8127	0.0000355	1.7823	0.0000259	1.7868
1.2860	0.0000190	1.8127	0.0000352	1.7823	0.0000257	1.7868
1.2870	0.0000188	1.8127	0.0000349	1.7823	0.0000255	1.7868
1.2880	0.0000186	1.8127	0.0000346	1.7823	0.0000254	1.7868
1.2890	0.0000185	1.8127	0.0000343	1.7823	0.0000252	1.7868
1.2900	0.0000183	1.8126	0.0000340	1.7823	0.0000250	1.7868
1.2910	0.0000181	1.8126	0.0000337	1.7823	0.0000248	1.7868
1.2920	0.0000179	1.8126	0.0000335	1.7822	0.0000246	1.7868
1.2930	0.0000177	1.8126	0.0000332	1.7822	0.0000244	1.7867
1.2940	0.0000175	1.8126	0.0000329	1.7822	0.0000242	1.7867
1.2950	0.0000174	1.8126	0.0000326	1.7822	0.0000240	1.7867
1.2960	0.0000172	1.8125	0.0000323	1.7822	0.0000238	1.7867
1.2970	0.0000170	1.8125	0.0000321	1.7822	0.0000236	1.7867
1.2980	0.0000171	1.8125	0.0000321	1.7821	0.0000236	1.7867
1.2990	0.0000167	1.8125	0.0000316	1.7821	0.0000233	1.7867
1.3000	0.0000165	1.8125	0.0000313	1.7821	0.0000231	1.7867
1.3010	0.0000166	1.8125	0.0000313	1.7821	0.0000231	1.7867

1.3020	0.0000164	1.8125	0.0000311	1.7821	0.0000229	1.7867
1.3030	0.0000162	1.8124	0.0000308	1.7821	0.0000227	1.7867
1.3040	0.0000161	1.8124	0.0000306	1.7820	0.0000225	1.7867
1.3050	0.0000159	1.8124	0.0000303	1.7820	0.0000223	1.7867
1.3060	0.0000157	1.8124	0.0000301	1.7820	0.0000221	1.7867
1.3070	0.0000156	1.8124	0.0000298	1.7820	0.0000220	1.7867
1.3080	0.0000154	1.8124	0.0000296	1.7820	0.0000218	1.7866
1.3090	0.0000151	1.8123	0.0000291	1.7820	0.0000214	1.7866
1.3100	0.0000151	1.8123	0.0000291	1.7819	0.0000214	1.7866
1.3110	0.0000150	1.8123	0.0000289	1.7819	0.0000212	1.7866
1.3120	0.0000148	1.8123	0.0000286	1.7819	0.0000211	1.7866
1.3130	0.0000147	1.8123	0.0000284	1.7819	0.0000209	1.7866
1.3140	0.0000143	1.8123	0.0000279	1.7819	0.0000206	1.7866
1.3150	0.0000144	1.8122	0.0000279	1.7819	0.0000206	1.7866
1.3160	0.0000142	1.8122	0.0000277	1.7818	0.0000204	1.7866
1.3170	0.0000141	1.8122	0.0000275	1.7818	0.0000202	1.7866
1.3180	0.0000140	1.8122	0.0000272	1.7818	0.0000201	1.7866
1.3190	0.0000139	1.8122	0.0000270	1.7818	0.0000199	1.7866
1.3200	0.0000138	1.8122	0.0000268	1.7818	0.0000197	1.7866
1.3210	0.0000136	1.8122	0.0000266	1.7818	0.0000196	1.7866
1.3220	0.0000135	1.8121	0.0000264	1.7817	0.0000194	1.7866
1.3230	0.0000134	1.8121	0.0000261	1.7817	0.0000192	1.7865
1.3240	0.0000133	1.8121	0.0000259	1.7817	0.0000191	1.7865
1.3250	0.0000132	1.8121	0.0000257	1.7817	0.0000189	1.7865
1.3260	0.0000131	1.8121	0.0000255	1.7817	0.0000187	1.7865
1.3270	0.0000130	1.8121	0.0000253	1.7817	0.0000186	1.7865
1.3280	0.0000129	1.8120	0.0000251	1.7816	0.0000184	1.7865
1.3290	0.0000128	1.8120	0.0000249	1.7816	0.0000182	1.7865
1.3300	0.0000127	1.8120	0.0000247	1.7816	0.0000180	1.7865
1.3310	0.0000126	1.8120	0.0000244	1.7816	0.0000179	1.7865
1.3320	0.0000125	1.8120	0.0000242	1.7816	0.0000177	1.7865
1.3330	0.0000125	1.8120	0.0000240	1.7816	0.0000176	1.7865
1.3340	0.0000124	1.8119	0.0000238	1.7815	0.0000174	1.7865
1.3350	0.0000123	1.8119	0.0000236	1.7815	0.0000173	1.7865
1.3360	0.0000124	1.8119	0.0000236	1.7815	0.0000173	1.7865
1.3370	0.0000121	1.8119	0.0000232	1.7815	0.0000170	1.7864
1.3380	0.0000120	1.8119	0.0000230	1.7815	0.0000168	1.7864
1.3390	0.0000121	1.8119	0.0000230	1.7815	0.0000168	1.7864
1.3400	0.0000119	1.8118	0.0000226	1.7814	0.0000165	1.7864
1.3410	0.0000118	1.8118	0.0000224	1.7814	0.0000164	1.7864
1.3420	0.0000118	1.8118	0.0000222	1.7814	0.0000163	1.7864
1.3430	0.0000119	1.8118	0.0000222	1.7814	0.0000163	1.7864
1.3440	0.0000118	1.8118	0.0000220	1.7814	0.0000161	1.7864

1.3450	0.0000116	1.8118	0.0000217	1.7814	0.0000159	1.7864
1.3460	0.0000117	1.8117	0.0000217	1.7813	0.0000159	1.7864
1.3470	0.0000117	1.8117	0.0000215	1.7813	0.0000157	1.7864
1.3480	0.0000117	1.8117	0.0000213	1.7813	0.0000156	1.7864
1.3490	0.0000116	1.8117	0.0000212	1.7813	0.0000155	1.7864
1.3500	0.0000116	1.8117	0.0000210	1.7813	0.0000154	1.7864
1.3510	0.0000115	1.8117	0.0000208	1.7813	0.0000153	1.7864
1.3520	0.0000115	1.8116	0.0000207	1.7812	0.0000151	1.7863
1.3530	0.0000115	1.8116	0.0000205	1.7812	0.0000150	1.7863
1.3540	0.0000114	1.8116	0.0000204	1.7812	0.0000149	1.7863
1.3550	0.0000114	1.8116	0.0000202	1.7812	0.0000148	1.7863
1.3560	0.0000114	1.8116	0.0000200	1.7812	0.0000147	1.7863
1.3570	0.0000112	1.8116	0.0000197	1.7812	0.0000144	1.7863
1.3580	0.0000113	1.8115	0.0000197	1.7811	0.0000144	1.7863
1.3590	0.0000113	1.8115	0.0000196	1.7811	0.0000143	1.7863
1.3600	0.0000113	1.8115	0.0000194	1.7811	0.0000142	1.7863
1.3610	0.0000112	1.8115	0.0000193	1.7811	0.0000141	1.7863
1.3620	0.0000112	1.8115	0.0000192	1.7811	0.0000140	1.7863
1.3630	0.0000114	1.8115	0.0000192	1.7811	0.0000140	1.7863
1.3640	0.0000112	1.8114	0.0000189	1.7810	0.0000138	1.7863
1.3650	0.0000112	1.8114	0.0000188	1.7810	0.0000137	1.7863
1.3660	0.0000113	1.8114	0.0000187	1.7810	0.0000136	1.7862
1.3670	0.0000113	1.8114	0.0000185	1.7810	0.0000135	1.7862
1.3680	0.0000113	1.8114	0.0000184	1.7810	0.0000134	1.7862
1.3690	0.0000114	1.8114	0.0000183	1.7809	0.0000133	1.7862
1.3700	0.0000114	1.8113	0.0000182	1.7809	0.0000133	1.7862
1.3710	0.0000114	1.8113	0.0000181	1.7809	0.0000132	1.7862
1.3720	0.0000115	1.8113	0.0000180	1.7809	0.0000131	1.7862
1.3730	0.0000116	1.8113	0.0000179	1.7809	0.0000130	1.7862
1.3740	0.0000116	1.8113	0.0000178	1.7809	0.0000129	1.7862
1.3750	0.0000117	1.8113	0.0000177	1.7808	0.0000128	1.7862
1.3760	0.0000118	1.8112	0.0000176	1.7808	0.0000127	1.7862
1.3770	0.0000118	1.8112	0.0000174	1.7808	0.0000126	1.7862
1.3780	0.0000119	1.8112	0.0000173	1.7808	0.0000125	1.7862
1.3790	0.0000120	1.8112	0.0000172	1.7808	0.0000124	1.7861
1.3800	0.0000121	1.8112	0.0000171	1.7808	0.0000123	1.7861
1.3810	0.0000122	1.8111	0.0000170	1.7807	0.0000122	1.7861
1.3820	0.0000123	1.8111	0.0000169	1.7807	0.0000121	1.7861
1.3830	0.0000124	1.8111	0.0000168	1.7807	0.0000120	1.7861
1.3840	0.0000126	1.8111	0.0000167	1.7807	0.0000119	1.7861
1.3850	0.0000127	1.8111	0.0000166	1.7807	0.0000118	1.7861
1.3860	0.0000128	1.8111	0.0000165	1.7806	0.0000117	1.7861
1.3870	0.0000129	1.8110	0.0000164	1.7806	0.0000116	1.7861

1.3880	0.0000130	1.8110	0.0000162	1.7806	0.0000115	1.7861
1.3890	0.0000132	1.8110	0.0000161	1.7806	0.0000115	1.7861
1.3900	0.0000133	1.8110	0.0000160	1.7806	0.0000114	1.7861
1.3910	0.0000134	1.8110	0.0000159	1.7806	0.0000113	1.7861
1.3920	0.0000136	1.8110	0.0000158	1.7805	0.0000112	1.7861
1.3930	0.0000137	1.8109	0.0000157	1.7805	0.0000111	1.7860
1.3940	0.0000138	1.8109	0.0000156	1.7805	0.0000111	1.7860
1.3950	0.0000140	1.8109	0.0000155	1.7805	0.0000110	1.7860
1.3960	0.0000141	1.8109	0.0000154	1.7805	0.0000109	1.7860
1.3970	0.0000142	1.8109	0.0000153	1.7804	0.0000109	1.7860
1.3980	0.0000144	1.8108	0.0000152	1.7804	0.0000108	1.7860
1.3990	0.0000145	1.8108	0.0000152	1.7804	0.0000108	1.7860
1.4000	0.0000147	1.8108	0.0000151	1.7804	0.0000107	1.7860
1.4010	0.0000148	1.8108	0.0000150	1.7804	0.0000107	1.7860
1.4020	0.0000150	1.8108	0.0000149	1.7804	0.0000106	1.7860
1.4030	0.0000151	1.8108	0.0000148	1.7803	0.0000106	1.7860
1.4040	0.0000151	1.8107	0.0000146	1.7803	0.0000104	1.7860
1.4050	0.0000153	1.8107	0.0000145	1.7803	0.0000104	1.7860
1.4060	0.0000155	1.8107	0.0000145	1.7803	0.0000104	1.7859
1.4070	0.0000159	1.8107	0.0000146	1.7803	0.0000104	1.7859
1.4080	0.0000159	1.8107	0.0000144	1.7802	0.0000103	1.7859
1.4090	0.0000161	1.8107	0.0000143	1.7802	0.0000103	1.7859
1.4100	0.0000166	1.8106	0.0000144	1.7802	0.0000104	1.7859
1.4110	0.0000169	1.8106	0.0000144	1.7802	0.0000103	1.7859
1.4120	0.0000169	1.8106	0.0000142	1.7802	0.0000102	1.7859
1.4130	0.0000172	1.8106	0.0000142	1.7802	0.0000102	1.7859
1.4140	0.0000177	1.8106	0.0000144	1.7801	0.0000103	1.7859
1.4150	0.0000179	1.8105	0.0000145	1.7801	0.0000103	1.7859
1.4160	0.0000180	1.8105	0.0000144	1.7801	0.0000102	1.7859
1.4170	0.0000185	1.8105	0.0000147	1.7801	0.0000103	1.7859
1.4180	0.0000189	1.8105	0.0000148	1.7801	0.0000103	1.7859
1.4190	0.0000190	1.8105	0.0000147	1.7800	0.0000102	1.7858
1.4200	0.0000194	1.8105	0.0000148	1.7800	0.0000102	1.7858
1.4210	0.0000198	1.8104	0.0000149	1.7800	0.0000103	1.7858
1.4220	0.0000205	1.8104	0.0000152	1.7800	0.0000104	1.7858
1.4230	0.0000207	1.8104	0.0000152	1.7800	0.0000103	1.7858
1.4240	0.0000213	1.8104	0.0000153	1.7800	0.0000103	1.7858
1.4250	0.0000218	1.8104	0.0000155	1.7799	0.0000104	1.7858
1.4260	0.0000225	1.8103	0.0000156	1.7799	0.0000104	1.7858
1.4270	0.0000234	1.8103	0.0000159	1.7799	0.0000106	1.7858
1.4280	0.0000241	1.8103	0.0000160	1.7799	0.0000106	1.7858
1.4290	0.0000248	1.8103	0.0000162	1.7799	0.0000106	1.7858
1.4300	0.0000255	1.8103	0.0000163	1.7798	0.0000107	1.7858

1.4310	0.0000260	1.8103	0.0000163	1.7798	0.0000106	1.7858
1.4320	0.0000269	1.8102	0.0000165	1.7798	0.0000107	1.7857
1.4330	0.0000277	1.8102	0.0000167	1.7798	0.0000108	1.7857
1.4340	0.0000286	1.8102	0.0000168	1.7798	0.0000108	1.7857
1.4350	0.0000296	1.8102	0.0000170	1.7797	0.0000109	1.7857
1.4360	0.0000306	1.8102	0.0000172	1.7797	0.0000110	1.7857
1.4370	0.0000316	1.8101	0.0000174	1.7797	0.0000111	1.7857
1.4380	0.0000327	1.8101	0.0000176	1.7797	0.0000112	1.7857
1.4390	0.0000338	1.8101	0.0000178	1.7797	0.0000114	1.7857
1.4400	0.0000349	1.8101	0.0000180	1.7797	0.0000115	1.7857
1.4410	0.0000361	1.8101	0.0000183	1.7796	0.0000117	1.7857
1.4420	0.0000374	1.8100	0.0000185	1.7796	0.0000119	1.7857
1.4430	0.0000387	1.8100	0.0000188	1.7796	0.0000121	1.7857
1.4440	0.0000404	1.8100	0.0000193	1.7796	0.0000126	1.7857
1.4450	0.0000414	1.8100	0.0000195	1.7796	0.0000127	1.7856
1.4460	0.0000424	1.8100	0.0000197	1.7795	0.0000129	1.7856
1.4470	0.0000442	1.8100	0.0000203	1.7795	0.0000134	1.7856
1.4480	0.0000457	1.8099	0.0000207	1.7795	0.0000138	1.7856
1.4490	0.0000476	1.8099	0.0000214	1.7795	0.0000144	1.7856
1.4500	0.0000487	1.8099	0.0000218	1.7795	0.0000148	1.7856
1.4510	0.0000503	1.8099	0.0000224	1.7794	0.0000153	1.7856
1.4520	0.0000518	1.8099	0.0000231	1.7794	0.0000159	1.7856
1.4530	0.0000529	1.8098	0.0000236	1.7794	0.0000164	1.7856
1.4540	0.0000548	1.8098	0.0000246	1.7794	0.0000173	1.7856
1.4550	0.0000563	1.8098	0.0000255	1.7794	0.0000181	1.7856
1.4560	0.0000582	1.8098	0.0000267	1.7793	0.0000191	1.7856
1.4570	0.0000586	1.8098	0.0000272	1.7793	0.0000197	1.7855
1.4580	0.0000608	1.8098	0.0000289	1.7793	0.0000212	1.7855
1.4590	0.0000615	1.8097	0.0000298	1.7793	0.0000221	1.7855
1.4600	0.0000626	1.8097	0.0000312	1.7793	0.0000233	1.7855
1.4610	0.0000636	1.8097	0.0000326	1.7792	0.0000244	1.7855
1.4620	0.0000645	1.8097	0.0000341	1.7792	0.0000255	1.7855
1.4630	0.0000652	1.8097	0.0000357	1.7792	0.0000265	1.7855
1.4640	0.0000658	1.8097	0.0000370	1.7792	0.0000273	1.7855
1.4650	0.0000663	1.8096	0.0000383	1.7792	0.0000278	1.7855
1.4660	0.0000667	1.8096	0.0000398	1.7792	0.0000280	1.7855
1.4670	0.0000669	1.8096	0.0000412	1.7791	0.0000279	1.7855
1.4680	0.0000670	1.8096	0.0000427	1.7791	0.0000275	1.7855
1.4690	0.0000670	1.8096	0.0000442	1.7791	0.0000268	1.7855
1.4700	0.0000669	1.8096	0.0000456	1.7791	0.0000258	1.7855
1.4710	0.0000671	1.8095	0.0000473	1.7791	0.0000249	1.7855
1.4720	0.0000663	1.8095	0.0000481	1.7790	0.0000235	1.7854
1.4730	0.0000659	1.8095	0.0000490	1.7790	0.0000223	1.7854

1.4740	0.0000654	1.8095	0.0000496	1.7790	0.0000211	1.7854
1.4750	0.0000648	1.8095	0.0000498	1.7790	0.0000200	1.7854
1.4760	0.0000642	1.8094	0.0000497	1.7790	0.0000190	1.7854
1.4770	0.0000635	1.8094	0.0000491	1.7790	0.0000182	1.7854
1.4780	0.0000633	1.8094	0.0000485	1.7789	0.0000176	1.7854
1.4790	0.0000621	1.8094	0.0000468	1.7789	0.0000168	1.7854
1.4800	0.0000614	1.8094	0.0000452	1.7789	0.0000163	1.7854
1.4810	0.0000607	1.8094	0.0000434	1.7789	0.0000159	1.7854
1.4820	0.0000599	1.8093	0.0000414	1.7789	0.0000156	1.7854
1.4830	0.0000592	1.8093	0.0000394	1.7789	0.0000154	1.7854
1.4840	0.0000585	1.8093	0.0000374	1.7788	0.0000153	1.7853
1.4850	0.0000583	1.8093	0.0000358	1.7788	0.0000153	1.7853
1.4860	0.0000572	1.8093	0.0000337	1.7788	0.0000151	1.7853
1.4870	0.0000565	1.8092	0.0000320	1.7788	0.0000150	1.7853
1.4880	0.0000563	1.8092	0.0000308	1.7788	0.0000151	1.7853
1.4890	0.0000552	1.8092	0.0000293	1.7787	0.0000149	1.7853
1.4900	0.0000542	1.8092	0.0000279	1.7787	0.0000147	1.7853
1.4910	0.0000540	1.8092	0.0000272	1.7787	0.0000149	1.7853
1.4920	0.0000534	1.8092	0.0000263	1.7787	0.0000149	1.7853
1.4930	0.0000528	1.8091	0.0000256	1.7787	0.0000149	1.7853
1.4940	0.0000518	1.8091	0.0000247	1.7786	0.0000147	1.7853
1.4950	0.0000512	1.8091	0.0000242	1.7786	0.0000148	1.7853
1.4960	0.0000510	1.8091	0.0000240	1.7786	0.0000150	1.7852
1.4970	0.0000504	1.8091	0.0000236	1.7786	0.0000150	1.7852
1.4980	0.0000499	1.8090	0.0000232	1.7786	0.0000151	1.7852
1.4990	0.0000493	1.8090	0.0000229	1.7785	0.0000152	1.7852
1.5000	0.0000487	1.8090	0.0000226	1.7785	0.0000152	1.7852
1.5010	0.0000482	1.8090	0.0000224	1.7785	0.0000153	1.7852
1.5020	0.0000477	1.8090	0.0000221	1.7785	0.0000154	1.7852
1.5030	0.0000472	1.8089	0.0000219	1.7785	0.0000155	1.7852
1.5040	0.0000467	1.8089	0.0000217	1.7784	0.0000156	1.7852
1.5050	0.0000466	1.8089	0.0000218	1.7784	0.0000158	1.7852
1.5060	0.0000457	1.8089	0.0000214	1.7784	0.0000158	1.7852
1.5070	0.0000456	1.8089	0.0000215	1.7784	0.0000160	1.7852
1.5080	0.0000447	1.8088	0.0000211	1.7784	0.0000159	1.7851
1.5090	0.0000443	1.8088	0.0000210	1.7783	0.0000160	1.7851
1.5100	0.0000442	1.8088	0.0000211	1.7783	0.0000162	1.7851
1.5110	0.0000434	1.8088	0.0000208	1.7783	0.0000161	1.7851
1.5120	0.0000430	1.8088	0.0000208	1.7783	0.0000162	1.7851
1.5130	0.0000425	1.8087	0.0000207	1.7783	0.0000162	1.7851
1.5140	0.0000422	1.8087	0.0000207	1.7782	0.0000162	1.7851
1.5150	0.0000420	1.8087	0.0000207	1.7782	0.0000162	1.7851
1.5160	0.0000417	1.8087	0.0000207	1.7782	0.0000162	1.7851

1.5170	0.0000414	1.8087	0.0000208	1.7782	0.0000162	1.7851
1.5180	0.0000411	1.8086	0.0000208	1.7782	0.0000162	1.7851
1.5190	0.0000409	1.8086	0.0000208	1.7781	0.0000161	1.7851
1.5200	0.0000406	1.8086	0.0000209	1.7781	0.0000160	1.7850
1.5210	0.0000404	1.8086	0.0000209	1.7781	0.0000160	1.7850
1.5220	0.0000401	1.8086	0.0000210	1.7781	0.0000159	1.7850
1.5230	0.0000399	1.8085	0.0000210	1.7781	0.0000158	1.7850
1.5240	0.0000397	1.8085	0.0000211	1.7780	0.0000157	1.7850
1.5250	0.0000399	1.8085	0.0000214	1.7780	0.0000158	1.7850
1.5260	0.0000393	1.8085	0.0000212	1.7780	0.0000155	1.7850
1.5270	0.0000391	1.8085	0.0000213	1.7780	0.0000154	1.7850
1.5280	0.0000389	1.8084	0.0000213	1.7779	0.0000153	1.7850
1.5290	0.0000390	1.8084	0.0000216	1.7779	0.0000153	1.7850
1.5300	0.0000385	1.8084	0.0000214	1.7779	0.0000150	1.7850
1.5310	0.0000383	1.8084	0.0000214	1.7779	0.0000149	1.7850
1.5320	0.0000385	1.8084	0.0000217	1.7779	0.0000148	1.7849
1.5330	0.0000379	1.8083	0.0000215	1.7778	0.0000145	1.7849
1.5340	0.0000377	1.8083	0.0000215	1.7778	0.0000143	1.7849
1.5350	0.0000379	1.8083	0.0000217	1.7778	0.0000142	1.7849
1.5360	0.0000374	1.8083	0.0000215	1.7778	0.0000138	1.7849
1.5370	0.0000372	1.8083	0.0000215	1.7778	0.0000135	1.7849
1.5380	0.0000374	1.8082	0.0000217	1.7777	0.0000133	1.7849
1.5390	0.0000369	1.8082	0.0000214	1.7777	0.0000129	1.7849
1.5400	0.0000368	1.8082	0.0000214	1.7777	0.0000126	1.7849
1.5410	0.0000366	1.8082	0.0000214	1.7777	0.0000123	1.7849
1.5420	0.0000369	1.8082	0.0000216	1.7777	0.0000122	1.7849
1.5430	0.0000371	1.8081	0.0000217	1.7776	0.0000121	1.7849
1.5440	0.0000363	1.8081	0.0000213	1.7776	0.0000116	1.7848
1.5450	0.0000362	1.8081	0.0000213	1.7776	0.0000114	1.7848
1.5460	0.0000361	1.8081	0.0000212	1.7776	0.0000112	1.7848
1.5470	0.0000360	1.8081	0.0000212	1.7776	0.0000110	1.7848
1.5480	0.0000359	1.8080	0.0000211	1.7775	0.0000108	1.7848
1.5490	0.0000357	1.8080	0.0000210	1.7775	0.0000107	1.7848
1.5500	0.0000356	1.8080	0.0000210	1.7775	0.0000105	1.7848
1.5510	0.0000359	1.8080	0.0000210	1.7775	0.0000105	1.7848
1.5520	0.0000354	1.8079	0.0000207	1.7775	0.0000102	1.7848
1.5530	0.0000353	1.8079	0.0000206	1.7774	0.0000101	1.7848
1.5540	0.0000356	1.8079	0.0000207	1.7774	0.0000100	1.7848
1.5550	0.0000352	1.8079	0.0000203	1.7774	0.0000098	1.7848
1.5560	0.0000351	1.8079	0.0000202	1.7774	0.0000096	1.7847
1.5570	0.0000350	1.8078	0.0000200	1.7773	0.0000095	1.7847
1.5580	0.0000349	1.8078	0.0000199	1.7773	0.0000094	1.7847
1.5590	0.0000352	1.8078	0.0000199	1.7773	0.0000093	1.7847

1.5600	0.0000348	1.8078	0.0000195	1.7773	0.0000091	1.7847
1.5610	0.0000347	1.8078	0.0000194	1.7773	0.0000090	1.7847
1.5620	0.0000347	1.8077	0.0000192	1.7772	0.0000088	1.7847
1.5630	0.0000346	1.8077	0.0000190	1.7772	0.0000087	1.7847
1.5640	0.0000349	1.8077	0.0000191	1.7772	0.0000087	1.7847
1.5650	0.0000344	1.8077	0.0000187	1.7772	0.0000085	1.7847
1.5660	0.0000347	1.8077	0.0000188	1.7772	0.0000086	1.7847
1.5670	0.0000346	1.8076	0.0000186	1.7771	0.0000085	1.7846
1.5680	0.0000345	1.8076	0.0000185	1.7771	0.0000084	1.7846
1.5690	0.0000341	1.8076	0.0000182	1.7771	0.0000082	1.7846
1.5700	0.0000344	1.8076	0.0000182	1.7771	0.0000083	1.7846
1.5710	0.0000343	1.8075	0.0000181	1.7771	0.0000082	1.7846
1.5720	0.0000339	1.8075	0.0000177	1.7770	0.0000080	1.7846
1.5730	0.0000338	1.8075	0.0000176	1.7770	0.0000079	1.7846
1.5740	0.0000337	1.8075	0.0000174	1.7770	0.0000078	1.7846
1.5750	0.0000336	1.8075	0.0000173	1.7770	0.0000077	1.7846
1.5760	0.0000335	1.8074	0.0000171	1.7769	0.0000076	1.7846
1.5770	0.0000334	1.8074	0.0000170	1.7769	0.0000076	1.7846
1.5780	0.0000333	1.8074	0.0000168	1.7769	0.0000075	1.7845
1.5790	0.0000333	1.8074	0.0000167	1.7769	0.0000074	1.7845
1.5800	0.0000336	1.8074	0.0000167	1.7769	0.0000074	1.7845
1.5810	0.0000335	1.8073	0.0000166	1.7768	0.0000073	1.7845
1.5820	0.0000331	1.8073	0.0000163	1.7768	0.0000071	1.7845
1.5830	0.0000331	1.8073	0.0000161	1.7768	0.0000070	1.7845
1.5840	0.0000331	1.8073	0.0000160	1.7768	0.0000069	1.7845
1.5850	0.0000334	1.8072	0.0000161	1.7768	0.0000070	1.7845
1.5860	0.0000337	1.8072	0.0000161	1.7767	0.0000070	1.7845
1.5870	0.0000330	1.8072	0.0000157	1.7767	0.0000067	1.7845
1.5880	0.0000333	1.8072	0.0000158	1.7767	0.0000067	1.7845
1.5890	0.0000333	1.8072	0.0000157	1.7767	0.0000067	1.7844
1.5900	0.0000333	1.8071	0.0000156	1.7766	0.0000066	1.7844
1.5910	0.0000333	1.8071	0.0000156	1.7766	0.0000065	1.7844
1.5920	0.0000332	1.8071	0.0000155	1.7766	0.0000065	1.7844
1.5930	0.0000332	1.8071	0.0000154	1.7766	0.0000064	1.7844
1.5940	0.0000328	1.8070	0.0000151	1.7766	0.0000063	1.7844
1.5950	0.0000328	1.8070	0.0000150	1.7765	0.0000062	1.7844
1.5960	0.0000328	1.8070	0.0000150	1.7765	0.0000062	1.7844
1.5970	0.0000331	1.8070	0.0000150	1.7765	0.0000062	1.7844
1.5980	0.0000331	1.8070	0.0000149	1.7765	0.0000062	1.7844
1.5990	0.0000331	1.8069	0.0000148	1.7764	0.0000061	1.7844
1.6000	0.0000331	1.8069	0.0000147	1.7764	0.0000061	1.7843
1.6010	0.0000331	1.8069	0.0000146	1.7764	0.0000060	1.7843
1.6020	0.0000331	1.8069	0.0000145	1.7764	0.0000060	1.7843

1.6030	0.0000331	1.8068	0.0000144	1.7764	0.0000060	1.7843
1.6040	0.0000331	1.8068	0.0000144	1.7763	0.0000059	1.7843
1.6050	0.0000331	1.8068	0.0000143	1.7763	0.0000059	1.7843
1.6060	0.0000331	1.8068	0.0000142	1.7763	0.0000058	1.7843
1.6070	0.0000331	1.8068	0.0000141	1.7763	0.0000058	1.7843
1.6080	0.0000331	1.8067	0.0000140	1.7762	0.0000057	1.7843
1.6090	0.0000335	1.8067	0.0000141	1.7762	0.0000058	1.7843
1.6100	0.0000335	1.8067	0.0000140	1.7762	0.0000058	1.7843
1.6110	0.0000335	1.8067	0.0000140	1.7762	0.0000057	1.7842
1.6120	0.0000335	1.8066	0.0000139	1.7762	0.0000057	1.7842
1.6130	0.0000336	1.8066	0.0000139	1.7761	0.0000057	1.7842
1.6140	0.0000335	1.8066	0.0000138	1.7761	0.0000056	1.7842
1.6150	0.0000335	1.8066	0.0000137	1.7761	0.0000056	1.7842
1.6160	0.0000332	1.8066	0.0000135	1.7761	0.0000055	1.7842
1.6170	0.0000331	1.8065	0.0000135	1.7760	0.0000055	1.7842
1.6180	0.0000331	1.8065	0.0000134	1.7760	0.0000054	1.7842
1.6190	0.0000331	1.8065	0.0000134	1.7760	0.0000054	1.7842
1.6200	0.0000335	1.8065	0.0000135	1.7760	0.0000055	1.7842
1.6210	0.0000335	1.8064	0.0000134	1.7760	0.0000055	1.7841
1.6220	0.0000334	1.8064	0.0000134	1.7759	0.0000054	1.7841
1.6230	0.0000334	1.8064	0.0000133	1.7759	0.0000054	1.7841
1.6240	0.0000330	1.8064	0.0000131	1.7759	0.0000053	1.7841
1.6250	0.0000330	1.8064	0.0000130	1.7759	0.0000053	1.7841
1.6260	0.0000330	1.8063	0.0000130	1.7758	0.0000053	1.7841
1.6270	0.0000330	1.8063	0.0000130	1.7758	0.0000053	1.7841
1.6280	0.0000334	1.8063	0.0000131	1.7758	0.0000053	1.7841
1.6290	0.0000334	1.8063	0.0000130	1.7758	0.0000053	1.7841
1.6300	0.0000333	1.8062	0.0000130	1.7757	0.0000053	1.7841
1.6310	0.0000333	1.8062	0.0000129	1.7757	0.0000053	1.7841
1.6320	0.0000333	1.8062	0.0000128	1.7757	0.0000053	1.7840
1.6330	0.0000333	1.8062	0.0000128	1.7757	0.0000053	1.7840
1.6340	0.0000333	1.8061	0.0000127	1.7757	0.0000052	1.7840
1.6350	0.0000333	1.8061	0.0000127	1.7756	0.0000052	1.7840
1.6360	0.0000332	1.8061	0.0000126	1.7756	0.0000052	1.7840
1.6370	0.0000332	1.8061	0.0000126	1.7756	0.0000052	1.7840
1.6380	0.0000332	1.8061	0.0000125	1.7756	0.0000052	1.7840
1.6390	0.0000331	1.8060	0.0000125	1.7755	0.0000052	1.7840
1.6400	0.0000331	1.8060	0.0000124	1.7755	0.0000052	1.7840
1.6410	0.0000331	1.8060	0.0000124	1.7755	0.0000051	1.7840
1.6420	0.0000330	1.8060	0.0000124	1.7755	0.0000051	1.7839
1.6430	0.0000330	1.8059	0.0000123	1.7754	0.0000051	1.7839
1.6440	0.0000330	1.8059	0.0000123	1.7754	0.0000051	1.7839
1.6450	0.0000334	1.8059	0.0000124	1.7754	0.0000052	1.7839

1.6460	0.0000334	1.8059	0.0000124	1.7754	0.0000052	1.7839
1.6470	0.0000335	1.8058	0.0000123	1.7754	0.0000051	1.7839
1.6480	0.0000335	1.8058	0.0000123	1.7753	0.0000051	1.7839
1.6490	0.0000335	1.8058	0.0000123	1.7753	0.0000051	1.7839
1.6500	0.0000335	1.8058	0.0000123	1.7753	0.0000051	1.7839
1.6510	0.0000336	1.8057	0.0000122	1.7753	0.0000051	1.7839
1.6520	0.0000336	1.8057	0.0000122	1.7752	0.0000051	1.7838
1.6530	0.0000336	1.8057	0.0000122	1.7752	0.0000051	1.7838
1.6540	0.0000336	1.8057	0.0000121	1.7752	0.0000051	1.7838
1.6550	0.0000337	1.8057	0.0000121	1.7752	0.0000050	1.7838
1.6560	0.0000337	1.8056	0.0000121	1.7751	0.0000050	1.7838
1.6570	0.0000337	1.8056	0.0000120	1.7751	0.0000050	1.7838
1.6580	0.0000337	1.8056	0.0000120	1.7751	0.0000050	1.7838
1.6590	0.0000341	1.8056	0.0000121	1.7751	0.0000051	1.7838
1.6600	0.0000341	1.8055	0.0000121	1.7750	0.0000051	1.7838
1.6610	0.0000338	1.8055	0.0000119	1.7750	0.0000050	1.7838
1.6620	0.0000338	1.8055	0.0000119	1.7750	0.0000050	1.7837
1.6630	0.0000342	1.8055	0.0000120	1.7750	0.0000051	1.7837
1.6640	0.0000342	1.8054	0.0000119	1.7750	0.0000051	1.7837
1.6650	0.0000343	1.8054	0.0000119	1.7749	0.0000051	1.7837
1.6660	0.0000343	1.8054	0.0000119	1.7749	0.0000051	1.7837
1.6670	0.0000343	1.8054	0.0000119	1.7749	0.0000051	1.7837
1.6680	0.0000344	1.8053	0.0000119	1.7749	0.0000051	1.7837
1.6690	0.0000341	1.8053	0.0000117	1.7748	0.0000050	1.7837
1.6700	0.0000341	1.8053	0.0000117	1.7748	0.0000050	1.7837
1.6710	0.0000342	1.8053	0.0000117	1.7748	0.0000050	1.7837
1.6720	0.0000342	1.8052	0.0000117	1.7748	0.0000050	1.7836
1.6730	0.0000346	1.8052	0.0000118	1.7747	0.0000051	1.7836
1.6740	0.0000347	1.8052	0.0000118	1.7747	0.0000051	1.7836
1.6750	0.0000348	1.8052	0.0000118	1.7747	0.0000051	1.7836
1.6760	0.0000349	1.8051	0.0000117	1.7747	0.0000051	1.7836
1.6770	0.0000346	1.8051	0.0000116	1.7746	0.0000050	1.7836
1.6780	0.0000350	1.8051	0.0000117	1.7746	0.0000051	1.7836
1.6790	0.0000347	1.8051	0.0000115	1.7746	0.0000050	1.7836
1.6800	0.0000351	1.8050	0.0000116	1.7746	0.0000051	1.7836
1.6810	0.0000355	1.8050	0.0000117	1.7745	0.0000052	1.7836
1.6820	0.0000356	1.8050	0.0000117	1.7745	0.0000051	1.7835
1.6830	0.0000353	1.8050	0.0000115	1.7745	0.0000050	1.7835
1.6840	0.0000354	1.8050	0.0000115	1.7745	0.0000050	1.7835
1.6850	0.0000358	1.8049	0.0000116	1.7744	0.0000051	1.7835
1.6860	0.0000359	1.8049	0.0000116	1.7744	0.0000051	1.7835
1.6870	0.0000356	1.8049	0.0000114	1.7744	0.0000050	1.7835
1.6880	0.0000360	1.8049	0.0000115	1.7744	0.0000051	1.7835

1.6890	0.0000357	1.8048	0.0000114	1.7744	0.0000050	1.7835
1.6900	0.0000361	1.8048	0.0000115	1.7743	0.0000051	1.7835
1.6910	0.0000359	1.8048	0.0000113	1.7743	0.0000050	1.7835
1.6920	0.0000359	1.8048	0.0000113	1.7743	0.0000050	1.7834
1.6930	0.0000356	1.8047	0.0000111	1.7743	0.0000049	1.7834
1.6940	0.0000361	1.8047	0.0000113	1.7742	0.0000050	1.7834
1.6950	0.0000365	1.8047	0.0000114	1.7742	0.0000051	1.7834
1.6960	0.0000362	1.8047	0.0000113	1.7742	0.0000050	1.7834
1.6970	0.0000366	1.8046	0.0000114	1.7742	0.0000051	1.7834
1.6980	0.0000367	1.8046	0.0000114	1.7741	0.0000051	1.7834
1.6990	0.0000372	1.8046	0.0000115	1.7741	0.0000051	1.7834
1.7000	0.0000365	1.8046	0.0000113	1.7741	0.0000050	1.7834
1.7010	0.0000370	1.8045	0.0000114	1.7741	0.0000050	1.7834
1.7020	0.0000371	1.8045	0.0000114	1.7740	0.0000051	1.7833
1.7030	0.0000372	1.8045	0.0000114	1.7740	0.0000051	1.7833
1.7040	0.0000373	1.8044	0.0000114	1.7740	0.0000051	1.7833
1.7050	0.0000374	1.8044	0.0000114	1.7740	0.0000051	1.7833
1.7060	0.0000380	1.8044	0.0000115	1.7739	0.0000052	1.7833
1.7070	0.0000374	1.8044	0.0000113	1.7739	0.0000050	1.7833
1.7080	0.0000379	1.8043	0.0000114	1.7739	0.0000051	1.7833
1.7090	0.0000380	1.8043	0.0000114	1.7739	0.0000052	1.7833
1.7100	0.0000382	1.8043	0.0000114	1.7738	0.0000052	1.7833
1.7110	0.0000383	1.8043	0.0000114	1.7738	0.0000052	1.7832
1.7120	0.0000385	1.8042	0.0000114	1.7738	0.0000052	1.7832
1.7130	0.0000386	1.8042	0.0000114	1.7738	0.0000052	1.7832
1.7140	0.0000388	1.8042	0.0000113	1.7737	0.0000053	1.7832
1.7150	0.0000385	1.8042	0.0000112	1.7737	0.0000052	1.7832
1.7160	0.0000390	1.8041	0.0000113	1.7737	0.0000053	1.7832
1.7170	0.0000392	1.8041	0.0000114	1.7737	0.0000053	1.7832
1.7180	0.0000393	1.8041	0.0000114	1.7736	0.0000053	1.7832
1.7190	0.0000394	1.8041	0.0000114	1.7736	0.0000053	1.7832
1.7200	0.0000400	1.8040	0.0000115	1.7736	0.0000054	1.7832
1.7210	0.0000397	1.8040	0.0000114	1.7736	0.0000053	1.7831
1.7220	0.0000395	1.8040	0.0000113	1.7735	0.0000053	1.7831
1.7230	0.0000396	1.8040	0.0000113	1.7735	0.0000053	1.7831
1.7240	0.0000398	1.8039	0.0000113	1.7735	0.0000053	1.7831
1.7250	0.0000407	1.8039	0.0000116	1.7735	0.0000055	1.7831
1.7260	0.0000404	1.8039	0.0000115	1.7734	0.0000054	1.7831
1.7270	0.0000406	1.8039	0.0000116	1.7734	0.0000054	1.7831
1.7280	0.0000403	1.8038	0.0000115	1.7734	0.0000054	1.7831
1.7290	0.0000405	1.8038	0.0000115	1.7734	0.0000054	1.7831
1.7300	0.0000411	1.8038	0.0000117	1.7733	0.0000055	1.7830
1.7310	0.0000409	1.8038	0.0000116	1.7733	0.0000054	1.7830

1.7320	0.0000407	1.8037	0.0000115	1.7733	0.0000054	1.7830
1.7330	0.0000417	1.8037	0.0000118	1.7733	0.0000056	1.7830
1.7340	0.0000419	1.8037	0.0000118	1.7732	0.0000056	1.7830
1.7350	0.0000417	1.8036	0.0000117	1.7732	0.0000055	1.7830
1.7360	0.0000419	1.8036	0.0000118	1.7732	0.0000055	1.7830
1.7370	0.0000425	1.8036	0.0000120	1.7731	0.0000057	1.7830
1.7380	0.0000427	1.8036	0.0000120	1.7731	0.0000057	1.7830
1.7390	0.0000429	1.8035	0.0000120	1.7731	0.0000057	1.7829
1.7400	0.0000432	1.8035	0.0000121	1.7731	0.0000057	1.7829
1.7410	0.0000430	1.8035	0.0000120	1.7730	0.0000057	1.7829
1.7420	0.0000432	1.8035	0.0000120	1.7730	0.0000057	1.7829
1.7430	0.0000439	1.8034	0.0000122	1.7730	0.0000058	1.7829
1.7440	0.0000445	1.8034	0.0000124	1.7730	0.0000060	1.7829
1.7450	0.0000439	1.8034	0.0000121	1.7729	0.0000058	1.7829
1.7460	0.0000442	1.8034	0.0000122	1.7729	0.0000059	1.7829
1.7470	0.0000445	1.8033	0.0000122	1.7729	0.0000059	1.7829
1.7480	0.0000443	1.8033	0.0000121	1.7729	0.0000059	1.7828
1.7490	0.0000455	1.8033	0.0000125	1.7728	0.0000061	1.7828
1.7500	0.0000453	1.8032	0.0000124	1.7728	0.0000060	1.7828
1.7510	0.0000455	1.8032	0.0000124	1.7728	0.0000061	1.7828
1.7520	0.0000458	1.8032	0.0000125	1.7728	0.0000061	1.7828
1.7530	0.0000456	1.8032	0.0000124	1.7727	0.0000061	1.7828
1.7540	0.0000463	1.8031	0.0000126	1.7727	0.0000062	1.7828
1.7550	0.0000465	1.8031	0.0000127	1.7727	0.0000062	1.7828
1.7560	0.0000477	1.8031	0.0000130	1.7727	0.0000065	1.7828
1.7570	0.0000471	1.8031	0.0000128	1.7726	0.0000063	1.7828
1.7580	0.0000474	1.8030	0.0000128	1.7726	0.0000063	1.7827
1.7590	0.0000469	1.8030	0.0000126	1.7726	0.0000062	1.7827
1.7600	0.0000481	1.8030	0.0000129	1.7725	0.0000064	1.7827
1.7610	0.0000484	1.8029	0.0000130	1.7725	0.0000064	1.7827
1.7620	0.0000491	1.8029	0.0000132	1.7725	0.0000065	1.7827
1.7630	0.0000489	1.8029	0.0000131	1.7725	0.0000065	1.7827
1.7640	0.0000496	1.8029	0.0000133	1.7724	0.0000066	1.7827
1.7650	0.0000494	1.8028	0.0000132	1.7724	0.0000065	1.7827
1.7660	0.0000497	1.8028	0.0000133	1.7724	0.0000066	1.7826
1.7670	0.0000505	1.8028	0.0000136	1.7724	0.0000067	1.7826
1.7680	0.0000504	1.8028	0.0000135	1.7723	0.0000066	1.7826
1.7690	0.0000507	1.8027	0.0000136	1.7723	0.0000066	1.7826
1.7700	0.0000510	1.8027	0.0000137	1.7723	0.0000066	1.7826
1.7710	0.0000514	1.8027	0.0000138	1.7723	0.0000067	1.7826
1.7720	0.0000512	1.8026	0.0000137	1.7722	0.0000066	1.7826
1.7730	0.0000520	1.8026	0.0000140	1.7722	0.0000067	1.7826
1.7740	0.0000523	1.8026	0.0000141	1.7722	0.0000068	1.7826

1.7750	0.0000531	1.8026	0.0000143	1.7721	0.0000069	1.7825
1.7760	0.0000529	1.8025	0.0000142	1.7721	0.0000068	1.7825
1.7770	0.0000533	1.8025	0.0000143	1.7721	0.0000069	1.7825
1.7780	0.0000536	1.8025	0.0000144	1.7721	0.0000069	1.7825
1.7790	0.0000540	1.8024	0.0000145	1.7720	0.0000069	1.7825
1.7800	0.0000544	1.8024	0.0000145	1.7720	0.0000070	1.7825
1.7810	0.0000543	1.8024	0.0000144	1.7720	0.0000069	1.7825
1.7820	0.0000552	1.8024	0.0000147	1.7720	0.0000071	1.7825
1.7830	0.0000556	1.8023	0.0000148	1.7719	0.0000071	1.7825
1.7840	0.0000560	1.8023	0.0000148	1.7719	0.0000072	1.7824
1.7850	0.0000569	1.8023	0.0000151	1.7719	0.0000073	1.7824
1.7860	0.0000573	1.8022	0.0000152	1.7718	0.0000074	1.7824
1.7870	0.0000577	1.8022	0.0000154	1.7718	0.0000074	1.7824
1.7880	0.0000582	1.8022	0.0000155	1.7718	0.0000075	1.7824
1.7890	0.0000587	1.8022	0.0000156	1.7718	0.0000076	1.7824
1.7900	0.0000592	1.8021	0.0000158	1.7717	0.0000076	1.7824
1.7910	0.0000597	1.8021	0.0000159	1.7717	0.0000077	1.7824
1.7920	0.0000602	1.8021	0.0000160	1.7717	0.0000077	1.7824
1.7930	0.0000602	1.8020	0.0000160	1.7717	0.0000077	1.7823
1.7940	0.0000612	1.8020	0.0000163	1.7716	0.0000079	1.7823
1.7950	0.0000617	1.8020	0.0000165	1.7716	0.0000079	1.7823
1.7960	0.0000622	1.8020	0.0000166	1.7716	0.0000080	1.7823
1.7970	0.0000627	1.8019	0.0000168	1.7715	0.0000081	1.7823
1.7980	0.0000632	1.8019	0.0000170	1.7715	0.0000081	1.7823
1.7990	0.0000642	1.8019	0.0000174	1.7715	0.0000084	1.7823
1.8000	0.0000641	1.8018	0.0000175	1.7715	0.0000084	1.7823
1.8010	0.0000641	1.8018	0.0000175	1.7714	0.0000084	1.7822
1.8020	0.0000647	1.8018	0.0000178	1.7714	0.0000085	1.7822
1.8030	0.0000658	1.8018	0.0000182	1.7714	0.0000088	1.7822
1.8040	0.0000665	1.8017	0.0000185	1.7714	0.0000089	1.7822
1.8050	0.0000677	1.8017	0.0000190	1.7713	0.0000092	1.7822
1.8060	0.0000679	1.8017	0.0000191	1.7713	0.0000092	1.7822
1.8070	0.0000686	1.8016	0.0000194	1.7713	0.0000094	1.7822
1.8080	0.0000699	1.8016	0.0000199	1.7712	0.0000096	1.7822
1.8090	0.0000706	1.8016	0.0000202	1.7712	0.0000098	1.7821
1.8100	0.0000714	1.8016	0.0000205	1.7712	0.0000099	1.7821
1.8110	0.0000728	1.8015	0.0000211	1.7712	0.0000102	1.7821
1.8120	0.0000736	1.8015	0.0000215	1.7711	0.0000104	1.7821
1.8130	0.0000744	1.8015	0.0000218	1.7711	0.0000106	1.7821
1.8140	0.0000756	1.8014	0.0000222	1.7711	0.0000108	1.7821
1.8150	0.0000756	1.8014	0.0000222	1.7710	0.0000107	1.7821
1.8160	0.0000756	1.8014	0.0000222	1.7710	0.0000106	1.7821
1.8170	0.0000775	1.8013	0.0000228	1.7710	0.0000110	1.7821

1.8180	0.0000771	1.8013	0.0000226	1.7710	0.0000107	1.7820
1.8190	0.0000786	1.8013	0.0000231	1.7709	0.0000109	1.7820
1.8200	0.0000796	1.8013	0.0000234	1.7709	0.0000110	1.7820
1.8210	0.0000818	1.8012	0.0000242	1.7709	0.0000113	1.7820
1.8220	0.0000829	1.8012	0.0000246	1.7708	0.0000114	1.7820
1.8230	0.0000827	1.8012	0.0000246	1.7708	0.0000113	1.7820
1.8240	0.0000846	1.8011	0.0000254	1.7708	0.0000116	1.7820
1.8250	0.0000859	1.8011	0.0000260	1.7708	0.0000118	1.7820
1.8260	0.0000867	1.8011	0.0000264	1.7707	0.0000118	1.7819
1.8270	0.0000879	1.8011	0.0000279	1.7707	0.0000125	1.7819
1.8280	0.0000878	1.8010	0.0000291	1.7707	0.0000130	1.7819
1.8290	0.0000878	1.8010	0.0000304	1.7706	0.0000135	1.7819
1.8300	0.0000878	1.8010	0.0000318	1.7706	0.0000141	1.7819
1.8310	0.0000872	1.8009	0.0000331	1.7706	0.0000147	1.7819
1.8320	0.0000896	1.8009	0.0000347	1.7706	0.0000155	1.7819
1.8330	0.0000914	1.8009	0.0000361	1.7705	0.0000163	1.7819
1.8340	0.0000923	1.8008	0.0000373	1.7705	0.0000169	1.7818
1.8350	0.0000952	1.8008	0.0000394	1.7705	0.0000181	1.7818
1.8360	0.0000960	1.8008	0.0000407	1.7704	0.0000188	1.7818
1.8370	0.0000980	1.8008	0.0000425	1.7704	0.0000200	1.7818
1.8380	0.0000999	1.8007	0.0000443	1.7704	0.0000212	1.7818
1.8390	0.0001003	1.8007	0.0000452	1.7704	0.0000220	1.7818
1.8400	0.0001013	1.8007	0.0000463	1.7703	0.0000231	1.7818
1.8410	0.0001021	1.8006	0.0000473	1.7703	0.0000240	1.7818
1.8420	0.0001035	1.8006	0.0000484	1.7703	0.0000252	1.7817
1.8430	0.0001032	1.8006	0.0000485	1.7703	0.0000258	1.7817
1.8440	0.0001027	1.8005	0.0000484	1.7702	0.0000263	1.7817
1.8450	0.0001048	1.8005	0.0000493	1.7702	0.0000275	1.7817
1.8460	0.0001040	1.8005	0.0000486	1.7702	0.0000277	1.7817
1.8470	0.0001038	1.8005	0.0000481	1.7701	0.0000280	1.7817
1.8480	0.0001021	1.8004	0.0000467	1.7701	0.0000277	1.7817
1.8490	0.0001030	1.8004	0.0000466	1.7701	0.0000281	1.7817
1.8500	0.0001018	1.8004	0.0000453	1.7701	0.0000277	1.7817
1.8510	0.0001018	1.8003	0.0000447	1.7700	0.0000277	1.7816
1.8520	0.0001018	1.8003	0.0000441	1.7700	0.0000276	1.7816
1.8530	0.0001012	1.8003	0.0000431	1.7700	0.0000272	1.7816
1.8540	0.0000999	1.8002	0.0000418	1.7699	0.0000266	1.7816
1.8550	0.0001000	1.8002	0.0000411	1.7699	0.0000264	1.7816
1.8560	0.0001001	1.8002	0.0000404	1.7699	0.0000262	1.7816
1.8570	0.0000981	1.8002	0.0000388	1.7699	0.0000254	1.7816
1.8580	0.0000981	1.8001	0.0000380	1.7698	0.0000251	1.7816
1.8590	0.0000961	1.8001	0.0000362	1.7698	0.0000242	1.7816
1.8600	0.0000955	1.8001	0.0000351	1.7698	0.0000236	1.7815

1.8610	0.0000955	1.8000	0.0000341	1.7697	0.0000232	1.7815
1.8620	0.0000957	1.8000	0.0000331	1.7697	0.0000227	1.7815
1.8630	0.0000945	1.8000	0.0000315	1.7697	0.0000217	1.7815
1.8640	0.0000942	1.7999	0.0000306	1.7697	0.0000211	1.7815
1.8650	0.0000946	1.7999	0.0000298	1.7696	0.0000205	1.7815
1.8660	0.0000951	1.7999	0.0000290	1.7696	0.0000199	1.7815
1.8670	0.0000944	1.7998	0.0000276	1.7696	0.0000189	1.7815
1.8680	0.0000943	1.7998	0.0000266	1.7695	0.0000180	1.7814
1.8690	0.0000944	1.7998	0.0000255	1.7695	0.0000170	1.7814
1.8700	0.0000959	1.7997	0.0000249	1.7695	0.0000164	1.7814
1.8710	0.0000955	1.7997	0.0000237	1.7694	0.0000154	1.7814
1.8720	0.0000945	1.7997	0.0000224	1.7694	0.0000142	1.7814
1.8730	0.0000941	1.7996	0.0000214	1.7694	0.0000133	1.7814
1.8740	0.0000958	1.7996	0.0000211	1.7694	0.0000129	1.7814
1.8750	0.0000982	1.7996	0.0000210	1.7693	0.0000127	1.7813
1.8760	0.0000971	1.7995	0.0000201	1.7693	0.0000119	1.7813
1.8770	0.0000961	1.7995	0.0000192	1.7693	0.0000112	1.7813
1.8780	0.0000972	1.7995	0.0000190	1.7692	0.0000110	1.7813
1.8790	0.0000963	1.7994	0.0000183	1.7692	0.0000104	1.7813
1.8800	0.0000967	1.7994	0.0000180	1.7692	0.0000102	1.7813
1.8810	0.0000993	1.7994	0.0000183	1.7691	0.0000104	1.7813
1.8820	0.0000992	1.7993	0.0000179	1.7691	0.0000101	1.7813
1.8830	0.0000998	1.7993	0.0000177	1.7691	0.0000100	1.7812
1.8840	0.0001003	1.7993	0.0000176	1.7690	0.0000100	1.7812
1.8850	0.0000996	1.7992	0.0000172	1.7690	0.0000097	1.7812
1.8860	0.0001009	1.7992	0.0000173	1.7690	0.0000098	1.7812
1.8870	0.0001022	1.7992	0.0000175	1.7690	0.0000100	1.7812
1.8880	0.0001028	1.7991	0.0000175	1.7689	0.0000101	1.7812
1.8890	0.0001022	1.7991	0.0000171	1.7689	0.0000099	1.7812
1.8900	0.0001043	1.7991	0.0000176	1.7689	0.0000103	1.7811
1.8910	0.0001065	1.7990	0.0000180	1.7688	0.0000107	1.7811
1.8920	0.0001058	1.7990	0.0000177	1.7688	0.0000105	1.7811
1.8930	0.0001059	1.7990	0.0000176	1.7688	0.0000106	1.7811
1.8940	0.0001074	1.7989	0.0000179	1.7687	0.0000109	1.7811
1.8950	0.0001061	1.7989	0.0000175	1.7687	0.0000107	1.7811
1.8960	0.0001085	1.7989	0.0000180	1.7687	0.0000112	1.7811
1.8970	0.0001110	1.7988	0.0000186	1.7686	0.0000117	1.7810
1.8980	0.0001113	1.7988	0.0000186	1.7686	0.0000118	1.7810
1.8990	0.0001139	1.7988	0.0000192	1.7686	0.0000124	1.7810
1.9000	0.0001135	1.7987	0.0000190	1.7685	0.0000124	1.7810
1.9010	0.0001138	1.7987	0.0000190	1.7685	0.0000125	1.7810
1.9020	0.0001141	1.7987	0.0000191	1.7685	0.0000127	1.7810
1.9030	0.0001160	1.7986	0.0000195	1.7684	0.0000131	1.7810

1.9040	0.0001179	1.7986	0.0000200	1.7684	0.0000136	1.7810
1.9050	0.0001207	1.7986	0.0000207	1.7684	0.0000143	1.7809
1.9060	0.0001212	1.7985	0.0000208	1.7684	0.0000144	1.7809
1.9070	0.0001217	1.7985	0.0000210	1.7683	0.0000146	1.7809
1.9080	0.0001222	1.7985	0.0000211	1.7683	0.0000148	1.7809
1.9090	0.0001268	1.7984	0.0000223	1.7683	0.0000158	1.7809
1.9100	0.0001273	1.7984	0.0000224	1.7682	0.0000160	1.7809
1.9110	0.0001287	1.7984	0.0000227	1.7682	0.0000164	1.7809
1.9120	0.0001286	1.7983	0.0000226	1.7682	0.0000164	1.7808
1.9130	0.0001326	1.7983	0.0000237	1.7681	0.0000173	1.7808
1.9140	0.0001324	1.7983	0.0000235	1.7681	0.0000173	1.7808
1.9150	0.0001349	1.7982	0.0000240	1.7681	0.0000177	1.7808
1.9160	0.0001364	1.7982	0.0000243	1.7680	0.0000180	1.7808
1.9170	0.0001362	1.7982	0.0000241	1.7680	0.0000179	1.7808
1.9180	0.0001378	1.7981	0.0000244	1.7680	0.0000182	1.7808
1.9190	0.0001386	1.7981	0.0000245	1.7679	0.0000183	1.7808
1.9200	0.0001421	1.7981	0.0000252	1.7679	0.0000189	1.7807
1.9210	0.0001440	1.7980	0.0000255	1.7679	0.0000192	1.7807
1.9220	0.0001460	1.7980	0.0000258	1.7678	0.0000195	1.7807
1.9230	0.0001488	1.7980	0.0000264	1.7678	0.0000200	1.7807
1.9240	0.0001507	1.7979	0.0000267	1.7678	0.0000202	1.7807
1.9250	0.0001509	1.7979	0.0000265	1.7677	0.0000201	1.7807
1.9260	0.0001528	1.7978	0.0000268	1.7677	0.0000203	1.7807
1.9270	0.0001557	1.7978	0.0000273	1.7677	0.0000208	1.7806
1.9280	0.0001586	1.7978	0.0000278	1.7677	0.0000212	1.7806
1.9290	0.0001617	1.7977	0.0000283	1.7676	0.0000216	1.7806
1.9300	0.0001639	1.7977	0.0000285	1.7676	0.0000217	1.7806
1.9310	0.0001662	1.7977	0.0000287	1.7676	0.0000219	1.7806
1.9320	0.0001686	1.7976	0.0000289	1.7675	0.0000220	1.7806
1.9330	0.0001691	1.7976	0.0000286	1.7675	0.0000217	1.7806
1.9340	0.0001715	1.7976	0.0000288	1.7675	0.0000218	1.7805
1.9350	0.0001739	1.7975	0.0000290	1.7674	0.0000219	1.7805
1.9360	0.0001764	1.7975	0.0000292	1.7674	0.0000220	1.7805
1.9370	0.0001788	1.7975	0.0000293	1.7674	0.0000220	1.7805
1.9380	0.0001812	1.7974	0.0000294	1.7673	0.0000221	1.7805
1.9390	0.0001826	1.7974	0.0000293	1.7673	0.0000219	1.7805
1.9400	0.0001861	1.7974	0.0000297	1.7673	0.0000221	1.7805
1.9410	0.0001908	1.7973	0.0000303	1.7672	0.0000226	1.7804
1.9420	0.0001923	1.7973	0.0000302	1.7672	0.0000224	1.7804
1.9430	0.0001960	1.7973	0.0000306	1.7672	0.0000226	1.7804
1.9440	0.0001998	1.7972	0.0000310	1.7671	0.0000229	1.7804
1.9450	0.0002013	1.7972	0.0000308	1.7671	0.0000227	1.7804
1.9460	0.0002029	1.7971	0.0000307	1.7671	0.0000224	1.7804

1.9470	0.0002057	1.7971	0.0000308	1.7670	0.0000224	1.7804
1.9480	0.0002086	1.7971	0.0000309	1.7670	0.0000224	1.7803
1.9490	0.0002116	1.7970	0.0000310	1.7670	0.0000224	1.7803
1.9500	0.0002136	1.7970	0.0000309	1.7669	0.0000223	1.7803
1.9510	0.0002190	1.7970	0.0000316	1.7669	0.0000227	1.7803
1.9520	0.0002243	1.7969	0.0000323	1.7669	0.0000232	1.7803
1.9530	0.0002261	1.7969	0.0000322	1.7668	0.0000230	1.7803
1.9540	0.0002290	1.7969	0.0000323	1.7668	0.0000231	1.7803
1.9550	0.0002319	1.7968	0.0000325	1.7668	0.0000232	1.7802
1.9560	0.0002323	1.7968	0.0000321	1.7667	0.0000229	1.7802
1.9570	0.0002363	1.7968	0.0000325	1.7667	0.0000232	1.7802
1.9580	0.0002426	1.7967	0.0000335	1.7667	0.0000240	1.7802
1.9590	0.0002427	1.7967	0.0000331	1.7666	0.0000236	1.7802
1.9600	0.0002449	1.7967	0.0000332	1.7666	0.0000237	1.7802
1.9610	0.0002456	1.7966	0.0000330	1.7666	0.0000235	1.7802
1.9620	0.0002474	1.7966	0.0000331	1.7665	0.0000235	1.7801
1.9630	0.0002515	1.7966	0.0000338	1.7665	0.0000240	1.7801
1.9640	0.0002538	1.7965	0.0000341	1.7665	0.0000243	1.7801
1.9650	0.0002548	1.7965	0.0000342	1.7664	0.0000243	1.7801
1.9660	0.0002556	1.7965	0.0000343	1.7664	0.0000243	1.7801
1.9670	0.0002548	1.7964	0.0000342	1.7664	0.0000241	1.7801
1.9680	0.0002551	1.7964	0.0000342	1.7663	0.0000241	1.7801
1.9690	0.0002551	1.7964	0.0000343	1.7663	0.0000241	1.7800
1.9700	0.0002562	1.7963	0.0000347	1.7663	0.0000243	1.7800
1.9710	0.0002559	1.7963	0.0000347	1.7662	0.0000243	1.7800
1.9720	0.0002556	1.7963	0.0000348	1.7662	0.0000242	1.7800
1.9730	0.0002540	1.7962	0.0000345	1.7662	0.0000239	1.7800
1.9740	0.0002536	1.7962	0.0000345	1.7661	0.0000239	1.7800
1.9750	0.0002532	1.7962	0.0000346	1.7661	0.0000238	1.7800
1.9760	0.0002565	1.7961	0.0000355	1.7661	0.0000245	1.7799
1.9770	0.0002545	1.7961	0.0000353	1.7660	0.0000242	1.7799
1.9780	0.0002549	1.7961	0.0000356	1.7660	0.0000244	1.7799
1.9790	0.0002541	1.7960	0.0000356	1.7660	0.0000243	1.7799
1.9800	0.0002520	1.7960	0.0000353	1.7659	0.0000240	1.7799
1.9810	0.0002498	1.7960	0.0000350	1.7659	0.0000238	1.7799
1.9820	0.0002502	1.7959	0.0000353	1.7659	0.0000239	1.7798
1.9830	0.0002493	1.7959	0.0000353	1.7658	0.0000239	1.7798
1.9840	0.0002481	1.7958	0.0000353	1.7658	0.0000239	1.7798
1.9850	0.0002493	1.7958	0.0000360	1.7657	0.0000243	1.7798
1.9860	0.0002467	1.7958	0.0000357	1.7657	0.0000241	1.7798
1.9870	0.0002466	1.7957	0.0000360	1.7657	0.0000243	1.7798
1.9880	0.0002451	1.7957	0.0000361	1.7656	0.0000243	1.7798
1.9890	0.0002413	1.7957	0.0000355	1.7656	0.0000238	1.7797

1.9900	0.0002413	1.7956	0.0000359	1.7656	0.0000241	1.7797
1.9910	0.0002400	1.7956	0.0000360	1.7655	0.0000241	1.7797
1.9920	0.0002412	1.7956	0.0000366	1.7655	0.0000247	1.7797
1.9930	0.0002401	1.7955	0.0000367	1.7655	0.0000247	1.7797
1.9940	0.0002366	1.7955	0.0000361	1.7654	0.0000243	1.7797
1.9950	0.0002367	1.7954	0.0000365	1.7654	0.0000246	1.7797
1.9960	0.0002356	1.7954	0.0000365	1.7654	0.0000247	1.7796
1.9970	0.0002332	1.7954	0.0000363	1.7653	0.0000245	1.7796
1.9980	0.0002343	1.7953	0.0000369	1.7653	0.0000249	1.7796
1.9990	0.0002342	1.7953	0.0000373	1.7653	0.0000252	1.7796
2.0000	0.0002328	1.7952	0.0000373	1.7652	0.0000252	1.7796
2.0010	0.0002327	1.7952	0.0000376	1.7652	0.0000254	1.7796
2.0020	0.0002303	1.7952	0.0000374	1.7652	0.0000252	1.7795
2.0030	0.0002290	1.7951	0.0000374	1.7651	0.0000252	1.7795
2.0040	0.0002276	1.7951	0.0000374	1.7651	0.0000252	1.7795
2.0050	0.0002273	1.7951	0.0000377	1.7650	0.0000254	1.7795
2.0060	0.0002271	1.7950	0.0000380	1.7650	0.0000256	1.7795
2.0070	0.0002258	1.7950	0.0000380	1.7650	0.0000255	1.7795
2.0080	0.0002246	1.7949	0.0000380	1.7649	0.0000255	1.7794
2.0090	0.0002236	1.7949	0.0000381	1.7649	0.0000255	1.7794
2.0100	0.0002237	1.7949	0.0000384	1.7649	0.0000257	1.7794
2.0110	0.0002238	1.7948	0.0000388	1.7648	0.0000259	1.7794
2.0120	0.0002229	1.7948	0.0000389	1.7648	0.0000259	1.7794
2.0130	0.0002231	1.7947	0.0000393	1.7648	0.0000262	1.7794
2.0140	0.0002228	1.7947	0.0000394	1.7647	0.0000262	1.7794
2.0150	0.0002202	1.7947	0.0000388	1.7647	0.0000258	1.7793
2.0160	0.0002188	1.7946	0.0000386	1.7646	0.0000256	1.7793
2.0170	0.0002208	1.7946	0.0000394	1.7646	0.0000261	1.7793
2.0180	0.0002206	1.7945	0.0000396	1.7646	0.0000262	1.7793
2.0190	0.0002203	1.7945	0.0000397	1.7645	0.0000263	1.7793
2.0200	0.0002212	1.7945	0.0000402	1.7645	0.0000267	1.7793
2.0210	0.0002198	1.7944	0.0000400	1.7645	0.0000266	1.7792
2.0220	0.0002208	1.7944	0.0000405	1.7644	0.0000270	1.7792
2.0230	0.0002217	1.7943	0.0000409	1.7644	0.0000273	1.7792
2.0240	0.0002215	1.7943	0.0000411	1.7644	0.0000275	1.7792
2.0250	0.0002215	1.7943	0.0000412	1.7643	0.0000276	1.7792
2.0260	0.0002236	1.7942	0.0000420	1.7643	0.0000283	1.7792
2.0270	0.0002234	1.7942	0.0000422	1.7642	0.0000285	1.7791
2.0280	0.0002245	1.7941	0.0000427	1.7642	0.0000289	1.7791
2.0290	0.0002233	1.7941	0.0000426	1.7642	0.0000288	1.7791
2.0300	0.0002233	1.7940	0.0000429	1.7641	0.0000290	1.7791
2.0310	0.0002245	1.7940	0.0000435	1.7641	0.0000295	1.7791
2.0320	0.0002248	1.7940	0.0000437	1.7641	0.0000297	1.7791

2.0330	0.0002239	1.7939	0.0000437	1.7640	0.0000296	1.7790
2.0340	0.0002252	1.7939	0.0000443	1.7640	0.0000301	1.7790
2.0350	0.0002266	1.7938	0.0000450	1.7639	0.0000305	1.7790
2.0360	0.0002279	1.7938	0.0000456	1.7639	0.0000309	1.7790
2.0370	0.0002280	1.7938	0.0000459	1.7639	0.0000311	1.7790
2.0380	0.0002268	1.7937	0.0000459	1.7638	0.0000310	1.7790
2.0390	0.0002303	1.7937	0.0000473	1.7638	0.0000320	1.7789
2.0400	0.0002302	1.7936	0.0000476	1.7638	0.0000321	1.7789
2.0410	0.0002300	1.7936	0.0000479	1.7637	0.0000323	1.7789
2.0420	0.0002275	1.7936	0.0000474	1.7637	0.0000320	1.7789
2.0430	0.0002275	1.7935	0.0000477	1.7636	0.0000321	1.7789
2.0440	0.0002312	1.7935	0.0000490	1.7636	0.0000331	1.7789
2.0450	0.0002326	1.7934	0.0000496	1.7636	0.0000336	1.7788
2.0460	0.0002292	1.7934	0.0000487	1.7635	0.0000329	1.7788
2.0470	0.0002296	1.7933	0.0000490	1.7635	0.0000330	1.7788
2.0480	0.0002323	1.7933	0.0000499	1.7635	0.0000338	1.7788
2.0490	0.0002313	1.7933	0.0000498	1.7634	0.0000336	1.7788
2.0500	0.0002338	1.7932	0.0000507	1.7634	0.0000344	1.7788
2.0510	0.0002353	1.7932	0.0000513	1.7633	0.0000349	1.7787
2.0520	0.0002354	1.7931	0.0000515	1.7633	0.0000351	1.7787
2.0530	0.0002356	1.7931	0.0000516	1.7633	0.0000353	1.7787
2.0540	0.0002348	1.7930	0.0000514	1.7632	0.0000353	1.7787
2.0550	0.0002352	1.7930	0.0000515	1.7632	0.0000355	1.7787
2.0560	0.0002308	1.7930	0.0000501	1.7632	0.0000346	1.7787
2.0570	0.0002324	1.7929	0.0000506	1.7631	0.0000352	1.7786
2.0580	0.0002378	1.7929	0.0000523	1.7631	0.0000367	1.7786
2.0590	0.0002383	1.7928	0.0000525	1.7630	0.0000370	1.7786
2.0600	0.0002375	1.7928	0.0000522	1.7630	0.0000370	1.7786
2.0610	0.0002392	1.7927	0.0000528	1.7630	0.0000377	1.7786
2.0620	0.0002398	1.7927	0.0000530	1.7629	0.0000380	1.7786
2.0630	0.0002403	1.7927	0.0000532	1.7629	0.0000383	1.7785
2.0640	0.0002381	1.7926	0.0000527	1.7628	0.0000379	1.7785
2.0650	0.0002396	1.7926	0.0000533	1.7628	0.0000384	1.7785
2.0660	0.0002425	1.7925	0.0000544	1.7628	0.0000393	1.7785
2.0670	0.0002442	1.7925	0.0000551	1.7627	0.0000398	1.7785
2.0680	0.0002433	1.7924	0.0000549	1.7627	0.0000397	1.7785
2.0690	0.0002438	1.7924	0.0000552	1.7627	0.0000400	1.7784
2.0700	0.0002468	1.7924	0.0000563	1.7626	0.0000408	1.7784
2.0710	0.0002497	1.7923	0.0000574	1.7626	0.0000417	1.7784
2.0720	0.0002487	1.7923	0.0000572	1.7625	0.0000416	1.7784
2.0730	0.0002478	1.7922	0.0000570	1.7625	0.0000414	1.7784
2.0740	0.0002468	1.7922	0.0000568	1.7625	0.0000413	1.7783
2.0750	0.0002509	1.7921	0.0000583	1.7624	0.0000425	1.7783

2.0760	0.0002486	1.7921	0.0000577	1.7624	0.0000420	1.7783
2.0770	0.0002490	1.7920	0.0000579	1.7623	0.0000422	1.7783
2.0780	0.0002469	1.7920	0.0000573	1.7623	0.0000416	1.7783
2.0790	0.0002525	1.7920	0.0000592	1.7623	0.0000431	1.7783
2.0800	0.0002517	1.7919	0.0000589	1.7622	0.0000428	1.7782
2.0810	0.0002521	1.7919	0.0000591	1.7622	0.0000428	1.7782
2.0820	0.0002524	1.7918	0.0000592	1.7621	0.0000429	1.7782
2.0830	0.0002527	1.7918	0.0000593	1.7621	0.0000430	1.7782
2.0840	0.0002594	1.7917	0.0000616	1.7621	0.0000447	1.7782
2.0850	0.0002570	1.7917	0.0000608	1.7620	0.0000441	1.7782
2.0860	0.0002561	1.7916	0.0000604	1.7620	0.0000438	1.7781
2.0870	0.0002499	1.7916	0.0000583	1.7619	0.0000422	1.7781
2.0880	0.0002566	1.7915	0.0000605	1.7619	0.0000439	1.7781
2.0890	0.0002594	1.7915	0.0000615	1.7619	0.0000446	1.7781
2.0900	0.0002596	1.7915	0.0000616	1.7618	0.0000447	1.7781
2.0910	0.0002585	1.7914	0.0000612	1.7618	0.0000444	1.7780
2.0920	0.0002598	1.7914	0.0000617	1.7617	0.0000448	1.7780
2.0930	0.0002573	1.7913	0.0000609	1.7617	0.0000443	1.7780
2.0940	0.0002561	1.7913	0.0000605	1.7617	0.0000441	1.7780
2.0950	0.0002590	1.7912	0.0000615	1.7616	0.0000450	1.7780
2.0960	0.0002619	1.7912	0.0000624	1.7616	0.0000458	1.7780
2.0970	0.0002638	1.7911	0.0000629	1.7615	0.0000464	1.7779
2.0980	0.0002631	1.7911	0.0000625	1.7615	0.0000463	1.7779
2.0990	0.0002623	1.7910	0.0000621	1.7615	0.0000462	1.7779
2.1000	0.0002616	1.7910	0.0000618	1.7614	0.0000461	1.7779
2.1010	0.0002649	1.7909	0.0000628	1.7614	0.0000470	1.7779
2.1020	0.0002682	1.7909	0.0000639	1.7613	0.0000480	1.7778
2.1030	0.0002690	1.7908	0.0000641	1.7613	0.0000482	1.7778
2.1040	0.0002673	1.7908	0.0000636	1.7612	0.0000477	1.7778
2.1050	0.0002696	1.7908	0.0000644	1.7612	0.0000483	1.7778
2.1060	0.0002652	1.7907	0.0000630	1.7612	0.0000471	1.7778
2.1070	0.0002714	1.7907	0.0000653	1.7611	0.0000488	1.7778
2.1080	0.0002708	1.7906	0.0000653	1.7611	0.0000487	1.7777
2.1090	0.0002741	1.7906	0.0000667	1.7610	0.0000497	1.7777
2.1100	0.0002760	1.7905	0.0000675	1.7610	0.0000504	1.7777
2.1110	0.0002767	1.7905	0.0000679	1.7610	0.0000506	1.7777
2.1120	0.0002732	1.7904	0.0000669	1.7609	0.0000498	1.7777
2.1130	0.0002805	1.7904	0.0000696	1.7609	0.0000519	1.7776
2.1140	0.0002741	1.7903	0.0000675	1.7608	0.0000504	1.7776
2.1150	0.0002771	1.7903	0.0000687	1.7608	0.0000514	1.7776
2.1160	0.0002772	1.7902	0.0000690	1.7607	0.0000517	1.7776
2.1170	0.0002816	1.7902	0.0000708	1.7607	0.0000531	1.7776
2.1180	0.0002807	1.7901	0.0000707	1.7607	0.0000529	1.7775

2.1190	0.0002842	1.7901	0.0000721	1.7606	0.0000539	1.7775
2.1200	0.0002851	1.7900	0.0000725	1.7606	0.0000542	1.7775
2.1210	0.0002932	1.7900	0.0000754	1.7605	0.0000564	1.7775
2.1220	0.0002874	1.7899	0.0000732	1.7605	0.0000548	1.7775
2.1230	0.0002871	1.7899	0.0000731	1.7605	0.0000548	1.7774
2.1240	0.0002867	1.7898	0.0000730	1.7604	0.0000548	1.7774
2.1250	0.0002906	1.7898	0.0000743	1.7604	0.0000561	1.7774
2.1260	0.0002946	1.7897	0.0000757	1.7603	0.0000573	1.7774
2.1270	0.0002901	1.7897	0.0000741	1.7603	0.0000562	1.7774
2.1280	0.0002971	1.7896	0.0000765	1.7602	0.0000582	1.7774
2.1290	0.0003028	1.7896	0.0000784	1.7602	0.0000599	1.7773
2.1300	0.0002999	1.7895	0.0000772	1.7602	0.0000592	1.7773
2.1310	0.0003012	1.7895	0.0000776	1.7601	0.0000597	1.7773
2.1320	0.0003040	1.7894	0.0000785	1.7601	0.0000607	1.7773
2.1330	0.0003039	1.7894	0.0000784	1.7600	0.0000609	1.7773
2.1340	0.0003051	1.7893	0.0000788	1.7600	0.0000614	1.7772
2.1350	0.0003019	1.7893	0.0000776	1.7599	0.0000607	1.7772
2.1360	0.0003091	1.7892	0.0000801	1.7599	0.0000629	1.7772
2.1370	0.0003046	1.7892	0.0000785	1.7599	0.0000617	1.7772
2.1380	0.0003133	1.7891	0.0000816	1.7598	0.0000644	1.7772
2.1390	0.0003090	1.7891	0.0000800	1.7598	0.0000632	1.7771
2.1400	0.0003119	1.7890	0.0000810	1.7597	0.0000643	1.7771
2.1410	0.0003164	1.7890	0.0000826	1.7597	0.0000658	1.7771
2.1420	0.0003193	1.7889	0.0000837	1.7596	0.0000669	1.7771
2.1430	0.0003164	1.7889	0.0000827	1.7596	0.0000662	1.7771
2.1440	0.0003165	1.7888	0.0000827	1.7595	0.0000663	1.7770
2.1450	0.0003185	1.7888	0.0000834	1.7595	0.0000669	1.7770
2.1460	0.0003206	1.7887	0.0000841	1.7595	0.0000675	1.7770
2.1470	0.0003212	1.7887	0.0000842	1.7594	0.0000675	1.7770
2.1480	0.0003218	1.7886	0.0000843	1.7594	0.0000676	1.7770
2.1490	0.0003300	1.7886	0.0000871	1.7593	0.0000700	1.7769
2.1500	0.0003241	1.7885	0.0000849	1.7593	0.0000683	1.7769
2.1510	0.0003320	1.7885	0.0000877	1.7592	0.0000708	1.7769
2.1520	0.0003292	1.7884	0.0000866	1.7592	0.0000701	1.7769
2.1530	0.0003311	1.7884	0.0000872	1.7591	0.0000708	1.7769
2.1540	0.0003315	1.7883	0.0000872	1.7591	0.0000710	1.7768
2.1550	0.0003416	1.7883	0.0000907	1.7591	0.0000741	1.7768
2.1560	0.0003361	1.7882	0.0000883	1.7590	0.0000724	1.7768
2.1570	0.0003415	1.7882	0.0000900	1.7590	0.0000741	1.7768
2.1580	0.0003406	1.7881	0.0000894	1.7589	0.0000740	1.7768
2.1590	0.0003397	1.7881	0.0000887	1.7589	0.0000739	1.7767
2.1600	0.0003355	1.7880	0.0000870	1.7588	0.0000729	1.7767
2.1610	0.0003376	1.7880	0.0000875	1.7588	0.0000738	1.7767

2.1620	0.0003429	1.7879	0.0000892	1.7587	0.0000757	1.7767
2.1630	0.0003454	1.7879	0.0000898	1.7587	0.0000767	1.7767
2.1640	0.0003466	1.7878	0.0000900	1.7587	0.0000770	1.7766
2.1650	0.0003415	1.7877	0.0000878	1.7586	0.0000754	1.7766
2.1660	0.0003428	1.7877	0.0000880	1.7586	0.0000757	1.7766
2.1670	0.0003538	1.7876	0.0000917	1.7585	0.0000789	1.7766
2.1680	0.0003502	1.7876	0.0000901	1.7585	0.0000777	1.7765
2.1690	0.0003563	1.7875	0.0000921	1.7584	0.0000795	1.7765
2.1700	0.0003544	1.7875	0.0000911	1.7584	0.0000788	1.7765
2.1710	0.0003607	1.7874	0.0000930	1.7583	0.0000807	1.7765
2.1720	0.0003618	1.7874	0.0000931	1.7583	0.0000810	1.7765
2.1730	0.0003710	1.7873	0.0000963	1.7582	0.0000840	1.7764
2.1740	0.0003720	1.7873	0.0000965	1.7582	0.0000845	1.7764
2.1750	0.0003644	1.7872	0.0000938	1.7581	0.0000823	1.7764
2.1760	0.0003685	1.7872	0.0000953	1.7581	0.0000839	1.7764
2.1770	0.0003661	1.7871	0.0000944	1.7581	0.0000834	1.7764
2.1780	0.0003719	1.7870	0.0000965	1.7580	0.0000855	1.7763
2.1790	0.0003708	1.7870	0.0000962	1.7580	0.0000855	1.7763
2.1800	0.0003731	1.7869	0.0000972	1.7579	0.0000866	1.7763
2.1810	0.0003789	1.7869	0.0000996	1.7579	0.0000889	1.7763
2.1820	0.0003782	1.7868	0.0000995	1.7578	0.0000891	1.7762
2.1830	0.0003761	1.7868	0.0000988	1.7578	0.0000889	1.7762
2.1840	0.0003860	1.7867	0.0001025	1.7577	0.0000925	1.7762
2.1850	0.0003805	1.7867	0.0001005	1.7577	0.0000912	1.7762
2.1860	0.0003907	1.7866	0.0001041	1.7576	0.0000950	1.7762
2.1870	0.0003938	1.7865	0.0001053	1.7576	0.0000965	1.7761
2.1880	0.0003813	1.7865	0.0001006	1.7575	0.0000930	1.7761
2.1890	0.0003969	1.7864	0.0001063	1.7575	0.0000986	1.7761
2.1900	0.0003968	1.7864	0.0001062	1.7574	0.0000991	1.7761
2.1910	0.0003981	1.7863	0.0001068	1.7574	0.0001001	1.7761
2.1920	0.0004136	1.7863	0.0001129	1.7573	0.0001058	1.7760
2.1930	0.0004056	1.7862	0.0001101	1.7573	0.0001037	1.7760
2.1940	0.0004064	1.7861	0.0001108	1.7572	0.0001046	1.7760
2.1950	0.0004089	1.7861	0.0001122	1.7572	0.0001060	1.7760
2.1960	0.0004078	1.7860	0.0001122	1.7571	0.0001063	1.7759
2.1970	0.0004034	1.7860	0.0001108	1.7571	0.0001055	1.7759
2.1980	0.0004135	1.7859	0.0001150	1.7570	0.0001096	1.7759
2.1990	0.0004239	1.7858	0.0001192	1.7570	0.0001138	1.7759
2.2000	0.0004234	1.7858	0.0001193	1.7570	0.0001143	1.7759
2.2010	0.0004248	1.7857	0.0001201	1.7569	0.0001153	1.7758
2.2020	0.0004297	1.7857	0.0001224	1.7569	0.0001176	1.7758
2.2030	0.0004309	1.7856	0.0001232	1.7568	0.0001185	1.7758
2.2040	0.0004340	1.7856	0.0001250	1.7568	0.0001200	1.7758

2.2050	0.0004430	1.7855	0.0001292	1.7567	0.0001234	1.7757
2.2060	0.0004448	1.7854	0.0001304	1.7567	0.0001240	1.7757
2.2070	0.0004467	1.7854	0.0001318	1.7566	0.0001244	1.7757
2.2080	0.0004529	1.7853	0.0001350	1.7566	0.0001260	1.7757
2.2090	0.0004457	1.7853	0.0001326	1.7565	0.0001227	1.7757
2.2100	0.0004501	1.7852	0.0001349	1.7565	0.0001233	1.7756
2.2110	0.0004586	1.7851	0.0001388	1.7564	0.0001252	1.7756
2.2120	0.0004617	1.7851	0.0001402	1.7564	0.0001247	1.7756
2.2130	0.0004729	1.7850	0.0001449	1.7563	0.0001268	1.7756
2.2140	0.0004758	1.7850	0.0001460	1.7563	0.0001262	1.7756
2.2150	0.0004786	1.7849	0.0001472	1.7562	0.0001254	1.7755
2.2160	0.0004770	1.7848	0.0001467	1.7562	0.0001230	1.7755
2.2170	0.0004855	1.7848	0.0001504	1.7561	0.0001240	1.7755
2.2180	0.0005004	1.7847	0.0001569	1.7561	0.0001269	1.7755
2.2190	0.0004944	1.7847	0.0001547	1.7560	0.0001229	1.7754
2.2200	0.0004951	1.7846	0.0001551	1.7560	0.0001210	1.7754
2.2210	0.0005049	1.7845	0.0001590	1.7559	0.0001216	1.7754
2.2220	0.0005150	1.7845	0.0001627	1.7559	0.0001222	1.7754
2.2230	0.0005210	1.7844	0.0001645	1.7558	0.0001214	1.7754
2.2240	0.0005211	1.7843	0.0001636	1.7558	0.0001186	1.7753
2.2250	0.0005278	1.7843	0.0001654	1.7557	0.0001176	1.7753
2.2260	0.0005476	1.7842	0.0001727	1.7557	0.0001205	1.7753
2.2270	0.0005504	1.7842	0.0001728	1.7556	0.0001183	1.7753
2.2280	0.0005474	1.7841	0.0001700	1.7556	0.0001141	1.7752
2.2290	0.0005559	1.7840	0.0001717	1.7555	0.0001132	1.7752
2.2300	0.0005785	1.7840	0.0001788	1.7555	0.0001161	1.7752
2.2310	0.0005791	1.7839	0.0001762	1.7554	0.0001127	1.7752
2.2320	0.0006034	1.7839	0.0001829	1.7554	0.0001157	1.7751
2.2330	0.0006110	1.7838	0.0001827	1.7553	0.0001144	1.7751
2.2340	0.0006013	1.7837	0.0001756	1.7553	0.0001088	1.7751
2.2350	0.0006216	1.7837	0.0001808	1.7552	0.0001116	1.7751
2.2360	0.0006275	1.7836	0.0001805	1.7552	0.0001108	1.7750
2.2370	0.0006352	1.7836	0.0001812	1.7551	0.0001110	1.7750
2.2380	0.0006502	1.7835	0.0001849	1.7551	0.0001133	1.7750
2.2390	0.0006659	1.7835	0.0001889	1.7550	0.0001162	1.7750
2.2400	0.0006639	1.7834	0.0001862	1.7550	0.0001150	1.7749
2.2410	0.0006810	1.7833	0.0001915	1.7549	0.0001193	1.7749
2.2420	0.0006749	1.7833	0.0001881	1.7549	0.0001182	1.7749
2.2430	0.0006736	1.7832	0.0001872	1.7548	0.0001191	1.7748
2.2440	0.0006739	1.7832	0.0001877	1.7547	0.0001210	1.7748
2.2450	0.0006837	1.7831	0.0001924	1.7547	0.0001262	1.7748
2.2460	0.0006938	1.7831	0.0001977	1.7546	0.0001322	1.7748
2.2470	0.0006850	1.7830	0.0001963	1.7546	0.0001340	1.7747

2.2480	0.0006960	1.7829	0.0002036	1.7545	0.0001422	1.7747
2.2490	0.0007102	1.7829	0.0002125	1.7545	0.0001522	1.7747
2.2500	0.0007245	1.7828	0.0002221	1.7544	0.0001634	1.7746
2.2510	0.0007275	1.7828	0.0002279	1.7544	0.0001721	1.7746
2.2520	0.0007202	1.7827	0.0002293	1.7543	0.0001777	1.7746
2.2530	0.0007263	1.7827	0.0002369	1.7543	0.0001882	1.7746
2.2540	0.0007291	1.7826	0.0002440	1.7542	0.0001979	1.7746
2.2550	0.0007509	1.7825	0.0002605	1.7542	0.0002143	1.7745
2.2560	0.0007459	1.7825	0.0002651	1.7541	0.0002208	1.7745
2.2570	0.0007396	1.7824	0.0002700	1.7541	0.0002265	1.7745
2.2580	0.0007323	1.7824	0.0002749	1.7540	0.0002308	1.7745
2.2590	0.0007266	1.7823	0.0002805	1.7540	0.0002351	1.7745
2.2600	0.0007251	1.7823	0.0002881	1.7539	0.0002401	1.7744
2.2610	0.0007178	1.7822	0.0002923	1.7539	0.0002418	1.7744
2.2620	0.0007317	1.7821	0.0003067	1.7538	0.0002513	1.7744
2.2630	0.0007395	1.7821	0.0003177	1.7538	0.0002575	1.7744
2.2640	0.0007262	1.7820	0.0003151	1.7537	0.0002529	1.7744
2.2650	0.0007392	1.7820	0.0003259	1.7537	0.0002582	1.7744
2.2660	0.0007248	1.7819	0.0003204	1.7537	0.0002513	1.7743
2.2670	0.0007052	1.7818	0.0003110	1.7536	0.0002412	1.7743
2.2680	0.0007198	1.7818	0.0003194	1.7536	0.0002444	1.7743
2.2690	0.0007108	1.7817	0.0003135	1.7535	0.0002373	1.7743
2.2700	0.0007044	1.7817	0.0003086	1.7535	0.0002307	1.7743
2.2710	0.0007109	1.7816	0.0003104	1.7534	0.0002287	1.7743
2.2720	0.0006864	1.7815	0.0002949	1.7534	0.0002141	1.7742
2.2730	0.0007002	1.7815	0.0002997	1.7533	0.0002136	1.7742
2.2740	0.0007086	1.7814	0.0003009	1.7533	0.0002102	1.7742
2.2750	0.0006784	1.7813	0.0002806	1.7532	0.0001921	1.7742
2.2760	0.0006735	1.7813	0.0002727	1.7532	0.0001829	1.7742
2.2770	0.0006736	1.7812	0.0002665	1.7531	0.0001750	1.7741
2.2780	0.0006717	1.7811	0.0002586	1.7531	0.0001661	1.7741
2.2790	0.0006625	1.7811	0.0002469	1.7530	0.0001550	1.7741
2.2800	0.0006583	1.7810	0.0002375	1.7530	0.0001457	1.7741
2.2810	0.0006542	1.7809	0.0002285	1.7529	0.0001370	1.7740
2.2820	0.0006595	1.7809	0.0002239	1.7529	0.0001315	1.7740
2.2830	0.0006594	1.7808	0.0002170	1.7528	0.0001253	1.7740
2.2840	0.0006618	1.7807	0.0002111	1.7528	0.0001204	1.7739
2.2850	0.0006450	1.7807	0.0001972	1.7527	0.0001115	1.7739
2.2860	0.0006409	1.7806	0.0001892	1.7527	0.0001068	1.7739
2.2870	0.0006350	1.7805	0.0001806	1.7526	0.0001025	1.7738
2.2880	0.0006324	1.7804	0.0001732	1.7525	0.0001000	1.7738
2.2890	0.0006300	1.7804	0.0001665	1.7525	0.0000983	1.7738
2.2900	0.0006394	1.7803	0.0001647	1.7524	0.0001003	1.7737

2.2910	0.0006437	1.7802	0.0001615	1.7524	0.0001017	1.7737
2.2920	0.0006328	1.7802	0.0001541	1.7523	0.0001002	1.7737
2.2930	0.0006071	1.7801	0.0001428	1.7522	0.0000954	1.7737
2.2940	0.0006122	1.7800	0.0001425	1.7522	0.0000980	1.7736
2.2950	0.0006196	1.7799	0.0001436	1.7521	0.0001010	1.7736
2.2960	0.0006173	1.7798	0.0001420	1.7520	0.0001015	1.7736
2.2970	0.0006039	1.7798	0.0001366	1.7520	0.0000987	1.7735
2.2980	0.0006073	1.7797	0.0001369	1.7519	0.0000993	1.7735
2.2990	0.0006444	1.7796	0.0001485	1.7519	0.0001073	1.7735
2.3000	0.0006564	1.7796	0.0001516	1.7518	0.0001081	1.7735
2.3010	0.0006044	1.7795	0.0001334	1.7517	0.0000930	1.7734
2.3020	0.0006002	1.7794	0.0001311	1.7517	0.0000890	1.7734
2.3030	0.0006050	1.7794	0.0001316	1.7516	0.0000867	1.7734
2.3040	0.0005956	1.7793	0.0001274	1.7516	0.0000811	1.7733
2.3050	0.0005881	1.7792	0.0001238	1.7515	0.0000761	1.7733
2.3060	0.0005850	1.7791	0.0001214	1.7514	0.0000720	1.7733
2.3070	0.0005889	1.7790	0.0001208	1.7514	0.0000695	1.7732
2.3080	0.0005793	1.7790	0.0001157	1.7513	0.0000646	1.7732
2.3090	0.0005768	1.7789	0.0001126	1.7513	0.0000614	1.7732
2.3100	0.0005784	1.7788	0.0001104	1.7512	0.0000594	1.7732
2.3110	0.0005800	1.7787	0.0001080	1.7511	0.0000578	1.7731
2.3120	0.0005776	1.7786	0.0001045	1.7511	0.0000557	1.7731
2.3130	0.0005823	1.7786	0.0001030	1.7510	0.0000549	1.7731
2.3140	0.0005680	1.7785	0.0000971	1.7509	0.0000513	1.7730
2.3150	0.0005678	1.7784	0.0000952	1.7509	0.0000503	1.7730
2.3160	0.0005705	1.7783	0.0000942	1.7508	0.0000497	1.7730
2.3170	0.0005821	1.7782	0.0000955	1.7507	0.0000508	1.7729
2.3180	0.0005869	1.7781	0.0000951	1.7507	0.0000509	1.7729
2.3190	0.0005740	1.7781	0.0000903	1.7506	0.0000483	1.7729
2.3200	0.0005730	1.7780	0.0000884	1.7505	0.0000476	1.7728
2.3210	0.0005737	1.7779	0.0000871	1.7505	0.0000473	1.7728
2.3220	0.0005700	1.7778	0.0000849	1.7504	0.0000464	1.7728
2.3230	0.0005823	1.7777	0.0000868	1.7504	0.0000479	1.7727
2.3240	0.0005940	1.7776	0.0000888	1.7503	0.0000495	1.7727
2.3250	0.0005824	1.7776	0.0000854	1.7502	0.0000475	1.7726
2.3260	0.0005923	1.7775	0.0000872	1.7502	0.0000488	1.7726
2.3270	0.0005935	1.7774	0.0000870	1.7501	0.0000488	1.7726
2.3280	0.0005836	1.7773	0.0000840	1.7500	0.0000470	1.7725
2.3290	0.0006023	1.7772	0.0000878	1.7500	0.0000496	1.7725
2.3300	0.0006217	1.7771	0.0000918	1.7499	0.0000523	1.7725
2.3310	0.0006257	1.7770	0.0000923	1.7498	0.0000527	1.7724
2.3320	0.0006104	1.7770	0.0000880	1.7498	0.0000501	1.7724
2.3330	0.0005979	1.7769	0.0000847	1.7497	0.0000479	1.7724

2.3340	0.0006157	1.7768	0.0000888	1.7496	0.0000505	1.7723
2.3350	0.0006246	1.7767	0.0000906	1.7496	0.0000519	1.7723
2.3360	0.0006225	1.7766	0.0000897	1.7495	0.0000514	1.7723
2.3370	0.0006151	1.7765	0.0000878	1.7494	0.0000502	1.7722
2.3380	0.0006221	1.7765	0.0000892	1.7494	0.0000512	1.7722
2.3390	0.0006134	1.7764	0.0000867	1.7493	0.0000496	1.7722
2.3400	0.0006166	1.7763	0.0000872	1.7492	0.0000498	1.7721
2.3410	0.0006214	1.7762	0.0000884	1.7491	0.0000504	1.7721
2.3420	0.0006146	1.7761	0.0000868	1.7491	0.0000493	1.7721
2.3430	0.0006243	1.7760	0.0000893	1.7490	0.0000509	1.7720
2.3440	0.0006407	1.7759	0.0000937	1.7489	0.0000539	1.7720
2.3450	0.0006261	1.7758	0.0000903	1.7489	0.0000519	1.7720
2.3460	0.0006322	1.7757	0.0000917	1.7488	0.0000530	1.7719
2.3470	0.0006611	1.7756	0.0000988	1.7487	0.0000576	1.7719
2.3480	0.0006733	1.7755	0.0001017	1.7487	0.0000594	1.7719
2.3490	0.0006724	1.7755	0.0001014	1.7486	0.0000591	1.7718
2.3500	0.0006527	1.7754	0.0000968	1.7485	0.0000559	1.7718
2.3510	0.0006584	1.7753	0.0000988	1.7484	0.0000569	1.7717
2.3520	0.0006804	1.7752	0.0001049	1.7484	0.0000607	1.7717
2.3530	0.0006783	1.7751	0.0001048	1.7483	0.0000605	1.7717
2.3540	0.0007059	1.7750	0.0001123	1.7482	0.0000653	1.7716
2.3550	0.0007372	1.7749	0.0001211	1.7482	0.0000709	1.7716
2.3560	0.0007170	1.7748	0.0001162	1.7481	0.0000676	1.7716
2.3570	0.0006979	1.7747	0.0001121	1.7480	0.0000647	1.7715
2.3580	0.0006985	1.7747	0.0001135	1.7480	0.0000653	1.7715
2.3590	0.0006917	1.7746	0.0001132	1.7479	0.0000646	1.7715
2.3600	0.0007014	1.7745	0.0001173	1.7478	0.0000664	1.7714
2.3610	0.0007229	1.7744	0.0001243	1.7477	0.0000702	1.7714
2.3620	0.0007351	1.7743	0.0001287	1.7477	0.0000723	1.7713
2.3630	0.0007389	1.7742	0.0001305	1.7476	0.0000729	1.7713
2.3640	0.0007445	1.7741	0.0001321	1.7475	0.0000736	1.7713
2.3650	0.0007636	1.7740	0.0001379	1.7474	0.0000768	1.7712
2.3660	0.0007850	1.7739	0.0001451	1.7474	0.0000808	1.7712
2.3670	0.0007863	1.7738	0.0001468	1.7473	0.0000812	1.7711
2.3680	0.0007914	1.7737	0.0001496	1.7472	0.0000822	1.7711
2.3690	0.0007682	1.7736	0.0001439	1.7472	0.0000782	1.7711
2.3700	0.0007454	1.7735	0.0001384	1.7471	0.0000743	1.7710
2.3710	0.0007613	1.7734	0.0001445	1.7470	0.0000775	1.7710
2.3720	0.0007725	1.7733	0.0001491	1.7469	0.0000799	1.7710
2.3730	0.0007859	1.7732	0.0001538	1.7469	0.0000826	1.7709
2.3740	0.0008073	1.7731	0.0001617	1.7468	0.0000870	1.7709
2.3750	0.0008413	1.7730	0.0001739	1.7467	0.0000941	1.7708
2.3760	0.0008407	1.7729	0.0001751	1.7466	0.0000948	1.7708

2.3770	0.0008216	1.7728	0.0001719	1.7466	0.0000928	1.7708
2.3780	0.0008148	1.7727	0.0001736	1.7465	0.0000936	1.7707
2.3790	0.0008223	1.7726	0.0001786	1.7464	0.0000966	1.7707
2.3800	0.0008434	1.7725	0.0001878	1.7463	0.0001024	1.7706
2.3810	0.0008581	1.7724	0.0001957	1.7462	0.0001071	1.7706
2.3820	0.0008789	1.7723	0.0002047	1.7462	0.0001125	1.7706
2.3830	0.0008731	1.7722	0.0002045	1.7461	0.0001124	1.7705
2.3840	0.0008639	1.7721	0.0002041	1.7460	0.0001119	1.7705
2.3850	0.0008624	1.7720	0.0002056	1.7459	0.0001125	1.7704
2.3860	0.0008906	1.7719	0.0002168	1.7459	0.0001189	1.7704
2.3870	0.0009157	1.7718	0.0002273	1.7458	0.0001247	1.7703
2.3880	0.0008939	1.7717	0.0002213	1.7457	0.0001206	1.7703
2.3890	0.0009049	1.7716	0.0002283	1.7456	0.0001237	1.7703
2.3900	0.0009302	1.7715	0.0002422	1.7455	0.0001304	1.7702
2.3910	0.0009338	1.7714	0.0002486	1.7455	0.0001325	1.7702
2.3920	0.0009416	1.7713	0.0002569	1.7454	0.0001355	1.7701
2.3930	0.0009096	1.7712	0.0002501	1.7453	0.0001300	1.7701
2.3940	0.0009425	1.7711	0.0002677	1.7452	0.0001384	1.7701
2.3950	0.0009780	1.7710	0.0002868	1.7452	0.0001476	1.7700
2.3960	0.0009563	1.7709	0.0002831	1.7451	0.0001442	1.7700
2.3970	0.0009998	1.7708	0.0003058	1.7450	0.0001553	1.7699
2.3980	0.0010120	1.7706	0.0003158	1.7449	0.0001588	1.7699
2.3990	0.0010079	1.7705	0.0003191	1.7449	0.0001582	1.7699
2.4000	0.0009953	1.7704	0.0003185	1.7448	0.0001550	1.7698
2.4010	0.0010512	1.7703	0.0003474	1.7447	0.0001669	1.7698
2.4020	0.0010184	1.7702	0.0003367	1.7446	0.0001577	1.7697
2.4030	0.0010121	1.7701	0.0003364	1.7445	0.0001539	1.7697
2.4040	0.0010413	1.7700	0.0003513	1.7445	0.0001574	1.7696
2.4050	0.0010641	1.7699	0.0003639	1.7444	0.0001586	1.7696
2.4060	0.0010658	1.7698	0.0003664	1.7443	0.0001547	1.7696
2.4070	0.0011055	1.7696	0.0003857	1.7442	0.0001586	1.7695
2.4080	0.0011223	1.7695	0.0003947	1.7442	0.0001576	1.7695
2.4090	0.0011237	1.7694	0.0003949	1.7441	0.0001541	1.7694
2.4100	0.0011253	1.7693	0.0003931	1.7440	0.0001510	1.7694
2.4110	0.0011262	1.7692	0.0003904	1.7439	0.0001480	1.7693
2.4120	0.0011294	1.7691	0.0003891	1.7438	0.0001458	1.7693
2.4130	0.0011107	1.7690	0.0003786	1.7438	0.0001393	1.7692
2.4140	0.0011563	1.7688	0.0003971	1.7437	0.0001439	1.7692
2.4150	0.0012060	1.7687	0.0004159	1.7436	0.0001472	1.7691
2.4160	0.0011914	1.7686	0.0004050	1.7435	0.0001380	1.7691
2.4170	0.0011852	1.7685	0.0003957	1.7434	0.0001306	1.7690
2.4180	0.0012317	1.7683	0.0004072	1.7434	0.0001324	1.7690
2.4190	0.0012715	1.7682	0.0004174	1.7433	0.0001347	1.7689

2.4200	0.0012580	1.7681	0.0004066	1.7432	0.0001304	1.7689
2.4210	0.0012162	1.7680	0.0003839	1.7431	0.0001219	1.7688
2.4220	0.0012591	1.7679	0.0003994	1.7430	0.0001273	1.7688
2.4230	0.0013098	1.7678	0.0004210	1.7429	0.0001345	1.7687
2.4240	0.0013078	1.7676	0.0004181	1.7429	0.0001317	1.7687
2.4250	0.0013122	1.7675	0.0004148	1.7428	0.0001284	1.7686
2.4260	0.0013354	1.7674	0.0004187	1.7427	0.0001279	1.7685
2.4270	0.0013298	1.7673	0.0004083	1.7426	0.0001238	1.7685
2.4280	0.0013799	1.7671	0.0004185	1.7425	0.0001282	1.7684
2.4290	0.0014113	1.7670	0.0004233	1.7424	0.0001302	1.7684
2.4300	0.0014138	1.7668	0.0004183	1.7423	0.0001293	1.7683
2.4310	0.0013941	1.7667	0.0004028	1.7422	0.0001246	1.7683
2.4320	0.0014438	1.7666	0.0004163	1.7421	0.0001297	1.7682
2.4330	0.0015271	1.7665	0.0004432	1.7420	0.0001406	1.7681
2.4340	0.0015791	1.7664	0.0004546	1.7419	0.0001468	1.7681
2.4350	0.0015438	1.7662	0.0004329	1.7418	0.0001400	1.7680
2.4360	0.0015247	1.7661	0.0004210	1.7418	0.0001367	1.7679
2.4370	0.0016238	1.7660	0.0004544	1.7417	0.0001509	1.7679
2.4380	0.0015738	1.7659	0.0004309	1.7416	0.0001426	1.7678
2.4390	0.0016068	1.7657	0.0004395	1.7415	0.0001466	1.7677
2.4400	0.0016193	1.7656	0.0004416	1.7414	0.0001483	1.7677
2.4410	0.0016648	1.7655	0.0004579	1.7413	0.0001549	1.7676
2.4420	0.0017001	1.7654	0.0004705	1.7412	0.0001602	1.7675
2.4430	0.0017746	1.7652	0.0005030	1.7411	0.0001733	1.7675
2.4440	0.0017173	1.7651	0.0004916	1.7409	0.0001689	1.7674
2.4450	0.0017678	1.7649	0.0005184	1.7408	0.0001810	1.7673
2.4460	0.0016723	1.7648	0.0004848	1.7407	0.0001703	1.7672
2.4470	0.0017138	1.7647	0.0005067	1.7406	0.0001804	1.7671
2.4480	0.0017872	1.7645	0.0005322	1.7405	0.0001928	1.7670

Hydronium jarosite			Sodium jarosite			Potassium jarosite		
cm^{-1}	k	n	cm^{-1}	k	n	cm^{-1}	k	n
262.3	1.18160	1.3201	225.6	0.69500	3.1699	100.3	0.01199	1.9126
264.2	1.08640	1.2823	227.6	0.85601	3.2196	102.2	0.01239	1.9160
266.1	0.99479	1.2584	229.5	1.05970	3.2367	104.1	0.01281	1.9195
268.1	0.90827	1.2466	231.4	1.30020	3.1914	106.1	0.01325	1.9232
270.0	0.82795	1.2449	233.4	1.54680	3.0520	108.0	0.01371	1.9271
271.9	0.75456	1.2515	235.3	1.74120	2.8119	109.9	0.01419	1.9312
273.9	0.68844	1.2644	237.2	1.82800	2.5119	111.9	0.01470	1.9354
275.8	0.62959	1.2821	239.1	1.79560	2.2203	113.8	0.01523	1.9399
277.7	0.57770	1.3030	241.1	1.67460	1.9887	115.7	0.01580	1.9447
279.6	0.53226	1.3259	243.0	1.50840	1.8374	117.6	0.01641	1.9497
281.6	0.49264	1.3499	244.9	1.33400	1.7653	119.6	0.01706	1.9550

283.5	0.45817	1.3744	246.9	1.17910	1.7608	121.5	0.01775	1.9606
285.4	0.42820	1.3987	248.8	1.06310	1.8064	123.4	0.01850	1.9665
287.4	0.40213	1.4225	250.7	0.99734	1.8823	125.4	0.01931	1.9728
289.3	0.37944	1.4458	252.6	0.98729	1.9683	127.3	0.02020	1.9796
291.2	0.35966	1.4682	254.6	1.03510	2.0434	129.2	0.02117	1.9869
293.1	0.34240	1.4899	256.5	1.13750	2.0809	131.1	0.02224	1.9946
295.1	0.32730	1.5107	258.4	1.27470	2.0487	133.1	0.02345	2.0031
297.0	0.31410	1.5308	260.4	1.39990	1.9269	135.0	0.02480	2.0122
298.9	0.30255	1.5500	262.3	1.45650	1.7371	136.9	0.02635	2.0222
300.9	0.29244	1.5685	264.2	1.42100	1.5358	138.9	0.02814	2.0331
302.8	0.28361	1.5863	266.1	1.31370	1.3710	140.8	0.03025	2.0453
304.7	0.27591	1.6034	268.1	1.16860	1.2610	142.7	0.03277	2.0588
306.6	0.26923	1.6200	270.0	1.01320	1.2047	144.6	0.03585	2.0741
308.6	0.26348	1.6360	271.9	0.86552	1.1935	146.6	0.03972	2.0916
310.5	0.25856	1.6516	273.9	0.73667	1.2159	148.5	0.04471	2.1120
312.4	0.25442	1.6668	275.8	0.63160	1.2598	150.4	0.05141	2.1360
314.4	0.25102	1.6816	277.7	0.55015	1.3149	152.4	0.06079	2.1650
316.3	0.24831	1.6961	279.6	0.48923	1.3738	154.3	0.07467	2.2011
318.2	0.24627	1.7104	281.6	0.44496	1.4324	156.2	0.09671	2.2473
320.1	0.24489	1.7244	283.5	0.41392	1.4884	158.1	0.13504	2.3084
322.1	0.24419	1.7384	285.4	0.39349	1.5409	160.1	0.20984	2.3899
324.0	0.24418	1.7523	287.4	0.38175	1.5895	162.0	0.37574	2.4819
325.9	0.24491	1.7661	289.3	0.37731	1.6337	163.9	0.72623	2.4410
327.8	0.24643	1.7800	291.2	0.37903	1.6731	165.9	0.92751	1.9537
329.8	0.24886	1.7939	293.1	0.38578	1.7072	167.8	0.60021	1.6318
331.7	0.25231	1.8080	295.1	0.39623	1.7354	169.7	0.33026	1.6688
333.6	0.25698	1.8223	297.0	0.40861	1.7573	171.6	0.21439	1.7701
335.6	0.26311	1.8367	298.9	0.42081	1.7734	173.6	0.17269	1.8620
337.5	0.27105	1.8512	300.9	0.43076	1.7848	175.5	0.17649	1.9422
339.4	0.28123	1.8657	302.8	0.43720	1.7940	177.4	0.23389	1.9965
341.3	0.29422	1.8798	304.7	0.44034	1.8040	179.4	0.30371	1.9506
343.3	0.31070	1.8929	306.6	0.44206	1.8171	181.3	0.27420	1.9010
345.2	0.33128	1.9036	308.6	0.44541	1.8344	183.2	0.23700	1.8569
347.1	0.35624	1.9101	310.5	0.45373	1.8551	185.1	0.15248	1.8807
349.1	0.38470	1.9094	312.4	0.46982	1.8765	187.1	0.11851	1.9369
351.0	0.41369	1.8989	314.4	0.49499	1.8943	189.0	0.10761	1.9882
352.9	0.43778	1.8777	316.3	0.52770	1.9030	190.9	0.10663	2.0358
354.8	0.45106	1.8490	318.2	0.56230	1.8981	192.9	0.11207	2.0833
356.8	0.45118	1.8199	320.1	0.58987	1.8804	194.8	0.12376	2.1334
358.7	0.44102	1.7970	322.1	0.60395	1.8584	196.7	0.14375	2.1894
360.6	0.42617	1.7831	324.0	0.60801	1.8437	198.6	0.17718	2.2546
362.6	0.41136	1.7770	325.9	0.61582	1.8403	200.6	0.23566	2.3324
364.5	0.39914	1.7764	327.8	0.64091	1.8352	202.5	0.34537	2.4206

366.4	0.39027	1.7788	329.8	0.67452	1.8020	204.4	0.55906	2.4804
368.3	0.38456	1.7825	331.7	0.67633	1.7403	206.4	0.88075	2.3415
370.3	0.38146	1.7862	333.6	0.63339	1.6969	208.3	0.96732	1.9153
372.2	0.38031	1.7894	335.6	0.58314	1.6962	210.2	0.70679	1.6534
374.1	0.38045	1.7916	337.5	0.55395	1.7227	212.1	0.45941	1.6521
376.1	0.38132	1.7926	339.4	0.55157	1.7566	214.1	0.32417	1.7326
378.0	0.38239	1.7925	341.3	0.57342	1.7839	216.0	0.25739	1.8173
379.9	0.38324	1.7913	343.3	0.61375	1.7937	217.9	0.22521	1.8928
381.8	0.38351	1.7893	345.2	0.66189	1.7765	219.9	0.21175	1.9603
383.8	0.38296	1.7868	347.1	0.70070	1.7292	221.8	0.20997	2.0229
385.7	0.38142	1.7839	349.1	0.71243	1.6615	223.7	0.21685	2.0833
387.6	0.37884	1.7811	351.0	0.69040	1.5936	225.6	0.23152	2.1438
389.6	0.37525	1.7787	352.9	0.64299	1.5434	227.6	0.25459	2.2068
391.5	0.37078	1.7769	354.8	0.58529	1.5173	229.5	0.28818	2.2740
393.4	0.36559	1.7759	356.8	0.52959	1.5123	231.4	0.33665	2.3473
395.3	0.35987	1.7758	358.7	0.48208	1.5215	233.4	0.40805	2.4272
397.3	0.35383	1.7768	360.6	0.44433	1.5389	235.3	0.51701	2.5096
399.2	0.34768	1.7789	362.6	0.41553	1.5598	237.2	0.68505	2.5732
401.1	0.34159	1.7820	364.5	0.39415	1.5818	239.1	0.91646	2.5556
403.1	0.33574	1.7861	366.4	0.37857	1.6033	241.1	1.11520	2.3911
405.0	0.33023	1.7911	368.3	0.36742	1.6234	243.0	1.15330	2.1848
406.9	0.32517	1.7969	370.3	0.35957	1.6420	244.9	1.11070	2.0823
408.8	0.32063	1.8036	372.2	0.35411	1.6588	246.9	1.10540	2.0563
410.8	0.31667	1.8108	374.1	0.35032	1.6739	248.8	1.15790	2.0346
412.7	0.31332	1.8187	376.1	0.34761	1.6874	250.7	1.24380	1.9758
414.6	0.31060	1.8271	378.0	0.34553	1.6996	252.6	1.32840	1.8662
416.6	0.30853	1.8360	379.9	0.34374	1.7108	254.6	1.38040	1.7149
418.5	0.30711	1.8454	381.8	0.34199	1.7211	256.5	1.38280	1.5458
420.4	0.30635	1.8551	383.8	0.34013	1.7308	258.4	1.33640	1.3839
422.3	0.30626	1.8652	385.7	0.33810	1.7404	260.4	1.25300	1.2459
424.3	0.30684	1.8756	387.6	0.33590	1.7499	262.3	1.14650	1.1383
426.2	0.30810	1.8864	389.6	0.33361	1.7596	264.2	1.02850	1.0617
428.1	0.31006	1.8976	391.5	0.33134	1.7698	266.1	0.90747	1.0141
430.1	0.31275	1.9090	393.4	0.32924	1.7804	268.1	0.78980	0.9924
432.0	0.31619	1.9209	395.3	0.32747	1.7915	270.0	0.68049	0.9929
433.9	0.32043	1.9331	397.3	0.32618	1.8033	271.9	0.58352	1.0109
435.8	0.32553	1.9457	399.2	0.32553	1.8155	273.9	0.50089	1.0414
437.8	0.33157	1.9588	401.1	0.32564	1.8283	275.8	0.43287	1.0793
439.7	0.33864	1.9723	403.1	0.32661	1.8414	277.7	0.37805	1.1205
441.6	0.34689	1.9863	405.0	0.32853	1.8549	279.6	0.33449	1.1624
443.6	0.35647	2.0008	406.9	0.33146	1.8685	281.6	0.30009	1.2035
445.5	0.36763	2.0159	408.8	0.33542	1.8821	283.5	0.27311	1.2430
447.4	0.38064	2.0315	410.8	0.34041	1.8957	285.4	0.25213	1.2807

449.3	0.39589	2.0476	412.7	0.34639	1.9090	287.4	0.23609	1.3165
451.3	0.41388	2.0640	414.6	0.35329	1.9220	289.3	0.22420	1.3506
453.2	0.43525	2.0805	416.6	0.36101	1.9345	291.2	0.21591	1.3830
455.1	0.46075	2.0966	418.5	0.36939	1.9466	293.1	0.21089	1.4141
457.1	0.49125	2.1111	420.4	0.37827	1.9581	295.1	0.20893	1.4439
459.0	0.52748	2.1223	422.3	0.38746	1.9692	297.0	0.21002	1.4727
460.9	0.56960	2.1278	424.3	0.39678	1.9801	298.9	0.21423	1.5003
462.8	0.61633	2.1239	426.2	0.40609	1.9910	300.9	0.22183	1.5269
464.8	0.66396	2.1076	428.1	0.41539	2.0025	302.8	0.23315	1.5521
466.7	0.70617	2.0777	430.1	0.42489	2.0151	304.7	0.24869	1.5755
468.6	0.73615	2.0378	432.0	0.43524	2.0296	306.6	0.26893	1.5961
470.6	0.75053	1.9954	433.9	0.44775	2.0469	308.6	0.29424	1.6127
472.5	0.75141	1.9586	435.8	0.46500	2.0674	310.5	0.32447	1.6232
474.4	0.74452	1.9314	437.8	0.49151	2.0900	312.4	0.35850	1.6249
476.3	0.73565	1.9143	439.7	0.53375	2.1084	314.4	0.39342	1.6153
478.3	0.72872	1.9050	441.6	0.59331	2.1049	316.3	0.42437	1.5930
480.2	0.72558	1.9008	443.6	0.64442	2.0578	318.2	0.44527	1.5597
482.1	0.72675	1.8994	445.5	0.64208	1.9911	320.1	0.45131	1.5210
484.1	0.73202	1.8991	447.4	0.59792	1.9589	322.1	0.44142	1.4844
486.0	0.74089	1.8986	449.3	0.55382	1.9670	324.0	0.41892	1.4571
487.9	0.75277	1.8970	451.3	0.52540	1.9967	325.9	0.38970	1.4429
489.8	0.76709	1.8939	453.2	0.51227	2.0360	327.9	0.35977	1.4427
491.8	0.78330	1.8887	455.1	0.51178	2.0800	329.8	0.33424	1.4561
493.7	0.80090	1.8814	457.1	0.52249	2.1269	331.7	0.31841	1.4833
495.6	0.81940	1.8716	459.0	0.54429	2.1759	333.6	0.32408	1.5261
497.6	0.83836	1.8592	460.9	0.57823	2.2261	335.6	0.39074	1.5648
499.5	0.85733	1.8442	462.8	0.62627	2.2761	337.5	0.44997	1.4816
501.4	0.87589	1.8267	464.8	0.69106	2.3230	339.4	0.43295	1.4551
503.3	0.89363	1.8066	466.7	0.77534	2.3615	341.3	0.43587	1.4036
505.3	0.91016	1.7842	468.6	0.88050	2.3835	343.3	0.39537	1.3758
507.2	0.92513	1.7595	470.6	1.00370	2.3769	345.2	0.38100	1.3683
509.1	0.93821	1.7328	472.5	1.13380	2.3292	347.1	0.36650	1.3371
511.1	0.94911	1.7044	474.4	1.24950	2.2342	349.1	0.32311	1.3112
513.0	0.95763	1.6746	476.3	1.32590	2.1008	351.0	0.27532	1.3118
514.9	0.96357	1.6437	478.3	1.34750	1.9535	352.9	0.23933	1.3262
516.8	0.96684	1.6121	480.2	1.31690	1.8201	354.8	0.21411	1.3439
518.8	0.96737	1.5802	482.1	1.24980	1.7195	356.8	0.19577	1.3610
520.7	0.96517	1.5482	484.1	1.16570	1.6587	358.7	0.18166	1.3768
522.6	0.96030	1.5165	486.0	1.08100	1.6355	360.6	0.17020	1.3913
524.6	0.95286	1.4855	487.9	1.00730	1.6432	362.6	0.16051	1.4047
526.5	0.94298	1.4553	489.8	0.95125	1.6738	364.5	0.15207	1.4173
528.4	0.93083	1.4263	491.8	0.91632	1.7197	366.4	0.14459	1.4293
530.3	0.91661	1.3987	493.7	0.90402	1.7744	368.3	0.13787	1.4409

532.3	0.90051	1.3725	495.6	0.91530	1.8322	370.3	0.13181	1.4521
534.2	0.88276	1.3481	497.6	0.95109	1.8872	372.2	0.12631	1.4630
536.1	0.86357	1.3254	499.5	1.01190	1.9323	374.1	0.12132	1.4738
538.1	0.84315	1.3046	501.4	1.09610	1.9576	376.1	0.11681	1.4844
540.0	0.82173	1.2856	503.3	1.19640	1.9519	378.0	0.11275	1.4949
541.9	0.79949	1.2686	505.3	1.29740	1.9072	379.9	0.10909	1.5054
543.8	0.77664	1.2535	507.2	1.37880	1.8270	381.8	0.10583	1.5157
545.8	0.75337	1.2404	509.1	1.42630	1.7277	383.8	0.10294	1.5261
547.7	0.72984	1.2291	511.1	1.44040	1.6296	385.7	0.10041	1.5363
549.6	0.70621	1.2196	513.0	1.43200	1.5455	387.6	0.09821	1.5466
551.6	0.68265	1.2119	514.9	1.41390	1.4779	389.6	0.09634	1.5569
553.5	0.65927	1.2059	516.8	1.39480	1.4231	391.5	0.09478	1.5672
555.4	0.63621	1.2016	518.8	1.37820	1.3753	393.4	0.09354	1.5775
557.3	0.61358	1.1988	520.7	1.36420	1.3300	395.3	0.09259	1.5879
559.3	0.59146	1.1975	522.6	1.35120	1.2845	397.3	0.09194	1.5983
561.2	0.56996	1.1976	524.6	1.33690	1.2375	399.2	0.09160	1.6089
563.1	0.54913	1.1989	526.5	1.31970	1.1893	401.1	0.09156	1.6195
565.1	0.52904	1.2015	528.4	1.29820	1.1407	403.1	0.09183	1.6303
567.0	0.50974	1.2051	530.3	1.27180	1.0930	405.0	0.09243	1.6412
568.9	0.49127	1.2098	532.3	1.24070	1.0475	406.9	0.09338	1.6524
570.8	0.47366	1.2154	534.2	1.20510	1.0050	408.8	0.09471	1.6637
572.8	0.45692	1.2219	536.1	1.16580	0.9664	410.8	0.09644	1.6752
574.7	0.44109	1.2292	538.1	1.12350	0.9321	412.7	0.09862	1.6870
576.6	0.42616	1.2373	540.0	1.07890	0.9025	414.6	0.10131	1.6991
578.6	0.41215	1.2460	541.9	1.03280	0.8775	416.6	0.10457	1.7115
580.5	0.39906	1.2554	543.8	0.98584	0.8572	418.5	0.10850	1.7242
582.4	0.38691	1.2653	545.8	0.93857	0.8415	420.4	0.11318	1.7373
584.3	0.37571	1.2759	547.7	0.89149	0.8301	422.3	0.11876	1.7506
586.3	0.36547	1.2870	549.6	0.84506	0.8229	424.3	0.12539	1.7642
588.2	0.35621	1.2986	551.6	0.79970	0.8197	426.2	0.13326	1.7779
590.1	0.34799	1.3108	553.5	0.75575	0.8201	428.1	0.14256	1.7917
592.1	0.34083	1.3236	555.4	0.71355	0.8239	430.1	0.15354	1.8053
594.0	0.33481	1.3368	557.3	0.67337	0.8308	432.0	0.16638	1.8182
595.9	0.33003	1.3507	559.3	0.63545	0.8403	433.9	0.18122	1.8300
597.8	0.32660	1.3651	561.2	0.59994	0.8521	435.8	0.19795	1.8398
599.8	0.32467	1.3802	563.1	0.56696	0.8659	437.8	0.21614	1.8467
601.7	0.32447	1.3958	565.1	0.53654	0.8812	439.7	0.23475	1.8500
603.6	0.32626	1.4121	567.0	0.50866	0.8977	441.6	0.25213	1.8491
605.6	0.33039	1.4288	568.9	0.48324	0.9151	443.6	0.26617	1.8447
607.5	0.33731	1.4459	570.8	0.46018	0.9331	445.5	0.27504	1.8383
609.4	0.34756	1.4632	572.8	0.43934	0.9515	447.4	0.27799	1.8330
611.3	0.36181	1.4802	574.7	0.42057	0.9701	449.3	0.27587	1.8314
613.3	0.38085	1.4960	576.6	0.40370	0.9887	451.3	0.27080	1.8358

615.2	0.40543	1.5095	578.6	0.38858	1.0072	453.2	0.26533	1.8470
617.1	0.43614	1.5188	580.5	0.37508	1.0256	455.1	0.26182	1.8648
619.1	0.47294	1.5212	582.4	0.36304	1.0439	457.1	0.26213	1.8886
621.0	0.51455	1.5133	584.3	0.35236	1.0619	459.0	0.26783	1.9177
622.9	0.55764	1.4918	586.3	0.34294	1.0797	460.9	0.28054	1.9515
624.8	0.59657	1.4549	588.2	0.33467	1.0972	462.8	0.30229	1.9893
626.8	0.62439	1.4039	590.1	0.32749	1.1146	464.8	0.33607	2.0301
628.7	0.63535	1.3443	592.1	0.32136	1.1319	466.7	0.38615	2.0713
630.6	0.62736	1.2838	594.0	0.31623	1.1490	468.6	0.45816	2.1073
632.6	0.60271	1.2300	595.9	0.31209	1.1662	470.6	0.55685	2.1253
634.5	0.56647	1.1875	597.8	0.30897	1.1833	472.5	0.67866	2.1036
636.4	0.52432	1.1578	599.8	0.30690	1.2005	474.4	0.79713	2.0188
638.3	0.48099	1.1400	601.7	0.30596	1.2180	476.3	0.86314	1.8760
640.3	0.43964	1.1320	603.6	0.30629	1.2357	478.3	0.84585	1.7249
642.2	0.40202	1.1314	605.6	0.30807	1.2537	480.2	0.76553	1.6182
644.1	0.36877	1.1359	607.5	0.31157	1.2722	482.1	0.66576	1.5719
646.1	0.33988	1.1438	609.4	0.31720	1.2912	484.1	0.57740	1.5728
648.0	0.31500	1.1537	611.3	0.32546	1.3107	486.0	0.51181	1.6013
649.9	0.29362	1.1648	613.3	0.33710	1.3305	487.9	0.46872	1.6431
651.8	0.27524	1.1763	615.2	0.35306	1.3503	489.8	0.44443	1.6903
653.8	0.25940	1.1881	617.1	0.37456	1.3691	491.8	0.43538	1.7392
655.7	0.24566	1.1997	619.1	0.40292	1.3852	493.7	0.43915	1.7881
657.6	0.23371	1.2110	621.0	0.43918	1.3958	495.6	0.45458	1.8363
659.6	0.22324	1.2220	622.9	0.48308	1.3961	497.6	0.48147	1.8829
661.5	0.21402	1.2327	624.8	0.53129	1.3807	499.5	0.52052	1.9271
663.4	0.20586	1.2429	626.8	0.57594	1.3455	501.4	0.57288	1.9665
665.3	0.19860	1.2527	628.7	0.60597	1.2922	503.3	0.63976	1.9978
667.3	0.19211	1.2621	630.6	0.61300	1.2304	505.3	0.72099	2.0150
669.2	0.18629	1.2712	632.6	0.59682	1.1728	507.2	0.81325	2.0108
671.1	0.18104	1.2799	634.5	0.56447	1.1285	509.1	0.90754	1.9788
673.1	0.17629	1.2882	636.4	0.52492	1.1001	511.1	0.99029	1.9188
675.0	0.17197	1.2963	638.3	0.48509	1.0857	513.0	1.04900	1.8400
676.9	0.16805	1.3040	640.3	0.44879	1.0815	514.9	1.08060	1.7577
678.8	0.16447	1.3114	642.2	0.41743	1.0841	516.8	1.09200	1.6844
680.8	0.16120	1.3186	644.1	0.39107	1.0909	518.8	1.09420	1.6239
682.7	0.15820	1.3256	646.1	0.36919	1.1000	520.7	1.09560	1.5733
684.6	0.15546	1.3323	648.0	0.35108	1.1103	522.6	1.09990	1.5268
686.5	0.15293	1.3388	649.9	0.33608	1.1212	524.6	1.10680	1.4794
688.5	0.15061	1.3451	651.8	0.32364	1.1321	526.5	1.11360	1.4279
690.4	0.14848	1.3513	653.8	0.31331	1.1429	528.4	1.11720	1.3716
692.3	0.14652	1.3572	655.7	0.30478	1.1536	530.3	1.11450	1.3111
694.3	0.14472	1.3630	657.6	0.29781	1.1640	532.3	1.10360	1.2487
696.2	0.14307	1.3686	659.6	0.29227	1.1742	534.2	1.08390	1.1866

698.1	0.14155	1.3740	661.5	0.28811	1.1842	536.1	1.05540	1.1272
700.0	0.14016	1.3793	663.4	0.28537	1.1938	538.1	1.01930	1.0725
702.0	0.13889	1.3845	665.3	0.28414	1.2031	540.0	0.97675	1.0238
703.9	0.13773	1.3896	667.3	0.28458	1.2116	541.9	0.92929	0.9820
705.8	0.13667	1.3945	669.2	0.28686	1.2191	543.8	0.87837	0.9474
707.8	0.13572	1.3993	671.1	0.29099	1.2247	545.8	0.82531	0.9204
709.7	0.13485	1.4040	673.1	0.29658	1.2275	547.7	0.77138	0.9007
711.6	0.13408	1.4086	675.0	0.30249	1.2264	549.6	0.71766	0.8882
713.5	0.13339	1.4130	676.9	0.30672	1.2211	551.6	0.66523	0.8824
715.5	0.13278	1.4174	678.8	0.30707	1.2129	553.5	0.61498	0.8830
717.4	0.13224	1.4217	680.8	0.30246	1.2041	555.4	0.56780	0.8891
719.3	0.13178	1.4259	682.7	0.29366	1.1973	557.3	0.52431	0.9002
721.3	0.13139	1.4299	684.6	0.28258	1.1937	559.3	0.48509	0.9153
723.2	0.13106	1.4339	686.5	0.27104	1.1934	561.2	0.45042	0.9336
725.1	0.13080	1.4378	688.5	0.26017	1.1957	563.1	0.42050	0.9542
727.0	0.13060	1.4417	690.4	0.25041	1.1995	565.1	0.39533	0.9764
729.0	0.13045	1.4454	692.3	0.24186	1.2044	567.0	0.37494	0.9994
730.9	0.13036	1.4491	694.3	0.23442	1.2099	568.9	0.35923	1.0226
732.8	0.13032	1.4526	696.2	0.22791	1.2156	570.8	0.34816	1.0452
734.8	0.13033	1.4561	698.1	0.22219	1.2214	572.8	0.34165	1.0665
736.7	0.13039	1.4595	700.0	0.21712	1.2272	574.7	0.33950	1.0855
738.6	0.13049	1.4629	702.0	0.21259	1.2329	576.6	0.34126	1.1011
740.5	0.13063	1.4661	703.9	0.20850	1.2386	578.6	0.34600	1.1120
742.5	0.13082	1.4693	705.8	0.20479	1.2442	580.5	0.35204	1.1171
744.4	0.13103	1.4724	707.8	0.20140	1.2497	582.4	0.35694	1.1159
746.3	0.13129	1.4755	709.7	0.19829	1.2550	584.3	0.35791	1.1093
748.3	0.13157	1.4784	711.6	0.19542	1.2603	586.3	0.35276	1.0997
750.2	0.13188	1.4813	713.5	0.19277	1.2655	588.2	0.34085	1.0905
752.1	0.13221	1.4841	715.5	0.19031	1.2706	590.1	0.32337	1.0845
754.0	0.13257	1.4869	717.4	0.18803	1.2756	592.1	0.30260	1.0836
756.0	0.13295	1.4896	719.3	0.18591	1.2805	594.0	0.28102	1.0882
757.9	0.13334	1.4922	721.3	0.18395	1.2854	595.9	0.26047	1.0976
759.8	0.13374	1.4947	723.2	0.18212	1.2902	597.8	0.24211	1.1107
761.8	0.13416	1.4972	725.1	0.18043	1.2950	599.8	0.22640	1.1266
763.7	0.13458	1.4996	727.0	0.17887	1.2997	601.7	0.21351	1.1443
765.6	0.13500	1.5020	729.0	0.17743	1.3043	603.6	0.20334	1.1634
767.5	0.13543	1.5043	730.9	0.17610	1.3089	605.6	0.19580	1.1835
769.5	0.13585	1.5065	732.8	0.17490	1.3134	607.5	0.19082	1.2044
771.4	0.13626	1.5087	734.8	0.17380	1.3179	609.4	0.18838	1.2260
773.3	0.13667	1.5108	736.7	0.17280	1.3223	611.3	0.18863	1.2482
775.3	0.13706	1.5129	738.6	0.17192	1.3267	613.3	0.19182	1.2712
777.2	0.13744	1.5150	740.5	0.17114	1.3311	615.2	0.19846	1.2950
779.1	0.13780	1.5169	742.5	0.17046	1.3354	617.1	0.20926	1.3194

781.0	0.13813	1.5189	744.4	0.16988	1.3396	619.1	0.22534	1.3441
783.0	0.13845	1.5208	746.3	0.16940	1.3438	621.0	0.24817	1.3684
784.9	0.13874	1.5227	748.3	0.16901	1.3480	622.9	0.27965	1.3905
786.8	0.13900	1.5245	750.2	0.16873	1.3521	624.8	0.32167	1.4070
788.8	0.13924	1.5263	752.1	0.16854	1.3562	626.8	0.37501	1.4119
790.7	0.13944	1.5281	754.0	0.16845	1.3602	628.7	0.43640	1.3968
792.6	0.13962	1.5299	756.0	0.16845	1.3642	630.6	0.49522	1.3540
794.5	0.13977	1.5317	757.9	0.16855	1.3681	632.6	0.53393	1.2847
796.5	0.13988	1.5335	759.8	0.16874	1.3720	634.5	0.53845	1.2039
798.4	0.13997	1.5352	761.8	0.16903	1.3758	636.4	0.50932	1.1331
800.3	0.14002	1.5370	763.7	0.16941	1.3795	638.3	0.45990	1.0858
802.3	0.14005	1.5388	765.6	0.16988	1.3832	640.3	0.40577	1.0639
804.2	0.14004	1.5406	767.5	0.17044	1.3868	642.2	0.35731	1.0616
806.1	0.14002	1.5424	769.5	0.17110	1.3904	644.1	0.31903	1.0718
808.0	0.13996	1.5442	771.4	0.17184	1.3939	646.1	0.29152	1.0884
810.0	0.13989	1.5460	773.3	0.17266	1.3973	648.0	0.27385	1.1073
811.9	0.13980	1.5479	775.3	0.17358	1.4007	649.9	0.26471	1.1260
813.8	0.13969	1.5498	777.2	0.17457	1.4039	651.8	0.26289	1.1425
815.8	0.13957	1.5517	779.1	0.17564	1.4071	653.8	0.26723	1.1551
817.7	0.13943	1.5537	781.0	0.17679	1.4101	655.7	0.27626	1.1621
819.6	0.13930	1.5557	783.0	0.17801	1.4131	657.6	0.28784	1.1618
821.5	0.13915	1.5577	784.9	0.17930	1.4160	659.6	0.29881	1.1534
823.5	0.13901	1.5598	786.8	0.18065	1.4188	661.5	0.30541	1.1374
825.4	0.13888	1.5619	788.8	0.18205	1.4214	663.4	0.30438	1.1167
827.3	0.13875	1.5641	790.7	0.18350	1.4239	665.3	0.29441	1.0955
829.3	0.13863	1.5663	792.6	0.18499	1.4264	667.3	0.27674	1.0779
831.2	0.13853	1.5685	794.5	0.18651	1.4286	669.2	0.25428	1.0663
833.1	0.13845	1.5708	796.5	0.18806	1.4308	671.1	0.23027	1.0612
835.0	0.13839	1.5732	798.4	0.18961	1.4328	673.1	0.20708	1.0618
837.0	0.13836	1.5756	800.3	0.19116	1.4347	675.0	0.18609	1.0664
838.9	0.13835	1.5780	802.3	0.19270	1.4365	676.9	0.16778	1.0738
840.8	0.13838	1.5805	804.2	0.19422	1.4381	678.8	0.15216	1.0828
842.8	0.13844	1.5830	806.1	0.19570	1.4396	680.8	0.13895	1.0926
844.7	0.13854	1.5855	808.0	0.19712	1.4410	682.7	0.12782	1.1027
846.6	0.13869	1.5881	810.0	0.19849	1.4423	684.6	0.11842	1.1129
848.5	0.13887	1.5907	811.9	0.19978	1.4435	686.5	0.11047	1.1227
850.5	0.13910	1.5934	813.8	0.20098	1.4445	688.5	0.10370	1.1323
852.4	0.13938	1.5961	815.8	0.20208	1.4455	690.4	0.09791	1.1415
854.3	0.13971	1.5988	817.7	0.20307	1.4464	692.3	0.09291	1.1503
856.3	0.14008	1.6015	819.6	0.20394	1.4472	694.3	0.08859	1.1587
858.2	0.14051	1.6043	821.5	0.20469	1.4480	696.2	0.08482	1.1668
860.1	0.14099	1.6071	823.5	0.20531	1.4488	698.1	0.08152	1.1745
862.0	0.14152	1.6099	825.4	0.20580	1.4495	700.0	0.07861	1.1818

864.0	0.14210	1.6127	827.3	0.20615	1.4503	702.0	0.07604	1.1888
865.9	0.14273	1.6155	829.3	0.20638	1.4511	703.9	0.07376	1.1956
867.8	0.14342	1.6183	831.2	0.20647	1.4519	705.8	0.07173	1.2020
869.8	0.14415	1.6212	833.1	0.20644	1.4528	707.8	0.06991	1.2082
871.7	0.14493	1.6240	835.0	0.20631	1.4538	709.7	0.06828	1.2142
873.6	0.14576	1.6269	837.0	0.20607	1.4548	711.6	0.06682	1.2199
875.5	0.14663	1.6297	838.9	0.20573	1.4560	713.5	0.06551	1.2255
877.5	0.14754	1.6326	840.8	0.20533	1.4573	715.5	0.06432	1.2308
879.4	0.14848	1.6354	842.8	0.20486	1.4587	717.4	0.06325	1.2360
881.3	0.14946	1.6382	844.7	0.20435	1.4602	719.3	0.06229	1.2410
883.3	0.15047	1.6411	846.6	0.20380	1.4619	721.3	0.06142	1.2459
885.2	0.15150	1.6439	848.5	0.20325	1.4638	723.2	0.06064	1.2506
887.1	0.15255	1.6467	850.5	0.20270	1.4658	725.1	0.05993	1.2551
889.0	0.15362	1.6495	852.4	0.20218	1.4679	727.0	0.05930	1.2596
891.0	0.15469	1.6523	854.3	0.20170	1.4702	729.0	0.05873	1.2639
892.9	0.15576	1.6551	856.3	0.20127	1.4727	730.9	0.05822	1.2682
894.8	0.15683	1.6579	858.2	0.20092	1.4752	732.8	0.05777	1.2723
896.8	0.15789	1.6608	860.1	0.20065	1.4780	734.8	0.05738	1.2763
898.7	0.15894	1.6636	862.0	0.20049	1.4808	736.7	0.05703	1.2802
900.6	0.15996	1.6665	864.0	0.20045	1.4838	738.6	0.05673	1.2841
902.5	0.16096	1.6694	865.9	0.20053	1.4869	740.5	0.05648	1.2878
904.5	0.16192	1.6723	867.8	0.20076	1.4901	742.5	0.05627	1.2915
906.4	0.16285	1.6753	869.8	0.20115	1.4933	744.4	0.05609	1.2951
908.3	0.16374	1.6783	871.7	0.20170	1.4967	746.3	0.05596	1.2986
910.3	0.16459	1.6814	873.6	0.20242	1.5001	748.3	0.05586	1.3021
912.2	0.16539	1.6846	875.5	0.20332	1.5035	750.2	0.05580	1.3055
914.1	0.16616	1.6879	877.5	0.20441	1.5070	752.1	0.05578	1.3089
916.0	0.16688	1.6914	879.4	0.20570	1.5104	754.0	0.05578	1.3121
918.0	0.16756	1.6949	881.3	0.20718	1.5139	756.0	0.05582	1.3154
919.9	0.16821	1.6987	883.3	0.20885	1.5173	757.9	0.05590	1.3185
921.8	0.16883	1.7025	885.2	0.21072	1.5206	759.8	0.05600	1.3217
923.8	0.16943	1.7066	887.1	0.21278	1.5239	761.8	0.05614	1.3247
925.7	0.17001	1.7109	889.0	0.21503	1.5271	763.7	0.05630	1.3278
927.6	0.17060	1.7154	891.0	0.21744	1.5301	765.6	0.05650	1.3307
929.5	0.17120	1.7202	892.9	0.22001	1.5330	767.5	0.05672	1.3337
931.5	0.17183	1.7252	894.8	0.22272	1.5357	769.5	0.05698	1.3366
933.4	0.17250	1.7305	896.8	0.22553	1.5382	771.4	0.05726	1.3394
935.3	0.17323	1.7361	898.7	0.22842	1.5405	773.3	0.05758	1.3422
937.3	0.17404	1.7420	900.6	0.23136	1.5425	775.3	0.05792	1.3450
939.2	0.17496	1.7482	902.5	0.23431	1.5443	777.2	0.05829	1.3477
941.1	0.17601	1.7548	904.5	0.23721	1.5459	779.1	0.05870	1.3504
943.0	0.17721	1.7618	906.4	0.24003	1.5472	781.0	0.05912	1.3530
945.0	0.17859	1.7692	908.3	0.24271	1.5483	783.0	0.05958	1.3556

946.9	0.18019	1.7770	910.3	0.24521	1.5492	784.9	0.06007	1.3582
948.8	0.18203	1.7852	912.2	0.24748	1.5499	786.8	0.06058	1.3607
950.8	0.18416	1.7939	914.1	0.24947	1.5505	788.8	0.06113	1.3632
952.7	0.18661	1.8030	916.0	0.25116	1.5510	790.7	0.06170	1.3656
954.6	0.18944	1.8127	918.0	0.25251	1.5515	792.6	0.06229	1.3680
956.5	0.19269	1.8229	919.9	0.25352	1.5520	794.5	0.06291	1.3703
958.5	0.19643	1.8336	921.8	0.25418	1.5527	796.5	0.06356	1.3727
960.4	0.20071	1.8449	923.8	0.25450	1.5536	798.4	0.06423	1.3749
962.3	0.20561	1.8568	925.7	0.25451	1.5548	800.3	0.06492	1.3771
964.3	0.21123	1.8694	927.6	0.25424	1.5563	802.3	0.06564	1.3793
966.2	0.21765	1.8825	929.5	0.25376	1.5582	804.2	0.06637	1.3814
968.1	0.22500	1.8964	931.5	0.25311	1.5605	806.1	0.06712	1.3835
970.0	0.23341	1.9110	933.4	0.25236	1.5634	808.0	0.06789	1.3855
972.0	0.24304	1.9263	935.3	0.25160	1.5668	810.0	0.06867	1.3875
973.9	0.25407	1.9422	937.3	0.25089	1.5707	811.9	0.06946	1.3894
975.8	0.26672	1.9589	939.2	0.25031	1.5752	813.8	0.07026	1.3913
977.8	0.28124	1.9763	941.1	0.24996	1.5802	815.8	0.07106	1.3931
979.7	0.29794	1.9942	943.0	0.24989	1.5858	817.7	0.07186	1.3949
981.6	0.31716	2.0127	945.0	0.25021	1.5920	819.6	0.07266	1.3966
983.5	0.33930	2.0314	946.9	0.25097	1.5986	821.5	0.07345	1.3982
985.5	0.36481	2.0501	948.8	0.25226	1.6057	823.5	0.07422	1.3998
987.4	0.39420	2.0683	950.8	0.25415	1.6132	825.4	0.07498	1.4014
989.3	0.42798	2.0855	952.7	0.25672	1.6210	827.3	0.07571	1.4028
991.3	0.46665	2.1007	954.6	0.26002	1.6291	829.3	0.07641	1.4043
993.2	0.51058	2.1129	956.5	0.26412	1.6374	831.2	0.07708	1.4057
995.1	0.55993	2.1203	958.5	0.26907	1.6457	833.1	0.07772	1.4070
997.0	0.61438	2.1212	960.4	0.27490	1.6540	835.0	0.07830	1.4083
999.0	0.67292	2.1135	962.3	0.28162	1.6621	837.0	0.07885	1.4096
1000.9	0.73358	2.0950	964.3	0.28923	1.6699	838.9	0.07933	1.4109
1002.8	0.79332	2.0643	966.2	0.29765	1.6771	840.8	0.07976	1.4121
1004.7	0.84815	2.0211	968.1	0.30677	1.6836	842.8	0.08013	1.4133
1006.7	0.89386	1.9666	970.0	0.31639	1.6892	844.7	0.08044	1.4145
1008.6	0.92682	1.9043	972.0	0.32626	1.6938	846.6	0.08069	1.4157
1010.5	0.94511	1.8389	973.9	0.33604	1.6974	848.5	0.08087	1.4169
1012.5	0.94901	1.7757	975.8	0.34532	1.7000	850.5	0.08098	1.4181
1014.4	0.94093	1.7189	977.8	0.35370	1.7019	852.4	0.08102	1.4194
1016.3	0.92482	1.6718	979.7	0.36078	1.7035	854.3	0.08101	1.4207
1018.2	0.90530	1.6352	981.6	0.36632	1.7053	856.3	0.08093	1.4220
1020.2	0.88681	1.6082	983.5	0.37024	1.7081	858.2	0.08079	1.4233
1022.1	0.87285	1.5881	985.5	0.37270	1.7128	860.1	0.08059	1.4247
1024.0	0.86539	1.5709	987.4	0.37419	1.7203	862.0	0.08034	1.4262
1026.0	0.86430	1.5521	989.3	0.37547	1.7314	864.0	0.08005	1.4277
1027.9	0.86714	1.5277	991.3	0.37766	1.7468	865.9	0.07972	1.4293

1029.8	0.86944	1.4951	993.2	0.38220	1.7670	867.8	0.07934	1.4310
1031.7	0.86589	1.4551	995.1	0.39100	1.7925	869.8	0.07894	1.4328
1033.7	0.85214	1.4109	997.0	0.40658	1.8231	871.7	0.07852	1.4346
1035.6	0.82645	1.3678	999.0	0.43237	1.8580	873.6	0.07807	1.4366
1037.5	0.79001	1.3308	1000.9	0.47286	1.8944	875.5	0.07762	1.4386
1039.5	0.74600	1.3036	1002.8	0.53299	1.9257	877.5	0.07716	1.4407
1041.4	0.69845	1.2875	1004.7	0.61449	1.9388	879.4	0.07670	1.4429
1043.3	0.65100	1.2824	1006.7	0.70666	1.9151	881.3	0.07625	1.4452
1045.2	0.60638	1.2867	1008.6	0.77820	1.8479	883.3	0.07580	1.4476
1047.2	0.56631	1.2987	1010.5	0.79830	1.7652	885.2	0.07538	1.4501
1049.1	0.53168	1.3165	1012.5	0.77498	1.7124	887.1	0.07497	1.4527
1051.0	0.50275	1.3384	1014.4	0.74776	1.7075	889.0	0.07460	1.4554
1053.0	0.47938	1.3631	1016.3	0.75158	1.7354	891.0	0.07425	1.4582
1054.9	0.46126	1.3898	1018.2	0.80210	1.7642	892.9	0.07394	1.4611
1056.8	0.44807	1.4176	1020.2	0.89004	1.7556	894.8	0.07367	1.4641
1058.7	0.43947	1.4461	1022.1	0.97232	1.6880	896.8	0.07345	1.4672
1060.7	0.43521	1.4750	1024.0	1.00370	1.5935	898.7	0.07328	1.4704
1062.6	0.43512	1.5041	1026.0	0.99957	1.5244	900.6	0.07315	1.4737
1064.5	0.43913	1.5331	1027.9	1.00830	1.4782	902.5	0.07309	1.4771
1066.5	0.44725	1.5619	1029.8	1.03360	1.4103	904.5	0.07309	1.4806
1068.4	0.45959	1.5902	1031.7	1.03050	1.3127	906.4	0.07315	1.4842
1070.3	0.47635	1.6179	1033.7	0.98557	1.2296	908.3	0.07329	1.4879
1072.2	0.49781	1.6446	1035.6	0.93758	1.1798	910.3	0.07349	1.4917
1074.2	0.52426	1.6698	1037.5	0.90731	1.1297	912.2	0.07378	1.4956
1076.1	0.55606	1.6927	1039.5	0.86190	1.0580	914.1	0.07416	1.4996
1078.0	0.59356	1.7127	1041.4	0.77703	0.9966	916.0	0.07462	1.5038
1080.0	0.63693	1.7284	1043.3	0.67457	0.9737	918.0	0.07518	1.5080
1081.9	0.68618	1.7384	1045.2	0.58072	0.9855	919.9	0.07584	1.5123
1083.8	0.74085	1.7409	1047.2	0.50565	1.0174	921.8	0.07661	1.5167
1085.7	0.79998	1.7341	1049.1	0.44910	1.0579	923.8	0.07750	1.5213
1087.7	0.86172	1.7161	1051.0	0.40737	1.1006	925.7	0.07851	1.5259
1089.6	0.92352	1.6852	1053.0	0.37673	1.1428	927.6	0.07965	1.5307
1091.5	0.98192	1.6411	1054.9	0.35432	1.1833	929.5	0.08093	1.5355
1093.5	1.03330	1.5841	1056.8	0.33814	1.2220	931.5	0.08236	1.5404
1095.4	1.07400	1.5164	1058.7	0.32683	1.2590	933.4	0.08393	1.5454
1097.3	1.10160	1.4411	1060.7	0.31947	1.2946	935.3	0.08566	1.5505
1099.2	1.11480	1.3620	1062.6	0.31548	1.3292	937.3	0.08755	1.5557
1101.2	1.11360	1.2829	1064.5	0.31451	1.3629	939.2	0.08960	1.5609
1103.1	1.09950	1.2072	1066.5	0.31636	1.3962	941.1	0.09181	1.5662
1105.0	1.07430	1.1371	1068.4	0.32099	1.4293	943.0	0.09416	1.5715
1107.0	1.04030	1.0741	1070.3	0.32850	1.4624	945.0	0.09665	1.5768
1108.9	0.99971	1.0191	1072.2	0.33908	1.4956	946.9	0.09925	1.5821
1110.8	0.95441	0.9722	1074.2	0.35304	1.5293	948.8	0.10193	1.5875

1112.7	0.90602	0.9332	1076.1	0.37085	1.5633	950.8	0.10466	1.5928
1114.7	0.85594	0.9018	1078.0	0.39313	1.5978	952.7	0.10739	1.5982
1116.6	0.80521	0.8776	1080.0	0.42063	1.6325	954.6	0.11007	1.6037
1118.5	0.75477	0.8599	1081.9	0.45436	1.6671	956.5	0.11266	1.6093
1120.5	0.70531	0.8482	1083.8	0.49543	1.7009	958.5	0.11511	1.6150
1122.4	0.65750	0.8421	1085.7	0.54523	1.7327	960.4	0.11740	1.6211
1124.3	0.61181	0.8408	1087.7	0.60504	1.7606	962.3	0.11950	1.6275
1126.2	0.56870	0.8438	1089.6	0.67608	1.7817	964.3	0.12145	1.6345
1128.2	0.52844	0.8504	1091.5	0.75865	1.7920	966.2	0.12327	1.6422
1130.1	0.49126	0.8601	1093.5	0.85165	1.7863	968.1	0.12503	1.6507
1132.0	0.45722	0.8722	1095.4	0.95121	1.7592	970.0	0.12683	1.6601
1134.0	0.42633	0.8862	1097.3	1.05040	1.7062	972.0	0.12879	1.6707
1135.9	0.39846	0.9016	1099.2	1.13940	1.6263	973.9	0.13104	1.6825
1137.8	0.37347	0.9179	1101.2	1.20830	1.5237	975.8	0.13376	1.6957
1139.7	0.35114	0.9348	1103.1	1.25000	1.4072	977.8	0.13711	1.7105
1141.7	0.33128	0.9520	1105.0	1.26280	1.2873	979.7	0.14132	1.7270
1143.6	0.31364	0.9694	1107.0	1.24960	1.1734	981.6	0.14664	1.7456
1145.5	0.29804	0.9867	1108.9	1.21620	1.0713	983.5	0.15340	1.7664
1147.5	0.28427	1.0040	1110.8	1.16860	0.9839	985.5	0.16204	1.7898
1149.4	0.27216	1.0210	1112.7	1.11200	0.9113	987.4	0.17317	1.8164
1151.3	0.26155	1.0378	1114.7	1.05050	0.8528	989.3	0.18771	1.8468
1153.2	0.25234	1.0544	1116.6	0.98697	0.8069	991.3	0.20709	1.8817
1155.2	0.24439	1.0707	1118.5	0.92329	0.7721	993.2	0.23366	1.9223
1157.1	0.23764	1.0867	1120.5	0.86075	0.7470	995.1	0.27155	1.9695
1159.0	0.23201	1.1025	1122.4	0.80032	0.7303	997.0	0.32818	2.0233
1161.0	0.22747	1.1181	1124.3	0.74259	0.7208	999.0	0.41707	2.0789
1162.9	0.22399	1.1334	1126.2	0.68813	0.7177	1000.9	0.55728	2.1139
1164.8	0.22156	1.1486	1128.2	0.63727	0.7200	1002.8	0.74451	2.0666
1166.7	0.22021	1.1637	1130.1	0.59036	0.7269	1004.7	0.87326	1.8922
1168.7	0.21997	1.1785	1132.0	0.54751	0.7375	1006.7	0.85019	1.7155
1170.6	0.22091	1.1932	1134.0	0.50883	0.7510	1008.6	0.77342	1.6446
1172.5	0.22313	1.2077	1135.9	0.47421	0.7666	1010.5	0.73317	1.6401
1174.5	0.22674	1.2220	1137.8	0.44349	0.7838	1012.5	0.73955	1.6474
1176.4	0.23189	1.2358	1139.7	0.41640	0.8019	1014.4	0.77716	1.6387
1178.3	0.23875	1.2492	1141.7	0.39265	0.8205	1016.3	0.82761	1.6021
1180.2	0.24747	1.2617	1143.6	0.37190	0.8393	1018.2	0.87260	1.5356
1182.2	0.25821	1.2730	1145.5	0.35386	0.8580	1020.2	0.89647	1.4465
1184.1	0.27098	1.2825	1147.5	0.33823	0.8765	1022.1	0.89060	1.3481
1186.0	0.28565	1.2896	1149.4	0.32476	0.8947	1024.0	0.85520	1.2551
1188.0	0.30175	1.2936	1151.3	0.31322	0.9125	1026.0	0.79687	1.1780
1189.9	0.31840	1.2937	1153.2	0.30344	0.9299	1027.9	0.72468	1.1220
1191.8	0.33431	1.2898	1155.2	0.29527	0.9468	1029.8	0.64714	1.0879
1193.7	0.34802	1.2822	1157.1	0.28861	0.9633	1031.7	0.57114	1.0736

1195.7	0.35832	1.2720	1159.0	0.28336	0.9794	1033.7	0.50130	1.0753
1197.6	0.36478	1.2610	1161.0	0.27949	0.9951	1035.6	0.44024	1.0887
1199.5	0.36790	1.2509	1162.9	0.27697	1.0103	1037.5	0.38866	1.1100
1201.5	0.36895	1.2427	1164.8	0.27583	1.0252	1039.5	0.34609	1.1360
1203.4	0.36936	1.2366	1166.7	0.27610	1.0396	1041.4	0.31150	1.1645
1205.3	0.37037	1.2322	1168.7	0.27785	1.0534	1043.3	0.28370	1.1940
1207.2	0.37276	1.2285	1170.6	0.28117	1.0667	1045.2	0.26152	1.2238
1209.2	0.37676	1.2246	1172.5	0.28617	1.0792	1047.2	0.24400	1.2534
1211.1	0.38218	1.2194	1174.5	0.29296	1.0907	1049.1	0.23036	1.2827
1213.0	0.38845	1.2121	1176.4	0.30164	1.1009	1051.0	0.22002	1.3118
1215.0	0.39472	1.2023	1178.3	0.31223	1.1093	1053.0	0.21254	1.3405
1216.9	0.40000	1.1897	1180.2	0.32467	1.1154	1054.9	0.20760	1.3693
1218.8	0.40329	1.1746	1182.2	0.33867	1.1185	1056.8	0.20502	1.3981
1220.7	0.40374	1.1576	1184.1	0.35370	1.1179	1058.7	0.20472	1.4273
1222.7	0.40074	1.1397	1186.0	0.36888	1.1131	1060.7	0.20671	1.4571
1224.6	0.39409	1.1217	1188.0	0.38295	1.1038	1062.6	0.21111	1.4878
1226.5	0.38396	1.1048	1189.9	0.39448	1.0900	1064.5	0.21818	1.5196
1228.5	0.37082	1.0898	1191.8	0.40205	1.0727	1066.5	0.22830	1.5529
1230.4	0.35540	1.0774	1193.7	0.40462	1.0532	1068.4	0.24208	1.5880
1232.3	0.33846	1.0677	1195.7	0.40178	1.0333	1070.3	0.26040	1.6253
1234.2	0.32079	1.0610	1197.6	0.39388	1.0145	1072.2	0.28450	1.6649
1236.2	0.30302	1.0569	1199.5	0.38184	0.9984	1074.2	0.31614	1.7069
1238.1	0.28569	1.0553	1201.5	0.36689	0.9857	1076.1	0.35788	1.7509
1240.0	0.26914	1.0558	1203.4	0.35030	0.9766	1078.0	0.41324	1.7957
1242.0	0.25364	1.0580	1205.3	0.33318	0.9710	1080.0	0.48667	1.8376
1243.9	0.23927	1.0615	1207.2	0.31635	0.9684	1081.9	0.58296	1.8693
1245.8	0.22611	1.0660	1209.2	0.30036	0.9684	1083.8	0.70376	1.8776
1247.7	0.21411	1.0713	1211.1	0.28552	0.9704	1085.7	0.84070	1.8438
1249.7	0.20323	1.0772	1213.0	0.27197	0.9738	1087.7	0.96769	1.7551
1251.6	0.19340	1.0834	1215.0	0.25974	0.9783	1089.6	1.05050	1.6236
1253.5	0.18453	1.0898	1216.9	0.24875	0.9836	1091.5	1.07460	1.4858
1255.5	0.17653	1.0964	1218.8	0.23893	0.9893	1093.5	1.05690	1.3732
1257.4	0.16932	1.1030	1220.7	0.23016	0.9953	1095.4	1.02510	1.2937
1259.3	0.16281	1.1096	1222.7	0.22233	1.0014	1097.3	0.99836	1.2370
1261.2	0.15695	1.1161	1224.6	0.21533	1.0076	1099.2	0.98212	1.1885
1263.2	0.15164	1.1225	1226.5	0.20906	1.0138	1101.2	0.97244	1.1372
1265.1	0.14685	1.1287	1228.5	0.20343	1.0199	1103.1	0.96159	1.0791
1267.0	0.14251	1.1349	1230.4	0.19837	1.0258	1105.0	0.94266	1.0156
1269.0	0.13858	1.1408	1232.3	0.19379	1.0316	1107.0	0.91206	0.9515
1270.9	0.13501	1.1467	1234.2	0.18965	1.0373	1108.9	0.86962	0.8920
1272.8	0.13178	1.1523	1236.2	0.18589	1.0428	1110.8	0.81753	0.8407
1274.7	0.12883	1.1578	1238.1	0.18247	1.0481	1112.7	0.75882	0.7999
1276.7	0.12616	1.1632	1240.0	0.17935	1.0533	1114.7	0.69662	0.7703

1278.6	0.12373	1.1684	1242.0	0.17648	1.0583	1116.6	0.63360	0.7516
1280.5	0.12151	1.1735	1243.9	0.17386	1.0632	1118.5	0.57210	0.7431
1282.5	0.11950	1.1784	1245.8	0.17144	1.0678	1120.5	0.51392	0.7435
1284.4	0.11767	1.1831	1247.7	0.16921	1.0724	1122.4	0.46048	0.7513
1286.3	0.11600	1.1877	1249.7	0.16715	1.0768	1124.3	0.41259	0.7649
1288.2	0.11449	1.1922	1251.6	0.16524	1.0811	1126.2	0.37061	0.7825
1290.2	0.11312	1.1966	1253.5	0.16347	1.0852	1128.2	0.33436	0.8027
1292.1	0.11188	1.2008	1255.5	0.16182	1.0892	1130.1	0.30341	0.8243
1294.0	0.11076	1.2049	1257.4	0.16028	1.0931	1132.0	0.27714	0.8463
1296.0	0.10976	1.2089	1259.3	0.15884	1.0968	1134.0	0.25491	0.8683
1297.9	0.10885	1.2128	1261.2	0.15750	1.1005	1135.9	0.23611	0.8898
1299.8	0.10805	1.2166	1263.2	0.15625	1.1040	1137.8	0.22021	0.9106
1301.7	0.10733	1.2202	1265.1	0.15507	1.1075	1139.7	0.20677	0.9307
1303.7	0.10670	1.2238	1267.0	0.15396	1.1108	1141.7	0.19541	0.9500
1305.6	0.10615	1.2273	1269.0	0.15292	1.1141	1143.6	0.18584	0.9685
1307.5	0.10567	1.2306	1270.9	0.15194	1.1172	1145.5	0.17781	0.9863
1309.5	0.10526	1.2339	1272.8	0.15102	1.1203	1147.5	0.17114	1.0034
1311.4	0.10492	1.2371	1274.7	0.15015	1.1233	1149.4	0.16569	1.0199
1313.3	0.10465	1.2402	1276.7	0.14933	1.1263	1151.3	0.16134	1.0359
1315.2	0.10443	1.2432	1278.6	0.14856	1.1291	1153.2	0.15802	1.0515
1317.2	0.10427	1.2461	1280.5	0.14782	1.1319	1155.2	0.15568	1.0666
1319.1	0.10416	1.2489	1282.5	0.14713	1.1346	1157.1	0.15432	1.0814
1321.0	0.10409	1.2516	1284.4	0.14647	1.1372	1159.0	0.15394	1.0959
1322.9	0.10408	1.2543	1286.3	0.14585	1.1398	1161.0	0.15457	1.1102
1324.9	0.10411	1.2569	1288.2	0.14526	1.1423	1162.9	0.15631	1.1242
1326.8	0.10418	1.2593	1290.2	0.14470	1.1448	1164.8	0.15924	1.1381
1328.7	0.10428	1.2618	1292.1	0.14417	1.1472	1166.7	0.16351	1.1517
1330.7	0.10442	1.2641	1294.0	0.14366	1.1495	1168.7	0.16931	1.1651
1332.6	0.10460	1.2663	1296.0	0.14318	1.1518	1170.6	0.17687	1.1780
1334.5	0.10480	1.2685	1297.9	0.14273	1.1541	1172.5	0.18642	1.1902
1336.4	0.10503	1.2706	1299.8	0.14229	1.1563	1174.5	0.19825	1.2014
1338.4	0.10528	1.2726	1301.7	0.14188	1.1584	1176.4	0.21255	1.2109
1340.3	0.10555	1.2745	1303.7	0.14149	1.1606	1178.3	0.22939	1.2180
1342.2	0.10584	1.2764	1305.6	0.14112	1.1626	1180.2	0.24850	1.2214
1344.2	0.10614	1.2782	1307.5	0.14076	1.1646	1182.2	0.26907	1.2201
1346.1	0.10645	1.2799	1309.5	0.14043	1.1666	1184.1	0.28953	1.2132
1348.0	0.10676	1.2815	1311.4	0.14011	1.1685	1186.0	0.30767	1.2003
1349.9	0.10708	1.2831	1313.3	0.13980	1.1704	1188.0	0.32102	1.1825
1351.9	0.10740	1.2846	1315.2	0.13951	1.1723	1189.9	0.32791	1.1623
1353.8	0.10771	1.2860	1317.2	0.13924	1.1741	1191.8	0.32817	1.1427
1355.7	0.10802	1.2873	1319.1	0.13898	1.1759	1193.7	0.32331	1.1264
1357.7	0.10832	1.2886	1321.0	0.13873	1.1777	1195.7	0.31584	1.1147
1359.6	0.10860	1.2898	1322.9	0.13849	1.1794	1197.6	0.30831	1.1074

1361.5	0.10886	1.2910	1324.9	0.13827	1.1811	1199.5	0.30269	1.1034
1363.4	0.10910	1.2921	1326.8	0.13805	1.1828	1201.5	0.30001	1.1008
1365.4	0.10932	1.2931	1328.7	0.13785	1.1844	1203.4	0.30038	1.0977
1367.3	0.10951	1.2941	1330.7	0.13766	1.1860	1205.3	0.30306	1.0922
1369.2	0.10967	1.2951	1332.6	0.13748	1.1876	1207.2	0.30649	1.0832
1371.2	0.10980	1.2960	1334.5	0.13731	1.1891	1209.2	0.30862	1.0702
1373.1	0.10990	1.2968	1336.4	0.13714	1.1906	1211.1	0.30735	1.0540
1375.0	0.10996	1.2976	1338.4	0.13699	1.1921	1213.0	0.30123	1.0364
1376.9	0.10999	1.2984	1340.3	0.13684	1.1936	1215.0	0.28995	1.0196
1378.9	0.10997	1.2992	1342.2	0.13671	1.1950	1216.9	0.27438	1.0056
1380.8	0.10993	1.2999	1344.2	0.13658	1.1964	1218.8	0.25611	0.9956
1382.7	0.10984	1.3007	1346.1	0.13646	1.1978	1220.7	0.23683	0.9899
1384.7	0.10972	1.3014	1348.0	0.13634	1.1992	1222.7	0.21793	0.9881
1386.6	0.10956	1.3021	1349.9	0.13623	1.2006	1224.6	0.20028	0.9894
1388.5	0.10937	1.3027	1351.9	0.13613	1.2019	1226.5	0.18436	0.9929
1390.4	0.10914	1.3034	1353.8	0.13604	1.2032	1228.5	0.17026	0.9980
1392.4	0.10888	1.3041	1355.7	0.13595	1.2045	1230.4	0.15795	1.0040
1394.3	0.10860	1.3048	1357.7	0.13587	1.2057	1232.3	0.14725	1.0107
1396.2	0.10828	1.3055	1359.6	0.13579	1.2070	1234.2	0.13798	1.0175
1398.2	0.10794	1.3062	1361.5	0.13572	1.2082	1236.2	0.12994	1.0245
1400.1	0.10758	1.3069	1363.4	0.13566	1.2094	1238.1	0.12296	1.0313
1402.0	0.10720	1.3076	1365.4	0.13560	1.2106	1240.0	0.11686	1.0380
1403.9	0.10680	1.3084	1367.3	0.13555	1.2117	1242.0	0.11152	1.0445
1405.9	0.10639	1.3091	1369.2	0.13550	1.2129	1243.9	0.10683	1.0508
1407.8	0.10597	1.3099	1371.2	0.13545	1.2140	1245.8	0.10268	1.0568
1409.7	0.10554	1.3107	1373.1	0.13541	1.2151	1247.7	0.09900	1.0626
1411.7	0.10510	1.3115	1375.0	0.13538	1.2162	1249.7	0.09572	1.0681
1413.6	0.10466	1.3123	1376.9	0.13535	1.2173	1251.6	0.09278	1.0734
1415.5	0.10422	1.3132	1378.9	0.13532	1.2184	1253.5	0.09014	1.0784
1417.4	0.10378	1.3140	1380.8	0.13530	1.2194	1255.5	0.08775	1.0833
1419.4	0.10335	1.3149	1382.7	0.13528	1.2205	1257.4	0.08559	1.0879
1421.3	0.10292	1.3158	1384.7	0.13527	1.2215	1259.3	0.08363	1.0924
1423.2	0.10249	1.3167	1386.6	0.13526	1.2225	1261.2	0.08184	1.0967
1425.2	0.10208	1.3177	1388.5	0.13525	1.2235	1263.2	0.08020	1.1008
1427.1	0.10168	1.3186	1390.4	0.13525	1.2244	1265.1	0.07869	1.1047
1429.0	0.10129	1.3195	1392.4	0.13525	1.2254	1267.0	0.07731	1.1085
1430.9	0.10091	1.3205	1394.3	0.13525	1.2263	1269.0	0.07603	1.1121
1432.9	0.10055	1.3215	1396.2	0.13526	1.2273	1270.9	0.07485	1.1156
1434.8	0.10021	1.3225	1398.2	0.13527	1.2282	1272.8	0.07375	1.1190
1436.7	0.09988	1.3235	1400.1	0.13528	1.2291	1274.7	0.07273	1.1223
1438.7	0.09957	1.3245	1402.0	0.13530	1.2300	1276.7	0.07178	1.1255
1440.6	0.09927	1.3255	1403.9	0.13532	1.2309	1278.6	0.07090	1.1285
1442.5	0.09900	1.3265	1405.9	0.13534	1.2318	1280.5	0.07007	1.1315

1444.4	0.09874	1.3275	1407.8	0.13537	1.2326	1282.5	0.06929	1.1343
1446.4	0.09850	1.3285	1409.7	0.13540	1.2335	1284.4	0.06857	1.1371
1448.3	0.09828	1.3295	1411.7	0.13543	1.2343	1286.3	0.06788	1.1398
1450.2	0.09808	1.3305	1413.6	0.13546	1.2351	1288.2	0.06724	1.1424
1452.2	0.09790	1.3316	1415.5	0.13550	1.2359	1290.2	0.06663	1.1449
1454.1	0.09774	1.3326	1417.4	0.13553	1.2367	1292.1	0.06606	1.1474
1456.0	0.09760	1.3336	1419.4	0.13557	1.2375	1294.0	0.06552	1.1497
1457.9	0.09748	1.3346	1421.3	0.13562	1.2383	1296.0	0.06501	1.1521
1459.9	0.09738	1.3356	1423.2	0.13566	1.2391	1297.9	0.06452	1.1543
1461.8	0.09729	1.3366	1425.2	0.13571	1.2398	1299.8	0.06406	1.1565
1463.7	0.09723	1.3376	1427.1	0.13576	1.2406	1301.7	0.06363	1.1586
1465.7	0.09718	1.3386	1429.0	0.13581	1.2413	1303.7	0.06321	1.1607
1467.6	0.09716	1.3396	1430.9	0.13586	1.2420	1305.6	0.06282	1.1628
1469.5	0.09715	1.3406	1432.9	0.13592	1.2427	1307.5	0.06244	1.1647
1471.4	0.09716	1.3415	1434.8	0.13598	1.2435	1309.5	0.06208	1.1667
1473.4	0.09718	1.3425	1436.7	0.13604	1.2442	1311.4	0.06174	1.1685
1475.3	0.09723	1.3434	1438.7	0.13610	1.2448	1313.3	0.06141	1.1704
1477.2	0.09729	1.3444	1440.6	0.13616	1.2455	1315.2	0.06110	1.1722
1479.2	0.09737	1.3453	1442.5	0.13623	1.2462	1317.2	0.06080	1.1739
1481.1	0.09746	1.3462	1444.4	0.13629	1.2469	1319.1	0.06052	1.1757
1483.0	0.09757	1.3471	1446.4	0.13636	1.2475	1321.0	0.06024	1.1773
1484.9	0.09770	1.3480	1448.3	0.13643	1.2482	1322.9	0.05998	1.1790
1486.9	0.09784	1.3489	1450.2	0.13650	1.2488	1324.9	0.05973	1.1806
1488.8	0.09800	1.3498	1452.2	0.13658	1.2494	1326.8	0.05949	1.1821
1490.7	0.09817	1.3507	1454.1	0.13665	1.2501	1328.7	0.05926	1.1837
1492.7	0.09836	1.3515	1456.0	0.13673	1.2507	1330.7	0.05904	1.1852
1494.6	0.09856	1.3523	1457.9	0.13681	1.2513	1332.6	0.05882	1.1867
1496.5	0.09877	1.3532	1459.9	0.13688	1.2519	1334.5	0.05862	1.1881
1498.4	0.09900	1.3540	1461.8	0.13697	1.2525	1336.4	0.05842	1.1895
1500.4	0.09924	1.3548	1463.7	0.13705	1.2530	1338.4	0.05823	1.1909
1502.3	0.09949	1.3555	1465.7	0.13713	1.2536	1340.3	0.05805	1.1923
1504.2	0.09976	1.3563	1467.6	0.13722	1.2542	1342.2	0.05787	1.1936
1506.2	0.10003	1.3571	1469.5	0.13730	1.2547	1344.2	0.05770	1.1949
1508.1	0.10032	1.3578	1471.4	0.13739	1.2553	1346.1	0.05754	1.1962
1510.0	0.10062	1.3585	1473.4	0.13748	1.2558	1348.0	0.05738	1.1975
1511.9	0.10093	1.3592	1475.3	0.13757	1.2564	1349.9	0.05722	1.1987
1513.9	0.10125	1.3599	1477.2	0.13766	1.2569	1351.9	0.05708	1.1999
1515.8	0.10158	1.3605	1479.2	0.13775	1.2574	1353.8	0.05693	1.2011
1517.7	0.10192	1.3612	1481.1	0.13784	1.2580	1355.7	0.05680	1.2023
1519.7	0.10227	1.3618	1483.0	0.13793	1.2585	1357.7	0.05666	1.2035
1521.6	0.10262	1.3624	1484.9	0.13803	1.2590	1359.6	0.05654	1.2046
1523.5	0.10299	1.3630	1486.9	0.13813	1.2595	1361.5	0.05641	1.2057
1525.4	0.10336	1.3636	1488.8	0.13822	1.2600	1363.4	0.05629	1.2068

1527.4	0.10374	1.3642	1490.7	0.13832	1.2605	1365.4	0.05617	1.2079
1529.3	0.10413	1.3647	1492.7	0.13842	1.2609	1367.3	0.05606	1.2089
1531.2	0.10452	1.3652	1494.6	0.13852	1.2614	1369.2	0.05595	1.2100
1533.2	0.10492	1.3657	1496.5	0.13862	1.2619	1371.2	0.05585	1.2110
1535.1	0.10532	1.3662	1498.4	0.13872	1.2623	1373.1	0.05574	1.2120
1537.0	0.10573	1.3667	1500.4	0.13882	1.2628	1375.0	0.05564	1.2130
1538.9	0.10614	1.3672	1502.3	0.13893	1.2632	1376.9	0.05555	1.2140
1540.9	0.10656	1.3676	1504.2	0.13903	1.2637	1378.9	0.05545	1.2150
1542.8	0.10698	1.3680	1506.2	0.13914	1.2641	1380.8	0.05536	1.2159
1544.7	0.10740	1.3684	1508.1	0.13924	1.2646	1382.7	0.05527	1.2168
1546.7	0.10783	1.3688	1510.0	0.13935	1.2650	1384.7	0.05519	1.2178
1548.6	0.10825	1.3691	1511.9	0.13945	1.2654	1386.6	0.05510	1.2187
1550.5	0.10868	1.3694	1513.9	0.13956	1.2658	1388.5	0.05502	1.2196
1552.4	0.10911	1.3698	1515.8	0.13967	1.2662	1390.4	0.05495	1.2204
1554.4	0.10954	1.3701	1517.7	0.13978	1.2666	1392.4	0.05487	1.2213
1556.3	0.10997	1.3703	1519.7	0.13989	1.2670	1394.3	0.05480	1.2222
1558.2	0.11040	1.3706	1521.6	0.14000	1.2674	1396.2	0.05472	1.2230
1560.2	0.11082	1.3708	1523.5	0.14011	1.2678	1398.2	0.05465	1.2238
1562.1	0.11125	1.3710	1525.4	0.14022	1.2682	1400.1	0.05459	1.2246
1564.0	0.11167	1.3712	1527.4	0.14034	1.2686	1402.0	0.05452	1.2255
1565.9	0.11208	1.3714	1529.3	0.14045	1.2690	1403.9	0.05445	1.2262
1567.9	0.11250	1.3716	1531.2	0.14056	1.2693	1405.9	0.05439	1.2270
1569.8	0.11290	1.3717	1533.2	0.14068	1.2697	1407.8	0.05433	1.2278
1571.7	0.11331	1.3718	1535.1	0.14079	1.2700	1409.7	0.05427	1.2286
1573.7	0.11371	1.3719	1537.0	0.14091	1.2704	1411.7	0.05421	1.2293
1575.6	0.11410	1.3720	1538.9	0.14102	1.2708	1413.6	0.05416	1.2301
1577.5	0.11448	1.3721	1540.9	0.14114	1.2711	1415.5	0.05410	1.2308
1579.4	0.11486	1.3721	1542.8	0.14126	1.2714	1417.4	0.05405	1.2315
1581.4	0.11523	1.3722	1544.7	0.14137	1.2718	1419.4	0.05400	1.2322
1583.3	0.11558	1.3722	1546.7	0.14149	1.2721	1421.3	0.05395	1.2329
1585.2	0.11593	1.3722	1548.6	0.14161	1.2724	1423.2	0.05390	1.2336
1587.2	0.11627	1.3722	1550.5	0.14173	1.2728	1425.2	0.05385	1.2343
1589.1	0.11660	1.3721	1552.4	0.14185	1.2731	1427.1	0.05380	1.2350
1591.0	0.11692	1.3721	1554.4	0.14197	1.2734	1429.0	0.05376	1.2357
1592.9	0.11723	1.3720	1556.3	0.14209	1.2737	1430.9	0.05371	1.2363
1594.9	0.11752	1.3719	1558.2	0.14221	1.2740	1432.9	0.05367	1.2370
1596.8	0.11780	1.3718	1560.2	0.14233	1.2743	1434.8	0.05362	1.2376
1598.7	0.11807	1.3717	1562.1	0.14245	1.2746	1436.7	0.05358	1.2383
1600.7	0.11833	1.3716	1564.0	0.14257	1.2749	1438.7	0.05354	1.2389
1602.6	0.11857	1.3715	1565.9	0.14269	1.2752	1440.6	0.05350	1.2395
1604.5	0.11880	1.3713	1567.9	0.14281	1.2755	1442.5	0.05346	1.2401
1606.4	0.11901	1.3712	1569.8	0.14293	1.2757	1444.4	0.05343	1.2407
1608.4	0.11921	1.3710	1571.7	0.14306	1.2760	1446.4	0.05339	1.2413

1610.3	0.11939	1.3708	1573.7	0.14318	1.2763	1448.3	0.05335	1.2419
1612.2	0.11955	1.3706	1575.6	0.14330	1.2766	1450.2	0.05332	1.2425
1614.2	0.11970	1.3704	1577.5	0.14343	1.2768	1452.2	0.05329	1.2431
1616.1	0.11984	1.3702	1579.4	0.14355	1.2771	1454.1	0.05325	1.2437
1618.0	0.11995	1.3700	1581.4	0.14367	1.2773	1456.0	0.05322	1.2442
1619.9	0.12006	1.3698	1583.3	0.14380	1.2776	1457.9	0.05319	1.2448
1621.9	0.12014	1.3696	1585.2	0.14392	1.2778	1459.9	0.05316	1.2453
1623.8	0.12021	1.3693	1587.2	0.14405	1.2781	1461.8	0.05313	1.2459
1625.7	0.12026	1.3691	1589.1	0.14417	1.2783	1463.7	0.05310	1.2464
1627.7	0.12029	1.3688	1591.0	0.14429	1.2786	1465.7	0.05307	1.2470
1629.6	0.12031	1.3686	1592.9	0.14442	1.2788	1467.6	0.05304	1.2475
1631.5	0.12031	1.3684	1594.9	0.14454	1.2790	1469.5	0.05301	1.2480
1633.4	0.12029	1.3681	1596.8	0.14467	1.2793	1471.4	0.05298	1.2485
1635.4	0.12025	1.3679	1598.7	0.14479	1.2795	1473.4	0.05296	1.2490
1637.3	0.12020	1.3676	1600.7	0.14492	1.2797	1475.3	0.05293	1.2496
1639.2	0.12013	1.3674	1602.6	0.14505	1.2799	1477.2	0.05291	1.2501
1641.2	0.12005	1.3671	1604.5	0.14517	1.2801	1479.2	0.05288	1.2505
1643.1	0.11995	1.3669	1606.4	0.14530	1.2804	1481.1	0.05286	1.2510
1645.0	0.11984	1.3666	1608.4	0.14542	1.2806	1483.0	0.05283	1.2515
1646.9	0.11970	1.3664	1610.3	0.14555	1.2808	1484.9	0.05281	1.2520
1648.9	0.11956	1.3662	1612.2	0.14568	1.2810	1486.9	0.05279	1.2525
1650.8	0.11940	1.3659	1614.2	0.14580	1.2812	1488.8	0.05277	1.2529
1652.7	0.11922	1.3657	1616.1	0.14593	1.2814	1490.7	0.05275	1.2534
1654.7	0.11903	1.3655	1618.0	0.14605	1.2815	1492.7	0.05272	1.2539
1656.6	0.11882	1.3653	1619.9	0.14618	1.2817	1494.6	0.05270	1.2543
1658.5	0.11861	1.3650	1621.9	0.14631	1.2819	1496.5	0.05268	1.2548
1660.4	0.11838	1.3648	1623.8	0.14643	1.2821	1498.4	0.05266	1.2552
1662.4	0.11813	1.3646	1625.7	0.14656	1.2823	1500.4	0.05264	1.2557
1664.3	0.11788	1.3644	1627.7	0.14669	1.2824	1502.3	0.05263	1.2561
1666.2	0.11761	1.3643	1629.6	0.14681	1.2826	1504.2	0.05261	1.2565
1668.2	0.11733	1.3641	1631.5	0.14694	1.2828	1506.2	0.05259	1.2570
1670.1	0.11704	1.3639	1633.4	0.14706	1.2830	1508.1	0.05257	1.2574
1672.0	0.11674	1.3638	1635.4	0.14719	1.2831	1510.0	0.05256	1.2578
1673.9	0.11644	1.3636	1637.3	0.14732	1.2833	1511.9	0.05254	1.2582
1675.9	0.11612	1.3635	1639.2	0.14744	1.2834	1513.9	0.05252	1.2587
1677.8	0.11579	1.3634	1641.2	0.14757	1.2836	1515.8	0.05251	1.2591
1679.7	0.11546	1.3633	1643.1	0.14770	1.2837	1517.7	0.05249	1.2595
1681.7	0.11511	1.3631	1645.0	0.14782	1.2839	1519.7	0.05248	1.2599
1683.6	0.11477	1.3631	1646.9	0.14795	1.2840	1521.6	0.05246	1.2603
1685.5	0.11441	1.3630	1648.9	0.14807	1.2842	1523.5	0.05245	1.2607
1687.4	0.11405	1.3629	1650.8	0.14820	1.2843	1525.4	0.05243	1.2611
1689.4	0.11368	1.3628	1652.7	0.14833	1.2844	1527.4	0.05242	1.2614
1691.3	0.11331	1.3628	1654.7	0.14845	1.2846	1529.3	0.05241	1.2618

1693.2	0.11293	1.3627	1656.6	0.14858	1.2847	1531.2	0.05239	1.2622
1695.1	0.11255	1.3627	1658.5	0.14870	1.2848	1533.2	0.05238	1.2626
1697.1	0.11217	1.3627	1660.4	0.14883	1.2850	1535.1	0.05237	1.2630
1699.0	0.11178	1.3627	1662.4	0.14895	1.2851	1537.0	0.05236	1.2633
1700.9	0.11139	1.3627	1664.3	0.14908	1.2852	1538.9	0.05234	1.2637
1702.9	0.11099	1.3627	1666.2	0.14920	1.2853	1540.9	0.05233	1.2641
1704.8	0.11060	1.3627	1668.2	0.14933	1.2854	1542.8	0.05232	1.2644
1706.7	0.11020	1.3627	1670.1	0.14945	1.2855	1544.7	0.05231	1.2648
1708.6	0.10981	1.3628	1672.0	0.14958	1.2857	1546.7	0.05230	1.2651
1710.6	0.10941	1.3628	1673.9	0.14970	1.2858	1548.6	0.05229	1.2655
1712.5	0.10901	1.3629	1675.9	0.14982	1.2859	1550.5	0.05228	1.2658
1714.4	0.10861	1.3630	1677.8	0.14995	1.2860	1552.4	0.05227	1.2662
1716.4	0.10822	1.3630	1679.7	0.15007	1.2861	1554.4	0.05226	1.2665
1718.3	0.10782	1.3631	1681.7	0.15019	1.2862	1556.3	0.05225	1.2669
1720.2	0.10742	1.3632	1683.6	0.15032	1.2863	1558.2	0.05224	1.2672
1722.1	0.10703	1.3634	1685.5	0.15044	1.2863	1560.2	0.05223	1.2675
1724.1	0.10664	1.3635	1687.4	0.15056	1.2864	1562.1	0.05223	1.2679
1726.0	0.10625	1.3636	1689.4	0.15069	1.2865	1564.0	0.05222	1.2682
1727.9	0.10586	1.3637	1691.3	0.15081	1.2866	1565.9	0.05221	1.2685
1729.9	0.10547	1.3639	1693.2	0.15093	1.2867	1567.9	0.05220	1.2688
1731.8	0.10509	1.3640	1695.1	0.15105	1.2868	1569.8	0.05219	1.2692
1733.7	0.10471	1.3642	1697.1	0.15117	1.2868	1571.7	0.05219	1.2695
1735.6	0.10434	1.3644	1699.0	0.15130	1.2869	1573.7	0.05218	1.2698
1737.6	0.10396	1.3646	1700.9	0.15142	1.2870	1575.6	0.05217	1.2701
1739.5	0.10359	1.3647	1702.9	0.15154	1.2871	1577.5	0.05217	1.2704
1741.4	0.10323	1.3649	1704.8	0.15166	1.2871	1579.4	0.05216	1.2707
1743.4	0.10287	1.3651	1706.7	0.15178	1.2872	1581.4	0.05216	1.2710
1745.3	0.10251	1.3653	1708.6	0.15190	1.2873	1583.3	0.05215	1.2713
1747.2	0.10216	1.3656	1710.6	0.15202	1.2873	1585.2	0.05215	1.2716
1749.1	0.10181	1.3658	1712.5	0.15214	1.2874	1587.2	0.05214	1.2719
1751.1	0.10146	1.3660	1714.4	0.15226	1.2874	1589.1	0.05214	1.2722
1753.0	0.10113	1.3662	1716.4	0.15237	1.2875	1591.0	0.05213	1.2725
1754.9	0.10079	1.3665	1718.3	0.15249	1.2875	1592.9	0.05213	1.2728
1756.9	0.10046	1.3667	1720.2	0.15261	1.2876	1594.9	0.05212	1.2731
1758.8	0.10014	1.3670	1722.1	0.15273	1.2876	1596.8	0.05212	1.2734
1760.7	0.09982	1.3672	1724.1	0.15285	1.2877	1598.7	0.05212	1.2737
1762.6	0.09950	1.3675	1726.0	0.15296	1.2877	1600.7	0.05211	1.2739
1764.6	0.09920	1.3677	1727.9	0.15308	1.2878	1602.6	0.05211	1.2742
1766.5	0.09889	1.3680	1729.9	0.15320	1.2878	1604.5	0.05211	1.2745
1768.4	0.09859	1.3683	1731.8	0.15331	1.2878	1606.4	0.05210	1.2748
1770.4	0.09830	1.3686	1733.7	0.15343	1.2879	1608.4	0.05210	1.2750
1772.3	0.09801	1.3688	1735.6	0.15354	1.2879	1610.3	0.05210	1.2753
1774.2	0.09773	1.3691	1737.6	0.15366	1.2879	1612.2	0.05210	1.2756

1776.1	0.09745	1.3694	1739.5	0.15377	1.2880	1614.2	0.05209	1.2758
1778.1	0.09718	1.3697	1741.4	0.15388	1.2880	1616.1	0.05209	1.2761
1780.0	0.09692	1.3700	1743.4	0.15400	1.2880	1618.0	0.05209	1.2764
1781.9	0.09666	1.3703	1745.3	0.15411	1.2880	1619.9	0.05209	1.2766
1783.9	0.09640	1.3706	1747.2	0.15422	1.2881	1621.9	0.05209	1.2769
1785.8	0.09615	1.3709	1749.1	0.15434	1.2881	1623.8	0.05209	1.2772
1787.7	0.09591	1.3712	1751.1	0.15445	1.2881	1625.7	0.05209	1.2774
1789.6	0.09567	1.3715	1753.0	0.15456	1.2881	1627.7	0.05209	1.2777
1791.6	0.09544	1.3718	1754.9	0.15467	1.2881	1629.6	0.05209	1.2779
1793.5	0.09521	1.3721	1756.9	0.15478	1.2881	1631.5	0.05209	1.2782
1795.4	0.09499	1.3724	1758.8	0.15489	1.2881	1633.4	0.05209	1.2784
1797.4	0.09478	1.3728	1760.7	0.15500	1.2881	1635.4	0.05209	1.2787
1799.3	0.09457	1.3731	1762.6	0.15511	1.2881	1637.3	0.05209	1.2789
1801.2	0.09436	1.3734	1764.6	0.15522	1.2882	1639.2	0.05209	1.2791
1803.1	0.09416	1.3737	1766.5	0.15533	1.2882	1641.2	0.05209	1.2794
1805.1	0.09397	1.3740	1768.4	0.15544	1.2882	1643.1	0.05209	1.2796
1807.0	0.09378	1.3744	1770.4	0.15554	1.2882	1645.0	0.05209	1.2799
1808.9	0.09359	1.3747	1772.3	0.15565	1.2881	1646.9	0.05209	1.2801
1810.9	0.09341	1.3750	1774.2	0.15576	1.2881	1648.9	0.05210	1.2803
1812.8	0.09324	1.3753	1776.1	0.15586	1.2881	1650.8	0.05210	1.2806
1814.7	0.09307	1.3757	1778.1	0.15597	1.2881	1652.7	0.05210	1.2808
1816.6	0.09291	1.3760	1780.0	0.15607	1.2881	1654.7	0.05210	1.2810
1818.6	0.09275	1.3763	1781.9	0.15618	1.2881	1656.6	0.05211	1.2813
1820.5	0.09260	1.3766	1783.9	0.15628	1.2881	1658.5	0.05211	1.2815
1822.4	0.09245	1.3770	1785.8	0.15639	1.2881	1660.4	0.05211	1.2817
1824.4	0.09230	1.3773	1787.7	0.15649	1.2880	1662.4	0.05211	1.2819
1826.3	0.09216	1.3776	1789.6	0.15659	1.2880	1664.3	0.05212	1.2822
1828.2	0.09203	1.3779	1791.6	0.15669	1.2880	1666.2	0.05212	1.2824
1830.1	0.09190	1.3783	1793.5	0.15680	1.2880	1668.2	0.05213	1.2826
1832.1	0.09178	1.3786	1795.4	0.15690	1.2880	1670.1	0.05213	1.2828
1834.0	0.09166	1.3789	1797.4	0.15700	1.2879	1672.0	0.05213	1.2830
1835.9	0.09154	1.3792	1799.3	0.15710	1.2879	1673.9	0.05214	1.2832
1837.9	0.09143	1.3796	1801.2	0.15720	1.2879	1675.9	0.05214	1.2834
1839.8	0.09132	1.3799	1803.1	0.15729	1.2878	1677.8	0.05215	1.2837
1841.7	0.09122	1.3802	1805.1	0.15739	1.2878	1679.7	0.05215	1.2839
1843.6	0.09113	1.3805	1807.0	0.15749	1.2878	1681.7	0.05216	1.2841
1845.6	0.09103	1.3809	1808.9	0.15759	1.2877	1683.6	0.05216	1.2843
1847.5	0.09094	1.3812	1810.9	0.15768	1.2877	1685.5	0.05217	1.2845
1849.4	0.09086	1.3815	1812.8	0.15778	1.2877	1687.4	0.05218	1.2847
1851.4	0.09078	1.3818	1814.7	0.15788	1.2876	1689.4	0.05218	1.2849
1853.3	0.09070	1.3821	1816.6	0.15797	1.2876	1691.3	0.05219	1.2851
1855.2	0.09063	1.3825	1818.6	0.15806	1.2875	1693.2	0.05219	1.2853
1857.1	0.09056	1.3828	1820.5	0.15816	1.2875	1695.1	0.05220	1.2855

1859.1	0.09050	1.3831	1822.4	0.15825	1.2874	1697.1	0.05221	1.2857
1861.0	0.09044	1.3834	1824.4	0.15834	1.2874	1699.0	0.05221	1.2859
1862.9	0.09038	1.3837	1826.3	0.15843	1.2873	1700.9	0.05222	1.2861
1864.9	0.09033	1.3840	1828.2	0.15853	1.2873	1702.9	0.05223	1.2863
1866.8	0.09028	1.3843	1830.1	0.15862	1.2872	1704.8	0.05224	1.2865
1868.7	0.09023	1.3846	1832.1	0.15871	1.2872	1706.7	0.05224	1.2867
1870.6	0.09019	1.3850	1834.0	0.15880	1.2871	1708.6	0.05225	1.2869
1872.6	0.09016	1.3853	1835.9	0.15888	1.2871	1710.6	0.05226	1.2871
1874.5	0.09012	1.3856	1837.9	0.15897	1.2870	1712.5	0.05227	1.2872
1876.4	0.09009	1.3859	1839.8	0.15906	1.2869	1714.4	0.05228	1.2874
1878.4	0.09006	1.3862	1841.7	0.15915	1.2869	1716.4	0.05229	1.2876
1880.3	0.09004	1.3865	1843.6	0.15923	1.2868	1718.3	0.05229	1.2878
1882.2	0.09002	1.3868	1845.6	0.15932	1.2867	1720.2	0.05230	1.2880
1884.1	0.09000	1.3871	1847.5	0.15940	1.2867	1722.1	0.05231	1.2882
1886.1	0.08999	1.3874	1849.4	0.15949	1.2866	1724.1	0.05232	1.2883
1888.0	0.08998	1.3877	1851.4	0.15957	1.2865	1726.0	0.05233	1.2885
1889.9	0.08997	1.3879	1853.3	0.15965	1.2865	1727.9	0.05234	1.2887
1891.9	0.08996	1.3882	1855.2	0.15974	1.2864	1729.9	0.05235	1.2889
1893.8	0.08996	1.3885	1857.1	0.15982	1.2863	1731.8	0.05236	1.2891
1895.7	0.08996	1.3888	1859.1	0.15990	1.2862	1733.7	0.05237	1.2892
1897.6	0.08997	1.3891	1861.0	0.15998	1.2862	1735.6	0.05238	1.2894
1899.6	0.08998	1.3894	1862.9	0.16006	1.2861	1737.6	0.05239	1.2896
1901.5	0.08999	1.3897	1864.9	0.16014	1.2860	1739.5	0.05240	1.2897
1903.4	0.09000	1.3899	1866.8	0.16021	1.2859	1741.4	0.05241	1.2899
1905.4	0.09002	1.3902	1868.7	0.16029	1.2859	1743.4	0.05243	1.2901
1907.3	0.09004	1.3905	1870.6	0.16037	1.2858	1745.3	0.05244	1.2903
1909.2	0.09006	1.3908	1872.6	0.16044	1.2857	1747.2	0.05245	1.2904
1911.1	0.09008	1.3910	1874.5	0.16052	1.2856	1749.1	0.05246	1.2906
1913.1	0.09011	1.3913	1876.4	0.16059	1.2855	1751.1	0.05247	1.2908
1915.0	0.09014	1.3916	1878.4	0.16067	1.2854	1753.0	0.05249	1.2909
1916.9	0.09017	1.3918	1880.3	0.16074	1.2853	1754.9	0.05250	1.2911
1918.9	0.09020	1.3921	1882.2	0.16081	1.2852	1756.9	0.05251	1.2913
1920.8	0.09024	1.3924	1884.1	0.16089	1.2852	1758.8	0.05252	1.2914
1922.7	0.09028	1.3926	1886.1	0.16096	1.2851	1760.7	0.05254	1.2916
1924.6	0.09032	1.3929	1888.0	0.16103	1.2850	1762.6	0.05255	1.2917
1926.6	0.09037	1.3931	1889.9	0.16110	1.2849	1764.6	0.05256	1.2919
1928.5	0.09041	1.3934	1891.9	0.16116	1.2848	1766.5	0.05258	1.2920
1930.4	0.09046	1.3936	1893.8	0.16123	1.2847	1768.4	0.05259	1.2922
1932.4	0.09051	1.3939	1895.7	0.16130	1.2846	1770.4	0.05260	1.2924
1934.3	0.09057	1.3941	1897.6	0.16137	1.2845	1772.3	0.05262	1.2925
1936.2	0.09062	1.3944	1899.6	0.16143	1.2844	1774.2	0.05263	1.2927
1938.1	0.09068	1.3946	1901.5	0.16150	1.2843	1776.1	0.05264	1.2928
1940.1	0.09074	1.3949	1903.4	0.16156	1.2842	1778.1	0.05266	1.2930

1942.0	0.09080	1.3951	1905.4	0.16163	1.2841	1780.0	0.05267	1.2931
1943.9	0.09086	1.3953	1907.3	0.16169	1.2840	1781.9	0.05269	1.2933
1945.9	0.09093	1.3956	1909.2	0.16175	1.2839	1783.9	0.05270	1.2934
1947.8	0.09100	1.3958	1911.1	0.16181	1.2838	1785.8	0.05272	1.2936
1949.7	0.09107	1.3960	1913.1	0.16187	1.2836	1787.7	0.05273	1.2937
1951.6	0.09114	1.3963	1915.0	0.16193	1.2835	1789.6	0.05275	1.2939
1953.6	0.09121	1.3965	1916.9	0.16199	1.2834	1791.6	0.05277	1.2940
1955.5	0.09129	1.3967	1918.9	0.16205	1.2833	1793.5	0.05278	1.2942
1957.4	0.09136	1.3969	1920.8	0.16211	1.2832	1795.4	0.05280	1.2943
1959.4	0.09144	1.3972	1922.7	0.16216	1.2831	1797.4	0.05281	1.2944
1961.3	0.09152	1.3974	1924.6	0.16222	1.2830	1799.3	0.05283	1.2946
1963.2	0.09161	1.3976	1926.6	0.16227	1.2829	1801.2	0.05285	1.2947
1965.1	0.09169	1.3978	1928.5	0.16233	1.2827	1803.1	0.05286	1.2949
1967.1	0.09177	1.3980	1930.4	0.16238	1.2826	1805.1	0.05288	1.2950
1969.0	0.09186	1.3982	1932.4	0.16244	1.2825	1807.0	0.05290	1.2952
1970.9	0.09195	1.3984	1934.3	0.16249	1.2824	1808.9	0.05291	1.2953
1972.9	0.09204	1.3986	1936.2	0.16254	1.2823	1810.9	0.05293	1.2954
1974.8	0.09213	1.3988	1938.1	0.16259	1.2821	1812.8	0.05295	1.2956
1976.7	0.09222	1.3990	1940.1	0.16264	1.2820	1814.7	0.05297	1.2957
1978.6	0.09232	1.3992	1942.0	0.16269	1.2819	1816.6	0.05299	1.2958
1980.6	0.09242	1.3994	1943.9	0.16273	1.2818	1818.6	0.05300	1.2960
1982.5	0.09251	1.3996	1945.9	0.16278	1.2816	1820.5	0.05302	1.2961
1984.4	0.09261	1.3998	1947.8	0.16283	1.2815	1822.4	0.05304	1.2962
1986.4	0.09271	1.4000	1949.7	0.16287	1.2814	1824.4	0.05306	1.2964
1988.3	0.09281	1.4002	1951.6	0.16292	1.2813	1826.3	0.05308	1.2965
1990.2	0.09292	1.4004	1953.6	0.16296	1.2811	1828.2	0.05310	1.2966
1992.1	0.09302	1.4006	1955.5	0.16300	1.2810	1830.1	0.05311	1.2968
1994.1	0.09312	1.4007	1957.4	0.16305	1.2809	1832.1	0.05313	1.2969
1996.0	0.09323	1.4009	1959.4	0.16309	1.2807	1834.0	0.05315	1.2970
1997.9	0.09334	1.4011	1961.3	0.16313	1.2806	1835.9	0.05317	1.2971
1999.9	0.09345	1.4013	1963.2	0.16317	1.2805	1837.9	0.05319	1.2973
2001.8	0.09356	1.4014	1965.1	0.16321	1.2803	1839.8	0.05321	1.2974
2003.7	0.09367	1.4016	1967.1	0.16325	1.2802	1841.7	0.05323	1.2975
2005.6	0.09378	1.4018	1969.0	0.16328	1.2801	1843.6	0.05325	1.2976
2007.6	0.09389	1.4019	1970.9	0.16332	1.2799	1845.6	0.05327	1.2978
2009.5	0.09401	1.4021	1972.9	0.16335	1.2798	1847.5	0.05329	1.2979
2011.4	0.09412	1.4023	1974.8	0.16339	1.2797	1849.4	0.05331	1.2980
2013.4	0.09424	1.4024	1976.7	0.16342	1.2795	1851.4	0.05333	1.2981
2015.3	0.09435	1.4026	1978.6	0.16346	1.2794	1853.3	0.05336	1.2982
2017.2	0.09447	1.4027	1980.6	0.16349	1.2792	1855.2	0.05338	1.2984
2019.1	0.09459	1.4029	1982.5	0.16352	1.2791	1857.1	0.05340	1.2985
2021.1	0.09471	1.4030	1984.4	0.16355	1.2789	1859.1	0.05342	1.2986
2023.0	0.09483	1.4032	1986.4	0.16358	1.2788	1861.0	0.05344	1.2987

2024.9	0.09495	1.4033	1988.3	0.16361	1.2787	1862.9	0.05346	1.2988
2026.9	0.09507	1.4035	1990.2	0.16363	1.2785	1864.9	0.05348	1.2990
2028.8	0.09520	1.4036	1992.1	0.16366	1.2784	1866.8	0.05351	1.2991
2030.7	0.09532	1.4037	1994.1	0.16369	1.2782	1868.7	0.05353	1.2992
2032.6	0.09544	1.4039	1996.0	0.16371	1.2781	1870.6	0.05355	1.2993
2034.6	0.09557	1.4040	1997.9	0.16374	1.2779	1872.6	0.05357	1.2994
2036.5	0.09569	1.4041	1999.9	0.16376	1.2778	1874.5	0.05360	1.2995
2038.4	0.09582	1.4043	2001.8	0.16378	1.2776	1876.4	0.05362	1.2996
2040.3	0.09595	1.4044	2003.7	0.16381	1.2775	1878.4	0.05364	1.2997
2042.3	0.09607	1.4045	2005.6	0.16383	1.2773	1880.3	0.05366	1.2999
2044.2	0.09620	1.4046	2007.6	0.16385	1.2772	1882.2	0.05369	1.3000
2046.1	0.09633	1.4048	2009.5	0.16387	1.2770	1884.1	0.05371	1.3001
2048.1	0.09646	1.4049	2011.4	0.16388	1.2769	1886.1	0.05374	1.3002
2050.0	0.09659	1.4050	2013.4	0.16390	1.2767	1888.0	0.05376	1.3003
2051.9	0.09672	1.4051	2015.3	0.16392	1.2766	1889.9	0.05378	1.3004
2053.8	0.09685	1.4052	2017.2	0.16393	1.2764	1891.9	0.05381	1.3005
2055.8	0.09698	1.4053	2019.1	0.16395	1.2763	1893.8	0.05383	1.3006
2057.7	0.09711	1.4054	2021.1	0.16396	1.2761	1895.7	0.05385	1.3007
2059.6	0.09724	1.4055	2023.0	0.16397	1.2759	1897.6	0.05388	1.3008
2061.6	0.09738	1.4056	2024.9	0.16399	1.2758	1899.6	0.05390	1.3009
2063.5	0.09751	1.4058	2026.9	0.16400	1.2756	1901.5	0.05393	1.3010
2065.4	0.09764	1.4059	2028.8	0.16401	1.2755	1903.4	0.05395	1.3011
2067.3	0.09777	1.4059	2030.7	0.16402	1.2753	1905.4	0.05398	1.3012
2069.3	0.09791	1.4060	2032.6	0.16403	1.2752	1907.3	0.05400	1.3013
2071.2	0.09804	1.4061	2034.6	0.16403	1.2750	1909.2	0.05403	1.3014
2073.1	0.09818	1.4062	2036.5	0.16404	1.2748	1911.1	0.05405	1.3015
2075.1	0.09831	1.4063	2038.4	0.16405	1.2747	1913.1	0.05408	1.3016
2077.0	0.09844	1.4064	2040.3	0.16405	1.2745	1915.0	0.05410	1.3017
2078.9	0.09858	1.4065	2042.3	0.16406	1.2744	1916.9	0.05413	1.3018
2080.8	0.09871	1.4066	2044.2	0.16406	1.2742	1918.9	0.05416	1.3019
2082.8	0.09885	1.4067	2046.1	0.16406	1.2740	1920.8	0.05418	1.3020
2084.7	0.09898	1.4067	2048.1	0.16406	1.2739	1922.7	0.05421	1.3021
2086.6	0.09912	1.4068	2050.0	0.16406	1.2737	1924.6	0.05423	1.3022
2088.6	0.09925	1.4069	2051.9	0.16406	1.2735	1926.6	0.05426	1.3023
2090.5	0.09939	1.4070	2053.8	0.16406	1.2734	1928.5	0.05429	1.3024
2092.4	0.09953	1.4070	2055.8	0.16406	1.2732	1930.4	0.05431	1.3025
2094.3	0.09966	1.4071	2057.7	0.16406	1.2730	1932.4	0.05434	1.3026
2096.3	0.09980	1.4072	2059.6	0.16405	1.2729	1934.3	0.05437	1.3027
2098.2	0.09993	1.4072	2061.6	0.16405	1.2727	1936.2	0.05439	1.3028
2100.1	0.10007	1.4073	2063.5	0.16404	1.2725	1938.1	0.05442	1.3029
2102.1	0.10020	1.4074	2065.4	0.16404	1.2724	1940.1	0.05445	1.3030
2104.0	0.10034	1.4074	2067.3	0.16403	1.2722	1942.0	0.05448	1.3031
2105.9	0.10047	1.4075	2069.3	0.16402	1.2720	1943.9	0.05450	1.3032

2107.8	0.10061	1.4075	2071.2	0.16401	1.2719	1945.9	0.05453	1.3032
2109.8	0.10074	1.4076	2073.1	0.16400	1.2717	1947.8	0.05456	1.3033
2111.7	0.10088	1.4076	2075.1	0.16399	1.2715	1949.7	0.05459	1.3034
2113.6	0.10101	1.4077	2077.0	0.16398	1.2714	1951.6	0.05462	1.3035
2115.6	0.10115	1.4077	2078.9	0.16396	1.2712	1953.6	0.05464	1.3036
2117.5	0.10128	1.4078	2080.8	0.16395	1.2710	1955.5	0.05467	1.3037
2119.4	0.10142	1.4078	2082.8	0.16394	1.2708	1957.4	0.05470	1.3038
2121.3	0.10155	1.4079	2084.7	0.16392	1.2707	1959.4	0.05473	1.3039
2123.3	0.10169	1.4079	2086.6	0.16390	1.2705	1961.3	0.05476	1.3039
2125.2	0.10182	1.4080	2088.6	0.16389	1.2703	1963.2	0.05479	1.3040
2127.1	0.10195	1.4080	2090.5	0.16387	1.2701	1965.1	0.05481	1.3041
2129.1	0.10209	1.4080	2092.4	0.16385	1.2700	1967.1	0.05484	1.3042
2131.0	0.10222	1.4081	2094.3	0.16383	1.2698	1969.0	0.05487	1.3043
2132.9	0.10235	1.4081	2096.3	0.16381	1.2696	1970.9	0.05490	1.3044
2134.8	0.10248	1.4081	2098.2	0.16379	1.2695	1972.9	0.05493	1.3044
2136.8	0.10262	1.4082	2100.1	0.16376	1.2693	1974.8	0.05496	1.3045
2138.7	0.10275	1.4082	2102.1	0.16374	1.2691	1976.7	0.05499	1.3046
2140.6	0.10288	1.4082	2104.0	0.16371	1.2689	1978.6	0.05502	1.3047
2142.6	0.10301	1.4083	2105.9	0.16369	1.2688	1980.6	0.05505	1.3048
2144.5	0.10314	1.4083	2107.8	0.16366	1.2686	1982.5	0.05508	1.3048
2146.4	0.10327	1.4083	2109.8	0.16363	1.2684	1984.4	0.05511	1.3049
2148.3	0.10340	1.4083	2111.7	0.16361	1.2682	1986.4	0.05514	1.3050
2150.3	0.10353	1.4083	2113.6	0.16358	1.2680	1988.3	0.05517	1.3051
2152.2	0.10366	1.4083	2115.6	0.16355	1.2679	1990.2	0.05520	1.3051
2154.1	0.10379	1.4084	2117.5	0.16352	1.2677	1992.1	0.05523	1.3052
2156.1	0.10391	1.4084	2119.4	0.16349	1.2675	1994.1	0.05526	1.3053
2158.0	0.10404	1.4084	2121.3	0.16345	1.2673	1996.0	0.05529	1.3054
2159.9	0.10417	1.4084	2123.3	0.16342	1.2672	1997.9	0.05532	1.3055
2161.8	0.10429	1.4084	2125.2	0.16338	1.2670	1999.9	0.05535	1.3055
2163.8	0.10442	1.4084	2127.1	0.16335	1.2668	2001.8	0.05538	1.3056
2165.7	0.10455	1.4084	2129.1	0.16331	1.2666	2003.7	0.05541	1.3057
2167.6	0.10467	1.4084	2131.0	0.16328	1.2664	2005.6	0.05545	1.3057
2169.6	0.10479	1.4084	2132.9	0.16324	1.2663	2007.6	0.05548	1.3058
2171.5	0.10492	1.4084	2134.8	0.16320	1.2661	2009.5	0.05551	1.3059
2173.4	0.10504	1.4084	2136.8	0.16316	1.2659	2011.4	0.05554	1.3060
2175.3	0.10516	1.4084	2138.7	0.16312	1.2657	2013.4	0.05557	1.3060
2177.3	0.10528	1.4084	2140.6	0.16308	1.2655	2015.3	0.05560	1.3061
2179.2	0.10541	1.4084	2142.6	0.16303	1.2654	2017.2	0.05563	1.3062
2181.1	0.10553	1.4084	2144.5	0.16299	1.2652	2019.1	0.05567	1.3062
2183.1	0.10565	1.4084	2146.4	0.16295	1.2650	2021.1	0.05570	1.3063
2185.0	0.10576	1.4084	2148.3	0.16290	1.2648	2023.0	0.05573	1.3064
2186.9	0.10588	1.4084	2150.3	0.16286	1.2646	2024.9	0.05576	1.3064
2188.8	0.10600	1.4084	2152.2	0.16281	1.2645	2026.9	0.05579	1.3065

2190.8	0.10612	1.4084	2154.1	0.16276	1.2643	2028.8	0.05583	1.3066
2192.7	0.10623	1.4083	2156.1	0.16271	1.2641	2030.7	0.05586	1.3066
2194.6	0.10635	1.4083	2158.0	0.16266	1.2639	2032.6	0.05589	1.3067
2196.6	0.10646	1.4083	2159.9	0.16261	1.2637	2034.6	0.05592	1.3068
2198.5	0.10658	1.4083	2161.8	0.16256	1.2636	2036.5	0.05596	1.3068
2200.4	0.10669	1.4083	2163.8	0.16251	1.2634	2038.4	0.05599	1.3069
2202.3	0.10680	1.4083	2165.7	0.16246	1.2632	2040.3	0.05602	1.3070
2204.3	0.10692	1.4082	2167.6	0.16240	1.2630	2042.3	0.05605	1.3070
2206.2	0.10703	1.4082	2169.6	0.16235	1.2628	2044.2	0.05609	1.3071
2208.1	0.10714	1.4082	2171.5	0.16229	1.2627	2046.1	0.05612	1.3072
2210.1	0.10725	1.4082	2173.4	0.16224	1.2625	2048.1	0.05615	1.3072
2212.0	0.10735	1.4081	2175.3	0.16218	1.2623	2050.0	0.05619	1.3073
2213.9	0.10746	1.4081	2177.3	0.16212	1.2621	2051.9	0.05622	1.3073
2215.8	0.10757	1.4081	2179.2	0.16206	1.2619	2053.8	0.05625	1.3074
2217.8	0.10768	1.4081	2181.1	0.16200	1.2617	2055.8	0.05629	1.3075
2219.7	0.10778	1.4080	2183.1	0.16194	1.2616	2057.7	0.05632	1.3075
2221.6	0.10788	1.4080	2185.0	0.16188	1.2614	2059.6	0.05635	1.3076
2223.6	0.10799	1.4080	2186.9	0.16182	1.2612	2061.6	0.05639	1.3076
2225.5	0.10809	1.4079	2188.8	0.16176	1.2610	2063.5	0.05642	1.3077
2227.4	0.10819	1.4079	2190.8	0.16169	1.2608	2065.4	0.05646	1.3078
2229.3	0.10829	1.4079	2192.7	0.16163	1.2607	2067.3	0.05649	1.3078
2231.3	0.10839	1.4078	2194.6	0.16156	1.2605	2069.3	0.05652	1.3079
2233.2	0.10849	1.4078	2196.6	0.16149	1.2603	2071.2	0.05656	1.3079
2235.1	0.10859	1.4077	2198.5	0.16143	1.2601	2073.1	0.05659	1.3080
2237.1	0.10869	1.4077	2200.4	0.16136	1.2599	2075.1	0.05663	1.3080
2239.0	0.10879	1.4077	2202.3	0.16129	1.2597	2077.0	0.05666	1.3081
2240.9	0.10888	1.4076	2204.3	0.16122	1.2596	2078.9	0.05669	1.3082
2242.8	0.10898	1.4076	2206.2	0.16115	1.2594	2080.8	0.05673	1.3082
2244.8	0.10907	1.4075	2208.1	0.16108	1.2592	2082.8	0.05676	1.3083
2246.7	0.10916	1.4075	2210.1	0.16100	1.2590	2084.7	0.05680	1.3083
2248.6	0.10926	1.4074	2212.0	0.16093	1.2588	2086.6	0.05683	1.3084
2250.6	0.10935	1.4074	2213.9	0.16086	1.2587	2088.6	0.05687	1.3084
2252.5	0.10944	1.4074	2215.8	0.16078	1.2585	2090.5	0.05690	1.3085
2254.4	0.10953	1.4073	2217.8	0.16071	1.2583	2092.4	0.05694	1.3085
2256.3	0.10962	1.4073	2219.7	0.16063	1.2581	2094.3	0.05697	1.3086
2258.3	0.10970	1.4072	2221.6	0.16055	1.2579	2096.3	0.05701	1.3086
2260.2	0.10979	1.4072	2223.6	0.16047	1.2577	2098.2	0.05704	1.3087
2262.1	0.10988	1.4071	2225.5	0.16039	1.2576	2100.1	0.05708	1.3087
2264.1	0.10996	1.4071	2227.4	0.16031	1.2574	2102.1	0.05711	1.3088
2266.0	0.11004	1.4070	2229.3	0.16023	1.2572	2104.0	0.05715	1.3088
2267.9	0.11013	1.4070	2231.3	0.16015	1.2570	2105.9	0.05718	1.3089
2269.8	0.11021	1.4069	2233.2	0.16007	1.2568	2107.8	0.05722	1.3089
2271.8	0.11029	1.4069	2235.1	0.15999	1.2567	2109.8	0.05725	1.3090

2273.7	0.11037	1.4068	2237.1	0.15990	1.2565	2111.7	0.05729	1.3090
2275.6	0.11045	1.4067	2239.0	0.15982	1.2563	2113.6	0.05732	1.3091
2277.6	0.11053	1.4067	2240.9	0.15973	1.2561	2115.6	0.05736	1.3091
2279.5	0.11061	1.4066	2242.8	0.15965	1.2559	2117.5	0.05739	1.3092
2281.4	0.11068	1.4066	2244.8	0.15956	1.2558	2119.4	0.05743	1.3092
2283.3	0.11076	1.4065	2246.7	0.15947	1.2556	2121.3	0.05747	1.3093
2285.3	0.11083	1.4065	2248.6	0.15938	1.2554	2123.3	0.05750	1.3093
2287.2	0.11091	1.4064	2250.6	0.15929	1.2552	2125.2	0.05754	1.3093
2289.1	0.11098	1.4064	2252.5	0.15920	1.2550	2127.1	0.05757	1.3094
2291.1	0.11105	1.4063	2254.4	0.15911	1.2549	2129.1	0.05761	1.3094
2293.0	0.11112	1.4062	2256.3	0.15902	1.2547	2131.0	0.05764	1.3095
2294.9	0.11119	1.4062	2258.3	0.15893	1.2545	2132.9	0.05768	1.3095
2296.8	0.11126	1.4061	2260.2	0.15883	1.2543	2134.8	0.05772	1.3096
2298.8	0.11133	1.4061	2262.1	0.15874	1.2541	2136.8	0.05775	1.3096
2300.7	0.11140	1.4060	2264.1	0.15865	1.2540	2138.7	0.05779	1.3097
2302.6	0.11146	1.4059	2266.0	0.15855	1.2538	2140.6	0.05783	1.3097
2304.6	0.11153	1.4059	2267.9	0.15845	1.2536	2142.6	0.05786	1.3097
2306.5	0.11159	1.4058	2269.8	0.15836	1.2534	2144.5	0.05790	1.3098
2308.4	0.11166	1.4058	2271.8	0.15826	1.2533	2146.4	0.05793	1.3098
2310.3	0.11172	1.4057	2273.7	0.15816	1.2531	2148.3	0.05797	1.3099
2312.3	0.11178	1.4056	2275.6	0.15806	1.2529	2150.3	0.05801	1.3099
2314.2	0.11184	1.4056	2277.6	0.15796	1.2527	2152.2	0.05804	1.3099
2316.1	0.11190	1.4055	2279.5	0.15786	1.2525	2154.1	0.05808	1.3100
2318.1	0.11196	1.4054	2281.4	0.15776	1.2524	2156.1	0.05812	1.3100
2320.0	0.11202	1.4054	2283.3	0.15766	1.2522	2158.0	0.05815	1.3100
2321.9	0.11208	1.4053	2285.3	0.15755	1.2520	2159.9	0.05819	1.3101
2323.8	0.11213	1.4052	2287.2	0.15745	1.2518	2161.8	0.05823	1.3101
2325.8	0.11219	1.4052	2289.1	0.15734	1.2517	2163.8	0.05826	1.3102
2327.7	0.11225	1.4051	2291.1	0.15724	1.2515	2165.7	0.05830	1.3102
2329.6	0.11230	1.4051	2293.0	0.15713	1.2513	2167.6	0.05834	1.3102
2331.6	0.11235	1.4050	2294.9	0.15703	1.2511	2169.6	0.05837	1.3103
2333.5	0.11240	1.4049	2296.8	0.15692	1.2510	2171.5	0.05841	1.3103
2335.4	0.11246	1.4049	2298.8	0.15681	1.2508	2173.4	0.05845	1.3103
2337.3	0.11251	1.4048	2300.7	0.15670	1.2506	2175.3	0.05848	1.3104
2339.3	0.11256	1.4047	2302.6	0.15659	1.2504	2177.3	0.05852	1.3104
2341.2	0.11261	1.4047	2304.6	0.15648	1.2503	2179.2	0.05856	1.3104
2343.1	0.11266	1.4046	2306.5	0.15637	1.2501	2181.1	0.05859	1.3105
2345.1	0.11270	1.4045	2308.4	0.15626	1.2499	2183.1	0.05863	1.3105
2347.0	0.11275	1.4045	2310.3	0.15615	1.2498	2185.0	0.05867	1.3105
2348.9	0.11280	1.4044	2312.3	0.15603	1.2496	2186.9	0.05870	1.3106
2350.8	0.11284	1.4043	2314.2	0.15592	1.2494	2188.8	0.05874	1.3106
2352.8	0.11289	1.4043	2316.1	0.15580	1.2492	2190.8	0.05878	1.3106
2354.7	0.11293	1.4042	2318.1	0.15569	1.2491	2192.7	0.05882	1.3107

2356.6	0.11297	1.4041	2320.0	0.15557	1.2489	2194.6	0.05885	1.3107
2358.6	0.11301	1.4041	2321.9	0.15546	1.2487	2196.6	0.05889	1.3107
2360.5	0.11306	1.4040	2323.8	0.15534	1.2486	2198.5	0.05893	1.3108
2362.4	0.11310	1.4040	2325.8	0.15522	1.2484	2200.4	0.05896	1.3108
2364.3	0.11314	1.4039	2327.7	0.15510	1.2482	2202.3	0.05900	1.3108
2366.3	0.11318	1.4038	2329.6	0.15498	1.2480	2204.3	0.05904	1.3108
2368.2	0.11322	1.4038	2331.6	0.15486	1.2479	2206.2	0.05908	1.3109
2370.1	0.11325	1.4037	2333.5	0.15474	1.2477	2208.1	0.05911	1.3109
2372.1	0.11329	1.4036	2335.4	0.15462	1.2475	2210.1	0.05915	1.3109
2374.0	0.11333	1.4036	2337.3	0.15450	1.2474	2212.0	0.05919	1.3110
2375.9	0.11336	1.4035	2339.3	0.15438	1.2472	2213.9	0.05922	1.3110
2377.8	0.11340	1.4034	2341.2	0.15425	1.2470	2215.8	0.05926	1.3110
2379.8	0.11344	1.4034	2343.1	0.15413	1.2469	2217.8	0.05930	1.3110
2381.7	0.11347	1.4033	2345.1	0.15401	1.2467	2219.7	0.05934	1.3111
2383.6	0.11350	1.4032	2347.0	0.15388	1.2465	2221.6	0.05937	1.3111
2385.6	0.11354	1.4032	2348.9	0.15376	1.2464	2223.6	0.05941	1.3111
2387.5	0.11357	1.4031	2350.8	0.15363	1.2462	2225.5	0.05945	1.3111
2389.4	0.11360	1.4031	2352.8	0.15350	1.2460	2227.4	0.05949	1.3112
2391.3	0.11363	1.4030	2354.7	0.15337	1.2459	2229.3	0.05952	1.3112
2393.3	0.11366	1.4029	2356.6	0.15325	1.2457	2231.3	0.05956	1.3112
2395.2	0.11369	1.4029	2358.6	0.15312	1.2456	2233.2	0.05960	1.3112
2397.1	0.11372	1.4028	2360.5	0.15299	1.2454	2235.1	0.05964	1.3113
2399.1	0.11375	1.4027	2362.4	0.15286	1.2452	2237.1	0.05967	1.3113
2401.0	0.11378	1.4027	2364.3	0.15273	1.2451	2239.0	0.05971	1.3113
2402.9	0.11381	1.4026	2366.3	0.15260	1.2449	2240.9	0.05975	1.3113
2404.8	0.11384	1.4026	2368.2	0.15246	1.2447	2242.8	0.05979	1.3114
2406.8	0.11386	1.4025	2370.1	0.15233	1.2446	2244.8	0.05982	1.3114
2408.7	0.11389	1.4024	2372.1	0.15220	1.2444	2246.7	0.05986	1.3114
2410.6	0.11392	1.4024	2374.0	0.15207	1.2443	2248.6	0.05990	1.3114
2412.6	0.11394	1.4023	2375.9	0.15193	1.2441	2250.6	0.05993	1.3114
2414.5	0.11397	1.4023	2377.8	0.15180	1.2439	2252.5	0.05997	1.3115
2416.4	0.11399	1.4022	2379.8	0.15166	1.2438	2254.4	0.06001	1.3115
2418.3	0.11402	1.4021	2381.7	0.15152	1.2436	2256.3	0.06005	1.3115
2420.3	0.11404	1.4021	2383.6	0.15139	1.2435	2258.3	0.06008	1.3115
2422.2	0.11407	1.4020	2385.6	0.15125	1.2433	2260.2	0.06012	1.3115
2424.1	0.11409	1.4020	2387.5	0.15111	1.2432	2262.1	0.06016	1.3116
2426.1	0.11411	1.4019	2389.4	0.15097	1.2430	2264.1	0.06020	1.3116
2428.0	0.11414	1.4019	2391.3	0.15084	1.2428	2266.0	0.06023	1.3116
2429.9	0.11416	1.4018	2393.3	0.15070	1.2427	2267.9	0.06027	1.3116
2431.8	0.11418	1.4017	2395.2	0.15056	1.2425	2269.8	0.06031	1.3116
2433.8	0.11420	1.4017	2397.1	0.15042	1.2424	2271.8	0.06035	1.3116
2435.7	0.11422	1.4016	2399.1	0.15027	1.2422	2273.7	0.06038	1.3117
2437.6	0.11425	1.4016	2401.0	0.15013	1.2421	2275.6	0.06042	1.3117

2439.5	0.11427	1.4015	2402.9	0.14999	1.2419	2277.6	0.06046	1.3117
2441.5	0.11429	1.4015	2404.8	0.14985	1.2418	2279.5	0.06050	1.3117
2443.4	0.11431	1.4014	2406.8	0.14971	1.2416	2281.4	0.06053	1.3117
2445.3	0.11433	1.4014	2408.7	0.14956	1.2415	2283.3	0.06057	1.3117
2447.3	0.11435	1.4013	2410.6	0.14942	1.2413	2285.3	0.06061	1.3118
2449.2	0.11437	1.4012	2412.6	0.14927	1.2412	2287.2	0.06064	1.3118
2451.1	0.11439	1.4012	2414.5	0.14913	1.2410	2289.1	0.06068	1.3118
2453.0	0.11441	1.4011	2416.4	0.14898	1.2409	2291.1	0.06072	1.3118
2455.0	0.11442	1.4011	2418.3	0.14884	1.2407	2293.0	0.06076	1.3118
2456.9	0.11444	1.4010	2420.3	0.14869	1.2406	2294.9	0.06079	1.3118
2458.8	0.11446	1.4010	2422.2	0.14854	1.2404	2296.8	0.06083	1.3118
2460.8	0.11448	1.4009	2424.1	0.14839	1.2403	2298.8	0.06087	1.3118
2462.7	0.11450	1.4009	2426.1	0.14825	1.2401	2300.7	0.06091	1.3119
2464.6	0.11452	1.4008	2428.0	0.14810	1.2400	2302.6	0.06094	1.3119
2466.5	0.11453	1.4008	2429.9	0.14795	1.2398	2304.6	0.06098	1.3119
2468.5	0.11455	1.4007	2431.8	0.14780	1.2397	2306.5	0.06102	1.3119
2470.4	0.11457	1.4007	2433.8	0.14765	1.2395	2308.4	0.06105	1.3119
2472.3	0.11459	1.4006	2435.7	0.14750	1.2394	2310.3	0.06109	1.3119
2474.3	0.11461	1.4006	2437.6	0.14735	1.2392	2312.3	0.06113	1.3119
2476.2	0.11462	1.4005	2439.5	0.14719	1.2391	2314.2	0.06116	1.3119
2478.1	0.11464	1.4005	2441.5	0.14704	1.2390	2316.1	0.06120	1.3119
2480.0	0.11466	1.4004	2443.4	0.14689	1.2388	2318.1	0.06124	1.3120
2482.0	0.11468	1.4004	2445.3	0.14674	1.2387	2320.0	0.06128	1.3120
2483.9	0.11469	1.4003	2447.3	0.14658	1.2385	2321.9	0.06131	1.3120
2485.8	0.11471	1.4003	2449.2	0.14643	1.2384	2323.8	0.06135	1.3120
2487.8	0.11473	1.4003	2451.1	0.14627	1.2382	2325.8	0.06139	1.3120
2489.7	0.11475	1.4002	2453.0	0.14612	1.2381	2327.7	0.06142	1.3120
2491.6	0.11476	1.4002	2455.0	0.14596	1.2380	2329.6	0.06146	1.3120
2493.5	0.11478	1.4001	2456.9	0.14581	1.2378	2331.6	0.06150	1.3120
2495.5	0.11480	1.4001	2458.8	0.14565	1.2377	2333.5	0.06153	1.3120
2497.4	0.11482	1.4000	2460.8	0.14550	1.2375	2335.4	0.06157	1.3120
2499.3	0.11483	1.4000	2462.7	0.14534	1.2374	2337.3	0.06161	1.3120
2501.3	0.11485	1.3999	2464.6	0.14518	1.2373	2339.3	0.06164	1.3120
2503.2	0.11487	1.3999	2466.5	0.14502	1.2371	2341.2	0.06168	1.3120
2505.1	0.11489	1.3999	2468.5	0.14486	1.2370	2343.1	0.06172	1.3121
2507.0	0.11491	1.3998	2470.4	0.14471	1.2369	2345.1	0.06175	1.3121
2509.0	0.11492	1.3998	2472.3	0.14455	1.2367	2347.0	0.06179	1.3121
2510.9	0.11494	1.3997	2474.3	0.14439	1.2366	2348.9	0.06183	1.3121
2512.8	0.11496	1.3997	2476.2	0.14423	1.2365	2350.8	0.06186	1.3121
2514.8	0.11498	1.3996	2478.1	0.14407	1.2363	2352.8	0.06190	1.3121
2516.7	0.11500	1.3996	2480.0	0.14391	1.2362	2354.7	0.06193	1.3121
2518.6	0.11502	1.3996	2482.0	0.14374	1.2361	2356.6	0.06197	1.3121
2520.5	0.11504	1.3995	2483.9	0.14358	1.2359	2358.6	0.06201	1.3121

2522.5	0.11506	1.3995	2485.8	0.14342	1.2358	2360.5	0.06204	1.3121
2524.4	0.11507	1.3994	2487.8	0.14326	1.2357	2362.4	0.06208	1.3121
2526.3	0.11509	1.3994	2489.7	0.14310	1.2355	2364.3	0.06212	1.3121
2528.3	0.11511	1.3994	2491.6	0.14293	1.2354	2366.3	0.06215	1.3121
2530.2	0.11513	1.3993	2493.5	0.14277	1.2353	2368.2	0.06219	1.3121
2532.1	0.11515	1.3993	2495.5	0.14261	1.2352	2370.1	0.06222	1.3121
2534.0	0.11517	1.3992	2497.4	0.14244	1.2350	2372.1	0.06226	1.3121
2536.0	0.11520	1.3992	2499.3	0.14228	1.2349	2374.0	0.06230	1.3121
2537.9	0.11522	1.3992	2501.3	0.14211	1.2348	2375.9	0.06233	1.3121
2539.8	0.11524	1.3991	2503.2	0.14195	1.2347	2377.8	0.06237	1.3121
2541.8	0.11526	1.3991	2505.1	0.14178	1.2345	2379.8	0.06240	1.3121
2543.7	0.11528	1.3991	2507.0	0.14162	1.2344	2381.7	0.06244	1.3121
2545.6	0.11530	1.3990	2509.0	0.14145	1.2343	2383.6	0.06247	1.3121
2547.5	0.11533	1.3990	2510.9	0.14128	1.2342	2385.6	0.06251	1.3121
2549.5	0.11535	1.3990	2512.8	0.14112	1.2340	2387.5	0.06254	1.3121
2551.4	0.11537	1.3989	2514.8	0.14095	1.2339	2389.4	0.06258	1.3121
2553.3	0.11539	1.3989	2516.7	0.14078	1.2338	2391.3	0.06262	1.3121
2555.3	0.11542	1.3988	2518.6	0.14061	1.2337	2393.3	0.06265	1.3121
2557.2	0.11544	1.3988	2520.5	0.14045	1.2335	2395.2	0.06269	1.3121
2559.1	0.11547	1.3988	2522.5	0.14028	1.2334	2397.1	0.06272	1.3121
2561.0	0.11549	1.3987	2524.4	0.14011	1.2333	2399.1	0.06276	1.3121
2563.0	0.11551	1.3987	2526.3	0.13994	1.2332	2401.0	0.06279	1.3121
2564.9	0.11554	1.3987	2528.3	0.13977	1.2331	2402.9	0.06283	1.3121
2566.8	0.11557	1.3986	2530.2	0.13960	1.2330	2404.8	0.06286	1.3121
2568.8	0.11559	1.3986	2532.1	0.13943	1.2328	2406.8	0.06290	1.3121
2570.7	0.11562	1.3986	2534.0	0.13926	1.2327	2408.7	0.06293	1.3121
2572.6	0.11564	1.3985	2536.0	0.13909	1.2326	2410.6	0.06297	1.3121
2574.5	0.11567	1.3985	2537.9	0.13892	1.2325	2412.6	0.06300	1.3121
2576.5	0.11570	1.3985	2539.8	0.13875	1.2324	2414.5	0.06304	1.3121
2578.4	0.11573	1.3984	2541.8	0.13858	1.2323	2416.4	0.06307	1.3121
2580.3	0.11576	1.3984	2543.7	0.13840	1.2322	2418.3	0.06310	1.3121
2582.3	0.11578	1.3984	2545.6	0.13823	1.2320	2420.3	0.06314	1.3120
2584.2	0.11581	1.3983	2547.5	0.13806	1.2319	2422.2	0.06317	1.3120
2586.1	0.11584	1.3983	2549.5	0.13789	1.2318	2424.1	0.06321	1.3120
2588.0	0.11587	1.3983	2551.4	0.13772	1.2317	2426.1	0.06324	1.3120
2590.0	0.11590	1.3982	2553.3	0.13754	1.2316	2428.0	0.06328	1.3120
2591.9	0.11593	1.3982	2555.3	0.13737	1.2315	2429.9	0.06331	1.3120
2593.8	0.11596	1.3982	2557.2	0.13720	1.2314	2431.8	0.06335	1.3120
2595.8	0.11600	1.3981	2559.1	0.13702	1.2313	2433.8	0.06338	1.3120
2597.7	0.11603	1.3981	2561.0	0.13685	1.2312	2435.7	0.06341	1.3120
2599.6	0.11606	1.3981	2563.0	0.13667	1.2311	2437.6	0.06345	1.3120
2601.5	0.11609	1.3980	2564.9	0.13650	1.2310	2439.5	0.06348	1.3120
2603.5	0.11613	1.3980	2566.8	0.13632	1.2308	2441.5	0.06351	1.3120

2605.4	0.11616	1.3980	2568.8	0.13615	1.2307	2443.4	0.06355	1.3120
2607.3	0.11620	1.3979	2570.7	0.13597	1.2306	2445.3	0.06358	1.3120
2609.3	0.11623	1.3979	2572.6	0.13580	1.2305	2447.3	0.06362	1.3119
2611.2	0.11627	1.3979	2574.5	0.13562	1.2304	2449.2	0.06365	1.3119
2613.1	0.11630	1.3978	2576.5	0.13545	1.2303	2451.1	0.06368	1.3119
2615.0	0.11634	1.3978	2578.4	0.13527	1.2302	2453.0	0.06372	1.3119
2617.0	0.11637	1.3978	2580.3	0.13509	1.2301	2455.0	0.06375	1.3119
2618.9	0.11641	1.3977	2582.3	0.13492	1.2300	2456.9	0.06378	1.3119
2620.8	0.11645	1.3977	2584.2	0.13474	1.2299	2458.8	0.06381	1.3119
2622.8	0.11649	1.3977	2586.1	0.13456	1.2298	2460.8	0.06385	1.3119
2624.7	0.11653	1.3976	2588.0	0.13439	1.2297	2462.7	0.06388	1.3119
2626.6	0.11656	1.3976	2590.0	0.13421	1.2296	2464.6	0.06391	1.3119
2628.5	0.11660	1.3976	2591.9	0.13403	1.2295	2466.5	0.06395	1.3118
2630.5	0.11664	1.3976	2593.8	0.13385	1.2294	2468.5	0.06398	1.3118
2632.4	0.11668	1.3975	2595.8	0.13368	1.2293	2470.4	0.06401	1.3118
2634.3	0.11673	1.3975	2597.7	0.13350	1.2292	2472.3	0.06404	1.3118
2636.3	0.11677	1.3975	2599.6	0.13332	1.2291	2474.3	0.06408	1.3118
2638.2	0.11681	1.3974	2601.5	0.13314	1.2291	2476.2	0.06411	1.3118
2640.1	0.11685	1.3974	2603.5	0.13296	1.2290	2478.1	0.06414	1.3118
2642.0	0.11689	1.3974	2605.4	0.13278	1.2289	2480.0	0.06417	1.3118
2644.0	0.11694	1.3973	2607.3	0.13261	1.2288	2482.0	0.06421	1.3117
2645.9	0.11698	1.3973	2609.3	0.13243	1.2287	2483.9	0.06424	1.3117
2647.8	0.11703	1.3973	2611.2	0.13225	1.2286	2485.8	0.06427	1.3117
2649.8	0.11707	1.3972	2613.1	0.13207	1.2285	2487.8	0.06430	1.3117
2651.7	0.11712	1.3972	2615.0	0.13189	1.2284	2489.7	0.06433	1.3117
2653.6	0.11716	1.3971	2617.0	0.13171	1.2283	2491.6	0.06436	1.3117
2655.5	0.11721	1.3971	2618.9	0.13153	1.2282	2493.5	0.06440	1.3117
2657.5	0.11726	1.3971	2620.8	0.13135	1.2281	2495.5	0.06443	1.3117
2659.4	0.11730	1.3970	2622.8	0.13117	1.2281	2497.4	0.06446	1.3116
2661.3	0.11735	1.3970	2624.7	0.13099	1.2280	2499.3	0.06449	1.3116
2663.3	0.11740	1.3970	2626.6	0.13081	1.2279	2501.3	0.06452	1.3116
2665.2	0.11745	1.3969	2628.5	0.13063	1.2278	2503.2	0.06455	1.3116
2667.1	0.11750	1.3969	2630.5	0.13045	1.2277	2505.1	0.06458	1.3116
2669.0	0.11755	1.3969	2632.4	0.13026	1.2276	2507.0	0.06461	1.3116
2671.0	0.11760	1.3968	2634.3	0.13008	1.2275	2509.0	0.06464	1.3115
2672.9	0.11765	1.3968	2636.3	0.12990	1.2275	2510.9	0.06468	1.3115
2674.8	0.11770	1.3968	2638.2	0.12972	1.2274	2512.8	0.06471	1.3115
2676.8	0.11775	1.3967	2640.1	0.12954	1.2273	2514.8	0.06474	1.3115
2678.7	0.11781	1.3967	2642.0	0.12936	1.2272	2516.7	0.06477	1.3115
2680.6	0.11786	1.3966	2644.0	0.12918	1.2271	2518.6	0.06480	1.3115
2682.5	0.11791	1.3966	2645.9	0.12900	1.2271	2520.5	0.06483	1.3114
2684.5	0.11797	1.3966	2647.8	0.12881	1.2270	2522.5	0.06486	1.3114
2686.4	0.11802	1.3965	2649.8	0.12863	1.2269	2524.4	0.06489	1.3114

2688.3	0.11808	1.3965	2651.7	0.12845	1.2268	2526.3	0.06492	1.3114
2690.3	0.11813	1.3964	2653.6	0.12827	1.2268	2528.3	0.06495	1.3114
2692.2	0.11819	1.3964	2655.5	0.12809	1.2267	2530.2	0.06498	1.3114
2694.1	0.11824	1.3964	2657.5	0.12790	1.2266	2532.1	0.06501	1.3113
2696.0	0.11830	1.3963	2659.4	0.12772	1.2265	2534.0	0.06504	1.3113
2698.0	0.11836	1.3963	2661.3	0.12754	1.2265	2536.0	0.06507	1.3113
2699.9	0.11842	1.3962	2663.3	0.12736	1.2264	2537.9	0.06509	1.3113
2701.8	0.11847	1.3962	2665.2	0.12717	1.2263	2539.8	0.06512	1.3113
2703.8	0.11853	1.3962	2667.1	0.12699	1.2262	2541.8	0.06515	1.3112
2705.7	0.11859	1.3961	2669.0	0.12681	1.2262	2543.7	0.06518	1.3112
2707.6	0.11865	1.3961	2671.0	0.12663	1.2261	2545.6	0.06521	1.3112
2709.5	0.11871	1.3960	2672.9	0.12644	1.2260	2547.5	0.06524	1.3112
2711.5	0.11877	1.3960	2674.8	0.12626	1.2260	2549.5	0.06527	1.3112
2713.4	0.11883	1.3959	2676.8	0.12608	1.2259	2551.4	0.06530	1.3111
2715.3	0.11889	1.3959	2678.7	0.12589	1.2258	2553.3	0.06533	1.3111
2717.3	0.11896	1.3958	2680.6	0.12571	1.2257	2555.3	0.06535	1.3111
2719.2	0.11902	1.3958	2682.5	0.12553	1.2257	2557.2	0.06538	1.3111
2721.1	0.11908	1.3958	2684.5	0.12535	1.2256	2559.1	0.06541	1.3111
2723.0	0.11914	1.3957	2686.4	0.12516	1.2255	2561.0	0.06544	1.3110
2725.0	0.11921	1.3957	2688.3	0.12498	1.2255	2563.0	0.06547	1.3110
2726.9	0.11927	1.3956	2690.3	0.12480	1.2254	2564.9	0.06549	1.3110
2728.8	0.11933	1.3956	2692.2	0.12461	1.2254	2566.8	0.06552	1.3110
2730.8	0.11940	1.3955	2694.1	0.12443	1.2253	2568.8	0.06555	1.3109
2732.7	0.11946	1.3955	2696.0	0.12425	1.2252	2570.7	0.06558	1.3109
2734.6	0.11953	1.3954	2698.0	0.12406	1.2252	2572.6	0.06560	1.3109
2736.5	0.11960	1.3954	2699.9	0.12388	1.2251	2574.5	0.06563	1.3109
2738.5	0.11966	1.3953	2701.8	0.12370	1.2250	2576.5	0.06566	1.3109
2740.4	0.11973	1.3953	2703.8	0.12351	1.2250	2578.4	0.06568	1.3108
2742.3	0.11979	1.3952	2705.7	0.12333	1.2249	2580.3	0.06571	1.3108
2744.3	0.11986	1.3952	2707.6	0.12314	1.2249	2582.3	0.06574	1.3108
2746.2	0.11993	1.3951	2709.5	0.12296	1.2248	2584.2	0.06576	1.3108
2748.1	0.12000	1.3951	2711.5	0.12278	1.2248	2586.1	0.06579	1.3107
2750.0	0.12007	1.3950	2713.4	0.12259	1.2247	2588.0	0.06582	1.3107
2752.0	0.12013	1.3949	2715.3	0.12241	1.2246	2590.0	0.06584	1.3107
2753.9	0.12020	1.3949	2717.3	0.12223	1.2246	2591.9	0.06587	1.3107
2755.8	0.12027	1.3948	2719.2	0.12204	1.2245	2593.8	0.06590	1.3106
2757.8	0.12034	1.3948	2721.1	0.12186	1.2245	2595.8	0.06592	1.3106
2759.7	0.12041	1.3947	2723.0	0.12168	1.2244	2597.7	0.06595	1.3106
2761.6	0.12048	1.3947	2725.0	0.12149	1.2244	2599.6	0.06597	1.3106
2763.5	0.12055	1.3946	2726.9	0.12131	1.2243	2601.5	0.06600	1.3105
2765.5	0.12062	1.3946	2728.8	0.12113	1.2243	2603.5	0.06602	1.3105
2767.4	0.12069	1.3945	2730.8	0.12094	1.2242	2605.4	0.06605	1.3105
2769.3	0.12076	1.3944	2732.7	0.12076	1.2242	2607.3	0.06607	1.3105

2771.2	0.12083	1.3944	2734.6	0.12058	1.2241	2609.3	0.06610	1.3104
2773.2	0.12091	1.3943	2736.5	0.12039	1.2241	2611.2	0.06612	1.3104
2775.1	0.12098	1.3942	2738.5	0.12021	1.2240	2613.1	0.06615	1.3104
2777.0	0.12105	1.3942	2740.4	0.12003	1.2240	2615.0	0.06617	1.3104
2779.0	0.12112	1.3941	2742.3	0.11984	1.2239	2617.0	0.06620	1.3103
2780.9	0.12120	1.3941	2744.3	0.11966	1.2239	2618.9	0.06622	1.3103
2782.8	0.12127	1.3940	2746.2	0.11948	1.2238	2620.8	0.06625	1.3103
2784.8	0.12134	1.3939	2748.1	0.11929	1.2238	2622.8	0.06627	1.3103
2786.7	0.12141	1.3939	2750.0	0.11911	1.2238	2624.7	0.06630	1.3102
2788.6	0.12149	1.3938	2752.0	0.11893	1.2237	2626.6	0.06632	1.3102
2790.5	0.12156	1.3937	2753.9	0.11874	1.2237	2628.5	0.06634	1.3102
2792.5	0.12163	1.3937	2755.8	0.11856	1.2236	2630.5	0.06637	1.3102
2794.4	0.12171	1.3936	2757.8	0.11838	1.2236	2632.4	0.06639	1.3101
2796.3	0.12178	1.3935	2759.7	0.11820	1.2235	2634.3	0.06641	1.3101
2798.2	0.12186	1.3935	2761.6	0.11801	1.2235	2636.3	0.06644	1.3101
2800.2	0.12193	1.3934	2763.5	0.11783	1.2235	2638.2	0.06646	1.3100
2802.1	0.12201	1.3933	2765.5	0.11765	1.2234	2640.1	0.06648	1.3100
2804.0	0.12208	1.3932	2767.4	0.11746	1.2234	2642.0	0.06651	1.3100
2806.0	0.12215	1.3932	2769.3	0.11728	1.2234	2644.0	0.06653	1.3100
2807.9	0.12223	1.3931	2771.2	0.11710	1.2233	2645.9	0.06655	1.3099
2809.8	0.12230	1.3930	2773.2	0.11692	1.2233	2647.8	0.06657	1.3099
2811.7	0.12238	1.3930	2775.1	0.11673	1.2232	2649.8	0.06659	1.3099
2813.7	0.12245	1.3929	2777.0	0.11655	1.2232	2651.7	0.06662	1.3098
2815.6	0.12253	1.3928	2779.0	0.11637	1.2232	2653.6	0.06664	1.3098
2817.5	0.12260	1.3927	2780.9	0.11619	1.2231	2655.5	0.06666	1.3098
2819.5	0.12268	1.3927	2782.8	0.11601	1.2231	2657.5	0.06668	1.3098
2821.4	0.12275	1.3926	2784.8	0.11582	1.2231	2659.4	0.06670	1.3097
2823.3	0.12283	1.3925	2786.7	0.11564	1.2231	2661.3	0.06673	1.3097
2825.2	0.12291	1.3924	2788.6	0.11546	1.2230	2663.3	0.06675	1.3097
2827.2	0.12298	1.3923	2790.5	0.11528	1.2230	2665.2	0.06677	1.3096
2829.1	0.12306	1.3923	2792.5	0.11510	1.2230	2667.1	0.06679	1.3096
2831.0	0.12313	1.3922	2794.4	0.11492	1.2229	2669.0	0.06681	1.3096
2833.0	0.12321	1.3921	2796.3	0.11473	1.2229	2671.0	0.06683	1.3096
2834.9	0.12328	1.3920	2798.2	0.11455	1.2229	2672.9	0.06685	1.3095
2836.8	0.12336	1.3919	2800.2	0.11437	1.2229	2674.8	0.06687	1.3095
2838.7	0.12343	1.3919	2802.1	0.11419	1.2228	2676.8	0.06689	1.3095
2840.7	0.12351	1.3918	2804.0	0.11401	1.2228	2678.7	0.06691	1.3094
2842.6	0.12358	1.3917	2806.0	0.11383	1.2228	2680.6	0.06693	1.3094
2844.5	0.12366	1.3916	2807.9	0.11365	1.2228	2682.5	0.06695	1.3094
2846.5	0.12373	1.3915	2809.8	0.11347	1.2227	2684.5	0.06697	1.3093
2848.4	0.12381	1.3914	2811.7	0.11329	1.2227	2686.4	0.06699	1.3093
2850.3	0.12388	1.3913	2813.7	0.11311	1.2227	2688.3	0.06701	1.3093
2852.2	0.12396	1.3913	2815.6	0.11293	1.2227	2690.3	0.06703	1.3093

2854.2	0.12403	1.3912	2817.5	0.11275	1.2227	2692.2	0.06705	1.3092
2856.1	0.12411	1.3911	2819.5	0.11257	1.2226	2694.1	0.06707	1.3092
2858.0	0.12418	1.3910	2821.4	0.11239	1.2226	2696.0	0.06709	1.3092
2860.0	0.12425	1.3909	2823.3	0.11221	1.2226	2698.0	0.06711	1.3091
2861.9	0.12433	1.3908	2825.2	0.11203	1.2226	2699.9	0.06712	1.3091
2863.8	0.12440	1.3907	2827.2	0.11185	1.2226	2701.8	0.06714	1.3091
2865.7	0.12447	1.3906	2829.1	0.11167	1.2225	2703.8	0.06716	1.3090
2867.7	0.12455	1.3905	2831.0	0.11149	1.2225	2705.7	0.06718	1.3090
2869.6	0.12462	1.3904	2833.0	0.11131	1.2225	2707.6	0.06720	1.3090
2871.5	0.12469	1.3903	2834.9	0.11113	1.2225	2709.5	0.06722	1.3089
2873.5	0.12477	1.3902	2836.8	0.11095	1.2225	2711.5	0.06723	1.3089
2875.4	0.12484	1.3902	2838.7	0.11077	1.2225	2713.4	0.06725	1.3089
2877.3	0.12491	1.3901	2840.7	0.11059	1.2225	2715.3	0.06727	1.3088
2879.2	0.12498	1.3900	2842.6	0.11042	1.2225	2717.3	0.06729	1.3088
2881.2	0.12506	1.3899	2844.5	0.11024	1.2224	2719.2	0.06730	1.3088
2883.1	0.12513	1.3898	2846.5	0.11006	1.2224	2721.1	0.06732	1.3087
2885.0	0.12520	1.3897	2848.4	0.10988	1.2224	2723.0	0.06734	1.3087
2887.0	0.12527	1.3896	2850.3	0.10970	1.2224	2725.0	0.06735	1.3087
2888.9	0.12534	1.3895	2852.2	0.10953	1.2224	2726.9	0.06737	1.3087
2890.8	0.12541	1.3894	2854.2	0.10935	1.2224	2728.8	0.06739	1.3086
2892.7	0.12548	1.3893	2856.1	0.10917	1.2224	2730.8	0.06740	1.3086
2894.7	0.12555	1.3892	2858.0	0.10900	1.2224	2732.7	0.06742	1.3086
2896.6	0.12562	1.3891	2860.0	0.10882	1.2224	2734.6	0.06743	1.3085
2898.5	0.12569	1.3890	2861.9	0.10864	1.2224	2736.5	0.06745	1.3085
2900.5	0.12576	1.3889	2863.8	0.10847	1.2224	2738.5	0.06746	1.3085
2902.4	0.12583	1.3888	2865.7	0.10829	1.2224	2740.4	0.06748	1.3084
2904.3	0.12590	1.3887	2867.7	0.10811	1.2224	2742.3	0.06750	1.3084
2906.2	0.12597	1.3886	2869.6	0.10794	1.2224	2744.3	0.06751	1.3084
2908.2	0.12603	1.3885	2871.5	0.10776	1.2224	2746.2	0.06753	1.3083
2910.1	0.12610	1.3884	2873.5	0.10759	1.2224	2748.1	0.06754	1.3083
2912.0	0.12617	1.3882	2875.4	0.10741	1.2224	2750.0	0.06755	1.3083
2914.0	0.12624	1.3881	2877.3	0.10723	1.2224	2752.0	0.06757	1.3082
2915.9	0.12630	1.3880	2879.2	0.10706	1.2224	2753.9	0.06758	1.3082
2917.8	0.12637	1.3879	2881.2	0.10688	1.2224	2755.8	0.06760	1.3082
2919.7	0.12643	1.3878	2883.1	0.10671	1.2224	2757.8	0.06761	1.3081
2921.7	0.12650	1.3877	2885.0	0.10654	1.2224	2759.7	0.06763	1.3081
2923.6	0.12656	1.3876	2887.0	0.10636	1.2224	2761.6	0.06764	1.3081
2925.5	0.12663	1.3875	2888.9	0.10619	1.2224	2763.5	0.06765	1.3080
2927.5	0.12669	1.3874	2890.8	0.10601	1.2224	2765.5	0.06767	1.3080
2929.4	0.12675	1.3873	2892.7	0.10584	1.2224	2767.4	0.06768	1.3080
2931.3	0.12682	1.3872	2894.7	0.10567	1.2224	2769.3	0.06769	1.3079
2933.2	0.12688	1.3871	2896.6	0.10549	1.2225	2771.2	0.06771	1.3079
2935.2	0.12694	1.3870	2898.5	0.10532	1.2225	2773.2	0.06772	1.3079

2937.1	0.12700	1.3869	2900.5	0.10515	1.2225	2775.1	0.06773	1.3078
2939.0	0.12706	1.3867	2902.4	0.10498	1.2225	2777.0	0.06774	1.3078
2941.0	0.12713	1.3866	2904.3	0.10480	1.2225	2779.0	0.06776	1.3078
2942.9	0.12719	1.3865	2906.2	0.10463	1.2225	2780.9	0.06777	1.3077
2944.8	0.12725	1.3864	2908.2	0.10446	1.2225	2782.8	0.06778	1.3077
2946.7	0.12730	1.3863	2910.1	0.10429	1.2225	2784.8	0.06779	1.3077
2948.7	0.12736	1.3862	2912.0	0.10412	1.2226	2786.7	0.06780	1.3076
2950.6	0.12742	1.3861	2914.0	0.10395	1.2226	2788.6	0.06781	1.3076
2952.5	0.12748	1.3860	2915.9	0.10377	1.2226	2790.5	0.06783	1.3075
2954.5	0.12754	1.3859	2917.8	0.10360	1.2226	2792.5	0.06784	1.3075
2956.4	0.12759	1.3857	2919.7	0.10343	1.2226	2794.4	0.06785	1.3075
2958.3	0.12765	1.3856	2921.7	0.10326	1.2227	2796.3	0.06786	1.3074
2960.2	0.12771	1.3855	2923.6	0.10309	1.2227	2798.2	0.06787	1.3074
2962.2	0.12776	1.3854	2925.5	0.10292	1.2227	2800.2	0.06788	1.3074
2964.1	0.12782	1.3853	2927.5	0.10275	1.2227	2802.1	0.06789	1.3073
2966.0	0.12787	1.3852	2929.4	0.10259	1.2227	2804.0	0.06790	1.3073
2968.0	0.12793	1.3851	2931.3	0.10242	1.2228	2806.0	0.06791	1.3073
2969.9	0.12798	1.3850	2933.2	0.10225	1.2228	2807.9	0.06792	1.3072
2971.8	0.12803	1.3849	2935.2	0.10208	1.2228	2809.8	0.06793	1.3072
2973.7	0.12809	1.3847	2937.1	0.10191	1.2228	2811.7	0.06794	1.3072
2975.7	0.12814	1.3846	2939.0	0.10174	1.2229	2813.7	0.06795	1.3071
2977.6	0.12819	1.3845	2941.0	0.10158	1.2229	2815.6	0.06796	1.3071
2979.5	0.12824	1.3844	2942.9	0.10141	1.2229	2817.5	0.06797	1.3071
2981.5	0.12829	1.3843	2944.8	0.10124	1.2230	2819.5	0.06798	1.3070
2983.4	0.12834	1.3842	2946.7	0.10108	1.2230	2821.4	0.06798	1.3070
2985.3	0.12839	1.3841	2948.7	0.10091	1.2230	2823.3	0.06799	1.3070
2987.2	0.12844	1.3840	2950.6	0.10074	1.2231	2825.2	0.06800	1.3069
2989.2	0.12849	1.3839	2952.5	0.10058	1.2231	2827.2	0.06801	1.3069
2991.1	0.12854	1.3837	2954.5	0.10041	1.2231	2829.1	0.06802	1.3069
2993.0	0.12859	1.3836	2956.4	0.10025	1.2232	2831.0	0.06802	1.3068
2995.0	0.12864	1.3835	2958.3	0.10008	1.2232	2833.0	0.06803	1.3068
2996.9	0.12868	1.3834	2960.2	0.09992	1.2232	2834.9	0.06804	1.3068
2998.8	0.12873	1.3833	2962.2	0.09975	1.2233	2836.8	0.06805	1.3067
3000.7	0.12878	1.3832	2964.1	0.09959	1.2233	2838.7	0.06805	1.3067
3002.7	0.12882	1.3831	2966.0	0.09943	1.2234	2840.7	0.06806	1.3067
3004.6	0.12887	1.3830	2968.0	0.09926	1.2234	2842.6	0.06807	1.3066
3006.5	0.12891	1.3829	2969.9	0.09910	1.2234	2844.5	0.06808	1.3066
3008.5	0.12896	1.3828	2971.8	0.09894	1.2235	2846.5	0.06808	1.3066
3010.4	0.12900	1.3827	2973.7	0.09877	1.2235	2848.4	0.06809	1.3065
3012.3	0.12904	1.3826	2975.7	0.09861	1.2236	2850.3	0.06809	1.3065
3014.2	0.12909	1.3825	2977.6	0.09845	1.2236	2852.2	0.06810	1.3065
3016.2	0.12913	1.3823	2979.5	0.09829	1.2237	2854.2	0.06811	1.3064
3018.1	0.12917	1.3822	2981.5	0.09813	1.2237	2856.1	0.06811	1.3064

3020.0	0.12922	1.3821	2983.4	0.09797	1.2238	2858.0	0.06812	1.3064
3022.0	0.12926	1.3820	2985.3	0.09781	1.2238	2860.0	0.06812	1.3063
3023.9	0.12930	1.3819	2987.2	0.09765	1.2239	2861.9	0.06813	1.3063
3025.8	0.12934	1.3818	2989.2	0.09749	1.2239	2863.8	0.06813	1.3063
3027.7	0.12938	1.3817	2991.1	0.09733	1.2240	2865.7	0.06814	1.3062
3029.7	0.12942	1.3816	2993.0	0.09717	1.2240	2867.7	0.06814	1.3062
3031.6	0.12947	1.3815	2995.0	0.09701	1.2241	2869.6	0.06815	1.3062
3033.5	0.12951	1.3814	2996.9	0.09685	1.2241	2871.5	0.06815	1.3061
3035.5	0.12955	1.3813	2998.8	0.09670	1.2242	2873.5	0.06816	1.3061
3037.4	0.12959	1.3812	3000.7	0.09654	1.2242	2875.4	0.06816	1.3061
3039.3	0.12963	1.3811	3002.7	0.09638	1.2243	2877.3	0.06816	1.3060
3041.2	0.12967	1.3810	3004.6	0.09622	1.2244	2879.2	0.06817	1.3060
3043.2	0.12971	1.3810	3006.5	0.09607	1.2244	2881.2	0.06817	1.3060
3045.1	0.12975	1.3809	3008.5	0.09591	1.2245	2883.1	0.06817	1.3059
3047.0	0.12979	1.3808	3010.4	0.09576	1.2246	2885.0	0.06818	1.3059
3049.0	0.12983	1.3807	3012.3	0.09560	1.2246	2887.0	0.06818	1.3059
3050.9	0.12986	1.3806	3014.2	0.09545	1.2247	2888.9	0.06818	1.3058
3052.8	0.12990	1.3805	3016.2	0.09529	1.2248	2890.8	0.06819	1.3058
3054.7	0.12994	1.3804	3018.1	0.09514	1.2248	2892.7	0.06819	1.3058
3056.7	0.12998	1.3803	3020.0	0.09499	1.2249	2894.7	0.06819	1.3058
3058.6	0.13002	1.3802	3022.0	0.09483	1.2250	2896.6	0.06819	1.3057
3060.5	0.13006	1.3801	3023.9	0.09468	1.2250	2898.5	0.06819	1.3057
3062.5	0.13010	1.3801	3025.8	0.09453	1.2251	2900.5	0.06820	1.3057
3064.4	0.13014	1.3800	3027.7	0.09438	1.2252	2902.4	0.06820	1.3056
3066.3	0.13018	1.3799	3029.7	0.09423	1.2253	2904.3	0.06820	1.3056
3068.2	0.13022	1.3798	3031.6	0.09408	1.2253	2906.2	0.06820	1.3056
3070.2	0.13027	1.3797	3033.5	0.09393	1.2254	2908.2	0.06820	1.3055
3072.1	0.13031	1.3797	3035.5	0.09378	1.2255	2910.1	0.06820	1.3055
3074.0	0.13035	1.3796	3037.4	0.09363	1.2256	2912.0	0.06820	1.3055
3076.0	0.13039	1.3795	3039.3	0.09348	1.2257	2914.0	0.06820	1.3054
3077.9	0.13043	1.3794	3041.2	0.09333	1.2258	2915.9	0.06821	1.3054
3079.8	0.13048	1.3794	3043.2	0.09319	1.2258	2917.8	0.06821	1.3054
3081.7	0.13052	1.3793	3045.1	0.09304	1.2259	2919.7	0.06821	1.3054
3083.7	0.13056	1.3792	3047.0	0.09289	1.2260	2921.7	0.06821	1.3053
3085.6	0.13061	1.3792	3049.0	0.09275	1.2261	2923.6	0.06821	1.3053
3087.5	0.13065	1.3791	3050.9	0.09260	1.2262	2925.5	0.06821	1.3053
3089.5	0.13070	1.3790	3052.8	0.09246	1.2263	2927.5	0.06821	1.3052
3091.4	0.13075	1.3790	3054.7	0.09231	1.2264	2929.4	0.06820	1.3052
3093.3	0.13079	1.3789	3056.7	0.09217	1.2265	2931.3	0.06820	1.3052
3095.2	0.13084	1.3789	3058.6	0.09203	1.2266	2933.2	0.06820	1.3052
3097.2	0.13089	1.3788	3060.5	0.09188	1.2267	2935.2	0.06820	1.3051
3099.1	0.13094	1.3787	3062.5	0.09174	1.2268	2937.1	0.06820	1.3051
3101.0	0.13100	1.3787	3064.4	0.09160	1.2269	2939.0	0.06820	1.3051

3103.0	0.13105	1.3786	3066.3	0.09146	1.2270	2941.0	0.06820	1.3050
3104.9	0.13110	1.3786	3068.2	0.09132	1.2271	2942.9	0.06820	1.3050
3106.8	0.13116	1.3785	3070.2	0.09118	1.2272	2944.8	0.06819	1.3050
3108.7	0.13122	1.3785	3072.1	0.09104	1.2273	2946.7	0.06819	1.3050
3110.7	0.13127	1.3785	3074.0	0.09091	1.2274	2948.7	0.06819	1.3049
3112.6	0.13133	1.3784	3076.0	0.09077	1.2275	2950.6	0.06819	1.3049
3114.5	0.13139	1.3784	3077.9	0.09063	1.2276	2952.5	0.06818	1.3049
3116.5	0.13146	1.3783	3079.8	0.09050	1.2278	2954.5	0.06818	1.3049
3118.4	0.13152	1.3783	3081.7	0.09036	1.2279	2956.4	0.06818	1.3048
3120.3	0.13159	1.3783	3083.7	0.09023	1.2280	2958.3	0.06818	1.3048
3122.2	0.13166	1.3782	3085.6	0.09010	1.2281	2960.2	0.06817	1.3048
3124.2	0.13173	1.3782	3087.5	0.08996	1.2282	2962.2	0.06817	1.3048
3126.1	0.13180	1.3782	3089.5	0.08983	1.2284	2964.1	0.06817	1.3047
3128.0	0.13187	1.3782	3091.4	0.08970	1.2285	2966.0	0.06816	1.3047
3130.0	0.13195	1.3781	3093.3	0.08957	1.2286	2968.0	0.06816	1.3047
3131.9	0.13203	1.3781	3095.2	0.08944	1.2288	2969.9	0.06815	1.3047
3133.8	0.13211	1.3781	3097.2	0.08931	1.2289	2971.8	0.06815	1.3046
3135.7	0.13220	1.3781	3099.1	0.08919	1.2290	2973.7	0.06815	1.3046
3137.7	0.13228	1.3781	3101.0	0.08906	1.2292	2975.7	0.06814	1.3046
3139.6	0.13237	1.3781	3103.0	0.08894	1.2293	2977.6	0.06814	1.3046
3141.5	0.13247	1.3781	3104.9	0.08881	1.2294	2979.5	0.06813	1.3045
3143.4	0.13256	1.3781	3106.8	0.08869	1.2296	2981.5	0.06813	1.3045
3145.4	0.13266	1.3781	3108.7	0.08857	1.2297	2983.4	0.06812	1.3045
3147.3	0.13277	1.3781	3110.7	0.08844	1.2299	2985.3	0.06812	1.3045
3149.2	0.13287	1.3781	3112.6	0.08832	1.2300	2987.2	0.06811	1.3045
3151.2	0.13298	1.3781	3114.5	0.08820	1.2302	2989.2	0.06811	1.3044
3153.1	0.13310	1.3781	3116.5	0.08809	1.2303	2991.1	0.06810	1.3044
3155.0	0.13321	1.3781	3118.4	0.08797	1.2305	2993.0	0.06810	1.3044
3156.9	0.13333	1.3781	3120.3	0.08785	1.2307	2995.0	0.06809	1.3044
3158.9	0.13346	1.3781	3122.2	0.08774	1.2308	2996.9	0.06808	1.3044
3160.8	0.13359	1.3781	3124.2	0.08763	1.2310	2998.8	0.06808	1.3043
3162.7	0.13373	1.3782	3126.1	0.08751	1.2312	3000.7	0.06807	1.3043
3164.7	0.13386	1.3782	3128.0	0.08740	1.2313	3002.7	0.06806	1.3043
3166.6	0.13401	1.3782	3130.0	0.08729	1.2315	3004.6	0.06806	1.3043
3168.5	0.13416	1.3782	3131.9	0.08719	1.2317	3006.5	0.06805	1.3043
3170.4	0.13431	1.3783	3133.8	0.08708	1.2319	3008.5	0.06804	1.3042
3172.4	0.13447	1.3783	3135.7	0.08697	1.2321	3010.4	0.06804	1.3042
3174.3	0.13464	1.3783	3137.7	0.08687	1.2323	3012.3	0.06803	1.3042
3176.2	0.13481	1.3784	3139.6	0.08677	1.2325	3014.2	0.06802	1.3042
3178.2	0.13499	1.3784	3141.5	0.08667	1.2326	3016.2	0.06801	1.3042
3180.1	0.13517	1.3785	3143.4	0.08657	1.2328	3018.1	0.06801	1.3042
3182.0	0.13536	1.3785	3145.4	0.08647	1.2330	3020.0	0.06800	1.3041
3183.9	0.13556	1.3786	3147.3	0.08638	1.2333	3022.0	0.06799	1.3041

3185.9	0.13577	1.3786	3149.2	0.08628	1.2335	3023.9	0.06798	1.3041
3187.8	0.13598	1.3787	3151.2	0.08619	1.2337	3025.8	0.06797	1.3041
3189.7	0.13620	1.3787	3153.1	0.08610	1.2339	3027.7	0.06797	1.3041
3191.7	0.13642	1.3788	3155.0	0.08602	1.2341	3029.7	0.06796	1.3041
3193.6	0.13666	1.3788	3156.9	0.08593	1.2343	3031.6	0.06795	1.3041
3195.5	0.13690	1.3789	3158.9	0.08585	1.2346	3033.5	0.06794	1.3041
3197.4	0.13715	1.3790	3160.8	0.08577	1.2348	3035.5	0.06793	1.3040
3199.4	0.13742	1.3790	3162.7	0.08569	1.2350	3037.4	0.06792	1.3040
3201.3	0.13769	1.3791	3164.7	0.08561	1.2353	3039.3	0.06791	1.3040
3203.2	0.13797	1.3791	3166.6	0.08554	1.2355	3041.2	0.06790	1.3040
3205.2	0.13825	1.3792	3168.5	0.08547	1.2358	3043.2	0.06790	1.3040
3207.1	0.13855	1.3793	3170.4	0.08540	1.2360	3045.1	0.06789	1.3040
3209.0	0.13886	1.3794	3172.4	0.08533	1.2363	3047.0	0.06788	1.3040
3210.9	0.13918	1.3794	3174.3	0.08527	1.2366	3049.0	0.06787	1.3040
3212.9	0.13952	1.3795	3176.2	0.08521	1.2368	3050.9	0.06786	1.3040
3214.8	0.13986	1.3796	3178.2	0.08515	1.2371	3052.8	0.06785	1.3040
3216.7	0.14021	1.3796	3180.1	0.08510	1.2374	3054.7	0.06784	1.3040
3218.7	0.14058	1.3797	3182.0	0.08505	1.2377	3056.7	0.06783	1.3040
3220.6	0.14096	1.3798	3183.9	0.08500	1.2380	3058.6	0.06782	1.3040
3222.5	0.14135	1.3798	3185.9	0.08496	1.2383	3060.5	0.06781	1.3040
3224.4	0.14176	1.3799	3187.8	0.08492	1.2386	3062.5	0.06780	1.3039
3226.4	0.14218	1.3800	3189.7	0.08488	1.2389	3064.4	0.06779	1.3039
3228.3	0.14261	1.3800	3191.7	0.08485	1.2392	3066.3	0.06778	1.3039
3230.2	0.14306	1.3801	3193.6	0.08482	1.2395	3068.2	0.06776	1.3039
3232.2	0.14352	1.3801	3195.5	0.08480	1.2398	3070.2	0.06775	1.3039
3234.1	0.14400	1.3802	3197.4	0.08478	1.2402	3072.1	0.06774	1.3039
3236.0	0.14449	1.3802	3199.4	0.08476	1.2405	3074.0	0.06773	1.3039
3237.9	0.14500	1.3803	3201.3	0.08475	1.2409	3076.0	0.06772	1.3039
3239.9	0.14553	1.3803	3203.2	0.08475	1.2412	3077.9	0.06771	1.3039
3241.8	0.14607	1.3804	3205.2	0.08475	1.2416	3079.8	0.06770	1.3040
3243.7	0.14663	1.3804	3207.1	0.08476	1.2420	3081.7	0.06769	1.3040
3245.7	0.14721	1.3804	3209.0	0.08477	1.2423	3083.7	0.06768	1.3040
3247.6	0.14780	1.3804	3210.9	0.08479	1.2427	3085.6	0.06766	1.3040
3249.5	0.14842	1.3804	3212.9	0.08482	1.2431	3087.5	0.06765	1.3040
3251.4	0.14905	1.3804	3214.8	0.08485	1.2435	3089.5	0.06764	1.3040
3253.4	0.14970	1.3804	3216.7	0.08490	1.2440	3091.4	0.06763	1.3040
3255.3	0.15037	1.3804	3218.7	0.08494	1.2444	3093.3	0.06762	1.3040
3257.2	0.15106	1.3804	3220.6	0.08500	1.2448	3095.2	0.06761	1.3040
3259.2	0.15177	1.3803	3222.5	0.08506	1.2453	3097.2	0.06759	1.3040
3261.1	0.15250	1.3803	3224.4	0.08514	1.2457	3099.1	0.06758	1.3040
3263.0	0.15325	1.3802	3226.4	0.08522	1.2462	3101.0	0.06757	1.3041
3264.9	0.15403	1.3801	3228.3	0.08531	1.2467	3103.0	0.06756	1.3041
3266.9	0.15482	1.3800	3230.2	0.08542	1.2472	3104.9	0.06755	1.3041

3268.8	0.15563	1.3799	3232.2	0.08553	1.2477	3106.8	0.06753	1.3041
3270.7	0.15647	1.3797	3234.1	0.08566	1.2482	3108.7	0.06752	1.3041
3272.7	0.15732	1.3796	3236.0	0.08580	1.2487	3110.7	0.06751	1.3041
3274.6	0.15820	1.3794	3237.9	0.08595	1.2492	3112.6	0.06750	1.3042
3276.5	0.15910	1.3792	3239.9	0.08611	1.2498	3114.5	0.06749	1.3042
3278.4	0.16001	1.3789	3241.8	0.08629	1.2503	3116.5	0.06747	1.3042
3280.4	0.16095	1.3787	3243.7	0.08648	1.2509	3118.4	0.06746	1.3042
3282.3	0.16191	1.3784	3245.7	0.08669	1.2515	3120.3	0.06745	1.3042
3284.2	0.16289	1.3780	3247.6	0.08692	1.2521	3122.2	0.06744	1.3043
3286.2	0.16388	1.3777	3249.5	0.08717	1.2528	3124.2	0.06743	1.3043
3288.1	0.16490	1.3773	3251.4	0.08743	1.2534	3126.1	0.06741	1.3043
3290.0	0.16593	1.3769	3253.4	0.08772	1.2541	3128.0	0.06740	1.3044
3291.9	0.16697	1.3764	3255.3	0.08803	1.2547	3130.0	0.06739	1.3044
3293.9	0.16804	1.3759	3257.2	0.08836	1.2554	3131.9	0.06738	1.3044
3295.8	0.16911	1.3754	3259.2	0.08871	1.2561	3133.8	0.06736	1.3044
3297.7	0.17020	1.3748	3261.1	0.08909	1.2569	3135.7	0.06735	1.3045
3299.7	0.17131	1.3742	3263.0	0.08950	1.2576	3137.7	0.06734	1.3045
3301.6	0.17242	1.3735	3264.9	0.08994	1.2584	3139.6	0.06733	1.3046
3303.5	0.17354	1.3728	3266.9	0.09042	1.2591	3141.5	0.06732	1.3046
3305.4	0.17466	1.3720	3268.8	0.09092	1.2599	3143.4	0.06731	1.3046
3307.4	0.17579	1.3712	3270.7	0.09147	1.2608	3145.4	0.06729	1.3047
3309.3	0.17692	1.3703	3272.7	0.09205	1.2616	3147.3	0.06728	1.3047
3311.2	0.17804	1.3694	3274.6	0.09268	1.2625	3149.2	0.06727	1.3048
3313.2	0.17917	1.3684	3276.5	0.09335	1.2634	3151.2	0.06726	1.3048
3315.1	0.18028	1.3674	3278.4	0.09407	1.2643	3153.1	0.06725	1.3049
3317.0	0.18139	1.3663	3280.4	0.09484	1.2652	3155.0	0.06724	1.3049
3318.9	0.18248	1.3651	3282.3	0.09567	1.2662	3156.9	0.06723	1.3050
3320.9	0.18356	1.3639	3284.2	0.09656	1.2671	3158.9	0.06722	1.3050
3322.8	0.18462	1.3627	3286.2	0.09751	1.2681	3160.8	0.06721	1.3051
3324.7	0.18565	1.3613	3288.1	0.09854	1.2691	3162.7	0.06720	1.3051
3326.7	0.18665	1.3599	3290.0	0.09964	1.2701	3164.7	0.06719	1.3052
3328.6	0.18763	1.3585	3291.9	0.10082	1.2712	3166.6	0.06718	1.3053
3330.5	0.18857	1.3570	3293.9	0.10209	1.2722	3168.5	0.06717	1.3053
3332.4	0.18946	1.3554	3295.8	0.10345	1.2733	3170.4	0.06716	1.3054
3334.4	0.19032	1.3538	3297.7	0.10491	1.2744	3172.4	0.06715	1.3055
3336.3	0.19113	1.3521	3299.7	0.10649	1.2755	3174.3	0.06714	1.3055
3338.2	0.19189	1.3504	3301.6	0.10818	1.2765	3176.2	0.06713	1.3056
3340.2	0.19259	1.3486	3303.5	0.11000	1.2776	3178.2	0.06712	1.3057
3342.1	0.19324	1.3468	3305.4	0.11195	1.2787	3180.1	0.06711	1.3058
3344.0	0.19382	1.3449	3307.4	0.11405	1.2797	3182.0	0.06711	1.3058
3345.9	0.19434	1.3430	3309.3	0.11631	1.2807	3183.9	0.06710	1.3059
3347.9	0.19479	1.3411	3311.2	0.11873	1.2817	3185.9	0.06709	1.3060
3349.8	0.19517	1.3391	3313.2	0.12132	1.2826	3187.8	0.06708	1.3061

3351.7	0.19548	1.3371	3315.1	0.12411	1.2834	3189.7	0.06708	1.3062
3353.7	0.19571	1.3350	3317.0	0.12709	1.2841	3191.7	0.06707	1.3063
3355.6	0.19586	1.3330	3318.9	0.13028	1.2847	3193.6	0.06707	1.3064
3357.5	0.19594	1.3309	3320.9	0.13368	1.2852	3195.5	0.06706	1.3065
3359.4	0.19593	1.3288	3322.8	0.13730	1.2855	3197.4	0.06706	1.3066
3361.4	0.19585	1.3267	3324.7	0.14115	1.2856	3199.4	0.06706	1.3067
3363.3	0.19568	1.3247	3326.7	0.14521	1.2855	3201.3	0.06705	1.3068
3365.2	0.19544	1.3226	3328.6	0.14949	1.2850	3203.2	0.06705	1.3069
3367.2	0.19511	1.3205	3330.5	0.15397	1.2843	3205.2	0.06705	1.3071
3369.1	0.19471	1.3184	3332.4	0.15864	1.2831	3207.1	0.06705	1.3072
3371.0	0.19422	1.3164	3334.4	0.16345	1.2815	3209.0	0.06705	1.3073
3372.9	0.19367	1.3143	3336.3	0.16838	1.2795	3210.9	0.06705	1.3074
3374.9	0.19303	1.3123	3338.2	0.17336	1.2769	3212.9	0.06705	1.3076
3376.8	0.19233	1.3104	3340.2	0.17834	1.2738	3214.8	0.06705	1.3077
3378.7	0.19155	1.3084	3342.1	0.18322	1.2701	3216.7	0.06706	1.3078
3380.7	0.19071	1.3065	3344.0	0.18793	1.2657	3218.7	0.06706	1.3080
3382.6	0.18981	1.3047	3345.9	0.19236	1.2607	3220.6	0.06706	1.3081
3384.5	0.18885	1.3029	3347.9	0.19641	1.2552	3222.5	0.06707	1.3083
3386.4	0.18783	1.3011	3349.8	0.19996	1.2490	3224.4	0.06708	1.3085
3388.4	0.18675	1.2994	3351.7	0.20292	1.2424	3226.4	0.06709	1.3086
3390.3	0.18563	1.2977	3353.7	0.20519	1.2354	3228.3	0.06710	1.3088
3392.2	0.18446	1.2961	3355.6	0.20670	1.2280	3230.2	0.06711	1.3090
3394.2	0.18325	1.2946	3357.5	0.20741	1.2205	3232.2	0.06712	1.3092
3396.1	0.18200	1.2931	3359.4	0.20728	1.2129	3234.1	0.06713	1.3093
3398.0	0.18071	1.2916	3361.4	0.20634	1.2054	3236.0	0.06715	1.3095
3399.9	0.17939	1.2902	3363.3	0.20461	1.1982	3237.9	0.06717	1.3097
3401.9	0.17805	1.2889	3365.2	0.20216	1.1913	3239.9	0.06719	1.3100
3403.8	0.17668	1.2876	3367.2	0.19907	1.1848	3241.8	0.06721	1.3102
3405.7	0.17530	1.2864	3369.1	0.19544	1.1788	3243.7	0.06723	1.3104
3407.7	0.17389	1.2853	3371.0	0.19135	1.1734	3245.7	0.06726	1.3106
3409.6	0.17247	1.2842	3372.9	0.18693	1.1685	3247.6	0.06728	1.3109
3411.5	0.17104	1.2831	3374.9	0.18226	1.1643	3249.5	0.06731	1.3111
3413.4	0.16960	1.2821	3376.8	0.17744	1.1606	3251.4	0.06734	1.3113
3415.4	0.16815	1.2812	3378.7	0.17255	1.1575	3253.4	0.06738	1.3116
3417.3	0.16671	1.2803	3380.7	0.16765	1.1549	3255.3	0.06742	1.3119
3419.2	0.16526	1.2795	3382.6	0.16282	1.1528	3257.2	0.06746	1.3122
3421.2	0.16381	1.2787	3384.5	0.15808	1.1511	3259.2	0.06750	1.3124
3423.1	0.16236	1.2780	3386.4	0.15348	1.1498	3261.1	0.06755	1.3127
3425.0	0.16093	1.2773	3388.4	0.14904	1.1489	3263.0	0.06760	1.3130
3426.9	0.15949	1.2767	3390.3	0.14478	1.1483	3264.9	0.06765	1.3134
3428.9	0.15807	1.2761	3392.2	0.14072	1.1479	3266.9	0.06771	1.3137
3430.8	0.15666	1.2755	3394.2	0.13685	1.1478	3268.8	0.06777	1.3140
3432.7	0.15525	1.2750	3396.1	0.13317	1.1479	3270.7	0.06784	1.3144

3434.7	0.15386	1.2745	3398.0	0.12969	1.1481	3272.7	0.06791	1.3148
3436.6	0.15249	1.2741	3399.9	0.12641	1.1485	3274.6	0.06799	1.3151
3438.5	0.15113	1.2737	3401.9	0.12331	1.1490	3276.5	0.06807	1.3155
3440.4	0.14978	1.2733	3403.8	0.12038	1.1496	3278.4	0.06816	1.3159
3442.4	0.14845	1.2730	3405.7	0.11762	1.1502	3280.4	0.06826	1.3164
3444.3	0.14713	1.2727	3407.7	0.11502	1.1510	3282.3	0.06836	1.3168
3446.2	0.14584	1.2724	3409.6	0.11258	1.1518	3284.2	0.06847	1.3173
3448.2	0.14456	1.2722	3411.5	0.11027	1.1526	3286.2	0.06859	1.3177
3450.1	0.14330	1.2720	3413.4	0.10810	1.1534	3288.1	0.06871	1.3182
3452.0	0.14205	1.2718	3415.4	0.10605	1.1543	3290.0	0.06885	1.3187
3453.9	0.14083	1.2716	3417.3	0.10412	1.1552	3291.9	0.06899	1.3193
3455.9	0.13962	1.2715	3419.2	0.10230	1.1561	3293.9	0.06915	1.3198
3457.8	0.13843	1.2713	3421.2	0.10058	1.1570	3295.8	0.06932	1.3204
3459.7	0.13726	1.2712	3423.1	0.09896	1.1579	3297.7	0.06950	1.3210
3461.7	0.13611	1.2712	3425.0	0.09742	1.1588	3299.7	0.06969	1.3216
3463.6	0.13498	1.2711	3426.9	0.09597	1.1596	3301.6	0.06990	1.3223
3465.5	0.13387	1.2710	3428.9	0.09459	1.1605	3303.5	0.07012	1.3230
3467.4	0.13277	1.2710	3430.8	0.09329	1.1614	3305.4	0.07037	1.3237
3469.4	0.13169	1.2710	3432.7	0.09205	1.1622	3307.4	0.07063	1.3244
3471.3	0.13063	1.2710	3434.7	0.09087	1.1631	3309.3	0.07091	1.3252
3473.2	0.12959	1.2710	3436.6	0.08976	1.1639	3311.2	0.07121	1.3260
3475.2	0.12857	1.2711	3438.5	0.08869	1.1647	3313.2	0.07154	1.3269
3477.1	0.12756	1.2711	3440.4	0.08768	1.1655	3315.1	0.07190	1.3278
3479.0	0.12657	1.2711	3442.4	0.08672	1.1663	3317.0	0.07228	1.3287
3480.9	0.12560	1.2712	3444.3	0.08580	1.1671	3318.9	0.07270	1.3297
3482.9	0.12465	1.2713	3446.2	0.08492	1.1678	3320.9	0.07316	1.3307
3484.8	0.12371	1.2714	3448.2	0.08408	1.1686	3322.8	0.07365	1.3318
3486.7	0.12278	1.2715	3450.1	0.08327	1.1693	3324.7	0.07419	1.3329
3488.7	0.12188	1.2716	3452.0	0.08250	1.1700	3326.7	0.07477	1.3341
3490.6	0.12098	1.2717	3453.9	0.08177	1.1707	3328.6	0.07542	1.3354
3492.5	0.12011	1.2718	3455.9	0.08106	1.1714	3330.5	0.07612	1.3367
3494.4	0.11925	1.2719	3457.8	0.08038	1.1720	3332.4	0.07689	1.3381
3496.4	0.11840	1.2720	3459.7	0.07973	1.1727	3334.4	0.07773	1.3396
3498.3	0.11756	1.2722	3461.7	0.07910	1.1733	3336.3	0.07866	1.3411
3500.2	0.11675	1.2723	3463.6	0.07850	1.1739	3338.2	0.07969	1.3428
3502.2	0.11594	1.2724	3465.5	0.07792	1.1745	3340.2	0.08082	1.3445
3504.1	0.11515	1.2726	3467.4	0.07736	1.1751	3342.1	0.08208	1.3463
3506.0	0.11437	1.2727	3469.4	0.07682	1.1757	3344.0	0.08347	1.3483
3507.9	0.11360	1.2729	3471.3	0.07630	1.1763	3345.9	0.08502	1.3503
3509.9	0.11285	1.2730	3473.2	0.07579	1.1768	3347.9	0.08675	1.3525
3511.8	0.11211	1.2732	3475.2	0.07531	1.1774	3349.8	0.08869	1.3548
3513.7	0.11138	1.2734	3477.1	0.07484	1.1779	3351.7	0.09086	1.3572
3515.7	0.11066	1.2735	3479.0	0.07438	1.1784	3353.7	0.09331	1.3598

3517.6	0.10996	1.2737	3480.9	0.07394	1.1789	3355.6	0.09607	1.3625
3519.5	0.10926	1.2739	3482.9	0.07351	1.1794	3357.5	0.09919	1.3654
3521.4	0.10858	1.2741	3484.8	0.07309	1.1799	3359.4	0.10274	1.3684
3523.4	0.10790	1.2742	3486.7	0.07269	1.1804	3361.4	0.10680	1.3716
3525.3	0.10724	1.2744	3488.7	0.07230	1.1808	3363.3	0.11145	1.3750
3527.2	0.10659	1.2746	3490.6	0.07192	1.1813	3365.2	0.11681	1.3785
3529.2	0.10594	1.2748	3492.5	0.07155	1.1818	3367.2	0.12301	1.3821
3531.1	0.10531	1.2750	3494.4	0.07119	1.1822	3369.1	0.13027	1.3858
3533.0	0.10468	1.2751	3496.4	0.07084	1.1826	3371.0	0.13881	1.3896
3534.9	0.10407	1.2753	3498.3	0.07049	1.1830	3372.9	0.14902	1.3933
3536.9	0.10346	1.2755	3500.2	0.07016	1.1835	3374.9	0.16137	1.3966
3538.8	0.10286	1.2757	3502.2	0.06984	1.1839	3376.8	0.17657	1.3991
3540.7	0.10227	1.2759	3504.1	0.06952	1.1843	3378.7	0.19549	1.3997
3542.6	0.10169	1.2761	3506.0	0.06921	1.1846	3380.7	0.21888	1.3962
3544.6	0.10112	1.2763	3507.9	0.06891	1.1850	3382.6	0.24617	1.3848
3546.5	0.10056	1.2765	3509.9	0.06861	1.1854	3384.5	0.27317	1.3611
3548.4	0.10000	1.2766	3511.8	0.06832	1.1858	3386.4	0.29091	1.3246
3550.4	0.09945	1.2768	3513.7	0.06804	1.1861	3388.4	0.29184	1.2835
3552.3	0.09891	1.2770	3515.7	0.06776	1.1865	3390.3	0.27801	1.2490
3554.2	0.09837	1.2772	3517.6	0.06749	1.1868	3392.2	0.25763	1.2255
3556.1	0.09785	1.2774	3519.5	0.06722	1.1872	3394.2	0.23694	1.2111
3558.1	0.09732	1.2776	3521.4	0.06696	1.1875	3396.1	0.21832	1.2026
3560.0	0.09681	1.2778	3523.4	0.06671	1.1878	3398.0	0.20207	1.1977
3561.9	0.09630	1.2780	3525.3	0.06646	1.1882	3399.9	0.18790	1.1950
3563.9	0.09580	1.2782	3527.2	0.06621	1.1885	3401.9	0.17545	1.1937
3565.8	0.09531	1.2783	3529.2	0.06597	1.1888	3403.8	0.16442	1.1934
3567.7	0.09482	1.2785	3531.1	0.06573	1.1891	3405.7	0.15461	1.1940
3569.6	0.09433	1.2787	3533.0	0.06550	1.1894	3407.7	0.14588	1.1951
3571.6	0.09386	1.2789	3534.9	0.06527	1.1897	3409.6	0.13811	1.1966
3573.5	0.09339	1.2791	3536.9	0.06505	1.1900	3411.5	0.13119	1.1985
3575.4	0.09292	1.2793	3538.8	0.06483	1.1903	3413.4	0.12502	1.2005
3577.4	0.09246	1.2795	3540.7	0.06461	1.1906	3415.4	0.11954	1.2027
3579.3	0.09200	1.2797	3542.6	0.06439	1.1908	3417.3	0.11465	1.2049
3581.2	0.09155	1.2798	3544.6	0.06418	1.1911	3419.2	0.11029	1.2072
3583.1	0.09111	1.2800	3546.5	0.06398	1.1914	3421.2	0.10640	1.2094
3585.1	0.09067	1.2802	3548.4	0.06377	1.1917	3423.1	0.10292	1.2116
3587.0	0.09023	1.2804	3550.4	0.06357	1.1919	3425.0	0.09980	1.2138
3588.9	0.08980	1.2806	3552.3	0.06337	1.1922	3426.9	0.09700	1.2159
3590.9	0.08938	1.2807	3554.2	0.06318	1.1924	3428.9	0.09448	1.2179
3592.8	0.08896	1.2809	3556.1	0.06298	1.1927	3430.8	0.09220	1.2198
3594.7	0.08854	1.2811	3558.1	0.06279	1.1929	3432.7	0.09014	1.2217
3596.6	0.08813	1.2813	3560.0	0.06260	1.1932	3434.7	0.08827	1.2234
3598.6	0.08772	1.2815	3561.9	0.06242	1.1934	3436.6	0.08657	1.2251

3600.5	0.08732	1.2816	3563.9	0.06224	1.1937	3438.5	0.08502	1.2268
3602.4	0.08692	1.2818	3565.8	0.06205	1.1939	3440.4	0.08361	1.2283
3604.4	0.08652	1.2820	3567.7	0.06188	1.1941	3442.4	0.08231	1.2298
3606.3	0.08613	1.2822	3569.6	0.06170	1.1943	3444.3	0.08112	1.2312
3608.2	0.08574	1.2824	3571.6	0.06153	1.1946	3446.2	0.08002	1.2325
3610.1	0.08536	1.2825	3573.5	0.06135	1.1948	3448.2	0.07901	1.2338
3612.1	0.08498	1.2827	3575.4	0.06118	1.1950	3450.1	0.07808	1.2350
3614.0	0.08460	1.2829	3577.4	0.06101	1.1952	3452.0	0.07721	1.2362
3615.9	0.08423	1.2830	3579.3	0.06085	1.1954	3453.9	0.07641	1.2373
3617.9	0.08386	1.2832	3581.2	0.06068	1.1956	3455.9	0.07566	1.2383
3619.8	0.08349	1.2834	3583.1	0.06052	1.1959	3457.8	0.07496	1.2393
3621.7	0.08313	1.2836	3585.1	0.06036	1.1961	3459.7	0.07431	1.2403
3623.6	0.08277	1.2837	3587.0	0.06020	1.1963	3461.7	0.07370	1.2412
3625.6	0.08241	1.2839	3588.9	0.06004	1.1965	3463.6	0.07313	1.2421
3627.5	0.08206	1.2841	3590.9	0.05988	1.1967	3465.5	0.07260	1.2430
3629.4	0.08171	1.2842	3592.8	0.05973	1.1968	3467.4	0.07209	1.2438
3631.4	0.08136	1.2844	3594.7	0.05958	1.1970	3469.4	0.07162	1.2445
3633.3	0.08102	1.2846	3596.6	0.05942	1.1972	3471.3	0.07117	1.2453
3635.2	0.08068	1.2847	3598.6	0.05927	1.1974	3473.2	0.07074	1.2460
3637.1	0.08034	1.2849	3600.5	0.05912	1.1976	3475.2	0.07034	1.2467
3639.1	0.08000	1.2851	3602.4	0.05898	1.1978	3477.1	0.06996	1.2473
3641.0	0.07967	1.2852	3604.4	0.05883	1.1980	3479.0	0.06960	1.2480
3642.9	0.07934	1.2854	3606.3	0.05868	1.1982	3480.9	0.06926	1.2486
3644.9	0.07902	1.2856	3608.2	0.05854	1.1983	3482.9	0.06893	1.2491
3646.8	0.07869	1.2857	3610.1	0.05840	1.1985	3484.8	0.06862	1.2497
3648.7	0.07837	1.2859	3612.1	0.05826	1.1987	3486.7	0.06832	1.2502
3650.6	0.07805	1.2860	3614.0	0.05812	1.1989	3488.7	0.06804	1.2508
3652.6	0.07773	1.2862	3615.9	0.05798	1.1990	3490.6	0.06776	1.2513
3654.5	0.07742	1.2864	3617.9	0.05784	1.1992	3492.5	0.06750	1.2517
3656.4	0.07711	1.2865	3619.8	0.05770	1.1994	3494.4	0.06725	1.2522
3658.4	0.07680	1.2867	3621.7	0.05756	1.1995	3496.4	0.06701	1.2526
3660.3	0.07649	1.2868	3623.6	0.05743	1.1997	3498.3	0.06678	1.2531
3662.2	0.07619	1.2870	3625.6	0.05729	1.1998	3500.2	0.06656	1.2535
3664.1	0.07588	1.2871	3627.5	0.05716	1.2000	3502.2	0.06635	1.2539
3666.1	0.07558	1.2873	3629.4	0.05703	1.2002	3504.1	0.06614	1.2543
3668.0	0.07529	1.2874	3631.4	0.05690	1.2003	3506.0	0.06594	1.2547
3669.9	0.07499	1.2876	3633.3	0.05677	1.2005	3507.9	0.06575	1.2550
3671.9	0.07470	1.2878	3635.2	0.05664	1.2006	3509.9	0.06556	1.2554
3673.8	0.07441	1.2879	3637.1	0.05651	1.2008	3511.8	0.06538	1.2557
3675.7	0.07412	1.2881	3639.1	0.05638	1.2009	3513.7	0.06521	1.2560
3677.6	0.07383	1.2882	3641.0	0.05625	1.2011	3515.7	0.06504	1.2564
3679.6	0.07354	1.2884	3642.9	0.05613	1.2012	3517.6	0.06488	1.2567
3681.5	0.07326	1.2885	3644.9	0.05600	1.2014	3519.5	0.06472	1.2570

3683.4	0.07298	1.2887	3646.8	0.05588	1.2015	3521.4	0.06456	1.2573
3685.4	0.07270	1.2888	3648.7	0.05575	1.2017	3523.4	0.06441	1.2575
3687.3	0.07242	1.2890	3650.6	0.05563	1.2018	3525.3	0.06426	1.2578
3689.2	0.07215	1.2891	3652.6	0.05551	1.2020	3527.2	0.06412	1.2581
3691.1	0.07187	1.2893	3654.5	0.05539	1.2021	3529.2	0.06398	1.2583
3693.1	0.07160	1.2894	3656.4	0.05527	1.2022	3531.1	0.06385	1.2586
3695.0	0.07133	1.2896	3658.4	0.05515	1.2024	3533.0	0.06371	1.2588
3696.9	0.07106	1.2897	3660.3	0.05503	1.2025	3534.9	0.06358	1.2591
3698.9	0.07080	1.2898	3662.2	0.05491	1.2026	3536.9	0.06346	1.2593
3700.8	0.07053	1.2900	3664.1	0.05479	1.2028	3538.8	0.06333	1.2595
3702.7	0.07027	1.2901	3666.1	0.05467	1.2029	3540.7	0.06321	1.2597
3704.6	0.07001	1.2903	3668.0	0.05456	1.2030	3542.6	0.06309	1.2599
3706.6	0.06975	1.2904	3669.9	0.05444	1.2032	3544.6	0.06298	1.2601
3708.5	0.06949	1.2906	3671.9	0.05433	1.2033	3546.5	0.06286	1.2603
3710.4	0.06923	1.2907	3673.8	0.05421	1.2034	3548.4	0.06275	1.2605
3712.4	0.06898	1.2908	3675.7	0.05410	1.2036	3550.4	0.06264	1.2607
3714.3	0.06872	1.2910	3677.6	0.05398	1.2037	3552.3	0.06253	1.2609
3716.2	0.06847	1.2911	3679.6	0.05387	1.2038	3554.2	0.06243	1.2611
3718.1	0.06822	1.2913	3681.5	0.05376	1.2039	3556.1	0.06232	1.2612
3720.1	0.06797	1.2914	3683.4	0.05365	1.2041	3558.1	0.06222	1.2614
3722.0	0.06772	1.2916	3685.4	0.05354	1.2042	3560.0	0.06212	1.2616
3723.9	0.06748	1.2917	3687.3	0.05342	1.2043	3561.9	0.06202	1.2617
3725.9	0.06723	1.2918	3689.2	0.05331	1.2044	3563.9	0.06192	1.2619
3727.8	0.06699	1.2920	3691.1	0.05320	1.2046	3565.8	0.06183	1.2620
3729.7	0.06675	1.2921	3693.1	0.05310	1.2047	3567.7	0.06173	1.2622
3731.6	0.06651	1.2922	3695.0	0.05299	1.2048	3569.6	0.06164	1.2623
3733.6	0.06627	1.2924	3696.9	0.05288	1.2049	3571.6	0.06154	1.2625
3735.5	0.06603	1.2925	3698.9	0.05277	1.2050	3573.5	0.06145	1.2626
3737.4	0.06580	1.2927	3700.8	0.05266	1.2052	3575.4	0.06136	1.2627
3739.4	0.06556	1.2928	3702.7	0.05256	1.2053	3577.4	0.06127	1.2628
3741.3	0.06533	1.2929	3704.6	0.05245	1.2054	3579.3	0.06119	1.2630
3743.2	0.06510	1.2931	3706.6	0.05235	1.2055	3581.2	0.06110	1.2631
3745.1	0.06487	1.2932	3708.5	0.05224	1.2056	3583.1	0.06101	1.2632
3747.1	0.06464	1.2933	3710.4	0.05214	1.2057	3585.1	0.06093	1.2633
3749.0	0.06441	1.2935	3712.4	0.05203	1.2058	3587.0	0.06084	1.2634
3750.9	0.06418	1.2936	3714.3	0.05193	1.2059	3588.9	0.06076	1.2636
3752.9	0.06396	1.2937	3716.2	0.05182	1.2061	3590.9	0.06068	1.2637
3754.8	0.06374	1.2939	3718.1	0.05172	1.2062	3592.8	0.06060	1.2638
3756.7	0.06351	1.2940	3720.1	0.05162	1.2063	3594.7	0.06052	1.2639
3758.6	0.06329	1.2941	3722.0	0.05152	1.2064	3596.6	0.06044	1.2640
3760.6	0.06307	1.2943	3723.9	0.05141	1.2065	3598.6	0.06036	1.2641
3762.5	0.06285	1.2944	3725.9	0.05131	1.2066	3600.5	0.06028	1.2642
3764.4	0.06263	1.2945	3727.8	0.05121	1.2067	3602.4	0.06020	1.2643

3766.4	0.06242	1.2947	3729.7	0.05111	1.2068	3604.4	0.06012	1.2643
3768.3	0.06220	1.2948	3731.6	0.05101	1.2069	3606.3	0.06005	1.2644
3770.2	0.06199	1.2949	3733.6	0.05091	1.2070	3608.2	0.05997	1.2645
3772.1	0.06177	1.2951	3735.5	0.05081	1.2071	3610.1	0.05990	1.2646
3774.1	0.06156	1.2952	3737.4	0.05071	1.2072	3612.1	0.05982	1.2647
3776.0	0.06135	1.2953	3739.4	0.05062	1.2073	3614.0	0.05975	1.2648
3777.9	0.06114	1.2954	3741.3	0.05052	1.2074	3615.9	0.05967	1.2648
3779.9	0.06093	1.2956	3743.2	0.05042	1.2075	3617.9	0.05960	1.2649
3781.8	0.06072	1.2957	3745.1	0.05032	1.2076	3619.8	0.05953	1.2650
3783.7	0.06051	1.2958	3747.1	0.05023	1.2077	3621.7	0.05946	1.2651
3785.6	0.06031	1.2960	3749.0	0.05013	1.2078	3623.6	0.05938	1.2651
3787.6	0.06010	1.2961	3750.9	0.05003	1.2079	3625.6	0.05931	1.2652
3789.5	0.05990	1.2962	3752.9	0.04994	1.2080	3627.5	0.05924	1.2653
3791.4	0.05970	1.2963	3754.8	0.04984	1.2081	3629.4	0.05917	1.2653
3793.4	0.05950	1.2965	3756.7	0.04975	1.2082	3631.4	0.05910	1.2654
3795.3	0.05929	1.2966	3758.6	0.04965	1.2083	3633.3	0.05903	1.2655
3797.2	0.05910	1.2967	3760.6	0.04956	1.2084	3635.2	0.05896	1.2655
3799.1	0.05890	1.2969	3762.5	0.04946	1.2085	3637.1	0.05889	1.2656
3801.1	0.05870	1.2970	3764.4	0.04937	1.2086	3639.1	0.05883	1.2657
3803.0	0.05850	1.2971	3766.4	0.04927	1.2087	3641.0	0.05876	1.2657
3804.9	0.05831	1.2972	3768.3	0.04918	1.2088	3642.9	0.05869	1.2658
3806.9	0.05811	1.2974	3770.2	0.04909	1.2089	3644.9	0.05862	1.2658
3808.8	0.05792	1.2975	3772.1	0.04900	1.2090	3646.8	0.05855	1.2659
3810.7	0.05773	1.2976	3774.1	0.04890	1.2091	3648.7	0.05849	1.2659
3812.6	0.05753	1.2977	3776.0	0.04881	1.2092	3650.6	0.05842	1.2660
3814.6	0.05734	1.2978	3777.9	0.04872	1.2093	3652.6	0.05835	1.2660
3816.5	0.05715	1.2980	3779.9	0.04863	1.2094	3654.5	0.05829	1.2661
3818.4	0.05696	1.2981	3781.8	0.04854	1.2095	3656.4	0.05822	1.2661
3820.4	0.05678	1.2982	3783.7	0.04845	1.2096	3658.4	0.05816	1.2662
3822.3	0.05659	1.2983	3785.6	0.04836	1.2096	3660.3	0.05809	1.2662
3824.2	0.05640	1.2985	3787.6	0.04827	1.2097	3662.2	0.05803	1.2663
3826.1	0.05622	1.2986	3789.5	0.04818	1.2098	3664.1	0.05796	1.2663
3828.1	0.05603	1.2987	3791.4	0.04809	1.2099	3666.1	0.05790	1.2664
3830.0	0.05585	1.2988	3793.4	0.04800	1.2100	3668.0	0.05783	1.2664
3831.9	0.05567	1.2990	3795.3	0.04791	1.2101	3669.9	0.05777	1.2664
3833.9	0.05548	1.2991	3797.2	0.04782	1.2102	3671.9	0.05770	1.2665
3835.8	0.05530	1.2992	3799.1	0.04773	1.2103	3673.8	0.05764	1.2665
3837.7	0.05512	1.2993	3801.1	0.04764	1.2104	3675.7	0.05758	1.2666
3839.6	0.05494	1.2994	3803.0	0.04756	1.2104	3677.6	0.05751	1.2666
3841.6	0.05476	1.2996	3804.9	0.04747	1.2105	3679.6	0.05745	1.2666
3843.5	0.05459	1.2997	3806.9	0.04738	1.2106	3681.5	0.05739	1.2667
3845.4	0.05441	1.2998	3808.8	0.04729	1.2107	3683.4	0.05732	1.2667
3847.4	0.05423	1.2999	3810.7	0.04721	1.2108	3685.4	0.05726	1.2667

3849.3	0.05406	1.3000	3812.6	0.04712	1.2109	3687.3	0.05720	1.2668
3851.2	0.05388	1.3002	3814.6	0.04703	1.2110	3689.2	0.05713	1.2668
3853.1	0.05371	1.3003	3816.5	0.04695	1.2110	3691.1	0.05707	1.2668
3855.1	0.05354	1.3004	3818.4	0.04686	1.2111	3693.1	0.05701	1.2669
3857.0	0.05336	1.3005	3820.4	0.04678	1.2112	3695.0	0.05695	1.2669
3858.9	0.05319	1.3006	3822.3	0.04669	1.2113	3696.9	0.05689	1.2669
3860.9	0.05302	1.3007	3824.2	0.04661	1.2114	3698.9	0.05682	1.2670
3862.8	0.05285	1.3009	3826.1	0.04652	1.2115	3700.8	0.05676	1.2670
3864.7	0.05268	1.3010	3828.1	0.04644	1.2115	3702.7	0.05670	1.2670
3866.6	0.05252	1.3011	3830.0	0.04635	1.2116	3704.6	0.05664	1.2670
3868.6	0.05235	1.3012	3831.9	0.04627	1.2117	3706.6	0.05658	1.2671
3870.5	0.05218	1.3013	3833.9	0.04619	1.2118	3708.5	0.05652	1.2671
3872.4	0.05202	1.3014	3835.8	0.04610	1.2119	3710.4	0.05646	1.2671
3874.4	0.05185	1.3016	3837.7	0.04602	1.2120	3712.4	0.05640	1.2672
3876.3	0.05169	1.3017	3839.6	0.04594	1.2120	3714.3	0.05634	1.2672
3878.2	0.05152	1.3018	3841.6	0.04585	1.2121	3716.2	0.05627	1.2672
3880.1	0.05136	1.3019	3843.5	0.04577	1.2122	3718.1	0.05621	1.2672
3882.1	0.05120	1.3020	3845.4	0.04569	1.2123	3720.1	0.05615	1.2672
3884.0	0.05104	1.3021	3847.4	0.04561	1.2124	3722.0	0.05609	1.2673
3885.9	0.05088	1.3023	3849.3	0.04553	1.2124	3723.9	0.05603	1.2673
3887.8	0.05072	1.3024	3851.2	0.04545	1.2125	3725.9	0.05597	1.2673
3889.8	0.05056	1.3025	3853.1	0.04536	1.2126	3727.8	0.05591	1.2673
3891.7	0.05040	1.3026	3855.1	0.04528	1.2127	3729.7	0.05585	1.2673
3893.6	0.05024	1.3027	3857.0	0.04520	1.2127	3731.6	0.05579	1.2674
3895.6	0.05008	1.3028	3858.9	0.04512	1.2128	3733.6	0.05573	1.2674
3897.5	0.04993	1.3029	3860.9	0.04504	1.2129	3735.5	0.05567	1.2674
3899.4	0.04977	1.3031	3862.8	0.04496	1.2130	3737.4	0.05561	1.2674
3901.3	0.04961	1.3032	3864.7	0.04488	1.2131	3739.4	0.05556	1.2674
3903.3	0.04946	1.3033	3866.6	0.04480	1.2131	3741.3	0.05550	1.2675
3905.2	0.04931	1.3034	3868.6	0.04472	1.2132	3743.2	0.05544	1.2675
3907.1	0.04915	1.3035	3870.5	0.04464	1.2133	3745.1	0.05538	1.2675
3909.1	0.04900	1.3036	3872.4	0.04456	1.2134	3747.1	0.05532	1.2675
3911.0	0.04885	1.3037	3874.4	0.04448	1.2134	3749.0	0.05526	1.2675
3912.9	0.04870	1.3038	3876.3	0.04441	1.2135	3750.9	0.05520	1.2675
3914.8	0.04855	1.3040	3878.2	0.04433	1.2136	3752.9	0.05514	1.2676
3916.8	0.04840	1.3041	3880.1	0.04425	1.2137	3754.8	0.05508	1.2676
3918.7	0.04825	1.3042	3882.1	0.04417	1.2137	3756.7	0.05502	1.2676
3920.6	0.04810	1.3043	3884.0	0.04409	1.2138	3758.6	0.05496	1.2676
3922.6	0.04795	1.3044	3885.9	0.04402	1.2139	3760.6	0.05491	1.2676
3924.5	0.04780	1.3045	3887.8	0.04394	1.2140	3762.5	0.05485	1.2676
3926.4	0.04766	1.3046	3889.8	0.04386	1.2140	3764.4	0.05479	1.2676
3928.3	0.04751	1.3047	3891.7	0.04378	1.2141	3766.4	0.05473	1.2677
3930.3	0.04736	1.3048	3893.6	0.04371	1.2142	3768.3	0.05467	1.2677

3932.2	0.04722	1.3050	3895.6	0.04363	1.2143	3770.2	0.05461	1.2677
3934.1	0.04708	1.3051	3897.5	0.04356	1.2143	3772.1	0.05456	1.2677
3936.1	0.04693	1.3052	3899.4	0.04348	1.2144	3774.1	0.05450	1.2677
3938.0	0.04679	1.3053	3901.3	0.04340	1.2145	3776.0	0.05444	1.2677
3939.9	0.04665	1.3054	3903.3	0.04333	1.2145	3777.9	0.05438	1.2677
3941.8	0.04650	1.3055	3905.2	0.04325	1.2146	3779.9	0.05432	1.2677
3943.8	0.04636	1.3056	3907.1	0.04318	1.2147	3781.8	0.05426	1.2677
3945.7	0.04622	1.3057	3909.1	0.04310	1.2148	3783.7	0.05421	1.2678
3947.6	0.04608	1.3058	3911.0	0.04303	1.2148	3785.6	0.05415	1.2678
3949.6	0.04594	1.3059	3912.9	0.04295	1.2149	3787.6	0.05409	1.2678
3951.5	0.04580	1.3060	3914.8	0.04288	1.2150	3789.5	0.05403	1.2678
3953.4	0.04567	1.3062	3916.8	0.04280	1.2150	3791.4	0.05398	1.2678
3955.3	0.04553	1.3063	3918.7	0.04273	1.2151	3793.4	0.05392	1.2678
3957.3	0.04539	1.3064	3920.6	0.04265	1.2152	3795.3	0.05386	1.2678
3959.2	0.04525	1.3065	3922.6	0.04258	1.2152	3797.2	0.05380	1.2678
3961.1	0.04512	1.3066	3924.5	0.04251	1.2153	3799.1	0.05374	1.2678
3963.1	0.04498	1.3067	3926.4	0.04243	1.2154	3801.1	0.05369	1.2678
3965.0	0.04485	1.3068	3928.3	0.04236	1.2155	3803.0	0.05363	1.2678
3966.9	0.04471	1.3069	3930.3	0.04229	1.2155	3804.9	0.05357	1.2678
3968.8	0.04458	1.3070	3932.2	0.04221	1.2156	3806.9	0.05351	1.2678
3970.8	0.04445	1.3071	3934.1	0.04214	1.2157	3808.8	0.05346	1.2679
3972.7	0.04431	1.3072	3936.1	0.04207	1.2157	3810.7	0.05340	1.2679
3974.6	0.04418	1.3073	3938.0	0.04200	1.2158	3812.6	0.05334	1.2679
3976.6	0.04405	1.3074	3939.9	0.04192	1.2159	3814.6	0.05329	1.2679
3978.5	0.04392	1.3075	3941.8	0.04185	1.2159	3816.5	0.05323	1.2679
3980.4	0.04379	1.3076	3943.8	0.04178	1.2160	3818.4	0.05317	1.2679
3982.3	0.04366	1.3078	3945.7	0.04171	1.2161	3820.4	0.05311	1.2679
3984.3	0.04353	1.3079	3947.6	0.04164	1.2161	3822.3	0.05306	1.2679
3986.2	0.04340	1.3080	3949.6	0.04157	1.2162	3824.2	0.05300	1.2679
3988.1	0.04327	1.3081	3951.5	0.04150	1.2163	3826.1	0.05294	1.2679
3990.1	0.04314	1.3082	3953.4	0.04142	1.2163	3828.1	0.05289	1.2679
3992.0	0.04302	1.3083	3955.3	0.04135	1.2164	3830.0	0.05283	1.2679
3993.9	0.04289	1.3084	3957.3	0.04128	1.2165	3831.9	0.05277	1.2679
3995.8	0.04276	1.3085	3959.2	0.04121	1.2165	3833.9	0.05272	1.2679
3997.8	0.04264	1.3086	3961.1	0.04114	1.2166	3835.8	0.05266	1.2679
3999.7	0.04251	1.3087	3963.1	0.04107	1.2167	3837.7	0.05260	1.2679
			3965.0	0.04100	1.2167	3839.6	0.05254	1.2679
			3966.9	0.04093	1.2168	3841.6	0.05249	1.2679
			3968.8	0.04086	1.2169	3843.5	0.05243	1.2679
			3970.8	0.04079	1.2169	3845.4	0.05237	1.2680
			3972.7	0.04072	1.2170	3847.4	0.05232	1.2680
			3974.6	0.04066	1.2171	3849.3	0.05226	1.2680
			3976.6	0.04059	1.2171	3851.2	0.05221	1.2680

			3978.5	0.04052	1.2172	3853.1	0.05215	1.2680
			3980.4	0.04045	1.2173	3855.1	0.05209	1.2680
			3982.3	0.04038	1.2173	3857.0	0.05204	1.2680
			3984.3	0.04031	1.2174	3858.9	0.05198	1.2680
			3986.2	0.04024	1.2175	3860.9	0.05192	1.2680
			3988.1	0.04018	1.2175	3862.8	0.05187	1.2680
			3990.1	0.04011	1.2176	3864.7	0.05181	1.2680
			3992.0	0.04004	1.2177	3866.6	0.05175	1.2680
			3993.9	0.03997	1.2177	3868.6	0.05170	1.2680
			3995.8	0.03991	1.2178	3870.5	0.05164	1.2680
			3997.8	0.03984	1.2178	3872.4	0.05159	1.2680
			3999.7	0.03977	1.2179	3874.4	0.05153	1.2680
						3876.3	0.05147	1.2680
						3878.2	0.05142	1.2680
						3880.1	0.05136	1.2680
						3882.1	0.05130	1.2680
						3884.0	0.05125	1.2680
						3885.9	0.05119	1.2680
						3887.8	0.05114	1.2680
						3889.8	0.05108	1.2680
						3891.7	0.05102	1.2680
						3893.6	0.05097	1.2680
						3895.6	0.05091	1.2680
						3897.5	0.05086	1.2680
						3899.4	0.05080	1.2680
						3901.3	0.05075	1.2680
						3903.3	0.05069	1.2680
						3905.2	0.05063	1.2680
						3907.1	0.05058	1.2680
						3909.1	0.05052	1.2680
						3911.0	0.05047	1.2680
						3912.9	0.05041	1.2680
						3914.8	0.05036	1.2680
						3916.8	0.05030	1.2680
						3918.7	0.05024	1.2680
						3920.6	0.05019	1.2680
						3922.6	0.05013	1.2680
						3924.5	0.05008	1.2680
						3926.4	0.05002	1.2680
						3928.3	0.04997	1.2680
						3930.3	0.04991	1.2680
						3932.2	0.04986	1.2680
						3934.1	0.04980	1.2680

						3936.1	0.04975	1.2680
						3938.0	0.04969	1.2680
						3939.9	0.04964	1.2680
						3941.8	0.04958	1.2680
						3943.8	0.04953	1.2680
						3945.7	0.04947	1.2680
						3947.6	0.04942	1.2680
						3949.6	0.04936	1.2680
						3951.5	0.04931	1.2680
						3953.4	0.04925	1.2680
						3955.3	0.04920	1.2680
						3957.3	0.04914	1.2680
						3959.2	0.04909	1.2680
						3961.1	0.04903	1.2680
						3963.1	0.04898	1.2680
						3965.0	0.04892	1.2680
						3966.9	0.04887	1.2680
						3968.8	0.04881	1.2680
						3970.8	0.04876	1.2680
						3972.7	0.04870	1.2680
						3974.6	0.04865	1.2680
						3976.6	0.04859	1.2680
						3978.5	0.04854	1.2680
						3980.4	0.04848	1.2680
						3982.3	0.04843	1.2680
						3984.3	0.04837	1.2680
						3986.2	0.04832	1.2680
						3988.1	0.04827	1.2680
						3990.1	0.04821	1.2680
						3992.0	0.04816	1.2680
						3993.9	0.04810	1.2680
						3995.8	0.04805	1.2680
						3997.8	0.04799	1.2680
						3999.7	0.04794	1.2680